Design, synthesis and evaluation of fluorescent probes for the diagnosis of Alzheimer's disease and Parkinson's disease

TECHNISCHE UNIVERSITÄT DARMSTADT

Vom Fachbereich Chemie
der Technischen Universität Darmstadt

zur Erlangung des akademischen Grades eines

Doctor rerum naturalium (Dr. rer. nat.)

genehmigte
Dissertation

vorgelegt von

Jiamin Gu, Ms. nat. sci.
Master der Naturwissenschaften
aus Jiangsu

Referent: Prof. Dr. Boris Schmidt
Korreferent: Prof. Dr. Katja Schmitz
Tag der Einreichung: 07. Januar 2013
Tag der mündlichen Prüfung: 18. Februar 2013

Darmstadt 2013
D17

The present work was done under the supervision of Prof. Dr. Boris Schmidt at the Clemens-Schöpf-Institute of Organic Chemistry and Biochemistry of the Technische Universität Darmstadt from January 2010 to December 2012.

Acknowledgements

The work embodied in this thesis was carried out from January 2010 until December 2012 at the Clemens Schöpf-Institute of Organic Chemistry and Biochemistry of the Technische Universität Darmstadt under the supervision of Prof. Dr. Boris Schmidt.

First of all, I would like to offer my utmost gratitude to Prof. Dr. Boris Schmidt for giving me the opportunity to come to Germany to work in his group and introducing me to the fascinating world of medicinal chemistry. I am very grateful to him for his constant help, advice, discussion and encouragement, which greatly contributed to solve problems I faced in my research work.

I am grateful to all my lab colleagues for the nice working atmosphere and for their sincerity and unfailing support. Special thanks to Dr. Fabio Lo Monte, Dr. Thomas Kramer and Dr. Stephanie Kolb for all the help rendered when I first started with my PhD. I would like to thank Upendra Rao Anumala for his valuable assistance in my study. I would also like to thank Birgit Keenan, thank you for all the help with organizational matters, regarding contract, visa etc.

I would like to thank all the employees of the institute, particularly to Dr. Reinhard Meusinger, Karin Jungk and Karl-Otto Runzheimer for their help with NMR and IR measurements; Christiane Rudolph and Gül Sahinalp for their help with mass measurements and Prof. Dr. Dencher for his help with UV-Vis spectrum analysis.

I am deeply grateful to Dr. Marlyse Okala Amombo and Dr. Fabio Lo Monte for critical reading of my dissertation. Their valuable advice and suggestions are gratefully acknowledged. Additionally, I would like to thank Stefan Göring for help with the German translations of the abstract.

I would also acknowledge the Federal German government and Bundesministerium für Bildung und Forschung (BMBF) for financial support. I am very grateful to Dr. Roland Heyny von Haußen, Jana Hölzer, Prof. Dr. Ingrid Hilger, Valérie Goetschy-Meyer and Dr. Christian Czech for their cooperation and biological testing.

I would like to thank all my friends, who supported me through my life. Last but not least, a big thanks to my family, especially my mother and father, for their concern and unconditional support. I would like to thank my wife, Qifang Wang, for your constantly supportive encouraging and unwavering love.

Partial results of this thesis have been published or submitted for publication:

1. Gu, J.; Anumala, U. R.; Lo Monte, F.; Kramer, T.; Heyny-von Haußen, R.; Holzer, J.; Goetschy-Meyer, V.; Mall, G.; Hilger, I.; Czech, C.; Schmidt, B.* 2-Styrylindolium based fluorescent probes visualize neurofibrillary tangles in Alzheimer's disease. *Bioorg. Med. Chem. Lett.* **2012**, *22*, 7667.

2. Lo Monte, F.*; Kramer, T.; Gu, J.; Brodrecht, M.; Pilakowski, J.; Fuertes, A.; Dominguez, J. M.; Plotkin, B.; Eldar-Finkelman, H.; Schmidt, B.* Structure-based optimization of oxadiazole-based GSK-3 inhibitors. *Eur. J. Med. Chem.* **2012**, accepted. DOI: 10.1016/j.ejmech.2012.06.006.

3. Lo Monte, F.*; Kramer, T.; Gu, J.; Anumala, U. R.; Marinelli, L.; La Pietra, V.; Novellino, E.; Franco, B.; Demedts, D.; Van Leuven, F.; Fuertes, A.; Dominguez, J. M.; Plotkin, B.; Eldar-Finkelman, H.; Schmidt, B* Identification of glycogen synthase kinase-3 inhibitors with a selective sting for glycogen synthase kinase-3α. *J. Med. Chem.* **2012**, *55*, 4407.

4. Schmidt, B.; Kieser, D.; Boländer, A.; Herms, J.; Heyny-von Haußen, R.; Gu, J. Compounds for diagnosing neurodegerative disease at the retina. *WO 2012041292*, **2012**.

5. Schmidt, B.; Kieser, D.; Boländer, A.; Herms, J.; Heyny-von Haußen, R.; Gu, J. Compounds for the diagnosis of neurodegenerative disorders on the olfactory epithelium. *WO 2012037928*, **2012**.

Zusammenfassung

Die Alzheimer Demenz (AD) und der Morbus-Parkinson (MP) sind die beiden meistbekannten, langsam fortschreitenden neurodegenerativen Erkrankungen. Kennzeichnend für beide Krankheiten sind proteinhaltige Ablagerungen, welche *post mortem* in den betroffenen Hirngeweben gefunden werden. Charakteristisch für die AD sind die beiden Proteine Amyloid-β (Aβ) und Tau, wohingegen für den MP Ablagerungen von α-Synuclein (ASN) in den Neuronen der *substantia nigra pars compacta* pathologisch kennzeichnend sind. Die Herstellung hirngängiger Substanzen in der AD, welche spezifisch an Aβ-Plaques und an den neurofibrillären Bündeln (NFTs) binden, sind nicht nur ein diagnostischer Ansatz, sondern auch ein erster Schritt in Richtung der Medikamentenentwicklung. Die derzeitige *in vivo* Diagnose der AD wird durch unzureichende Sensitivität und Spezifität der diagnostischen Methoden beeinträchtigt, weshalb eine neue nicht-invasive Bildgebung zur Früherkennung der AD benötigt wird. Derzeit gibt es unterschiedliche Verbindungsklassen für die Detektion der Aβ-Plaques, jedoch ist nur eine geringe Anzahl an Substanzen für den pathologischen Nachweis der NFTs bekannt. In dieser Arbeit wurden erfolgreich fluoreszierende Liganden unterschiedliche Substanzklassen der Thiazole, der Bisstyrole, der Spiropyrane, der Trimethincyanine oder auch der Indolyle für die Detektion der Aβ-Plaques und der NFTs in Hirngeweben von AD Patienten synthetisiert. Die Visualisierung der selektiv gebundenen Substanzen an Aβ-Plaques oder NFTs im Hippocampus eines AD-Gehirns erfolgte mittels eines Fluoreszenzmikroskops. Zur Bestimmung der Bindungsaffinität wurde ein neuer kompetitiver Thiazin Red R Assay eingesetzt. Des Weiteren wurden potentielle Verbindungen *in vitro* in einem hepatozellulären Karzinom-Assay (HepG2) sowie in einem Zebrafisch-Embryo Toxizitäts-Assay untersucht. Hierbei zeigten die Substanzen keine oder geringfügige Zytotoxizität bei entsprechender Konzentration auf, wodurch die Evaluation in einem *in vivo* Maus-Modell gegeben ist. Darüber hinaus ist die Detektion nasaler Tauablagerungen mittels dieser fluoreszenter Liganden in der Nasenschleimhaut möglich. Nach entsprechender Präparation erzeugen diese eine entsprechende Fluoreszenzmarkierung der entsprechenden Pathogene, wodurch eine Frühdiagnose ermöglicht wird. Gleichzeitig wurden ausgewählte Substanzen als potentielle Liganden für die Bindung an ASN in MP untersucht. Durch PET- bzw. SPECT-Bildgebung können weitere radioaktiv markierte Analoga als Sonden für Aβ, Tau und ASN dienen.

Contents

Abbreviations

3D	Three-dimensional
Å	Angstrom
AD	Alzheimer's disease
AIBN	2,2'-Azobis(isobutyronitrile)
AICD	APP intracellular domain
ApoE	Apolipoprotein E
APP	Amyloid precursor protein
Ar	Aryl
ASN	α-Synuclein
Aβ	β-Amyloid
$A\beta_{40}$	40-Amino-acid-long peptide
$A\beta_{42}$	42-Amino-acid-long peptide
BACE	β-Site APP cleaving enzyme
BBB	Blood-brain barrier
bpm	Beats per minute
BSc	Boris Schmidt substance database code
CaMK-II	Calcium-calmodulin-dependent kinase-II
CDK-5	Cyclin-dependent kinase-5
CK-1	Casein kinase-1
CNS	Central nervous system
CR	Congo red
CT	Computed tomography
C-terminal	Carboxy-terminal
CTF	Carboxy-terminal fragments
d	Doublet

DAPI	Fluorescence dye: 4',6-diamidino-2-phenylindole
DMSO	Dimethyl sulfoxide
dpf	Days post-fertilization
E	Exon
EC_{50}	Effective doses
Et	Ethyl
EtOAc	Ethyl acetate
FITC	Fluorescent dye: fluorescein
g	Gram
GSK-3	Glycogen synthase kinase-3
GSMs	γ-Secretase modulators
HE	Hydroxyethylene
HEA	Hydroxyethylamine
HepG2	Liver hepatocellular carcinoma cell assay
hpf	Hours post-fertilization
HPLC	High-performance liquid chromatography
Hz	Hertz
IC_{50}	Half maximal inhibitory concentration
IMPY	6-Iodo-2-(4'-dimethylamino)phenyl-imidazo[1,2-*a*]pyridine
IR	Infrared
J	Coupling constant
kDa	Kilodalton
LBs	Lewy bodies
LC_{50}	Lethality concentration
LNs	Lewy neurites
LRRK2	Leucine-rich repeat kinase 2
m	Multiplet

MAPs	Microtubule-associated proteins
MAPT	Microtubule-associated protein tau
MARK	Microtubule affinity-regulating kinase
MB	Methylene blue
ME	Merocyanine
Me	Methyl
mp	Melting point
MPM	Multiphoton microscopy
MRI	Magnetic resonance imaging
MW	Molecular weight
N-terminal	Amino-terminal
NBS	*N*-Bromosuccinimide
NFTs	Neurofibrillary tangles
NIH	National Institutes of Health
NMP	*N*-Methyl-2-pyrrolidon
NMR	Nuclear magnetic resonance
NSAIDs	Non-steroidal anti-inflammatory drugs
PD	Parkinson’s disease
PDPK	Proline-directed protein kinase
PEG	Polyethylene glycol
PET	Positron emission tomography
Ph	Phenyl
PHFs	Paired helical filaments
PIB	Pittsburgh Compound-B
PINK 1	PTEN-induced protein kinase 1
PKA	cAMP dependent protein kinase
PRD	Proline-rich domain

PRKN	Parkin
Pro	Proline
PS	Presenilins
RH	Rhodanine
s	Singlet
SAR	Structure-activity relationship
SB	Styrylbenzenes
Ser	Serine
SFs	Straight filaments
SP	Spiropyran
SPECT	Single-photon emission computed tomography
SPs	Senile plaques
t	Triplet
$t_{1/2}$	Half-life
TH	Thiohydantoin
THF	Tetrahydrofuran
Thr	Threonine
ThS	Thioflavin S
ThT	Thioflavin T
TI	Teratogenic index
TICT	Twisted internal charge-transfer
TLC	Thin layer chromatography
Tyr	Tyrosine
UCH-L1	Ubiquitin C-terminal hydrolase like 1
UV	Ultraviolet
WSG	Water soluble groups
λ_{max}	Wavelength of maximum absorption

1. Introduction

1.1. Alzheimer's disease

In 1906, Dr. Alois Alzheimer, a German pathologist, discovered lesions in the brain of a woman who died with dementia at age 56. Alzheimer's disease (AD) was first described by Dr. Alzheimer and named after him. Today, one hundred years later, AD is becoming the most common form of dementia affecting millions of elderly people, which can be caused by a lot of progressive disorders that affect memory, thinking, behavior, the ability to perform the everyday activities and eventually by disturbances in reasoning, planning, language and perception.[1-3]

One major risk factor of AD progression is age, and most individuals with the disease are age 65 or older. After age 65, the possibility of developing dementia roughly doubles every five years. It was estimated that 36 million people were living with AD and other dementias all over the world in 2011, this number will rise up to 66 million by 2030 and 115 million by 2050.[4] It is noteworthy that almost 60% of the patients live in low and middle income countries currently, and the number will increase to 70% by 2050. According to the World Alzheimer Report 2010, it was proposed that the worldwide costs of dementia were more than 600 billion US dollars in 2010, which amounts to more than 1% of global GDP in that year.[5] The average social costs are 33 thousands per person with dementia every year, which is even higher than the annual income in Germany.

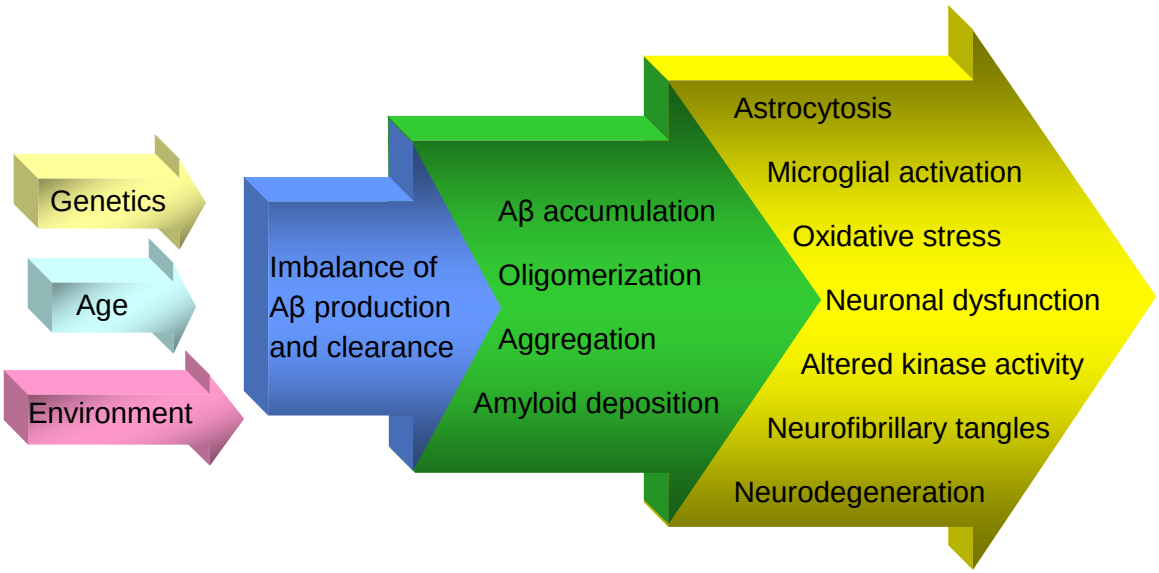

Figure 1.1 The amyloid cascade hypothesis of Alzheimer's disease

The risk factors for AD include age and genetics regarding the etiology of AD. Other possible environmental factors are level of education, sex, head injury, exposure to heavy metals and toxins.[6] Even positive family heredity will affect and cause dementia (**Figure 1.1**).[1,7]

Post-mortem analysis of human brains provided the mechanisms of disease and potential interventions. A century ago, Dr. Alzheimer started to describe the disease by two kinds of abnormal proteins in patients' brains: senile plaques (SPs) and neurofibrillary tangles (NFTs) (**Figure 1.2**).[7-9] Currently, scientists generally agree that SPs and NFTs are major hallmarks of AD.[10,11] SPs are composed of the β-amyloid (Aβ) peptide, a fragment of the amyloid precursor protein (APP), whereas the NFTs are comprised of the hyperphosphorylated form of the microtubule-associated protein tau.

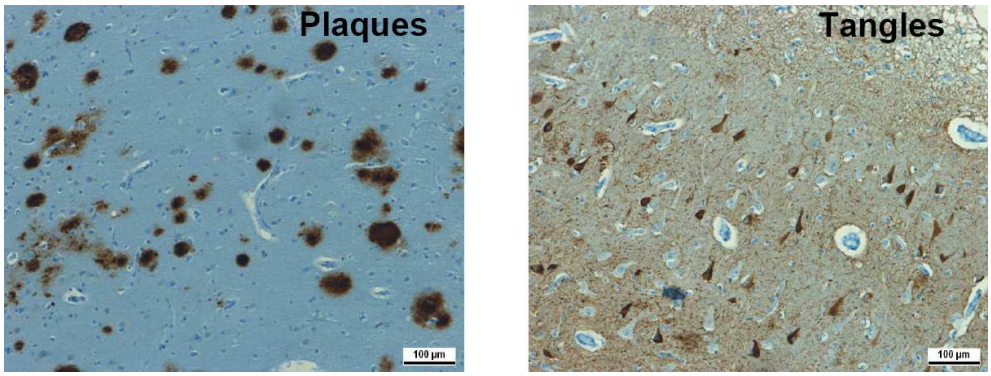

Figure 1.2 Immunohistochemical staining with antibodies against Aβ plaques (left) and NFTs (right)

A deeper understanding of different cellular functions of hallmarks will help us to study the diagnostic and therapeutic methods for AD.

1.1.1. Overview of amyloid precursor protein processing enzymes and products

The pathology of AD has been studied intensely in the last two decades. Although the real mechanisms to cause AD are not fully understood, according to the amyloid cascade hypothesis, it is widely believed that the uncontrolled clumping of Aβ plaques is one of the cardinal factors to cause AD.[12,13] The deposition of Aβ is related to an imbalance between its production and clearance. The excess Aβ is believed to be a main contributor to the dysfunction and degeneration of neurons that occurs in AD.[14] Aβ plaque formation is a neuropathological hallmark which is found in the brain of patients with AD.

APP is a type-1 membrane protein with a large extracellular portion, which is expressed in various mammalian cells. The biochemical studies of APP and the presenilins (PS) have greatly enhanced the understanding of the molecular pathways leading to Aβ generation.[15,16]

The major component of Aβ plaques are small 38- to 42-amino-acid-long β-amyloid peptides. They are generated by the stepwise cleavage of APP, which is a transmembrane glycoprotein of undetermined function.[8] APP can be processed by α-, β- and γ-secretases. Aβ protein is generated by the successive action of β-secretase and γ-secretase. These two secretases serve to release various isoforms of the Aβ peptide. Aβ is prone to aggregation, giving rise to toxic species, including dimers, oligomers and fibrils. The most aggregation-prone $A\beta_{42}$ isoform aggregates faster to form toxic oligomers and deposits as Aβ plaques.

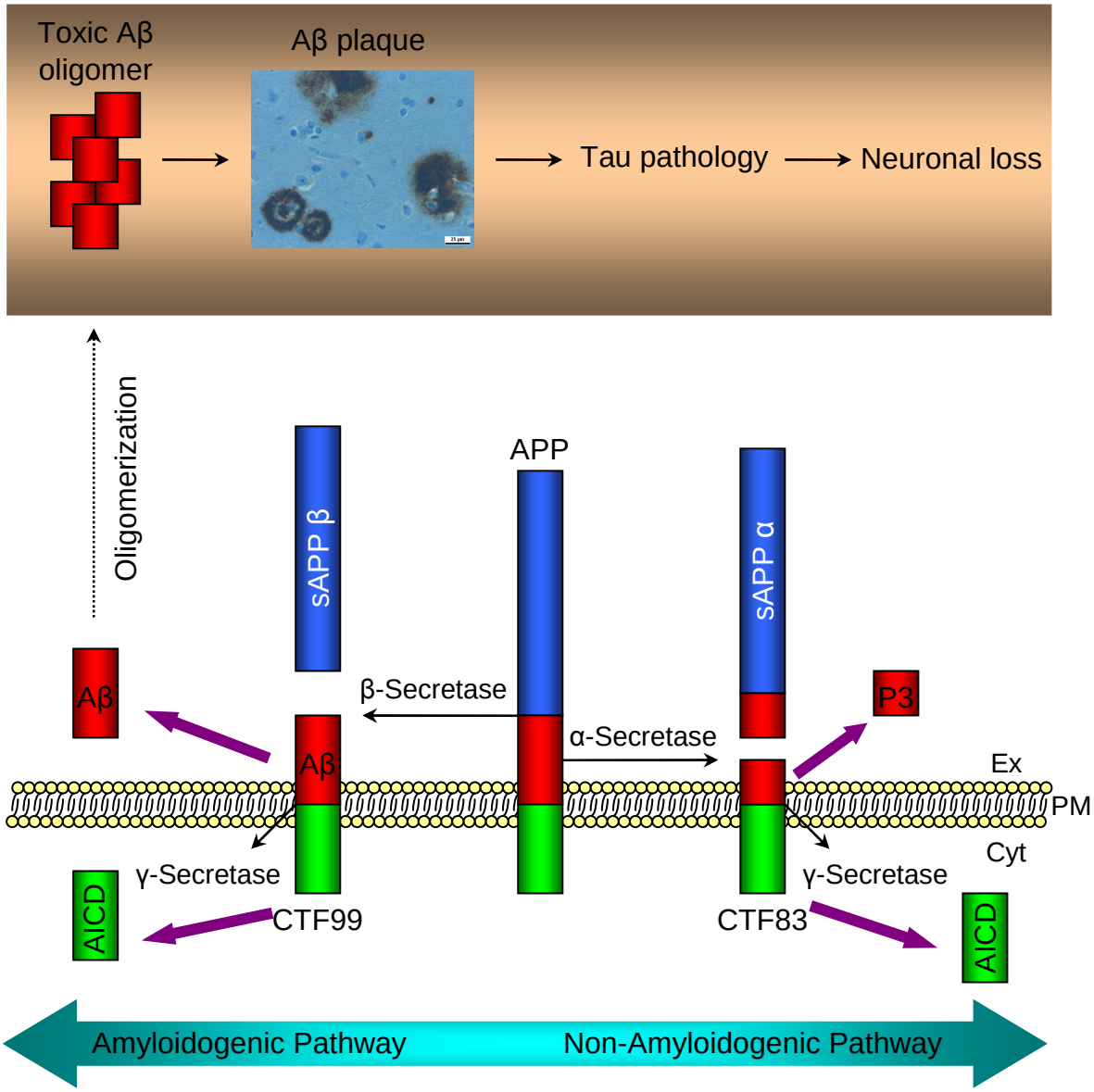

Figure 1.3 The APP processing and cleavage products. Aβ fragments oligomerize and fibrillize leading to AD pathology (left and upper panel). APP: amyloid precursor protein; CTF: carboxy-terminal fragments; AICD: APP intracellular domain; Ex: extracellular; PM: plasma membrane; Cyt: cytosol.

A simplified APP processing is depicted in **Figure 1.3**.[3,7,17-22] The non-amyloidogenic APP processing pathway (right) involves cleavages by α- and γ-secretases resulting in the generation of a long secreted form of APP (sAPP*α*). The amyloidogenic APP processing pathway (left) involves cleavages by β- and γ-secretases resulting in the generation of a long secreted form of APP (sAPPβ). The carboxy-terminal fragments (CTF) generated by *α*- and β-secretase are called CTF83 and CTF99, respectively.[23] γ-Secretase cleavage of CTF83 and CTF99 in the membrane results in the generation of P3 and Aβ, respectively, as well as the amino-terminal (N-terminal) APP intracellular domain (AICD).

β-secretase and β-cleavage

β-Site APP cleaving enzyme 1 (BACE1), was first identified and characterized as β-secretase in AD in 1999 by five research groups from industry and academia.[24] It is a type I transmembrane aspartyl protease with its active site on the luminal side of the membrane. Certainly, BACE1 exhibited all the known characteristics of β-secretase. The 501 amino acid sequence of BACE1 bears the hallmark features of eukaryotic aspartic proteases of the pepsin family.[25,26] β-Secretase cleaves APP in its extracellular domain and leaves a fragment called CTF99, which is further cleaved by the transmembrane γ-secretase complex that includes presenilin. It was also reported that BACE1 can also cleave APP at a more carboxy-terminal (C-terminal) position to result in CTF89.[17]

A related enzyme, BACE2, exerts β-secretase activity, but it is expressed at very low levels in the brain and is mostly restricted to glial cells.[27,28]

γ-secretase and γ-cleavage

γ-Secretase is a high-molecular-weight protein complex and the detailed structure is still unknown. It cleaves APP at multiple sites and in sequential steps to generate Aβ peptides of different lengths, as well as the N-terminal AICD (**Figure 1.4**). There are two major Aβ species that are being formed: the 40-amino-acid-long peptide ($A\beta_{40}$) and the more aggregation-prone 42-amino-acid-long peptide ($A\beta_{42}$). It has been shown that under physiological conditions, $A\beta_{40}$ constitutes nearly 90% of the total amount of Aβ. Besides, the dominant γ-cleavage site at $A\beta_{40}$ and $A\beta_{42}$ residues, ζ-cleavage at 46 and ε-cleavage at 49 residues are also thought to be mediated by γ–secretase.[21,29-31]

The monomeric Aβ (molecular weight ~4 kDa) is produced mainly in neurons from APP (molecular weight ~120 kDa) via sequential scission by the enzymes β- and γ-secretase.[14] Great progress has been made in characterizing molecules involved in APP processing and functions of APP cleavage products. Nevertheless, Aβ remains the main suspect in AD

pathogenesis. Understanding of the process would help us to explore the diagnostic and therapeutic methods in the future.

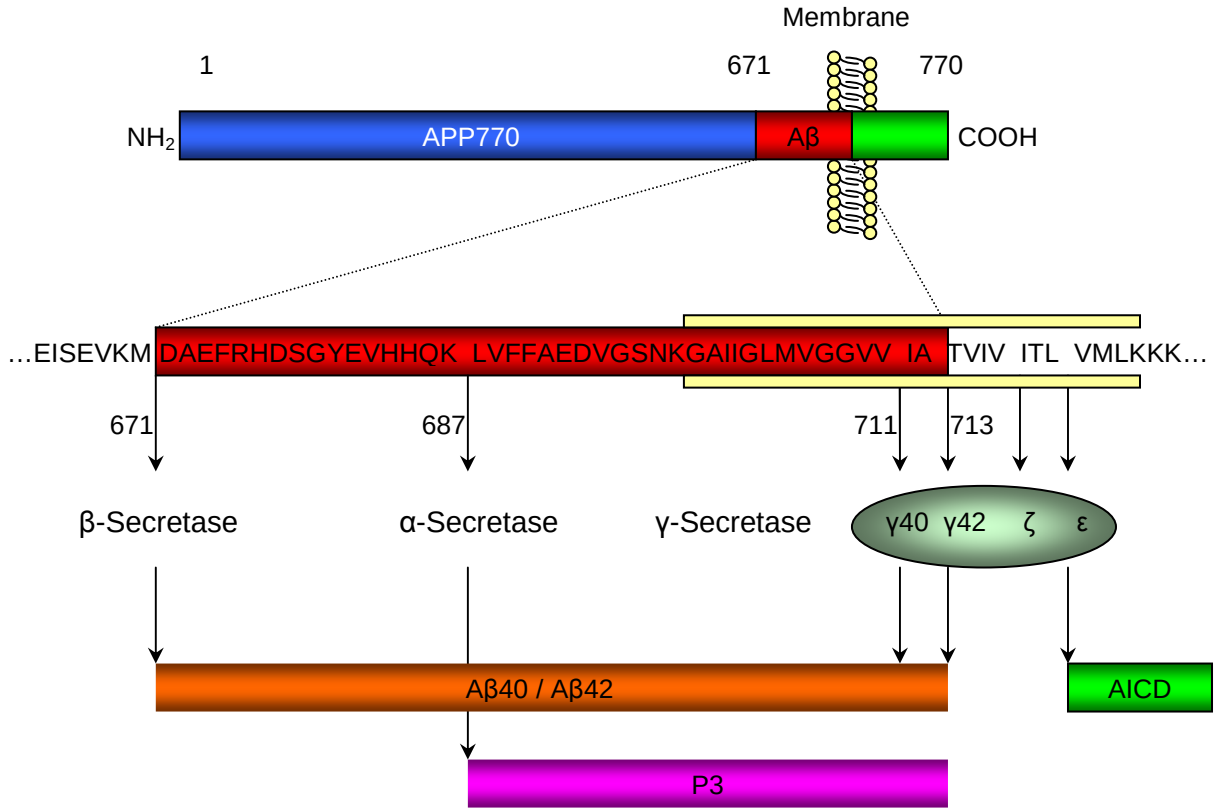

Figure 1.4 The role of β-secretase and γ-secretase in the proteolytic processing of APP.

1.1.2. The role of tau in Alzheimer's disease

NFTs are another major pathologic hallmark of AD. In normal cells tau regulates the assembly and maintenance of the structural stability of microtubules. However, tau becomes abnormally phosphorylated, aggregates into paired helical filaments (PHFs) and loses its ability to maintain the microtubule tracks in the diseased brain.[32] Afterwards, the free tau molecules aggregate into PHFs to form NFTs.[33]

Tau contains three major domains: an N-terminal projection domain, a C-terminal domain of microtubule binding repeats and a short tail sequence. In the adult human central nervous system (CNS), there are six tau isoforms, about 352- to 441-amino-acid-long residues (**Figure 1.5**). Tau isoforms are likely to have specific functions related to the absence or presence of regions encoded by the cassette exons 2, 3 and 10. The two 29-amino acid sequences encoded by exons 2 and 3 (E2 and E3) give rise to different lengths of the N-terminal part of Tau proteins. These two additional inserts are highly acidic. They are followed by a basic proline-rich domain (PRD).[13,34,35] Exon 10 encodes an additional microtubule binding repeat, resulting in isoforms with either three- (3R) or four- (4R)

microtubule binding internal repeats.[36] Splicing generates two series of tau isoforms, each containing either 3R or 4R microtubule-binding repeats (M1-M4) with differential affinity for microtubules.[13,19] The 3R or 4R is made of a highly conserved 18-amino acid repeat. It has been demonstrated that 3R tau isoforms also bind less tightly than 4R tau to microtubules.[37] In normal brain, the 3R/4R tau ratios for both mRNA and protein are almost equal. The role of altered 3R/4R tau ratio in AD remains controversial. Several findings suggested that increased 3R tau may contribute to AD, because 3R, but not 4R, tau contributes to the increased phosphorylated tau levels in brain.[38] However, the tau transgenic mice available for the *in vivo* experiment are all based on the 4R tau repeat and deposit very little amounts of tau.[39] The 3R tau isoforms are predominant in neonatal mouse whereas in adult mouse the 4R isoforms are predominant.[40,41] This shortcoming may limit the use of mouse models for the *in vivo* evaluation of tau imaging agents.

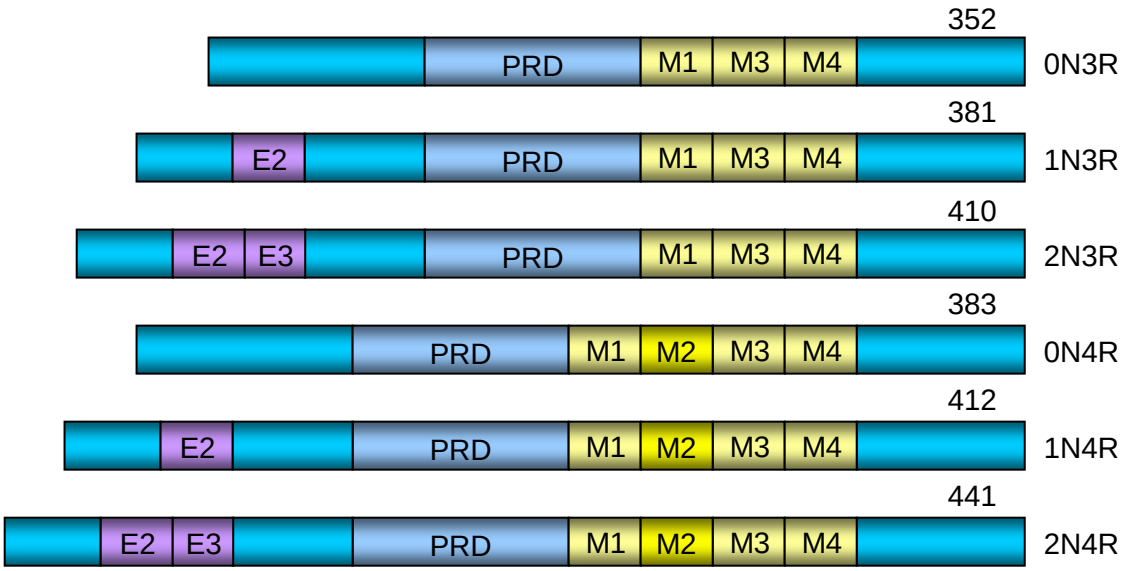

Figure 1.5 In the human CNS, the alternative splicing of exons 2, 3 and 10 generates six tau isoforms which ranges in size from 352- to 441-amino acids. Lack of E2 and E3 leads to 0N tau isoforms, whereas inclusion of E2 gives rise to 1N and inclusion of both E2 and E3 produce 2N tau isoforms. M1–M4 corresponding to the four imperfect-repeat microtubule binding domains in which M2 is encoded by exon 10. Absence of M2 gives 3R tau and inclusion results in 4R tau isoforms.

The microtubule-associated protein tau is the main component of NFTs. In the normal state, it is a hydrophilic, soluble protein that promotes microtubule assembly and stabilization. However, pathological forms of tau are abnormally phosphorylated at certain residues and significantly reduced affinity for microtubules. Currently, there is limited knowledge about the impact of phosphorylation on tau function. Generally, it negatively regulates the binding of tau to microtubules.[9] It is known that tau is one of the microtubule-associated proteins (MAPs) that stabilize neuronal microtubules for their role in the development of cell processes, the

establishment of cell polarity and intracellular transport. In the healthy brain, only two or three residues on tau are phosphorylated. The degree of phosphorylated tau depends on the activities of protein kinases and phosphatases. But in AD and other tauopathies, the phosphorylation level of tau is much higher, with approximately nine phosphates in every molecule.[18,42] The abnormal hyperphosphorylation of tau may result in the upregulation of tau kinases or downregulation of tau phosphatases in AD brains. Some of them may regulate its microtubule-binding properties. Several groups reported recently that tau has 84 putative phosphorylation sites including 45 serines (Ser), 35 threonines (Thr) and 4 tyrosines (Tyr).[8] Hyperphosphorylation of tau may occur at different putative Ser, Thr, and Tyr residues through a disruption of the equilibrium of tau kinases and tau phosphatases activity.[33] Especially, the phosphorylation of orthologous residues in the adjacent microtubule-binding repeats at Ser262 and Ser356 has been suggested to detach tau from microtubules.[43] Indeed, hyperphosphorylated tau accumulates in the somatodendritic compartment of neurons, aggregates and eventually forms NFTs.[8]

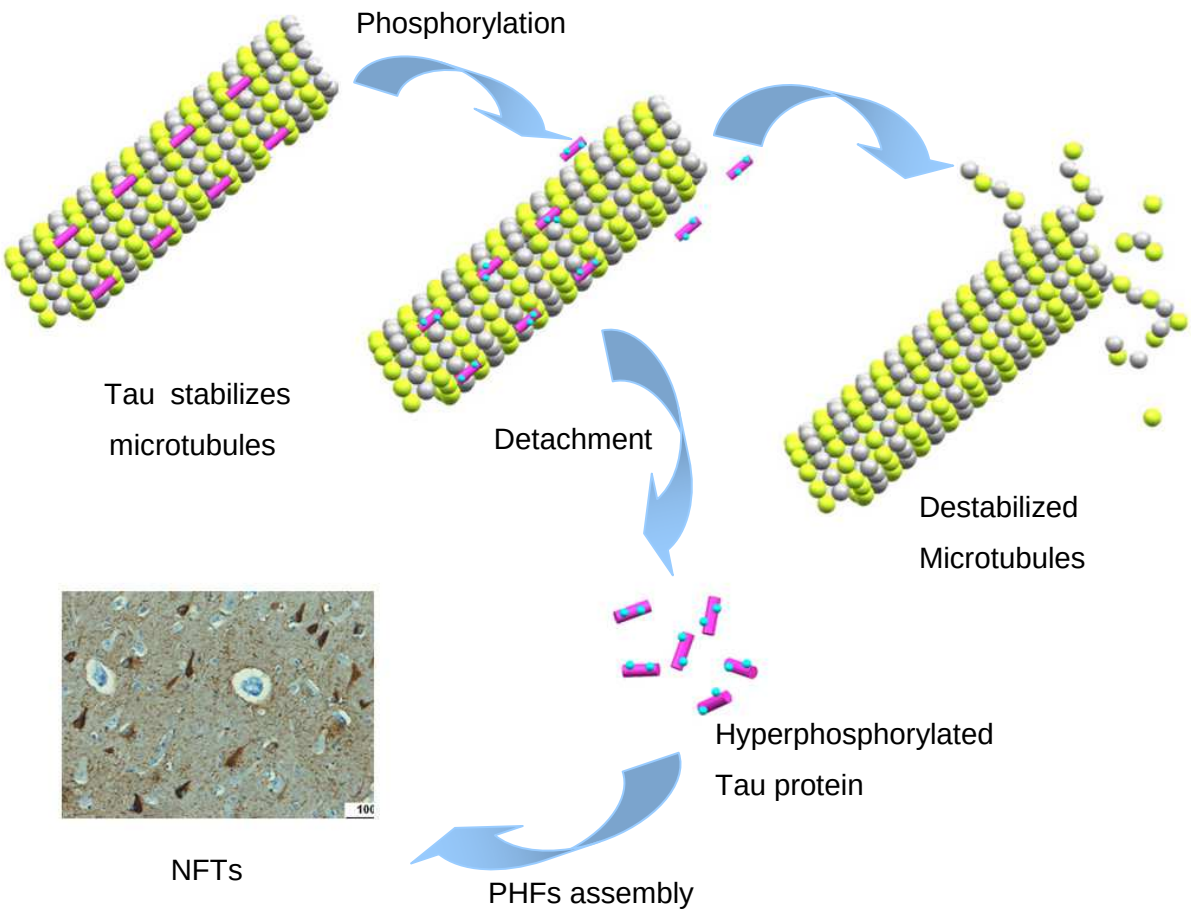

Figure 1.6 Proposed model of tau leads to neurofibrillary tangle formation.

Tau phosphorylation has been demonstrated to cause decreased binding and destabilization of microtubules, and hyperphosphorylated tau from AD brains fails to bind microtubules. Hence, functions of tau that involve microtubules, such as microtubule stabilization and the regulation of axonal transport may be compromised, possibly contributing to disease. Indeed, the majority of studies suggest that hyperphosphorylation of tau is a major contributor to the pathologic progression that leads to tangle formation.[13]

There are three kinds of NFT can be recognized morphologically: pretangles, intracellular tangles and extracellular (ghost) tangles. It is reported that intracellular tangles were 3R/4R tau-positive, however most pretangles were 4R tau-positive and ghost tangles were 3R tau-positive. These evidences suggested that isoforms of tau aggregates may shift from a 4R tau-predominant formation to a 3R tau-predominant formation during the development of NFT.[44] Phosphorylated Ser101 plays an important role in the formation of ghost tangles and pretangles. The ghost tangles appeared as loose bundles of fibers and located in the neuropil when intracellular tangles are exposed extracellularly. More and more evidences indicated that hyperphosphorylated tau is toxic to neurons and this toxicity is associated with the induction of cell death.[44-46]

Different from the antibody against paired helical filaments, the antibodies against tau and phosphorylated neurofilaments do not stain ghost tangles. It suggested that the loss of specific epitopes during the progression of the disease may cause the inability to detect ghost tangles by immunohistochemistry.[47] However, ghost tangles were clearly visualized with *Thiazine Red R*. The affinities of these probes to aggregated tau and $A\beta_{40}$ were determined by displacement of the reference dye *Thiazine Red R*, hence IC_{50} data obtained in the competition assay are reported rather than K_i values. *Thiazine Red R* was selected as reference ligand for the displacement assay, because it was previously shown to be superior to Thioflavin S or immune histochemical detection of aggregated Tau and $A\beta_{40}$.[48,49] It was shown to be an accurate maker for β-pleated sheet structures and to reliably stain Aβ plaques and diffuse NFTs (K_d for aggregated $A\beta_{40}$ = 49 nM and K_d for aggregated tau = 18 nM). It was reported that the *in vitro* binding affinity (K_i) of Methoxy-X04 (**Chapter 1.3.2**) is 26.8 nM.[50] The same compound was measured in *Thiazine Red R* assay and IC_{50} values are shown in experiment sections.

1.2. Therapeutic approaches to Alzheimer's disease

1.2.1. β-Secretase as a therapeutic target for Alzheimer's disease

Currently, the reduction of Aβ levels in the brain is an attractive clinical approach to treat AD. According to the amyloid cascade hypothesis, it is believed that β-secretase is the first protease that processes APP in the pathway leading to the production of Aβ.[51] For this reason, β-secretase is an attractive therapeutic target for the development of inhibitor drugs. The development of β-secretase inhibitors has been pursued more than a decade.

There are some factors that should be taken into consideration for the development of a viable β-secretase inhibitor. Generally, drugs for β-secretase should be small, potent and display low toxicity. They must exhibit favorable selective transition state analogues with good membrane penetration and pharmaceutical properties.[26,52-54] Besides, the inhibitor should express sufficient lipophilicity to efficiently cross the blood–brain barrier (BBB) to achieve high concentrations in the brain.[24]

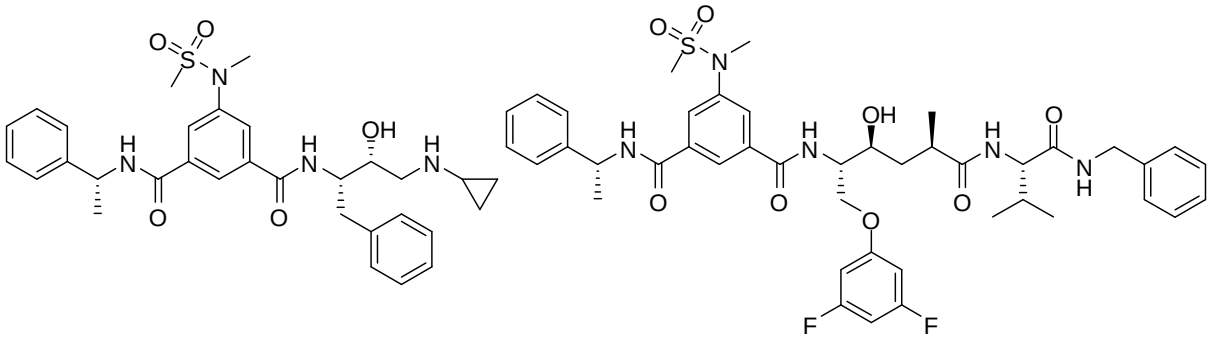

Figure 1.7 Hydroxyethylamine (HEA) and Hydroxyethylene (HE) BACE1 inhibitors

Since the identification of β-secretase in 1999, a series of β-secretase inhibitors had been employed.[55] So far, several promising inhibitors have entered early phase clinical trials (**Figure 1.7**). The overall progress in the field permits some optimism that this structure-based design strategy will lead to better compounds. It seems that β-secretase inhibitors may be a valuable and important therapeutic target for the treatment of AD.

1.2.2. γ-Secretase as a therapeutic target for Alzheimer's disease

As previously discussed, γ-secretase is a rationale target for the treatment of AD because it regulates the final step of the Aβ formation. The main form of Aβ contains 40 amino acids, but the carboxy-terminal-extended species, made up of 42 residues, is also produced at the same time. The longer form is more prone to aggregate into fibrils and $A\beta_{42}$ makes up the

major component of SPs. Selective lowering of $A\beta_{42}$ levels with small molecule γ-secretase modulators (GSMs), such as some non-steroidal anti-inflammatory drugs (NSAIDs),[56] a holds promise in the treatment of AD.

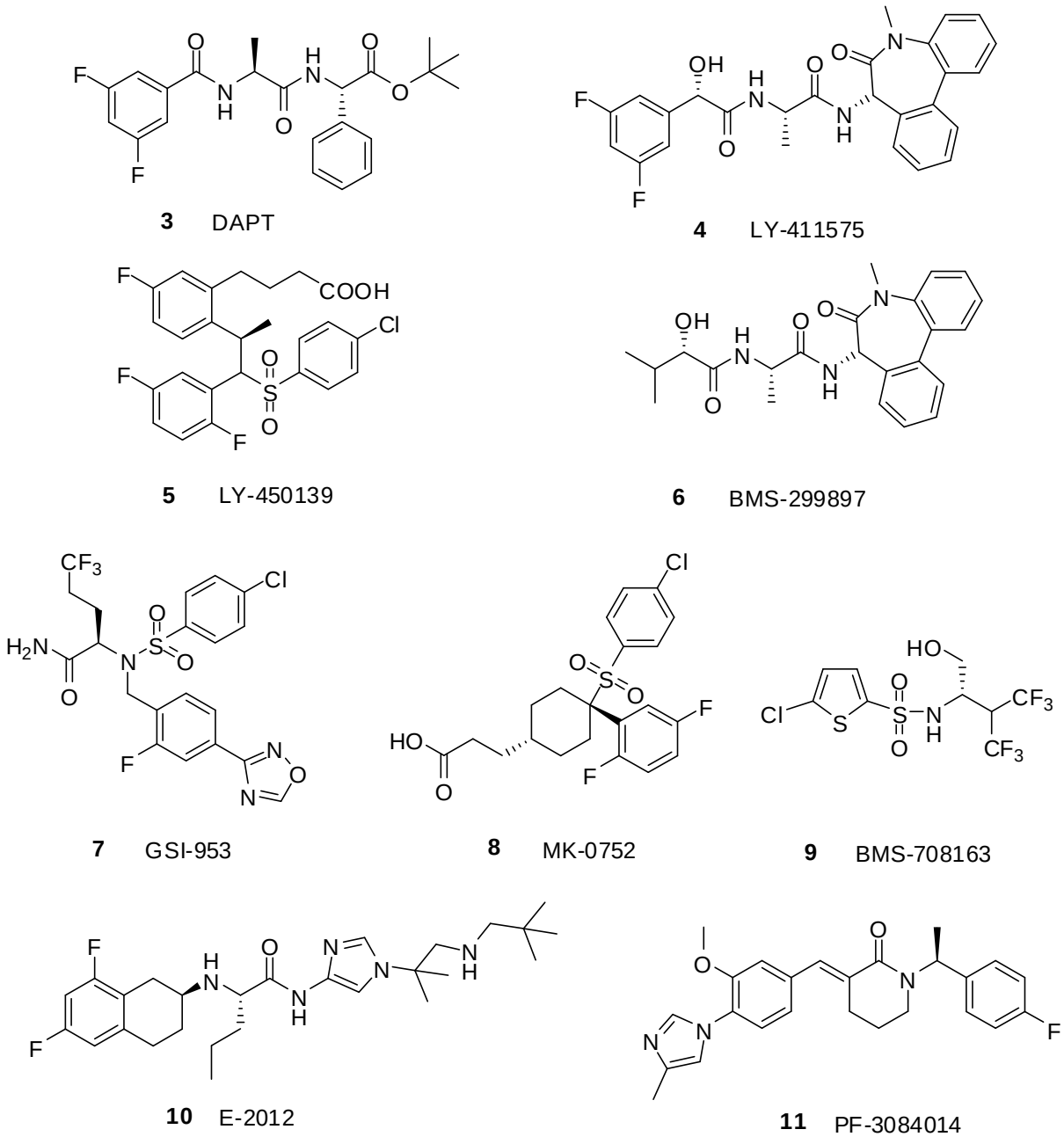

Figure 1.8 Structures of γ-Secretase inhibitors.

In short, γ-secretase is a complicated and unusual proteolytic complex. However, several classes of potent inhibitors have been discovered and evaluated. Currently, at least six compounds have entered clinical development. In 2001, the first *in vivo* testing of a γ-secretase inhibitor involved the dipeptidic compound DAPT (*N*-[*N*- (3,5-difluorophenacetyl)-*L*-alanyl]-*S*-phenylglycine *t*-butyl ester) (**3**) was reported, which was developed by Elan and Eli

Lilly (**Figure 1.8**). The benzodiazepine analog LY-411575 (**4**) and benzolactam semagacestat (LY-450139) (**5**), which were developed by Eli Lilly, are others potent, orally available and active γ-secretase inhibitors which have been tested extensively *in vivo*.[57-59] LY-411575 is one of the most potent γ-secretase inhibitors yet reported, with an IC_{50} value of 119 pmol/L for the inhibition of Aβ production in APP overexpressing HEK293 cells. LY-450139 is a functional γ-secretase inhibitor that has been tested in the human Phase II trial.[60] Bristol-Myers Squibb (BMS) and the former SIBIA Neurosciences developed the sulfonamide inhibitor BMS-299897 (**6**) as the first γ-secretase inhibitor to reach clinical trials. This compound displays an IC_{50} = 7 nmol/L in the inhibition of Aβ production in APP-overexpressing HEK293 cells. However, human testing of BMS-299897 started in 2001, but clinical data have never been fully reported. The long-lasting lack of data on its clinical development indicate that it has been abandoned.[61] Besides, five other γ-secretase inhibitors, GSI-953 (**7**), MK-0752 (**8**), BMS-708163 (**9**), E-2012 (**10**) and PF-3084014 (**11**) already entered the clinical trials.[62,63]

1.2.3. Tau as a therapeutic target for Alzheimer's disease

NFTs are one of the pathological hallmarks of AD and primarily composed of aggregates of hyperphosphorylated forms of the MAPs tau. Tau phosphorylation is believed to initiate or facilitate dissociation from microtubules leading to microtubule destabilization, decay of cellular transport properties and cell death.

The last decade has witnessed the rise of interest in inhibitors of tau aggregation as potential target of drugs for therapeutic purposes in AD. Numerous researches in tau therapeutics are in process. Some of the principal lines to investigate tau in neurodegenerative disease have been implemented.[64] First, reduction or prevention of the abnormal tau hyperphosphorylation through inhibition of specific protein kinases, such as glycogen synthase kinase-3 (GSK-3), cyclin-dependent kinase-5 (CDK-5), casein kinase-1 (CK-1), cAMP dependent protein kinase (PKA), calcium-calmodulin-dependent kinase-II (CaMK-II), and microtubule affinity-regulating kinase family (MARK).[19,33] Second, the prevention of disassembly of tau aggregates into PHFs. Furthermore, the development of tau immunotherapy and anti-inflammatory therapy as a means of controlling pathogenesis and preserving neuronal function in disease was suggested to be a valid strategy.

1.2.3.1. Drug development targeting the kinase in Alzheimer's disease

GSK-3

Glycogen synthase kinase 3 (GSK-3), a tau kinase with a plethora of other substrates, is able to phosphorylate both non-Ser/Thr-Pro sites and Ser/Thr-Pro sites. There are two

related isoforms of GSK-3 encoded by two independent genes, GSK-3α and GSK-3β, which share 98% homology in their catalytic domains and have similar biochemical properties.[65,66] GSK-3 is highly enriched in the human brain and recent research indicates that the GSK-3β isoform is a key kinase required for the abnormal hyperphosphorylation of tau.[67] However, several investigations suggest GSK-3α as a potential target for the treatment of AD and other CNS diseases.[68,69]

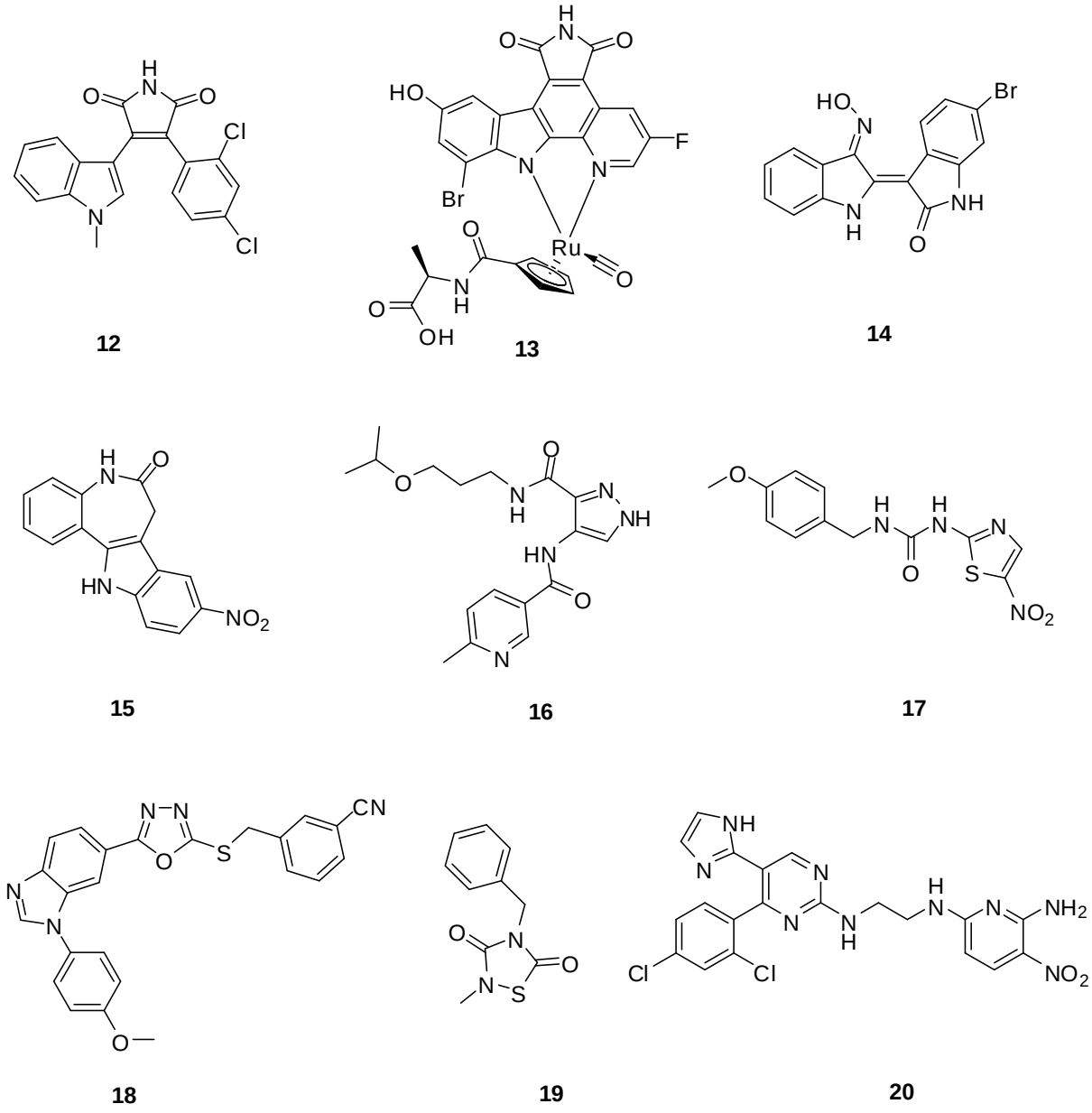

Figure 1.9 Small-molecule inhibitors of GSK-3.

Lithiumchloride was the first GSK-3 inhibitor to be discovered, but the mechanism of action is still not well understood. Indeed, during the last decade, various types of small organic molecules as GSK-3 inhibitors have been published (**Figure 1.9**). A wide range of molecules

that inhibit GSK-3 have been evaluated such as maleimide derivatives (**12**), staurosporine and organometallic inhibitors (**13**), indole derivatives (**14**), paullone derivatives (**15**), pyrazolamide derivatives (**16**), thiazole derivatives (**17**), oxadiazole derivatives (**18**), thiadiazolindiones (**19**) and furopyrimidine derivatives (**20**).[70,71] Currently, some GSK-3 inhibitors pass through preclinical or clinical trials with the therapeutic indication AD.

CDK-5

CDK-5 is a 33 kDa heavy proline-directed protein kinase (PDPK), which phosphorylates Ser/Thr residues immediately preceding a proline residue. It has also been associated with the development of neurofibrillary pathology because of its overexpression in a mouse model. Further results have shown to induce tau hyperphosphorylation and tangle formation. Additionally, due to the GSK-3 overactivity in the double transgenic mice and colocalized with both aggregated tau and CDK-5, it implied that CDK-5 may also act directly, indirectly or in concert with GSK-3.[72]

Others kinases

Altogether, it seems that numerous kinase interactions cause the abnormal tau hyperphosphorylation. It is believed that more than one kinase is involved in tau phosphorylation. The net effect of different kinases will be focus of research in the next decade.

1.2.3.2. Small molecule inhibitors of tau aggregation

Under normal conditions tau is a very soluble protein that does not readily aggregate into filaments. In AD, protein aggregation processes have been implicated in neuronal dysfunction and cytotoxicity. Tau aggregation is a potential mediator of neurodegeneration. Further development of small molecules to reduce tau aggregate formation and/or enhance their clearance will be an efficient pathway to treat AD.

Interestingly, the first drug, which is currently evaluated in clinical trials and directly modulates tau, is methylene blue (MB) (**21**) (RemberTM). In 1996, MB was first found to inhibit tau-tau binding through the repeat domain. In 2008, Wischik's team reported inhibitors of tau aggregation as potential therapy for AD.[64]

In 2004, Jeff Kuret's lab developed a cyanine dye named N744 (**22**), which was found to inhibit tau fibrillization and promote disaggregation of mature synthetic filaments *in vitro*.[73] They found that inhibitors, which include thiacarbocyanine dyes, can inhibit recombinant tau fibrillization in the presence of anionic surfactant aggregation inducers. In 2007, Kuret's lab synthesized and characterized a cyclic bis-thiacarbocyanine molecule containing two

thiacarbocyanine moieties (**23**) to evaluate tau fibrillization inhibitory activity.[74,75] The bis-thiacarbocyanine was evaluated in the action of cyanine-mediated inhibition of tau aggregation, which inhibited the aggregation of full-length tau protein with >4-fold better potency than the monomer N744 (**Figure 1.10**).

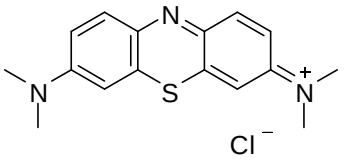

21 Methylene blue

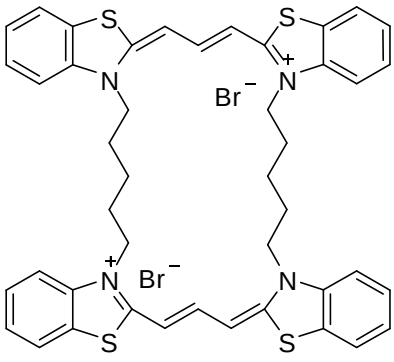

23 Bis-thiacarbocyanine

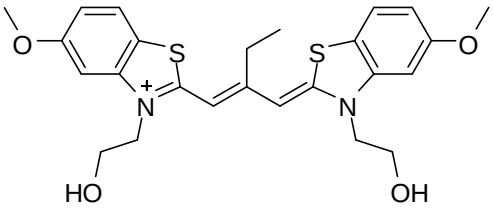

22 N744

Figure 1.10 Tau aggregation inhibitors.

In brief, small molecule inhibitors of tau aggregation serve as important research tools and possibly as basis for potential new therapeutics. Searching in the National Institute of Health (NIH) clinical trial database demonstrates that more than 950 clinical trials have been conducted or are ongoing (search for “tauopathy” in the www.clinicaltrials.gov, in 18.12.2012). Most of these studies are mainly directed to find new AD treatments or diagnostics. Fortunately, some new classes of drugs that have been previously tested in preclinical tau models are now being tested in different clinical trial phases at present. By pursuing these lines of study, a viable therapy for AD and related tauopathies may be achieved.

1.3. Molecular imaging in Alzheimer's disease

Imaging biomarkers hold great promise for diagnosing disease, monitoring disease progression, tracking therapeutic effect, and improving our knowledge of pathophysiology.[76] Molecular imaging allows repetitive, non-invasive assessment in biological and biochemical processes in living subjects. Therefore, this technology could enhance the understanding of disease and identify drug activity during the preclinical and clinical stage of drug development (**Figure 1.11**). The parallel paths for the development of therapeutic drugs and diagnostic agents raise exciting opportunities to develop technology and to improve the

efficiency. It contributed to selected candidates which seem most likely to be successful or to halt the drug development which would eventually fail. It will significantly save time and cost to improve the overall drug development process.[77-79]

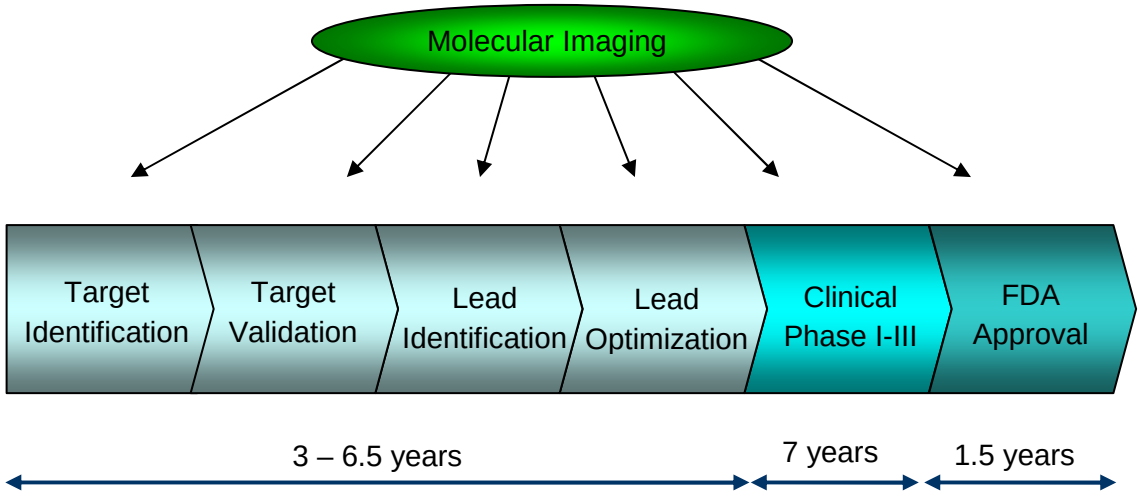

Figure 1.11 Drug developments is a long process that generally spans about 10 to 15 years, but molecular imaging can help in many steps of the process.

The key considerations for the imaging compounds include target validation, identification of suitable candidate compounds with high affinity and uptake at the target site, adequate clearance and low potential toxicity.[80] Habitually, the exploration of imaging agents starts with the design and synthesis of novel and unique probes which can directly interact with specific molecular targets, such as a receptor, transporter or enzyme. With conception and creation, iterative modification of knowing structure is the main approach to obtain the new compounds as imaging agent which selectively bind to the target. Additionally, the bioactivity such as the sensitivity of detection and specificity of interaction, pharmacokinetics of delivery, and signal-to-noise ratio will be characterized by appropriate *in vitro* and *in vivo* assays which are important for the imaging agent performance.

Imaging agents can be aimed at targets, such as Aβ, tau or α-synuclein (ASN), which play critical roles in neurodegenerative diseases. However, imaging agents do not modify the functional targets of the disease. This technology may also be used in the earlier stage of the disease to detect the hallmarks. It will provide valuable time for effective prevention, treatment and reduce or avoid the pain of the disease. Development of molecular imaging probes is essential for the application of multimodal molecular imaging techniques in the drug development processes. Currently, some probes are widely used in rodents or larger animals. Once the imaging agent has passed through preclinical testing, it would be ultimately used in clinical trials, such as positron emission tomography (PET), single-photon

emission computed tomography (SPECT), magnetic resonance imaging (MRI) and ultrasound.[77]

With the advances in the development of imaging agents, molecular imaging is believed to play an important role in accelerating and improving drug development in the future.

1.3.1. Molecular imaging techniques in Alzheimer's disease

Imaging techniques offer a non-invasive or minimally invasive method for visualizing, characterizing, and quantifying anatomical structures and physiological processes at cellular and subcellular levels. Early symptoms of the disease may be detected by imaging technologies. Generally, molecular imaging can provide early and clear identification of fundamental biological and biochemical processes such as the cause, location and extent of the disease. Over the past two decades, neuroimaging techniques such as computed tomography (CT), PET, SPECT, MRI and multiphoton microscopy (MPM) have increasingly been employed to detect AD, to clarify the neuropathology and to monitor disease progression *in vivo*.

Structural imaging techniques such as CT and MRI are often done to exclude some causes of dementia, such as normal pressure hydrocephalus or some special lesions like tumors. At the same time, they can help to clarify the diagnosis by detecting areas with atrophy or vascular lesions in the early stage of disease. While CT provides good spatial resolution, the MRI provides comparable resolution with far better contrast. Because of greater accuracy, manipulability and precision, MRI has more recently surpassed CT in diagnosis of AD.[31,81]

PET and SPECT have been extensively evaluated as diagnostic procedures for AD. They can image and detect the concentrations of neuroreceptors, transporters, and neurotransmitters in the picomolar range *in vivo*.[82] As well it serves to define a patient's pathological status when the neurological symptoms can not be explained by CT or MRI. PET and SPECT are often used as extremely sensitive noninvasive imaging techniques to label the molecules with positron emitting radionucleotides.[83] The radioisotopes decay will result in the emission of detectable γ-rays. Afterwards, the tomographic reconstruction techniques are used to obtain three-dimensional (3D) images.[84] γ-ray emitting isotopes such as [^{15}O], [^{13}N], [^{11}C] and [^{18}F] have widely been used in PET. However, these positron emitters have very short half-lives ([^{15}O], $t_{1/2}$ = 2.1 min; [^{13}N], $t_{1/2}$ = 10.0 min, [^{11}C], $t_{1/2}$ = 20.1 min; [^{18}F], $t_{1/2}$ = 110 min). Among these, [^{11}C] and [^{18}F] are more frequently used to replace hydrogen or a hydroxyl group on substrates to target receptors.[85] Meanwhile, compounds labeled with longer half-lives isotopes such as [^{99m}Tc] ($t_{1/2}$ = 6h) or [^{125}I] ($t_{1/2}$ = 13h) are commonly used in SPECT imaging. In comparison to the PET, SPECT is more widespread

in clinical settings because there is no need for an on-site cyclotron. In addition, SPECT has lower costs compared with PET imaging.

Table 1.1 Advantages and limitations of different imaging techniques.

Imaging techniques	Advantage	Disadvantage
Optical imaging	• High-throughput screening • High sensitivity	• Limited clinical translation • Low depth penetration
PET	• Clinical translation • High sensitivity • Noninvasive	• Costs • Limited spatial resolution
SPECT	• Clinical translation • High sensitivity • Noninvasive	• Limited spatial resolution
MRI	• Clinical translation • Relatively High resolution • Noninvasive	• Costs • Imaging time • low sensitivity
CT	• High spatial resolution • Clinical translation	• No target-specific imaging • Radiation • Poor soft-tissue contrast
Ultrasound imaging	• Clinical translation • High spatial and temporal resolution • Low costs	• Operator dependency • Targeted imaging limited to vascular compartment
MPM	• High signal to noise ratio • Very high resolution	• Invasive

In general, each imaging technique has some advantages as well as limitations (**Table 1.1**). The combination of different imaging techniques provides great promise for the effective diagnosis of the disease. Actually, all imaging techniques are rather complementary than competitive. Currently, neuroimaging techniques have more and more been used to detect effects in the AD brains. There is still a demand for effective biomarkers in AD to improve the diagnosis and to detect disease progression, to monitor the therapeutic effects and to predict future dementia prior to onset of cognitive decline.[31]

1.3.2. Imaging agents for the detection of Aβ plaques

Excessive Aβ aggregation forms Aβ plaques in the brain and plays one of the most important roles in the early pathological stage of AD.[86] In this case, with noninvasive technologies, Aβ plaques bear potential to be a useful biomarker for the early diagnosis of AD. For this reason, it may be used to evaluate the clinical efficacy of therapies.

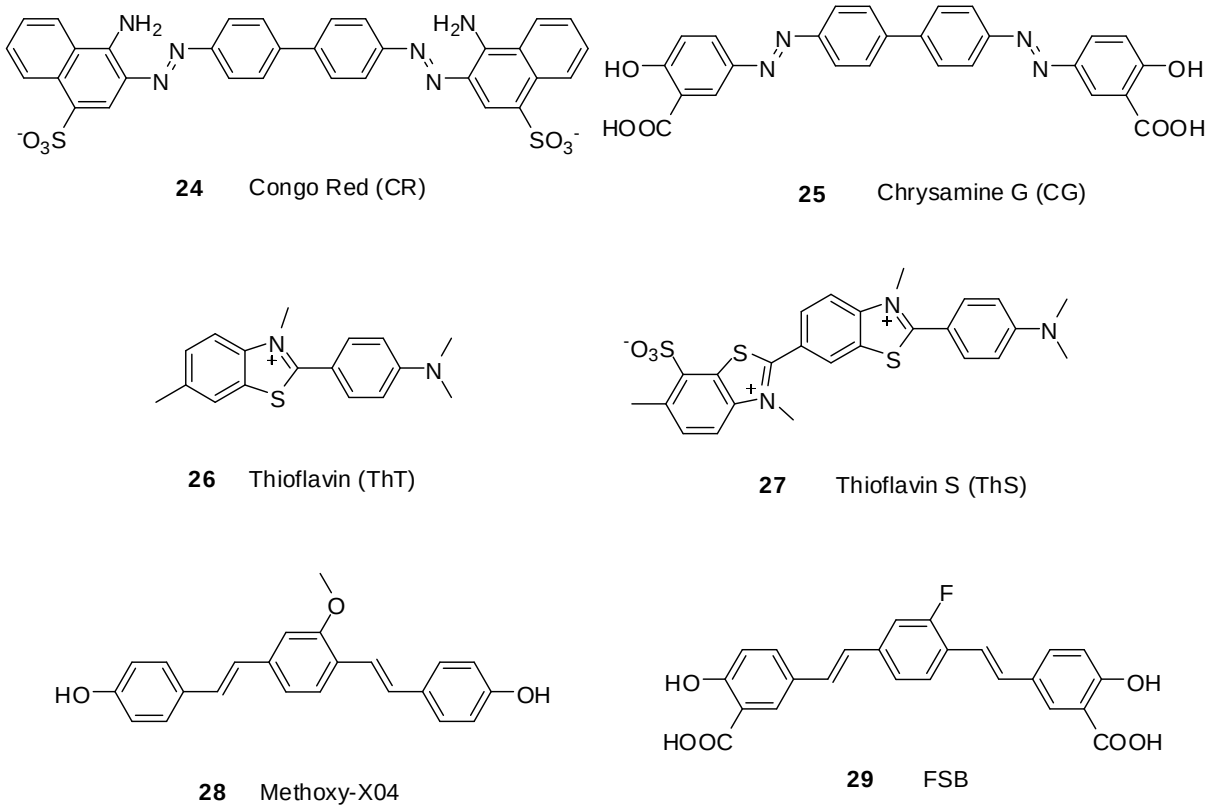

Figure 1.12 Organic dyes widely used for the histological staining of Aβ plaques.

In the past ten years, several research groups synthesized a large number of small molecule compounds as candidates for amyloid imaging agents (**Figure 1.12**).[50,87-92] Some of these derivatives exhibit high binding affinities to Aβ plaques and display excellent brain pharmacokinetic profiles.[93] Generally, the imaging agents should meet the following conditions: first, effectively image Aβ plaques; second, have good reproducibility in many subjects and clinical settings; third, widely appropriate for specific task; and fourth, easily cross the BBB with the property of rapid clearance from the brain. However, only a few agents were able to satisfy these requirements right now.[94]

Several lead compounds have been studied, such as Congo red (CR) (**24**), benzothiazole derivatives (**26**), 6-dialkylamino-2-naphthylethylidenemalononitrile (DDNP) derivatives (**31**), styrylbenzene (SB) derivatives (**32**) and vinylbenzoxazole derivatives (**33**) (**Figure 1.12** and **Figure 1.13**).[90,95] The candidates differ in binding characteristics and in their brain uptake.

Some of the agents have recently led to promising *in vivo* imaging of Aβ plaques in patients with AD.[96]

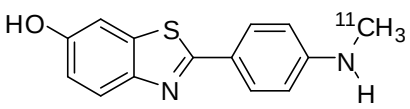

30 [^{11}C]PIB

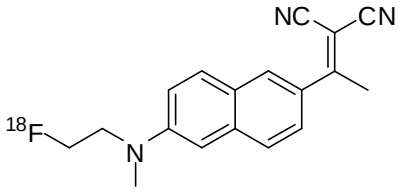

31 [^{18}F]FDDNP

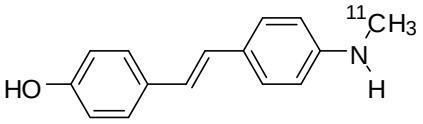

32 [^{11}C]SB-13

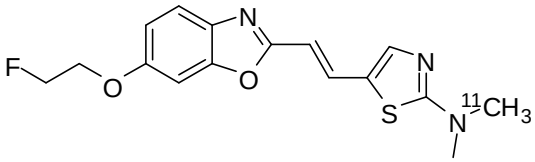

33 [^{11}C]BF-227

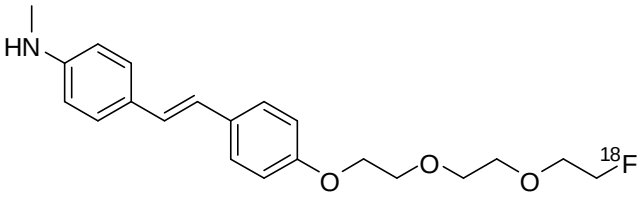

34 [^{18}F]BAY94-9172

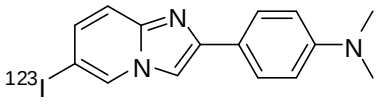

35 [^{123}I]IMPY

Figure 1.13 PET and SPECT imaging probes for Aβ plaques.

The most studied amyloid PET imaging probe [*N*-methyl-^{11}C]$_2$-(4'-methylaminophenyl)-6-hydroxybenzothiazole, also called Pittsburgh Compound-B (^{11}C-PIB) (**30**) had advanced research in AD.[97-99] So far, at least four other amyloid PET ligands have been evaluated with PET in AD patients (**Figure 1.13**), such as [^{18}F]-1,1-dicyano-2-[6-(dimethylamino)-2-naphtalenyl] propene (^{18}F-FDDNP) (**31**),[100,101] [^{11}C]4-*N*-methylamino-4´-hydroxystilbene (^{11}C-SB13) (**32**),[102] [^{11}C]2-(2-[2-dimethylaminothiazol-5-yl]ethenyl)-6-(2-[fluoro]ethoxy)benzoxazole (^{11}C-BF-227) (**33**)[103] and [^{18}F]-Florbetaben (^{18}F-BAY94-9172) (**34**).[104] These derivatives show excellent binding affinities with K_d values of < 10 nM for aggregates of $A\beta_{40}$.[105]

Because of the long half-lives ([^{99m}Tc] and [^{125}I]) of positron emitters and other advantages over PET, a series of Aβ specific imaging agents and their related derivatives were synthesized for SPECT. But to our knowledge, until now only [^{123}I]-6-iodo-2-(4'-dimethylamino)phenyl-imidazo[1,2-*a*]pyridine ([^{123}I]IMPY) (**35**) have been tested in humans (**Figure 1.13**).[106] It is regrettable that [^{123}I]IMPY (**35**) ultimately failed in the clinical trials. At this point, it is urgent to develop novel Aβ specific imaging agents for SPECT.

1.3.3. Imaging agents for the detection of neurofibrillary tangles

While many imaging probes for Aβ plaques have been developed in the last decade, it is inconceivable that only few compounds for targeting NFTs have been reported.

Neurofibrillary lesions appear at certain sites decades before the onset of dementia in AD. They are highly correlated with AD symptoms and proved as a potential surrogate marker for the detection of disease at very early stages. It is believed that NFTs detection should lead to the early diagnosis of AD and estimate the severity stage of disease. Besides, the relation of tau aggregates to neurodegeneration and cognitive decline in AD also provides a potential surrogate marker for the disease. In the view of these superiorities, *in vivo* imaging of NFTs is needed and should be a necessary complement to the imaging of Aβ plaques as useful tool for the early and accurate diagnosis of AD.[107]

Requirements for the ideal tau imaging agent should meet the following principal criteria. First, they require sufficient permeability to the BBB after intravenous injection while simultaneously being subject to rapid clearance from normal brain tissue. Because the major PET radionuclides ^{11}C and ^{18}F have very short half-lives, it will contribute to detect the specific binding *in vivo*. Second, the imaging agent should express excellent affinity for NFTs and sensitivity to be detected. Last but not least, in order to make sure the neuritic lesion spatial distribution would not be covered up or confounded by other lesions in the brain, imaging agents must bind tau aggregates with sufficient selectivity or low nonspecific binding to other lesions.[107,108]

Until now only few reports are published on the development of imaging probes which target NFTs (**Figure 1.14**). The first tau aggregate binding agent Thioflavin T (**26**) was recognized on the basis of direct fluorescence in tissues. However, the toxicity and inability to cross the BBB limited further tests *in vivo*. Afterwards, several papers have reported FSB (**29**), FDDNP (**31**), curcumin (**36**), neutral benzothiazole derivatives (**30**, **37** and **38**), thiohydantoin (TH) (**39**), rhodanine (RH) (**40**), benzimidazole (**41**) derivatives, carbazole derivatives (**42**) and quinolines (**43**-**45**) as candidate probes for *in vivo* imaging of tau pathology in AD.

Multitracer PET imaging use FDDNP (**31**) and neutral ThT derivatives such as PIB (**30**) to reveal some complex disease progression in AD. In spite of low specific binding, they could provide significant information about the differences in topographical distribution between FDDNP-PET and PIB-PET images and assist to understand the distributions of Aβ plaques and NFTs in both subjects with or without AD.[109]

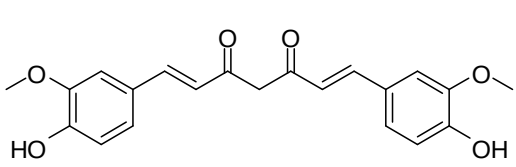

36 Curcumin

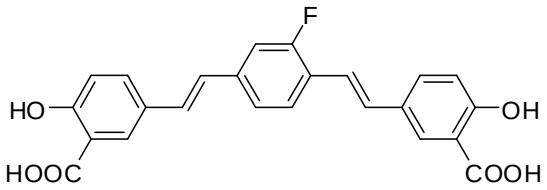

29 FSB

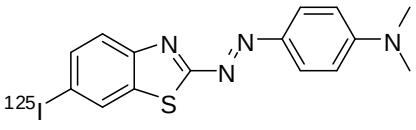

37 [^{125}I]PDB

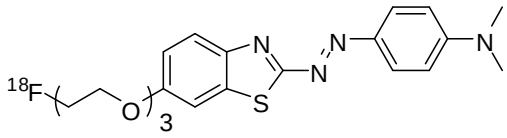

38 [^{18}F]FPPDB

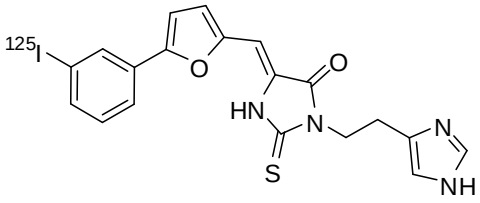

39 [^{125}I]TH2

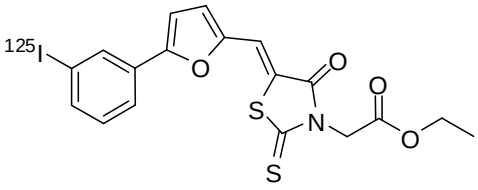

40 [^{125}I]RH1

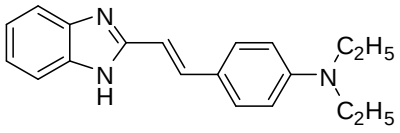

41 BF-126

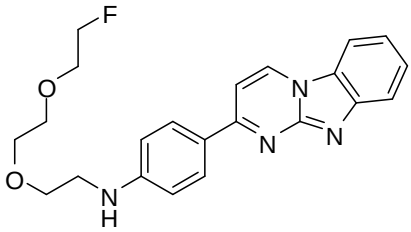

42 T557

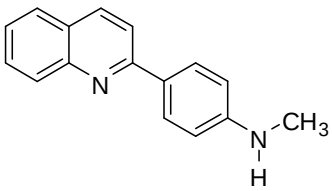

43 BF-158

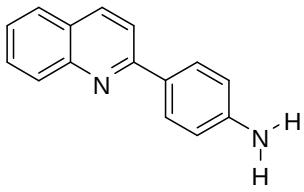

44 BF-170

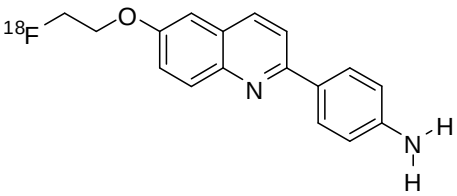

45 [^{18}F]THK523

Figure 1.14 Imaging probes for targeting NFTs.

Okamura *et al*. introduced some novel compounds such as 4-[2-(2-benzoimidazolyl)ethenyl]-*N*,*N*-diethylbenzenamine (BF-126) (**41**), 2-[(4-methylamino)phenyl]quinoline (BF-158) (**43**) and 2-(4-aminophenyl)quinoline (BF-170) (**44**) as candidate compounds for *in vivo* imaging of tau pathology in the AD brain. These agents are injected intravenously into normal mice and exhibit excellent brain uptake and fast clearance from normal brain tissue.[108] Besides,

these probes display relatively higher binding affinity to tau fibril comparing with the binding affinity to Aβ fibrils.

In the past few years, our group and Saji *et al*. developed several phenyldiazenyl benzothiazole derivatives, for example [^{125}I]4-((6-iodobenzo[*d*]thiazol-2-yl)diazenyl)-*N*,*N*-dimethylaniline (PDB) (**37**) and [^{18}F]4-((6-(2-(2-(2-fluoroethoxy)ethoxy)ethoxy)-benzo[*d*]thiazol-2-yl)diazenyl)-*N*,*N*-dimethylaniline (FPPDB) (**38**), also with a series of thiohydantoin (**39**) and rhodanine (**40**) derivatives as candidate probes targeting NFTs.[110-112] Several compounds displayed high uptake after 2 min post-injection and a relatively fast washout from mice brain. It was observed that these probes may be suitable for PET imaging of NFTs in the brain of AD patients.

All of these compounds together with FSB (**29**) and curcumin (**36**) are not specific in binding to NFTs. They also bind to Aβ plaques in the brain.[39,107] Currently, the preclinical tests of THK-523 (**45**) exhibited up to 10-fold higher binding affinity for NFTs over Aβ aggregates. The high affinity and selectivity for tau pathology, both *in vitro* and *in vivo*, indicate that radio-labeled THK523 (**45**) may fulfill ligand criteria for human imaging trials.[113]

At present, no PET/SPECT imaging agents have been used to evaluate the tau pathology in the brain of AD patients.[112] Thus, PET/SPECT imaging agents with greater affinity and selectivity for NFTs are still required. *In vivo* imaging of tau pathology will provide new insight into tau aggregation in the human brain.

1.3.4. A general model for ligand binding to cross-β-sheet aggregates

Amyloid aggregates are hallmarks of neurodegenerative diseases such as AD and Parkinson's disease (PD). The formation of amyloid fibrils assembled from a wide variety of peptides and proteins such as Aβ peptides, tau proteins and ASN are adopt an in-register parallel cross-β-sheet conformation.[114-117] It has been proven that β-strands are the predominant secondary structural elements, yet 3D topology of these arrangements results in different strains of Aβ aggregates.

The intracellular filaments consist of PHFs and straight filaments (SFs). An early investigation by X-ray diffraction of bulk fibers made from preparations of PHFs showed evidence for a cross-β structure.[116] The β-sheets in amyloid fibrils have a cross-β orientation, which means that the β-strand segments arrange approximately perpendicularly to the long axes of the fibrils. At the same time, the inter-strand hydrogen bonds should be directed approximately parallel to the long axes.[118] According to current research, the side chains on each side of the β-sheet form neat rows, which are also called 'binding channels'. They run along the fibril and perpendicular to the strands. It has been reported that the width of

'binding channels' is the distance between every second residue and the average β-sheet is 6.50-6.95 Å (**Figure 1.15**, **b**).[119]

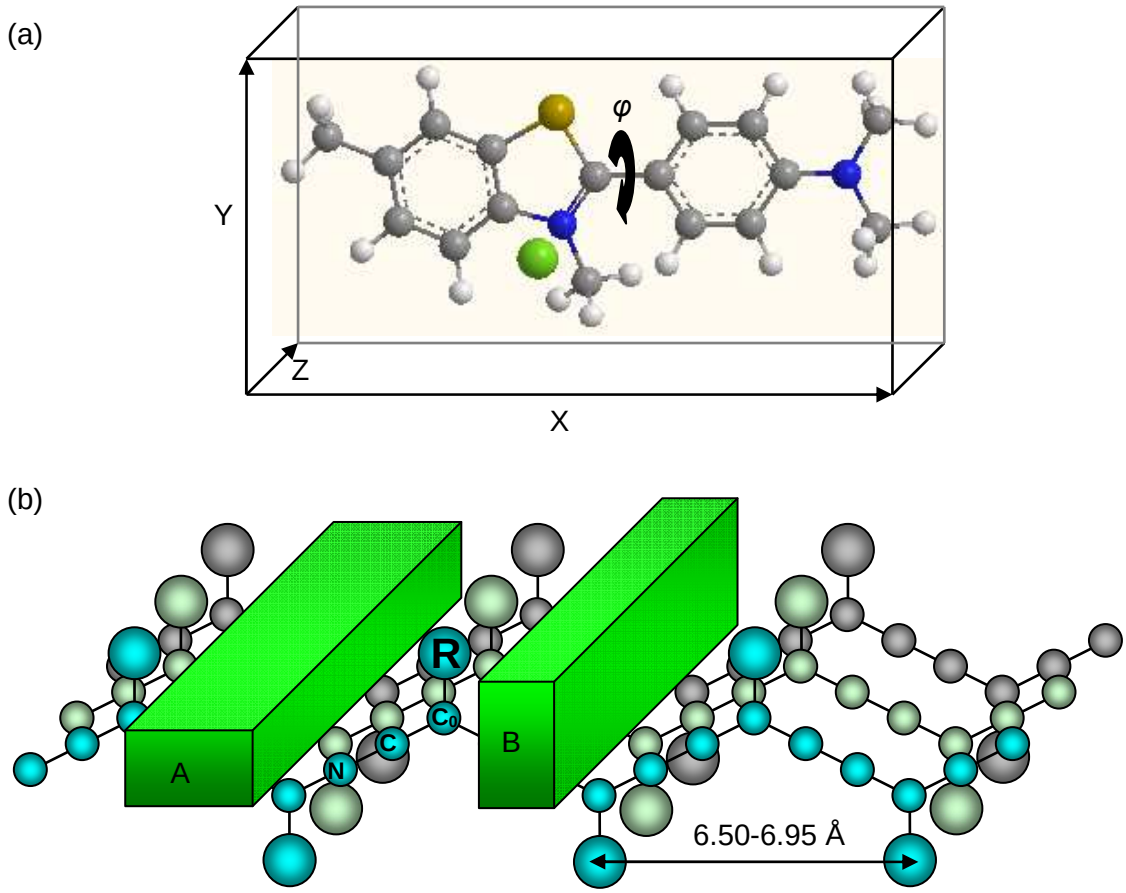

Figure 1.15 (a) Schematic representation of the x-, y-, and z-principal axes of the ThT. Molecular dimensions were obtained via ChemDraw and Chem3D software (b) Schematic representation of a cross-β-sheet and possible position of dye molecules (green cubes) in the 'binding channel'. The molecule interacts with the fibril by binding mode A or B. The backbone atoms (N, C, and C_0) and the side chain (R) for one residue are indicated. The hydrogen bonds are not listed and this scheme is valid for both parallel and anti-parallel sheets.

Several models have been proposed for the interactions between imaging agents and amyloid fibrils.[114] However, the exact mechanism and interaction are still unknown. On the basis of molecular dynamics simulations and direct binding studies, some reports focus on ThT and other cyanine dyes to elucidate the binding mode to Aβ, tau and ASN. Detection of these fibrils is usually achieved by measuring the significantly enhanced fluorescence after the specific fluorescent probes bind to fibrils. The results suggest that the probe binds to the fibrils with its long axes, parallel to the fibril axes, by embedding into the "binding channel" which runs along the filament surface.

Krebs *et al*. proposed a general model to clarify binding of ThT to amyloid fibrils. Afterwards, Volkova *et al*. used this model to study ASN with cyanine dyes.[114,119,120] Both of them

calculated the molecular dimensions as x-, y-, and z-principal axes lengths to estimate the correlation between the size as well as properties of imaging probe and its ability to interact selectively with fibrils. It was assumed that the imaging probe with favorable molecular dimensions may insert into the "binding channel" effectively. Generally, the molecular dimensions (y-, and/or z-axes) should not exceed 6.5 Å, the supposed width of "binding channel" (**Figure 1.15**, **b**).

Quantum-chemical calculations of the ThT conformation indicated that it has a noticeable nonplanar conformation in the ground state S_0 and the torsion angle φ between the benzothiazole and the dimethylaminobenzene rings is about 37°. In the excited singlet state S_1, a twisted internal charge-transfer (TICT) process takes place which results in a transition from the fluorescent state to the nonfluorescent TICT state. Hereby the angle φ between the benzothiazole and the benzene rings changes from 37° to 90° (**Figure 1.15**, **a**).[121] The dimensions value of ThT is in the ground state (x = 15.2 Å; y = 6.1 Å; z = 4.3 Å) suggested that the dye inserted itself into the binding channel with its shortest axes perpendicular to the fibril axes (**Figure 1.15**, **b**). As soon as the ThT located in the rather rigid microenvironment of amyloid fibrils, the interactions should lead to immobilization of the dye in the "binding channel" and further limit intramolecular dye rotation because of the steric hindrance. This result would prevent the excited state to be quenched and even enhance the fluorescence intensity.

In conclusion, the hypothesis suggested that imaging probes with favorable molecular dimension values, approximately 3 Å along z-axes and up to 6.5 Å along y-axes, could preferentially insert into 'binding channels' with their x-axes parallel to the fibril axes, closely surrounded by the fibrils side chains (**Figure 1.15**, **b**).[120] With knowledge of the structural constraints amyloid fibrils it will be possible to guide the design of novel imaging agents which bind to targets more specifically and which will give us insight into the aggregation process.

1.4. α-Synuclein and Parkinson's disease

PD is the second most common neurodegenerative disorder after AD. It is estimated that PD affects about 1-2% of the population over the age of 65 years worldwide. The clinical symptoms of PD include tremor at rest, rigidity on passive movement, bradykinesia and hypokinesia.[122,123] The typical pathological hallmarks of PD are characterized by the deficiency of dopaminergic neurons from the pars compacta of the substantia nigra, and the formation of fibrillar aggregates composed of ASN and other proteinaceous substances such

as Lewy bodies (LBs) and Lewy neurites (LNs) in the brainstem and cortical areas (**Figure 1.16**).[124,125] All of them contribute to the major clinical symptoms of PD.[126]

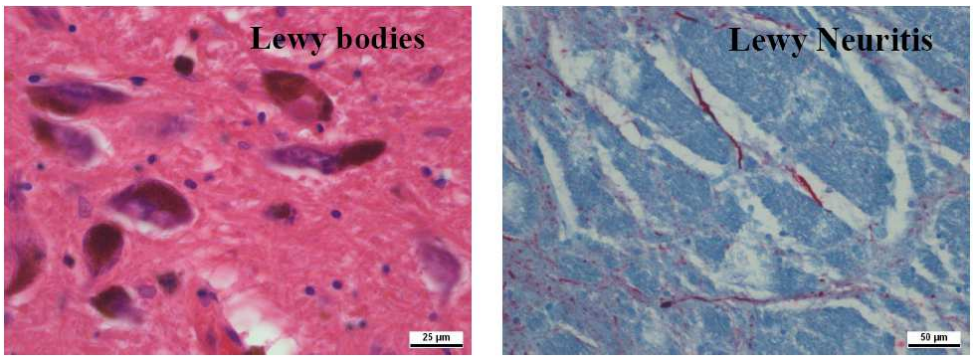

Figure 1.16 Immunohistochemical staining with antibodies against Lewy bodies (left) and Lewy Neurites (right).

So far, 13 genetic loci, PARK1-13, have been suggested for the rare forms of PD such as autosomal dominant and autosomal recessive PD. The identification of several single gene mutations linked to PD, such as ASN, ubiquitin C-terminal hydrolase like 1 (UCH-L1), parkin (PRKN), leucine-rich repeat kinase 2 (LRRK2), PTEN-induced protein kinase 1 (PINK 1), microtubule-associated protein tau (MAPT) and oncogene DJ-1 genes, contribute to understand the pathogenesis of the disease.[127-130] The combination of genetic and environmental factors is likely to be implicated in producing abnormal protein aggregation within specific groups of neurons, leading to cell dysfunction and death.[129] These will improve our understanding of the mechanisms leading to inherited and idiopathic forms of PD.[130]

1.4.1. Pathological role of α-synuclein in Parkinson's disease

ASN is a small (14.5 kDa), abundant, highly soluble, intrinsically disordered and natively unfolded protein. It is mainly expressed in neurons of the central nervous system and localized at presynaptic terminals in close proximity to synaptic vesicles.[131] Structurally ASN is composed of 140 amino acids and distributed in three different parts (**Figure 1.17**). First, the amphipathic N-terminal region (residues 1-60), shows imperfect KTKEGV repeats which are involved in lipid binding. Second, the highly hydrophobic self-aggregating sequence of residues 61-95 is supposed to be responsible for ASN aggregation and β-sheet formation. Third, the acidic C-terminal region (residues 96-140) which is rich in Pro, Asp and Glu residues plays a critical role to regulate fibril formation.[132-134]

The human ASN protein plays an important role in the etiology of PD. While natively unfolded proteins may lack static conformers containing extended regions of *α*-helix and β-sheet, the oligomeric conformation will gradually be converted to β-sheet-rich fibrillar structures.[131] The fibrillar aggregates of ASN are formations of heavily insoluble polymers of

protein observed in LBs and LNs.[135] In the most of the patients, these two synucleinopathies are easy to differentiate clinically by the predominance of extrapyramidal motor features in PD patients. They are believed to be the most cardinal hallmarks of PD.[136] In fact, LBs contain many proteins, including neurofilaments and other cytoskeletal proteins, suggesting that there are co-precipitants, which might be important in aggregation. However, ASN is thought to be the most sensitive marker for LBs and necessary for their formation.

MDVFMKGL S**K**A**KEGV**VAAA E**KTK**Q**GV**AEAA G**KTKEGV**LYVG

S**KTKEGV**VHGV ATVA E**KTKE**Q**V**TNVG GAVVT**GV**TAVA Q**KT**V**EG**AGSIA

AATGFVKKDQLGKNEEGAPQEGILEDMPVDPDNEAYEMPSEEGYQDYEPEA

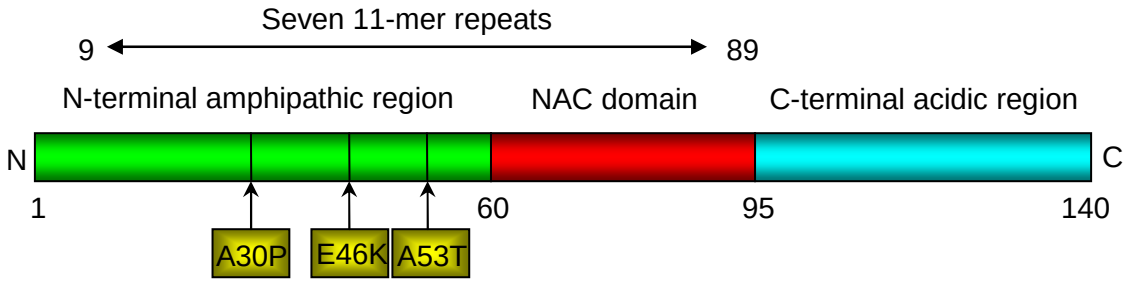

Figure 1.17 Primary structure of ASN. The imperfect 11-mer repeats are emphasized. There are three different regions of the protein which are indicated in the ASN sequence (bottom). The N-terminal amphipathic region (green) contains most of the repeats and the three point mutations linked to autosomal dominant early-onset PD. The central non-amyloid-β component (NAC) (red) encompasses the most hydrophobic residues and promotes aggregation. The C-terminal acidic region (blue) tends to decrease protein aggregation.

Three ASN mutations (A53T, A30P and E46K) associated to autosomal dominant early-onset PD have been published (**Figure 1.17**).[127,131,137] In order to explore the differential neurotoxicity between the various forms of ASN, it is necessary to identify the mechanisms of toxicity and to understand the role of ASN in PD. Some researchers believe that LBs are neurotoxic while others have deemed that oligomers, not fibrils, are even more toxic. *In vitro* finding suggests that fibril formation is accelerated by the E46K and A53T mutation. In contrast, the A30P mutation increases the total rate of aggregation of ASN, while on the other hand, it slows the rate of formation of mature filaments. Presently, it has been debated that particular species of ASN are toxic.[124,137-139] Apparently, ASN is a protein with a natural tendency to aggregate into oligomers. These oligomers can further aggregate into fibrils that are deposited as LBs and LNs. It is important in PD and help to clarify both genetic and nongenetic factors which increase this aggregation.

In brief, mutations variably produce either oligomers or fibrils. Such evidence may be used to design diagnostic tools and therapeutics aiming at the prevention or reduction of toxic ASN aggregates in the brain. Thus, the inhibition of ASN oligomerization and aggregation may produce a therapy for both sporadic and inherited PD.[129,134] Furthermore, the identification of ASN deregulation in synucleinopathies may help the development of effective treatments.

1.4.2. Clinical diagnosis and treatment of Parkinson's disease

PD is also characterized by a progressive loss of nigrostriatal dopaminergic neurons associated with intracellular Lewy inclusion bodies. LBs are hallmark lesions of PD that appear in dopaminergic neurons of the substantia nigra and other brain regions.[140] Although the real cause of the degeneration is not known, in order to improve the clinical diagnosis of PD, some clinical criteria have been established, and most experts use the UK Parkinson's Disease Society's Brain Bank diagnostic criteria.[122,129] The major clinical syndrome of PD pathology is the loss of the dopaminergic neurons in the substantia nigra pars compacta (SNc) which results in striatal dopamine deficiency, as well as dysfunction of non-dopaminergic pathways, including serotonin, noradrenaline, and acetylcholine neuronal systems. For the past two decades, neuroimaging techniques such as PET, SPECT, MRI and transcranial sonography (TCS) have more and more been evolved to detect PD and to elucidate the neuropathological mechanisms, compensatory responses, fundamental symptoms, treatment associated complications, and monitor the disease progression *in vivo*.[141-143] Functional imaging approaches such as PET and SPECT have been successfully employed to detect dopaminergic dysfunction in PD and monitor PD progression, which is reflected by changes of levodopa, glucose metabolism and dopamine transporter binding in the brain. Structural changes in the substantia nigra of PD patients can be detected with both TCS and diffusion tensor MRI.[143]

For almost half a century, levodopa combined with a peripheral dopa decarboxylase inhibitor has been regarded as the gold standard and most effective therapy for the treatment of PD.[141,144-146] As noted above, ASN is the major fibrillary component of LBs and LNs, which are the pathologic hallmarks of PD (**Figure 1.18**). It also makes ASN an excellent candidate to monitor prodromal PD. Therefore, several therapeutic strategies aim to inhibit filament formation and promote filament clearance.[140,147,148] Several studies have described small organic molecules that inhibit the filament formation, for example catecholamines, porphyrin phthalocyanine, the polyphenol baicalein and the anti-tuberculosis drug rifampicin.[149] Currently, mutations in the LRRK2, DJ-1, PINK1 and Parkin gene are targets of drug development at major pharmaceutical companies.[150]

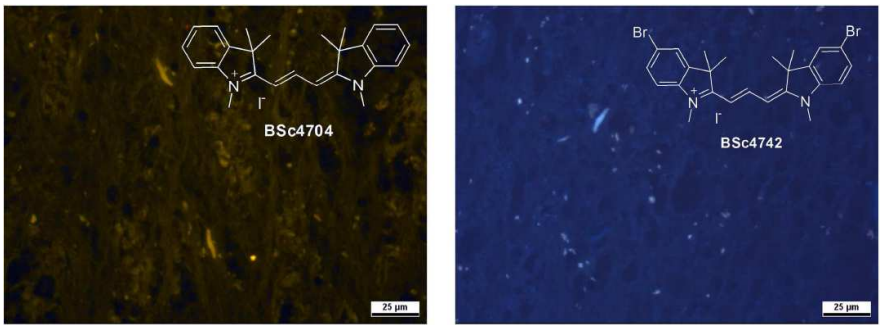

Figure 1.18 Imaging of ASN aggregates by cyanine dyes (Tissues: midbrain; Patient: male, 87 years old, PD).

1.5. Zebrafish as a good model in neurodegeneration disease

The mouse has become the pre-eminent model for human physiology and disease. However, several factors limit its use in large-scale genetic and therapeutic screening. National and international government agencies have called to reduce, refine or replace mammalian species in toxicological tests with alternative methods, even with non-mammalian models.[151] Currently, the zebrafish (*Danio rerio*) has been concerned as a classical tractable vertebrate and embryological model for human disease.[152] There are a number of favorable features that make it an excellent alternative model for biomedical and behavioral genetics studies, including its small size, high fecundity, rapid external development, optical transparency during early embryogenesis, permeability to small molecules, amenability to high-throughput screening, and genetic similarity to humans.[153,154]

1.5.1. The husbandry of zebrafish (*Danio rerio*)

Comprehensive understanding of the zebrafish in their native environment, such as habitat preferences, reproductive behaviors, and diet is important for both the improvement of husbandry standards and the optimization of their use in physiological and pharmacological studies. The zebrafish is native to South Asia and broadly distributed in the lower reaches of the major river drainages of India, Bangladesh, Nepal, Myanmar and Pakistan. This geographic region is characterized by its monsoon climate with pronounced rainy and dry seasons.[155] Understanding the habitat types and zebrafish behavior in the wild allows to optimize the husbandry and to control laboratory conditions.

Olfactory cues play an important role in zebrafish reproduction and spawning behavior. Males release pheromones into the water.[156] When the females are stimulated by the pheromones, this will cause ovulation, which is followed by female release of postovulatory pheromones. As soon as males sense pheromones, the fish will express chasing behavior which triggers mating and spawning. Moreover, according to recent research nutrition,

feeding, water quality and genetic management could also determine the reproductive success in zebrafish.

Figure 1.19 The husbandry of zebrafish (A and B) and representative examples of zebrafish spawning technology (C-E) in our lab.

The embryos are selected and transferred to a 10 L tank. In laboratory conditions, zebrafish larvae naturally hatch within 2.5–3 days post-fertilization (dpf). After hatching, they stick to hard surfaces by means of specialized cells on the head, displaying low levels of spontaneous activity. The larvae have the ability to swim after 5-7 dpf. The zebrafish usually attains its sexual maturity within 3–6 months post fertilization in laboratory settings and females housed with males spawn once a week (**Figure 1.19**).

In our group, the zebrafish is bred and maintained according to the methods described by Christiane Nuesslein-Volhard and Ralf Dahm.[157] Briefly, the zebrafish is raised on 14-h light-10-h dark cycles at 26.0 ± 0.5°C. The zebrafish are fed twice per day, about 3 to 5 mg/fish aquarium fish food (Tetra ™) as well as white/red mosquito larvae for adults. The juveniles are fed 0.1-0.3 mg/fish aquarium fish food. In addition, bloodworms, which are an important component of the diet of wild zebrafish, are supplied once a week. In order to maintain adequate water quality, 30-50% of water is exchanged every week.

1.5.2. Zebrafish as a tool in Alzheimer's disease research

The mouse is the main model used to model neurodegenerative pathology. However, non-mammalian species have become very popular alternative organisms in neurotoxicological study. Some non-mammals provide facile husbandry and share relevant physiological and pharmacological properties with human beings.[151,158] As a model organism, the zebrafish

presents many advantages to study human disease. The vertebrate zebrafish genome and anatomy indicate ~420 million years of divergence from the human lineage. Thus, most human genes have clearly identifiable orthologues in zebrafish.[159]

Small molecule screening takes advantages of the small size, permeability and optical transparency of the zebrafish embryo in the early stage.[160] The effects can be observed in the transparent embryos using microscopy. As a result, defects in numerous organ systems including the CNS and BBB have been identified.[151] Therefore, the zebrafish is a favorite model organism for developmental geneticists and high-throughput screenings in applications including small molecule discovery and toxicology research.[152,161]

According to the hypothesis, the pathologic hallmarks of AD are extracellular Aβ plaques and intracellular NFTs. Early-onset AD is associated with three gene mutations involved in Aβ proteolysis displaying autosomal-dominant inheritance pattern in humans: APP, Presenilin 1 (PS1), and Presenilin 2 (PS2). Late-onset AD is linked to a number of genetic risk factors including the apolipoprotein E (ApoE), neuronal sortilin-related receptor (SORL1) and MAPT.[159,162] Except MAPT, other human genes have been found with a high percent of amino acid similarity in zebrafish.[163] Two paralogues of MAPT in zebrafish, named *mapta* and *maptb* has been identified. Both of *mapta* and *maptb* mRNAs were expressed in the developing CNS. The zebrafish CNS is comparable to human CNS: the zebrafish CNS also contains microglia, cells with astrocytic properties, oligodendrocytes, myelin and the BBB. It implicates that the zebrafish shows conservation of basic brain organization and several key neuroanatomical and neurochemical pathways with relevance to neurological human diseases.[164] Moreover, zebrafish embryos develop BBB functions by 3 dpf. Although the BBB may not be fully mature until 5 dpf, however, it has a structure similar to that in higher vertebrates. The functioning BBB in the transparent embryo brain can still serve as model to study drug permeation in the nervous system and efficacy of CNS drugs.[165]

The zebrafish is an excellent model transiently expressing mutant human tau. It assists to understand the MAPT contribution to tau pathology and tau redistribution from neuronal axons to neuronal soma forming pathogenic neurofibrillary tangles. Current research suggested that the mouse models express only 4R tau in the brain. This feature limited comprehensive and accurate study of tauopathies like AD. Conversely, like human tau, the zebrafish tau isoforms with different kinds of microtubule-binding repeats are expressed in the CNS.[166] Changes in the subcellular ratio of 3R and 4R isoforms can cause the pathological consequences in mammals. Therefore, the major production of the 4R or 6R isoforms from *mapta* and of the 3R isoforms from *maptb* suggests that zebrafish embryos will be a valuable tool to study the discrete functions and interactions of the 3R and 4R MAPT isoforms.[167] The various and externally fertilized embryos of the zebrafish are easily

subjected to the methods for manipulating gene and protein activity, like injection of antisense oligonucleotides, mRNAs or transgenes. These technologies may be applied to arrayed in microtitre plates to screen drug libraries.

The mouse is a typical animal model, but *in vivo* whole animal imaging requires some special techniques and complex manipulations. Oppositely, the zebrafish has a long transparent period (almost 3 weeks) during early development and short generation times (2-3 months) for *in vivo* imaging in a variety of biological investigations. Currently, some groups use fluorescent probes to stain the tau protein in transgenic fish to monitor progression of pathology and genetic inheritance *in vivo*.[168,169] This technology has potential applications for the zebrafish imaging. Using the transgenic zebrafish to express fluorescent proteins *in vivo* suggested that the zebrafish is a valuable tool for the spatio-temporal detection and analysis of many biological processes.[170]

1.5.3. The use of *in vivo* zebrafish assays in drug toxicity screening

The mammalian models like mouse remain the gold standard for evaluating developmental toxicity. Nevertheless, acceptance of zebrafish as a toxicology model is increasing in the USA and Europe. In the process of looking for alternative models for toxicity testing, the zebrafish offers several noteworthy advantages including low costs, small amount of drugs required, convenience of drug treatment, short treatment time, easy husbandry in large numbers, limitless range of morphological and functional assays, optically transparent embryo and good correlation between results in mammals and humans.

Compared with other animal models, rapid development is one of the most significant advantages for assessing compound developmental toxicity in zebrafish (**Figure 1.20**). The precursor cells and tissues of the brain, eyes, heart and musculature will be established at 24 hours post-fertilization (hpf). Basically, most of the internal organs, such as the cardiovascular system, gut, liver and kidney, develop rapidly in the first 24-48 hpf and the zebrafish completes embryogenesis in the first 72 hpf. Since the stages for initiating and terminating compound treatment are vital parameters for evaluating toxicity, the organogenesis is essentially completed within the first 5 days of development. This stage is usually used to terminate compound treatment. Usually, the stage for compound treatment is about 6 hpf but not later than 24 hpf. Due to transparency, organs of zebrafish can be easily visualized *in vivo* by light microscopy without use of complicated dissecting procedures. Furthermore, chemicals can be directly added to the solution of embryonic development to simplify the drug dispensing and promote high-throughput screening. For these reasons, zebrafish permit highly efficient phenotype analysis and fast *in vivo* drug screening.

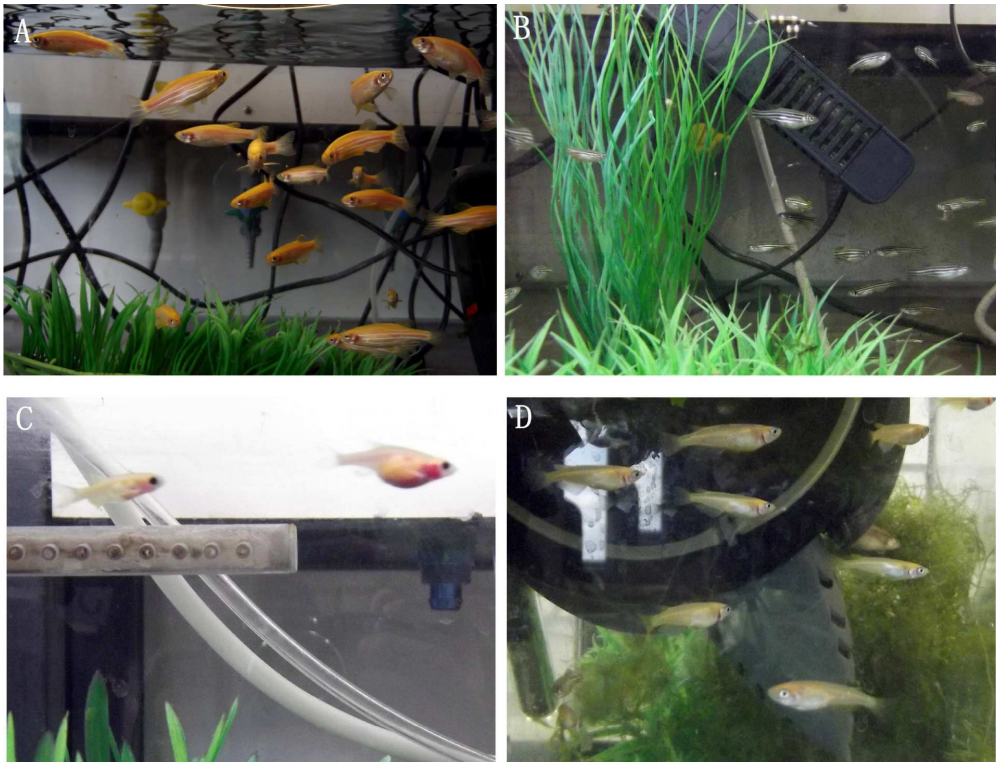

Figure 1.20 Four kinds of fish used to study toxicity in our lab. Gold zebrafish (A), wild-type zebrafish (B), casper (C) and medaka (D).

Shorter treatment time increases throughput and is normally sufficient for evaluating compound toxicity in the cardiovascular system, nervous system and specific sections in the brain. Cardiotoxicity, neurotoxicity, digestive system, genotoxicity, DNA microarrays and metabolic enzymes are in the habit of determining compound toxicity.[171-174] The lethality concentration (LC_{50}), toxicity concentration (also called effective doses) (EC_{50}) and % apoptosis are mostly used as parameters for toxicity studies.[156] The percent incidence and teratogenic index (TI), which defined as the LC_{50}/EC_{50} ratio, were used to clarify the effects of hazardous chemicals.

2. Objectives

Novel non-invasive imaging may improve the *in vivo* diagnosis of Alzheimer's disease (AD). Currently, several compounds have been developed in order to detect β-amyloid (Aβ) plaque pathologies in brains of AD patients. However, only few compounds have been reported which can specifically target neurofibrillary tangles (NFTs). Therefore, the main objective of my work presented in this thesis was to design and synthesize series of imaging probes which specifically bind to Aβ plaques or NFTs. These compounds may be used in the future as potential *in vivo* imaging markers for the diagnosis of AD. Based on this purpose, the following tasks were carried out:

- Design and synthesis of various fluorescent dyes with sensitivity and specificity to detect Aβ plaques or NFTs.
- *In vitro* histological evaluation of different sets of probes, visible by fluorescence microscopy, using hippocampus sections of AD patient brains.
- Quantification of the binding affinity of several active probes by a new competitive *Thiazine Red R* displacement assay.
- Selected candidates were profiled in the *in vitro* liver hepatocellular carcinoma cell assay and in the *in vivo* wild-type zebrafish embryo development assay for toxicological studies.
- The solubilities of candidate probes were evaluated in order to optimize these compounds for further use as potential *in vivo* agents for the diagnosis of AD.
- Selected tau active probes were applied to detect tau deposits in the olfactory epithelium tissues.

Due to the lack of imaging probes for the detection of α-synuclein aggregates in Parkinson's disease (PD), the second aim of this thesis was to explore and evaluate some fluorescent probes for effectively visualization of α-synuclein aggregates. These compounds may be used as potential biomarkers for the early detection of PD.

3. Results and Discussion

An ideal noninvasive imaging biomarker may be used to evaluate the efficacy of therapeutic agents and to diagnose the AD in the early stage. However, current probes tend to have relatively poor selectivity. Thus, modification of known structures and development of next generation imaging probes will be an important step to accelerate our understanding of AD. The investigation of a clinically useful radiolabeled derivative has become subject of worldwide research.[175] There are two fundamental principles for the development of molecular probes to image Aβ plaques and NFTs in cases of AD. First, molecules should be able to bind specifically to SPs or NFTs with high affinities in both *in vitro* and *in vivo* studies. Second, they should have adequate lipophilicities to cross the BBB. From the point of view of molecular design the association of imaging probes with small molecule inhibitors should be of high importance. Based on previous research there is a strong possibility that small-molecule inhibitors of Aβ or tau aggregation will provide sufficient guidelines for the core-structural design. Finally, the novel probes may be used for the imaging of Aβ plaques or NFTs.[176] It is important to recognize that the core structure may be responsible for its binding affinity to proteins. *In vitro* binding affinity should be taken as the first standard for a rational probe design. Thus, small molecules that bind to Aβ such as CR (**24**), ThT (**26**) and curcumin (**36**) are important tools to study Aβ aggregation and will serve as core structures for further optimization of imaging probes.

3.1. Design, synthesis and evaluation of benzothiazole derivatives for Aβ and tau imaging

3.1.1. Design, synthesis and evaluation of phenyldiazenyl benzothiazole derivatives

Over the past ten years, several AD imaging agents were developed for PET and SPECT. Theoretically the core structure of these probes can be assembled by two building blocks: an aromatic moiety comprised of two or more aromatic rings as well as a linker that may also serve as an affinity binding modifier.[176] The most commonly used agents for Aβ imaging *in vitro* include CR (**24**) and ThT (**26**).[177] However, ThT (**26**) contains a positively charged quaternary heterocyclic nitrogen which may limit the compound to cross the BBB.[177] To overcome this problem Klunk *et al.* synthesized a number of neutral ThT analogs without the methyl group on the nitrogen of the thiazole ring. These uncharged compounds did not only retain binding ability, but showed 6-fold increased binding affinity for aggregated Aβ. It was also observed that removal of the charge improved the lipophilicity and showed very good

brain penetration.[178] Further research suggested that removal of the methyl group on the 6-carbon of the benzothiazole moiety does not effect the affinity.[179] The removal of one of the two methyl groups on the amine nitrogen in the 4'-position significantly increases the affinity for Aβ, with the best result having a 40-fold improved affinity.[180] It was reported that CR (**24**) directly binds to Aβ, blocks aggregation and fibril formation *in vitro*. However, the large structure prevents itself to cross the BBB and be further used for *in vivo* studies.[175]

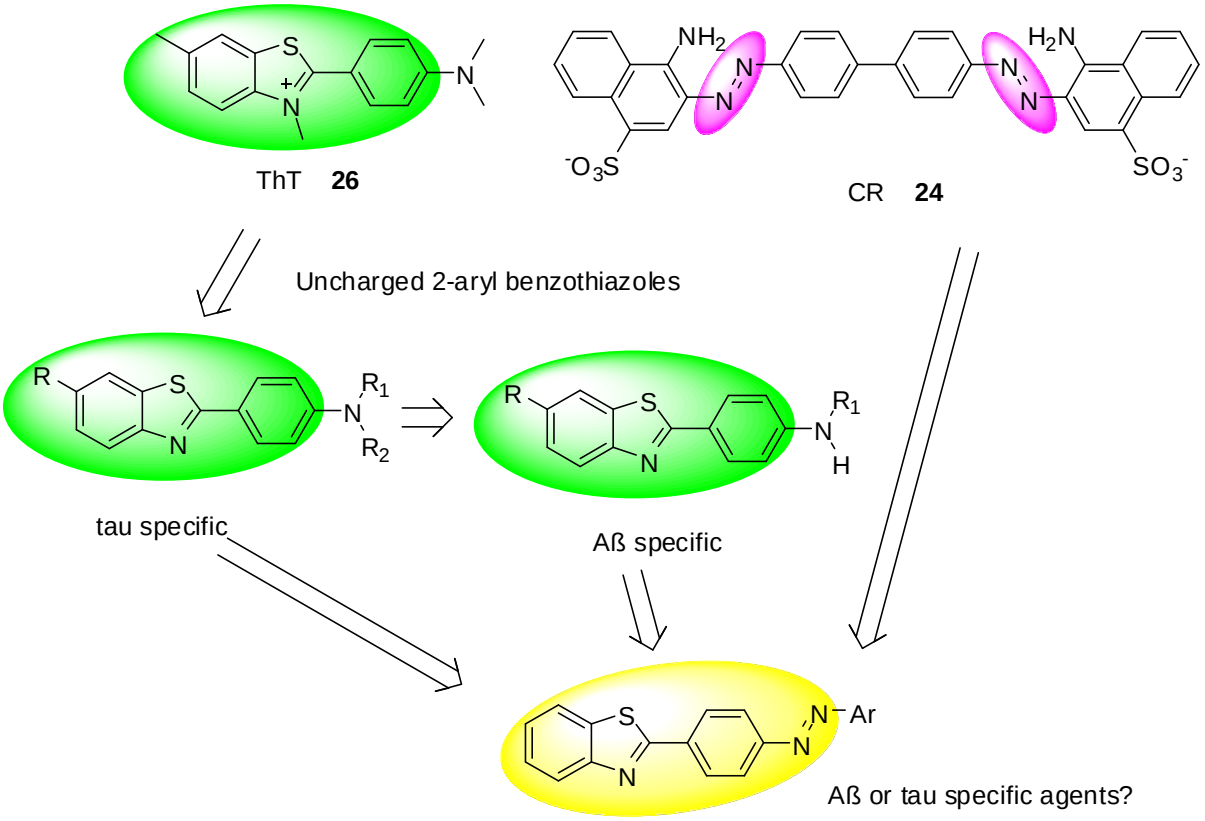

Figure 3.1 Design strategy for phenyldiazenyl benzothiazoles.

According to pervious research, ThT (**26**) is a non-specific imaging marker of Aβ aggregates. It binds to many types of proteins such as tau and ASN. Thus, the combination of the core structure of ThT (2-aryl benzothiazole) and the azobenzene of CR may be attractive to design novel scaffolds with high affinity and selectivity to the targets. It may provide an excellent chance to develop new probes for the detection of Aβ or tau aggregates in AD (**Figure 3.1**). The terminal aryl groups on this scaffold may improve the affinity and the specificity of these probes. It was reported that compounds with a *N*,*N*-dimethyl group may display higher binding affinity to tau than to Aβ aggregates, while compounds with a terminal *N*-methyl group have higher binding affinity to Aβ.[180,181] In order to investigate the novel scaffold for the imaging of Aβ plaques and NFTs in AD brain, seven phenyldiazenyl benzothiazoles have been synthesized and evaluated in post-mortem brain tissues (**Table 3.1**).

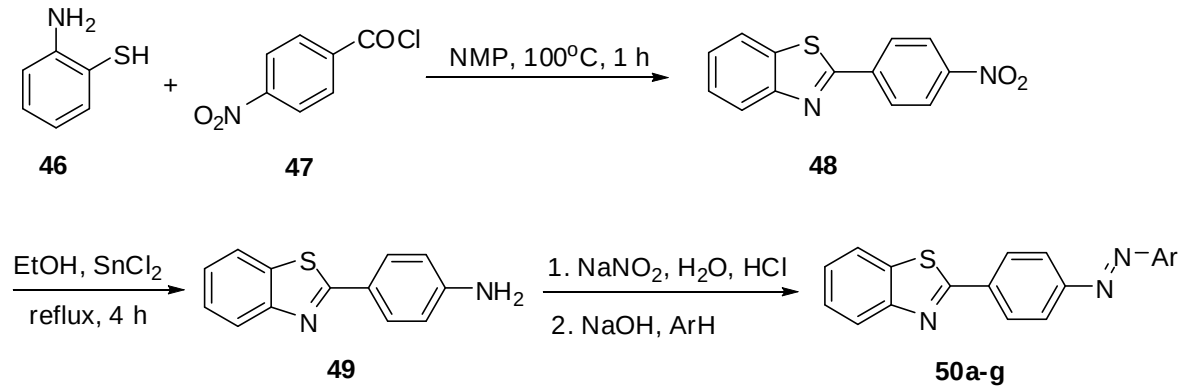

Scheme 3.1 Synthesis of phenyldiazenyl benzothiazole derivatives.

Table 3.1 Structures and properties of phenyldiazenyl benzothiazoles

Entry	BSc No.	Ar	*c*Log*P*[a]	Yield (%)[b]	Staining effect[c]
50a	**BSc4211**	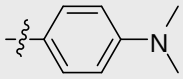	7.02	71	Aβ: **-** NFT: **-**
50b	**BSc4212**	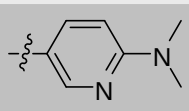	6.40	63	Aβ: **-** NFT: **-**
50c	**BSc4213**	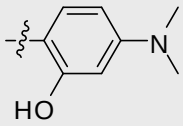	6.63	67	Aβ: **-** NFT: **-**
50d	**BSc4214**	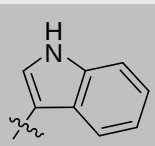	6.28	46	Aβ: **-** NFT: **-**
50e	**BSc4215**	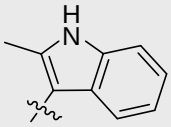	6.62	49	Aβ: **-** NFT: **-**
50f	**BSc4295**	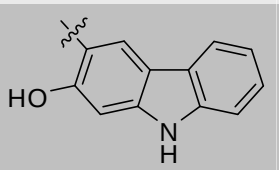	6.94	81	Aβ: **-** NFT: **-**
50g	**BSc4296**	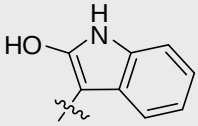	6.08	48	Aβ: **-** NFT: **-**

[a] Determined by CS ChemOffice 10.0; [b] Isolated yields; [c] **-** stands for no staining.

The commercially available 4-nitrobenzoyl chloride (**47**) was treated with 2-aminobenzenethiol (**46**) at 100 °C in NMP to afford the 2-(4-nitrophenyl)benzo[*d*]thiazole (**48**). Due to its poor solubility in organic solvents, this compound was only characterized by HPLC. By reduction of the aromatic nitro group using stannous chloride, 4-(benzo[*d*]thiazol-2-yl) aniline **49** was obtained in 92% yield. The key process involved initial diazotization of **49** with sodium nitrite in hydrochloric acid solution to furnish the diazonium salt (**Scheme 3.1**). Followed by coupling with aryl compounds, all of the phenyldiazenyl benzothiazole derivatives in **Table 3.1** (**50a-g**) were purified by column chromatography and characterized by NMR spectroscopy and mass spectrometry. Compounds **50d-g** with a free secondary amine may improve the solubility in buffer solution. This property may affect the interaction between probes and proteins.[182]

The introduction of a hydroxyl group in the *ortho* position of the azo group (**50c**, **50f** and **50g**) may form intramolecular hydrogen bonds within the molecule. It may hinder the free rotation of the molecule and make it more rigid. Therefore, it may improve the optical properties for Aβ plaques or NFTs imaging. Aromatic α-hydroxy azo compounds may undergo fast intramolecular proton transfer between the enol azo form **50c** and the keto hydrazone form **50c'** (**Scheme 3.2**). This equilibrium has been studied by a variety of spectroscopic techniques. The ^{1}H-NMR and ^{13}C-NMR showed that the neutral form of this substance almost completely adopts the enol azo form rather than the keto hydrazone form in solution.

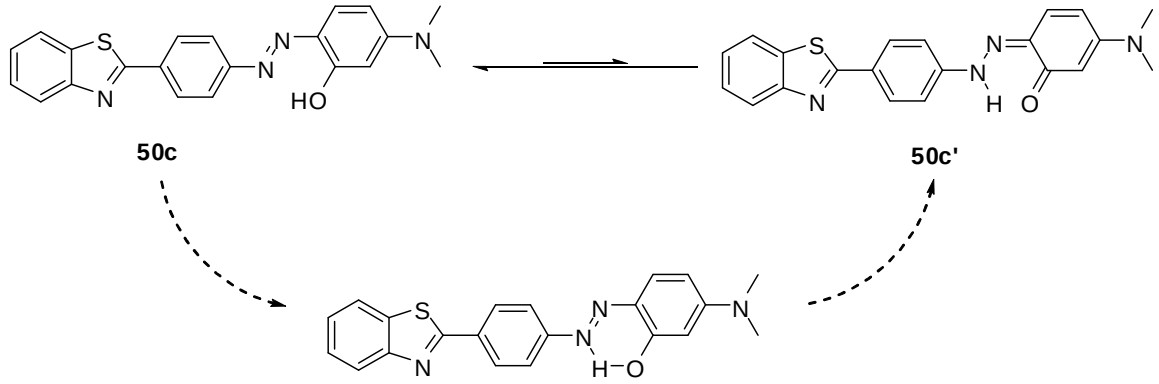

Scheme 3.2 The enol azo form **50c** and the keto hydrazone **50c'**.

Unlike ThT and its analogs, all of these phenyldiazenyl benzothiazoles (**50a-g**) are colored but not fluorescent. In order to investigate the binding effect of these dyes (**50a-g**) to Aβ plaques and NFTs, probes were evaluated by staining hippocampal sections of human AD brain tissue and analyzed by fluorescence microscopy. However, neither Aβ plaques nor NFTs were detected by fluorescence microscopy using the DAPI- or FITC-filters. Recently, Saji *et al.* reported that phenyldiazenyl benzothiazoles with strong binding affinity toward tau aggregates. Several probes may be used as potential PET imaging agents *in vivo*.[110,111,183]

This suggests that our dyes may also bind to Aβ plaques and/or NFTs, while the fluorescence properties will limit the detection by the DAPI- or FITC-filters employed in fluorescence microscopy.

3.1.2. Synthesis and evaluation of phenylhydrazone benzothiazole derivatives for Aβ and tau imaging

The phenyldiazenyl benzothiazoles did not exhibit fluorescence upon binding to the proteins. To overcome this limitation, this work focused on the synthesis and optimization of a hydrazone linkage strategy to enhance the photophysical properties of these probes by extending the π system.[181] Subsequently, different terminal aryl substituents were explored on the hydrazone group. It was found that the phenylhydrazone benzothiazoles can be synthesized in a one-pot reaction from the hydrazine formation to produce **52a-v** in isolated yields ranged from 44 % to 81 % (**Table 3.2**). The *E-Z* configurated isomers were synthesized by known methods, or with slight modifications, which are depicted in **Scheme 3.3**.

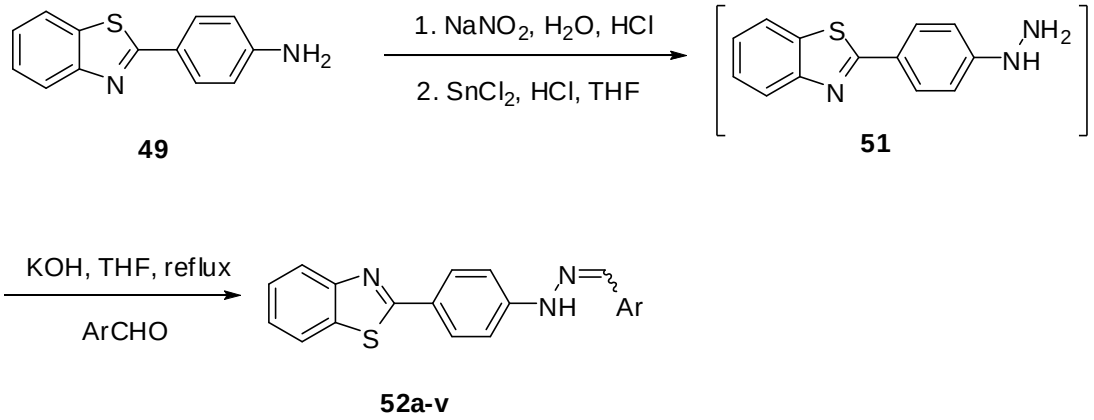

Scheme 3.3 Synthesis of phenylhydrazone benzothiazole derivatives.

The hydrazine **51** was coupled with a range of aldehydes to afford hydrazone derivatives. The reaction was monitored by thin layer chromatography (TLC) and HPLC. After purification by column chromatography these products were characterized by NMR spectroscopy and mass spectrometry. In the ^{1}H-NMR spectra of these probes, the proton signals of the NH group were observed as a singlet at 10.48-11.45 ppm and the proton of the N=CH group was observed as a singlet at 7.84-8.22 ppm. Furthermore, ^{13}C-NMR spectra revealed that these probes lack the signals of the methylene group. All of these data indicate that probes adopted the hydrazone form **52 I** but not the azo form **52 II** (**Scheme 3.4**). The NH group of the hydrazone may be useful to improve the affinity to Aβ plaques and to lower the calculated Log*P* values to appropriate range, which may contribute to cross the BBB *in vivo*.

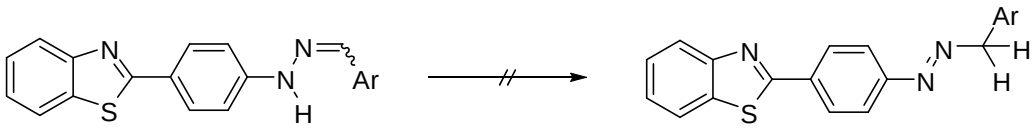

52 I **52 II**

Scheme 3.4 The hydrazone form and the azo form of phenylhydrazone benzothiazoles.

Notably, substituent changes in the electron donor group may affect the intensity of fluorescence emission upon binding to targets. Initially, these probes with different substitutents at various positions of the phenyl group (**52a-l** and **52o**) were evaluated by neuropathological staining of AD brain sections. The structure-activity relationship (SAR) analysis revealed that most of these probes were weak in staining Aβ plaques and/or NFTs. The NH group of the hydrazone may be important to increase the fluorescence and binding affinity to proteins in comparison to the azo compounds. Compounds **52j** and **52l** showed that the hydroxyl group in the *para* position may affect the visualization of Aβ aggregates. The comparison of **52e-f** with **52j** indicates that one electron-withdrawing group only in the phenyl ring is not sufficient to warrant target affinity. The comparison of compound **52k** with compounds **52d**, **52g** and **52o** suggested that probes bear electron-donating groups in the *meta* and the *para* positions, showed a relative good activity towards Aβ aggregates. It is assumed that an electron-donating group such as methylamino, dimethylamino, methoxy, methylthio or hydroxy groups in the *meta* and the *para* positions may play an important role for binding affinity to Aβ plaques and/or NFTs. The electron-donating atoms (N, O, S) may enhance the hydrogen bond between the substituents and proteins. However, the exchange of various substituents at the phenyl ring does not significantly affect the imaging effects. This indicates that the aryl ring does not have a major impact on binding.

Table 3.2 Structures and properties of phenylhydrazone benzothiazoles.

Entry	BSc No.	Ar	*c*Log*P*[a]	Yield (%)[b]	Staining effect[c]
52a	**BSc4216**	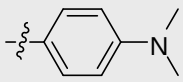	7.02	76	Aβ: **+** NFT: **-**
52b	**BSc4217**	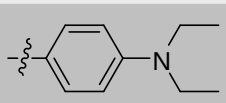	6.40	73	Aβ: **-** NFT: **-**
52c	**BSc4219**	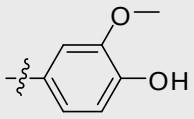	6.63	46	Aβ: **+** NFT: **-**

52d	**BSc4220**	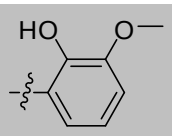	6.28	53	Aβ: **++** NFT: **-**
52e	**BSc4297**	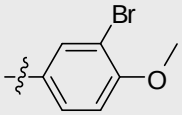	6.62	80	Aβ: **-** NFT: **-**
52f	**BSc4298**	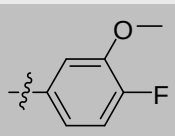	6.94	78	Aβ: **+** NFT: **++**
52g	**BSc4299**	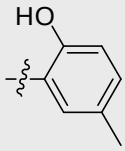	6.08	50	Aβ: **+** NFT: **-**
52h	**BSc4300**	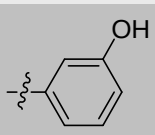	5.30	61	Aβ: **+** NFT: **-**
52i	**BSc4301**	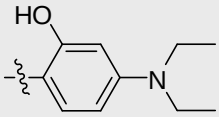	6.26	81	Aβ: **-** NFT: **-**
52j	**BSc4302**	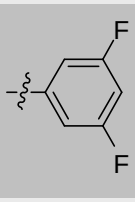	6.00	80	Aβ: **-** NFT: **-**
52k	**BSc4303**	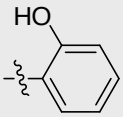	5.30	68	Aβ: **-** NFT: **-**
52l	**BSc4304**	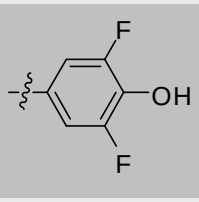	5.61	61	Aβ: **++** NFT: **-**
52m	**BSc4330**	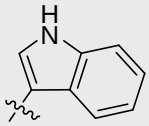	5.23	52	Aβ: **+++** NFT: **-**
52n	**BSc4331**	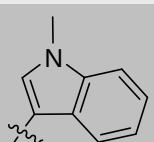	5.46	48	Aβ: **-** NFT: **-**

52o	**BSc4332**	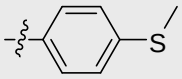	6.13	71	Aβ: **++** NFT: **-**
52p	**BSc4333**	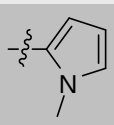	4.47	44	Aβ: **+++** NFT: **++**
52q	**BSc4334**	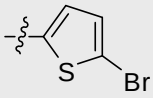	6.38	73	Aβ: **++** NFT: **+++**
52r	**BSc4335**	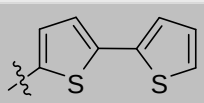	7.38	66	Aβ: **+++** NFT: **-**
52s	**BSc4336**	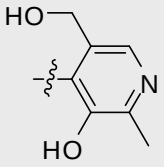	4.09	75	Aβ: **-** NFT: **-**
52t	**BSc4337**	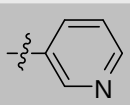	4.35	78	Aβ: **+** NFT: **+**
52u	**BSc4342**	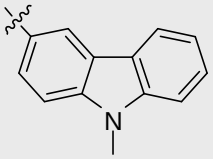	6.52	67	Aβ: **+++** NFT: **+**
52v	**BSc4565**	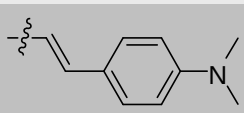	5.86	46	Aβ: **++** NFT: **-**

[a] Determined by CS ChemOffice 10.0; [b] Isolated yields; [c] **+++** stands for efficient staining, **++** stands for normal staining, **+** stands for weak staining and **-** stands for no staining.

The *in vitro* staining assay revealed that probes with terminal phenyl substituents poorly stained Aβ plaques and NFTs. To overcome this shortcoming, we intended to improve the fluorescence intensity of these probes to improve histology results. It was reported that the π-conjugation length affects the fluorescence emission efficiency.[184] For this purpose, compound **52u** has been synthesized by an 8-methyl-9*H*-carbazole domain replacement of the terminal phenyl ring. Remarkably, Aβ plaques and NFTs were clearly observed by fluorescence microscopy (**Figure 3.2**). Furthermore, the replacement of the carbazole moiety with the indole moiety (**52m)** and 2,2'-bithiophene moiety (**52r)** led to probes that showed excellent visualization of Aβ plaques in human brain sections. However, no NFTs have been observed by fluorescence microscopy. Probes **52p-q** and **52s-t** display diminished π-

conjugation of the five- or six-membered heterocyclics to the aromatic core. The *in vitro* staining assay indicated that Aβ plaques and NFTs were clearly stained with these probes (**52p-q** and **52s-t**) as shown in **Figure 3.2**. It was assumed that the electron-donating atoms (N, O, S) of the heterocyclics may form hydrogen bonds between probe and proteins and thus improve the binding affinity.

Additionally, we synthesized compound **50v** which features an extended π conjugation between the hydrazone and the terminal phenyl ring. The comparision of probe **50v** (**Figure 3.2**, **T**) with probe **50a** (**Figure 3.2**, **A**) did not provide distinct biological profiles against Aβ plaques. It implies that the effective π conjugation may not be a crucial factor in fluorescence imaging.

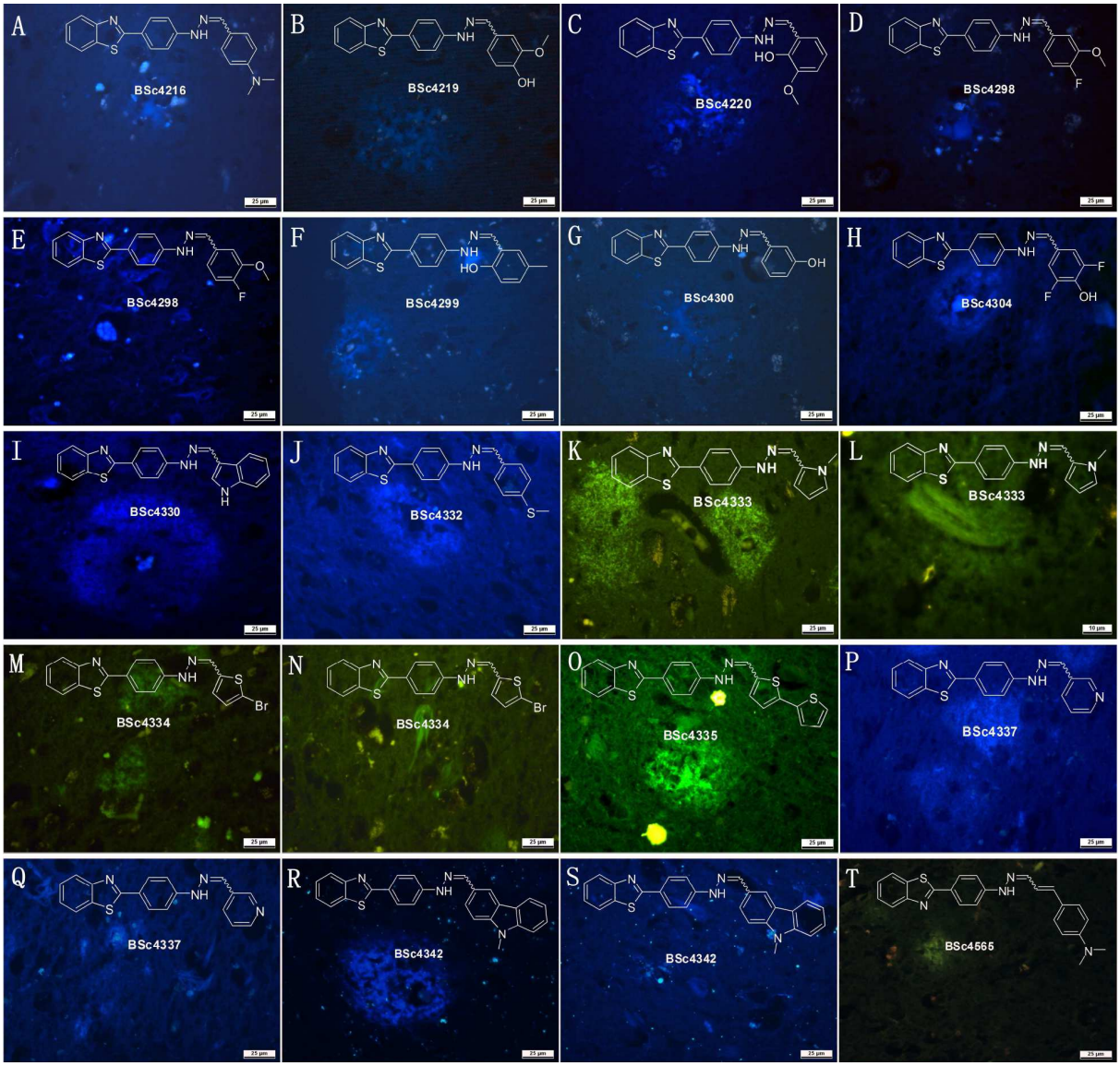

Figure 3.2 Neuropathological staining of brain sections from the hippocampus of an AD patient (Tissues: hippocampus; Patient: female, 89 years old; CERAD Score: 3; NFTs-level: V).

To quantify the binding affinity of these probes, a new *Thiazine Red R* displacement assay has been developed and selected candidates were profiled toxicologically. The probes **52l-m**, **52o** and **52r** stained Aβ plaques clearly in human brain tissues as seen in the *in vitro* staining assay, whereas NFTs in the same brain sections were not visualized. This observation stands in contrast to the activity in the *Thiazine Red R* displacement assay, where compound **52l-m**, **52o** and **52r** present almost equipotent affinity to aggregated tau and $A\beta_{40}$. The lack of NFT staining in the human brain sections may be due to interference with the fluorescence properties upon binding to tau aggregates, e.g. a fluorescence reduction or effect on the Stokes shift, which limit the detection by the DAPI- or FITC-filters employed in fluorescence microscopy.

Compound **52p** displayed ~2-5-fold higher affinity to tau aggregates and ~8-20-fold higher affinity to $A\beta_{40}$ aggregates than the rest of the compounds in this series. Remarkably, these probes displayed ~5-25-fold higher affinity to tau aggregates and ~7-140-fold higher affinity to $A\beta_{40}$ aggregates than PIB (**30**), which was used in the same system for comparison. It indicates sufficient affinity of these probes for the imaging of tau and Aβ aggregates *in vivo*.

Five of these phenylhydrazone benzothiazoles (**52p-r**, **52t** and **52u**) have been evaluated further at different concentrations in the wild-type zebrafish embryo development assay. These embryos were collected and maintained in E2 medium at 26 °C. Afterwards, the embryos were treated with solutions containing 5 μM and 10 μM of compounds at 50-75% epiboly, approximately 6-8 hpf. The phenotypes were observed using the Axio Scope A1 microscope system from Carl Zeiss at 24 hpf and 72 hpf (**Figure 3.3**) to explore their *in vivo* cytotoxicity.

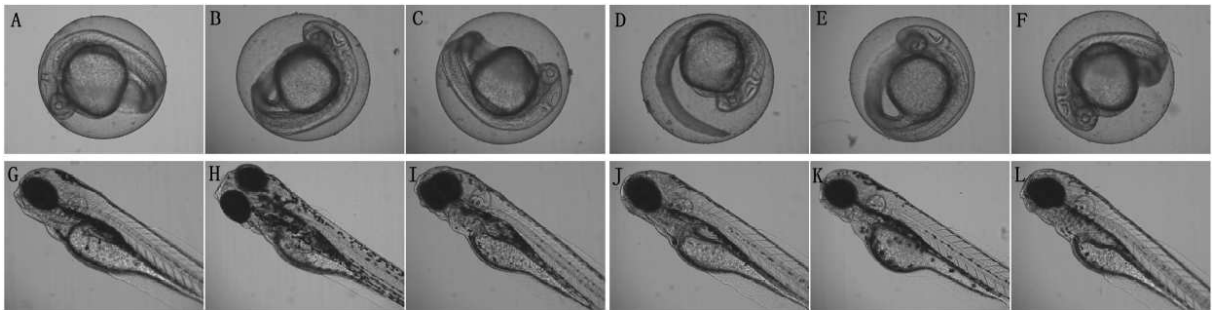

Figure 3.3 *In vivo* cytotoxicity studies of embryos of wild-type zebrafish with 10 μM phenylhydrazone benzothiazoles after 24 (A-F) and 72 (G-L) hpf. Controlled (A and G), Probe **52p** (B and H), **52q** (C and I), **52r** (D and J), **52t** (E and K) and **52u** (F and L).

It was found that the embryos developed well at different concentrations up to 10 μM at 24 hpf and 72 hpf and did not display any lesions in eyes, yolks, tail and heart beat (~60-70 bpm after 24 hpf and ~140-150 bpm after 72 hpf). This evidence suggests that phenylhydrazone

benzothiazoles have negligible cytotoxicity against zebrafish embryos which indicates sufficient safety for *in vivo* evaluation in mouse models.

3.2. Synthesis and evaluation of imidazo[1,2-*a*]pyridines and imidazo[1,2-*a*]pyrimidines based probes for tau imaging

3.2.1. Synthesis and evaluation of imidazo[1,2-*a*]pyridine derivatives for tau imaging

[^{123}I]IMPY (**35**) has been characterized as a potential ligand for SPECT-based imaging of Aβ plaques in the past decade. *In vivo* biodistribution after an intravenous injection of [^{125}I]IMPY in normal mice showed a high initial brain uptake and fast washout.[106,185] However, the signal-to-noise ratio for Aβ plaques labeling is not as high as that of [^{11}C]PIB (**30**). The low contrast limited its use in clinical trails. As mentioned before, the removal of one of these two methyl groups on the amine in the 4'-position, such as PIB, significantly increases the affinity toward Aβ aggregates. Hence, we planned to remove either one or two substituents on the nitrogen in the 4'-position of 4-(imidazo[1,2-*a*]pyridin-2-yl)aniline and evaluate the derivatives by staining of AD brain sections. Additionally, it may reduce the lipophilicity to an appropriate level and thus to promote the probe to penetrate the BBB in humans.

We selected the -CH_2CF_3 group as a substituent of the amino group for further research. The CF_3 group enjoys a privileged role in the field of medicinal chemistry because its incorporation into small molecules frequently improves efficacy. It promotes electrostatic interactions with biological targets, improves cellular membrane permeability and increases robustness of the oxidative metabolism of drugs.[186] It is reported that the electronic inductive effect of the 2,2,2-trifluoroethyl residue is equal to the inductive effect of the hydrogen atom. In some respects, the -$NHCH_2CF_3$ residue in the derivatives behaves like a primary amine.[187] Moreover, the fluoride compound is easy to be radiolabeled. It may serve as precursor probe for PET and MRI imaging *in vivo*.

The commercially available 2-aminopyridine **53** and α-bromoketone **54** were refluxed in EtOH to form imidazo[1,2-*a*]pyridines **55** in good yield. The free anilin **56** (**BSc4485**) was readily prepared via **55** by reduction with stannous chloride. To a solution of **56** in trifluoroacetic acid was added trifluoroacetic anhydride under ice-cooling. The resulting solution was stirred at room temperature overnight to afford the mono-substituted anilin **57** (**BSc4436**) in 86 % yield.[188] Finally, the reduction of compound **57** with $LiAlH_4$ in THF afforded the 2,2,2-trifluoroethyl substituted compound **58** (**BSc4439**) (**Scheme 3.5**).

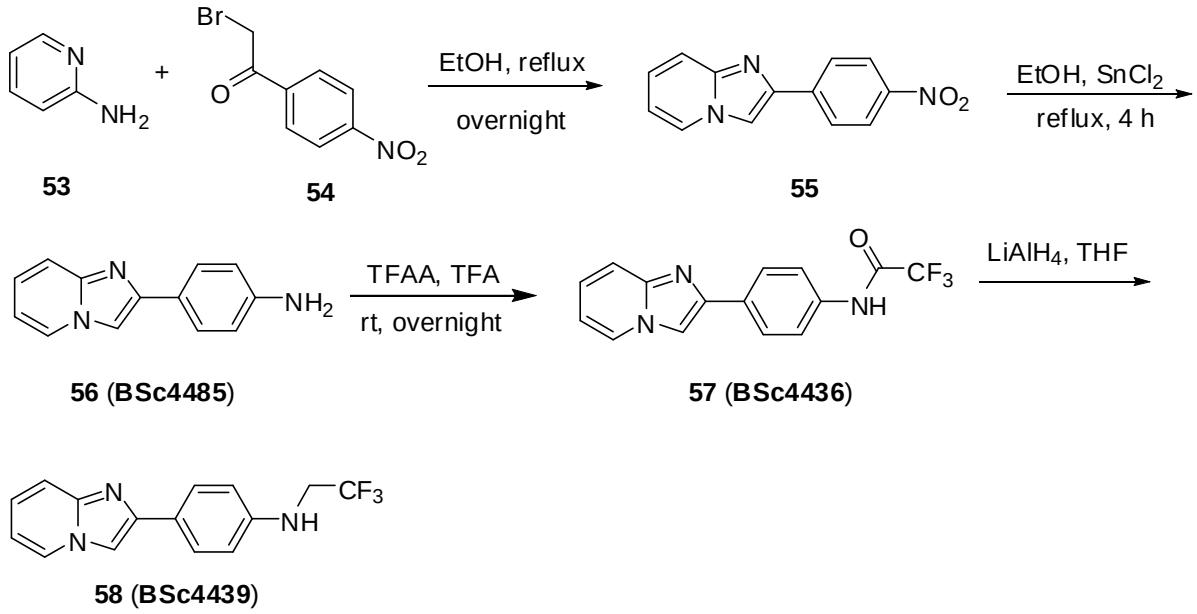

Scheme 3.5 Synthesis of imidazo[1,2-*a*]pyridines

To further investigate the binding effects to Aβ plaques and/or NFTs in AD brain sections, we performed neuropathological fluorescent staining with compounds **56**, **57** and **58**. However, all of these three compounds failed to detect Aβ plaques by fluorescence microscopy. However, a weak NFT staining was observed for compounds **56** and **57** (**Figure 3.4**, **A and B**). Probe **58** stained the NFTs but the fluorescence was absent. It was assumed that in the presence of 2,2,2-trifluoroethyl residue the fluorescence may be quenched upon binding to tau aggregates.

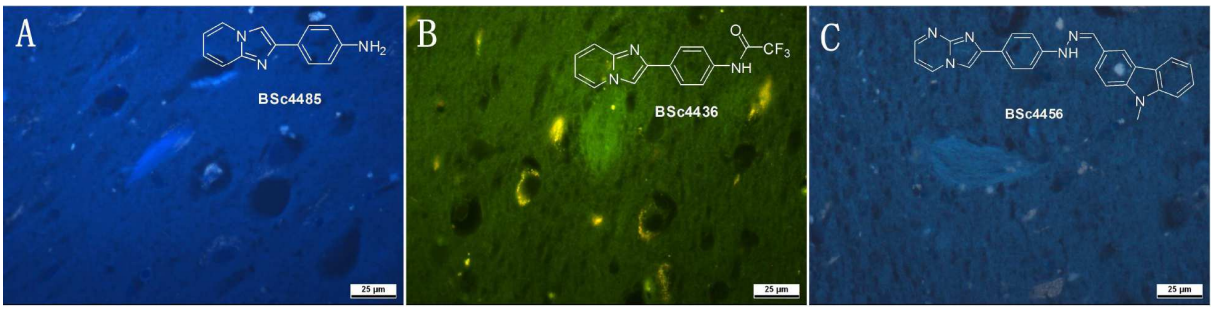

Figure 3.4 *In vitro* histochemical staining of postmortem AD brain tissues with compounds **56**, **57** and **70**. (Tissues: hippocampus; Patient: female, 89 years old; CERAD Score: 3; NFTs-level: V)

3.2.2. Synthesis and evaluation of imidazo[1,2-*a*]pyridines derivatives based on [8+2] cycloaddition reaction

Imidazo[1,2-*a*]pyridines displayed poor contrast between NFTs and background (**Chapter 3.2.1**). In order to achieve the necessary improvement for imaging, it was planned to increase the fluorescence intensity of molecules by extension of the π conjugation. The efficient [8+2] cycloaddition of imidazo[1,2-*a*]pyridines with electron-deficient 2π systems

was recently reported. A number of tetracyclic compounds, which exhibit interesting photophysical properties, were synthesized.[189]

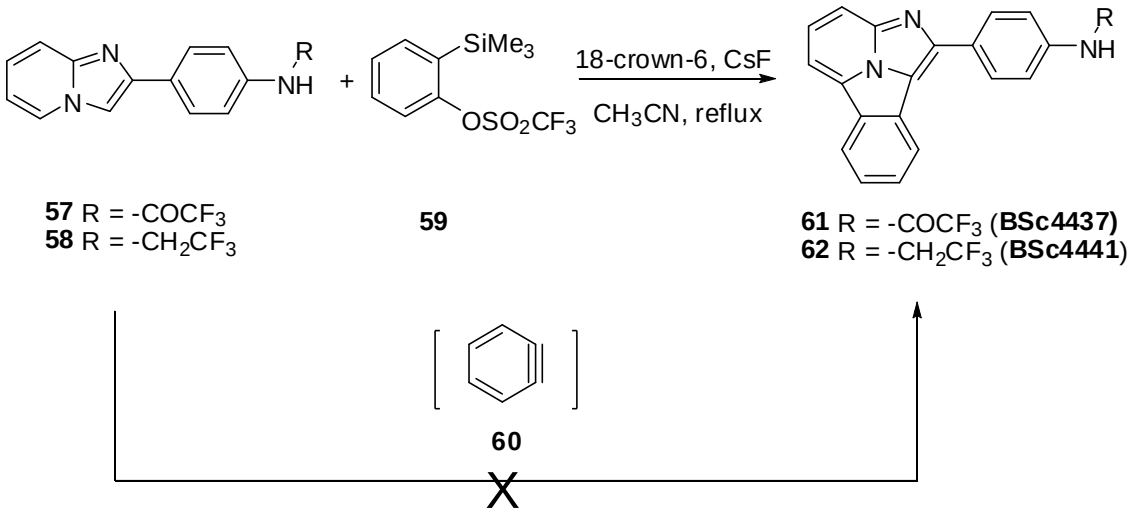

Scheme 3.6 Synthesis of the imidazo[1,2-*a*]pyridines by 2-(trimethylsilyl)phenyl trifluoromethanesulfonate.

The bicyclic heterocycles **57** (**BSc4436**) and **58** (**BSc4439**) are suitable substrates for [8+2] cycloaddition reaction. The reactions are feasible under classical heating using 2-(trimethylsilyl)phenyl triflates **59** as benzyne precursors. The heating process promoted the *ortho*-elimination of **59** in the presence of CsF and 18-crown-6. The [8+2] cycloaddition of the intermediate *o*-benzyne with imidazo[1,2-*a*]pyridines yield compound **61** (**BSc4437**) and **62** (**BSc4441**) in moderate isolated overall yields (**Scheme 3.6**). In order to improve the efficiency of the reaction, microwave irradiation was investigated. However, it did not significantly affect the reaction yields. The benzyne precursor **59** was replaced by an economic substance to reduce the costs. The *o*-benzyne intermediate **60** was achieved by thermal decomposition of benzendiazonium 2-carboxylate which was obtained by aprotic diazotization of 2-aminobenzoic acid in THF.[190] We investigated the direct reaction between *o*-benzyne and bicyclic heterocycles compounds **57** and **58** under microwave irradiation and classical heating conditions.[191] However, [8+2] cycloaddition products were not observed by HPLC.

As shown in **Scheme 3.7**, initially, we intended to substitute a phenyl group on the primary amine of **56**. Nevertheless, the reaction did not convert to compound **65** but underwent [8+2] cycloaddition to form the compound **64** (**BSc4484**). It suggested that bromobenzene **63** converted to the *o*-benzyne under thermodynamic condition. The *o*-benzyne further reacted with the imidazo[1,2-*a*]pyridines **56** to form tetracyclic compound **64** in the presence of *t*-BuOK.

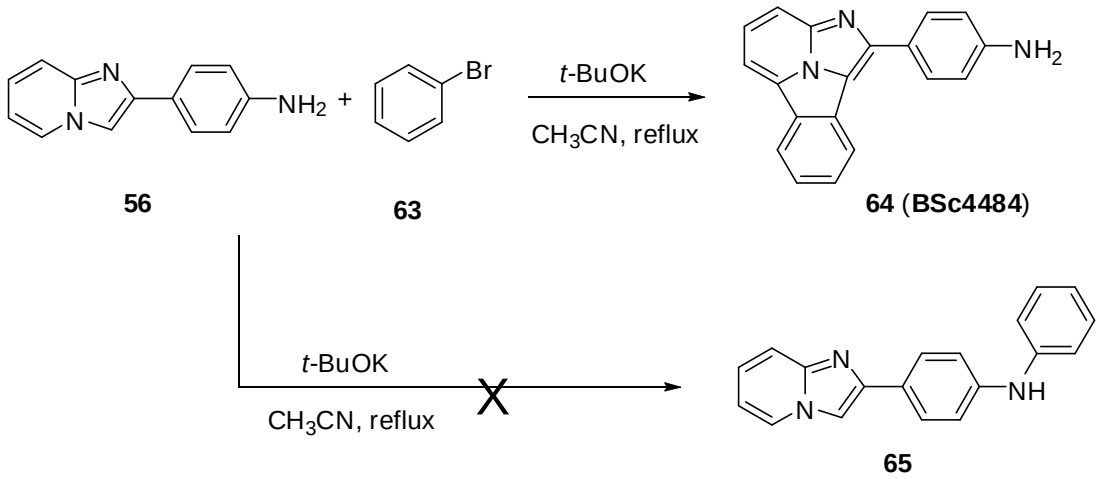

Scheme 3.7 Synthesis of imidazo[1,2-*a*]pyridine derivative **64**.

To demonstrate that the [8+2] cycloaddition derivatives enhance the fluorescence to bicyclic imidazo[1,2-*a*]pyridines, we studied the photophysical properties of compounds **57**, **58**, **61** and **62**. All of these four compounds were prepared as 1.0 μmol/mL solution in EtOH. The color photographs of these compounds were obtained upon irradiation the solution with the UV lamp (365 nm) (**Figure 3.5**). It is consistent with the underlying assumption that the tetracyclic compounds have higher fluorescence intensity than the bicyclic compounds. Comparision of compounds **57**, **61** with compounds **58**, **62** suggested that the fluorescence may significantly be enhanced by reducing the electron-withdrawing ability of the substituent on the amine group.

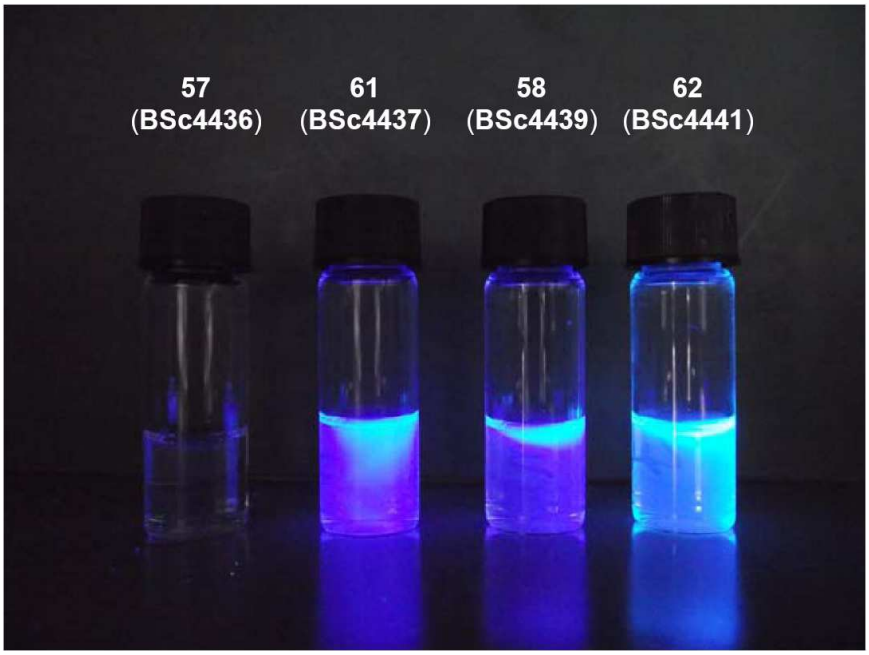

Figure 3.5 Photographs of **57** (**BSc4436**), **61** (**BSc4437**), **58** (**BSc4439**) and **62** (**BSc4441**) (from left to right) with UV (365 nm,) illumination. The concentration is 1 μmol/mL.

These tetracyclic probes were evaluated using post-mortem AD brain tissues. However, they failed to detect Aβ plaques and NFTs by fluorescence microscopy. It was assumed that the three dimensions of the tetracyclic compounds are too large to allow insertion into the binding channel of Aβ or tau fibrils, which may cause them to be inactive in imaging assay.

3.2.3. Synthesis and evaluation of imidazo[1,2-*a*]pyrimidine derivatives for tau imaging

The results of the phenylhydrazone benzothiazoles (**Chapter 3.1.2**) suggested to modify imidazo[1,2-*a*]pyridines **56** and imidazo[1,2-*a*]pyrimidine **68** with phenylhydrazone moiety. However, only the hydrophilic imidazo[1,2-*a*]pyrimidine derivative **68** can be substituted with a hydrazone moiety. The compound **70** (**BSc4456**) was synthesized using the same procedures depicted in **Chapter 3.1.2**. The pyrimidin-2-amine **66** and *α*-bromoketone **54** were refluxed in EtOH to form the imidazo[1,2-*a*] pyrimidine **67**. Followed by reduction with stannous chloride, the free amino compound **68** was obtained in quantitative yield. Employing a one-pot synthesis, compound **70** was purified by column chromatography and characterized by NMR spectroscopy.

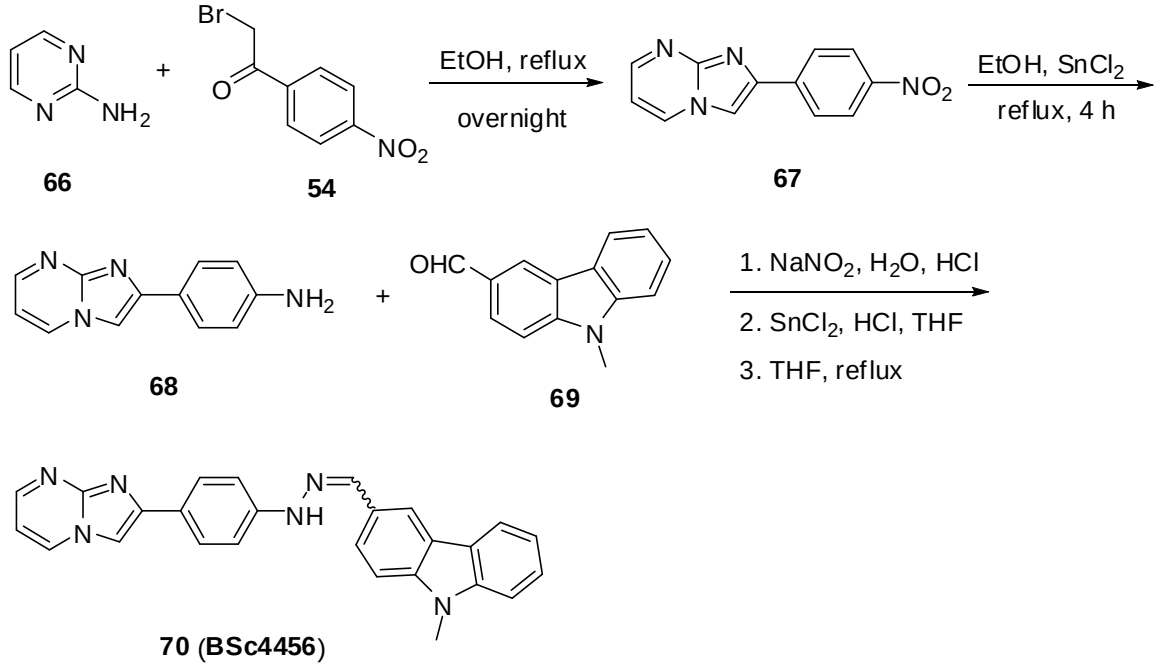

Scheme 3.8 Synthetic route for imidazo[1,2-*a*] pyrimidine derivative **70**.

To further confirm the binding affinity of compound **70** to Aβ plaques and NFTs, a fluorescent staining of AD brain sections was carried out. A selective but weak NFTs staining was observed by fluorescence microscopy (**Figure 3.4**, **C**). Taken together, it was assumed that the low contrast may be due to the relatively low binding affinity for tau aggregates, which

may cause the fast washout from AD brain sections. The low signal-to-noise ratio is an adverse factor which limits the use of these compounds for NFT imaging *in vivo*.

3.3. Synthesis and evaluation of tetrazine derivatives as potential imaging probes in Alzheimer's disease

1,2,4,5-Tetrazine, so-called *s*-tetrazine, is a well established heterocycle, which was discovered more than 100 years ago. It contains an electron poor aryl ring with four nitrogens. *S*-Tetrazines are attractive molecules that can be used as strong electron acceptors. Because of the four electronegative nitrogen atoms in the aryl ring they have a relatively high reversible reduction potential. Recently, *s*-tetrazines have been applied in various functional molecular systems, such as polymers and metal complexes.[192] It was reported that all the *s*-tetrazines are highly colored, while the electroactive heterocycles exhibit a very high electron affinity.[193] In many cases, the first excited state of *s*-tetrazines has a very long decay time, involving a forbidden n-π* transition in the timescale of 10-160 ns. It is noteworthy that many *s*-tetrazines are known to display high fluorescence quantum yields because of the substitution with heteroatoms such as chlorine and oxygen.[192] Some of these derivatives display fluorescence properties in the crystalline state, which positively makes them as the smallest organic fluorophores and therefore attractive for imaging applications.[194] Taken together, this class of compounds may be used to develop some imaging agents for the detection of Aβ plaques and NFTs in AD.

We anticipated that the bis-pyrazole **74** (**BSc4338**) may display higher affinity than the highly fluorescent bis-heteroatom compounds. As shown in **Scheme 3.9**, the reaction of guanidine hydrochloride **71** and hydrazine hydrate in dioxane gave triaminoguanidine **72** in quantitative yield. Upon reacting with acetylacetone to give compound **73**, the solid was oxidized with sodium nitrite to afford the red fluorescent compound **74**. Furthermore, we utilized this scaffold to synthesize tetrazines **75a-c** (**BSc4339**, **BSc4340** and **BSc4341**) via nucleophilic substitution. It was found that only one pyrazole group of compound **74** can be replaced with phenylamine under classical heating or microwave condition in the presence of acetonitrile. However, the second substitution can not proceed even with forcing reaction conditions.

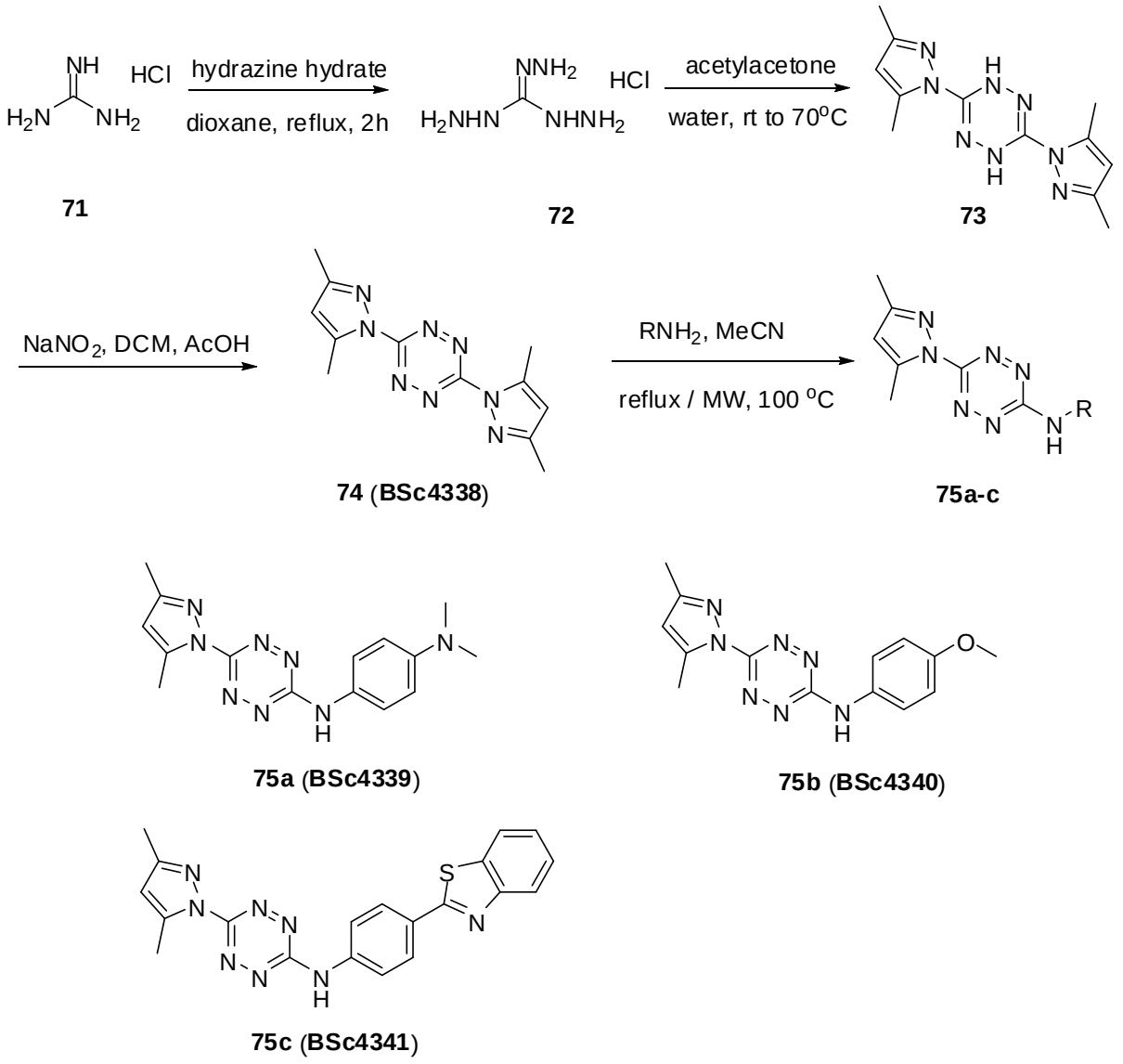

Scheme 3.9 Synthesis of tetrazines and structures of **74** and **75a-c**.

Unexpectedly, the aryl substituted compounds **75a-c** are highly colored but poorly fluorescent. Compounds **74** and **75a-c** were evaluated by neuropathological staining of AD brain sections. The brain tissues were investigated by fluorescence microscopy employing a DAPI- or FITC- filters. The *in vitro* staining experiments showed that the red fluorescent compound **74** poorly stained NFTs. It was assumed that fluorescence may be quenched upon binding to tau aggregates. On the other hand, the weakly fluorescent compounds **75a-c** stained Aβ plaques and NFTs as shown in **Figure 3.6**. It was hypothesized that tetrazines may have a relative binding affinity toward Aβ and tau aggregates *in vitro*. However, the lack of sufficient fluorescence properties limits them to be used as imaging probes for the detection of Aβ plaques and NFTs *in vitro*.

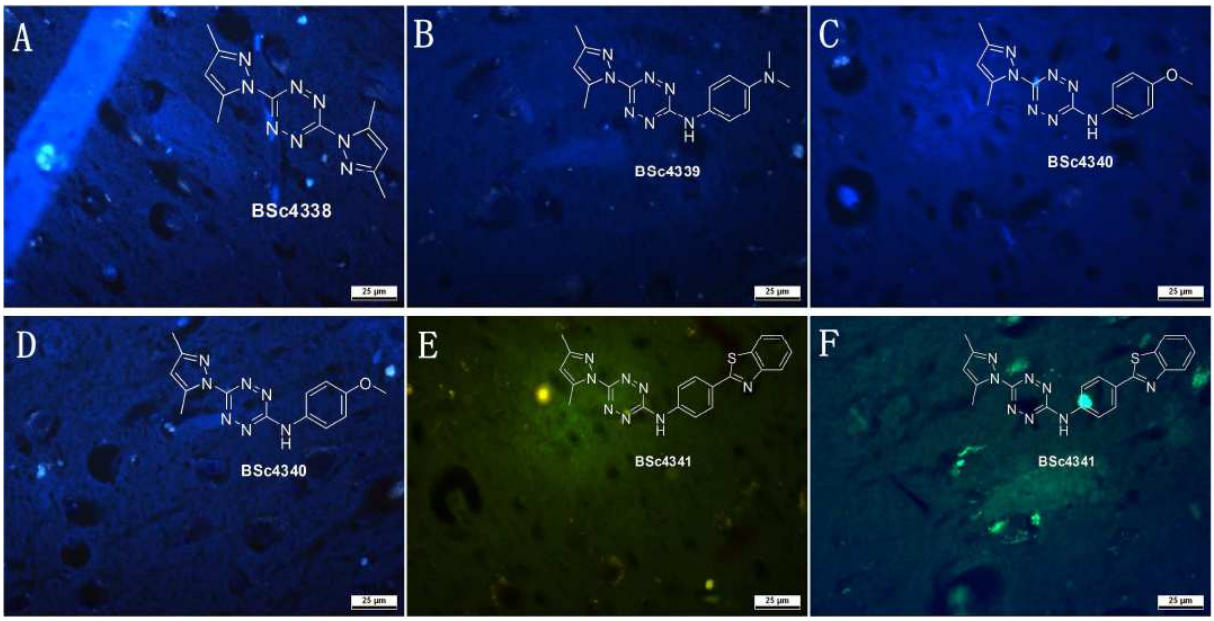

Figure 3.6 *In vitro* histochemical staining of postmortem AD brain tissues with **74** (**BSc4338**) and **75a-c** (**BSc4339**, **BSc4340** and **BSc4341**) (Tissues: hippocampus; Patient: female, 89 years old; CERAD Score: 3; NFTs-level: V).

3.4. Design, synthesis and evaluation of bisstyryl derivatives for Aβ and tau imaging

A design strategy was applied to arrive at molecules with large two-photon absorption cross-section. The bisstyrylbenzenes with donor-π-acceptor-π-donor structural motifs exhibit exceptionally large two-photon absorption cross-section values. The enhanced value allows lower laser intensities to be used for excitation and reduces optical damage to preserve the tissue.[195] The two-photon absorption cross-section correlates with the electron affinity of the central ring. The higher the reduction potential on the central ring, the higher the two-photon absorption cross-section.[196] Based on these guiding principles, a series of donor-π-donor derivatives containing substituted phenyl as the π-core have been investigated. Generally, the donors are connect to the π-core by C=C bonds. The highly conjugated molecules with extended π-system result in strong fluorescence, which could be induced by absorption of either one or two photons and high excitation intensity. The strong two-photon excited fluorescence and stimulated emission are attractive factors for the fluorescence imaging of Aβ plaques and NFTs in AD brain.

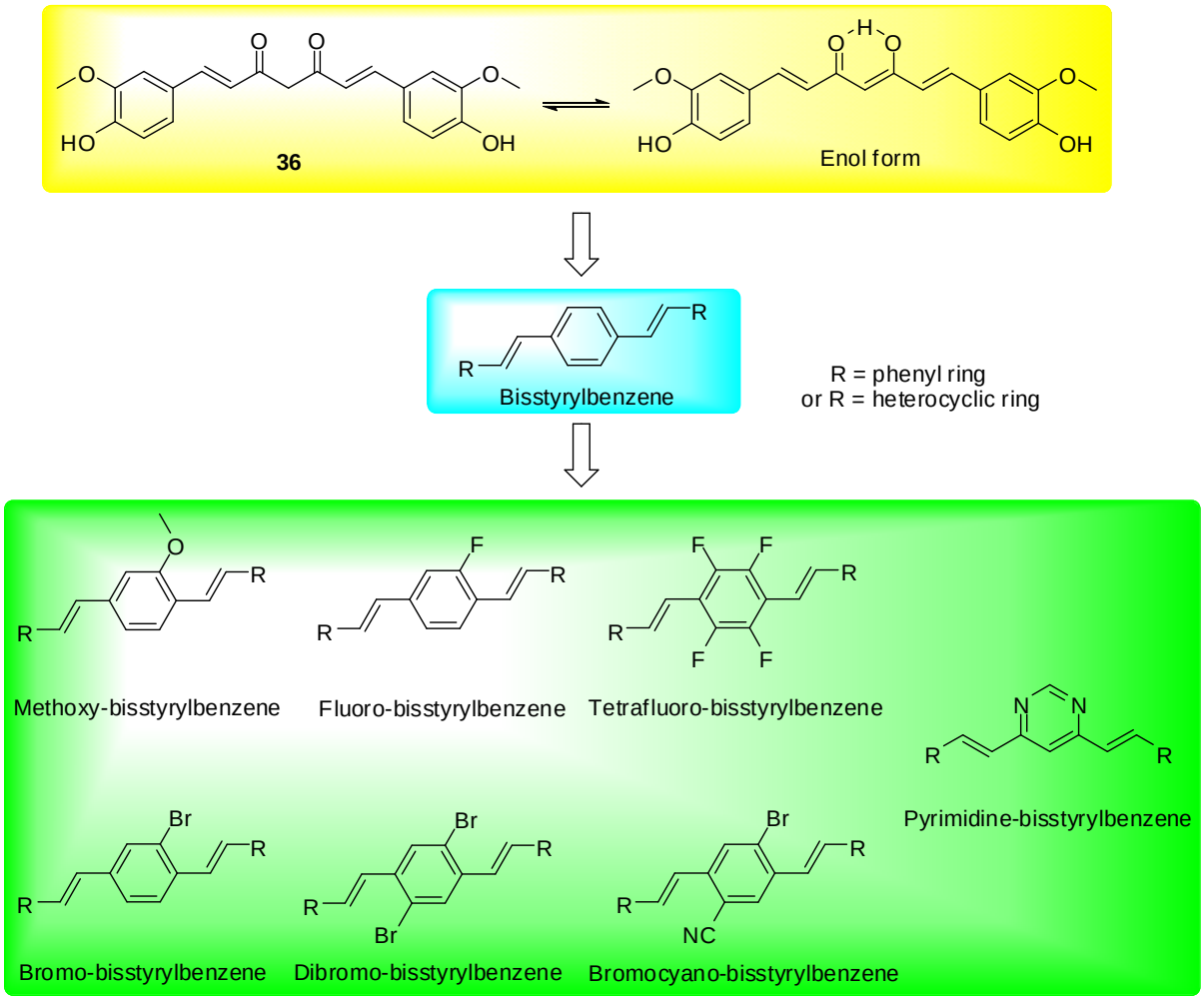

Figure 3.7 Design strategies for the bisstyryl derivatives as imaging probes.

The presence of Aβ aggregates in the human retina was reported by several groups, yet is subject to ongoing debate. Curcumin is currently used in imaging evalutions and suggested the identification of Aβ deposits in the mouse retina. The Aβ deposits have been monitored in the mouse retina by fluorescence microscopy after high dosage of curcumin.[197,198] However, systemic application of curcumin to humans at the necessary concentration is likely to cause adverse events. It is reported that curcumin is photo labile and toxic to most human cell lines > 50 µmol/L.

Generally, curcumin can exist in several tautomeric forms, such as the 1,3-diketo form and the enol forms (**Figure 3.7**). The enol form of curcumin is more energetically stable in the solid phase and in solution. Based on the structure of curcumin and Congo Red (CR) many bisstyryl derivatives have been synthesized in the past decade.[50,95,199-202] The aromatic cores with a high electron-withdrawing character as acceptor connect with the terminal donor group resulting in a highly fluorescent push-pull system. Excitingly, several compounds displaying good affinities to Aβ aggregates have been studied in mice experiments *in vivo*. Only few

compounds for targeting NFTs have been reported. The lack of NFTs specific fluorescent probes imposes a limit on the *in vivo* quantification of neurofibrillary pathology in AD patients. Hence, the challenge still remains to develop novel fluorescent probes with improved affinity and selectivity to NFTs. For this reason, further modification of known scaffolds that affect the lipophilicity and fluorescence properties may improve the imaging probes to enable them for *in vitro*, *in vivo* and clinical applications. In this study we synthesized many bisstyryl derivatives with different core structures as π-center (**Figure 3.7**). The histological and toxicological evaluation guided the optimization of these probes for the detection of Aβ plaques and NFTs *in vivo*.

3.4.1. Synthesis and evaluation of 1,4-bisstyryl-2-methoxybenzene derivatives for Aβ and tau imaging

Because of the appropriate lipophilicity and excellent fluorescence properties, Methoxy-X04 can successfully stain Aβ and tau aggregates in the postmortem sections of AD brain. In 2002, Klunk *et al.* reported that Methoxy-X04 (**28**) enters the brain and retains sufficent binding affinity for Aβ *in vitro*.[50] *In vivo* imaging of Aβ plaques in the transgenic mouse brain suggested that [^{11}C]Methoxy-X04 is a viable candidate for *in vivo* application.[203] However, no Methoxy-X04 derivatives specially targeting NFTs have been reported until now.

In the present study, we employed 2-methoxybenzene as π-center core. The replacement of the phenol group by substituted phenyl ring or heterocyclic ring may lead to molecules with high conjugation length and excellent fluorescence properties. Moreover, the functional groups may affect the lipophilicity and the specificity for tau aggregates.

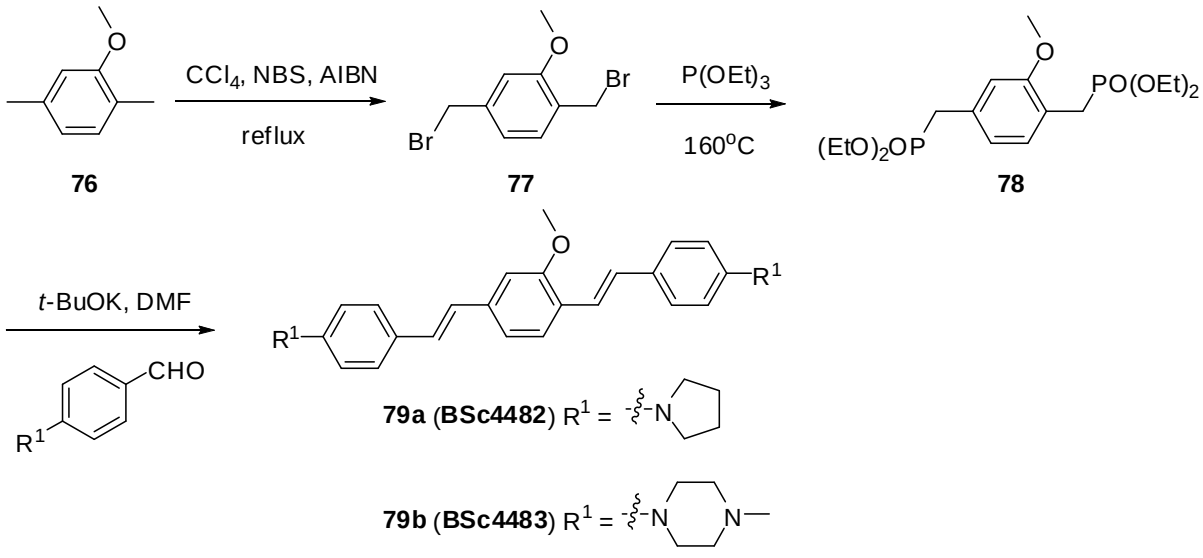

Scheme 3.10 Synthesis of 1,4-bisstyryl-2-methoxybenzenes **79a-b**.

1,4-Bisstyryl-2-methoxybenzenes were obtained by using the procedure described by Klunk *et al*. with several modifications.[50] Initially, the 1,4-bis(bromomethyl)-2-methoxybenzene intermediate **77** was obtained through benzylic bromination of 2-methoxy-1,4-dimethylbenzene **76** in the presence of *N*-bromosuccinimide (NBS) and 2,2'-azobis(isobutyronitrile) (AIBN). The compound **78** was synthesized in quantitative yield by employing a Michaelis–Arbuzov reaction (**Scheme 3.10**).

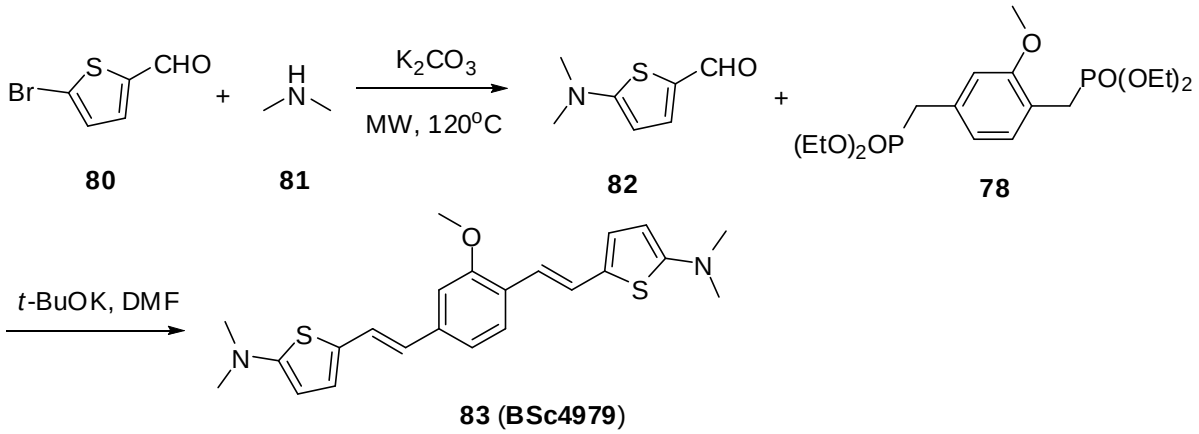

Scheme 3.11 Synthesis of 1,4-bisstyryl-2-methoxybenzenes **83**.

As illustrated in **Scheme 3.11** we synthesized 5-(dimethylamino)thiophene-2-carbaldehyde **82** by the nucleophilic aryl substitution of 5-bromothiophene-2-carbaldehyde **80** in the presence of K_2CO_3 and dimethylamine (40% in water). The product was obtained using microwave radiation in the Biotage Initiator 300 (1h, 120 °C). The key step was the Wittig–Horner coupling reaction between phosphonate **78** and corresponding benzaldehydes that produced 1,4-bisstyryl-2-methoxybenzenes (**79a-b** and **83**) as a sole products (**Scheme 3.10** and **Scheme 3.11**). These compounds were purified by column chromatography and characterized by NMR spectroscopy. The products are generated as *trans* isomers within the limits of NMR detection by the coupling constant for the vinylic protons (J = 16.0-16.5 Hz) in the ^{1}H-NMR spectra. It was found that all of these derivatives exhibit excellent fluorescence under UV light.

Probe **79a** (**BSc4482**) with a 1-pyrrolidine moiety stains Aβ plaques clearly but only minimally stains NFTs. In order to reduce lipophilicity and to improve the water solubility, probe **79b** (**BSc4483**) bearing a 4-methylpiperazine group was synthesized. In contrast, probe **79b** improved the staining effect on NFTs but stains amyloid to a lesser extent. Probe **83** (**BSc4979**) was obtained by the replacement of the donor group by a 5-(dimethylamino)thiophene moiety. Excitingly, numerous NFTs can be clearly observed in the post-mortem brain tissue of AD patient (**Figure 3.8**, **F**). Furthermore, the central core

plaques were detected in the same tissue with high contrast relative to the background (**Figure 3.8**, **B**).

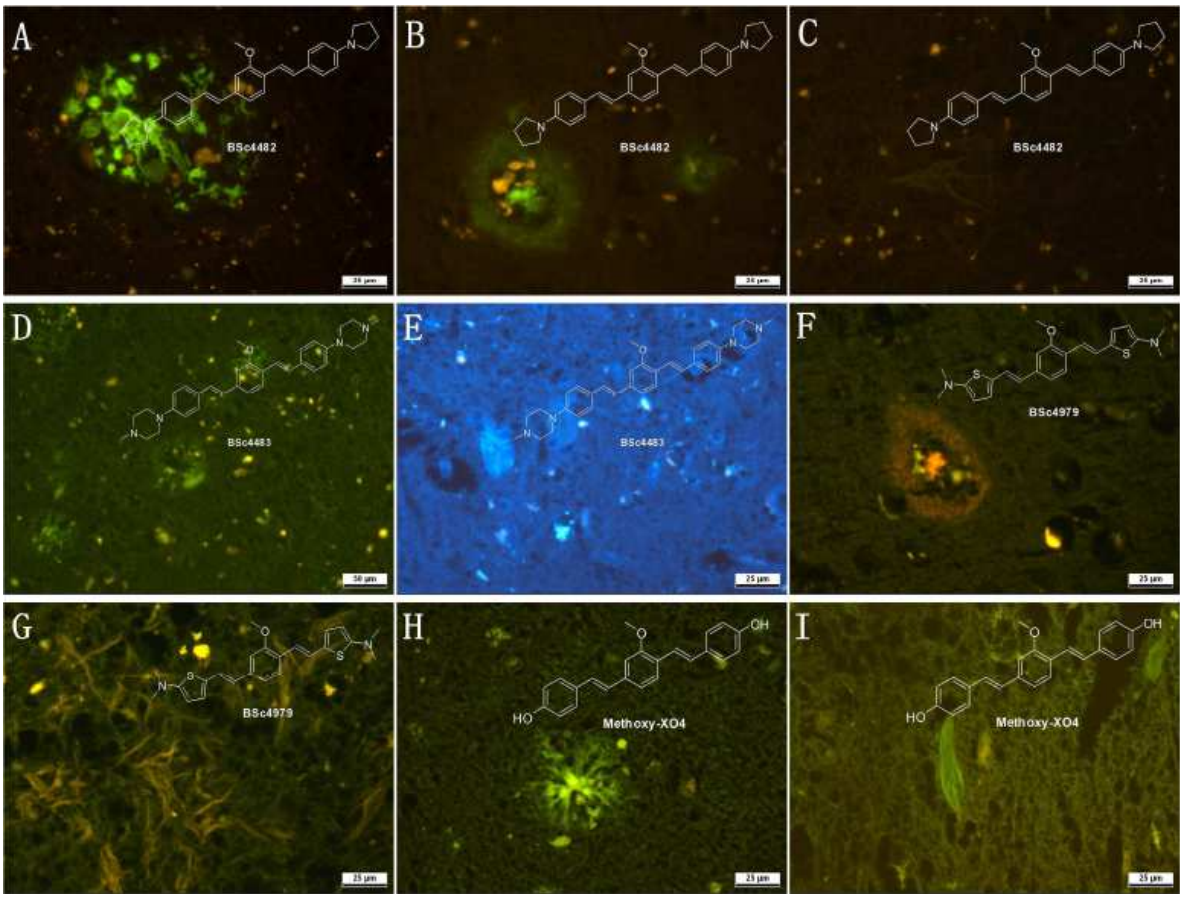

Figure 3.8 *In vitro* histochemical staining of postmortem AD brain tissues with 1,4-bisstyryl-2-methoxybenzenes (Tissues: hippocampus; Patient: male, 71 or 89 years old; CERAD Score: 3; NFTs-level: V).

The compound with good staining in the series **83** was tested in an *in vitro* binding assay. It provided excellent IC_{50} values for $A\beta_{40}$-aggregates and tau aggregates. The displacement ability of these 1,4-bisstyryl-2-methoxybenzene derivatives was compared against the known probes Methoxy-X04 under same assay conditions. It displayed ~5-fold higher affinity to $A\beta_{40}$ aggregates and ~3-fold higher affinity to tau aggregates in comparison to Methoxy-X04. It indicates sufficient affinity of this probe for imaging of Aβ and tau aggregates *in vivo*. Furthermore, it may be radiolabeled with $^{11}CH_3$, ^{18}F and ^{123}I at the N position and evaluated as PET and SPECT radioligands for Aβ and tau imaging *in vivo*.

In order to demonstrate the cytotoxicity of compound **83**, we performed a wild-type zebrafish embryo development assay. Due to the poor solubility in distilled water, these embryos were treated with solutions containing 1 μM of compound **83** at 6-8 hpf. The phenotypes were compared at 24 hpf and 72 hpf. It was found that the embryos developed well at 24 hpf and 72 hpf, and did not display any lesions in eyes, yolks, tail and heart beat (**Figure 3.9**).

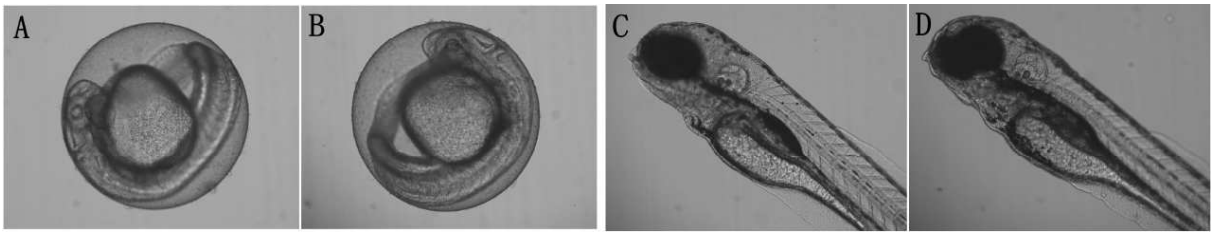

Figure 3.9 *In vivo* cytotoxicity studies of embryos of wild-type zebrafish in 1 µM probe **83** at 24 hpf and 72 hpf. Controlled (A and C) and probe **83** (B and D).

The absorption spectrum indicated that the absorption maximum of probes **79a** and **79b** were 407.0 and 390.5 nm in EtOH, respectively. They are close to the value of Methoxy-X04 (λ = 380 nm in methanol).[204] On the other hand, it was found that compound **83** shows a redshifted absorption spectrum (λ = 434.0 nm in ethanol) due to the introduction of the terminal *N*,*N*-dimethylthiophen-2-amine unit.

We hypothesized that this redshift is preferable. It may place the fluorescence emission in the ideal viewing region. This result may facilitate the detection of Aβ or tau aggregates by the DAPI- or FITC-filters employed in fluorescence microscopy. Taken together, these results indicate that fluorescent probes with good photophysical properties and high affinity may assist to handle and be applicable in biological and histological staining.

3.4.2. Synthesis and evaluation of 1,4-bisstyryl-2-bromobenzene and 1,4-bisstyryl-2,5-dibromobenzene derivatives for the detection of Aβ plaques

Recently a lot of attention has been directed toward the derivatization of CR to develop small molecules as potential diagnostic tools for AD. (*E*,*E*)-1-Bromo-2,5-bis(3-hydroxycarbonyl-4-hydroxy)styrylbenzene (BSB) has been reported by Skovronsky and coworkers as a typical ligand which sensitively labels SPs in AD brain sections. Furthermore, it could detect Aβ plaques with high specificity in a mouse model of AD. However, it was also reported that NFTs can be stained brightly with BSB both *in vitro* and *in vivo*.[202,205] Additionally, the carboxylic acid moiety of BSB derivatives would be mostly ionized in the physiological pH range, which may reduce its ability to cross the BBB in humans.

As shown in **Scheme 3.12**, the replacement of the salicylic acid moiety by a 1-methyl-1*H*-pyrrole moiety resulted in 2,2'-(1*E*,1'*E*)-2,2'-(2-bromo-1,4-phenylene)bis(ethene-2,1-diyl)bis(1-methyl-1*H*-pyrrole) **88** (**BSc4575**). Bis(diethylphosphonate) **86** was coupled with 1-methyl-1*H*-pyrrole-2-carbaldehyde **87** to afford the (*E*,*E*)-isomer **88** as the sole product which has been characterized by ^{1}H-NMR spectroscopy.

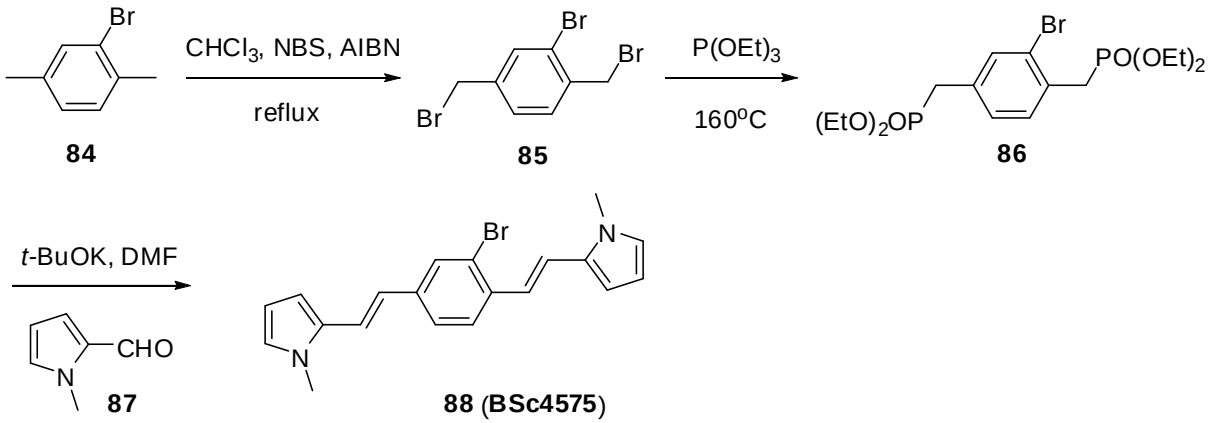

Scheme 3.12 Synthesis of 1,4-bisstyryl-2-bromobenzene derivative **88**.

The red shift of the absorption maximum in the two-photon excitation spectra and the cross-section value mainly depend on the electron deficiency on the central benzene ring. In order to improve the cross-section value and the photostability, we replaced the electron-withdrawing central ring. The 1,4-bisstyryl-2,5-dibromobenzenes **92a-c** (**BSc4575**, **BSc4576** and **BSc4580**) in **Scheme 3.13** were obtained using previously reported procedures. Alternatively, bis(diethylphosphonate) **91** was used for the Wittig-Horner reaction with corresponding aldehydes and the compounds **92a-c** were obtained as the sole product in good yields. According to the ^{1}H-NMR and HPLC spectrum, there were no other isomers present.

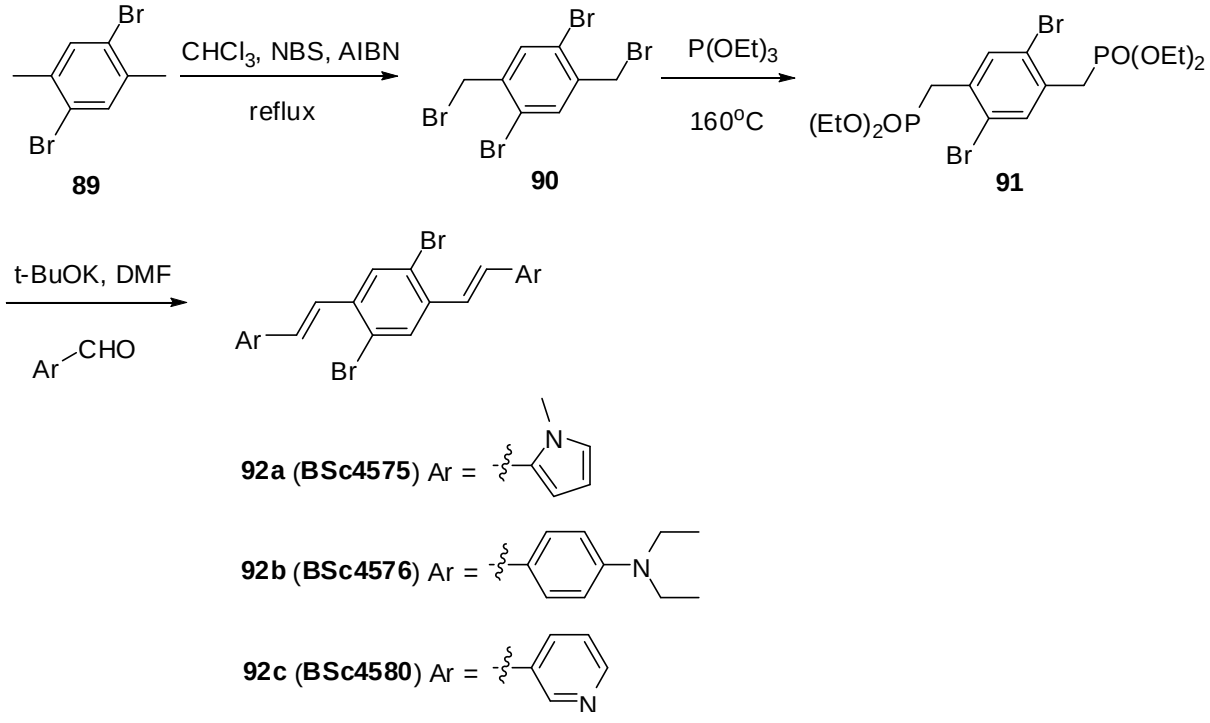

Scheme 3.13 Synthesis and structures of 1,4-bisstyryl-2,5-dibromobenzenes **92a-c**.

The compounds **88** and **92a-c** displayed poor solubility in buffer solution or in DMSO. This creates significant challenges for further *in vitro* and *in vivo* studies of these compounds. In order to address this shortcoming, we further modified the product by replacing the bromine with an amide group on the central core. The compound **94** (**BSc4574**) was synthesized using the procedure described by Jiang *et al* with few modifications.[206] With the replacement of the catalyst palladium (II) chloride and triphenylphosphine by bis(triphenylphosphine)palladium(II) dichloride, the reaction was carried out using the aryl bromide **92a** and isocyanides **93** in the presence of CsF and DMSO (**Scheme 3.14**) under a mild reaction condition.

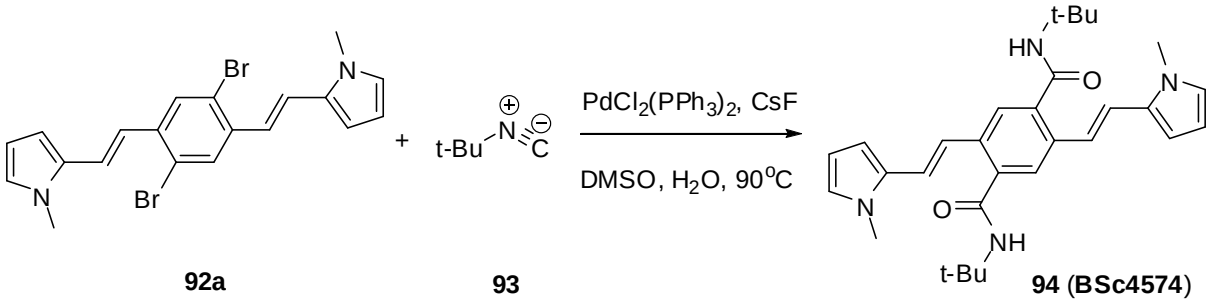

92a **93** **94** (**BSc4574**)

Scheme 3.14 Synthesis of amide via palladium-catalyzed amidation of 1,4-bisstyryl-2,5-dibromobenzene derivative.

All of these five probes have been evaluated for the fluorescent staining of Aβ plaques and NFTs in postmortem AD brain sections (**Figure 3.10**). Probes **92b** and **94** selectively labeled Aβ plaques in the brain tissues. However, probes **88**, **92a** and **92c** failed to detect Aβ plaques and NFTs by the fluorescence microscopy. It was assumed that the lipophilicity may affect the staining results of these probes. Further modification of probes **88** and **92b-c** aimed to improve the hydrophilicity of these scaffolds.

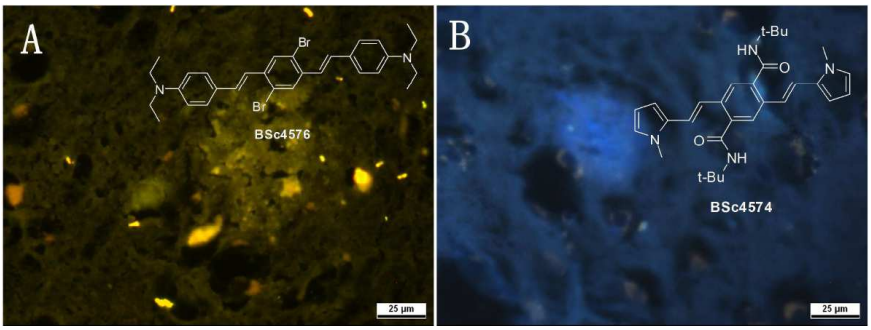

Figure 3.10 *In vitro* histochemical staining of postmortem AD brain tissues with **92b** and **94** (Tissues: hippocampus; Patient: male, 71 years old; CERAD Score: 3; NFTs-level: V).

3.4.3. Synthesis and evaluation of 1,4-bisstyryl-2-fluorobenzene and 1,2,4,5-tetrafluoro-3,6-bisstyrylbenzene derivatives for Aβ and tau imaging

3.4.3.1. Synthesis and evaluation of 1,4-bisstyryl-2-fluorobenzene derivatives for Aβ and tau imaging

According to the heavy atom effect, the fluorescence intensity of fluoro-substitution is usually greater than that of corresponding bromo-substituted compounds. In order to replace the bromine on the central ring, we planned to exploit an analogous compound to BSB that contains a fluoro group. In addition, in an *in vivo* experiment, the probe with smaller molecular weight may be favorable for improving the ability to penetrate the BBB and the rapid clearance from the brain. Currently, ^{18}F-labeled ligands have been developed to overcome the limitation of short half-life of ^{11}C. The fluoro-substituted probes may have the potential to be used as PET/MRI agents to detect Aβ or tau aggregates in AD.[199]

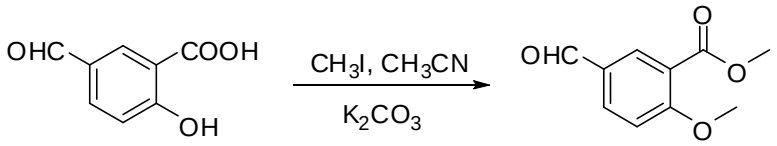

95 **96**

Scheme 3.15 Synthesis of methyl 5-formyl-2-methoxybenzoate **96**.

The acidic hydrogen of carboxyl and hydroxyl groups may not be compatible with the Wittig-Horner reaction. They were protected by methylation of 5-formyl-2-hydroxybenzoic acid **95** in acetonitrile at room temperature, which formed the compound **96** in quantitative yield (**Scheme 3.15**). The progress of the reaction was monitored by TLC and HPLC. After the completion of the reaction, the solution was concentrated under reduced pressure and the product was purified by column chromatography.

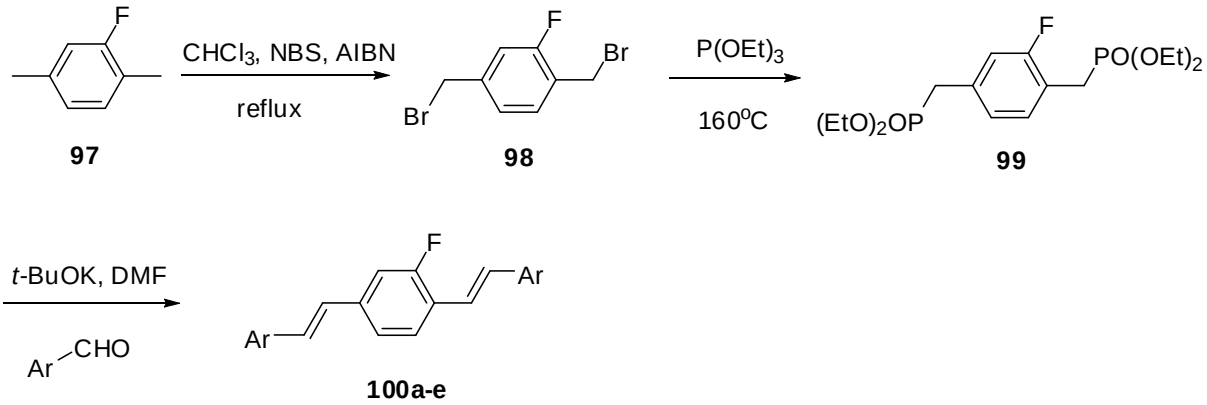

97 **98** **99**

100a-e

Scheme 3.16 Synthesis of 1,4-bisstyryl-2-fluorobenzenes **100a-e**.

Table 3.3 Structures and properties of 1,4-bisstyryl-2-fluorobenzenes **100a-e**.

Entry	BSc No.	Ar	Yield/%	*c*Log*P*[a]	MW[a]	Staining effect[b]
100a	**BSc4740**	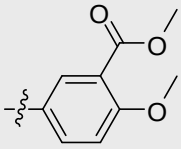	57	5.96	476.2	Aβ: **+++** NFT: **+++**
100b	**BSc4975**	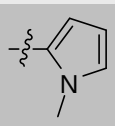	55	4.13	306.2	Aβ: **+** NFT: **++**
100c	**BSc4976**	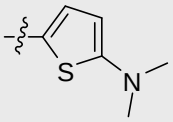	39	7.48	398.1	Aβ: **-** NFT: **+**
100d	**BSc4977**	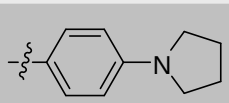	62	7.77	438.2	Aβ: **+++** NFT: **++**
100e	**BSc4978**	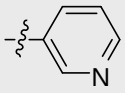	66	3.90	302.1	Aβ: **+++** NFT: **+**

[a] Determined by CS ChemOffice 10.0; [b] **+++** stands for efficient staining, **++** stands for normal staining, **+** stands for weak staining, **-** stands for no staining.

The synthetic pathway for preparing compounds **100a-e** is depicted in **Scheme 3.16**. The 2-fluoro-1,4-dimethylbenzene **97** was brominated using NBS under mild condition to generate the dibromide **98**. Followed by Michaelis–Arbuzov reaction to form the bisdiethylphosphonate **99** in high yield, the key step was carried out by base catalyzed Wittig-Horner reaction. The corresponding benzaldehydes and compound **99** were reacted in DMF at 80 °C to form the compounds **100a-e** (**Table 3.3**). Finally, compounds **100a-e** were purified by column chromatography and characterized by NMR spectroscopy. All of these compounds display excellent fluorescence under UV light, which allows them to be used to detect Aβ and tau aggregates in AD brain tissue.

To confirm the binding affinities of these derivatives for Aβ plaques and NFTs in the brain, *in vitro* fluorescent staining of brain sections from AD patients was carried out. In postmortem brain tissue many NFTs were clearly stained with **100a** and **100d** as seen in the *in vitro* assay (**Figure 3.11**, **A** and **F**), whereas Aβ plaques can be observed in the same brain section from hippocampus (**Figure 3.11**, **B** and **G**). The 1-methyl-1*H*-pyrrole derivative **100b** stains NFTs superior to Aβ plaques (**Figure 3.11**, **C** and **D**). In contrast, the pyridine

derivative **100e** strongly stains Aβ plaques but poorly stains NFTs (**Figure 3.11**, **H** and **I**). Especially, probe **100c** selectively binds to NFTs (**Figure 3.11**, **E**). On the basis of histological staining of Aβ plaques and NFTs, the staining effect seems to be determined by the styryl substituent of the probe. Based on these results, further radiolabeled these probes may be applied as PET radioligands for Aβ plaques and/or NFT imaging *in vivo*.

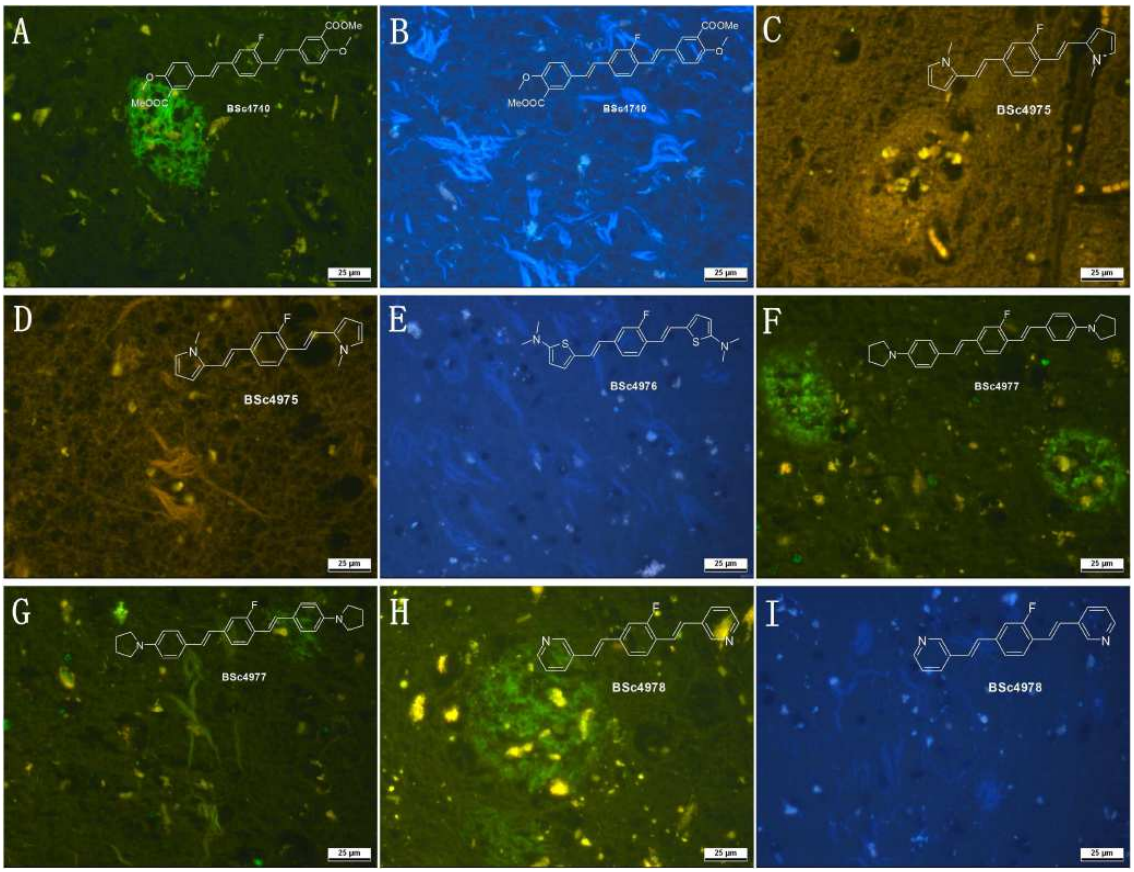

Figure 3.11 *In vitro* histochemical staining of postmortem AD brain tissues with 1,4-bisstyryl-2-fluorobenzenes (Tissues: hippocampus; Patient: males, 71 and 72 years old; CERAD Score: 3; NFTs-level: V).

To quantify the binding affinities of **100b** and **100d-e** for $A\beta_{40}$ and tau aggregates, a new *Thiazine Red R* displacement assay was carried out. Probe **100b** displayed higher binding affinity for both $A\beta_{40}$ and tau aggregates. It is noteworthy that compound **100d** displays > 5-fold higher affinity to tau over $A\beta_{40}$. This result is consistent with the underlying assumption that probe with a 4-phenylpyrrolidine moiety may be conducive to present a specific affinity for tau aggregates in AD brain sections. Unfortunately, the binding affinities of probe **100e** for $A\beta_{40}$ and tau aggregates are out of the range of valid values.

3.4.3.2. Synthesis and evaluation of 1,2,4,5-tetrafluoro-3,6-bisstyrylbenzene derivatives for the detection of Aβ plaques

Higuchi *et al*. have proposed the monofluoro bisstyrylbenzene derivative FSB for the visualization of Aβ plaques in APP transgenic mice by ^{19}F-MRI. However, the low sensitivity of ^{19}F-MRI limits its further use to detect Aβ plaques in human brain.[207] In order to overcome this limitation and to enhance two photon excitation, we planned to design several bisstyrylbenzene ligands with a highly fluorinated tetrafluorophenyl core. Flaherty *et al*. reported that the binding affinity of the tetrafluorophenyl bisstyrylbenzene derivative increased 360-fold in comparison to its monofluorophenyl counterpart. Besides, it suggested that bisstyrylbenzenes with carboxylic acid functional groups have lower Aβ binding affinities than their neutral counterparts.[95] Hence, we were interested to develop several tetrafluorphenyl bisstyryl derivatives to investigate their ability to detect Aβ plaques and NFTs in postmortem sections.

The bisstyrylbenzene derivatives **104a-h** were synthesized using the procedures described by Flaherty *et al*. as shown in **Scheme 3.17**. The 1,4-bis(bromomethyl)-2,3,5,6-tetrafluorobenzene **102** was obtained in a one-step benzylic bromination of commercially available compound **101** using NBS and AIBN. The coupling precursor bisdiethylphosphonate **103** was prepared by the Michaelis–Arbuzov reaction between compound **102** and triethyl phosphite. Finally, the bisstyrylbenzene ligands **104a-h** (**Table 3.4**) were obtained using the classic Wittig-Horner coupling between bisdiethylphosphonate and corresponding aldehydes in DMF at 80 °C for 16 h. All of these compounds were recrystallized from EtOAc and further characterized by NMR spectroscopy. The ^{1}H-NMR spectrum revealed that the two doublets correspond to *trans* configured olefinic protons with a large coupling constant (J = 16.5-17.0 Hz). However, several compounds (**104b** and **104e-f**) could not be characterized by ^{13}C-NMR spectroscopy. This was due to poor solubility.

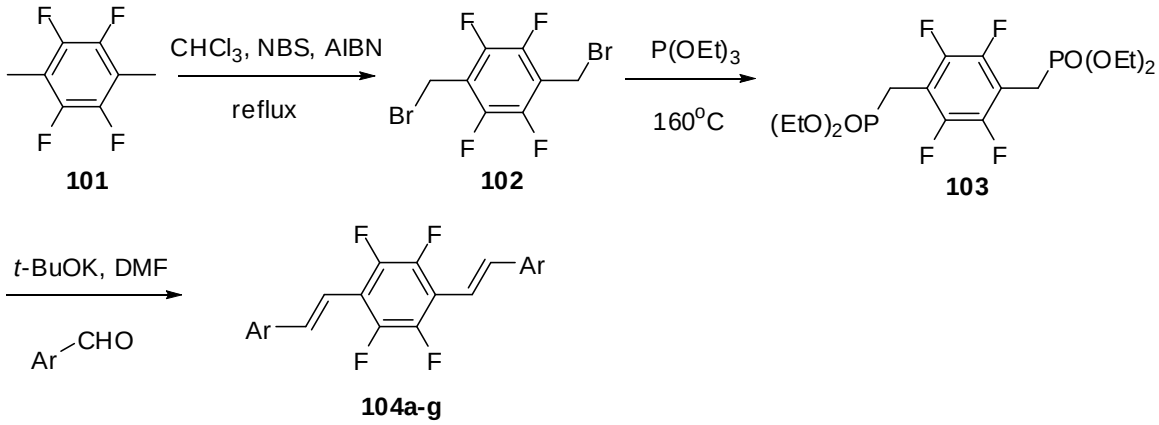

Scheme 3.17 Synthesis of 1,2,4,5-tetrafluoro-3,6-bisstyrylbenzenes **104a-g**.

Table 3.4 Structures and properties of 1,2,4,5-tetrafluoro-3,6-bisstyrylbenzenes **104a-g**.

Entry	BSc No.	Ar	Yield/%	*c*Log*P*[a]	MW[a]	Staining effect[b]
104a	**BSc4566**	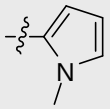	69	4.61	360.4	Aβ: **-** NFT: **-**
104b	**BSc4567**	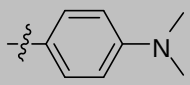	65	7.62	440.5	Aβ: **+++** NFT: **-**
104c	**BSc4569**	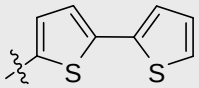	66	10.44	530.6	Aβ: **+++** NFT: **-**
104d	**BSc4570**	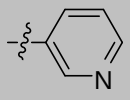	62	4.37	356.3	Aβ: **+** NFT: **-**
104e	**BSc4571**	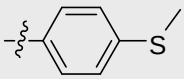	59	7.93	446.5	Aβ: **++** NFT: **-**
104f	**BSc4572**	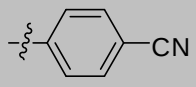	53	7.11	404.4	Aβ: **-** NFT: **-**
104g	**BSc4573**	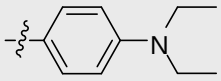	59	8.97	496.6	Aβ: **-** NFT: **-**

[a] Determined by CS ChemOffice 10.0; [b] **+++** stands for efficient staining, **++** stands for normal staining, **+** stands for weak staining and **-** stands for no staining.

The qualitative selective binding of the fluorescent probes to Aβ plaques was evaluated in the primary screen on hippocampal sections of human AD brain tissue and analyzed by fluorescence microscopy. Remarkably, numerous fluorescent spots were detected by the probes **104b-c** (**Figure 3.12**, **A** and **B**). These results reveal that probes **104b-c** are useful as specific fluorescent probes for the detection of Aβ aggregates in the brain sections of AD patient. Probes **104d-e** resulted in faint plaque staining. In addition, due to the poor solubility, we observed tiny crystals of compounds **104d-e** on the brain sections (**Figure 3.12**, **C** and **D**). Unfortunately, probes **104a** and **104f-g** failed to detect Aβ plaques and NFTs by fluorescence microscopy. These results indicate that the electron-donor groups or electron-withdrawing groups in the *para* position of styryl groups may not affect the staining results.

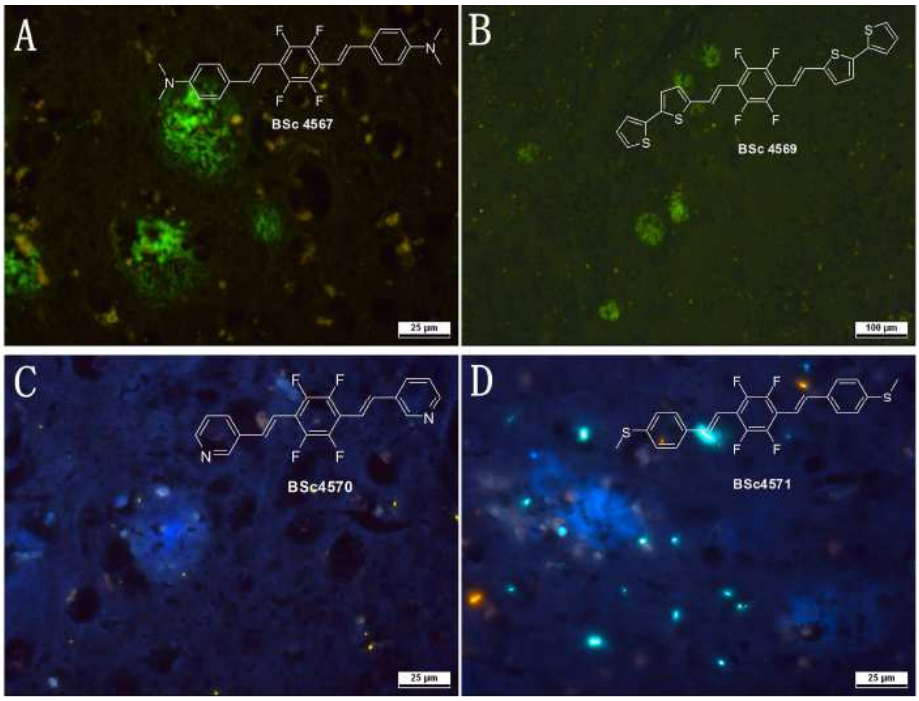

Figure 3.12 *In vitro* histochemical staining of postmortem AD brain tissues with 1,2,4,5-tetrafluoro-3,6-bisstyrylbenzenes (Tissues: hippocampus; Patient: male, 71 years old; CERAD Score: 3; NFTs-level: V).

The selected compound **100a** and two of 1,2,4,5-tetrafluoro-3,6-bisstyrylbenzenes **104b-c** have been further evaluated at different concentrations in the wild-type zebrafish embryo development assay. The embryos incubated with compound **100a** developed well and no lesions were found at different concentrations up to 5 µM at 24 hpf and 72 hpf (**Figure 3.13**, **B** and **G**). However, the juvenile fish incubated with 10 µM of compound **100a** showed spinal curvature after 72 hpf (**Figure 3.13**, **H**). This result suggested that probe **100a** might be cytotoxic at concentrations higher than 5 µM. On the other hand, due to the poor solubility, the embryos were only treated with 1 µM of probes **104b-c**. The passable results have shown that these embryos developed well in the presence of 1 µM probes **104b-c** at 24 hpf and 72 hpf (**Figure 3.12**). The cytotoxicity study suggested that these probes have negligible cytotoxicity against zebrafish embryos at the same concentration that was used for histology experiments on human AD brain tissue (1 µM). In conclusion, further modification should aim to improve the solubility of these compounds.

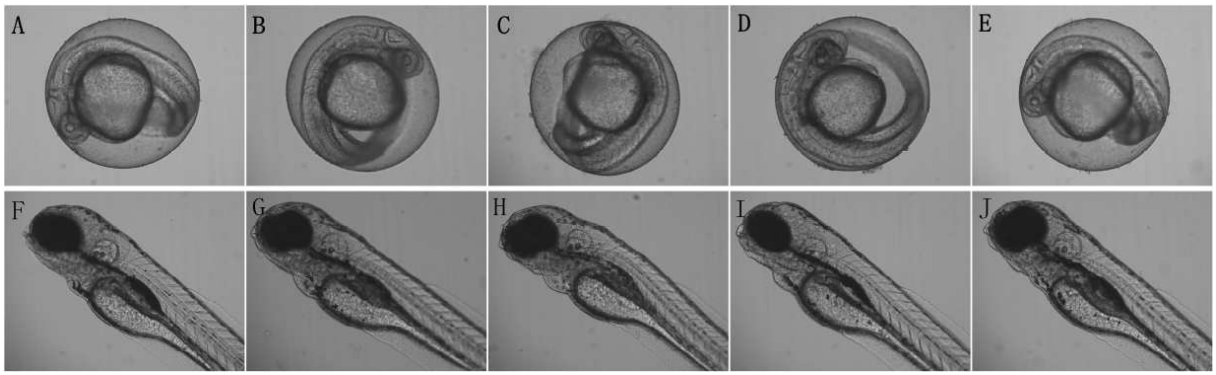

Figure 3.13 *In vivo* cytotoxicity studies of embryos of wild-type zebrafish with 5 μM (B and G) and 10 (C and H) μM **100a** and embryos with 1 μM **104b-c** at 24 hpf and 72 hpf. Controlled (A and C), probe **104b** (D and I) and probe **104b** (E and J).

3.4.4. Synthesis and evaluation of 1,4-bisstyryl-2-bromo-5-cyanobenzene derivatives for Aβ and tau imaging

It is reported that introduction of the fluorophore group on the central ring may enhance the two-photon absorption cross-section value.[208] For this purpose, we synthesized a series of 1,4-bisstyryl-2-bromo-5-cyanobenzenes as to exploit the effect for the detection of Aβ aggregates and NFTs in human postmortem sections. Subsequently, different substituents on the *para* position of styryl groups were explored to investigate the interaction with Aβ or tau aggregates.

The mono-cyano substituted compounds **108a-e** were synthesized in four steps. A mixture of commercially available 1,4-dibromo-2,5-dimethylbenzene **89** and an equivalent of CuCN in DMF at 80 °C for 1 h afforded the mono-cyano substrate **105**. The reaction was monitored by TLC and the product was purified by column chromatography. Followed by benzylic bromination and Michaelis–Arbuzov reaction, bisdiethylphosphonate **107** was coupled with the corresponding aldehydes in DMF at 80 °C to afford the 1,4-bisstyryl-2-bromo-5-cyanobenzenes **108a-e** (**Scheme 3.18**, **Table 3.5**). The products were recrystalled from EtOAc and characterized by NMR spectroscopy.

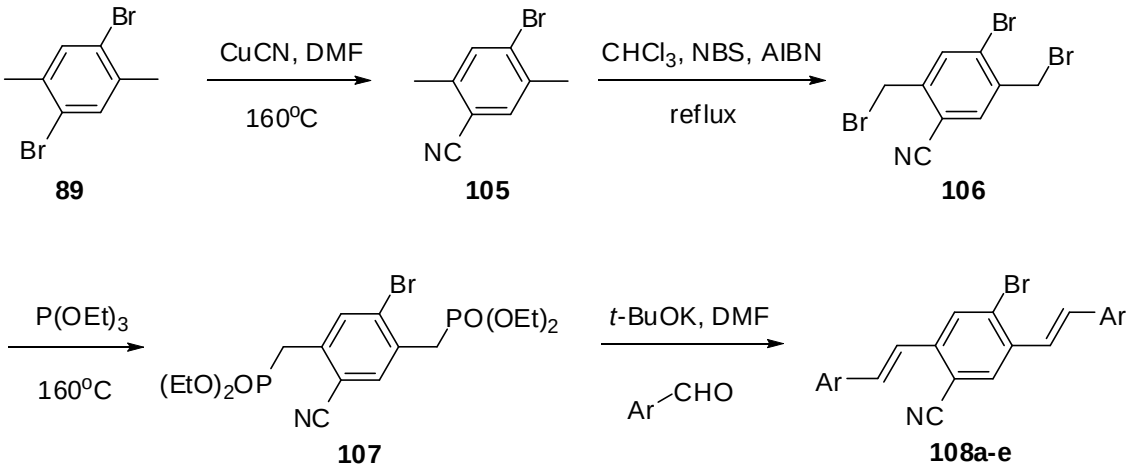

Scheme 3.18 Synthesis of 1,4-bisstyryl-2-bromo-5-cyanobenzenes **108a-e**.

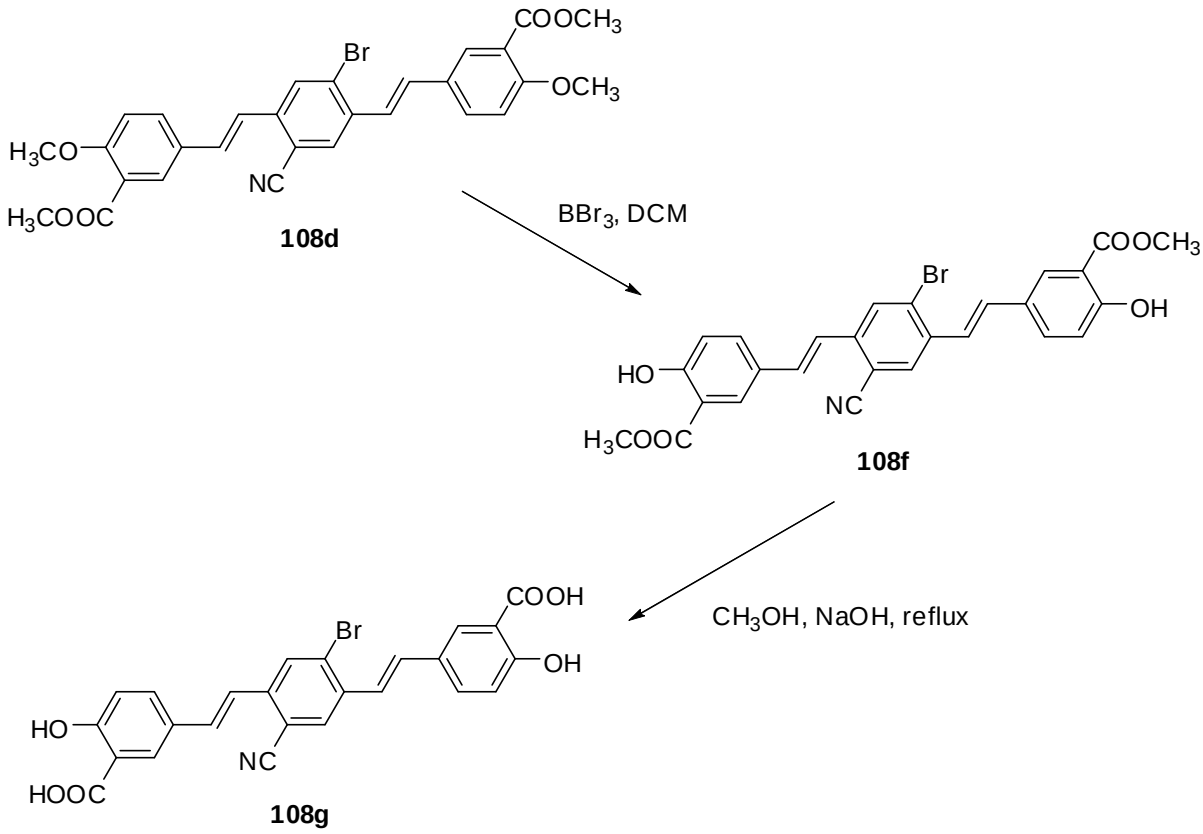

Scheme 3.19 Synthesis of 1,4-bisstyryl-2-bromo-5-cyanobenzenes**108f-g**.

The phenolic bis-styrylbenzene **108f** was obtained by subsequent boron tribromide demethylation in dichloromethane at room temperature (**Scheme 3.19**, **Table 3.5**). Due to the poor solubility, the compound **108f** was only characterized by mass spectrometry and the purity was analyzed by HPLC. Finally, the deprotected salicylic acid derivative **108g** was obtained by ester hydrolysis and the conformation was determined by ^{1}H-NMR.

Table 3.5 Structures and properties 1,4-bisstyryl-2-bromo-5-cyanobenzenes**108a-g**.

Entry	BSc No.	Ar	Yield/%	*c*Log*P*[a]	MW[a]	Staining effect[b]
108a	**BSc4577**	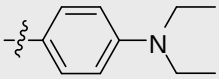	77	9.20	528.5	Aβ: **++** NFT: **-**
108b	**BSc4578**	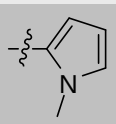	73	4.84	392.3	Aβ: **-** NFT: **-**
108c	**BSc4580**	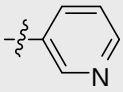	82	4.60	388.3	Aβ: **++** NFT: **+**
108d	**BSc4581**	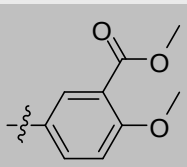	66	6.66	562.4	Aβ: **++** NFT: **-**
108e	**BSc4582**	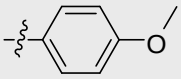	69	7.02	446.3	Aβ: **+** NFT: **-**
108f	**BSc4642**	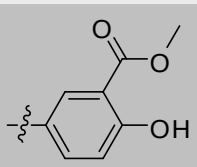	97	6.14	534.4	Aβ: **+++** NFT: **++**
108g	**BSc4702**	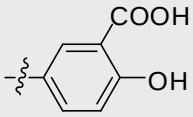	84	5.61	506.3	Aβ: **++** NFT: **++**

[a] Determined by CS ChemOffice 10.0; [b] **+++** stands for efficient staining, **++** stands for normal staining, **+** stands for weak staining, **-** stands for no staining.

The biological evaluation of these compounds for Aβ plaques and NFTs was accomplished by fluorescent staining of brain sections (**Figure 3.14**). Probes **108a** and **108d-e** stained Aβ plaques specifically but with poor contrast to the background in AD brain sections. Due to the poor solubility, tiny crystals of compound **108a** on brain sections were observed by fluorescence microscopy. In addition, probes **108c** and **108f-g** were observed to bind to Aβ plaques and NFTs in AD brain tissues. Especially, at the beginning, probes **108f** and **108g** labeled Aβ plaques and NFTs clearly. However, the fluorescence was prone to photobleaching within few seconds. It was assumed that the presence of the phenolic moiety or active hydrogen on this scaffold may restore the fluorescence in the bleached region upon binding to the proteins. To our surprise, the most soluble compound (**108b**) in this set failed to detect both Aβ and tau aggregates. It indicates that lipophilicity may not affect the staining

effects of these ligands. However, the poor solubility and permeability are adverse properties which limit the potential use of these compounds *in vivo*.

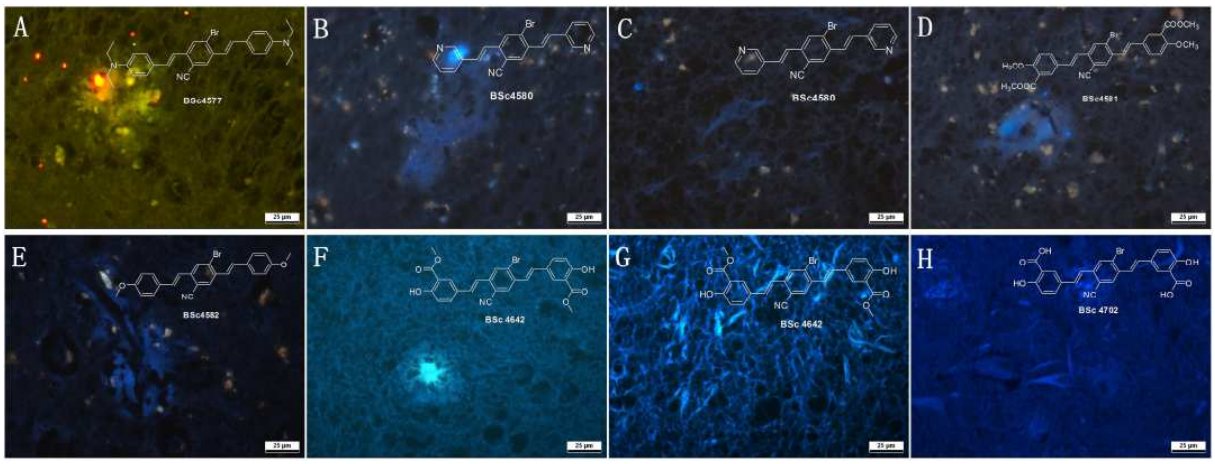

Figure 3.14 *In vitro* histochemical staining of postmortem AD brain tissues with 1,4-bisstyryl-2-bromo-5-cyanobenzenes (Tissues: hippocampus; Patient: male, 71 years old; CERAD Score: 3; NFTs-level: V).

3.4.5. Synthesis and evaluation of bis(arylvinyl)pyrimidine derivatives as imaging probes for Aβ and tau imaging

According to previous studies by our group, the replacement of the central ring of the Methoxy-X04 by pyrimidine as aromatic core may lead to molecules with a enlarged π-conjugation. The bis(arylvinyl)pyrimidines displayed good fluorescence properties in an *in vitro* binding experiment.[49] Nevertheless, the poor solubility (< 0.1 g/L) might limit the use in living human subjects. In order to address this shortcoming, we focused on the introduction of different functional groups to improve physicochemical properties and reduce lipophilicity of probes.

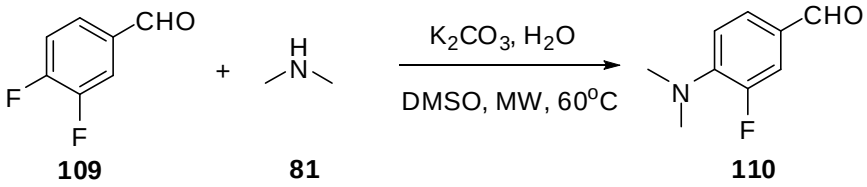

Scheme 3.20 Synthesis of 4-(dimethylamino)-3-fluorobenzaldehyde **110**.

In this series, aldehydes **82**, **110** and **113** were not commercially available. As shown in **Scheme 3.20**, in the presence of K_2CO_3, 4-(dimethylamino)-3-fluorobenzaldehyde **110** was prepared by the 3,4-difluorobenzaldehyde **109** and dimethylamine solution (40% in water) under microwave irradiation. In addition, CuI-catalyzed coupling reaction was carried out

using *L*-proline as promoter. The reaction of 4-bromobenzaldehyde **111** and 2-aminoethanol **112** proceeded at 80 °C under microwave condition to form 4-(2-hydroxyethylamino) benzaldehyde **113** in 93 % yield (**Scheme 3.21**).

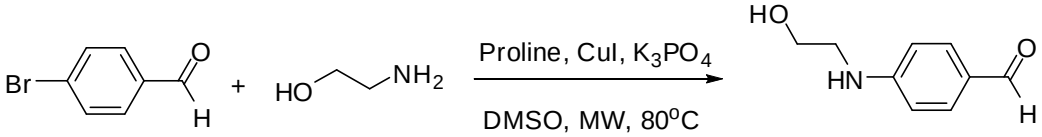

111 **112** **113**

Scheme 3.21 Synthesis of 4-(2-hydroxyethylamino)benzaldehyde **113**.

According to the previously reported procedure, bis(arylvinyl)pyrimidines **115a-d** were formed in an atom efficient reaction by condensation of 4,6-dimethylpyrimidine **114** and aryl aldehydes. The experimental procedure is straightforward and rather economic because it does not require any organic solvent.[209] The reaction was carried out in 5 M NaOH solution using Aliquat 336 as phase transfer catalyst. According to the coupling constant (*J* = 15.0-16.0 Hz) in ^{1}H-NMR spectroscopy (**Table 3.6**), purification by column chromatography provided the *trans* isomers only.

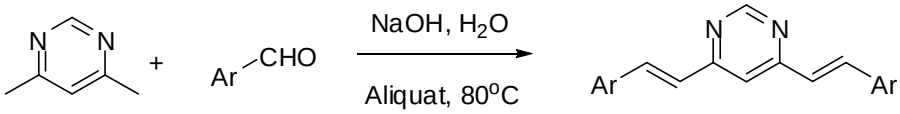

114 **115a-d**

Scheme 3.22 Synthesis of bis(arylvinyl)pyrimidines **115a-d**.

In order to evaluate the binding effects to Aβ plaques and NFT in AD brain sections, we performed neuropathological fluorescent staining with these bis(arylvinyl)pyrimidines (**Figure 3.15**). The most soluble probe **115a** clearly binds to Aβ and tau aggregates. In addition, probes **115b** and **115d** displayed selectivity for NFTs in hippocampal tissue sections from AD human brain. This suggested these compounds may be used as tau specific fluorescent probe for *in vivo* quantification of neurofibrillary pathology. Further radiolabeling of **115b** and **115d** may extend their use to the *in vivo* imaging of tau aggregates in the brain. Unfortunately, probe **115c** failed to detect Aβ plaques and NFTs by fluorescence microscopy. However, bromine-containing moiety may be used to synthesize the ^{125}I-labeled radioligand for tau imaging *in vitro* and *in vivo*.

Table 3.6 Structures and properties of bis(arylvinyl)pyrimidines.

Entry	BSc No.	Ar	Yield/%	*c*Log*P*[a]	MW[a]	Staining effect[b]
115a	**BSc4919**	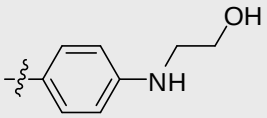	82	3.29	402.2	Aβ: **+++** NFT: **++**
115b	**BSc4921**	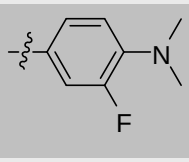	77	6.21	406.2	Aβ: **-** NFT: **+**
115c	**BSc4959**	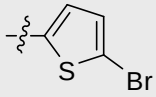	62	6.71	451.9	Aβ: **-** NFT: **-**
115d	**BSc4960**	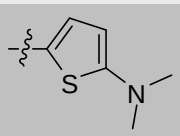	76	6.24	382.1	Aβ: **-** NFT: **+++**

[a] Determined by CS ChemOffice 10.0; [b] **+++** stands for efficient staining, **++** stands for normal staining, **+** stands for weak staining and **-** stands for no staining.

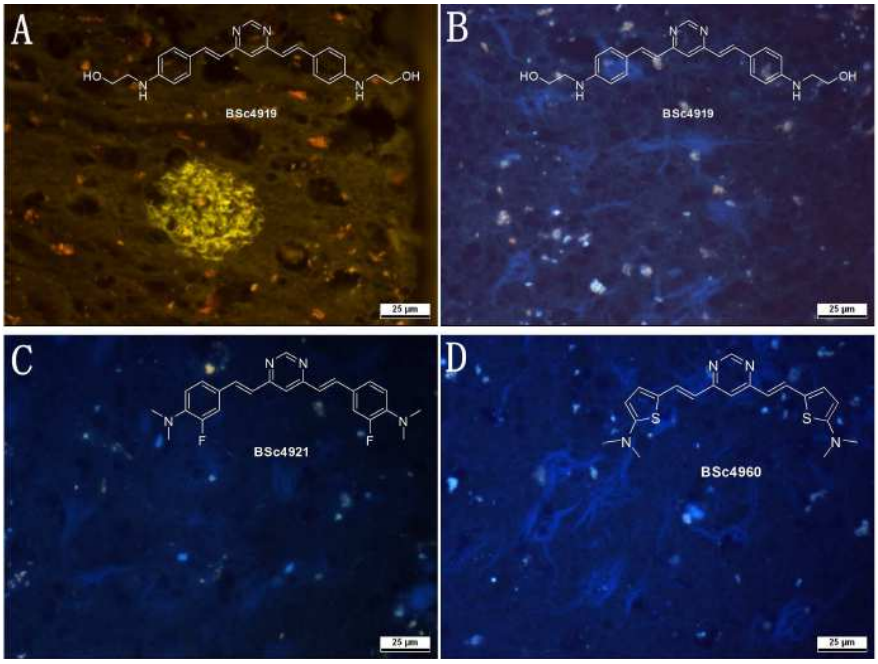

Figure 3.15 *In vitro* histochemical staining of postmortem AD brain tissues with bis(arylvinyl)pyrimidines (Tissues: hippocampus; Patient: male, 72 years old; CERAD Score: 3; NFTs-level: V).

Three compounds were tested in a new *in vitro* affinity assay to determine the IC_{50} values versus *Thiazine Red R* displacement from aggregated tau and $A\beta_{40}$. It was found that probe **115a** showed 5.4-fold higher affinity to aggregated tau over $A\beta_{40}$. In contrast, probes **115b** and **115d** displayed the opposite performance. The probe **115b** displayed 1.4-fold higher affinity for tau aggregates. Remarkably, probe **115d** displayed excellent affinity to both $A\beta_{40}$ and tau aggregates in the low-nanomolar range, which suggested sufficient affinity of the probe for imaging of tau aggregates *in vivo*.

To investigate the cytotoxicity of bis(arylvinyl)pyrimidines, probe **115a** was evaluated at different concentrations in the wild-type zebrafish embryo development assay. As shown in **Figure 3.16**, the embryos developed well and no lesions were found at different concentrations up to 10 μM at 24 hpf and 72 hpf. It implied that probe **115a** displays negligible cytotoxicity at the corresponding concentrations. Further modification with improved solubility may further this series as potential *in vivo* imaging agents for AD.

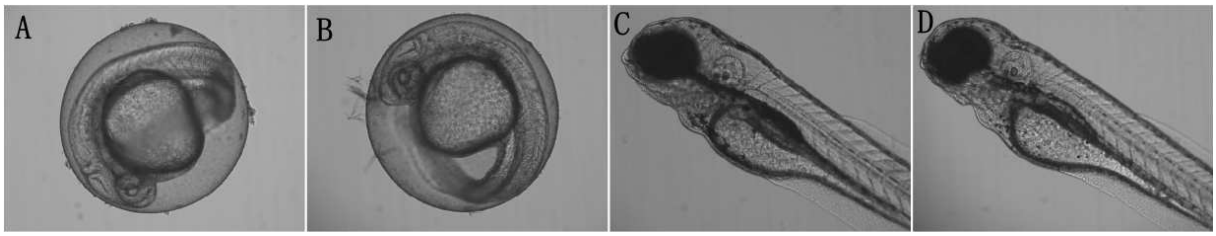

Figure 3.16 *In vivo* cytotoxicity studies of embryos of wild-type zebrafish in 10 μM with **115a** at 24 hpf and 72 hpf. Controlled (A and C) and probe **115a** (B and D).

3.5. Design, synthesis and evaluation of spiropyran derivatives as specific tau imaging probes

3.5.1. Design, synthesis and spectroscopy of spiropyran derivatives

In the past few decades, thermochromic and photochromic indolinobenzospiropyrans have been suggested as classic photoswitchable molecules. They show reversibe structural conversion between the closed spiropyran (**SP**) form and the opened merocyanine (**ME**) form upon external optical, thermal, or chemical stimulations. They have been widely utilized for colorimetric and fluorescent detections of chemical or biological species.[210] Generally, **SP** molecules are known to be unstable, whereas **ME** molecules are relatively stable, either thermally or photochemically.[211]

The initial idea was that **SP** dye may engage in specific interaction to bind to Aβ or tau aggregates. Furthermore, the external optical stimulation may promote the conversion from

the **SP** component to the corresponding **ME** conformation. As a result, the fluorescent species may be detected by fluorescence microscopy or other imaging technologies. Toward this goal, we employed a series of fluorescent photoswitch dyes, which were applied to detect Aβ and tau aggregates in AD brain sections.

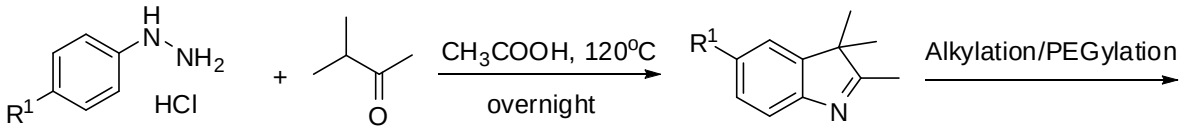

116a: R^1 = H
116b: R^1 = F
116c: R^1 = Br
116d: R^1 = OCH_3

117

118a: R^1 = H
118b: R^1 = F
118c: R^1 = Br
118d: R^1 = OCH_3

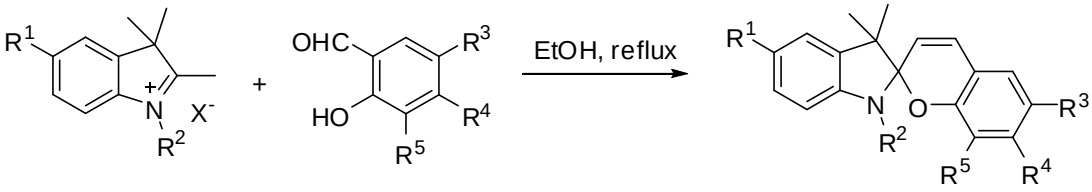

119a: R^1 = H, R^2 = CH_3, X = I
119b: R^1 = H, R^2 = *n*-Bu, X = I
119c: R^1 = F, R^2 = CH_3, X = I
119d: R^1 = Br, R^2 = CH_3, X = I
119e: R^1 = OCH_3, R^2 = CH_3, X = I
119f: R^1 = H, R^2 = $CH_2CH_2OCH_3$, X = Cl

120a-l

R^1 = H, F, Br, OCH_3
R^2 = CH_3, *n*-Bu, -$CH_2CH_2OCH_3$
R^3 = H, OH, NO_2, CH_3, F, CH_3
R^4 = H, $N(CH_2CH_3)_2$
R^5 = H, OCH_3

Scheme 3.23 Synthesis of spiropyran derivatives.

As shown in **Scheme 3.23** and **Table 3.7**, the indolinospiropyrans were synthesized in three steps starting from the commercially available phenylhydrazines **116a-d** and 3-methyl-2-butanone **117**. Typically, they were condensed to generate the intermediate hydrazone and further converted by Fischer indole synthesis to obtain the 3*H*-indoles **118a-d**. Methylation of compounds **118a-d** in acetonitrile under reflux formed the indolium **119a** and **119c-e** as colorless solids in quantitative yields. The colorless solids were used in the following step without further purification. In addition, indolenine **118a** and 1-iodobutane were stirred under reflux in ethylmethylketone to obtain the indolium **119b** as pale yellow solid in a yield of 73 %. After PEGylation with 2-methoxyethyl 4-methylbenzenesulfonate in the N-position of compound **118a**, the crude product was purified by column chromatography. Finally, the salicylaldehydes condensed with **119a-f** via a carbinol intermediate to form the spiropyrans **120a-l** in moderate yields.

Table 3.7 Structures and staining effect of spiropyran derivatives.

Entry	BSc No.	R^1	R^2	R^3	R^4	R^5	Staining effect[a]
120a	**BSc4452**	H	Me	H	$N(Et)_2$	H	Aβ: **-** NFT: **+++**
120b	**BSc4453**	H	Me	H	H	OMe	Aβ: **-** NFT: **-**
120c	**BSc4454**	H	Me	OH	H	H	Aβ: **-** NFT: **-**
120d	**BSc4455**	H	Me	NO_2	H	H	Aβ: **-** NFT: **+**
120e	**BSc4487**	H	Me	F	H	H	Aβ: **-** NFT: **-**
120f	**BSc4488**	H	Me	H	H	H	Aβ: **-** NFT: **-**
120g	**BSc4489**	H	Me	Me	H	H	Aβ: **-** NFT: **-**
120h	**BSc4744**	H	n-Bu	H	$N(Et)_2$	H	Aβ: **-** NFT: **+++**
120i	**BSc4807**	F	Me	H	$N(Et)_2$	H	Aβ: **-** NFT: **-**
120j	**BSc4808**	Br	Me	H	$N(Et)_2$	H	Aβ: **+** NFT: **+**
120k	**BSc4809**	OMe	Me	H	$N(Et)_2$	H	Aβ: **+** NFT: **-**
120l	**BSc4903**	H	CH_2CH_2OMe	H	$N(Et)_2$	H	Aβ: **-** NFT: **+++**

[a] **+++** stands for efficient staining, **+** stands for weak staining, **-** stands for no staining.

The compound **120d** was used as an example to study and evaluate the absorbance values of each conformation via UV spectroscopy. The structures of each conformation have been characterized using ^{1}H-NMR and ^{13}C-NMR spectroscopic data.

The absorption spectrum of a colorless solution of **SP 120d** in EtOH displayed the maximum absorption wavelength around 320 nm, but it did not show any bands at wavelengths greater than 450 nm. In order to study the ring closure state, **120d** was first irradiated in EtOH for 1 h by sunlight. However, the maximum absorption wavelength at ~330 nm suggested that the compound almost completely adopted the **SP** form in solution. Furthermore, upon illumination of this solution with ultraviolet light (365 nm, 220 V, 50 Hz) for 1 h, the colorless **SP** switches to the dark purple **ME**. The appearance of an absorption band at 539 nm in this process may be due to the ring opening form lead to a large planar π-system. Furthermore, upon addition of 10% CH_3COOH to the purple **ME** solution, **ME** switched completely to the yellow-green **MEH$^+$**. Consistently, the absorption band at 539 nm disappeared (**Figure 3.17**). Finally, upon irradiation with visible light, **MEH$^+$** released a proton and switched to **SP** state in the anticlockwise cycle (**Figure 3.18**).[210,212]

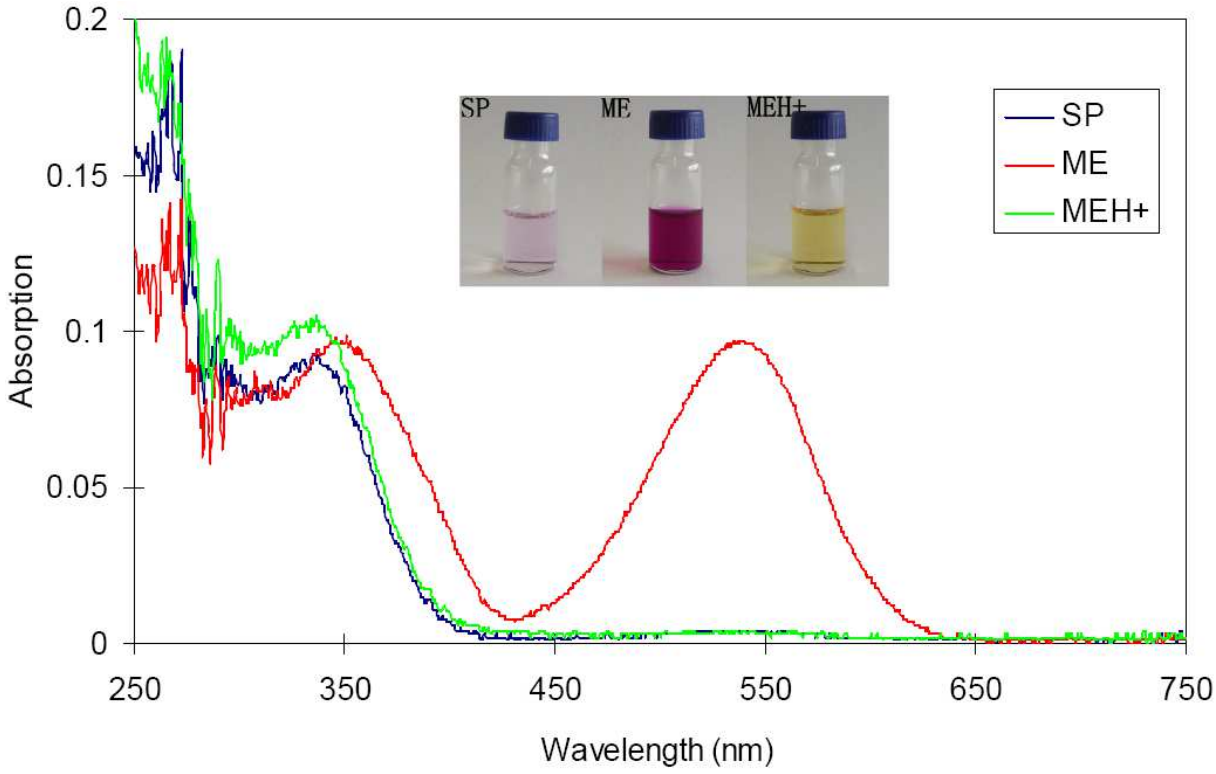

Figure 3.17 The absorption spectra of a solution of 10 μM **120d** in EtOH (blue) and the same solution after irradiation with ultraviolet light (red), as well as addition of 10% CH_3COOH (green).

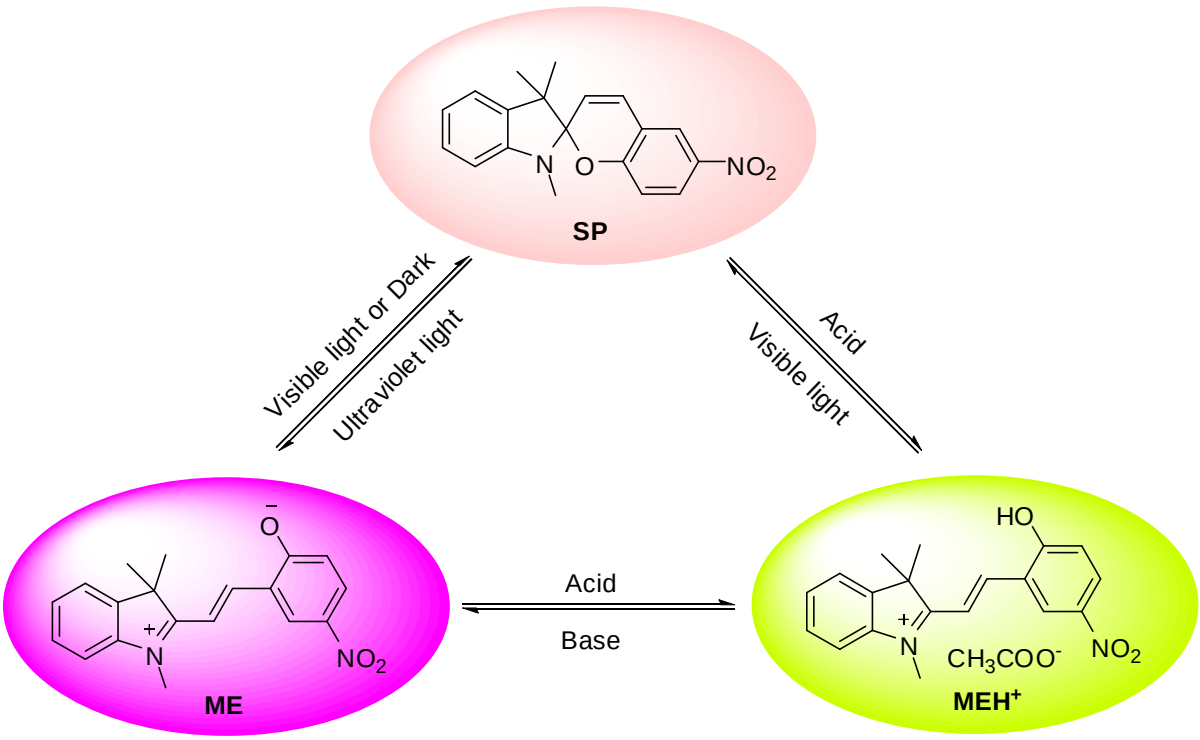

Figure 3.18 The switching cycle associated with three states of **120d**.

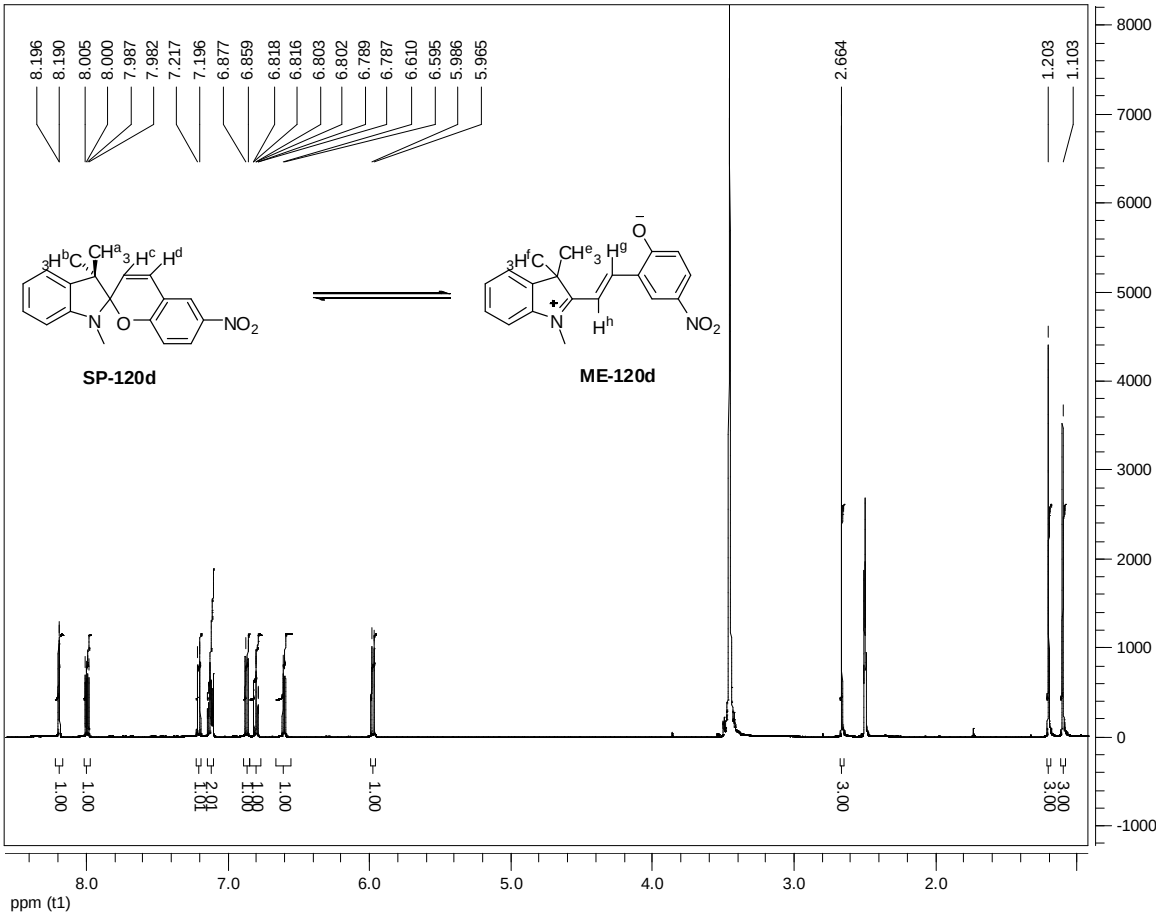

Figure 3.19 The ^{1}H-NMR spectrum of compound **120d**.

The structures of the condensed products have been characterized by ^{1}H-NMR and ^{13}C-NMR spectroscopic data. The chiral spirocenter of **120d** imposed two different environments on the methyl protons H^a and H^b. However, in case of the **ME** conformation, the methyl protons H^e and H^f are place in the same chemical environments, the loss of the chiral spirocenter simplifies the NMR signal. As a result, two distinct singlets were observed at 1.20 ppm and 1.10 ppm in ^{1}H-NMR spectrum, which corresponded to the methyl protons H^a and H^b, respectively (**Figure 3.19**). Additionally, two doublets at 5.97 ppm and 7.20 ppm corresponded to olefinic protons H^c and H^d, respectively. The relatively smaller coupling constant of 10.5 Hz suggested that these two protons are in a *cis*-arrangement relative to the interposed double bond. On the other hand, the coupling constant for the olefinic protons of H^g and H^h are around 16 Hz. In fact, the conformation of **SP** was forced into a *cis* configuration, but **ME** is proned to adopt *trans* configuration.

3.5.2. Evaluation of spiropyran derivatives as specific tau imaging probes

To confirm the selectivity of **SP** derivatives for the detection of Aβ plaques and NFTs in the brain, *in vitro* staining of hippocampal sections from human postmortem AD was carried out. Initially, probes **120a-g** with different acceptor or donor substituents (R^3-R^5) on the aryl ring have been studied. The results indicate that compounds **120a** and **120d** selectively stained NFTs in human brain sections (**Figure 3.20**, **B** and **C**). In addition, probe **120a** provided a good contrast versus Aβ plaques and background (**Figure 3.20**, **A** and **B**).

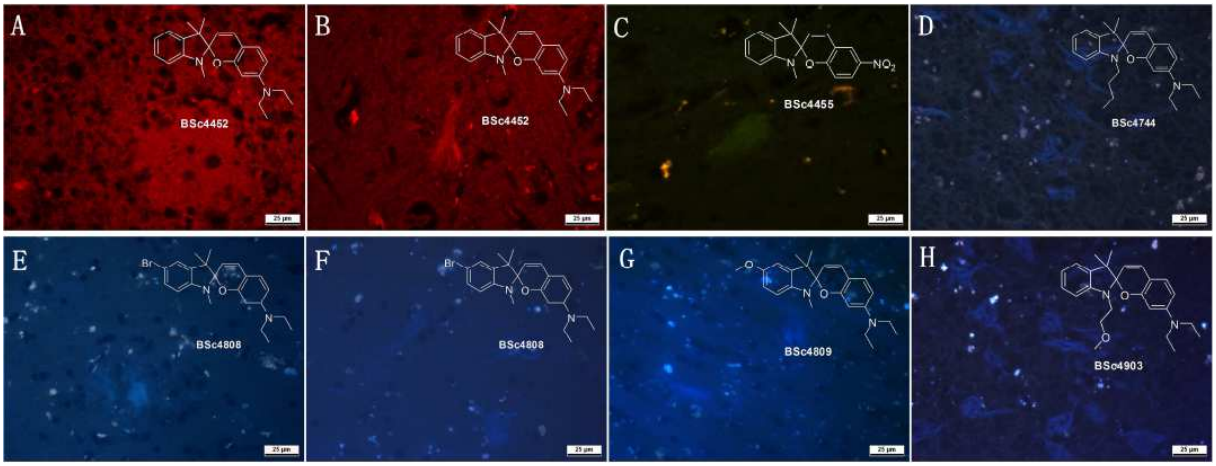

Figure 3.20 *In vitro* histochemical staining of postmortem AD brain tissues with spiropyrans (Tissues: hippocampus; Patient: male, 71 years old; CERAD Score: 3; NFTs-level: V).

Considering these results, we explored the strategy to construct fluorescent derivatives based on these scaffold. The probe **120a** was selected as a standard compound by changing the substituents on the 1'-position of the indole ring. Probes **120h** and **120l** were synthesized according to our previously synthetic procedure. Obviously, numerous NFTs

were detected by fluorescence microscopy. The SAR analysis revealed that probes with a diethylamine group in the 7-position may play a critical role in visualization of NFTs in AD brain sections. Furthermore, compounds **120i-k** were synthesized to investigate the effect of the different functional groups on the 5'-position of indole ring. However, these probes faintly stained tau aggregates, while probe **120j** also weakly stained Aβ plaques in postmortem tissue (**Figure 3.20**). The absorption spectrum showed that efficacious probes **120a**, **120h**, **120j** and **120l** adopt **ME** conformations (λ_{max} ≈ 550 nm) in EtOH, while inactive derivatives may correspond to **SP** conformations (λ_{max} ≈ 300 nm). It was assumed that the **ME** conformation rather than the **SP** conformation may be responsible for the binding of Aβ and tau aggregates. These data suggested that probes with diethylamine group on the 7-position but without substitution on the 5'-position of indole ring may be an ideal scaffold for selective binding to NFTs. Further modifications on the 1'-position of indole ring may improve the solubility of these compounds.

In order to quantify the cytotoxicity of compounds **120a** and **120h**, we performed a zebrafish embryo development assay (**Figure 3.21**). The embryos were treated with solutions containing compounds at 6-8 hpf, and the phenotypes were compared at 24 hpf. The embryos developed well and no lesions were found at different concentrations up to 5 μM at 24 hpf and 72 hpf. In addition, we profiled the probe **120a** in a liver hepatocellular carcinoma cell assay (HepG2) *in vitro* to evaluate the cytotoxicity in human cells. The EC_{50} was calculated via the best-fitted trendline of cell vitality as a function of dye concentration. It showed an EC_{50} > 20 μM after 24 h of incubation. These results suggested that **SP** derivatives display negligible cytotoxicity against zebrafish embryos and HepG2 at the concentration employed for the histology experiments on human AD brain tissue (1 μM). These probes may be suitable for further *in vivo* applications.

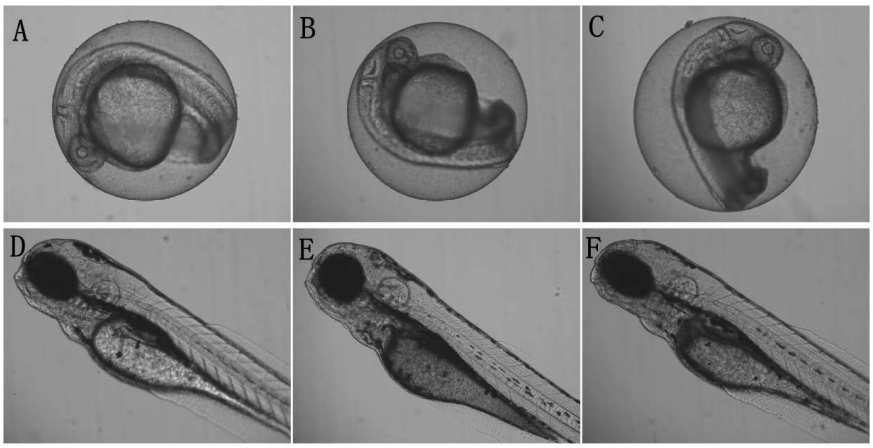

Figure 3.21 *In vivo* cytotoxicity studies of embryos of wild-type zebrafish with **120a** and **120h** at 24 hpf and 72 hpf. Controlled (A and D), probe **120a** (B and E) and probe **120h** (C and F).

3.6. Design, synthesis and evaluation of merocyanine derivatives for Aβ and tau imaging

3.6.1. Design, synthesis and properties of merocyanine derivatives

The lead structure for AD imaging was selected from a set of established high fluorescent dyes and evaluated for the silk dying properties versus wool reserve, which indicated β-sheet binding of dye. The cyanines were advanced due to their structural analogies to known tau ligands and evaluated against other lead structures, such as bisstilbenes and squaric acid derivatives.[49,213] However, the bisstilbenes displayed limited solubility and the squaric acid derivatives did not display sufficient binding.[204,214] The ring-opening **ME** formed a extended planar π-system, which may lead to improved photostability and fluorescence intensity (**Chapter 3.5.2**). In order to achieve this purpose, we designed and synthesized a series of low cytotoxic, water-soluble **ME** derivatives as potential diagnostic tools for the detection of NFTs in AD.

The synthesis of 3,3-dimethyl-2-styrylindolium derivatives employed known methods or slight modifications thereof,[215] which is depicted in **Scheme 3.24**. The key transformation to the target 3,3-dimethyl-2-styrylindolium derivatives **121a-k** (**Table 3.8**) was achieved by the Knoevenagel condensation of the *N*-alkylated indolium backbone **119a-e** and corresponding aldehydes in ethanol under reflux. Furthermore, compounds **121i-k** introduced an additional acceptor or donor group on the 5-positon of the cationic indolium moiety. All of these compounds were isolated in good yields by standard chromatographic purification on silica gel.

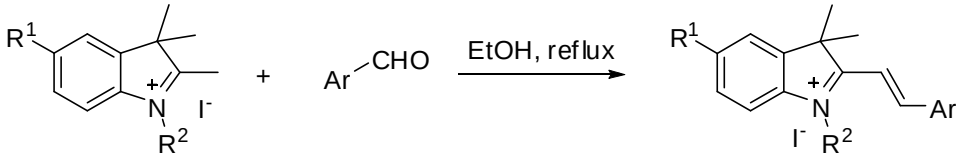

119a-e **121a-k**

Scheme 3.24 Synthesis of 3,3-dimethyl-2-styrylindolium derivatives.

The ^{1}H-NMR spectrum revealed that the two doublets at 8.56-8.20 ppm and 7.59-7.17 ppm correspond to the *trans* configured olefinic protons with a large coupling constant (*J* = 15.5-16.5 Hz). According to the ^{1}H-NMR spectra, the 3,3'-geminal methyl protons are placed in the same chemical environment because they appeared as a singlet at 1.78-1.73 ppm for the six equivalent methyl protons. This observation was confirmed by the ^{13}C-NMR spectra.

Table 3.8 Structures and affinity data of indolium derivatives

Entry	BSc No.	R^1	R^2	Ar	*c*Log*P*[a]	MW[b]	Staining effect[c]
121a	**BSc4743**	H	*n*-Bu	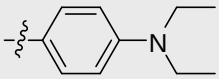	3.58	502.5	Aβ: **+** NFT: **+++**
121b	**BSc4745**	H	Me	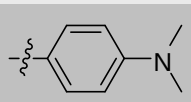	1.39	432.3	Aβ: **+** NFT: **++**
121c	**BSc4746**	H	Me	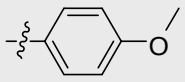	1.34	419.3	Aβ: **-** NFT: **+++**
121d	**BSc4747**	H	Me	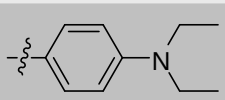	2.14	460.4	Aβ: **-** NFT: **+++**
121e	**BSc4748**	H	Me	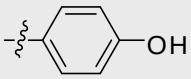	0.81	405.3	Aβ: **+** NFT: **+++**
121f	**BSc4749**	H	Me	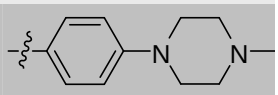	1.28	487.4	Aβ: **+** NFT: **+++**
121g	**BSc4750**	H	Me	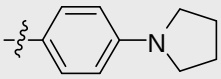	1.79	458.4	Aβ: **+** NFT: **+++**
121h	**BSc4751**	H	Me	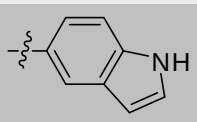	1.52	428.3	Aβ: **+** NFT: **+++**
121i	**BSc4815**	F	Me	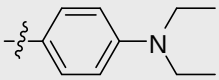	2.28	478.4	Aβ: **+** NFT: **-**
121j	**BSc4816**	OMe	Me	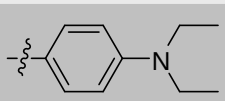	2.17	490.4	Aβ: **+** NFT: **-**
121k	**BSc4817**	Br	Me	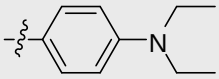	2.92	539.3	Aβ: **++** NFT: **-**

[a] Log*P* values were calculated using the Molinspiration Cheminformatics software (V2011. 04); [b] Determined by CS ChemOffice 10.0; [c] **+++** stands for efficient staining, **++** stands for normal staining, **+** stands for weak staining, **-** stands for no staining.

In order to investigate the effect of the geminal methyl groups on visualization of Aβ and tau aggregates, we replaced one of the geminal methyls with an ethyl moiety to twist the alkyl plane. 3-methyl-3'-ethyl-2-styrylindolium derivatives were prepared by a route similar to the

previous experiment (**Scheme 3.24**). The phenylhydrazine hydrochloride **116a** has been condensed with 3-methylpentan-2-one **122** to yield the corresponding hydrazones and further converted by Fischer indole synthesis to obtain cyclized compound **123**. Methylation of the indolenine in acetonitrile under reflux formed the indolium **124** in quantitative yield, which was used without further purification in the next step. Finally, compounds **125a-d** were obtained in good yields by the Knoevenagel condensation between indolium **124** and corresponding aldehydes in refluxing ethanol. The products were purified by column chromatography and characterized by NMR spectroscopy. The compounds adopt *trans* configuration as assigned by the coupling constants for the olefinic protons ^{1}H-NMR spectra (J = 15.0-16.0 Hz).

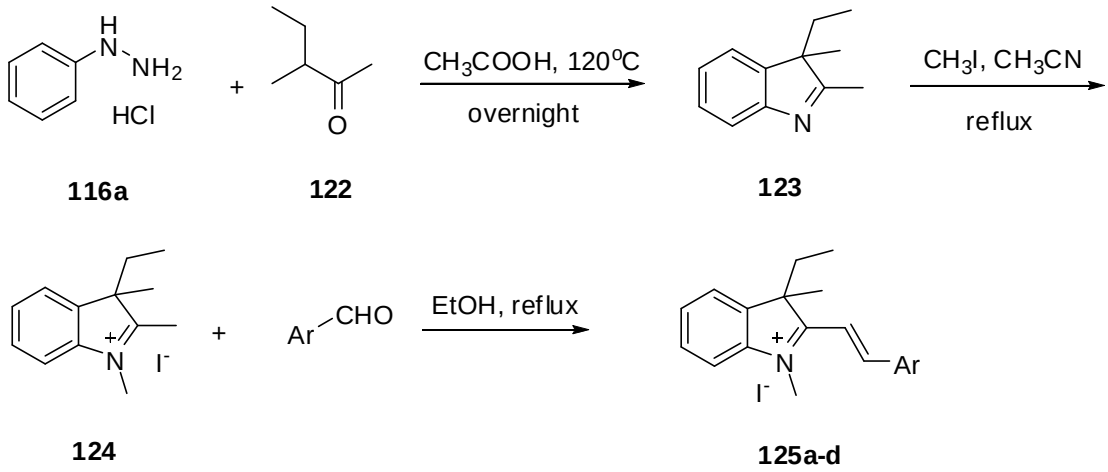

Scheme 3.25 Synthesis of 3-methyl-3'-ethyl-2-styrylindolium derivatives.

Table 3.9 Structures and affinity data of indolium derivatives.

Entry	BSc No.	Ar	*c*Log*P*[a]	MW[b]	Staining effect[c]
123a	**BSc4813**	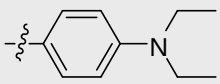	2.46	474.4	Aβ: **++** NFT: **+**
123b	**BSc4814**	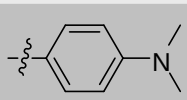	1.71	446.4	Aβ: **++** NFT: **-**
123c	**BSc4865**	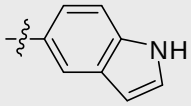	1.81	442.3	Aβ: **-** NFT: **-**
123d	**BSc4866**	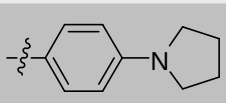	2.11	472.4	Aβ: **++** NFT: **-**

[a] Log*P* values were calculated using the Molinspiration Cheminformatics software (V2011. 04); [b] Determined by CS ChemOffice 10.0; [c] **++** stands for normal staining, **+** stands for weak staining, **-** stands for no staining.

Moreover, in order to obtain a better understanding of the influence of 3,3'-geminal methyl moiety, we synthesized two compounds comprising a cationic benzoxazolium acceptor. The pyrrolidin electron-donating functionality was introduced to bias affinity to tau aggregates. The synthetic routes to compounds **129** (**BSc4905**) and **131** (**BSc4906**) are depicted in **Scheme 3.26**.

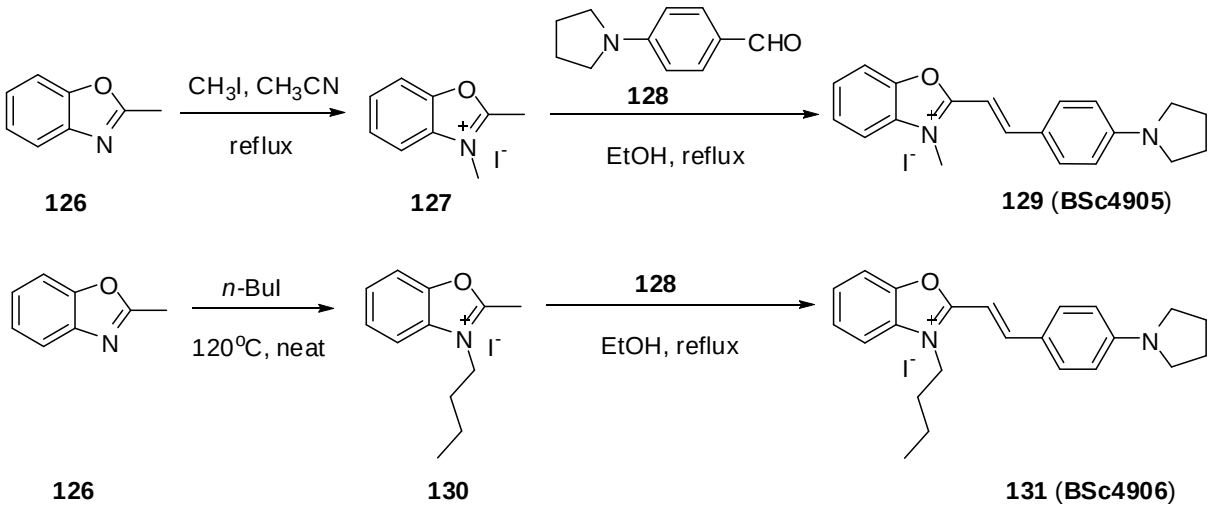

Scheme 3.26 Synthesis of 3-methyl-3'-ethyl-2-styrylindolium derivatives.

The mixture of commercially available 2-methylbenzo[*d*]oxazole **126** and iodomethane was stirred in refluxing acetonitrile to afford the 2,3-dimethylbenzo[*d*]oxazol-3-ium iodide **127**. Alternatively, compound **126** and 1-iodobutane were heated at 120 °C without any solvent to form 3-butyl-2-methylbenzo[*d*]oxazol-3-ium iodide **130**. Followed by Knoevenagel condensation with 4-(pyrrolidin-1-yl)benzaldehyde **128**, compounds **129** and **131** were obtained in good yields.

Probes with appropriate lipophilicity and low molecular weights may display sufficient permeability to cross the BBB and rapid clearance from the body, when they were used as an *in vivo* probe.[216] The calculated Log*P* values of these compounds in **Table 3.8** and **Table 3.9** were found to be in the range of 0.81 and 3.58. In addition, the calculated Log*P* values of compounds **128** and **129** are 1.18 and 2.62, respectively. All of Log*P* values have been calculated using the Molinspiration Cheminformatics software (V2011. 04). In addition, the molecular weights of 3,3-dialkyl-2-styrylindolium iodide derivatives are below 540 Daltons (**Table 3.8** and **Table 3.9**). Simultaneously, the molecular weights of probes **129** and **131** determined by CS ChemOffice 10.0 gave 432.3 and 474.4 Daltons, respectively. Taken together, these properties are in the range of accepted lipophilicity criteria for the BBB permeation after intravenous injection. These observations suggested merocyanine probes as potential *in vivo* imaging agents for neurodegeneration diseases.

3.6.2. Evaluation of merocyanine derivatives as imaging probes for Aβ and tau imaging

The qualitative selective binding of fluorescent probes to Aβ plaques and NFTs was evaluated in the primary screen on hippocampal sections of human AD brain tissue and analyzed by fluorescence microscopy. This low throughput screen secured binding of these probes to tau aggregates in human AD pathology, as different tau isoforms may result in different binding sites on *in vitro* aggregates or tau transgenic mouse models.[217] The 2-styryl-indolium probes **121a-h** stain NFTs in human tissue (**Figure 3.22**) and provide a good contrast versus Aβ plaques and background, especially probes **121a**, **121d** and **121g**. These probes displayed an excellent staining of NFTs (**Figure 3.22**, **B**, **F** and **J**) in comparison to Aβ plaques (**Figure 3.22**, **A**, **E** and **I**). The results suggested a good affinity to the NFTs, which required quantification in a ligand binding assay to both Aβ and tau aggregates. Remarkably, the probes **121a-h** stained NFTs strongly in human tissue as observed by fluorescence microscopy, whereas plaques in the same brain preparations were stained just weakly. This observation stands in contrast to the activity in the *Thiazine Red R* displacement assay, where compound **121a** displayed almost equipotent affinity to $A\beta_{40}$-aggregates and tau aggregates (**Table 3.10**). The lack of potent plaque staining in the human tissue preparations may be due to interference with the fluorescence properties upon plaque binding, e.g. a fluorescence reduction or effect on the Stokes shift, which limit the detection by the DAPI- or FITC-filters employed in fluorescence microscopy. Besides, the *Thiazine Red R* assay may not reflect the binding sites in human tissues. However, these results indicate that 3,3-dimethyl-2-styrylindolium probes **121a-h** may be useful for the post mortem detection of NFTs in the brain of AD patients.[214]

The probes with different substitutents in the 5-position of cationic indolium core (**121i-k**) were evaluated by neuropathological staining of AD brain sections. However, only Aβ plaques were observed by fluorescence microscopy (**Figure 3.22**, **L**, **M** and **N**). On the basis of histological staining, probe **123a** depicted an excellent Aβ plaques staining while only faintly staining NFTs. Additionally, 3-methyl-3'-ethyl-2-styrylindolium derivatives **123b** and **123d** intensely and specificilly stained Aβ plaques on postmortem AD brain sections. In conclusion, the red emission dyes **121i-k**, **123a-b** and **123d** may prevent interference with autofluorescence from tissue and other small molecule components in the assay system. Further radiolabeling of these probes may result in specific PET radioligands for Aβ plaques imaging *in vivo*.

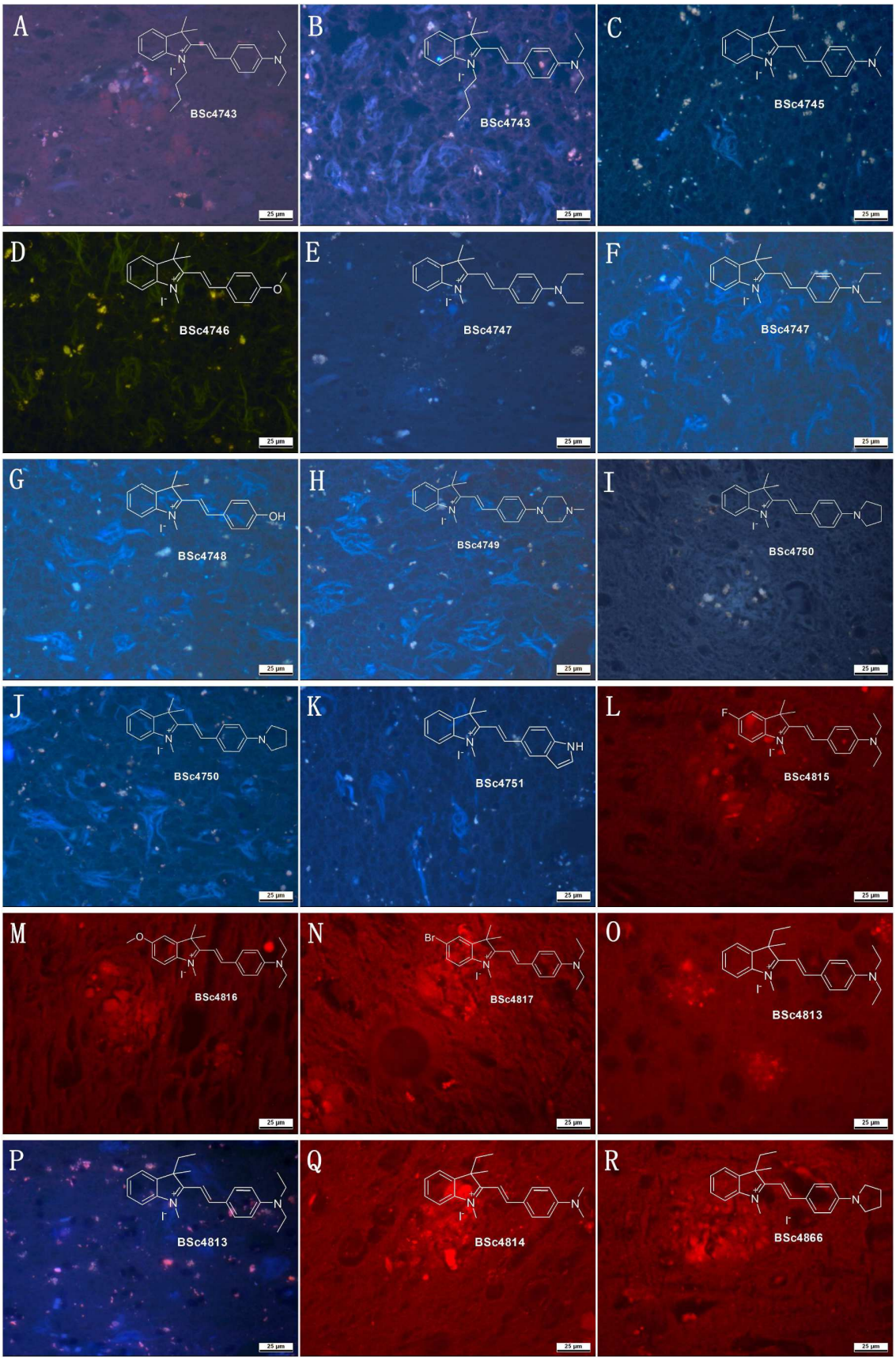

Figure 3.22 *In vitro* histochemical staining of postmortem AD brain tissues with **ME** derivatives (Tissues: hippocampus; Patient: male, 71 years old; CERAD Score: 3; NFTs-level: V).

However, benzoxazolium derivatives **129** and **131** failed to detect Aβ plaques and NFTs by fluorescence microscopy. Only astrocytes have been stained and observed by fluorescence microscopy. Therefore, it is hypothesized that the indolium core may play an important role in the recognition of Aβ and tau aggregates in the hippocampal sections of AD brain. Furthermore, the probes with 3,3'-geminal methyl moiety but without electron-donating or electron-withdrawing group in the 5-position of the indolium core may exhibit remarkable selectivity for tau aggregates. In contrast, probes with a 3,3'-geminal methyl moiety and electron-donating or electron-withdrawing group in the 5-positions of the indolium core may allow to detect Aβ plaques in postmortem brain tissue.

At the same time, we further evaluated the solubility of these tau specific probes. The solubility of the *N*-methylated probes **121a-g** is higher than 0.5 g/L while the value of probe **121h** is greater than 0.25 g/L at 25 °C in distilled water. According to the calculated Log*P* values in **Table 3.8**, the lipophilicity increased which is due to the introduction of a bulky structure on the 1-position of the indole ring (**121a**). Thus, the *N*-butylated probe **121a** only displayed a solubility of > 0.1 g/L at 25 °C in distilled water. It is consistent with the underlying assumption that, in some respects, the Log*P* value may relate to solubility in water. Particularly, probe **121f** with the 1-methyl-4-phenylpiperazine moiety significantly increases the solubility in aqueous media (> 1.0 g/L) in comparison to the rest of the compounds. The solubility of established imaging agents: FDDNP, Methoxy-X04 and BF-158, are in the same range or inferior to the solubility of these 3,3-dimethyl-2-styrylindolium derivatives.[214]

Table 3.10 Competitive *Thiazine Red R* displacement from Tau aggregates for probes **121a**, **121g**, Methoxy-X04, FDDNP, PIB and BF158.[214]

Compound	Aggr.Tau-IC_{50}/nM	Aggr. $A\beta_{40}$-IC_{50}/nM
121a	1.41	1.37
121g	5.10	ND
Methoxy-X04	246	140
FDDNP	1635	1467
PIB	3255	5190
BF-158	>10000	>10000

ND, not determined due to spectral overlap with the reference compound in the displacement assay.

Unfortunately, the affinity of most probes to tau aggregates could not be quantified in the competition binding assays *in vitro*. This was due to spectral overlap with the reference ligand *Thiazine Red R*. *Thiazine Red R* was selected as reference ligand for the displacement assay, because it was shown to be superior to ThS or immune histochemical detection of aggregated Tau and $A\beta_{40}$.[48] The affinity of the probes **121a** and **121g** to Tau aggregates was determined indirectly (IC_{50} values of 5.1 nM and 1.4 nM, respectively) in the displacement assay for Tau affinity versus the reference ligand *Thiazine Red R*. Remarkably, the pyrrolidyl substituent results in higher affinity than *N*,*N*-diethyl derivative. This may be due to the locked conformation of the *N*-alkyl chain. In addition, the displacement ability of these 2- styrylindolium derivatives was compared against the standard probes, such as Methoxy-X04, FDDNP, PIB and BF-158, under the same assay conditions. Significantly, 3,3-dimethyl-2-styrylindolium derivatives **121a** and **121g** displayed ~50-7000 fold higher affinity to tau aggregates (**Table 3.10**). This indicates sufficient affinity of these probes for imaging of tau aggregates *in vivo*. Furthermore, the series may be radiolabeled with $^{11}CH_3$, ^{18}F and ^{123}I at either O or N position and evaluated as PET and SPECT radioligands for NFT-imaging *in vivo*.[214]

Four of the 3,3-dimethyl-2-styrylindolium compounds (**121a, 121c-d** and **121g**) have been further evaluated at different concentrations in the wild-type zebrafish embryo development assay.[214] The embryos developed well and no lesions were found at different concentrations up to 10 µM at 24 hpf. After 72 hpf, only the juvenile fish incubated with compound **121a** have shown small lesions in the yolk sac (**Figure 3.23**, **G**). The HepG2 cell proliferation assay of these four compounds was used to evaluate the cytotoxicity in human cells. The EC_{50} were calculated via the best-fitted trendline of cell vitality as a function of dye concentration. Compounds **121a, 121c-d** and **121g** showed EC_{50} values of 0.93, 10.93, 8.57 and 8.31 µM, respectively, after 24 h incubation. Compound **121a** displayed higher cytotoxicity in both assays than other compounds in this series. Both cytotoxicity studies suggested that 3,3-dimethyl-2-styrylindolium probes have negligible cytotoxicity against zebrafish embryos and HepG2 at the concentration employed for the histology experiments on human AD brain tissue (1 µM).

Taken together these results suggest that 3,3-dimethyl-2-styrylindolium compounds should be advanced to *in vivo* mice experiments in transgenic mice. However, the 4R tau transgenic mice available to the project are all based on the 4R tau repeat and deposit very little amounts of Tau. Moreover, these 4R Tau mouse models seem to be void of the tau aggregate binding site present in humans.[39,181] The presence of at least two different binding sites on tau aggregates was demonstrated for the tau probe THK523 recently.[113]

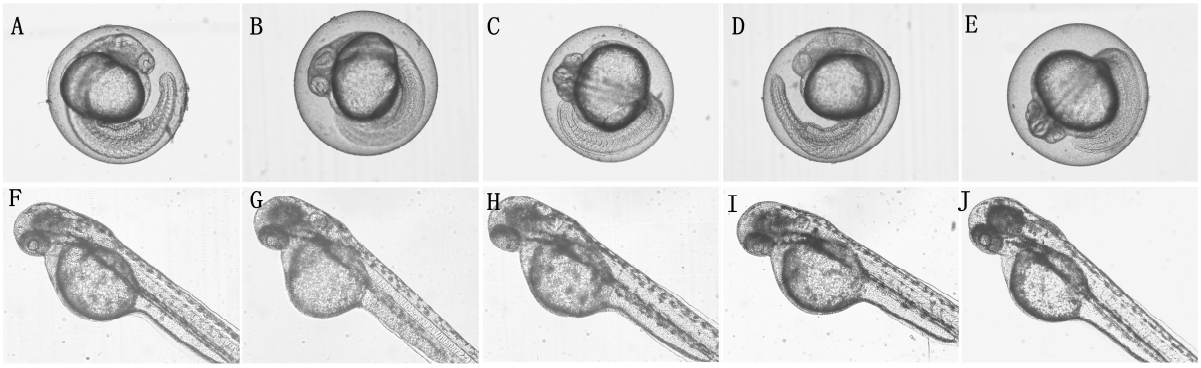

Figure 3.23 *In vivo* cytotoxicity studies of embryos of wild-type zebrafish with 3,3-dimethyl-2-styrylindolium compounds after 24 (A-E) and 72 (F-G) hpf. Controlled (A and F), **121a** (B and G), **121c** (C and H), **121d** (D and I) and **121g** (E and J).

In conclusion, we have developed a series of water soluble 3,3-dimethyl-2-styrylindolium probes for fluorescence imaging of NFTs in human AD brain. The results of the *in vitro* fluorescent staining protocol used brain sections of AD patient. They suggest potent NFT imaging and low nonspecific binding. The cytotoxicity experiments with wild-type zebrafish embryos and HepG2 cells suggest that these probes may be suitable for further *in vivo* applications. This indicates sufficient safety for *in vivo* evaluation in mouse models.[214]

3.7. Design, synthesis and evaluation of trimethine cyanine derivatives for Aβ and tau imaging

3.7.1. Design, synthesis of trimethine cyanine derivatives

In the past decade the histological staining of Aβ aggregates by fluorescent dyes is crucial for the diagnosis of AD. The fluorescent compounds ThT (**26**), ThS (**27**) and CR (**24**) are the most used dyes for the detection of amyloid aggregates *in vitro*. However, CR is not a fluorescent dye, while ThT and ThS are blue-emission dyes that may interfere with autofluorescence from tissue or some small molecule components in the assay system.[218,213] Thus, the design of new selective dyes capable to detecte hallmark proteins is important for the basic pathology research in AD. In order to achieve this purpose, we evaluated cyanine dyes as more sensitive and benign probes to stain biological tissue. Especially, cyanine dyes have high affinity for Aβ or tau aggregates, which implied that these compounds may be suitable as fluorescent probes for the *in vivo* diagnosis of AD.[213,219]

As shown in **Scheme 3.27**, 4-nitrophenyl hydrazine **132** and 3-methylbutan-2-one **117** were condensed and followed by Fischer indole synthesis to obtain the indole **133**.

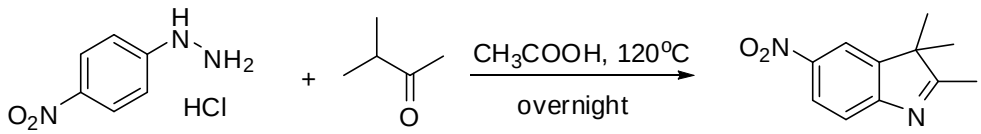

132 **117** **133**

Scheme 3.27 Synthesis of 2,3,3-trimethyl-5-nitro-3*H*-indole.

Several indolium salts have been synthesized as shown in **Chapter 3.5.1**. In addition, methylation of the compound **133** with iodomethane in acetonitrile formed the indolium **134a** in good yield (**Scheme 3.28**). Indolenine **118a** and 1-bromodecane were refluxed in acetonitrile for 4 days to prepare the indolium salts **134b** as waxy solid. Furthermore, 2-(2-(2-methoxyethoxy)ethoxy)ethanol, 2-(2-methoxyethoxy)ethanol and 3-methoxypropan-1-ol were reacted with 4-toluene sulfonyl chloride to form the corresponding 4-methylbenzenesulfonates. After PEGylation on the *N* position of indolenine **118a**, the products **134c-e** were purified by column chromatography and characterized by NMR spectroscopy.

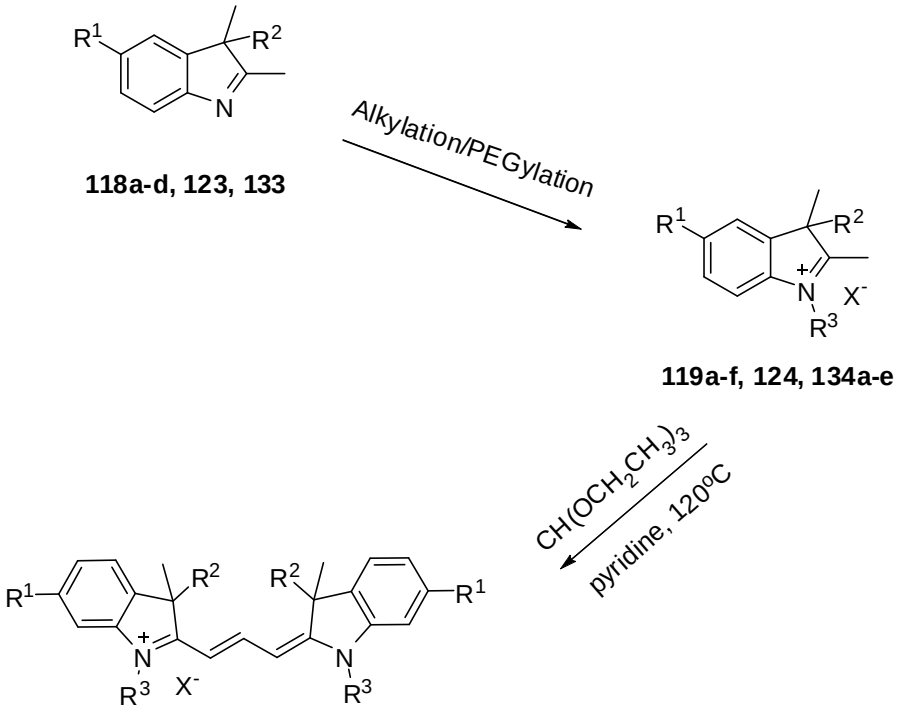

118a-d, 123, 133

119a-f, 124, 134a-e

135a-l

R^1 = H, F, Br, OCH_3, NO_2
R^2 = CH_3, CH_2CH_3
R^3 = CH_3, *n*-Bu, *n*-decyl, $CH_2CH_2OCH_3$, $(CH_2CH_2O)_2CH_3$, $(CH_2CH_2O)_3CH_3$, $CH_2CH_2CH_2OCH_3$
X = Cl, Br, I, TsO

Scheme 3.28 Synthesis of trimethine cyanines **135a-l**.

Table 3.11 Structures, calculated Log*P* and staining effect of trimethine cyanines

Entry	BSc No.	R^1	R^2	R^3	X	*c*Log*P*[a]	Staining effect[b]
135a	**BSc4704**	H	CH_3	CH_3	I	2.77	Aβ: **-** NFT: **+++**
135b	**BSc4705**	NO_2	CH_3	CH_3	I	2.64	Aβ: **+** NFT: **++**
135c	**BSc4737**	H	CH_3	*n*-decyl	Br	9.55	Aβ: **+** NFT: **+++**
135d	**BSc4738**	H	CH_3	$(CH_2CH_2O)_3CH_3$	Cl	1.93	Aβ: **+** NFT: **+**
135e	**BSc4739**	H	CH_3	*n*-Bu	I	5.64	Aβ: **+** NFT: **++**
135f	**BSc4741**	H	CH_3	$CH_2CH_2OCH_3$	Cl	2.74	Aβ: **+** NFT: **+++**
135g	**BSc4742**	Br	CH_3	CH_3	I	4.34	Aβ: **-** NFT: **+++**
135h	**BSc4806**	F	CH_3	CH_3	I	3.05	Aβ: **-** NFT: **+**
135i	**BSc4810**	OCH_3	CH_3	CH_3	I	2.84	Aβ: **+++** NFT: **-**
135j	**BSc4811**	H	Et	CH_3	I	3.42	Aβ: **-** NFT: **+**
135k	**BSc4818**	H	CH_3	$(CH_2CH_2O)_2CH_3$	TsO	2.33	Aβ: **-** NFT: **-**
135l	**BSc4920**	H	CH_3	$CH_2CH_2CH_2OCH_3$	Cl	3.28	Aβ: **-** NFT: **++**

[a] Log*P* values were calculated using the Molinspiration Cheminformatics software (V2011. 04); [b] **+++** stands for efficient staining, **++** stands for normal staining, **+** stands for weak staining and **-** stands for no staining.

In the presence of pyridine as a base and solvent, the trimethine cyanines were formed by a condensation reaction between triethyl orthoformate and the corresponding indolium salts (**Scheme 3.28**). A series of cyanine dyes has been synthesized as summarized in **Table 3.11**. According to the coupling constants of the olefinic protons (*J* = 13.0-13.5 Hz), symmetric trimethine cyanines adopt the thermodynamically favorable *trans* conformer. During chromatography, the tosylate counterion of **135d**, **135f** and **135l** were exchanged for chloride ions once the mobile phase involved 2% triethylamine. The process has been judged by absence of tosylate protons in the ^{1}H-NMR spectra.[220]

Table 3.12 Structures, properties and staining effect of trimethine cyanine based on benzothiazolium and benzoxazolium.

Entry	BSc No.	R^1	X	Y	*c*Log*P*[a]	MW[b]	Staining effect[b]
138a	**BSc4706**	CH_3	I	S	1.77	464.4	Aβ: **+++** NFT: **+**
138b	**BSc4867**	$CH_2CH_2O_3CH_3$	TsO	S	1.74	596.8	Aβ: **-** NFT: **-**
138c	**BSc4868**	$(CH_2CH_2O)_3CH_3$	TsO	S	0.92	773.0	Aβ: **+** NFT: **-**
138d	**BSc4904**	CH_3	I	O	0.48	432.3	Aβ: **-** NFT: **-**
138e	**BSc4907**	*n*-Bu	I	O	3.36	516.4	Aβ: **-** NFT: **-**

[a] Log*P* values were calculated using the Molinspiration Cheminformatics software (V2011. 04); [b] Determined by CS ChemOffice 10.0. [c] **+++** stands for efficient staining, **++** stands for normal staining, **+** stands for weak staining, **-** stands for no staining.

By further replacement of the indolium cores with benzothiazolium or benzoxazolium, we synthesized five trimethines as shown in **Scheme 3.29** and **Table 3.12**. The commercially available 2-methylbenzo[*d*]thiazole **136** and iodomethane were refluxed in acetonitrile to afford the 2,3-dimethylbenzo[*d*]thiazol-3-ium iodide **137a**, which can be used in the next step without further purification. Additionally, PEGylation of 2-methylbenzo[*d*]thiazole **136** with 2-methoxyethyl 4-methylbenzenesulfonate and 2-(2-(2-methoxyethoxy)ethoxy)ethyl 4-methylbenzenesulfonate was carried out to synthesize the benzothiazolium salts **137b-c**, respectively. Similarly, cyanine dyes **138a-e** were readily prepared via the classical route

involving the condensation of the heterocyclic quaternary salts (**127**, **130** and **137a-c**) with triethyl orthoformate in dry pyridine. Consistently, the structures adopt the *trans* configuration, which is indicated by the coupling constant of the olefinic protons around 12.5-13.5 Hz. However, in the case of absence of triethylamine in the mobile phase for column chromatography, the tosylate moiety was retained (**138b-c**). The results were confirmed by tosylate protons in the ^{1}H-NMR spectra.

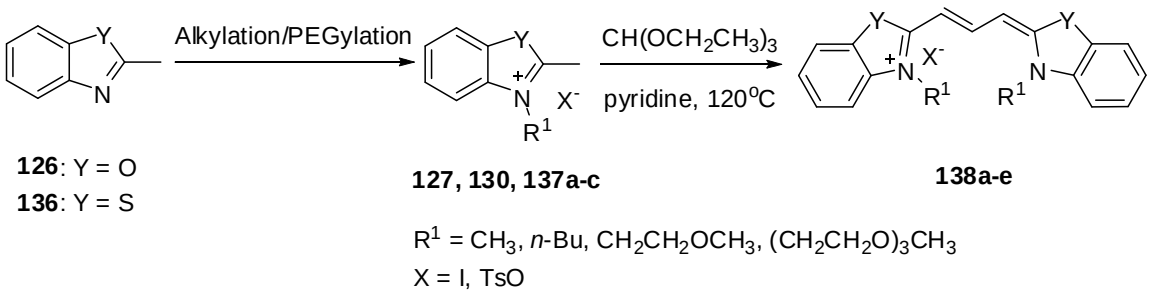

Scheme 3.29 Synthesis of trimethine cyanines based on benzothiazolium and benzoxazolium cores.

3.7.2. Evaluation of trimethine cyanine derivatives as specific Aβ or tau imaging probes

In order to evaluate the ability to visualize Aβ plaques and NFTs, hippocampus sections from confirmed AD cases were stained with the trimethine cyanines and evaluated by fluorescence microscopy (**Figure 3.24**). It is noteworthy that the trimethine cyanine derivative **135a** displayed a remarkably higher selectivity for aggregated tau. With the replacement of the methyl group on the nitrogen of indolenine with different length alkyl chains, probes **135c** and **135e** stained NFTs in human tissue strongly as observed by fluorescence microscopy, whereas plaques in the same brain preparations were stained just weakly. However, the long alkyl chains increase the Log*P* values, which may lead to reduce the solubility in some respects. To overcome this limitation, we introduced the poly(ethylene glycol) moieties on the nitrogen position of indolenine (**135d**, **135f** and **135k-l**). By increasing the length of poly(ethylene glycol) moieties, compound **135d** (> 1.0 g/L) is more soluble in distilled water than compound **135f** (> 0.5 g/L). Oppositely, probe **135f** exhibited a better staining to tau aggregates in comparison to probe **135d**. These results indicate that the binding effect may not be associated with the lipophilicity of our probes. On the other hand, the probe **135k** with tosylate moiety failed to detect Aβ and tau aggregates by fluorescence microscopy. It was hypothesized that the size of the tosylate counterion is bigger than the chloride ion, which exceeds the width of 'binding channel' in unsullied staining protocols. Finally, the steric hindrance may prevent the probe to interact with Aβ or tau aggregates. Furthermore, compounds bearing an electron-donating or an electron-withdrawing group at the 5-position of indolium core were investigated. In the presence of an electron-withdrawing group, probes

135b (NO_2) and **135g** (Br) displayed excellent NFTs staining while only faintly staining Aβ plaques. However, probe **135h** with a fluoro-substitutent poorly stained tau aggregates with low contrast to the background. In the presence of the electron-donating group such as OCH_3, probe **135i** displayed a remarkably higher staining of Aβ plaques.

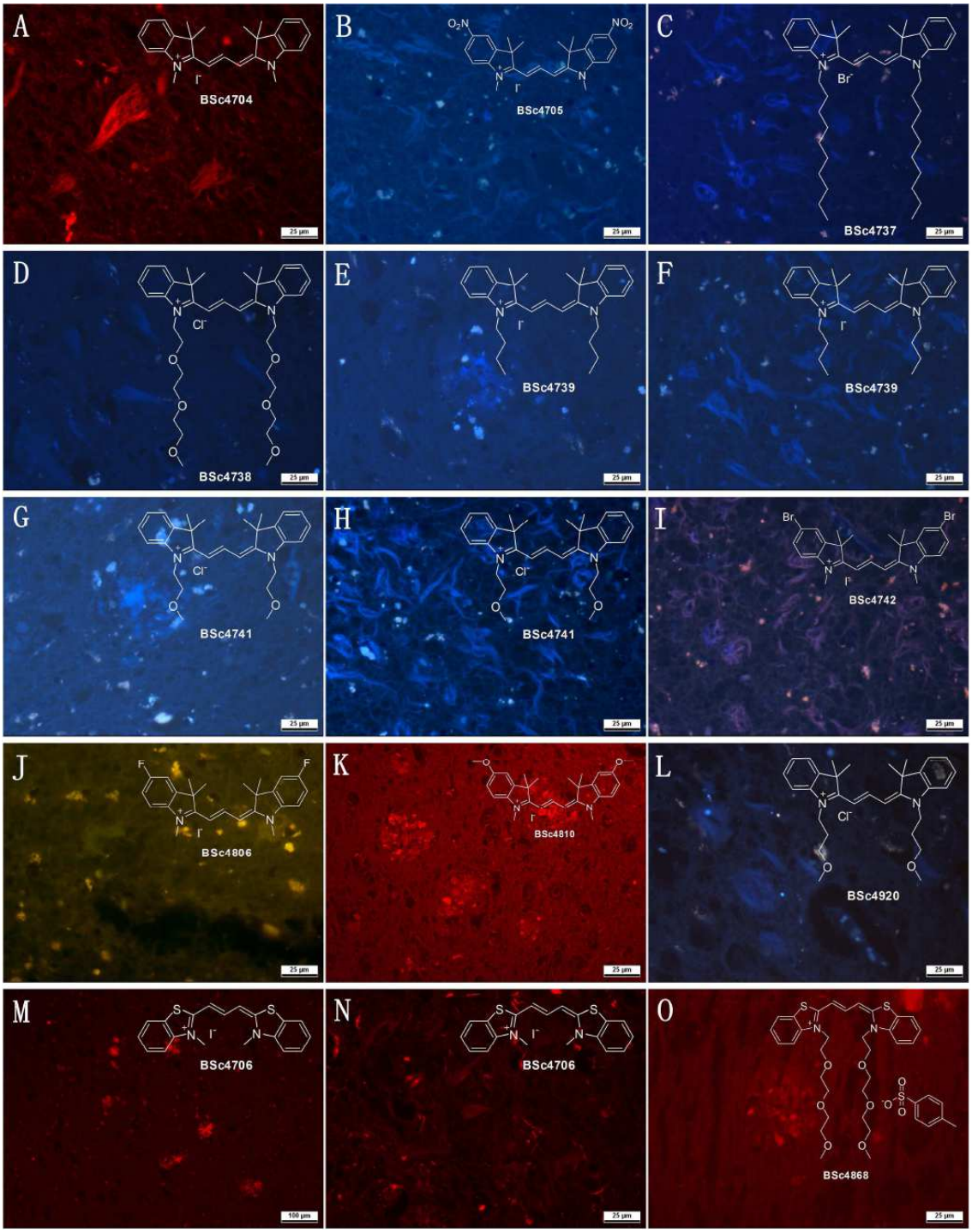

Figure 3.24 *In vitro* histochemical staining of postmortem AD brain tissues with **ME** derivatives (Tissues: hippocampus; Patient: male, 71 years old; CERAD Score: 3; NFTs-level: V).

Moreover, we performed neuropathological fluorescent staining with the benzothiazolium cyanine dye **138a**. Many NFTs were clearly stained with probe **138a** as seen in the *in vitro* assay. However, replacement of the methyl group on the nitrogen of the indolenine benzothiazole with different length of poly(ethylene glycol) moieties gave negative staining results. It was found that only probe **138c** poorly stained Aβ plaques with low contrast to the background. In addition, replacement of the sulfur atom with oxygen at the Y position of benzothiazolium (**Scheme 3.29**), provided the probes **138d-e**, which failed to detect Aβ and tau aggregates in postmortem AD brain tissues. These results suggest that 3,3-geminal methyl of these scaffolds may be important for the selective visualization of NFTs by fluorescence microscopy.

The affinity of most probes to Aβ or tau aggregates could not be quantified due to spectral overlap with the reference ligand *Thiazine Red R*. Fortunately, the affinities of several probes to tau aggregates were determined indirectly in the displacement assay for tau affinity versus the reference ligand *Thiazine Red R* using aggregated recombinant human microtubule associated tau protein purified from *E. coli* and aggregated synthetic $A\beta_{40}$ as reported previously. Probes **135a**, **135e** and **135g** showed ~1480-10000 fold higher affinity to tau aggregates in comparison to the value of PIB under the same assay conditions. It indicates sufficient affinity of probes for further imaging of tau aggregates *in vivo*.

Five trimethine cyanines (**135a, 135c** and **135e-g**) have been further evaluated in the wild-type zebrafish embryo development assay. It was found that the embryos treated with probes **135a, 135c** and **135e-f** developed well at different concentrations up to 10 μM at 24 hpf. However, probe **135g** showed cytotoxicity at 10 μM at 24 hpf, while the embryos developed well at 5 μM concentration. In the same concentration the juvenile fish incubated with compounds **135c** and **135f** developed well until 72 hpf. Unfortunately, in the presence of probes **135a**, **135e** and **135g**, the juveniles stopped growing and died at 2 dpf (**Figure 3.25**).

Seven compounds were evaluated for their cytotoxicity in the HepG2 cell proliferation assay. The EC_{50} values of compounds **135a-g** and **135l** were thus obtained. Both cytotoxicity studies concluded that tau selectivity probes **135a** and **135g** have negligible cytotoxicity against zebrafish embryos and HepG2 at the concentration employed for the histology experiments on human AD brain tissue (1 μM).

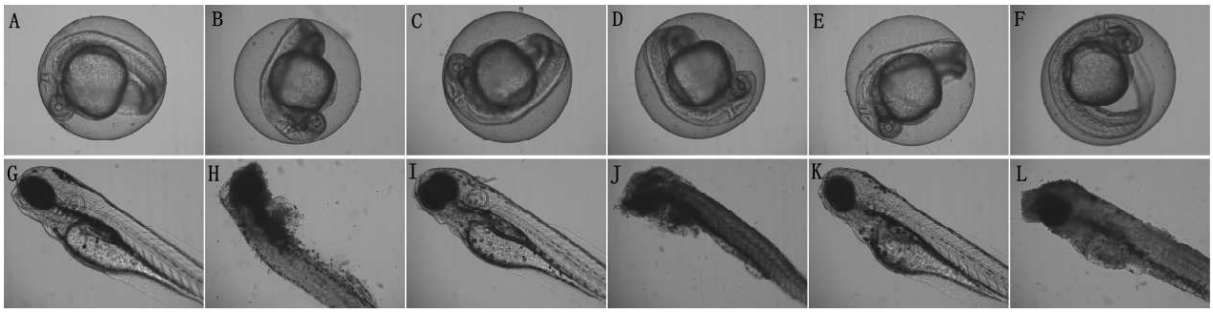

Figure 3.25 *In vivo* cytotoxicity studies of embryos of wild-type zebrafish with 5 µM (F and L) or 10 µM (B-E and H-K) trimethine cyanines after 24 (A-F) and 72 (G-K) hpf. Controlled (A and G), **135a** (B and H), **135c** (C and I), **135e** (D and J), **135f** (E and K) and **135g** (F).

The tau specific imaging probes **135a-g**, **135i** and **135l** were evaluated for solubility in distilled water. The solubilities of **135a**, **135d**, **135f** and **135l** are higher than 0.5 g/L while the rest of probes are lower than 0.1 g/L in distilled water at 25 °C. However, the solubility of established imaging agents: FDDNP, Methoxy-X04 and BF-158, is in the same range or inferior to the solubility of our trimethine cyanines.

On the basis of histological staining of Aβ plaques and NFTs, the trimethine cyanines **135a-g**, **135i** and **135l** stained NFTs in human tissue strongly as detected by fluorescence microscopy, whereas plaques in the same brain preparations were not stained or just stained weakly. These results suggest that cyanine dyes **135a-g**, **135i** and **135l** may be applied as potential fluorescent probes for the detection of tau deposits on the olfactory epithelium of AD patients. Furthermore, these probes may be radiolabeled with $^{11}CH_3$, ^{18}F and ^{123}I at the nitrogen position and evaluated as PET and SPECT radioligands for NFT-imaging *in vivo*.

3.8. Synthesis and evaluation of *N*-2-aryl-1,2,3-triazole derivatives as specific tau imaging probes

As a new class of UV/blue-light-emitting fluorophores, the *N*-2-aryl-1,2,3-triazoles may provide tunable emission and flexible Stokes shift through planar intramolecular charge transfer. In spite of both *N*-1-aryl-1,2,3-triazoles and *N*-2-aryl-1,2,3-triazoles gave a strong absorption, only the *N*-2-analogous showed excellent fluorescence emission in the UV/blue range with high efficiency in different solvents.[221,222] For these reasons, the symmetrical *N*-2-aryl-1,2,3-triazoles are more potent ligands than unsymmetrical *N*-1-analogous in biological imaging (**Figure 3.26**). It was reported that *N*-2-aryl-triazole displayed ~17-fold higher intensity than *N*-1-aryl isomer. [221,222] This observation suggested the possible use of *N*-2-aryl-1,2,3-triazoles as fluorescent probes for the detection of Aβ and tau aggregates in AD.

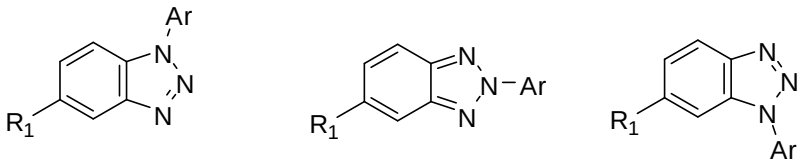

N-1-substituted *N*-2-substituted *N*-3-substituted

Figure 3.26 The isomers of *N*-substituted-1,2,3-triazoles.

Previous research in our group suggested that compounds with a dimethylamino and diethylamino group may display good affinity to tau aggregates. In the present work, we have synthesized several *N*-2-aryl-triazoles containing dimethylamino or diethylamino on the 4-position of the 2-aryl ring. In addition, we investigated the effect of the electron-donating or electron-withdrawing group on the 5-position of benzotriazole ring for staining. The synthetic route used to prepare *N*-2-aryl-triazoles was shown in **Scheme 3.30**.[223]

Obviously, *N*-1-substituted or *N*-3-substituted 1,2,3-triazoles can be efficiently prepared by general reaction conditions. In contrast, regioselective synthesis of *N*-2-substituted-1,2,3-triazoles in good yields is still a challenge for organic chemists. The synthesis of *N*-2-substituted-1,2,3-triazoles is outlined in **Scheme 3.30**. The process involved initial diazotization of 4-substituted-2-nitroanilines **139a-d** with sodium nitrite in hydrochloride solution to form the diazonium salt. Followed by coupling with the molar equivalent of *N*,*N*-dimethylaniline or *N*,*N*-diethylaniline at 0-5 °C, the reactions were carried out immediately with a change in color from pale yellow to deep brown to afford the corresponding azo compounds **141a-g**.

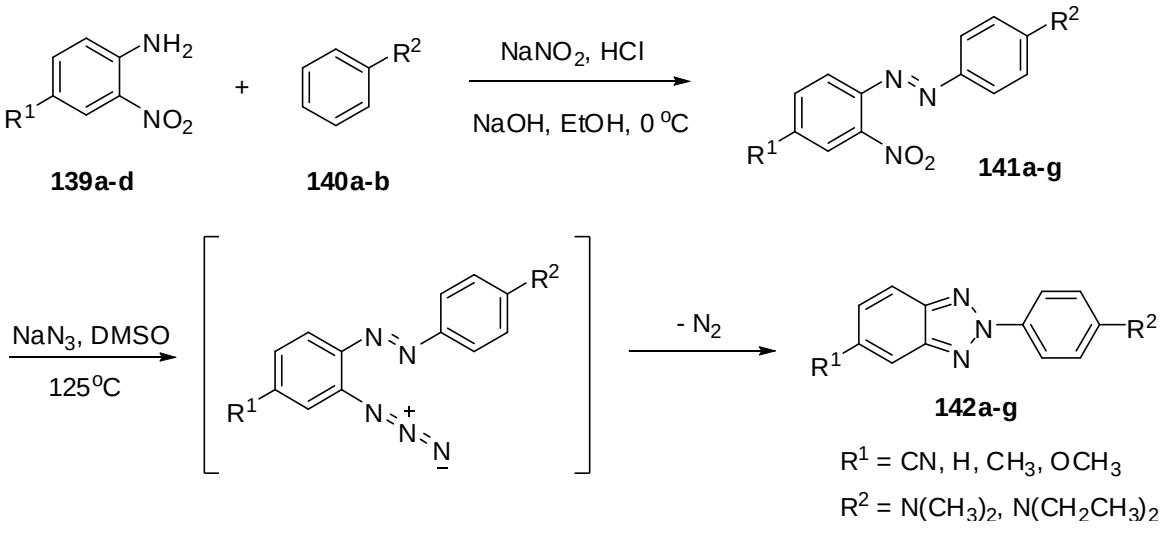

Scheme 3.30 Synthesis of benzo[*d*][1,2,3]triazol derivatives.

Table 3.13 Structures, properties and staining effect of benzo[*d*][1,2,3]triazoles.

Entry	BSc No.	R^1	R^2	*c*Log*P*[a]	MW[a]	Staining effect[b]
142a	**BSc4954**	CN	$N(CH_3)_2$	3.81	263.3	Aβ: **+** NFT: **+++**
142b	**BSc4955**	H	$N(CH_3)_2$	3.78	238.3	Aβ: **+** NFT: **+++**
142c	**BSc4956**	H	$N(CH_2CH_3)_2$	4.45	266.3	Aβ: **++** NFT: **++**
142d	**BSc4957**	CH_3	$N(CH_3)_2$	4.26	252.3	Aβ: **+** NFT: **+++**
142e	**BSc4958**	CH_3	$N(CH_2CH_3)_2$	4.94	280.4	Aβ: **+** NFT: **+**
142f	**BSc5043**	OCH_3	$N(CH_3)_2$	3.65	268.3	Aβ: **-** NFT: **-**
142g	**BSc5044**	OCH_3	$N(CH_2CH_3)_2$	4.33	296.4	Aβ: **-** NFT: **-**

[a] Determined by CS ChemOffice 10.0. [b] **+++** stands for efficient staining, **++** stands for normal staining, **+** stands for weak staining, **-** stands for no staining.

As shown in **Scheme 3.30**, the reaction of 2-nitroazobenzenes with sodium azide obtained the intermediates, which immediately released nitrogen under thermodynamic condition to afford the *N*-2-aryl-1,2,3-triazoles **142a-g** (**Table 3.13**). The *N*-2-aryl-1,2,3-triazoles were purified by column chromatography and characterized by NMR spectroscopy.

To further confirm the binding of -2-aryl-1,2,3-triazoles for NFTs in the AD brain, fluorescent staining was carried out by using of brain tissue sections (**Figure 3.27**). It was found that many NFTs were clearly stained with **142a-e** as seen in the *in vitro* assay, whereas Aβ plaques in the same brain sections were stained just weakly. To our surprise, probes **142f-g** with methoxy in the 5-position of benzotriazole ring failed to detect both Aβ and tau aggregates by fluorescence microscopy.

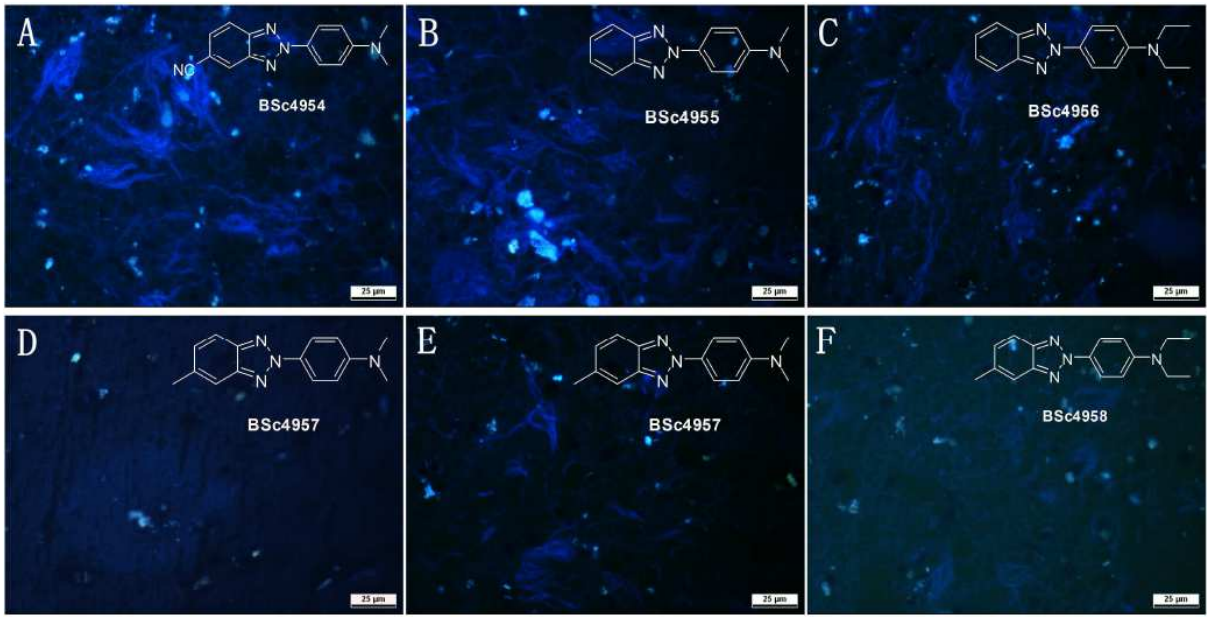

Figure 3.27 *In vitro* histochemical staining of postmortem AD brain tissues with *N*-2-aryl-1,2,3-triazoles (Tissues: hippocampus; Patient: male, 72 years old; CERAD Score: 3; NFTs-level: V).

The affinities of these probes **142b-e** to Aβ and tau aggregates were determined in the displacement assay for Aβ and tau affinity versus the reference ligand *Thiazine Red R*. Unfortunately, the affinities of probes **142b-d** to Aβ and tau aggregates could not be quantified because the values were out of the measureable range. It is noteworthy that probe **142e** shown the higher binding affinity for both Aβ and tau aggregates in the low- to mid-nanomolar range. It displayed ~17-fold higher affinity to tau aggregates in comparison to PIB which uses the same system for comparison.

Compounds **142c-d** have been further evaluated at different concentrations in the wild-type zebrafish embryo development assay (**Figure 3.28**). The embryos were treated with solutions containing compounds at 6-8 hpf, and the phenotypes were compared at 24 hpf and 72 hpf. It was found that the embryos developed well and did not display any lesions in eyes, yolks, tail and heart beat at different concentrations up to 10 μM. The cytotoxicity analysis proposes that *N*-2-aryl-1,2,3-triazoles have negligible cytotoxicity against wild-type zebrafish embryos at the concentration employed for the histology experiments on human AD brain tissue (1 μM).

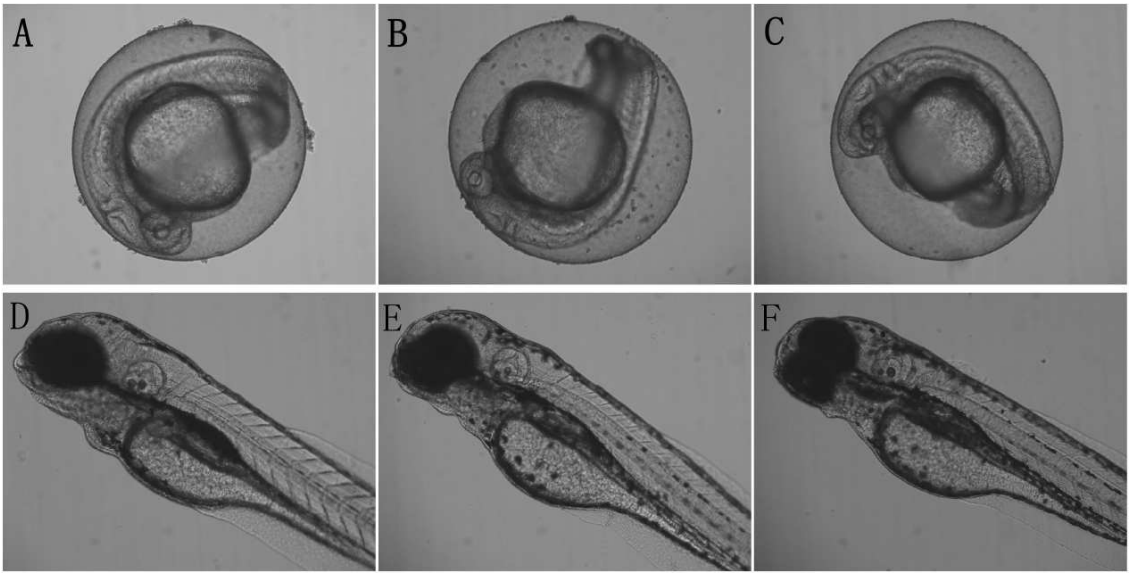

Figure 3.28 *In vivo* cytotoxicity studies of embryos of wild-type zebrafish with 10 µM *N*-2-aryl-1,2,3-triazoles at 24 hpf and 72 hpf. Controlled (A and D) probe **142c** (B and E) and probe **142d** (C and F).

In conclusion, we sought that *N*-2-aryl-1,2,3-triazoles containing a dimethylamino/diethylamino group in the 4-position of the 2-aryl ring have good fluorescence characteristics appropriate for the detection of tau aggregates in the brain tissue. The *in vitro* binding assay and the cytotoxicity experiments with zebrafish embryos suggest that *N*-2-aryl-1,2,3-triazoles may be used as potential imaging agents for tau pathology in AD.

3.9. Nasal mucous membranes as a potential diagnosing approach for Alzheimer's disease

A key obstacle in the development of diagnostics for AD is the blockage of drug entrance into the CNS by the BBB. From 1970s, there was a range of publications starting to clarify the neural connection between nasal mucosa and brain.[224,225] Due to the absence of a BBB between nose and brain, it suggested that the nasal cavity may enable drugs to access the brain and the nervous system by pathways involving the olfactory epithelium and the olfactory bulb. Therefore, the human olfactory system may be conducive to diagnose and treat brain disorders, such as AD and PD (**Figure 3.29**).

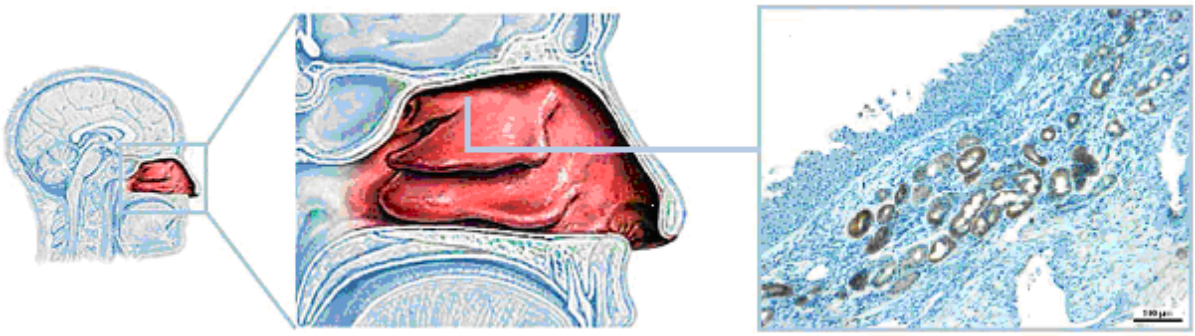

Figure 3.29 Nasal mucous membranes, a type of tissue that lines the nasal cavity, and immunohistochemical staining with antibodies against tau deposits on the olfactory epithelium tissues.

Comparing 20 confirmed AD patients and 5 healthy controls, our group discovered that the typical nasal tau-protein may deposit in nasal mucous membranes, particularly in the nasal Bowman's glands and olfactory epithelium.[204,226] The severity of tau accumulation in the Bowman's glands and its correlation to AD is subject to ongoing investigation.[49] However, this observation has shown potential for the noninvasive diagnosis of AD via changes in the olfactory epithelium in the early stages of disease.[227]

Table 3.14 Staining effect of selected probes on olfactory epithelium tissues.

Entry	BSc No.	Staining effect[a]
52p	**BSc4333**	**-**
52q	**BSc4334**	**-**
52u	**BSc4342**	**-**
83	**BSc4979**	**-**
100a	**BSc4740**	**+**
100b	**BSc4975**	**++**
115a	**BSc4919**	**+++**
115d	**BSc4960**	**+++**
142c	**BSc4956**	**++**
[a] **+++** stands for efficient staining, **++** stands for normal staining, **+** stands for weak staining, **-** stands for no staining.		

Several tau probes identified by brain histology (**Table 3.14** and **Table 3.15**) were used for the detection of tau deposits on the olfactory epithelium tissues *in vitro*. Unexpectedly, the phenylhydrazone benzothiazoles (**52p-q** and **52u**) and 1,4-bisstyryl-2-methoxybenzenes (**83**) failed to stain tau deposits. It was assumed that the high lipophilicity and poor water solubility limit these probes to penetrate the tissues, which lead to insufficient imaging. Thus, the poor cell permeability of imaging probe may prevent the visualization of tau deposits on the olfactory epithelium tissues.

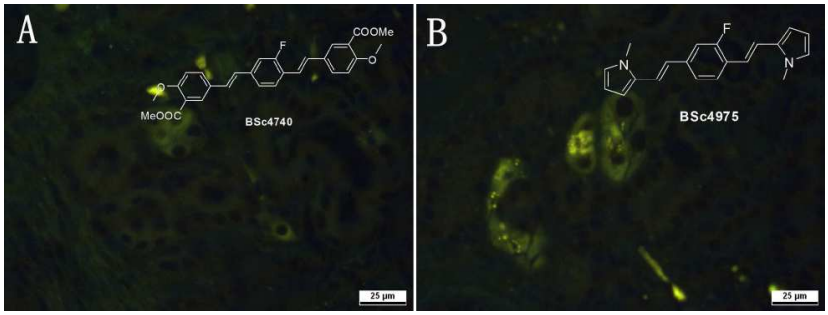

Figure 3.30 *In vitro* histochemical staining of postmortem AD olfactory epithelium tissues with 1,4-bisstyryl-2-methoxybenzenes (Tissues: olfactory epithelium; Patient: male, 78 years old; Braak: V, CERAD Score: 3).

The *N*-2-aryl-1,2,3-triazole derivative (**142c**), the 1,4-bisstyryl-2-fluorobenzenes (**100a-b**) and the bis(arylvinyl)pyrimidines (**115a** and **115d**) stained tau deposits on the olfactory epithelium tissues (**Figure 3.30** and **Figure 31**). As detected by fluorescence microscopy, in human olfactory epithelium tissue, the *N*-2-aryl-1,2,3-triazoles stained tau deposits strongly in comparison to bisstyryl derivatives. These results indicate that the relatively efficacious compounds (**115a**, **115d** and **142c**) may exhibit greater cell permeability, whereas less cell permeability compounds (**100a-b**) poorly stained tau deposits and limited the detection by the DAPI- or FITC-filters employed in fluorescence microscopy.

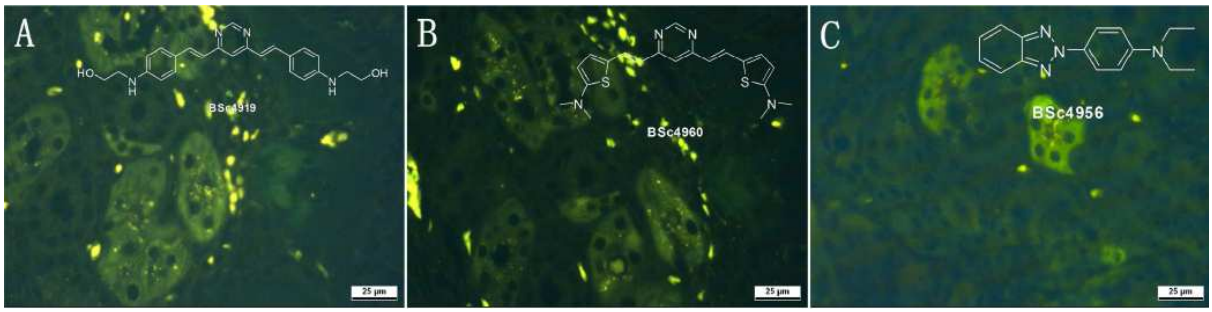

Figure 3.31 *In vitro* histochemical staining of postmortem AD olfactory epithelium tissues with bis(arylvinyl)pyrimidines and *N*-2-aryl-1,2,3-triazoles (Tissues: olfactory epithelium; Patient: male, 78 years old; Braak: V, CERAD Score: 3).

Table 3.15 Staining effect of selected cyanine dyes on olfactory epithelium tissues.

Entry	BSc No.	Staining effect[a]
120a	**BSc4452**	**+++**
120h	**BSc4744**	**+++**
121a	**BSc4743**	**+++**
121d	**BSc4747**	**+++**
121g	**BSc4750**	**+++**
135a	**BSc4704**	**+++**
135c	**BSc4737**	**+++**
135e	**BSc4739**	**+++**
135g	**BSc4742**	**+++**
[a] **+++** stands for efficient staining.		

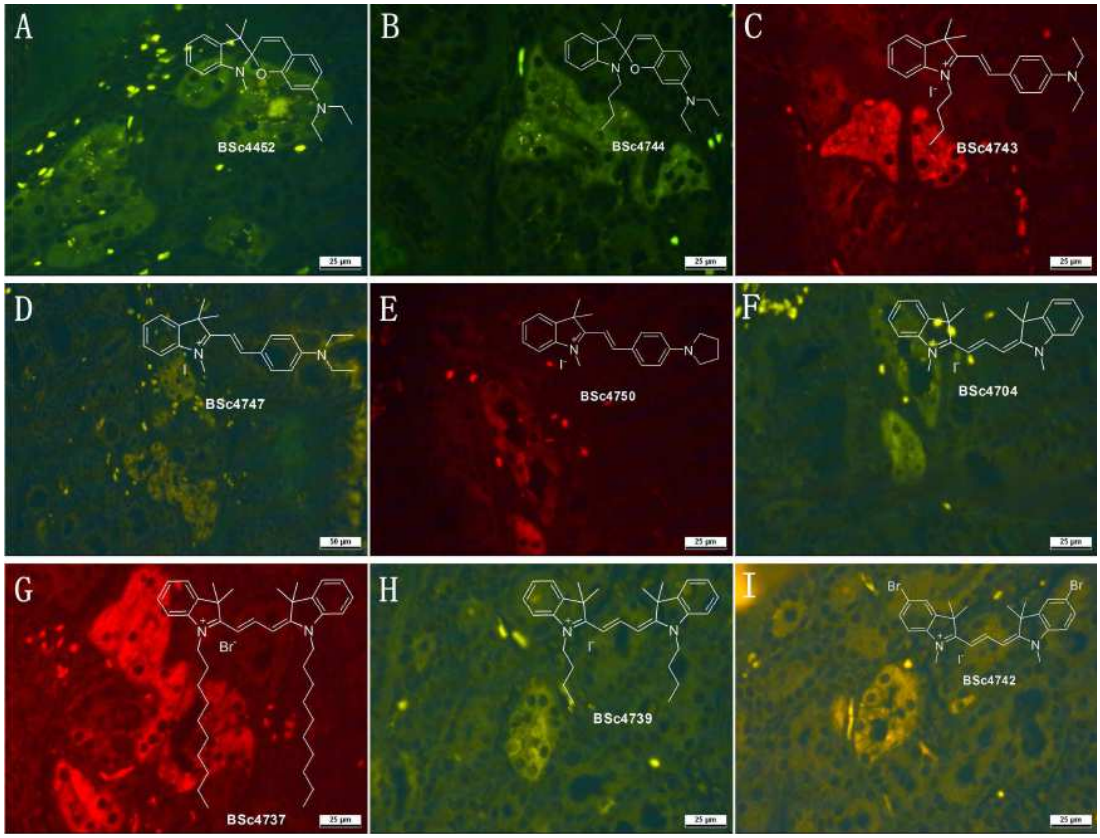

Figure 3.32 *In vitro* histochemical staining of postmortem AD olfactory epithelium tissues with spiropyrans and cyanine dyes (Tissues: olfactory epithelium; Patient: male, 78 years old; Braak: V, CERAD Score: 3).

Remarkably, many tau deposits were clearly stained with the spiropyrans (**120a**, **120h** and **120l**), merocyanines (**121a**, **121d** and **121g**) and trimethine cyanines (**135a**, **135c**, **135e** and **135g**) as seen in the *in vitro* assay (**Figure 3.32**). The tau deposits can be observed by fluorescence microscopy under green and red filters (more details see experimental sections). These results suggested that cyanine dyes were efficacious fluorescent probes for the detection of tau deposits on the olfactory epithelium tissues. The good solubility in water and negligible cytotoxicity suggested that these probes may be suitable for further *in vivo* applications in the near future.

In conclusion, we developed six classes of fluorescent probes to detect nasal tau-protein deposits. Since olfactory epithelium and olfactory bulb are not confined by the BBB, the efficiency of the drug depends on cell permeability rather than brain penetration. Therefore, the fluorescent labeling and histological examination suggested that nasal mucous membranes may be a potential tool for the detection of AD in the early stages.

3.10. Evaluation imaging probes to detect α-synuclein aggregates for Parkinson's disease

ASN is a component of LBs which are found in the brain of PD patients. ASN has been widely studied since 1997. Afterwards, plenty of articles describing the role of ASN in PD have been published.[137] In contrast to AD imaging agents, until now, only a handful of studies regarding fluorescent probes for the detection of ASN have been reported.

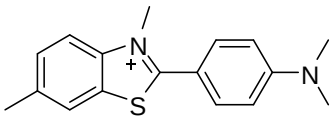

26 ThT

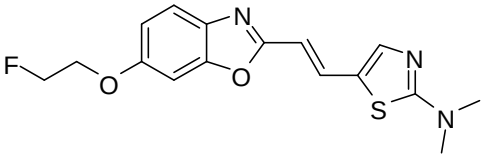

143 BF-227

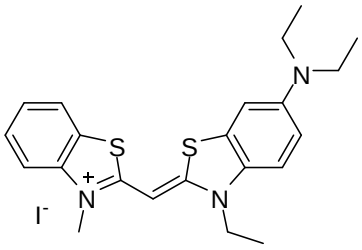

144 T-284

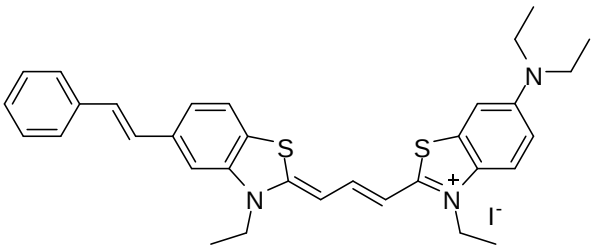

145 SH-516

Figure 3.33 Imaging agents for the detection of ASN aggregates *in vitro*.

The fluorescent compound ThT (**26**) is the most classic fluorescent dye which used for detection of amyloid structures including ASN. Besides, BF-227 (**143**) can be used for the detection of ASN-positive LBs and LNs via *in vitro* postmortem examination. In addition, cyanine dyes T-284 (**144**) and SH-516 (**145**) (**Figure 3.33**) were examined as sensitive and specific fluorescent probes for monitoring and characterizing ASN aggregations *in vitro*.[228-230]

Table 3.16 Staining effects of trimethine cyanine dyes for AD and PD.

Entry	BSc No.	Staining effect in AD and PD brain sections[a]		
135a	**BSc4704**	Aβ: **-**	NFT: **+++**	ASN: **++**
135b	**BSc4705**	Aβ: **+**	NFT: **++**	ASN: **-**
135c	**BSc4737**	Aβ: **+**	NFT: **+++**	ASN: **-**
135d	**BSc4738**	Aβ: **+**	NFT: **+**	ASN: **+++**
135e	**BSc4739**	Aβ: **+**	NFT: **++**	ASN: **++**
135f	**BSc4741**	Aβ: **+**	NFT: **+++**	ASN: **++**
135g	**BSc4742**	Aβ: **-**	NFT: **+++**	ASN: **+++**
135h	**BSc4806**	Aβ: **-**	NFT: **+**	ASN: **+++**
135i	**BSc4810**	Aβ: **+++**	NFT: **-**	ASN: **+++**
135j	**BSc4811**	Aβ: **-**	NFT: **-**	ASN: **+++**
135k	**BSc4818**	Aβ: **-**	NFT: **-**	ASN: **-**
135l	**BSc4920**	Aβ: **-**	NFT: **++**	ASN: **+++**
138b	**BSc4867**	Aβ: **-**	NFT: **-**	ASN: **++**
138c	**BSc4868**	Aβ: **+**	NFT: **-**	ASN: **+++**
138d	**BSc4904**	Aβ: **-**	NFT: **-**	ASN: **+++**
138e	**BSc4907**	Aβ: **-**	NFT: **-**	ASN: **-**

[a] **+++** stands for efficient staining, **++** stands for normal staining, **+** stands for weak staining, **-** stands for no staining.

The cyanine dyes exhibit a significant increase in fluorescence intensity in the presence of fibrillar ASN.[120] Unfortunately, cyanine dyes have shown potential as fluorescent probes for detection of biomolecules (DNA, lipid and protein) which indicates unselective binding. With the aim of searching novel fluorescent probe for the detection of ASN aggregates, we

explored strategies to construct fluorescent derivatives based on the compounds **144** and **145**.

We conducted a histochemical staining of postmortem PD brain tissues with 16 trimethine cyanines (**Table 3.16**). The stained brain tissues were investigated under a fluorescence microscopy employing DAPI- and FITC-filters. Excitingly, these *in vitro* assays revealed that 12 trimethine cyanine dyes effectively stained hallmark lesions of PD including LBs and LNs (**Figure 3.34**). Numerous fluorescent spots were observed in the sections of substantia nigra from PD brain. It indicates the potential application of trimethine cyanine dyes as imaging agents for the detection of ASN aggregates in PD. Meanwhile, different substituents in 1-position or 5-position of the indolium cores did not have a significant impact on histological staining. It is noteworthy that probes **135j**, **138b** and **138d** could specifically detect ASN aggregates by fluorescence microscopy while they failed to detect Aβ plaques or NFTs in AD subjects under same assay conditions. The ongoing radiolabeling of these probes as PET or SPECT imaging agents may be conducive to diagnose PD in the early stages.

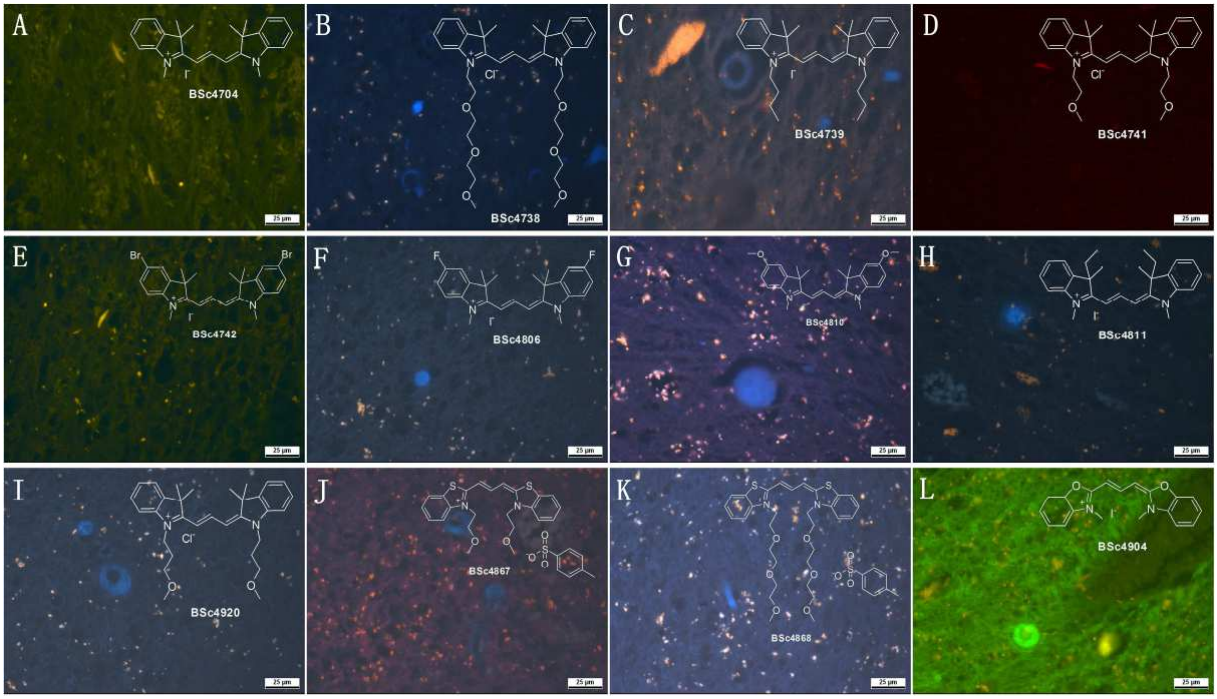

Figure 3.34 *In vitro* histochemical staining of postmortem PD brain tissues with trimethine cyanines (Tissues: midbrain; Patient: male, 76 years old).

However, the probes **135b-c**, **135k** and **138e** failed to detect ASN aggregates by fluorescence microscopy. The fact that ASN aggregates are undetectable by these fluorescent dyes may be due to the lower density of LBs or LNs presented in the brain sections (around four times lower than Aβ plaques and NFTs in AD). However, this assumption needs to be confirmed by further experiments.

Furthermore, the biological evaluation of 6 **ME** derivatives based on indolium cores were accomplished by fluorescent staining of PD brain sections (**Table 3.17**). It was found that five probes intensely stained ASN aggregates under these assay conditions (**Figure 3.35**, **A**-**E**). It appears that the chain length of the PEGylation or alkylation has no affect on the staining results. Simultaneously, the introduction of an electron-donating or electron-withdrawing group in the 5-position of cationic indolium core reduced unspecific binding and improved the visualization of ASN aggregates in the PD brain sections. However, the replacement of one of the geminal methyl groups by an ethyl moiety in the 3-position, probe **123b** stained ASN aggregates in human midbrain tissue strongly as observed by fluorescence microscopy, while **123d** failed to detect human midbrain ASN aggregates by fluorescence microscopy. We hypothesized that this result may be caused by the density of ASN aggregates in postmortem substantia nigra sections from PD brain.

Table 3.17 Staining effects of **ME** dyes.

Entry	BSc No.	Staining effect in AD and PD brain sections[a]		
121a	**BSc4743**	Aβ: **+**	NFT: **+++**	ASN: **++**
121b	**BSc4745**	Aβ: **+**	NFT: **++**	ASN: **+++**
121j	**BSc4816**	Aβ: **+**	NFT: **-**	ASN: **+++**
121k	**BSc4817**	Aβ: **++**	NFT: **-**	ASN: **+++**
123b	**BSc4814**	Aβ: **++**	NFT: **-**	ASN: **+++**
123d	**BSc4866**	Aβ: **++**	NFT: **-**	ASN: **-**

[a] **+++** stands for efficient staining, **++** stands for normal staining, **+** stands for weak staining, **-** stands for no staining.

Finally, the *N*-2-aryl-1,2,3-triazoles **142a-g** were examined by neuropathological staining of PD brain sections. Unfortunately, these derivatives did not stain ASN aggregates in the human brain section but poorly stained nerve fibrils with a low contrast to the background (**Figure 3.35**, **F**).

From the above results, it can be concluded that the cyanine moiety may play a critical role in the binding to ASN aggregates. The charged aryl group may contribute to increased fluorescence upon binding to aggregated ASN. Further research on cyanine dyes as potential imaging agents for ASN aggregates in PD is needed. These data provide a direction for the development of non-invasive agents for early *in vivo* detection of ASN aggregates in PD using PET and SPECT.

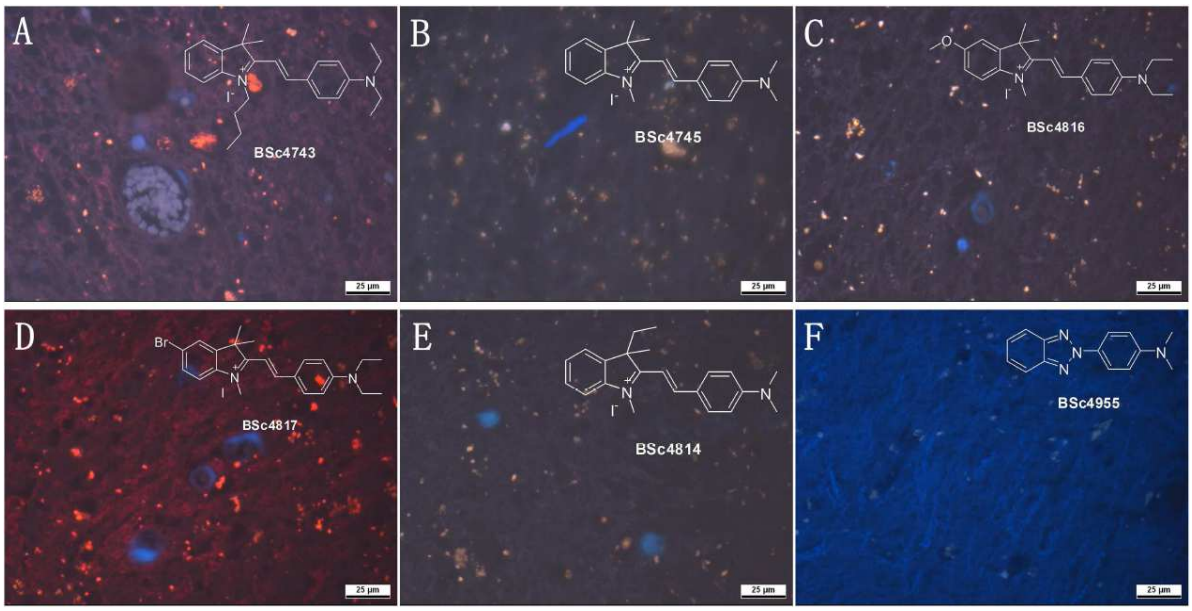

Figure 3.35 *In vitro* histochemical staining of postmortem PD brain tissues with **ME** dyes (Tissues: midbrain; Patient: male, 76 years old).

4. Summary

Design, synthesis and evaluation of potential imaging agents for Alzheimer's disease

Based on the modification of known structures with good binding affinities to β-sheet rich proteins, we prepared a diverse set of imaging agents for the detection of β-amyloid (Aβ) plaques and neurofibrillary tangles (NFTs) in Alzheimer's disease (AD). This resulted in six sets of probes, such as benzothiazoles, bis(styryl) derivatives, spiropyrans, indolium derivatives, trimethine cyanines and *N*-2-aryl-1,2,3-triazoles, which clearly stained Aβ plaques and NFTs in human tissues as observed by fluorescence microscopy. Several compounds provided highly specific visualization of Aβ plaques or NFTs in brain tissues of AD patients.

Due to the absence of fluorescence, the phenyldiazenyl benzothiazoles (**50a-g**) failed to visualize Aβ plaques and NFTs in the neuropathological staining of AD brain sections (**Chapter 3.1.1**). In order to overcome this shortcoming, we developed a set of fluorescent phenylhydrazone benzothiazoles (**52a-v**). The histological results of the probes **52f**, **52p-q** and **52t-u** displayed excellent staining of both Aβ plaques and NFTs (**Chapter 3.1.2**) (**Figure 4.1**). In addition, probes **52a**, **52c-d**, **52g-h**, **52l-o**, **52r** and **52v** specifically visualize Aβ plaques. It is noteworthy that the replacement of terminal phenyl groups by heteroaryls may increase fluorescence intensity upon binding to the targets. These compounds can provide improved signal-to-noise ratio for Aβ plaques and NFTs in comparison to IMPY derivatives (**Chapter 3.2.1**). The cytotoxicity analysis suggested that phenylhydrazone benzothiazoles have negligible cytotoxicity against zebrafish embryos at the concentration employed for further *in vivo* applications.

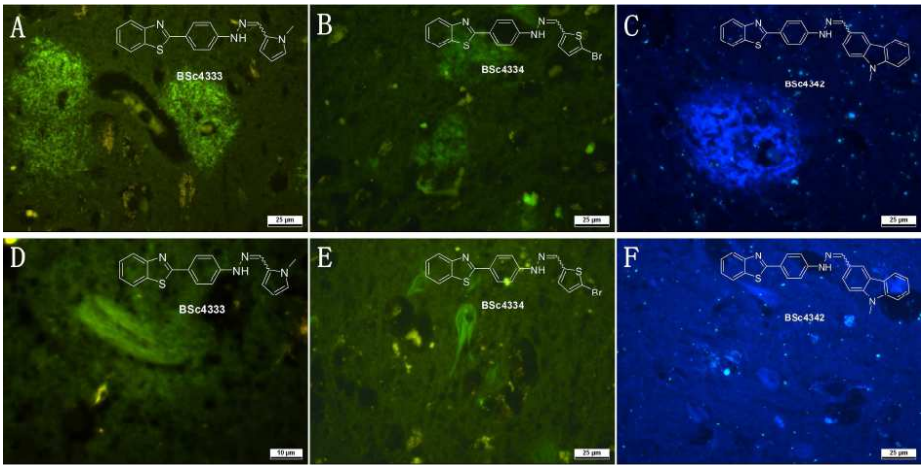

Figure 4.1 *In vitro* histochemical staining of phenylhydrazone benzothiazoles **52p** (**BSc4333**), **52p** (**BSc4334**) and **52u** (**BSc4342**) to Aβ plaques (A-C) and NFTs (D-E) (Tissues: hippocampus; Patient: female, 89 years old; CERAD Score: 3; NFTs-level: V).

Furthermore, we evaluated imidazo[1,2-*a*]pyridines (**Chapter 3.2.1**), imidazo[1,2-*a*]pyrimidines (**Chapter 3.2.3**) and tetrazines (**Chapter 3.3**) for the histological staining of Aβ plaques and NFTs in postmortem AD brain sections. The imaging results indicate that these probes exhibit remarkable selectivity for tau aggregates *in vitro*. However, lack of fluorescence properties upon target binding and low signal-to-noise ratio may limit them for the visualization of NFTs in the brain of AD patients. However, due to the steric hindrance, the [8+2] cycloaddition tetracyclics (**61**, **62** and **65**) may lose their capacity to fit into the fibril "binding channel", which causes them to be inactive in the imaging assay.

Due to the excellent optical properties, we designed and synthesized several bisstyryl derivatives to evaluate the staining of AD postmortem brain sections. It appears that 1,2,4,5-tetrafluoro-3,6-bisstyrylbenzenes **104b-c** clearly and specific stained Aβ plaques in AD brain sections (**Chapter 3.4.3**). In contrast, the bis(arylvinyl)pyrimidine derivative **115d** selectively binds NFTs in the hippocampal sections of human AD brain (**Chapter 3.4.5**). Additionally, the 1,4-bisstyryl-2-methoxybenzenes **83** and 4-bisstyryl-2-fluorobenzenes **100a** can be used to stain both Aβ and tau aggregates and provide a good contrast versus background (**Figure 4.2**). These results suggest that bisstyryl derivatives may be developed as potential ligands for imaging Aβ or tau aggregates in AD. However, the poor solubility (< 0.1 g/mL) and permeability are adverse properties which limits their use *in vivo*. In order to solve this major problem, it is necessary to find an effective way to improve the solubility and meet the lipophilicity criterion.

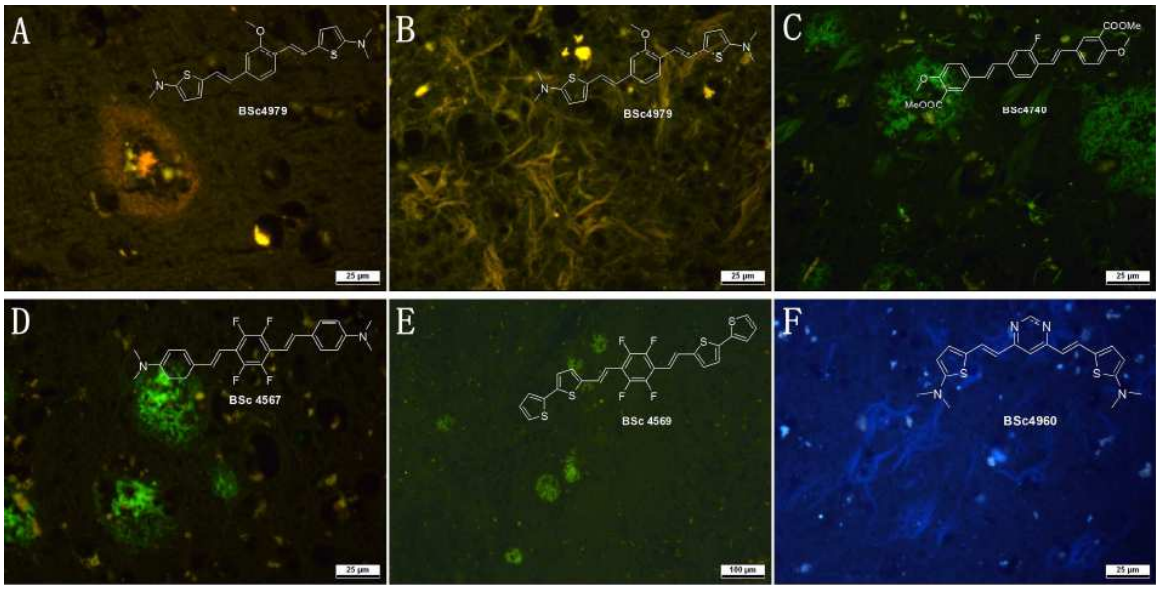

Figure 4.2 *In vitro* histochemical staining of bisstyryl derivatives **83** (**BSc4979**), **100a** (**BSc4740**), **104b** (**BSc4567**), **104c** (**BSc4569**) and **115d** (**BSc4960**) (Tissues: hippocampus; Patient: male, 71 or 72 years old; CERAD Score: 3; NFTs-level: V).

The spiropyrans **120a**, **120h** and **120l**, with a diethylamine group on the 7-position and different substituents on the 1'-position of the indole-ring, stained NFTs in human tissue clearly as observed by fluorescence microscopy, whereas plaques in the same brain preparations were not stained (**Chapter 3.5**) (**Figure 4.3**). Based on these structures, we further synthesized and evaluated water soluble merocyanines as specific Aβ or tau imaging agents (**Chapter 3.6**). The probes with a 3,3'-geminal methyl moiety (**121a-h**) exhibit highly specific staining to NFTs (**Figure 4.3**), which provides a good contrast versus Aβ plaques and background. However, the replacement of one of the geminal methyls by ethyl (**123a-b** and **133d**) or the substitution of different function groups on the 5-position of the indolium core (**121i-k**), specifically labels Aβ plaques in AD brain tissues. Furthermore, cytotoxicity studies with wild-type zebrafish embryos and liver hepatocellular carcinoma cells (HepG2) indicate that spiropyrans and merocyanines were sufficiently safe for further *in vivo* evaluation in mouse models.

We evaluated trimethine cyanine dyes as sensitive and specific probes for the detection of Aβ and tau aggregates by fluorescence microscopy (**Chapter 3.7**). We performed neuropathological fluorescent staining to confirm the ability to bind to Aβ plaques and NFT in postmortem AD brain sections. Probes **135a-g** stain NFTs in human tissue and provide a good contrast versus Aβ plaques and background (**Figure 4.3**). The wild-type zebrafish embryo development assay indicated no adverse events at 5 μM at 24 hpf. Especially, PEGylation at the *N* position of indolenine may improve the solubility of these compounds. It provides a guideline to optimize these compounds for potential use as *in vivo* imaging agents for the diagnosis of AD.

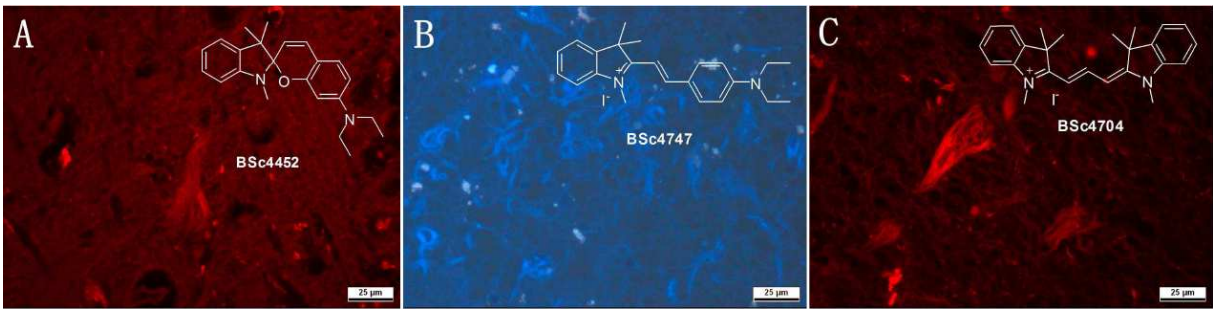

Figure 4.3 *In vitro* histochemical staining of tau specific dyes **120a** (**BSc4452**), **121d** (**BSc4747**) and **135a** (**BSc4704**) (Tissues: hippocampus; Patient: male, 71 years old; CERAD Score: 3; NFTs-level: V).

To confirm the specific binding of *N*-2-substituted-1,2,3-triazoles to NFTs *in vitro*, neuropathological staining was performed on the brain sections of AD patients. The NFTs were clearly stained by compounds **142a-e**, whereas Aβ plaques in the same brain sections

were stained just weakly (**Chapter 3.8**). The cytotoxicity experiments with zebrafish embryos suggest that these probes may be suitable for further *in vivo* applications in future.

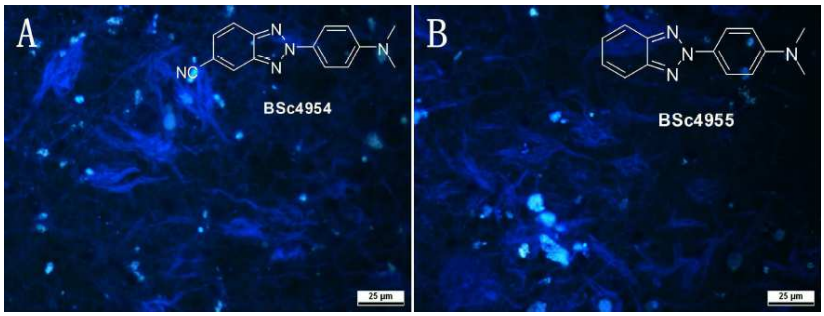

Figure 4.4 *In vitro* histochemical staining of *N*-2-substituted-1,2,3-triazoles **142a** (**BSc4954**) and **142b** (**BSc4955**) (Tissues: hippocampus; Patient: male, 72 years old; CERAD Score: 3; NFTs-level: V).

The affinities of these probes to aggregated tau and $A\beta_{40}$ were determined by displacement of the reference dye *Thiazine Red R*, thus IC_{50} data obtained in the competition assay are reported rather than *Ki* values. Significantly, phenylhydrazone benzothiazoles, bisstyryl derivatives, spiropyrans and cyanine dyes displayed ~7-10000 fold higher affinity for $A\beta_{40}$/tau aggregates in comparison to known compounds. This indicates sufficient affinity of these probes for the imaging of Aβ or tau aggregates *in vivo*.

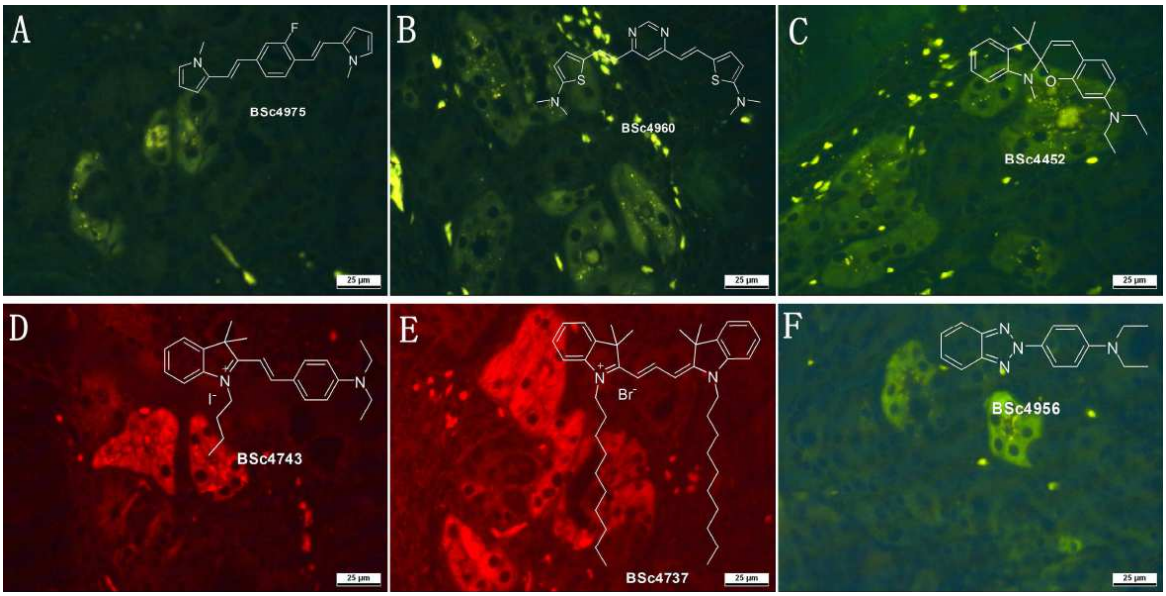

Figure 4.5 *In vitro* histochemical staining of selected probes **100b** (**BSc4975**), **115d** (**BSc4960**), **120a** (**BSc4452**), **121a** (**BSc4743**), **135c** (**BSc4737**) and **142c** (**BSc4956**) for the detection of tau aggregates on the olfactory epithelium tissues (Tissues: olfactory epithelium; Patient: male, 78 years old; Braak: V, CERAD Score: 3).

20 probes for tau aggregates were selected and investigated as potential imaging agents for the detection of tau deposits in the olfactory epithelium tissue *in vitro* (**Chapter 3.9**). It is noteworthy that the *N*-2-aryl-1,2,3-triazole (**142c**), the 1,4-bisstyryl-2-fluorobenzenes (**100a-b**) and the bis(arylvinyl)pyrimidines (**115a** and **115d**) stain tau deposits in the olfactory epithelium tissues. Furthermore, the spiropyrans (**120a**, **120h** and **120l**), the merocyanines (**121a**, **121d** and **121g**) and the trimethine cyanines (**135a**, **135c**, **135e** and **135g**) exhibit good to excellent staining of tau deposits and provide a good contrast versus background. They were clearly observed by fluorescence microscopy using green and red filters (**Figure 4.5**). Since olfactory epithelium and olfactory bulb are not confined by the BBB, the fluorescent labeling suggested that nasal mucous membranes may give assess to detection method for the diagnosis of AD in the early stages.

In conclusion, we successfully designed and synthesized sets of imaging agents for the selective detection of Aβ plaques and NFTs in postmortem AD brain sections. Selected candidates displayed higher affinity in the *in vitro* experiments in comparison to standard probes, such as PIB and Methoxy-X04. The cytotoxicity experiments with wild-type zebrafish embryos and HepG2 cells suggested that these probes displayed negligible cytotoxicity at the concentration employed for the histology experiments on human AD brain tissue (1 µM). Taken together, these results suggest that our candidates may be advanced to *in vivo* mice experiments in transgenic mice. These preferably fluorescent probes may be suitable for the detection of tau deposits on the olfactory epithelium of AD patients. Further optimization and radiolabeling of these probes may provide PET/SPECT imaging radiotracer for Aβ plaques and/or NFT imaging *in vivo*.

Table 4.1 The 10 most tau selective dyes.

Entry	BSc No.	*c*Log*P*	MW[a]	Histochemical staining
120a	**BSc4452**	6.80[a]	348.5	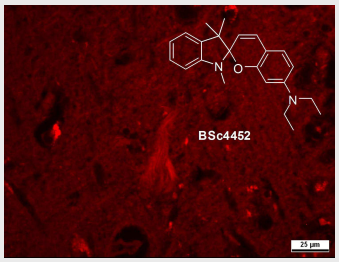
120l	**BSc4903**	6.64[a]	392.5	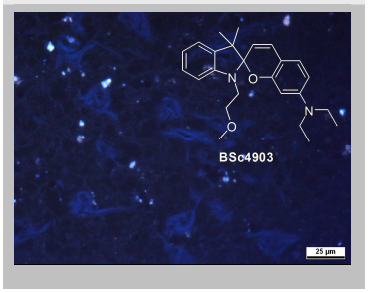

121a	**BSc4743**	3.58[a]	502.5	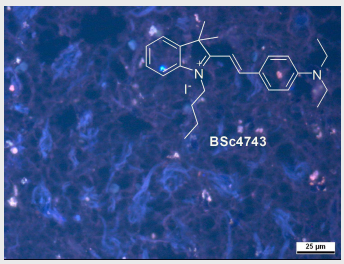
121d	**BSc4747**	2.14[b]	460.4	
121g	**BSc4750**	1.79[b]	458.4	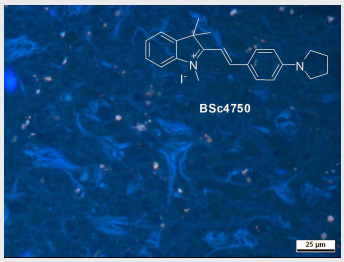
135a	**BSc4704**	2.77[b]	484.4	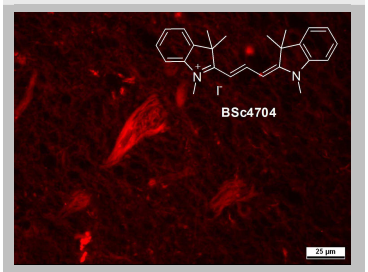
135e	**BSc4739**	5.64[b]	586.6	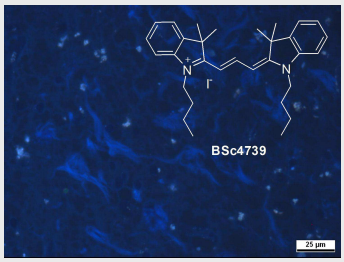
135f	**BSc4741**	2.74[b]	481.1	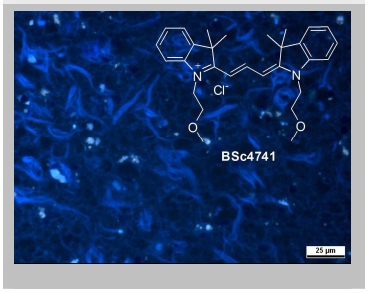

142a	**BSc4954**	3.81[a]	263.3	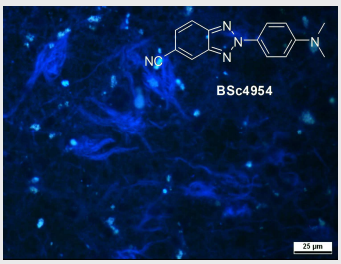
142b	**BSc4955**	3.78[a]	238.3	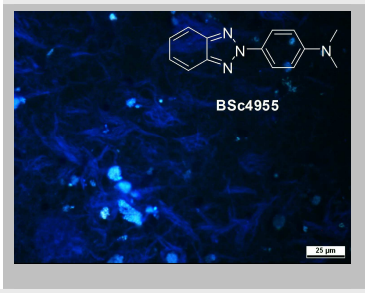

[a] Determined by CS ChemOffice 10.0; [b] Log*P* values were calculated using the Molinspiration Cheminformatics software (V2011. 04).

Evaluation of imaging probes to detect α-synuclein aggregates in Parkinson's disease

The second part of this thesis attempted to investigate several imaging agents for the detection of ASN aggregates in postmortem Parkinson's disease (PD) brain sections (**Chapter 3.9**). It was found that 12 trimethine cyanine dyes and 5 merocyanine dyes strongly labeled ASN aggregates in the sections of substantia nigra. However, all the *N*-2-aryl-1,2,3-triazoles failed to detect ASN aggregates by fluorescence microscopy. It indicated that cyanine moiety may play a critical role in binding to ASN aggregates *in vitro*.

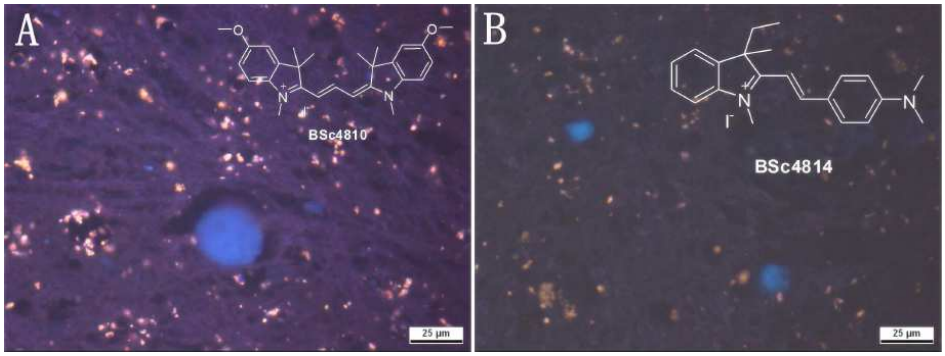

Figure 4.6 *In vitro* histochemical staining of cyanine dyes **135i** (**BSc4810**) and **123b** (**BSc4814**) to ASN aggregates (Tissues: midbrain; Patient: male, 76 years old).

5. Outlook

We successfully examined several imaging agents for the detection of Aβ plaques or NFTs in postmortem AD brain sections. Some of the results have been published or filed for patent application. At the same time, we evaluated cyanine dyes as sensitive probes for the detection of ASN aggregates *in vitro*. Therefore, further optimization of these compounds may have broad application prospects in neurodegenerative disease in future.

The efficacy of central nervous system drugs for AD and PD depends on the sufficient lipophilicity to cross the BBB and enable rapid clearance from brain. Besides, poor solubility and cell permeability may limit their diagnostic potential for tau aggregates on the olfactory epithelium *in vivo*. In order to meet the solubility criteria and cross the BBB in humans, future work will have to focus on improved solubility of these compounds in aqueous media.

Generally, the solubility of these imaging agents in water may be achieved by PEGylation. In addition, the introduction of a terminal 4-phenylpiperazine moiety is another feasible option to increase the solubility (**Figure 5.1**). These feasible approaches provide directions for improved of drug solubility.

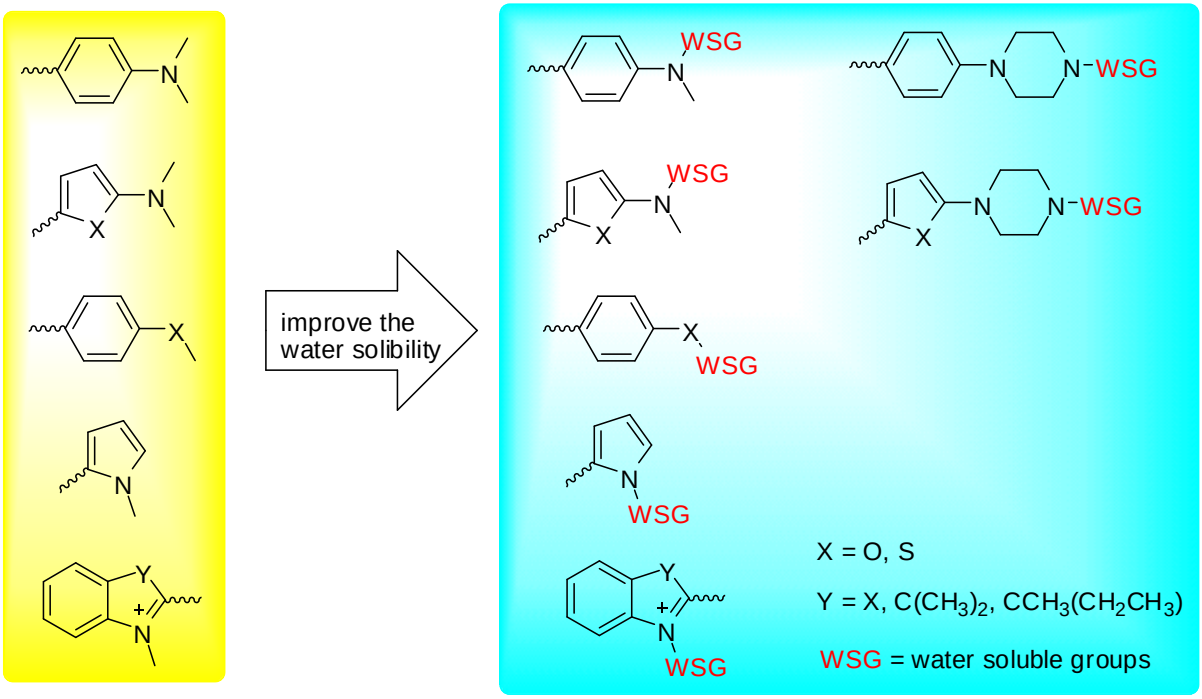

Figure 5.1 Examples of optimization to improve the solubility of these structures.

Compounds **104b-c** selectively visualize Aβ plaques in human brain tissue. The high fluorine contentmay make them particularly valuable for the development of a noninvasive probe for early detection of AD because all the fluorine atoms are chemically equivalent. By improving the water solubility, all of these probes may be used as imaging agents for the detection of Aβ aggregates.

On the basis of increased solubility, the continuing research may focus on the development of radiolabeled compounds which can be applied as highly selective and specific PET/SPECT radiotracer for Aβ plaques or NFT imaging *in vivo* (**Figure 5.2**).

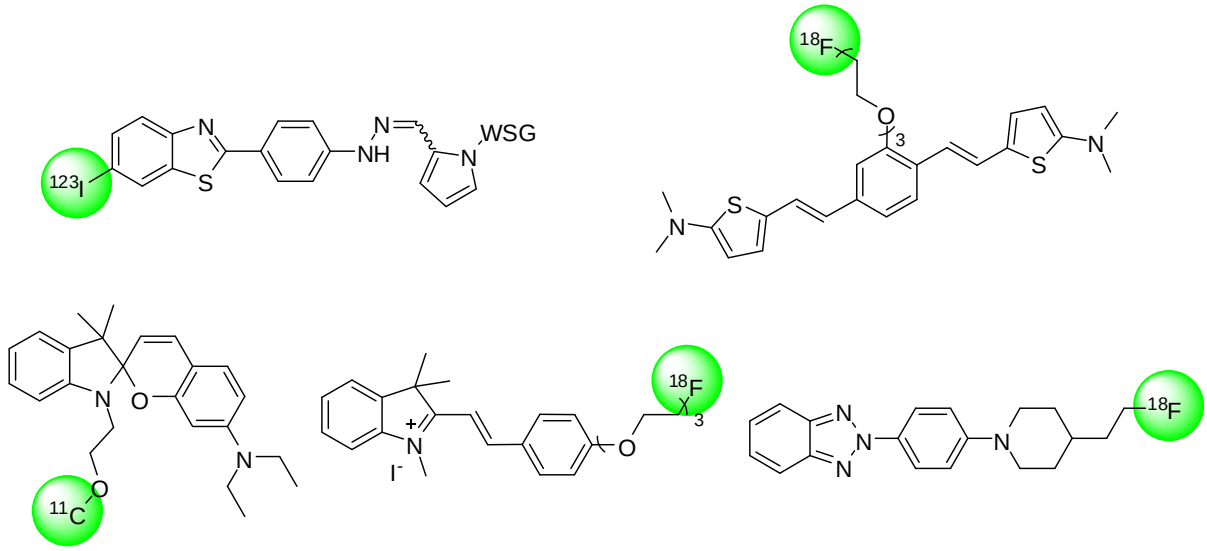

Figure 5.2 Examples of potential radiolabeled chemical structures for PET and SPECT imaging.

The boron-containing compounds, with fluorescence covering a wide range from pure blue (450 nm) to saturated red (670 nm), have a wide range of applications as fluorescent probes in biological systems.[231] The luminescent organic boron derivatives based on *N*,*N*- and *N*,*O*-chelated boron complexes show excellent photophysical properties such as thermal and photochemical stability and high fluorescence quantum yield.[232,233] Because of the poor staining effects of the phenylhydrazone benzothiazoles in **Chapter 3.1.2** and the merocyanines in **Chapter 3.6**, additional structural changes (**Figure 5.3**) to form a rigid boronchelate fluorescent core may modify the fluorescence properties and improve their suitability for Aβ or tau imaging.

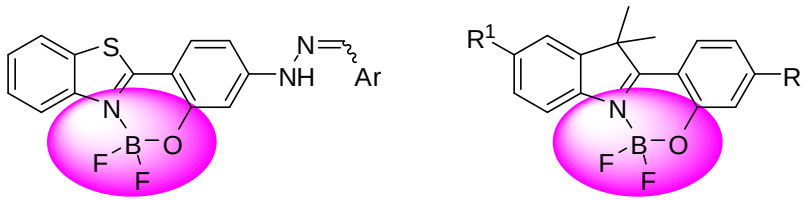

Figure 5.3 The *N*,*O*-chelated boron derivatives.

6. Experimental section

6.1. General Information

Melting points were measured by a Mettler FP5/51. The ^{1}H-NMR spectra were recorded on a Bruker DRX 500 spectrometer at 500 MHz. The ^{13}C-NMR spectra were recorded on a Bruker DRX 500 spectrometer at 125 MHz. Chemical shifts were reported downfield from Me_4Si. IR was performed by PerkinElmer FT-IR spectrometer PARAGON 1000PC. UV-Vis spectra were recorded by Shimadzu UV-2401PC. Mass spectrometry was performed on a MAT 95 double focussing sector field MS. Elemental analyses were performed by Elementar Vario EL. Flash column chromatography was carried out with Merck silica gel 60 (15-40 mm). Thin-layer chromatography (TLC) was carried out with aluminum sheets precoated with silica gel 60 F254 (0.2 mm, Merck). Chromatographic spots were visualized by UV light. All commercially available chemicals were used without further purification.

6.2. Synthesis of benzothiazole derivatives

6.2.1. General procedures for synthesis of phenyldiazenyl benzothiazole derivatives

2-(4-Nitrophenyl)benzo[*d*]thiazol (48)

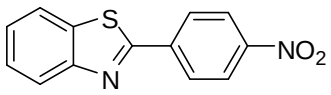

4-Nitrobenzoyl chloride (5.60 g, 30.0 mmol, 1.0 eq) was added to a solution of 2-aminobenzothiol (3.2 mL, 30.0 mmol, 1.0 eq) in NMP (30 mL) by small portions under ice-cooling. The reaction mixture was stirred at 100 °C for 2 h. After cooling down to room temperature, the mixture was added to ice water and treated with aqueous ammonia solution to pH=8-9. Precipitates were filtered off and washed with cold EtOH. 7.28 g of 2-(4-nitrophenyl)benzo[*d*]thiazol was obtained as a yellow solid (yield: 95 %).

4-(Benzo[*d*]thiazol-2-yl) aniline (49)

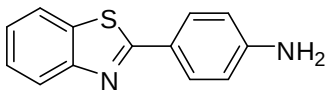

Tin chloride (7.40 g, 39.0 mmol, 5.0 eq) was added to a solution of 2-(4-nitrophenyl) benzo[*d*]thiazol (2.00 g, 7.8 mmol, 1.0 eq) in EtOH (20 mL). The reaction was stirred and refluxed overnight. When the mixture was cooled to room temperature, the solvent was

evaporated *in vacuo*. The residue was dissolved in ethyl acetate, washed with NaOH solution (2 N, 3 x 30 mL), distilled H_2O (2 x 30 mL) and brine (30 mL). The organic phase was dried over Na_2SO_4. After filtration, the solvent was evaporated *in vacuo* to afford 1.62 g of 4-(benzo[*d*]thiazol-2-yl) aniline as yellow solid.

Yield: 92 %. **^{1}H-NMR (300 MHz, $CDCl_3$)**: δ = 8.00 (d, *J* = 8.1 Hz, 1H), 7.90 (d, *J* = 8.7 Hz, 2H), 7.85 (d, *J* = 7.8 Hz, 1H), 7.45 (td, *J* = 8.1 Hz, *J* = 1.2 Hz, 1H), 7.32 (td, *J* = 8.1 Hz, *J* = 1.2 Hz, 1H), 6.74 (d, *J* = 9.0 Hz, 2H), 3.95 (s, 2H) ppm. **^{13}C-NMR (75 MHz, $CDCl_3$)**: δ = 168.5, 154.3, 149.2, 134.6, 129.1, 126.0, 124.4, 124.0, 122.5, 121.4, 114.8 ppm. **MS (EI, 70 eV)**: *m/z* = 226 $[M]^+$.

General procedure for azo coupling reaction

A solution of $NaNO_2$ (76 mg, 1.1 mmol, 1.1 eq) in water (1 mL) was added dropwise to an ice-cold solution of 4-(benzo[*d*]thiazol-2-yl)aniline (226 mg, 1.0 mmol, 1.0 eq) in 6 N HCl (1 mL), and the temperature was controlled under 5 °C. The reaction was stirred for 5 min and added to a solution of the corresponding aromatic compound (1.1 mmol, 1.1 eq) in a mixture of 6 N HCl (1.0 mL) and water (1.0 mL). Followed by 30 min of stirring at room temperature, the reaction mixture was poured onto a mixture of ice water (20 mL) and 6 N NaOH solution (2 mL). Precipitates were filtered off and washed with cold water. The crude product was purified by column chromatography (SiO_2; ethyl acetate: cyclohexane = 1:10) to furnish the corresponding compound with yields of 46-81 % (**Table 3.1**).

(*E*)-4-((4-(Benzo[*d*]thiazol-2-yl)phenyl)diazenyl)-*N*,*N*-dimethylaniline (50a)

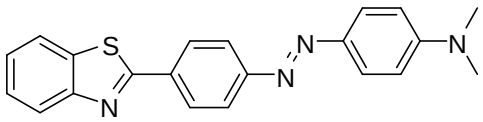

BSc4211

Yield: 71 %. **^{1}H-NMR (500 MHz, $CDCl_3$)**: δ = 8.21 (d, *J* = 8.5 Hz, 2H), 8.09 (d, *J* = 8.0 Hz, 1H), 7.96 (d, *J* = 9.0 Hz, 2H), 7.92 (d, *J* = 9.0 Hz, 3H), 7.51 (td, *J* = 8.0 Hz, *J* = 1.0 Hz, 1H), 7.40 (td, *J* = 8.0 Hz, *J* = 1.0 Hz, 1H), 6.78 (d, *J* = 8.0 Hz, 1H), 3.12 (s, 6H) ppm. **^{13}C-NMR (125 MHz, $CDCl_3$)**: δ = 163.7, 154.3, 153.7, 148.3, 134.0, 128.3, 126.4, 126.0, 125.4, 125.2, 123.3, 122.8, 121.6, 115.5, 111.5, 40.3 ppm. **MS (EI, 70 eV)**: *m/z* = 358 $[M]^+$. **UV/Vis (Ethanol)**: λ_{max} = 445.5 nm.

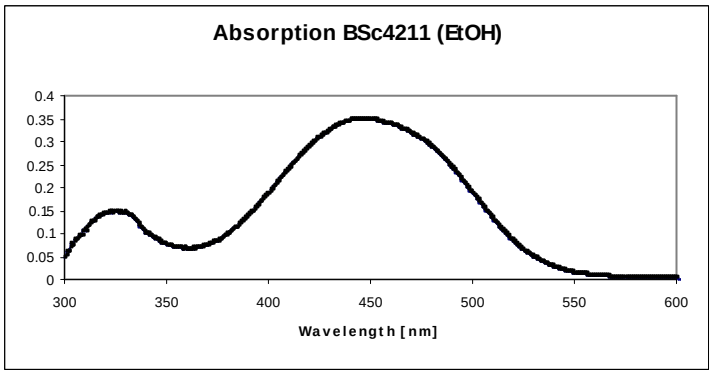

(*E*)-5-((4-(Benzo[*d*]thiazol-2-yl)phenyl)diazenyl)-*N*,*N*-dimethylpyridin-2-amine (50b)

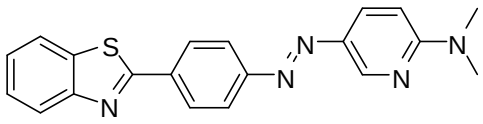

BSc4212

Yield: 63 %. **^{1}H-NMR (300 MHz, $CDCl_3$)**: δ = 8.85 (d, *J* = 2.1 Hz, 1H), 8.22 (d, *J* = 6.0 Hz, 2H), 8.12-8.04 (m, 2H), 7.99-7.90 (m, 3H), 7.51 (td, *J* = 8.4 Hz, *J* = 1.2 Hz, 1H), 7.40 (td, *J* = 8.4 Hz, *J* = 1.2 Hz, 1H), 6.61 (d, *J* = 9.4 Hz, 1H), 3.25 (s, 6H) ppm. **MS (EI, 70 eV)**: *m/z* = 359 $[M]^+$. **UV/Vis (Ethanol)**: λ_{max} = 424.0 nm.

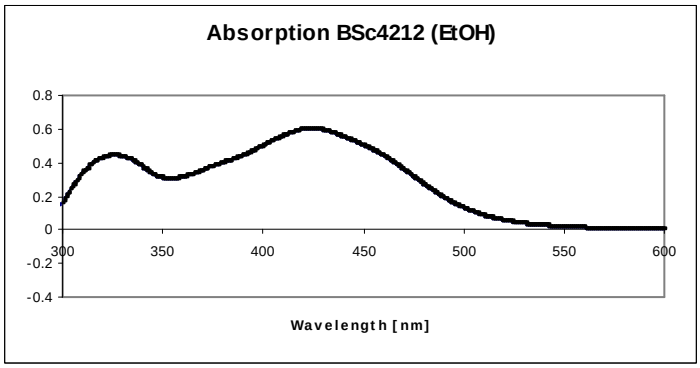

(*E*)-2-((4-(Benzo[*d*]thiazol-2-yl)phenyl)diazenyl)-5-(dimethylamino)phenol (50c)

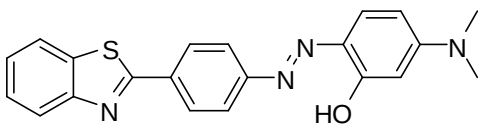

BSc4213

Yield: 67 %. **^{1}H-NMR (500 MHz, $CDCl_3$)**: δ = 14.94 (s, 1H), 8.17 (d, *J* = 8.5 Hz, 2H), 8.08 (d, *J* = 7.5 Hz, 1H), 7.91 (d, *J* = 8.0 Hz, 1H), 7.80 (d, *J* = 8.5 Hz, 2H), 7.53 (d, *J* = 9.5 Hz, 1H), 7.50 (td, *J* = 8.0 Hz, *J* = 1.0 Hz, 1H), 7.39 (td, *J* = 8.0 Hz, *J* = 1.0 Hz, 1H), 6.46 (dd, *J* = 9.5 Hz, *J* = 3.0 Hz, 1H), 6.07 (d, *J* = 3.0 Hz, 1H), 3.13 (s, 6H) ppm. **^{13}C-NMR (125 MHz, $CDCl_3$)**: δ = 167.3, 161.2, 155.0, 154.3, 150.7, 135.1, 135.1, 132.5, 131.9, 128.3, 126.4, 125.2, 123.2, 121.6, 120.5, 107.2, 98.5, 40.3 ppm. **MS (EI, 70 eV)**: *m/z* = 374 $[M]^+$. **UV/Vis (Ethanol)**: λ_{max} = 478.0 nm.

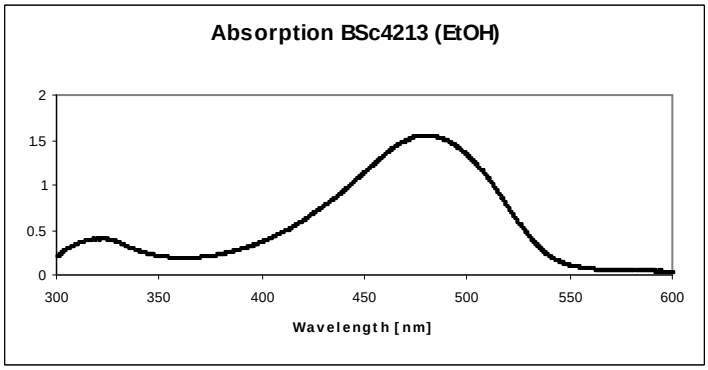

(*E*)-2-(4-((1*H*-Indol-3-yl)diazenyl)phenyl)benzo[*d*]thiazole (50d)

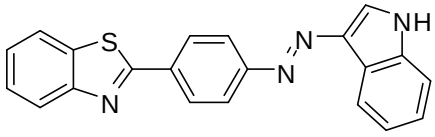

BSc4214

Yield: 46 %. **^{1}H-NMR (500 MHz, $CDCl_3$)**: δ = 8.66 (s, 1H), 8.62-8.57 (m, 1H), 8.24 (d, *J* = 8.5 Hz, 2H), 8.12-8.08 (m, 2H), 8.01 (d, *J* = 8.5 Hz, 2H), 7.93 (d, *J* = 7.5 Hz, 1H), 7.51 (td, *J* = 8.0 Hz, *J* = 1.0 Hz, 1H), 7.45-7.33 (m, 4H) ppm. **^{13}C-NMR (125 MHz, $CDCl_3$)**: δ = 167.5, 165.8, 154.3, 151.4, 137.4, 136.3, 135.9, 135.20, 133.8 131.5, 128.3, 126.4, 125.3, 124.7, 123.4, 123.2, 122.5, 121.6, 111.4 ppm. **MS (EI, 70 eV)**: *m/z* = 354 $[M]^+$. **UV/Vis (Ethanol)**: λ_{max} = 400.0 nm.

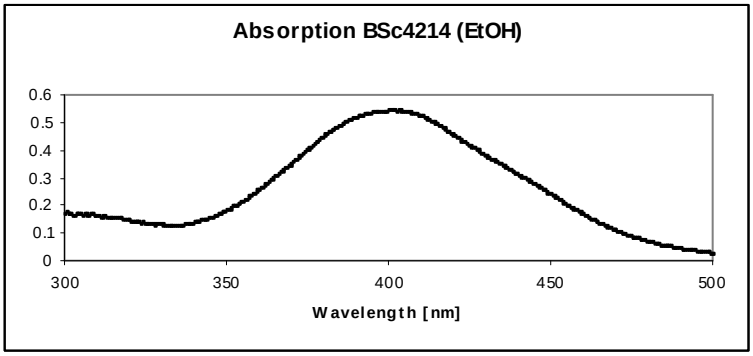

(*E*)-2-(4-((2-Methyl-1*H*-indol-3-yl)diazenyl)phenyl)benzo[*d*]thiazole (50e)

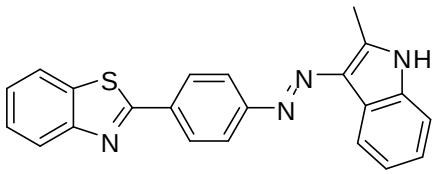

BSc4215

Yield: 49 %. **^{1}H-NMR (500 MHz, $CDCl_3$)**: δ = 8.56 (d, *J* = 8.0 Hz, 1H), 8.42 (s, 1H), 8.21 (d, *J* = 7.5 Hz, 2H), 8.10 (d, *J* = 8.0 Hz, 1H), 8.00 (d, *J* = 7.5 Hz, 2H), 7.82 (d, *J* = 8.0 Hz, 1H), 7.51 (td, *J* = 8.0 Hz, *J* = 1.0 Hz, 1H), 7.40 (td, *J* = 8.0 Hz, *J* = 1.0 Hz, 1H), 7.34-7.24 (m, 3H), 2.87 (s, 3H) ppm. **^{13}C-NMR (125 MHz, $CDCl_3$)**: δ = 167.7, 155.8, 154.3, 144.00, 135.2, 135.1, 133.5, 133.2, 128.3, 126.4, 125.2, 123.8, 123.2, 122.6, 122.3, 121.6, 119.5, 110.5, 29.4 ppm. **MS (EI, 70 eV)**: *m/z* = 368 $[M]^+$. **UV/Vis (Ethanol)**: λ_{max} = 412.0 nm.

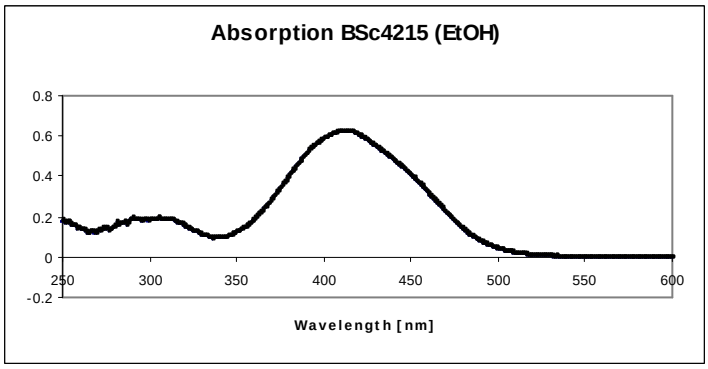

(*E*)-3-((4-(Benzo[*d*]thiazol-2-yl)phenyl)diazenyl)-9*H*-carbazol-2-ol (50f)

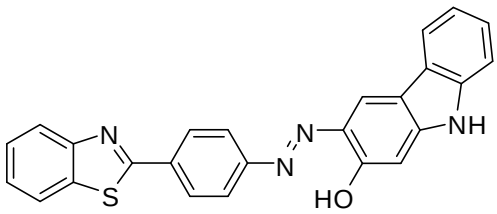

BSc4295

Yield: 81 %. **^{1}H-NMR (500 MHz, d_6-DMSO)**: δ = 12.30 (s, 1H), 11.56 (s, 1H), 9.62 (s, 1H), 8.30 (d, *J* = 9.0 Hz, 2H), 8.20-8.08 (m, 5H), 7.58 (d, *J* = 8.0 Hz, 1H), 7.50 (d, *J* = 8.0 Hz, 1H), 7.45 (d, *J* = 7.5 Hz, 1H), 7.37 (d, *J* = 8.0 Hz, 1H), 7.20 (d, *J* = 8.0 Hz, 1H), 6.96 (s, 1H) ppm. **^{13}C-NMR (125 MHz, d_6-DMSO)**: δ = 166.2, 154.3, 153.6, 152.5, 144.5, 140.8, 134.6, 133.6, 133.4, 128.3, 126.7, 125.6, 123.1, 122.9, 122.6, 122.3, 120.3, 120.1, 119.8, 117.6, 111.1, 96.9 ppm. **MS (EI, 70 eV)**: *m/z* = 420 $[M]^+$. **UV/Vis (Ethanol)**: λ_{max} = 455.0 nm.

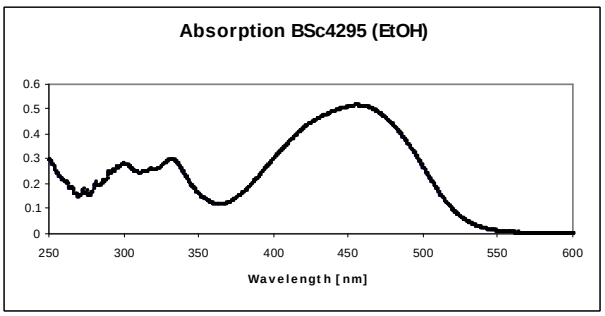

(*E*)-3-((4-(Benzo[*d*]thiazol-2-yl)phenyl)diazenyl)-1*H*-indol-2-ol (50g)

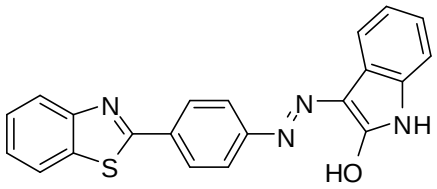

BSc4296

Yield: 48 %. **^{1}H-NMR (500 MHz, d_6-DMSO)**: δ = 12.88 (s, 1H), 11.08 (s, 1H), 8.13-8.06 (m, 3H), 8.02 (d, *J* = 7.5 Hz, 1H), 7.62-7.57 (m, 3H), 7.53 (td, *J* = 8.5 Hz, *J* = 1.5 Hz, 1H), 7.43 (td, *J* = 8.0 Hz, *J* = 1.0 Hz, 1H), 7.28 (td, *J* = 7.5 Hz, *J* = 1.0 Hz, 1H), 7.08 (td, *J* = 7.5 Hz, *J* = 1.0 Hz, 1H), 6.94 (d, *J* = 8.0 Hz, 1H) ppm. **^{13}C-NMR (125 MHz, d_6-DMSO)**: δ = 166.8, 163.0, 153.6, 145.0, 140.3, 134.1, 129.4, 129.1, 128.6, 126.4, 125.0, 122.4, 122.1, 121.9, 120.8, 119.0, 114.5, 110.6 ppm. **MS (EI, 70 eV)**: *m/z* = 370 $[M]^+$. **UV/Vis (Ethanol)**: λ_{max} = 408.0 nm.

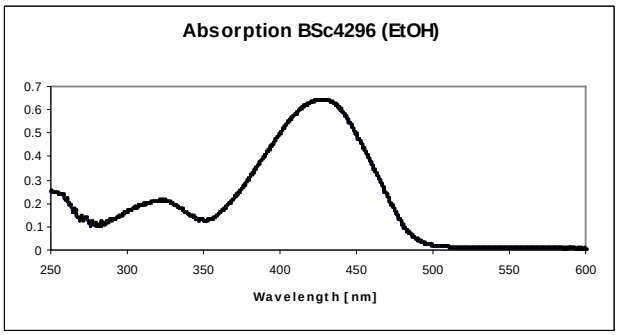

6.2.2. General procedures for synthesis of phenylhydrazone benzothiazole derivatives

A solution of $NaNO_2$ (76 mg, 1.1 mmol, 1.1 eq) in water (1 mL) was added to an ice-cold solution of 4-(benzo[*d*]thiazol-2-yl) aniline (226 mg, 1.0 mmol, 1.0 eq) in 6 N HCl (1 mL), and the temperature was controlled under 5 °C. The reaction was stirred for 5 min and added slowly to a solution of $SnCl_2 \cdot 2H_2O$ in HCl (conc., 0.5 mL) at -5 °C. The reaction mixture was stirred at room temperature for 1 h.

Corresponding aldehydes (1 mmol, 1.0 eq) was dissolved in 30 ml THF, the solution of aldehydes were added to phenylhydrazine. The reaction mixture was stirred and refluxed for 2 hours. When it was cooled, the mixture was extracted with THF twice. The organic phase was dried over Na_2SO_4, filtered, and concentrated. The residue was purified by column chromatography (SiO_2; ethyl acetate: cyclohexane = 1:1) to furnish the corresponding compound with the yields of 44-81 % (**Table 3.2**).

4-((2-(4-(Benzo[*d*]thiazol-2-yl)phenyl)hydrazono)methyl)-*N*,*N*-dimethylaniline (52a)

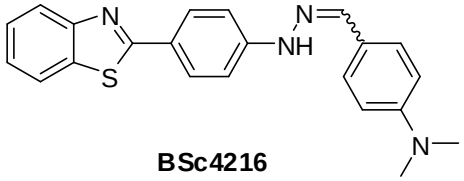

BSc4216

Yield: 76 %. **^{1}H-NMR (500 MHz, d_6-DMSO)**: δ = 10.53 (s, 1H), 8.06 (d, *J* = 8.1 Hz, 1H), 7.97-7.90 (m, 3H), 7.87 (s, 1H), 7.55-7.45 (m, 3H), 7.37 (td, *J* = 7.8 Hz, *J* = 0.9 Hz, 1H), 7.14 (d, *J* = 9.0 Hz, 2H), 6.75 (d, *J* = 9.0 Hz, 2H), 2.96 (s, 6H) ppm. **^{13}C-NMR (125 MHz, d_6-DMSO)**: δ = 167.7, 153.9, 150.6, 128.2, 140.2, 133.8, 128.7, 127.3, 126.3, 124.5, 122.9, 122.3, 120.0, 121.9, 112.0, 111.7, 39.9 ppm. **MS (EI, 70 eV)**: *m/z* = 372 $[M]^+$. **UV/Vis (Ethanol)**: λ_{max} = 403.0 nm.

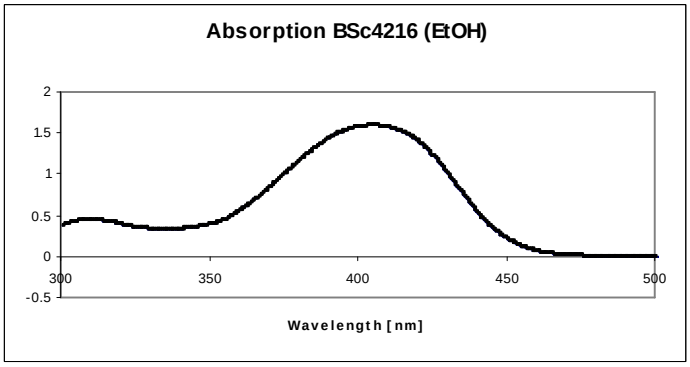

***In vitro* neuropathological staining of AD brain sections**: Tissues: hippocampus; Patient: female, 89 years old; CERAD Score: 3; NFTs-level: V.

4-((2-(4-(Benzo[*d*]thiazol-2-yl)phenyl)hydrazono)methyl)-*N*,*N*-diethylaniline (52b)

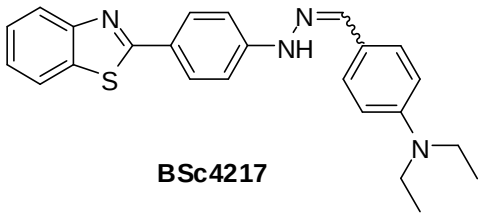

BSc4217

Yield: 73 %. **^{1}H-NMR (500 MHz, d_6-DMSO)**: δ = 10.48 (s, 1H), 8.05 (d, *J* = 7.5 Hz, 1H), 7.95-7.91 (m, 3H), 7.84 (s, 1H), 7.50-7.46 (m, 3H), 7.37 (td, *J* = 8.0Hz, *J* = 1.5 Hz, 1H), 7.13 (d, *J* = 8.5 Hz, 2H), 6.69 (d, *J* = 9.0 Hz, 2H), 3.41-3.35 (m, 4H), 1.11 (d, *J* = 7.5 Hz, 6H) ppm. **^{13}C-NMR (125 MHz, d_6-DMSO)**: δ = 167.6, 153.8, 148.1, 147.8, 140.2, 133.7, 128.6, 127.5, 127.5, 126.2, 124.4, 122.1, 121.9, 121.8, 111.5, 111.2, 43.6, 12.4 ppm. **MS (EI, 70 eV)**: *m/z* = 400 $[M]^+$. **UV/Vis (Ethanol)**: λ_{max} = 407.5 nm.

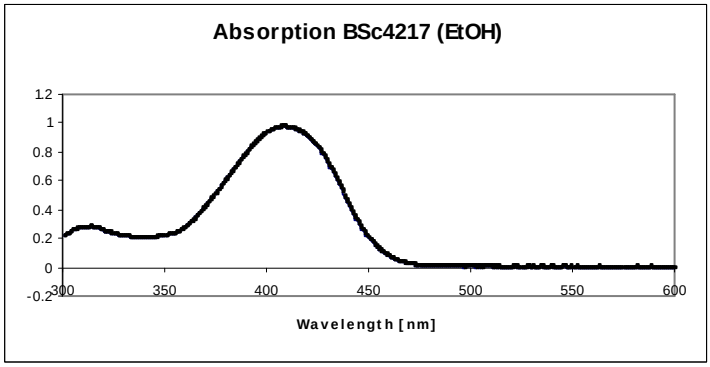

***In vitro* neuropathological staining of AD brain sections**: Tissues: hippocampus; Patient: female, 89 years old; CERAD Score: 3; NFTs-level: V.

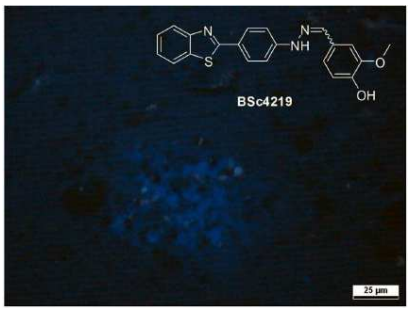

4-((2-(4-(Benzo[*d*]thiazol-2-yl)phenyl)hydrazono)methyl)-2-methoxyphenol (52c)

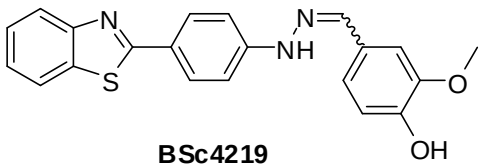

BSc4219

Yield: 46 %. **^{1}H-NMR (300 MHz, d_6-DMSO)**: δ = 10.64 (s, 1H), 9.93 (s, 1H), 8.06 (d, *J* = 8.1 Hz, 1H), 7.99-7.91 (m, 3H), 7.87 (s, 1H), 7.49 (t, *J* = 7.8 Hz, 1H), 7.37 (t, *J* = 7.8 Hz, 1H), 7.30 (d, *J* = 1.8 Hz, 1H), 7.18 (d, *J* = 8.7 Hz, 2H), 7.07 (dd, *J* = 8.1 Hz, *J* = 1.8 Hz, 1H), 6.81 (d, *J* = 8.1 Hz, 1H), 3.85 (s, 3H) ppm. **^{13}C-NMR (75 MHz, d_6-DMSO)**: δ = 167.6, 153.8, 148.0, 147.9, 147.6, 139.6, 133.8, 128.9, 128.7, 126.7, 126.3, 124.5, 122.6, 121.9, 120.2, 115.5, 111.8, 108.8, 55.5 ppm. **MS (EI, 70 eV)**: *m/z* = 375 $[M]^+$. **UV/Vis (Ethanol)**: λ_{max} = 384.5 nm.

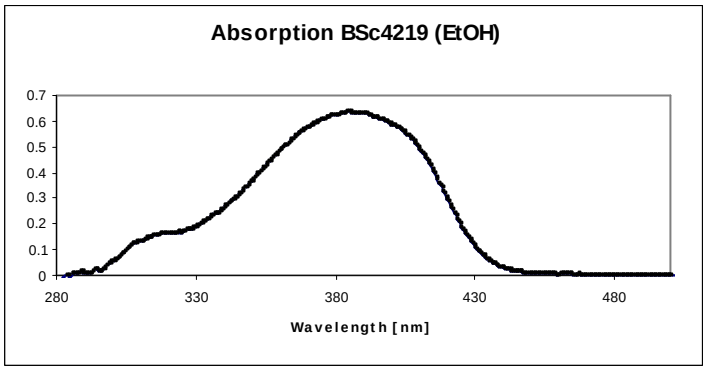

2-((2-(4-(Benzo[*d*]thiazol-2-yl)phenyl)hydrazono)methyl)-6-methoxyphenol (50d)

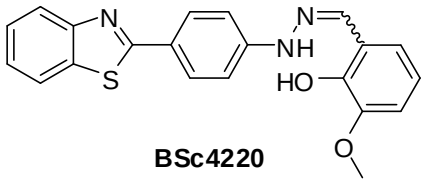

BSc4220

Yield: 53 %. **^{1}H-NMR (300 MHz, d_6-DMSO)**: δ = 10.87 (s, 1H), 9.73 (s, 1H), 8.28 (s, 1H), 8.07 (d, *J* = 7.8 Hz, 1H), 8.01-7.94 (m, 3H), 7.49 (td, *J* = 8.1 Hz, *J* = 1.2 Hz, 1H), 7.39 (td, *J* = 8.1 Hz, *J* = 1.2 Hz, 1H), 7.29 (dd, *J* = 7.8 Hz, *J* = 1.5 Hz, 1H), 7.14 (d, *J* = 8.7 Hz, 2H), 6.95 (dd, *J* = 8.1 Hz, *J* = 1.5 Hz, 1H), 6.84 (t, *J* = 7.8 Hz, 1H), 3.82 (s, 3H) ppm. **^{13}C-NMR (75 MHz, d_6-DMSO)**: δ = 167.4, 153.7, 147.8, 147.3, 145.1, 137.8, 133.8, 128.8, 126.3, 124.6, 123.2, 122.0, 120.9, 119.1, 118.2, 112.0, 111.9, 55.8 ppm. **MS (EI, 70 eV)**: *m/z* = 375 $[M]^+$. **UV/Vis (Ethanol)**: λ_{max} = 384.0 nm.

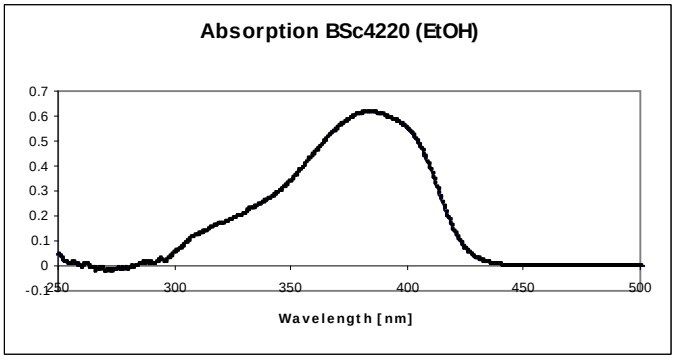

***In vitro* neuropathological staining of AD brain sections**: Tissues: hippocampus; Patient: female, 89 years old; CERAD Score: 3; NFTs-level: V.

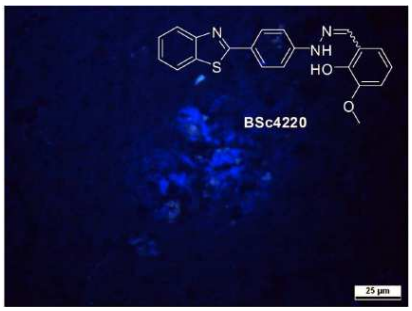

2-(4-(2-(3-Bromo-4-methoxybenzylidene)hydrazinyl)phenyl)benzo[*d*]thiazole (52e)

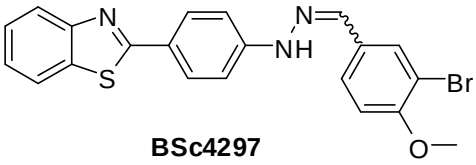

BSc4297

Yield: 80 %. **^{1}H-NMR (500 MHz, d_6-DMSO)**: δ = 10.81 (s, 1H), 8.07 (d, *J* = 8.0 Hz, 1H), 7.98-7.93 (m, 4H), 7.89 (s, 1H), 7.66 (dd, *J* = 8.5Hz, *J* = 2.0 Hz, 1H), 7.49 (td, *J* = 8.0Hz, *J* = 1.0 Hz, 1H), 7.38 (td, *J* = 8.0Hz, *J* = 1.0 Hz, 1H), 7.20 (d, *J* = 8.5 Hz, 2H), 7.17 (d, *J* = 8.5 Hz, 1H), 3.89 (s, 3H) ppm. **^{13}C-NMR (125 MHz, d_6-DMSO)**: δ = 167.5, 155.5, 153.7, 147.7, 137.2, 133.8, 129.7, 129.4, 128. 7, 126.9, 126.3, 124.5, 123.1, 121.9, 112.7, 112.0, 111.1, 56.3 ppm. **MS (EI, 70 eV)**: *m/z* = 439 [*M*+2]$^{+}$. **UV/Vis (Ethanol)**: λ_{max} = 386.0 nm.

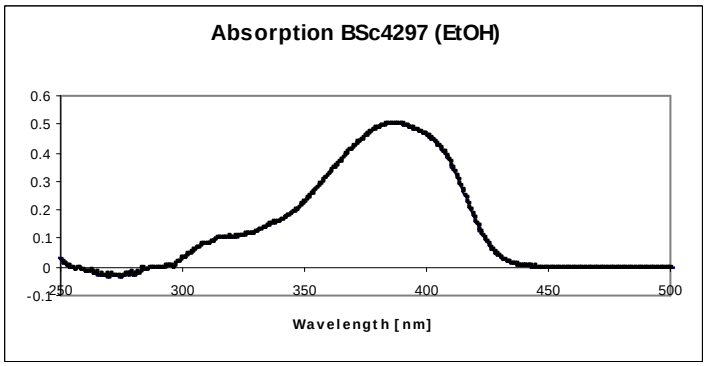

2-(4-(2-(4-Fluoro-3-methoxybenzylidene)hydrazinyl)phenyl)benzo[*d*]thiazole (52f)

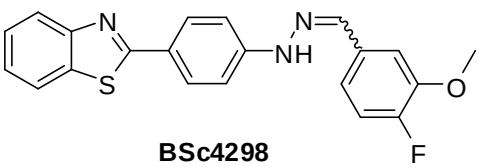

BSc4298

Yield: 78 %. **^{1}H-NMR (500 MHz, d_6-DMSO)**: δ = 10.85 (s, 1H), 8.07 (d, *J* = 8.0 Hz, 1H), 7.98-7.94 (m, 3H), 7.94 (s, 1H), 7.51-7.47 (m, 2H), 7.38 (td, *J* = 8.0Hz, *J* = 1.0 Hz, 1H), 7.27-7.21 (m, 4H), 3.93 (s, 3H) ppm. **^{13}C-NMR (125 MHz, d_6-DMSO)**: δ = 167.5, 153.7, 152.6, 150.7, 147.6, 147.4, 137.9, 133.8, 132.3, 128.6, 126.3, 124.6, 123.2, 1221.0, 119.0, 116.1, 112.1, 110.3, 55.9 ppm. **MS (EI, 70 eV)**: *m/z* = 377 $[M]^+$. **UV/Vis (Ethanol)**: λ_{max} = 383.5 nm.

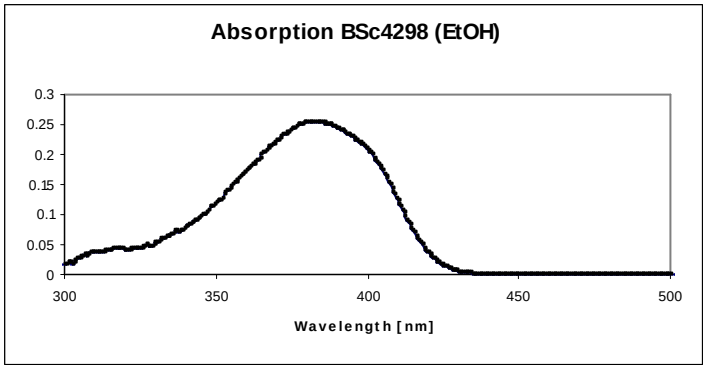

***In vitro* neuropathological staining of AD brain sections**: Tissues: hippocampus; Patient: female, 89 years old; CERAD Score: 3; NFTs-level: V.

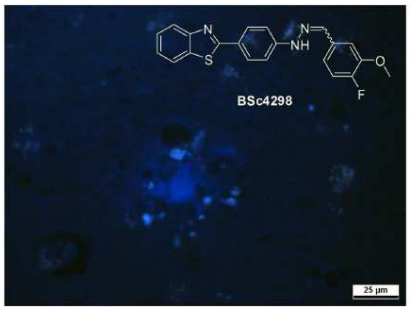

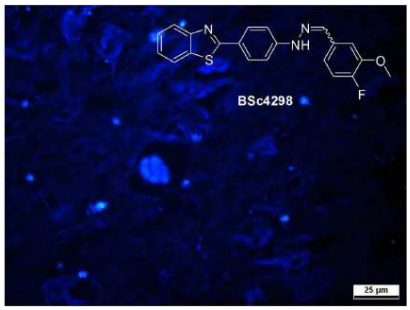

2-((2-(4-(Benzo[*d*]thiazol-2-yl)phenyl)hydrazono)methyl)-4-methylphenol (52g)

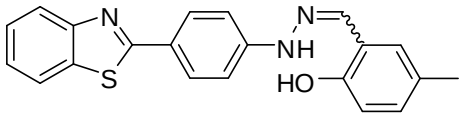

BSc4299

Yield: 50 %. **^{1}H-NMR (500 MHz, d_6-DMSO)**: δ = 10.84 (s, 1H), 10.05 (s, 1H), 8.23 (s, 1H), 8.06 (d, *J* = 8.0 Hz, 1H), 8.00-7.94 (m, 3H), 7.49 (td, *J* = 8.0 Hz, *J* = 1.0 Hz, 1H), 7.46 (d, *J* = 2.0 Hz, 1H), 7.38 (td, *J* = 8.0 Hz, *J* = 1.0 Hz, 1H), 7.13 (d, *J* = 8.5 Hz, 2H), 7.02-6.98 (m, 1H), 6.80 (d, *J* = 8.0 Hz, 1H), 2.25 (s, 3H) ppm. **^{13}C-NMR (125 MHz, d_6-DMSO)**: δ = 167.4, 153.7, 153.5, 147.3, 138.3, 133.8, 130.4, 128.8, 127.8, 126.7, 126.3, 124.6, 123.1, 120.00, 121.9, 120.1, 115.8, 111.8, 20.0 ppm. **MS (EI, 70 eV)**: *m/z* = 359 $[M]^+$. **UV/Vis (Ethanol)**: λ_{max} = 384.0 nm.

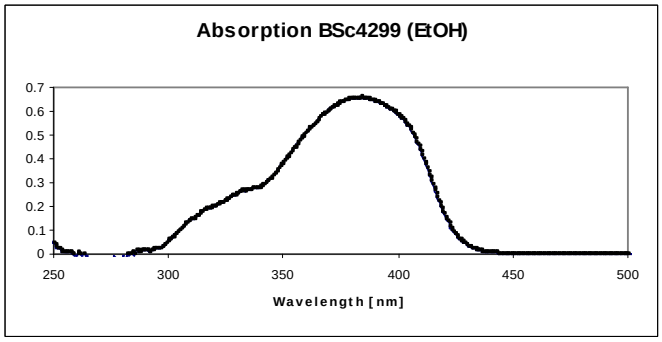

***In vitro* neuropathological staining of AD brain sections**: Tissues: hippocampus; Patient: female, 89 years old; CERAD Score: 3; NFTs-level: V.

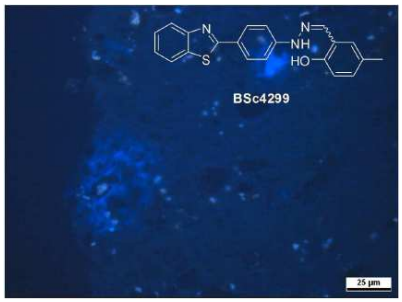

3-((2-(4-(Benzo[*d*]thiazol-2-yl)phenyl)hydrazono)methyl)phenol (52h)

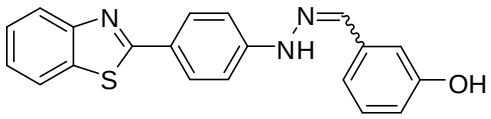

BSc4300

Yield: 61 %. **^{1}H-NMR (300 MHz, d_6-DMSO)**: δ = 10.79 (s, 1H), 9.50 (s, 1H), 8.06 (d, *J* = 8.1 Hz, 1H), 8.00-7.93 (m, 3H), 7.89 (s, 1H), 7.49 (td, *J* = 8.1 Hz, *J* = 1.2 Hz, 1H), 7.38 (td, *J* = 7.8 Hz, *J* = 1.2 Hz, 1H), 7.25-7.14 (m, 4H), 7.09 (d, *J* = 7.8 Hz, 1H), 6.78-6.72 (m, 1H) ppm. **^{13}C-NMR (75 MHz, d_6-DMSO)**: δ = 167.5, 157.5, 153.7, 147.7, 139.0, 136.5, 133.8, 129.6, 128.7, 126.3, 124.6, 123.1, 122.0, 117.5, 115.8, 112.0, 111.8 ppm. **MS (EI, 70 eV)**: *m/z* = 345 $[M]^+$. **UV/Vis (Ethanol)**: λ_{max} = 385.0 nm.

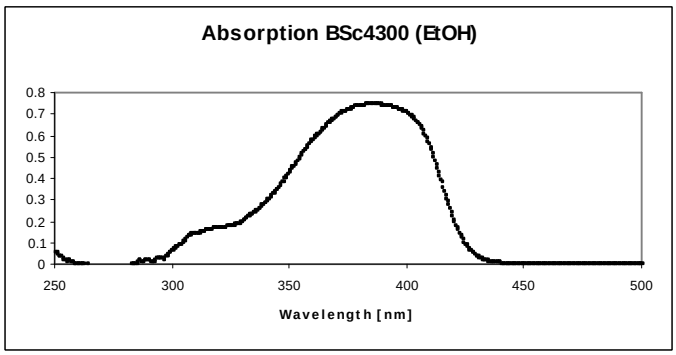

2-((2-(4-(Benzo[*d*]thiazol-2-yl)phenyl)hydrazono)methyl)-5-(diethylamino)phenol (52i)

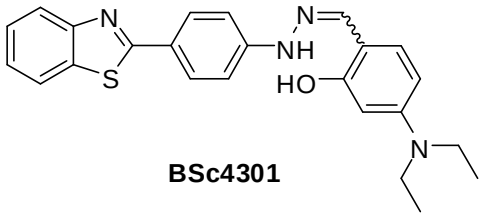

BSc4301

Yield: 81 %. **^{1}H-NMR (300 MHz, d_6-DMSO)**: δ = 10.54 (s, 1H), 10.44 (s, 1H), 8.10 (s, 1H), 8.06 (d, *J* = 8.1 Hz, 1H), 7.95 (d, *J* = 8.7 Hz, 3H), 7.49 (td, *J* = 8.1 Hz, *J* = 1.2 Hz, 1H), 7.38 (td, *J* = 8.1 Hz, *J* = 1.2 Hz, 1H), 7.29 (d, *J* = 8.7 Hz, 1H), 7.02 (d, *J* = 8.7 Hz, 2H), 6.27 (dd, *J* = 8.7 Hz, *J* = 2.4 Hz, 1H), 6.15 (d, *J* = 2.4 Hz, 1H), 3.42-3.27 (m, 4H), 1.11 (t, *J* = 7.2 Hz, 6H) ppm. **^{13}C-NMR (75 MHz, d_6-DMSO)**: δ = 167.5, 157.8, 153.8, 149.1, 147.4, 141.7, 133.8, 129.3, 128. 8, 126.2, 124.5, 122.3, 121.9, 111.2, 107.7, 103.7, 97.5, 43.7, 12.5 ppm. **MS (EI, 70 eV)**: *m/z* = 416 $[M]^+$. **UV/Vis (Ethanol)**: λ_{max} = 405.0 nm.

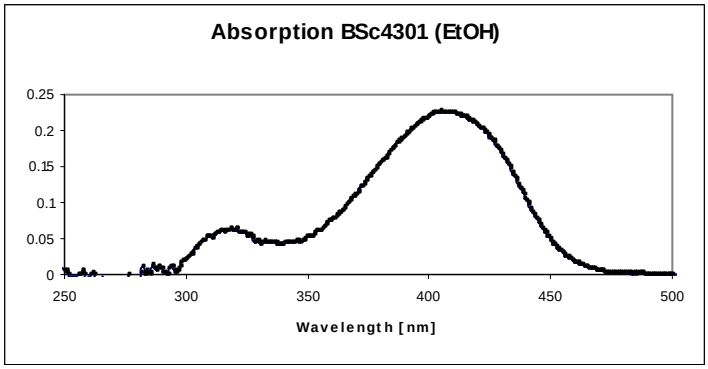

2-(4-(2-(3,5-Difluorobenzylidene)hydrazinyl)phenyl)benzo[*d*]thiazole (52j)

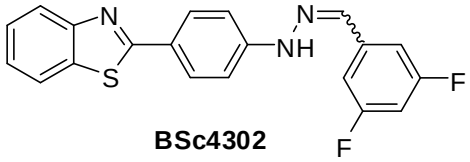

BSc4302

Yield: 80 %. **^{1}H-NMR (300 MHz, d_6-DMSO)**: δ = 11.10 (s, 1H), 8.07 (d, *J* = 7.8 Hz, 1H), 8.02-7.95 (m, 3H), 7.93 (s, 1H), 7.50 (td, *J* = 8.4 Hz, *J* = 1.2 Hz, 1H), 7.45-7.35 (m, 3H), 7.27 (d, *J* = 9.0 Hz, 2H), 7.17 (m, 1H) ppm. **^{13}C-NMR (75 MHz, d_6-DMSO)**: δ = 167.7, 164.3 (d, *J* = 13.4 Hz), 161.0(d, *J* = 13.6 Hz), 153.7, 147.2, 139.2 (t, *J* = 9.9 Hz), 136.0, 133.9, 128.6, 126.3, 124.7, 123.9, 122.0 (d, *J* = 7.1 Hz), 112.5, 108.5 (d, *J* = 25.8 Hz), 103.26 (t, *J* = 26.1 Hz) ppm. **MS (EI, 70 eV)**: *m/z* = 365 $[M]^+$. **UV/Vis (Ethanol)**: λ_{max} = 385.0 nm.

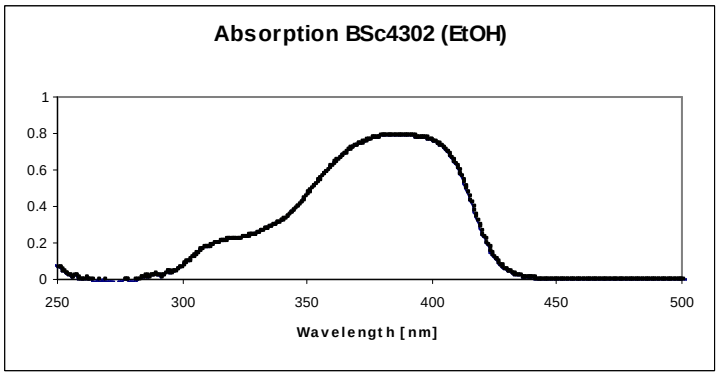

2-((2-(4-(Benzo[*d*]thiazol-2-yl)phenyl)hydrazono)methyl)phenol (52k)

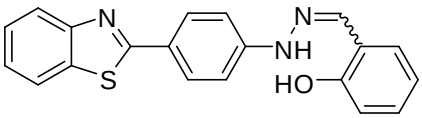

BSc4303

Yield: 68 %. **^{1}H-NMR (300 MHz, d_6-DMSO)**: δ = 10.87 (s, 1H), 10.28 (s, 1H), 8.27 (s, 1H), 8.07 (d, *J* = 7.8 Hz, 1H), 8.02-7.93 (m, 3H), 7.66 (dd, *J* = 7.8 Hz, *J* = 1.5 Hz, 1H), 7.49 (td, *J* = 8.1 Hz, *J* = 1.2 Hz, 1H), 7.38 (td, *J* = 8.1 Hz, *J* = 1.2 Hz, 1H), 7.24-7.11 (m, 3H), 6.93-6.85 (m, 2H) ppm. **^{13}C-NMR (75 MHz, d_6-DMSO)**: δ = 167.4, 155.6, 153.7, 147.3, 138.1, 133.8, 129.7, 128.8, 126.7, 126.3, 124.6, 123.2, 122.0, 121.9, 120.5, 119.4, 115.9, 111.8 ppm. **MS (EI, 70 eV)**: *m/z* = 345 $[M]^+$. **UV/Vis (Ethanol)**: λ_{max} = 384.5 nm.

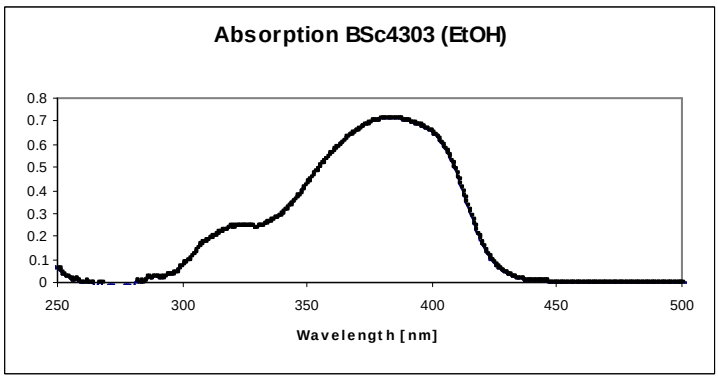

4-((2-(4-(Benzo[*d*]thiazol-2-yl)phenyl)hydrazono)methyl)-2,6-difluorophenol (52l)

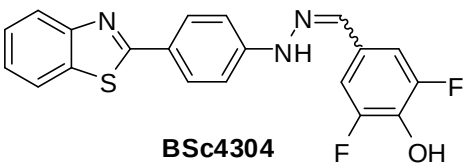

BSc4304

Yield: 61 %. **^{1}H-NMR (300 MHz, d_6-DMSO)**: δ = 10.87 (s, 1H), 10.47 (s, 1H), 8.07 (d, *J* = 7.2 Hz, 1H), 7.99-7.92 (m, 3H), 7.84 (s, 1H), 7.50 (td, *J* = 8.4 Hz, *J* = 1.5 Hz, 1H), 7.42-7.34 (m, 3H), 7.21 (d, *J* = 8.7 Hz, 2H) ppm. **^{13}C-NMR (75 MHz, d_6-DMSO)**: δ = 167.5, 154.0 (d, *J* = 7.5 Hz), 153.7, 150.8, 147.6, 136.8, 133.9 (d, *J* = 16.4 Hz), 133.8, 128.7, 126.3 (d, *J* = 8.6 Hz), 124.6, 123.2, 122.0 (d, *J* = 2.4 Hz), 109.3, 109.2 ppm. **MS (EI)**: *m/z* = 381 $[M]^+$. **UV/Vis (Ethanol)**: λ_{max} = 386.0 nm.

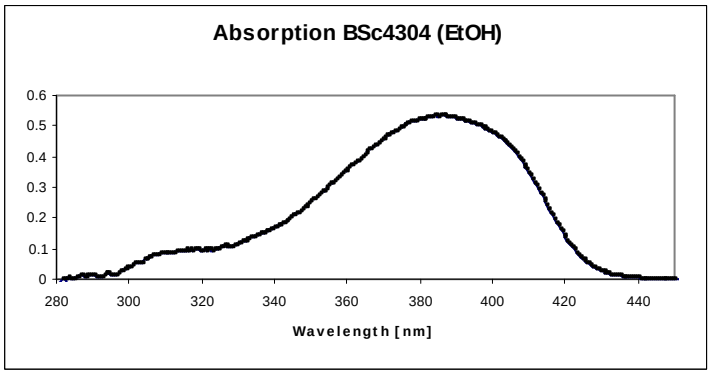

***In vitro* neuropathological staining of AD brain sections**: Tissues: hippocampus; Patient: female, 89 years old; CERAD Score: 3; NFTs-level: V.

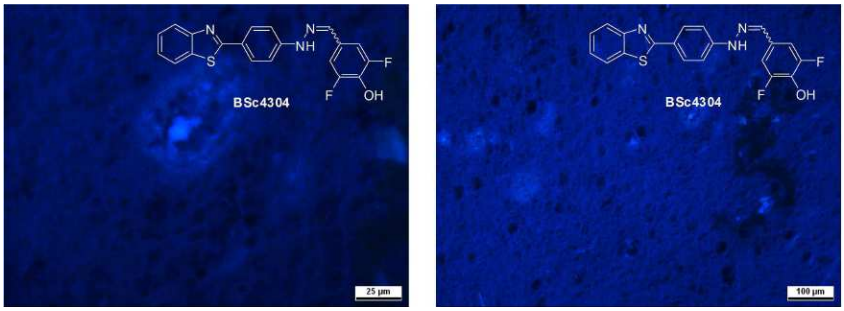

2-(4-(2-((1*H*-Indol-3-yl)methylene)hydrazinyl)phenyl)benzo[*d*]thiazole (52m)

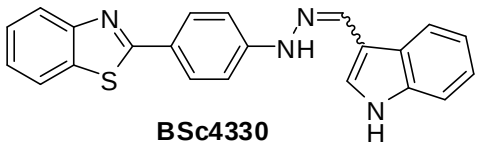

BSc4330

Yield: 52 %. **^{1}H-NMR (500 MHz, d_6-DMSO)**: δ = 11.43 (s, 1H), 10.44 (s, 1H), 8.30-8.25 (m, 1H), 8.22 (s, 1H), 8.06 (d, *J* = 8.0, 1H), 7.97 (d, *J* = 9.0, 2H), 7.94 (d, *J* = 8.0, 1H), 7.72 (d, *J* = 2.0 Hz, 1H), 7.52-7.34 (m, 3H), 7.25-7.14 (m, 4H) ppm. **^{13}C-NMR (125 MHz, d_6-DMSO)**: δ = 167.8, 153.9, 148.4, 146.2, 137.3, 137.0, 133.8, 128.9, 128.4, 126.3, 124.5, 124.2, 122.4, 121.9, 121.9, 121.6, 120.2, 112.4, 111.8, 111.4 ppm. **MS (EI, 70 eV)**: *m/z* = 368 $[M]^+$. **UV/Vis (Ethanol)**: λ_{max} = 398.0 nm.

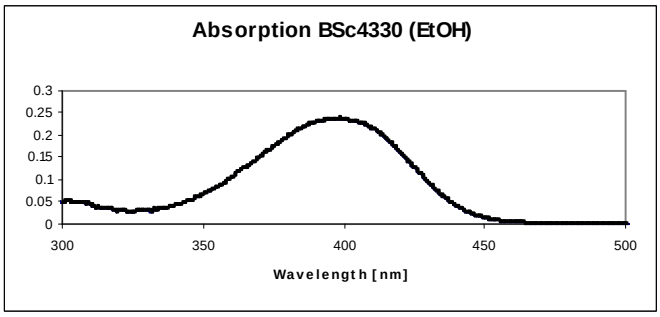

***In vitro* neuropathological staining of AD brain sections**: Tissues: hippocampus; Patient: female, 89 years old; CERAD Score: 3; NFTs-level: V.

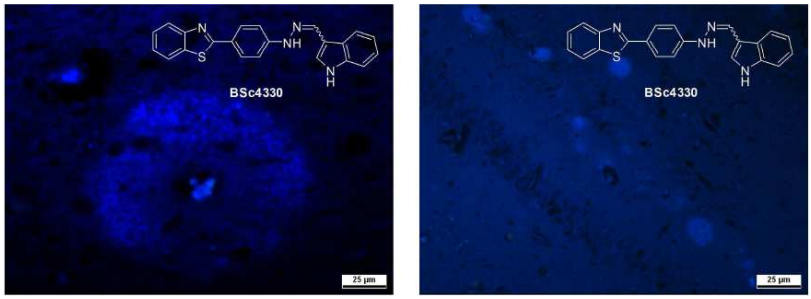

2-(4-(2-((1-Methyl-1H-indol-3-yl)methylene)hydrazinyl)phenyl)benzo[*d*]thiazole (52n)

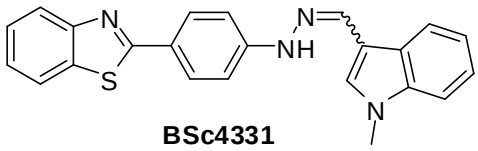

BSc4331

Yield: 48 %. **^{1}H-NMR (500 MHz, d_6-DMSO)**: δ = 11.45 (s, 1H), 8.29 (d, *J* = 7.5, 1H), 8.19 (s, 1H), 8.05 (d, *J* = 7.5, 1H), 7.97 (d, *J* = 8.5, 2H), 7.94 (d, *J* = 8.0, 1H), 7.71 (s, 1H), 7.52-7.45 (m, 2H), 7.37 (td, *J* = 8.0 Hz, *J* = 1.0 Hz, 1H), 7.28 (td, *J* = 8.0 Hz, *J* = 1.0 Hz, 1H), 7.24 (td, *J* = 8.0 Hz, *J* = 1.0 Hz, 1H), 7.17 (d, *J* = 8.5 Hz, 2H), 3.82 (s, 3H) ppm. **^{13}C-NMR (125 MHz, d_6-DMSO)**: δ = 167.7, 153.8, 148.3, 137.4, 136.6, 133.7, 130.0, 128.8, 126.2, 124.5, 124.4, 122.4, 121.9, 121.9, 121.8, 121.7, 120.4, 111.3, 110.0, 32.6 ppm. **MS (EI, 70 eV)**: *m/z* = 382 $[M]^+$. **UV/Vis (Ethanol)**: λ_{max} = 397.0 nm.

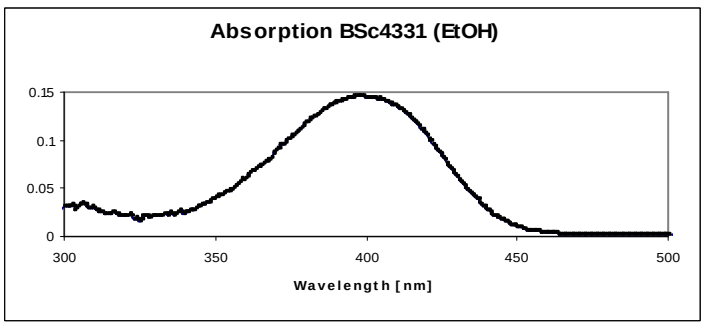

2-(4-(2-(4-(Methylthio)benzylidene)hydrazinyl)phenyl)benzo[*d*]thiazole (52o)

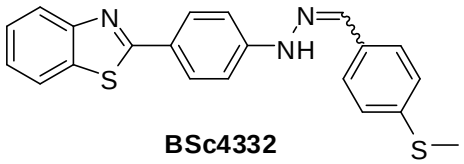

BSc4332

Yield: 71 %. **^{1}H-NMR (500 MHz, d_6-DMSO)**: δ = 10.96 (s, 1H), 8.06 (d, *J* = 7.5, 1H), 7.98-7.93 (m, 4H), 7.63 (d, *J* = 8.5, 2H), 7.49 (td, *J* = 8.5 Hz, *J* = 1.5 Hz, 1H), 7.38 (td, *J* = 8.5 Hz, *J* = 1.5 Hz, 1H), 7.29 (d, *J* = 8.5 Hz, 2H), 7.21 (d, *J* = 9.0 Hz, 2H), 2.51 (s, 3H) ppm. **^{13}C-NMR (125 MHz, d_6-DMSO)**: δ = 167.5, 153.7, 147.7, 138.6, 138.4, 133.8, 131.9, 128.6, 126.3, 126.3, 125.8, 124.5, 123.0, 121.9, 112.0, 14.4 ppm. **MS (EI, 70 eV)**: *m/z* = 375 $[M]^+$. **UV/Vis (Ethanol)**: λ_{max} = 393.5 nm.

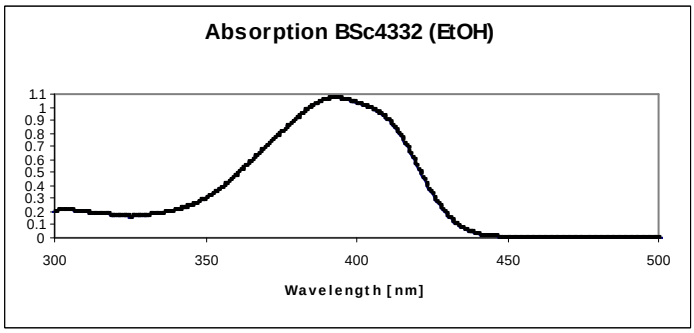

***In vitro* neuropathological staining of AD brain sections**: Tissues: hippocampus; Patient: female, 89 years old; CERAD Score: 3; NFTs-level: V.

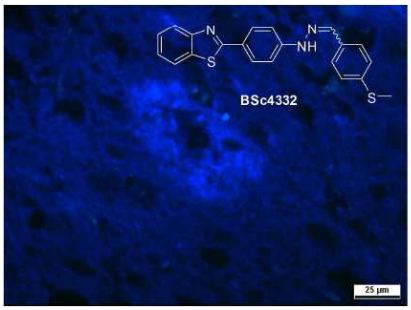

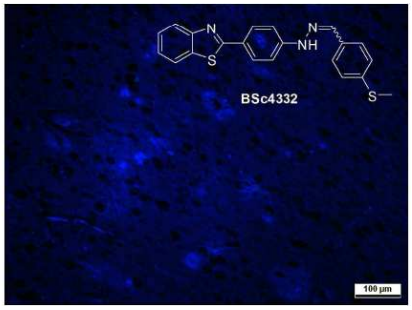

2-(4-(2-((1-Methyl-1H-pyrrol-2-yl)methylene)hydrazinyl)phenyl)benzo[*d*]thiazole (52p)

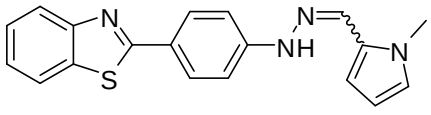

BSc4333

Yield: 44 %. **^{1}H-NMR (500 MHz, d_6-DMSO)**: δ = 10.49 (s, 1H), 8.04 (d, *J* = 8.0, 1H), 7.96-7.90 (m, 4H), 7.48 (td, *J* = 8.0 Hz, *J* = 1.0 Hz, 1H), 7.37 (td, *J* = 8.0 Hz, *J* = 1.0 Hz, 1H), 7.09

(d, *J* = 8.5 Hz, 2H), 6.90 (t, *J* = 2.0 Hz, 1H), 6.40-6.37 (m, 1H), 6.08-6.06 (m, 1H), 3.90 (s, 3H) ppm. **^{13}C-NMR (125 MHz, d_6-DMSO)**: δ = 167.6, 153.8, 148.0, 133.8, 133.2, 128.7, 126.7, 124.4, 122.3, 121.9, 112.5, 111.6, 107.8, 36.2 ppm. **MS (EI, 70 eV)**: *m/z* = 332 $[M]^+$. **UV/Vis (Ethanol)**: λ_{max} = 396.0 nm.

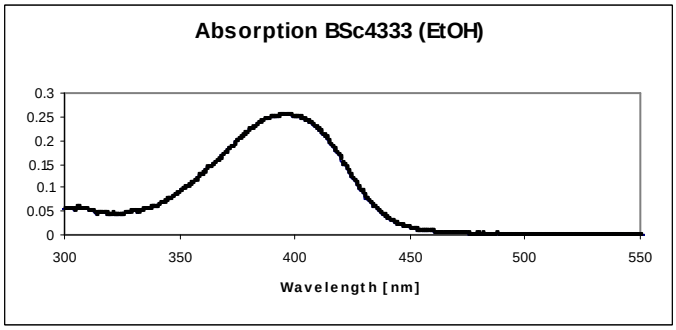

***In vitro* neuropathological staining of AD brain sections**: Tissues: hippocampus; Patient: female, 89 years old; CERAD Score: 3; NFTs-level: V.

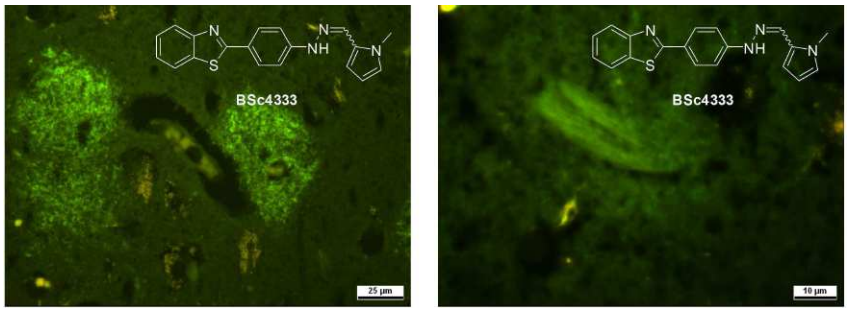

2-(4-(2-((5-Bromothiophen-2-yl)methylene)hydrazinyl)phenyl)benzo[*d*]thiazole (52q)

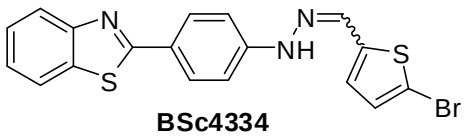

BSc4334

Yield: 73 %. **^{1}H-NMR (500 MHz, d_6-DMSO)**: δ = 11.04 (s, 1H), 8.10 (s, 1H), 8.06 (d, *J* = 7.5 Hz, 1H), 7.96 (d, *J* = 8.5, 3H), 7.49 (td, *J* = 8.0 Hz, *J* = 1.0 Hz, 1H), 7.38 (td, *J* = 8.0 Hz, *J* = 1.0 Hz, 1H), 7.20 (d, *J* = 4.0 Hz, 1H), 7.15-7.11 (m, 3H) ppm. **^{13}C-NMR (125 MHz, d_6-DMSO)**: δ = 167.4, 153.7, 147.1, 142.2, 133.8, 133.3, 131.0, 128.7, 127.9, 126.3, 124.6, 123.4, 122.0, 121.9, 112.1, 111.9 ppm. **MS (EI, 70 eV)**: *m/z* = 415 $[M+2]^+$. **UV/Vis (Ethanol)**: λ_{max} = 398.5 nm.

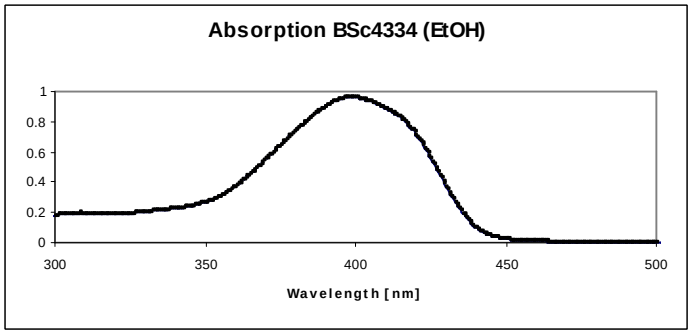

***In vitro* neuropathological staining of AD brain sections**: Tissues: hippocampus; Patient: female, 89 years old; CERAD Score: 3; NFTs-level: V.

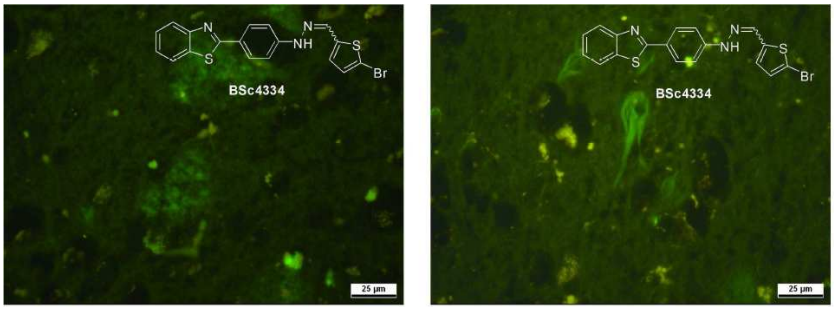

2-(4-(2-(2,2'-Bithiophen-5-ylmethylene)hydrazinyl)phenyl)benzo[*d*]thiazole (52r)

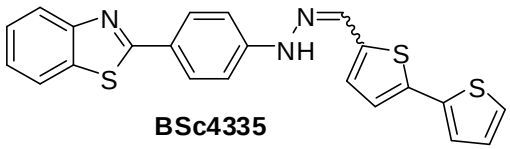

BSc4335

Yield: 66 %. **^{1}H-NMR (500 MHz, d_6-DMSO)**: δ = 11.14 (s, 1H), 8.17 (s, 1H), 8.06 (d, *J* = 8.0 Hz, 1H), 7.99-7.94 (m, 3H), 7.54 (dd, *J* = 5.0 Hz, *J* = 1.0 Hz, 1H), 7.49 (td, *J* = 8.0 Hz, *J* = 1.0 Hz, 1H), 7.40-7.36 (m, 2H), 7.26 (d, *J* = 4.0 Hz, 1H), 7.24 (d, *J* = 4.0 Hz, 1H), 7.17 (d, *J* = 9.0 Hz, 2H), 7.13-7.10 (m, 1H) ppm. **^{13}C-NMR (125 MHz, d_6-DMSO)**: δ = 167.5, 153.7, 147.2, 139.1, 136.4, 136.3, 133.8, 128.7, 128.6, 128.4, 126.3, 125.7, 124.6, 124.3, 124.2, 123.3, 120.0, 121.9, 112.0 ppm. **MS (EI, 70 eV)**: *m/z* = 417 $[M]^+$. **UV/Vis (Ethanol)**: λ_{max} = 420.5 nm.

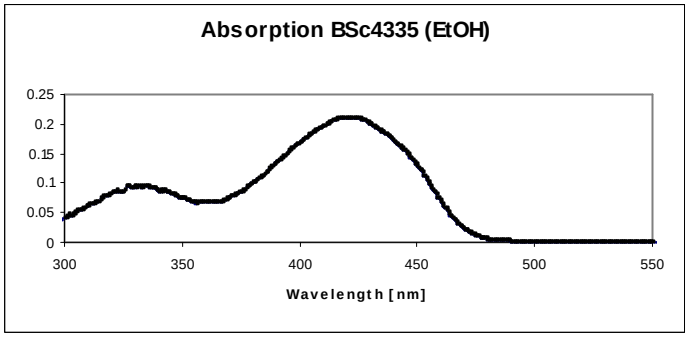

***In vitro* neuropathological staining of AD brain sections**: Tissues: hippocampus; Patient: female, 89 years old; CERAD Score: 3; NFTs-level: V.

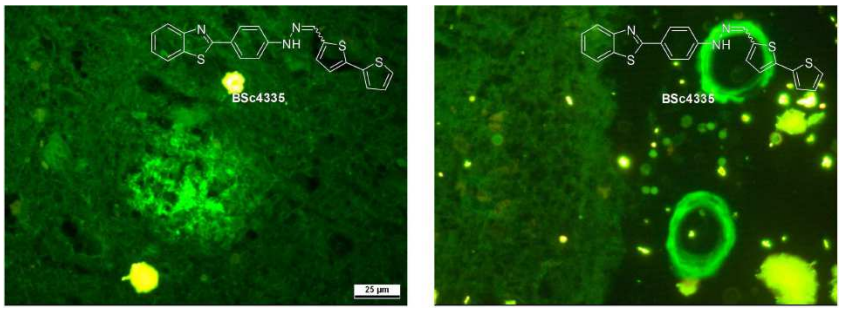

4-((2-(4-(Benzo[*d*]thiazol-2-yl)phenyl)hydrazono)methyl)-5-(hydroxymethyl)-2-methylpyridin-3-ol (52s)

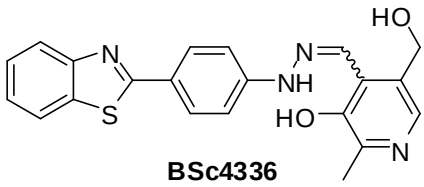

BSc4336

Yield: 75 %. **^{1}H-NMR (500 MHz, d_6-DMSO)**: δ = 11.42 (s, 1H), 11.26 (s, 1H), 8.52 (s, 1H), 8.09 (d, *J* = 7.5 Hz, 1H), 8.05 (d, *J* = 9.0 Hz, 2H), 7.99 (d, *J* = 7.5 Hz, 1H), 7.96 (s, 1H), 7.50 (td, *J* = 8.0 Hz, *J* = 1.0 Hz, 1H), 7.40 (td, *J* = 8.0 Hz, *J* = 1.0 Hz, 1H), 7.12 (d, *J* = 9.0 Hz, 2H), 5.34 (t, *J* = 5.5 Hz, 1H), 4.63 (d, *J* = 5.5 Hz, 2H), 2.44 (s, 3H) ppm. **^{13}C-NMR (125 MHz, d_6-DMSO)**: δ = 167.1, 153.7, 149.2, 146.4, 145.8, 139.0, 138.4, 133.9, 131.3, 129.0, 126.3, 124.8, 124.5, 122.1, 122.0, 121.3, 112.2, 59.0, 18.8 ppm. **MS (EI, 70 eV)**: *m/z* = 390 $[M]^+$. **UV/Vis (Ethanol)**: λ_{max} = 394.0 nm.

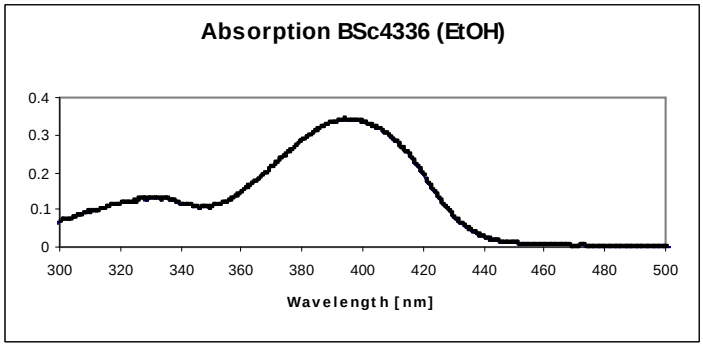

2-(4-(2-(Pyridin-3-ylmethylene)hydrazinyl)phenyl)benzo[*d*]thiazole (52t)

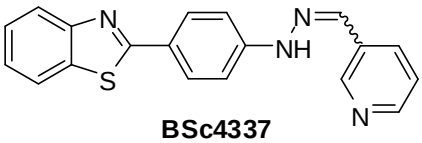

BSc4337

Yield: 78 %. **^{1}H-NMR (500 MHz, d_6-DMSO)**: δ = 11.06 (s, 1H), 8.85 (d, *J* = 2.0 Hz, 1H), 8.51 (dd, *J* = 5.0 Hz, *J* = 2.0 Hz, 1H), 8.12 (dt, *J* = 8.0 Hz, *J* = 2.0 Hz, 1H), 8.07 (d, *J* = 8.0 Hz, 1H), 8.00-7.95 (m, 4H), 7.50 (td, *J* = 8.0 Hz, *J* = 1.0 Hz, 1H), 7.46-7.42 (m, 1H), 7.39 (td, *J* = 8.0 Hz, *J* = 1.0 Hz, 1H), 7.25 (d, *J* = 8.5 Hz, 2H) ppm. **^{13}C-NMR (125 MHz, d_6-DMSO)**: δ = 167.4, 153.7, 149.0, 147.6, 147.3, 135.6, 133.8, 132.2, 131.1, 128.7, 126.3, 124.6, 123.7, 123.6, 122.0, 121.9, 112.3 ppm. **MS (EI, 70 eV)**: *m/z* = 330 $[M]^+$. **UV/Vis (Ethanol)**: λ_{max} = 387.0 nm.

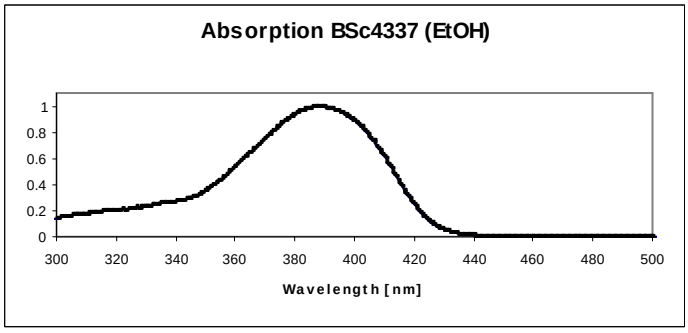

***In vitro* neuropathological staining of AD brain sections**: Tissues: hippocampus; Patient: female, 89 years old; CERAD Score: 3; NFTs-level: V.

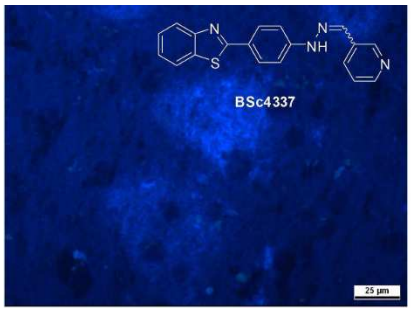

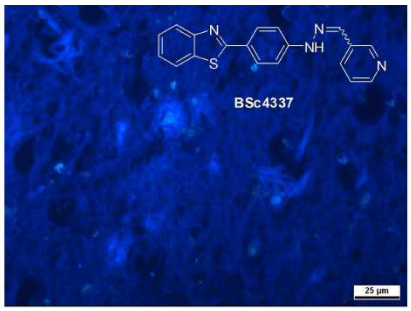

2-(4-(2-((9-Methyl-9*H*-carbazol-3-yl)methylene)hydrazinyl)phenyl)benzo[*d*]thiazole (52u)

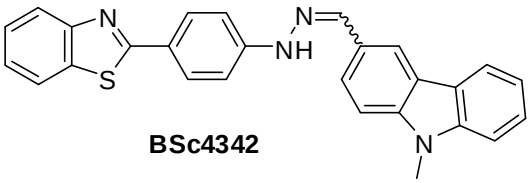

BSc4342

Yield: 67 %. **^{1}H-NMR (500 MHz, d_6-DMSO)**: δ= 10.86 (s, 1H), 8.43 (s, 1H), 8.24 (d, *J* = 8.0 Hz, 1H), 8.18 (s, 1H), 8.07 (d, *J* = 8.0 Hz, 1H), 7.97 (d, *J* = 9.0 Hz, 2H), 7.96 (d, *J* = 8.0 Hz, 1H), 7.92 (dd, *J* = 8.5 Hz, *J* = 1.5 Hz, 1H), 7.65 (d, *J* = 8.5 Hz, 1H), 7.61 (d, *J* = 8.5 Hz, 1H), 7.52-7.47 (m, 2H), 7.38 (td, *J* = 8.0 Hz, *J* = 1.0 Hz, 1H), 7.28-7.23 (m, 3H), 3.91 (s, 3H) ppm. **^{13}C-NMR (125 MHz, d_6-DMSO)**: δ= 167.6, 153.8, 148.1, 140.9, 140.8, 140.4, 133.8, 128.7, 126.4, 126.2, 125.9, 124.5, 123.8, 123.7, 122.5, 122.1, 121.9, 121.5, 120.4, 119.4, 118.7, 111.8, 109.5, 109.3, 29.0 ppm. **MS (EI, 70 eV)**: *m/z* = 432 $[M]^+$. **UV/Vis (Ethanol)**: λ_{max} = 387.0 nm.

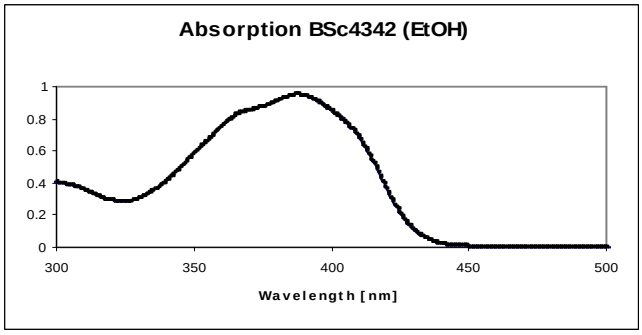

***In vitro* neuropathological staining of AD brain sections**: Tissues: hippocampus; Patient: female, 89 years old; CERAD Score: 3; NFTs-level: V.

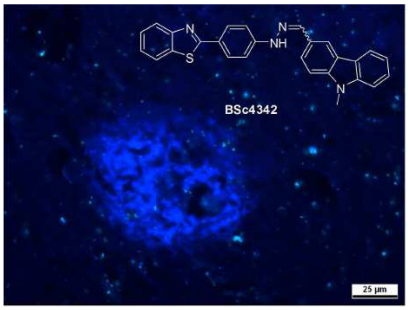

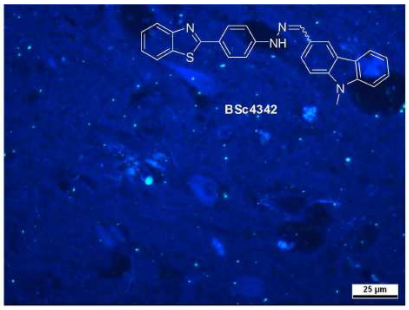

4-(3-(2-(4-(Benzo[*d*]thiazol-2-yl)phenyl)hydrazono)prop-1-enyl)-*N*,*N*-dimethylaniline (52v)

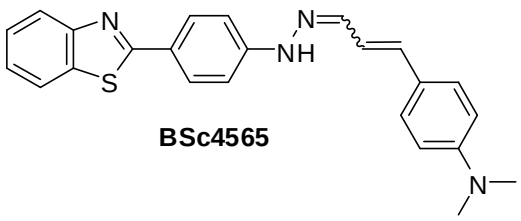

BSc4565

Yield: 46 %. **^{1}H-NMR (500 MHz, d_6-DMSO)**: δ = 10.60 (s, 1H), 8.06 (d, *J* = 7.5 Hz, 1H), 7.95-7.91 (m, 3H), 7.76 (d, *J* = 7.5 Hz, 1H), 7.48 (td, *J* = 8.5 Hz, *J* = 1.5 Hz, 1H), 7.42-7.35 (m, 3H), 7.09 (d, *J* = 8.5 Hz, 2H), 6.80-6.76 (m, 2H), 6.70 (d, *J* = 9.0 Hz, 2H), 2.94 (s, 6H) ppm.

^{13}C-NMR (125 MHz, d_6-DMSO): δ = 167.5, 156.1, 153.7, 150.1, 142.7, 135.5, 132.8, 128.6, 128.5, 127.7, 126.2, 125.2, 124.3, 122.6, 121.9, 121.3, 112.0, 111.7 ppm. **MS (EI, 70 eV)**: *m/z* = 398 $[M]^+$. **UV/Vis (Ethanol)**: λ_{max} = 412.5 nm.

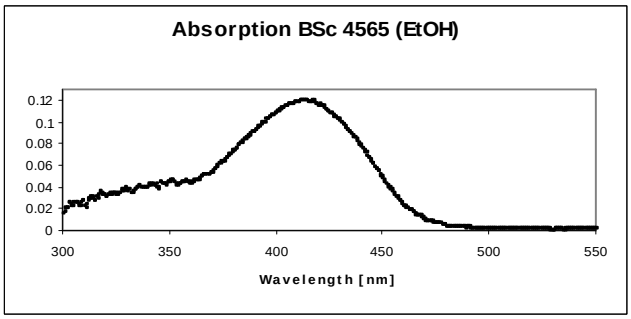

***In vitro* neuropathological staining of AD brain sections**: Tissues: hippocampus; Patient: female, 89 years old; CERAD Score: 3; NFTs-level: V.

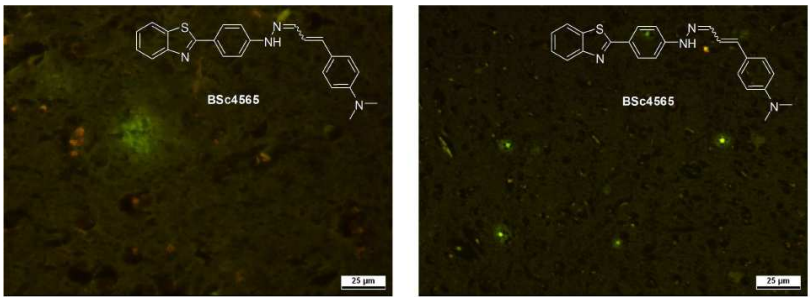

6.3. Synthesis of imidazo[1,2-*a*]pyridines and imidazo[1,2-*a*]pyrimidines derivatives

6.3.1. General procedures for synthesis of imidazo[1,2-*a*]pyridines derivatives

2-(4-Nitrophenyl)imidazo[1,2-*a*]pyridine (55)

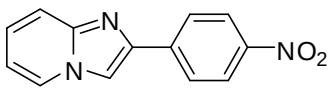

A mixture of 2-aminopyridine (0.94 g, 10.0 mmol, 1.0 eq) and α-bromoketone (2.44 g, 10.0 mmol, 1.0 eq) was refluxed in ethanol (40 mL) overnight. The solvent was evaporated *in vacuo*. 5 N NaOH was added to adjust pH > 10, precipitates were filtered off and washed with brine and cooled ethyl acetate. The compound was dried under the high vacuum pump and 2.26 g of 2-(4-nitrophenyl)imidazo[1,2-*a*]pyridine was obtained as yellow solid.

Yield: 95 %. **^{13}C-NMR (125 MHz, d_6-DMSO)**: δ = 146.4, 141.9, 140.4, 127.2, 126.2, 125.9, 124.1, 116.9, 112.9, 111.6 ppm. **MS (EI, 70 eV)**: *m/z* = 239 $[M]^+$.

4-(Imidazo[1,2-*a*]pyridin-2-yl)aniline (56)

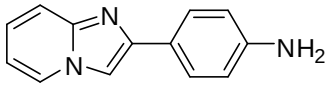

BSc4485

To a suspension of 2-(4-nitrophenyl)imidazo[1,2-*a*]pyridine (2.39 g, 10 mmol, 1.0 eq) in 20 ml ethanol, $SnCl_2$ (9.48 g, 50 mmol, 5.0 eq) were added. The mixture was heated to reflux temperature overnight. After cooling down to room temperature, the solvent was evaporated *in vacuo*. 5 N NaOH was added to adjust pH > 10. The mixture was extracted with ethyl acetate and washed with brine (3 x 30 mL), dried over Na_2SO_4. After filtration, the solution was evaporated to obtain 2.09 g of 4-(imidazo[1,2-*a*]pyridin-2-yl)aniline as yellow solid (yield: quant.).

^{1}H-NMR (500 MHz, d_6-DMSO): δ = 8.43 (dt, *J* = 6.5 Hz, *J* = 1.0 Hz, 1H), 8.10 (s, 1H), 7.62 (dt, *J* = 8.5 Hz, *J* = 2.0 Hz, 2H), 7.48 (dd, *J* = 9.0 Hz, *J* = 0.5 Hz, 1H), 7.20-7.15 (m, 1H), 6.82 (td, *J* = 6.5 Hz, *J* = 1.0 Hz, 1H), 6.62 (dt, *J* = 8.5 Hz, *J* = 2.0 Hz, 2H), 5.22-5.17 (m, 2H) ppm. **^{13}C-NMR (125 MHz, d_6-DMSO)**: δ = 148.6, 145.6, 144.7, 126.7, 126.5, 124.4, 121.6, 116.0, 114.0, 111.9, 106.8 ppm. **MS (EI, 70 eV)**: *m/z* = 209 $[M]^+$. **UV/Vis (Ethanol)**: λ_{max} = 340.5 nm.

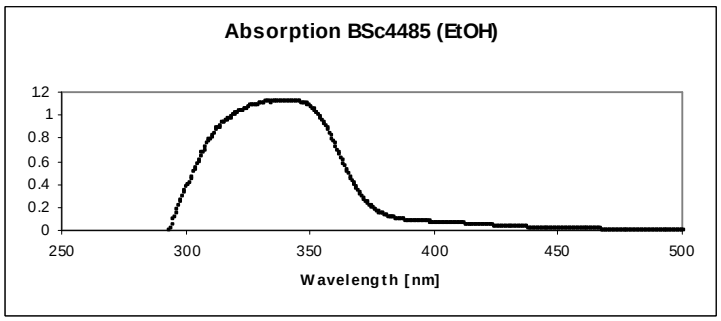

***In vitro* neuropathological staining of AD brain sections**: Tissues: hippocampus; Patient: female, 89 years old; CERAD Score: 3; NFTs-level: V.

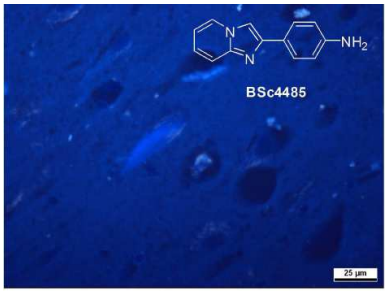

2,2,2-Trifluoro-*N*-(4-(imidazo[1,2-*a*]pyridin-2-yl)phenyl)acetamide (57)

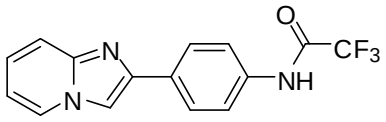

BSc4436

To a solution of 4-(imidazo[1,2-*a*]pyridin-2-yl)aniline (209 mg, 1 mmol, 1.0 eq) in 1 mL trifluoroacetic acid (TFA) was added trifluoroacetic anhydride (TFAA) (424 mg, 2.2 mmol, 2.2 eq) under ice-bath. The resulting solution was stirred at room temperature overnight and the reaction mixture was added into ice-water. The residue were collected by filtration, and washed with brine (2 x 30 mL). The residue was purified by recrystallization to afford the 2,2,2-trifluoro-*N*-(4-(imidazo[1,2-*a*]pyridin-2-yl)phenyl)acetamide 261 mg.

Yield: 86 %. **^{1}H-NMR (500 MHz, d_6-DMSO)**: δ = 11.32 (s, 1H), 8.52 (dt, *J* = 7.0 Hz, *J* = 1.0 Hz, 1H), 8.38 (s, 1H), 8.00 (d, *J* = 9.0 Hz, 2H), 7.75 (d, *J* = 9.0 Hz, 2H), 7.57 (dd, *J* = 9.0 Hz, *J* = 1.0 Hz, 1H), 7.27-7.22 (m, 1H), 6.89 (td, *J* = 7.0 Hz, *J* = 1.5 Hz, 1H) ppm. **^{13}C-NMR (125 MHz, d_6-DMSO)**: δ = 154.5, 154.5, 144.8, 143.6, 135.9, 131.2, 126.8, 126.0, 124.9, 121.1, 116.5, 112.2, 109.0 ppm. **MS (EI, 70 eV)**: *m/z* = 305 $[M]^+$. **UV/Vis (Ethanol)**: λ_{max} = 418.0 nm.

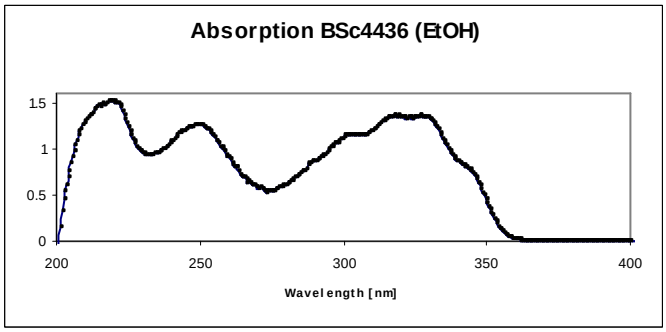

***In vitro* neuropathological staining of AD brain sections**: Tissues: hippocampus; Patient: female, 89 years old; CERAD Score: 3; NFTs-level: V.

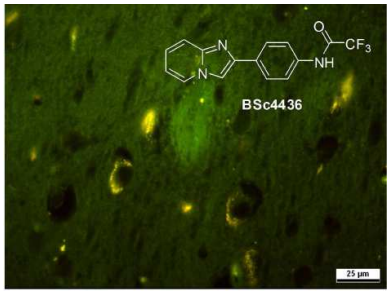

4-(Imidazo[1,2-*a*]pyridin-2-yl)-*N*-(2,2,2-trifluoroethyl)aniline (58)

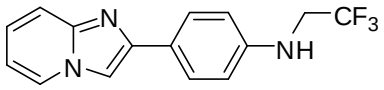

BSc4439

A solution of 2,2,2-trifluoro-*N*-(4-(imidazo[1,2-*a*]pyridin-2-yl)phenyl)acetamide (305 mg, 1 mmol, 1.0 eq) in anhydrous THF (0.5 mL) was added dropwise to an ice-cooled suspension of $LiAlH_4$ (152 mg, 4 mmol, 4.0 eq) in THF (0.5 mL). The reaction mixture was refluxed overnight. After cooled in ice-bath, the mixture was alkalized with 10% NaOH solution and extracted with ethyl acetate. The organic layer was washed with brine and dried over Na_2SO_4. After filtration, the solvent was evaporated. The residue was purified by column chromatography (SiO_2; dichloromethane: methanol = 10:1) to furnish 276 mg of 4-(imidazo[1,2-*a*]pyridin-2-yl)-*N*-(2,2,2-trifluoroethyl)aniline.

Yield: 95 %. **^{1}H-NMR (500 MHz, d_6-DMSO)**: δ = 8.46 (dt, *J* = 7.0 Hz, *J* = 1.0 Hz, 1H), 8.17 (s, 1H), 7.73 (d, *J* = 9.0 Hz, 2H), 7.50 (dd, *J* = 9.0 Hz, *J* = 0.5 Hz, 1H), 7.20-7.15 (m, 1H), 6.83 (td, *J* = 7.0 Hz, *J* = 1.5 Hz, 1H), 6.80 (d, *J* = 9.0 Hz, 2H), 6.37 (t, *J* = 7.0 Hz, 1H), 4.00-3.91 (m, 2H) ppm. **^{13}C-NMR (125 MHz, d_6-DMSO)**: δ = 147.2, 145.1, 144.5, 126.5, 126.4, 124.1, 123.0, 116.0, 112.4, 111.7, 107.0, 44.1, 43.8 ppm. **MS (EI, 70 eV)**: *m/z* = 291 $[M]^+$. **UV/Vis (Ethanol)**: λ_{max} = 333.5 nm.

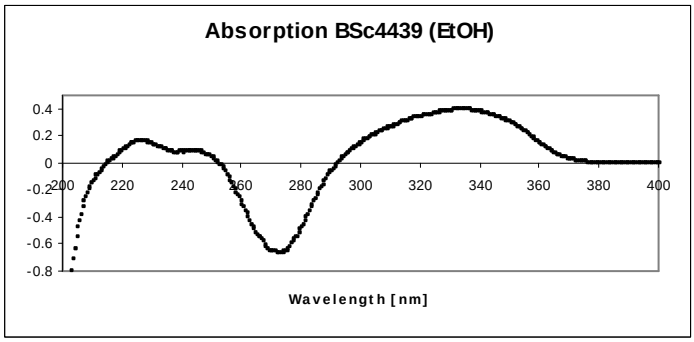

Method A of [8+2] cycloaddition reaction

Under the protection of inert gas, bromobenzene (15.7 mg, 0.1 mmol, 1.0 eq) was added to a mixture of corresponding substrates (0.1 mmol, 1.0 eq), *t*-BuOK (22.4 mg, 0.2 mmol, 2 eq) in 2 ml acetonitrile. The reaction was refluxed overnight. The resulting mixture was dissolved in ethyl acetate and washed with brine (2 x 30 mL). The solvent was evaporated *in vacuo*, and the residue was purified by flash chromatography (SiO_2; ethyl acetate: cyclohexane = 1:2) to obtain pure [8+2] cycloaddition products **61** and **62**.

1-(4-(2,2,2-Trifluoroacetyl)phenyl)benzo[*a*]imidazo[5,1,2-*cd*]indolizine (61)

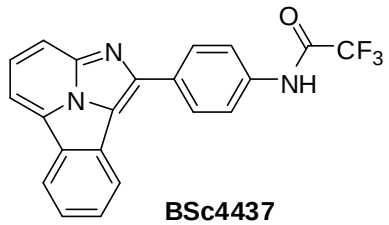

BSc4437

Yield: 45 %. **^{1}H-NMR (500 MHz, d_6-DMSO)**: δ = 11.53 (s, 1H), 8.70 (d, *J* = 8.0 Hz, 1H), 8.62 (d, *J* = 8.0 Hz, 1H), 8.47-8.43 (m, 3H), 8.19 (d, *J* = 8.0 Hz, 1H), 8.12 (dd, *J* = 8.5 Hz, *J* = 7.5 Hz, 1H), 8.03 (d, *J* = 8.5 Hz, 2H), 7.91 (td, *J* = 8.5 Hz, *J* = 1.0 Hz, 1H), 7.75 (td, *J* = 8.5 Hz, *J* = 1.0 Hz, 1H) ppm. **MS (EI, 70 eV)**: *m/z* = 379 $[M]^+$. **UV/Vis (Ethanol)**: λ_{max} = 418.0 nm.

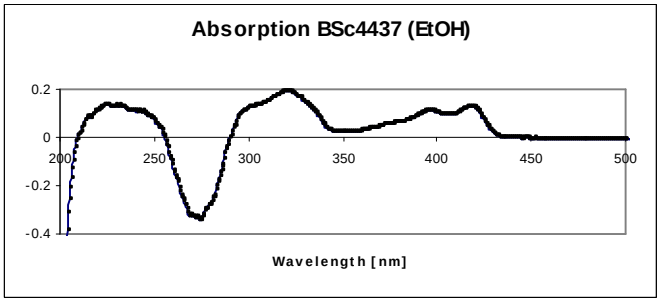

1-(4-(2,2,2-Trifluoroethyl)phenyl)benzo[*a*]imidazo[5,1,2-*cd*]indolizine (62)

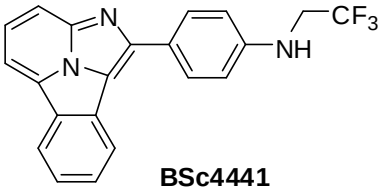

BSc4441

Yield: 41 %. **^{1}H-NMR (500 MHz, d_6-DMSO)**: δ = 8.66 (d, *J* = 8.0 Hz, 1H), 8.51 (d, *J* = 8.5 Hz, 1H), 8.37 (d, *J* = 8.0 Hz, 1H), 8.20 (d, *J* = 7.5 Hz, 2H), 8.10-8.03 (m, 2H), 7.87 (td, *J* = 8.0 Hz, *J* = 1.0 Hz, 1H), 7.69 (td, *J* = 8.0 Hz, *J* = 1.0 Hz, 1H), 7.04 (d, *J* = 8.5 Hz, 2H), 6.77 (t, *J* = 7.0 Hz, 1H), 4.12-4.01 (m, 2H) ppm. **^{13}C-NMR (125 MHz, d_6-DMSO)**: δ = 148.6, 146.7, 139.0, 130.2, 129.2, 129.1, 129.0, 127.7, 126.5, 124.4, 123.7, 122.7, 120.4, 118.5, 112.8, 112.0, 109.0, 43.9, 43.6 ppm. **MS (EI, 70 eV)**: *m/z* = 365 $[M]^+$. **UV/Vis (Ethanol)**: λ_{max} = 425.0 nm.

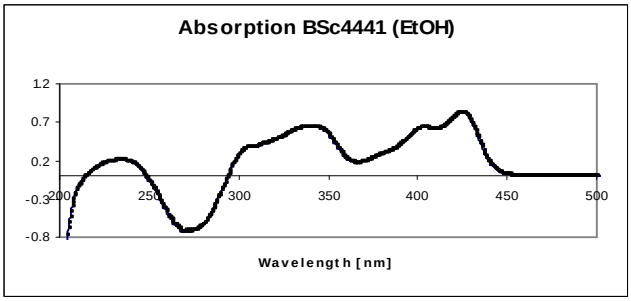

Method B of [8+2] cycloaddition reaction

Under the protection of inert gas, the benzyne precursor 2-(trimethylsilyl)phenyl trifluoromethane sulfonate (59.6 mg, 0.2 mmol, 2.0 eq) was added to a mixture of corresponding substrates (0.1 mmol, 1.0 eq), 18-crown-6 (0.11 g, 0.2 mmol, 2.0 eq) and CsF (30.4 mg, 0.2 mmol, 2.0 eq) in 2 ml of acetonitrile. The reaction was refluxed overnight. The resulting mixture was dissolved in ethyl acetate and washed with brine (2 x 30 mL). The solvent was evaporated *in vacuo*, and the residue was purified by flash chromatography (SiO_2; ethyl acetate: cyclohexane = 1:2) to obtain the corresponding pure [8+2] cycloaddition product.

1-(4-Aminophenyl)benzo[*a*]imidazo[5,1,2-*cd*]indolizine (64)

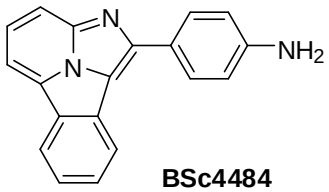

BSc4484

Yield: 42 %. **^{1}H-NMR (500 MHz, d_6-DMSO)**: δ = 8.66 (d, *J* = 8.0 Hz, 1H), 8.51 (d, *J* = 8.5 Hz, 1H), 8.36 (dd, *J* = 6.0 Hz, *J* = 2.0 Hz, 1H), 8.11 (d, *J* = 8.5 Hz, 2H), 8.07-8.01 (m, 2H), 7.87 (td, *J* = 8.5 Hz, *J* = 1.0 Hz, 1H), 7.68 (td, *J* = 8.5 Hz, *J* = 0.5 Hz, 1H), 6.84 (d, *J* = 8.5 Hz, 2H), 5.67 (s, 2H) ppm. **MS (EI, 70 eV)**: *m/z* = 283 $[M]^+$.

***In vitro* neuropathological staining of AD brain sections**: Tissues: hippocampus; Patient: female, 89 years old; CERAD Score: 3; NFTs-level: V.

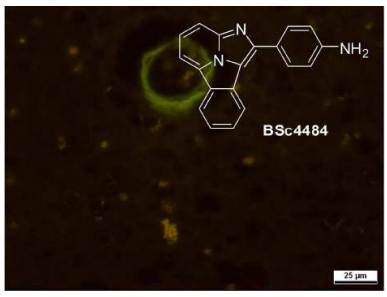

6.3.2. General procedures for synthesis of imidazo[1,2-*a*]pyrimidines derivatives

2-(4-Nitrophenyl)imidazo[1,2-*a*]pyrimidine (67)

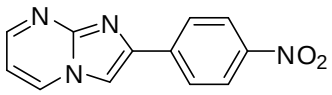

A mixture of pyrimidin-2-amine (0.95 g, 10.0 mmol, 1.0 eq) and α-bromoketone (2.44 g, 10.0 mmol, 1.0 eq) was refluxed in ethanol (40 mL) overnight. The solvent was evaporated *in vacuo*. 5 N NaOH was added to adjust pH > 10, Precipitates were filtered off and washed with brine and cooled ethyl acetate. The compound was dried under the high vacuum to obtain 2-(4-nitrophenyl)imidazo[1,2-*a*]pyrimidine as yellow solid, which was used in next step without further purification.

4-(Imidazo[1,2-*a*]pyrimidin-2-yl)aniline (68)

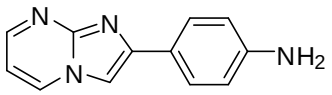

To a suspension of 2-(4-nitrophenyl)imidazo[1,2-*a*]pyrimidine (2.40 g, 10 mmol, 1.0 eq) in 20 ml ethanol, $SnCl_2$ (9.48 g, 50 mmol, 5.0 eq) was added. The suspension was heated to reflux temperature overnight. After cooling down to room temperature, the solvent was evaporated *in vacuo*. 5 N NaOH was to adjusted to pH > 10, the mixture was extracted with ethyl acetate, washed with brine (3 x 30 mL) and dried over Na_2SO_4. After filtration, the solvent was evaporated to obtain 2.10 g of 4-(imidazo[1,2-*a*]pyridin-2-yl)aniline as yellow solid (yield: quant.).

^{1}H-NMR (500 MHz, d_6-DMSO): δ = 8.87 (dd, *J* = 6.5 Hz, *J* = 2.0 Hz, 1H), 8.42 (dd, *J* = 4.0 Hz, *J* = 2.0 Hz, 1H), 8.09 (s, 1H), 7.68 (d, *J* = 9.0 Hz, 2H), 6.97 (dd, *J* = 6.5 Hz, *J* = 4.0 Hz, 1H), 6.65 (d, *J* = 8.5 Hz, 2H), 5.33 (s, 2H) ppm. **^{13}C-NMR (125 MHz, d_6-DMSO)**: δ = 149.1, 148.9, 147.8, 146.7, 134.1, 126.7, 120.8, 113.7, 108.2, 104.8 ppm.

A solution of $NaNO_2$ (76 mg, 1.1 mmol, 1.0 eq) in water (1 mL) was added to an ice-cold mixture of 4-(imidazo[1,2-*a*]pyridin-2-yl)aniline (210 mg, 1.0 mmol, 1.0 eq) in 6 N HCl (1mL), and the temperature was controlled to stay below 5 °C. The reaction was stirred for 5 min and added slowly to a solution of $SnCl_2 \cdot 2H_2O$ in HCl (conc., 0.5mL) at -5 °C. The reaction mixture was stirred at room temperature for 1 h. 9-Methyl-9*H*-carbazole-3-carbaldehyde (209

mg, 1 mmol, 1.0 eq) was dissolved in 30 ml THF and added to the reaction. The reaction mixture was stirred and refluxed for 2 hours. When it was cooled, the mixture was extracted with THF twice. The organic phase was dried over Na_2SO_4, filtered, and concentrated. The residue was purified by column chromatography (SiO_2; dichloromethane: methanol = 20:1) to furnish 162 mg of product as yellow-green solid.

3-((2-(4-(Imidazo[1,2-*a*]pyrimidin-2-yl)phenyl)hydrazono)methyl)-9-methyl-9*H*-carbazole (70)

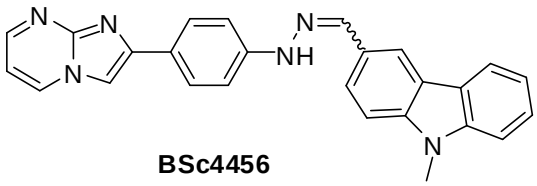

BSc4456

Yield: 41 %. **^{1}H-NMR (500 MHz, d_6-DMSO)**: δ = 10.40 (s, 1H), 8.92 (dd, *J* = 7.5 Hz, *J* = 2.0 Hz, 1H), 8.47 (dd, *J* = 4.0 Hz, *J* = 2.0 Hz, 1H), 8.40 (d, *J* = 1.5 Hz, 1H), 8.24(d, *J* = 8.0 Hz, 1H), 8.21 (s, 1H), 8.10 (s, 1H), 7.92-7.87 (m, 3H), 7.63 (d, *J* = 9.0 Hz, 1H), 7.60 (d, *J* = 8.5 Hz, 1H), 7.49 (td, *J* = 8.5 Hz, *J* = 1.5 Hz, 1H), 7.26-7.19 (m, 3H), 7.01 (dd, *J* = 7.5 Hz, *J* = 4.0 Hz, 1H), 3.90 (s, 3H) ppm. **^{13}C-NMR (125 MHz, d_6-DMSO)**: δ = 149.2, 147.9, 146.2, 145.7, 140.9, 140.6, 138.6, 134.3, 126.8, 126.8, 125.8, 123.5, 123.3, 122.1, 121.9, 120.4, 118.9, 118.3, 111.8, 109.4, 109.2, 108.4, 105.5, 29.0 ppm. **MS (EI, 70 eV)**: *m/z* = 416 $[M]^+$. **UV/Vis (Ethanol)**: λ_{max} = 397.0 nm.

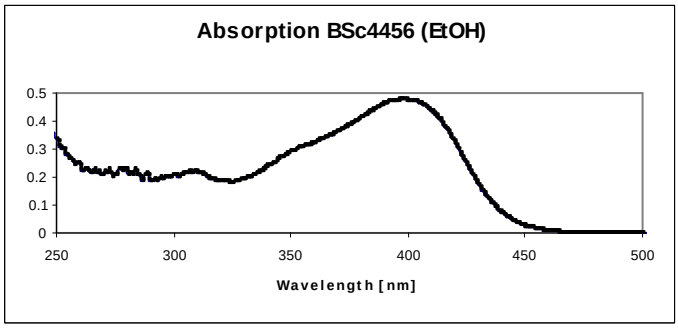

***In vitro* neuropathological staining of AD brain sections**: Tissues: hippocampus; Patient: female, 89 years old; CERAD Score: 3; NFTs-level: V.

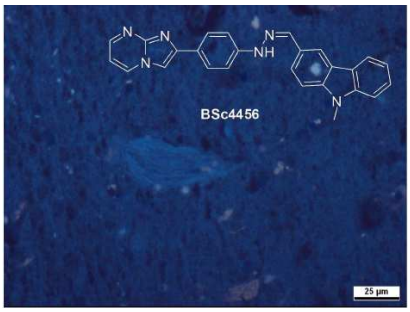

6.4. Synthesis of tetrazine derivatives

Triaminoguanidine monohydrochloride (72)

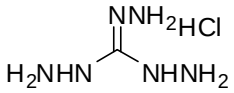

To a suspension of guanidine monohydrochloride (9.55 g, 100 mmol, 1.0 eq) in 1,4-dioxane (50 mL) was added hydrazine monohydrate (15.5 g, 310 mmol, 3.1 eq) slowly. The reaction mixture was heated to reflux for 2 hours during which colorless precipitates formed. When the reaction mixture was cooled down to room temperature, the solid was collected by suction filtration, washed with 1,4-dioxane and dried under high vacuum overnight to afford 13.57 g of title compound as a colorless solid (yield: 97 %).

3,6-Bis(3,5-dimethyl-1*H*-pyrazol-1-yl)-1,4-dihydro-1,2,4,5-tetrazine (73)

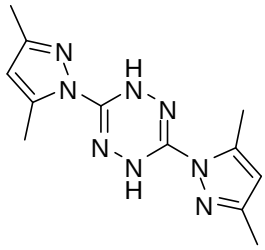

To slurry of triaminoguanidine monohydrochloride (7.03 g, 50.0 mmol, 1.0 eq) in 50 ml distilled water was added acetylacetone (10.00 g, 100.0 mmol, 2.0 eq). The reaction mixture was stirred at room temperature for 30 minutes. The solution turned to pale yellow then to a clear orange, followed by precipitate formation. The reaction mixture was then heated up to 70 ^{o}C for 4 hours till the orange precipitates formed. The reaction was cooled down to the room temperature. The solid was filtered off, washed with water and dried under the high vacuum to give 6.04 g of pure product as a yellow solid.

Yield: 89 %. **^{1}H-NMR (500 MHz, d_6-DMSO)**: δ = 8.84 (s, 2H), 8.15 (s, 2H), 2.40 (s, 6H), 2.17 (s, 6H) ppm. **^{13}C-NMR (125 MHz, d_6-DMSO)**: δ = 149.3, 145.2, 141.6, 109.3, 13.2, 12.8 ppm. **MS (EI, 70 eV)**: *m/z* = 272 $[M]^+$.

3,6-Bis(3,5-dimethyl-1*H*-pyrazol-1-yl)-1,2,4,5-tetrazine (74)

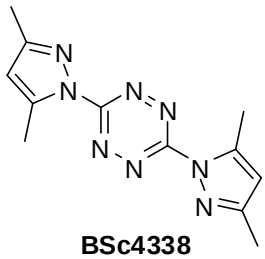

BSc4338

3,6-Bis(3,5-dimethyl-1*H*-pyrazol-1-yl)-1,2,4,5-tetrazine (2.72 g, 10 mmol, 1.0 eq) was suspended in the 5 % solution of $NaNO_2$ (40 mL, 2.9 eq) and dichloromethane (4 mL). The mixture was placed in the ice bath, and acetic acid (1.5 mL) was added to the mixture. The mixture was stirred overnight. The mixture was extracted with dichloromethane, washed with base and brine, dried over Na_2SO_4. After filtration, the solvent was evaporated *in vacuo*. The residue was washed with diethyl ether to give 2.17g of product as a pink solid.

Yield: 80 %. **^{1}H-NMR (300 MHz, $CDCl_3$)**: δ = 6.18 (s, 2H), 2.70 (s, 6H), 2.38 (s, 6H) ppm. **^{13}C-NMR (75 MHz, $CDCl_3$)**: δ = 159.4, 154.6, 143.9, 112.0, 14.8, 14.0 ppm. **MS (EI, 70 eV)**: *m/z* = 270 $[M]^+$. **UV/Vis (Ethanol)**: λ_{max} = 303.5 nm.

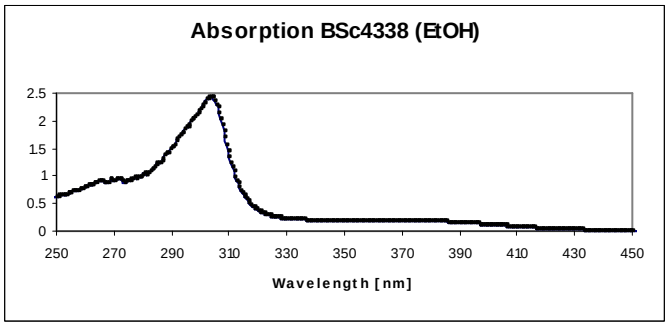

***In vitro* neuropathological staining of AD brain sections**: Tissues: hippocampus; Patient: female, 89 years old; CERAD Score: 3; NFTs-level: V.

General procedure for nucleophilic substitution

A mixture of 3,6-bis(3,5-dimethyl-1*H*-pyrazol-1-yl)-1,2,4,5-tetrazine (270 mg, 1.0 mmol), and corresponding aldehyde (2.0 mmol) was refluxed in MeCN (3 mL) for 16 h or under microwave condition for 1 h. The solvent was removed *in vacuo* and the residue was purified by recrystallization to obtain corresponding tetrazine compounds **75a-c**.

***N*^{1}-(6-(3,5-Dimethyl-1*H*-pyrazol-1-yl)-1,2,4,5-tetrazin-3-yl)-*N*^{4},*N*^{4}-dimethylbenzene-1,4-diamine (75a)**

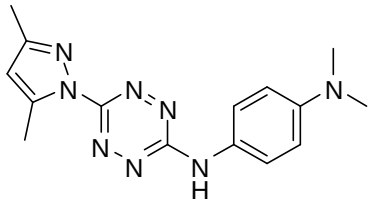

BSc4339

Yield: 92 %. **^{1}H-NMR (500 MHz, d_6-DMSO)**: δ = 10.66 (s, 1H), 7.52 (d, *J* = 9.0 Hz, 2H), 6.78 (d, *J* = 9.0 Hz, 2H), 6.20 (s, 1H), 2.89 (s, 6H), 2.52 (s, 3H), 2.23 (s, 3H) ppm. **^{13}C-NMR (125 MHz, d_6-DMSO)**: δ = 160.3, 156.6, 150.1, 147.4, 141.3, 127.2, 121.7, 112.6, 108.5, 40.3, 13.24, 12.3 ppm. **MS (EI, 70 eV)**: *m/z* = 310 $[M]^+$. **UV/Vis (Ethanol)**: λ_{max} = 325.5 nm.

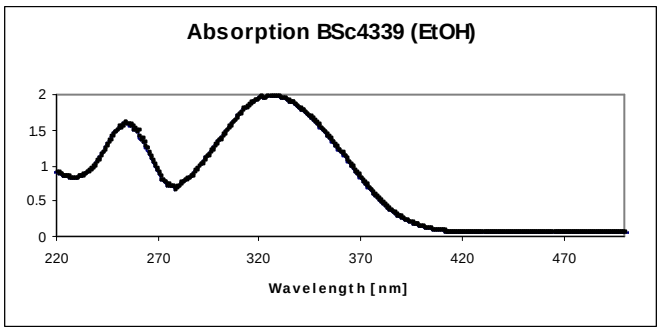

***In vitro* neuropathological staining of AD brain sections**: Tissues: hippocampus; Patient: female, 89 years old; CERAD Score: 3; NFTs-level: V.

6-(3,5-Dimethyl-1*H*-pyrazol-1-yl)-*N*-(4-methoxyphenyl)-1,2,4,5-tetrazin-3-amine (75b)

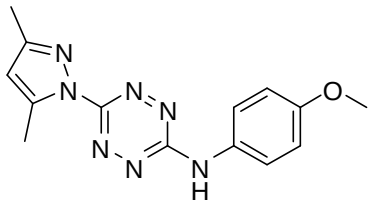

BSc4340

Yield: 96 %. **^{1}H-NMR (500 MHz, d_6-DMSO)**: δ = 10.81 (s, 1H), 7.64 (d, *J* = 9.0 Hz, 2H), 6.99 (d, *J* = 9.0 Hz, 2H), 6.21 (s, 1H), 3.76 (s, 3H), 2.44 (s, 3H), 2.24 (s, 3H) ppm. **^{13}C-NMR (125 MHz, d_6-DMSO)**: δ = 160.4, 156.9, 155.7, 150.3, 141.5, 131.0, 121.8, 114.1, 108.8, 53.7, 13.4, 12.5 ppm. **MS (EI, 70 eV)**: *m/z* = 397 $[M]^+$. **UV/Vis (Ethanol)**: λ_{max} = 315.5 nm.

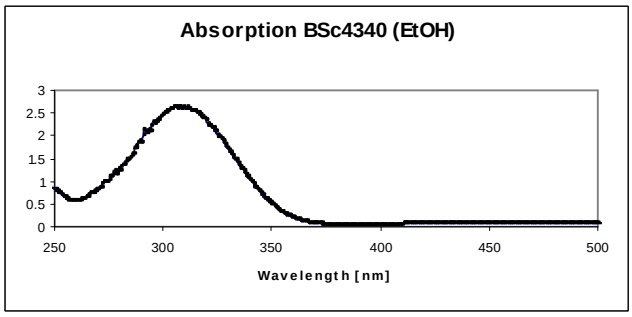

***In vitro* neuropathological staining of AD brain sections**: Tissues: hippocampus; Patient: female, 89 years old; CERAD Score: 3; NFTs-level: V.

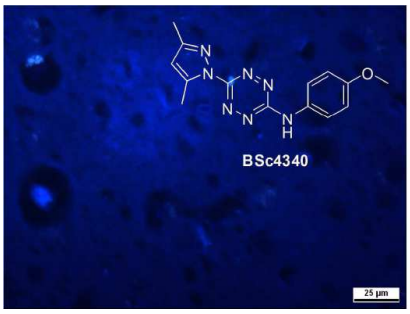

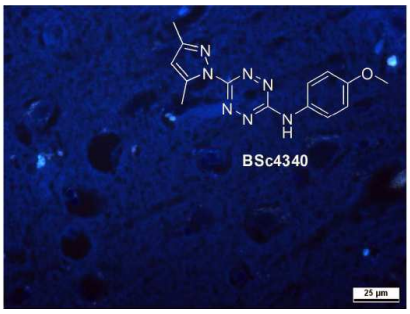

***N*-(4-(Benzo[*d*]thiazol-2-yl)phenyl)-6-(3,5-dimethyl-1*H*-pyrazol-1-yl)-1,2,4,5-tetrazin-3-amine (75c)**

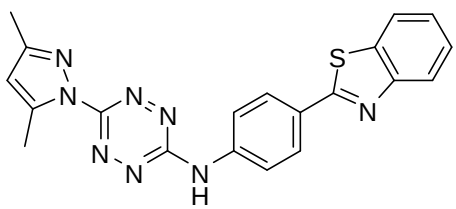

BSc4341

Yield: 34 %. **^{1}H-NMR (500 MHz, d_6-DMSO)**: δ = 10.45 (s, 1H), 8.18-8.11 (m, 3H), 8.04 (d, *J* = 8.0 Hz, 1H), 7.99 (d, *J* = 8.5 Hz, 2H), 7.54 (td, *J* = 8.5 Hz, *J* = 1.5 Hz, 1H), 7.45 (td, *J* = 8.5 Hz, *J* = 1.5 Hz, 1H), 6.26 (s, 1H), 2.50 (s, 3H), 2.26 (s, 3H) ppm. **^{13}C-NMR (125 MHz, d_6-DMSO)**: δ = 166.9, 160.4, 157.1, 153.7, 150.8, 141.9, 141.3, 134.3, 128.2, 127.5, 126.6, 125.3, 122.6, 122.3, 119.6, 109.3, 13.4, 12.8 ppm. **MS (EI, 70 eV)**: *m/z* = 400 $[M]^+$. **UV/Vis (Ethanol)**: λ_{max} = 344.5 nm.

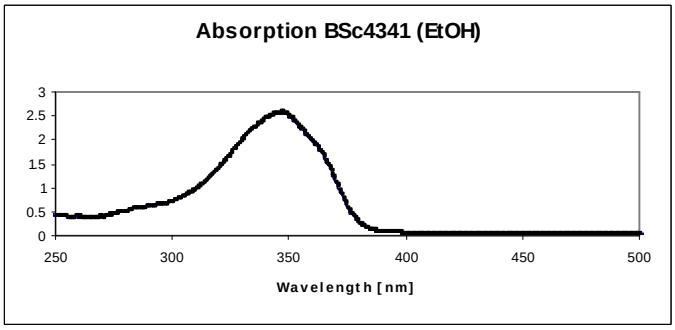

***In vitro* neuropathological staining of AD brain sections**: Tissues: hippocampus; Patient: female, 89 years old; CERAD Score: 3; NFTs-level: V.

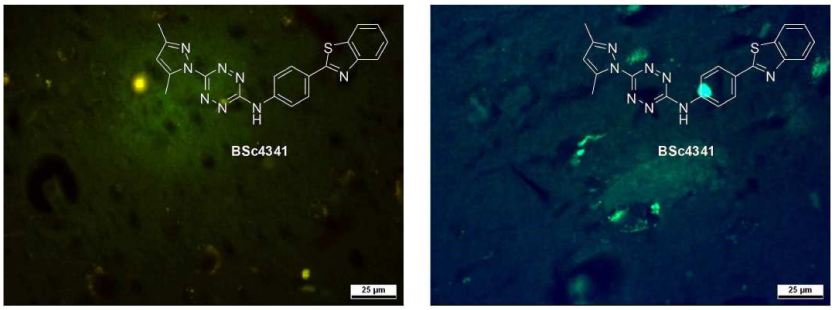

6.5. Synthesis of bisstyryl derivatives

6.5.1. Synthesis of 1,4-bisstyryl-2-methoxybenzene derivatives

5-(Dimethylamino)thiophene-2-carbaldehyde (82)

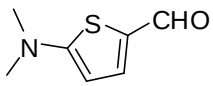

A mixture of 5-bromothiophene-2-carbaldehyde (191 mg, 1.0 mmol, 1.0 eq), 30 % dimethylamine solution (750 mg, 5.0 mmol, 5.0 eq) and potassium carbonate (414 mg, 3.0 mmol, 3.0 eq) was stirred for 1 h at 120 °C under microwave irradiation. Reaction mixture was cooled down to room temperature, the residue was purified by column chromatography (SiO_2; ethyl acetate: cyclohexane = 1:1) to afford 0.96 g of title compound.

Yield: 62 %. **^{1}H-NMR (500 MHz, d_6-DMSO)**: δ = 9.41 (s, 1H), 7.67 (d, *J* = 4.5 Hz, 1H), 6.11 (d, *J* = 4.5 Hz, 1H), 3.06 (s, 6H) ppm. **^{13}C-NMR (125 MHz, d_6-DMSO)**: δ = 179.4, 167.4, 141.3, 125.3, 103.4, 41.6 ppm.

Tetraethyl (2-methoxy-1,4-phenylene)bis(methylene)diphosphonate

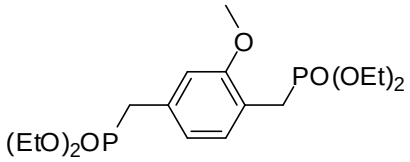

To a stirred solution of 2-methoxy-1,4-dimethylbenzene (1.36 g, 10.0 mmol, 1.0 eq) in CCl_4 (30 mL) was added NBS (6.23 g, 35.0 mmol, 3.5 eq) and AIBN (0.23 g, 1.4 mmol, 0.14 eq) at room temperature. The reaction mixture was refluxed for 15 h. The cooled reaction mixture was then washed with H_2O and dried over $MgSO_4$. After removal of the solvent *in vacuo*, the residue was crystallized from cyclohexane to afford the 1,4-bis(bromomethyl)-2-methoxybenzene, which was used in the next reaction without further purification.

A mixture of triethyl phosphite (2.49 g, 15.0 mmol, 3.0 eq) and 1,4-bis(bromomethyl)-2-methoxybenzene (1.47 g, 5.0 mmol, 1.0 eq) was heated to 160 °C for 6 h. The residue was purified by column chromatography (SiO_2; ethyl acetate: cyclohexane = 1:10) to afford the title compound in quantitative yield.

^{1}H-NMR (500 MHz, d_6-DMSO): δ = 7.16 (dd, *J* = 7.5 Hz, *J* = 2.0 Hz, 1H), 6.92 (s, 1H), 6.82 (d, *J* = 7.5 Hz, 1H), 4.00-3.87 (m, 8H), 3.77 (s, 3H), 3.24-3.09 (m, 4H), 1.20-1.12 (m, 12H) ppm. **^{13}C-NMR (125 MHz, d_6-DMSO)**: δ = 156.5, 132.1, 130.5, 121.5, 118.2, 118.2, 112.3, 61.2 (d, *J* = 16.5 Hz), 55.3, 32.2 (d, *J* = 134.8 Hz), 25.4 (d, *J* = 137.0 Hz), 16.1 (t, *J* = 3.3 Hz) ppm.

General procedure for Wittig-Horner coupling

The *t*-BuOK (168 mg, 1.5 mmol, 3.0 eq) was added to a stirred solution of tetraethyl (2-methoxy-1,4-phenylene)bis(methylene)diphosphonate (198 mg, 0.5 mmol, 1.0 eq) in DMF (4 mL) at room temperature. The mixture was stirred under argon for 5 min. Then corresponding aldehyde (1.0 mmol, 2.0 eq) was added to the mixture, and further reacted at room temperature overnight. The reaction was then quenched with H_2O (10 mL). Precipitates were filtered off and purified by column chromatography (SiO_2; ethyl acetate: cyclohexane = 1:2) to afford the corresponding compound with yields of 47-63 %.

1,1'-(4,4'-(1*E*,1'*E*)-2,2'-(2-Methoxy-1,4-phenylene)bis(ethene-2,1-diyl)bis(4,1-phenylene))dipyrrolidine (79a)

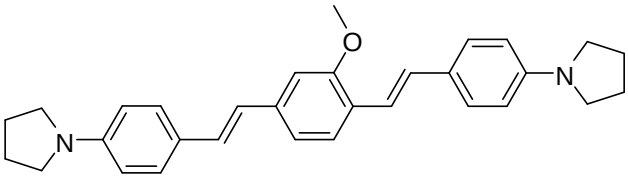

BSc4882

Yield: 63 %. **^{1}H-NMR (500 MHz, $CDCl_3$)**: δ = 7.53 (d, *J* = 8.5 Hz, 1H), 7.42 (t, *J* = 8.5 Hz, 4H), 7.25 (d, *J* = 16.5 Hz, 1H), 7.09-6.97 (m, 4H), 6.87 (d, *J* = 16.5 Hz, 1H), 6.59-6.52 (m, 4H), 3.94 (s, 3H), 3.36-3.28 (m, 8H), 2.05-1.98 (m, 8H) ppm. **^{13}C-NMR (125 MHz, $CDCl_3$)**: δ = 156.7, 147.5, 137.8, 128.8, 128.5, 127.7, 127.7, 126.0, 125.8, 123.7, 118.9, 118.2, 111.8, 108.2, 55.6, 47.6, 25.5 ppm. **MS (EI, 70 eV)**: *m/z* = 450 $[M]^+$. **UV/Vis (Ethanol)**: λ_{max} = 407.0 nm.

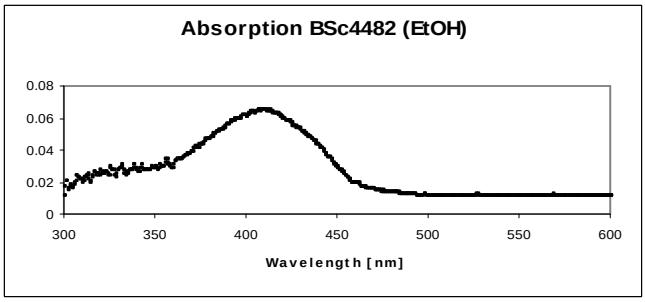

***In vitro* neuropathological staining of AD brain sections**: Tissues: hippocampus; Patient: male, 71 years old; CERAD Score: 3; NFTs-level: V.

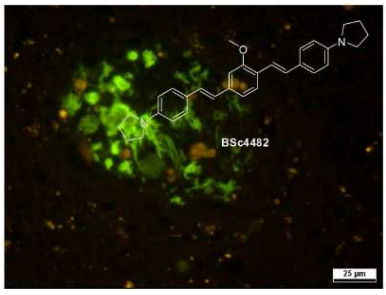

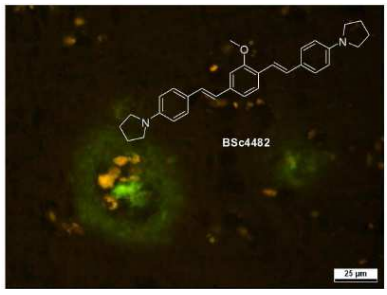

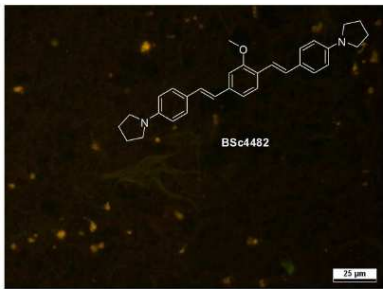

4,4'-(4,4'-(1*E*,1'*E*)-2,2'-(2-Methoxy-1,4-phenylene)bis(ethene-2,1-diyl)bis(4,1-phenylene))bis(1-methylpiperazine) (79b)

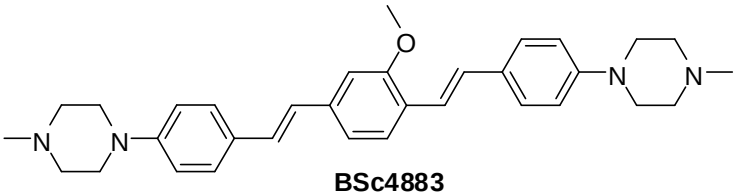

BSc4883

Yield: 47 %. **^{1}H-NMR (500 MHz, $CDCl_3$)**: δ= 7.54 (d, *J* = 8.0 Hz, 1H), 7.44 (t, *J* = 8.0 Hz, 4H), 7.32 (d, *J* = 16 Hz, 1H), 7.10-6.88 (m, 9H), 3.93 (s, 3H), 3.29-3.23 (m, 8H), 2.60 (t, *J* = 5.0 Hz, 8H), 2.37 (s, 6H) ppm. **^{13}C-NMR (125 MHz, $CDCl_3$)**: δ = 156.8, 150.6, 150.4, 137.8, 129.6, 128.7, 128.4, 128.1, 127.4, 126.1, 126.0, 125.8, 120.3, 119.1, 115.8, 115.7, 108.4, 55.6, 55.0, 48.7, 48.6, 46.1, 45.8, 8.8 ppm. **MS (EI, 70 eV)**: *m/z* = 508 $[M]^+$. **UV/Vis (Ethanol)**: λ_{max} = 388.0 nm.

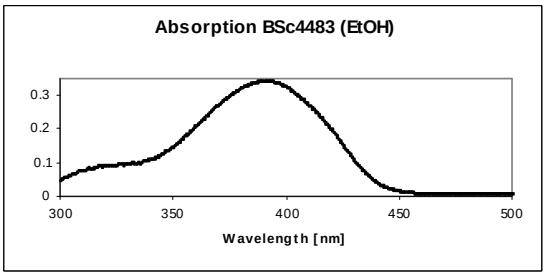

***In vitro* neuropathological staining of AD brain sections**: Tissues: hippocampus; Patient: male, 71 years old; CERAD Score: 3; NFTs-level: V.

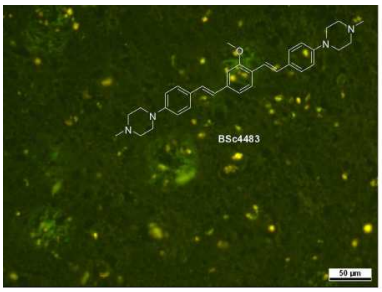

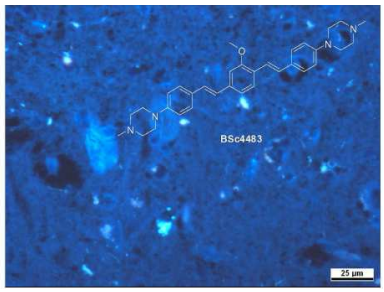

5,5'-(1*E*,1'*E*)-2,2'-(2-Methoxy-1,4-phenylene)bis(ethene-2,1-diyl)bis(*N*,*N*-dimethylthiophen-2-amine) (83)

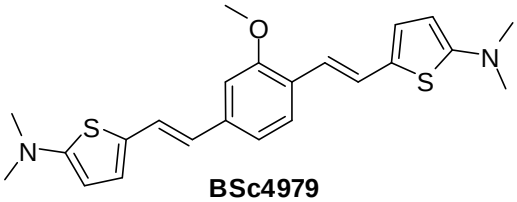

BSc4979

Yield: 53 %. **^{1}H-NMR (500 MHz, d_6-DMSO)**: δ = 7.45 (d, *J* = 8.5 Hz, 1H), 7.27 (d, *J* = 16.0 Hz, 1H), 7.20 (d, *J* = 16.0 Hz, 1H), 7.06 (d, *J* = 1.0 Hz, 1H), 7.00 (d, *J* = 8.0 Hz, 1H), 6.83 (d, *J* = 4.0 Hz, 1H), 6.78 (d, *J* = 4.0 Hz, 1H), 6.68 (d, *J* = 16.0 Hz, 1H), 6.45 (d, *J* = 16.0 Hz, 1H), 5.82 (d, *J* = 4.0 Hz, 1H), 5.79 (d, *J* = 4.0 Hz, 1H), 3.87 (s, 3H), 2.91 (s, 6H), 2.90 (s, 6H) ppm. **^{13}C-NMR (125 MHz, d_6-DMSO)**: δ = 158.1, 157.8, 155.8, 136.9, 128.3, 127.9, 127.5, 126.6, 125.0, 124.1, 122.6, 122.5, 121.5, 118.2, 115.8, 107.8, 102.0, 102.0, 55.3, 42.0, 41.9 ppm. **UV/Vis (Ethanol)**: λ_{max} = 434.0 nm.

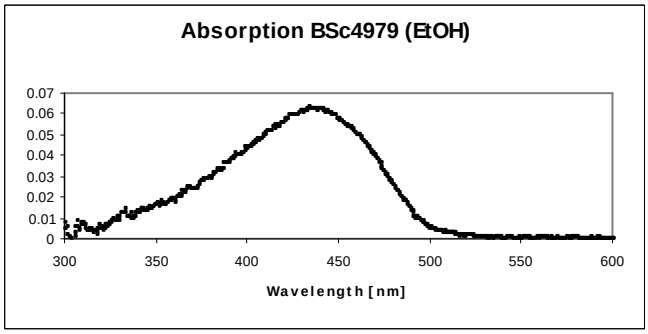

***In vitro* neuropathological staining of AD brain sections**: Tissues: hippocampus; Patient: male, 71 years old; CERAD Score: 3; NFTs-level: V.

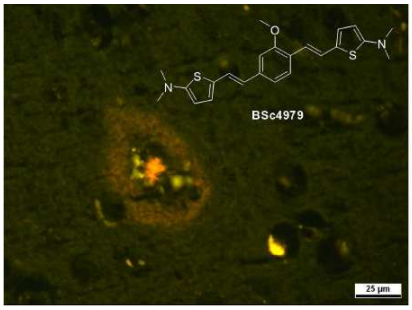

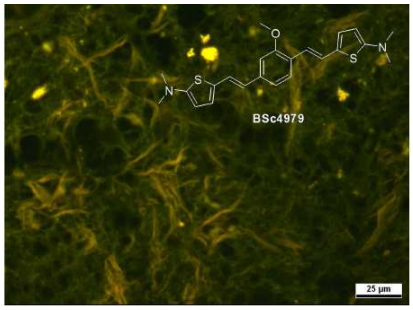

6.5.2. Synthesis of 1,4-bisstyryl-2-bromobenzene and 1,4-bisstyryl-2,5-dibromobenzene derivatives

6.5.2.1. Synthesis of 1,4-bisstyryl-2-bromobenzene derivative

2,2'-(1*E*,1'*E*)-2,2'-(2-Bromo-1,4-phenylene)bis(ethene-2,1-diyl)bis(1-methyl-1*H*-pyrrole) (88)

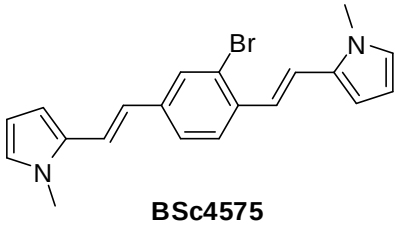

BSc4575

The *t*-BuOK (168 mg, 1.5 mmol, 3.0 eq) was added to a stirred solution of tetraethyl (2-bromo-1,4-phenylene)bis(methylene)diphosphonate (229 mg, 0.5 mmol, 1.0 eq) in DMF (4 mL) at room temperature. The mixture was stirred for 5 min under argon. Then 1-methyl-1*H*-pyrrole-2-carbaldehyde (109 mg, 1.0 mmol, 2.0 eq) was added to the mixture, which was further stirred at room temperature overnight. The reaction was then quenched with H_2O (10 mL). Precipitates were filtered off and purified by column chromatography (SiO_2; dichloromethane: methanol = 10:1) to afford the title compound 96 mg.

Yield: 52 %. **^{1}H-NMR (500 MHz, $CDCl_3$)**: δ = 7.66 (d, *J* = 1.5 Hz, 1H), 7.55 (d, *J* = 8.0 Hz, 1H), 7.33 (dd, *J* = 8.0 Hz, *J* = 2.0 Hz, 1H), 7.19 (d, *J* = 16.0 Hz, 1H), 6.93 (t, *J* = 15.5 Hz, 2H), 6.76 (d, *J* = 16.0 Hz, 1H), 6.68-6.64 (m, 2H), 6.56 (dd, *J* = 4.0 Hz, *J* = 1.5 Hz, 1H), 6.51 (dd, *J* = 4.0 Hz, *J* = 1.5 Hz, 1H), 6.19-6.15 (m, 2H), 3.72 (s, 3H), 3.71 (s, 3H) ppm. **^{13}C-NMR (125 MHz, $CDCl_3$)**: δ = 138.1, 125.7, 131.9, 131.7, 130.0, 125.8, 125.1, 124.3, 124.1, 124.0, 123.8, 119.1, 117.8, 108.5, 108.1, 107.3, 34.4, 34.2 ppm. **UV/Vis (Ethanol)**: λ_{max} = 395.0 nm.

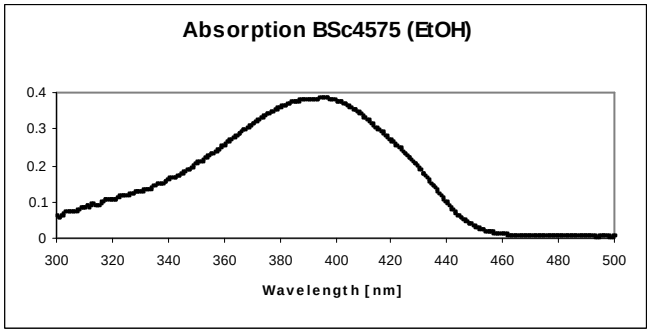

6.5.2.2. Synthesis of 1,4-bisstyryl-2,5-dibromobenzene derivatives

Tetraethyl (2,5-dibromo-1,4-phenylene)bis(methylene)diphosphonate (91)

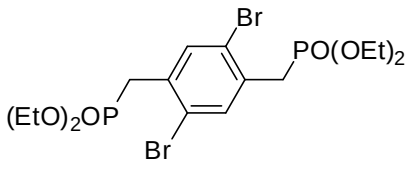

To a stirred solution of 1,4-dibromo-2,5-dimethylbenzene (2.64 g, 10.0 mmol, 1.0 eq) in $CHCl_3$ (30 mL) was added NBS (6.23 g, 35.0 mmol, 3.5 eq) and AIBN (0.23 g, 1.4 mmol, 0.14 eq) at room temperature. The reaction mixture was refluxed for 15 h. The cooled reaction mixture was then washed with H_2O and dried over $MgSO_4$. After removal of the solvent *in vacuo*, the residue was crystallized from cyclohexane to afford the 1,4-dibromo-2,5-bis(bromomethyl)benzene, which was used in the next reaction without further purification.

A mixture of triethyl phosphite (2.49 g, 15.0 mmol, 3.0 eq) and 1,4-dibromo-2,5-bis(bromomethyl)benzene (2.11 g, 5.0 mmol, 1.0 eq) was heated to 160 °C for 6 h. The residue was purified by column chromatography (SiO_2; ethyl acetate: cyclohexane = 1:10) to afford 2.11 g of title compound.

Yield: 79 %. **^{1}H-NMR (500 MHz, d_6-DMSO)**: δ = 7.65 (d, *J* = 2.0 Hz, 2H), 4.01-3.94 (m, 8H), 3.39 (d, *J* = 20.5 Hz, 4H), 1.18 (t, *J* = 7.0 Hz, 12H) ppm. **^{13}C-NMR (125 MHz, d_6-DMSO)**: δ = 134.9, 132.7, 122.8, 61.6, 31.7(d, *J* = 135.8 Hz), 16.0 ppm. **MS (EI, 70 eV)**: *m/z* = 535 $[M+1]^+$.

General procedure for Wittig-Horner coupling

The *t*-BuOK (168 mg, 1.5 mmol, 3.0 eq) was added to a stirred solution of tetraethyl (2,5-dibromo-1,4-phenylene)bis(methylene)diphosphonate (268 mg, 0.5 mmol, 1.0 eq) in DMF (4 mL) at room temperature. The mixture was stirred for 5 min under argon. Then the corresponding aldehyde (1.0 mmol, 2.0 eq) was added to the mixture, which was further stirred at room temperature overnight. The reaction was then quenched with H_2O (10 mL), and the precipitates were filtered off, the residue was purified by column chromatography (SiO_2; dichloromethane: methanol = 10:1) to afford the **92a-c** in moderate yields.

6.5.2.3. Synthesis of 1,4-bisstyryl-2,5-dibromobenzene derivatives

2,2'-(1*E*,1'*E*)-2,2'-(2,5-Dibromo-1,4-phenylene)bis(ethene-2,1-diyl)bis(1-methyl-1*H*-pyrrole) (92a)

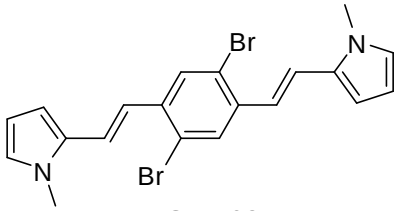

BSc4568

Yield: 45 %. **^{1}H-NMR (500 MHz, $CDCl_3$)**: δ = 7.78 (s, 2H), 7.09 (d, *J* = 16 Hz, 2H), 6.90 (d, *J* = 15.5 Hz, 2H), 6.68 (s, 2H), 6.58 (d, *J* = 3.0 Hz, 2H), 6.18 (t, *J* = 3.0 Hz, 2H), 3.74 (s, 6H) ppm. **^{13}C-NMR (125 MHz, $CDCl_3$)**: δ = 137.1, 131.5, 129.4, 124.7, 122.6, 122.5, 120.1, 108.7, 108.5, 34.4 ppm. **UV/Vis (Ethanol)**: λ_{max} = 401.0 nm.

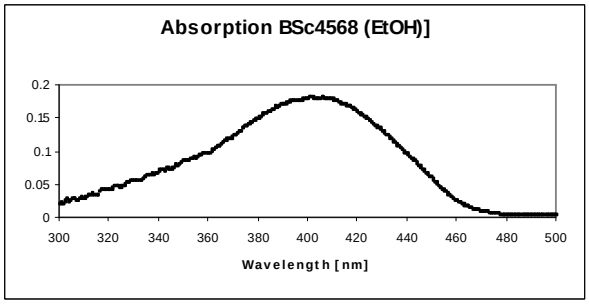

4,4'-(1*E*,1'*E*)-2,2'-(2,5-Dibromo-1,4-phenylene)bis(ethene-2,1-diyl)bis(*N*,*N*-diethylaniline) (92b)

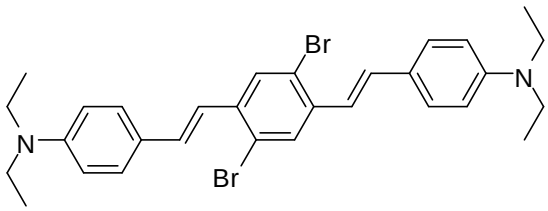

BSc4576

Yield: 37 %. **^{1}H-NMR (500 MHz, $CDCl_3$)**: δ = 7.82 (s, 2H), 7.42 (d, *J* = 9.0 Hz, 4H), 7.12 (d, *J* = 16.0 Hz, 2H), 6.96 (d, *J* = 16.0 Hz, 2H), 6.67 (d, *J* = 9.0 Hz, 4H), 3.43-3.36 (m, 8H), 1.19 (t, *J* = 7.0 Hz, 12H) ppm. **^{13}C-NMR (125 MHz, $CDCl_3$)**: δ = 147.9, 137.1, 131.8, 129.5, 128.4, 124.1, 122.5, 120.7, 111.6, 44.4, 12.7 ppm. **UV/Vis (Ethanol)**: λ_{max} = 422.0 nm.

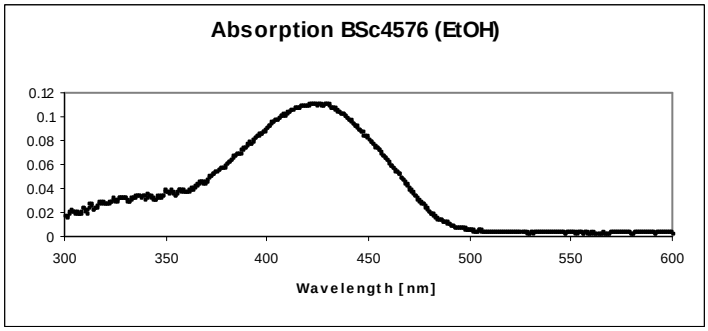

***In vitro* neuropathological staining of AD brain sections**: Tissues: hippocampus; Patient: male, 71 years old; CERAD Score: 3; NFTs-level: V.

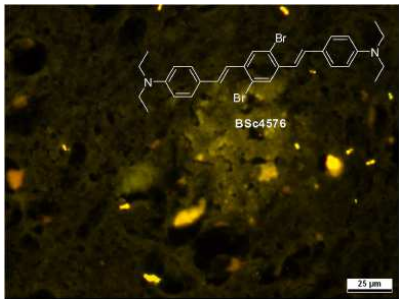

3,3'-(1*E*,1'*E*)-2,2'-(2,5-Dibromo-1,4-phenylene)bis(ethene-2,1-diyl)dipyridine (92c)

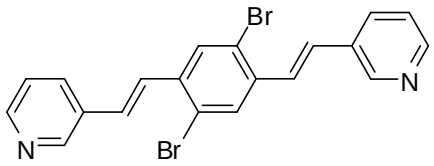

BSc4583

Yield: 52 %. **^{1}H-NMR (500 MHz, $CDCl_3$)**: δ = 8.76 (d, *J* = 2.0 Hz, 2H), 8.55 (dd, *J* = 4.5 Hz, *J* = 1.5 Hz, 2H), 7.91-7.87 (m, 4H), 7.43 (d, *J* = 16.0 Hz, 2H), 7.33 (dd, *J* = 8.0 Hz, *J* = 5.0 Hz, 2H), 7.05 (d, *J* = 16.0 Hz, 2H) ppm. **^{13}C-NMR (125 MHz, $CDCl_3$)**: δ = 149.4, 148.9, 137.3, 133.1, 132.2, 130.6, 128.8, 127.8, 123.7, 123.2 ppm. **UV/Vis (Ethanol)**: λ_{max} = 350.0 nm.

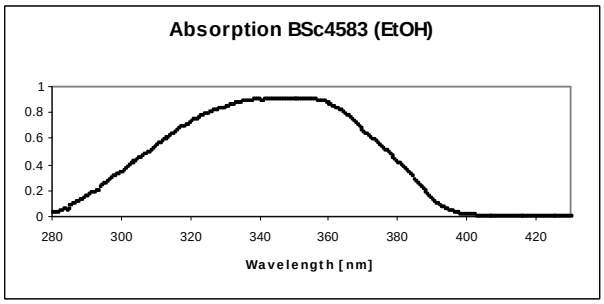

6.5.2.4. Synthesis of amides via palladium-catalyzed amidation of aryl bromides

***N*^{1},*N*^{4}-Di-*tert*-butyl-2,5-bis((*E*)-2-(1-methyl-1*H*-pyrrol-2-yl)vinyl)terephthalamide (94)**

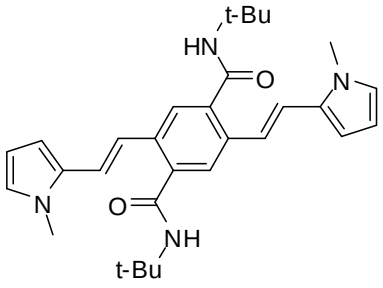

BSc4574

To the mixture of **92a** (**BSc4568)** (111.5 mg, 0.25 mmol, 1.0 eq) and $PdCl_2(PPh_3)_2$ (17.6 mg, 0.025 mmol, 0.1 eq) in 2.0 ml DMSO was added successively CsF (76 mg, 0.5 mmol, 2.0 eq) and H_2O (0.1 mL). After stirring for 5 min, 2-isocyano-2-methylpropane (52 mg, 0.625 mmol, 2.5 eq) was added. The reaction mixture was stirred at 90°C for 16h. The reaction mixture was extracted with dichloromethane, and then the combined organic layers were washed with brine, dried over Na_2SO_4. After filtration, the solvent was evaporated *in vacuo*, the residue was purified by column chromatography (SiO_2; ethyl acetate: cyclohexane = 1:3) to give 33 mg of pure product.

Yield: 27 %. **^{1}H-NMR (500 MHz, $CDCl_3$)**: δ = 7.63 (s, 2H), 7.05 (d, *J* = 16.0 Hz, 2H), 6.98 (d, *J* = 16.0 Hz, 2H), 6.67-6.64 (m, 2H), 6.49 (dd, *J* = 4.0 Hz, *J* = 1.5 Hz, 2H), 6.17-6.14 (m, 2H), 5.61 (s, 2H), 3.71 (s, 6H), 1.49 (s, 18H) ppm. **^{13}C-NMR (125 MHz, $CDCl_3$)**: δ = 168.7, 137.6, 133.5, 131.7, 124.3, 124.2, 121.1, 119.8, 108.6, 107.6, 52.2, 34.4, 28.9 ppm. **UV/Vis (Ethanol)**: λ_{max} = 377.5 nm.

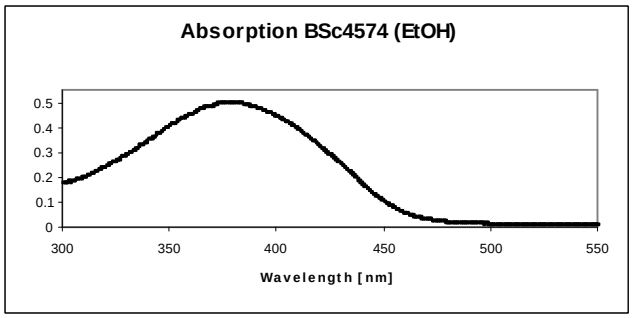

***In vitro* neuropathological staining of AD brain sections**: Tissues: hippocampus; Patient: male, 71 years old; CERAD Score: 3; NFTs-level: V.

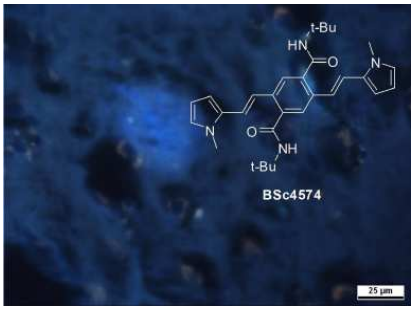

6.5.3. Synthesis of 1,4-bisstyryl-2-fluorobenzene and 1,2,4,5-tetrafluoro-3,6-bisstyrylbenzene derivatives

6.5.3.1. Synthesis of methyl 5-formyl-2-methoxybenzoate

Methyl 5-formyl-2-methoxybenzoate (96)

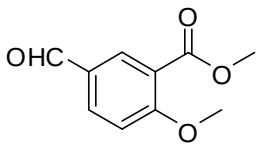

To a stirred solution of formyl salicylic acid (166 mg, 1.0 mmol, 1.0 eq) in DMF (1 mL) at room temperature was added CH_3I (568 mg, 4.0 mmol, 4.0 eq). The reaction mixture was stirred for 2 days. The reaction mixture was extracted with EtOAc, washed with H_2O and dried over $MgSO_4$. After filtration, the solvent was evaporated *in vacuo*, the residue was

purified by column chromatography (SiO_2; ethyl acetate: cyclohexane = 1:3) to afford 190 mg of title compound.

Yield: 98 %. **^{1}H-NMR (500 MHz, d_6-DMSO)**: δ = 9.92-9.90 (s, 1H), 8.20-8.18 (d, *J* = 2.0 Hz, 1H), 8.10-8.06 (dd, *J* = 8.5 Hz, *J* = 2.5 Hz, 1H), 7.38-7.35 (d, *J* = 9.0 Hz, 1H), 3.95-3.93 (s, 3H), 3.83-3.81 (s, 3H) ppm. **^{13}C-NMR (125 MHz, d_6-DMSO)**: δ = 190.9, 165.1, 162.5, 134.7, 132.4, 128.6, 120.3, 113.0, 56.4, 52.1 ppm. **MS (EI)**: *m/z* = 194 $[M]^+$.

6.5.3.2. Synthesis of 1,4-bisstyryl-2-fluorobenzene derivatives

Tetraethyl (2-fluoro-1,4-phenylene)bis(methylene)diphosphonate (99)

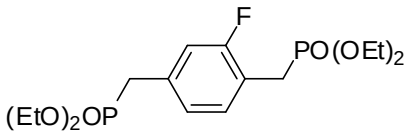

To a stirred solution of 2-fluoro-1,4-dimethylbenzene (1.24 g, 10.0 mmol, 1.0 eq) in $CHCl_3$ (30 mL) was added NBS (6.23 g, 35.0 mmol, 3.5 eq) and AIBN (0.23 g, 1.4 mmol, 0.14 eq) at room temperature. The reaction mixture was refluxed for 15 h. The cooled reaction mixture was then washed with H_2O and dried over $MgSO_4$. After filtration, the solvent was evaporated *in vacuo*, the residue was crystallized from cyclohexane to afford the 1,4-bis(bromomethyl)-2-fluorobenzene, which was used in the next reaction without further purification.

A mixture of triethyl phosphite (2.49 g, 15.0 mmol, 3.0 eq) and 1,4-bis(bromomethyl)-2-fluorobenzene (1.41 g, 5.0 mmol, 1.0 eq) was heated to 160 °C for 6 h. The residue was purified by column chromatography (SiO_2; ethyl acetate: cyclohexane = 1:10) to afford the title compound in quantitative yield.

^{1}H-NMR (500 MHz, d_6-DMSO): δ = 7.29 (td, *J* = 8.0 Hz, *J* = 2.5 Hz, 1H), 7.12-7.05 (m, 2H), 3.99-3.91 (m, 8H), 3.28-3.15 (m, 4H), 1.17 (t, *J* = 7.0 Hz, 12H) ppm. **^{13}C-NMR (125 MHz, d_6-DMSO)**: δ = 159.9 (brd, *J* = 247.5 Hz), 133.4 (brs), 131.6 (d, *J* = 2.8 Hz), 125.5 (t, *J* = 3.1 Hz), 117.4 (brs), 116.3 (brd, *J* = 19.1 Hz), 61.4 (brs), 32.1, 31.0, 25.7, 24.6, 16.0 (brs) ppm.

General procedure for Wittig-Horner coupling

The *t*-BuOK (168 mg, 1.5 mmol, 3.0 eq) was added to a stirred solution of tetraethyl (2-fluoro-1,4-phenylene)bis(methylene)diphosphonate (198 mg, 0.5 mmol, 1.0 eq) in DMF (4 mL) at room temperature. The mixture was stirred for 5 min under argon. Then

corresponding aldehyde (1.0 mmol, 2.0 eq) was added to the mixture, which was further stirred at room temperature overnight. The reaction was then quenched with H_2O (10 mL), and the precipitates were filtered off, the residue was purified by column chromatography (SiO_2; dichloromethane: methanol = 10:1) to afford the corresponding compound in moderate yields (**Table 3.3**).

Dimethyl 5,5'-(1*E*,1'*E*)-2,2'-(2-fluoro-1,4-phenylene)bis(ethene-2,1-diyl)bis(2-methoxy benzoate) (100a)

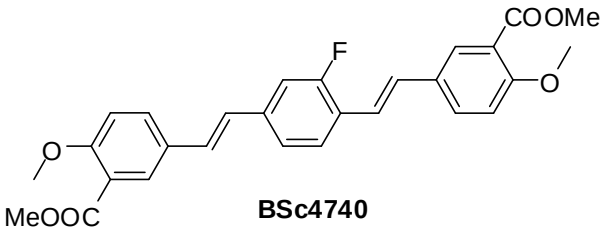

BSc4740

Yield: 57 %. **^{1}H-NMR (500 MHz, $CDCl_3$)**: δ = 7.97 (dd, *J* = 4.5 Hz, *J* = 2.5 Hz, 2H), 7.63 (dd, *J* = 9.0 Hz, *J* = 2.5 Hz, 1H), 7.60 (dd, *J* = 9.0 Hz, *J* = 2.5 Hz, 1H), 7.54 (d, *J* = 8.0 Hz, 1H), 7.25 (dd, *J* = 8.0 Hz, *J* = 1.5 Hz, 1H), 7.20 (dd, *J* = 7.0 Hz, *J* = 1.5 Hz, 1H), 7.14 (d, *J* = 3.5 Hz, 2H), 7.04-6.96 (m, 4H), 3.93 (s, 6H), 3.93 (s, 6H) ppm. **^{13}C-NMR (125 MHz, $CDCl_3$)**: δ = 166.5, 160.8 (brd, *J* = 247.9 Hz), 158.8, 158.8, 138.3, 138.3, 131.4 (d, *J* = 10.5 Hz), 129.9, 129.8, 129.7, 129.3, 129.1, 129.1, 128.2, 127.1 (d, *J* = 3.8 Hz), 126.4, 124.2 (d, *J* = 12.9 Hz), 122.4, 120.4 (d, *J* = 4.1 Hz), 119.9, 113.0 (d, *J* = 22.9 Hz), 112.4, 56.2, 52.1. **UV/Vis (Ethanol)**: λ_{max} = 366.0 nm.

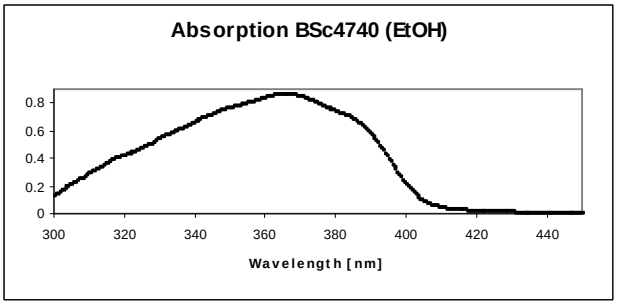

***In vitro* neuropathological staining of AD brain sections**: Tissues: hippocampus; Patient: male, 71 years old; CERAD Score: 3; NFTs-level: V.

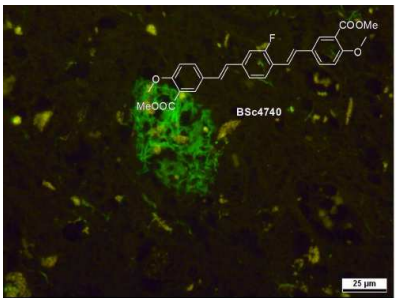

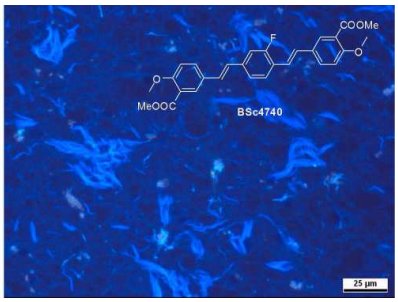

***In vitro* neuropathological staining of AD olfactory epithelium sections**: Tissues: olfactory epithelium; Patient: male, 78 years old; Braak: V, CERAD Score: 3.

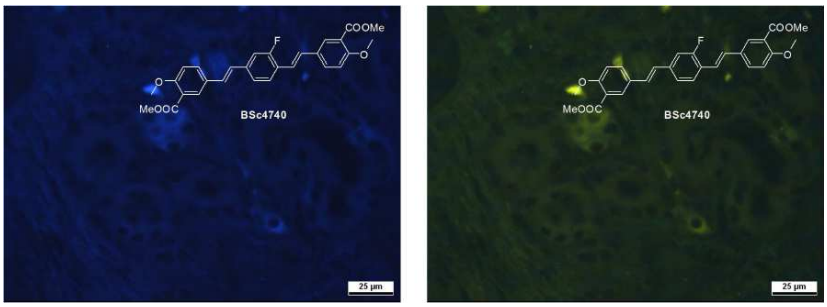

2,2'-(1*E*,1'*E*)-2,2'-(2-Fluoro-1,4-phenylene)bis(ethene-2,1-diyl)bis(1-methyl-1*H*-pyrrole) (100b)

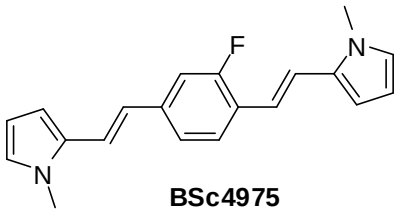

BSc4975

Yield: 55 %. **^{1}H-NMR (500 MHz, d_6-DMSO)**: δ = 7.72 (t, *J* = 8.0 Hz, 1H), 7.45 (dd, *J* = 13.0 Hz, *J* = 1.0 Hz, 1H), 7.33 (dd, *J* = 8.0 Hz, *J* = 1.0 Hz, 1H), 7.24 (d, *J* = 5.0 Hz, 1H), 7.20 (d, *J* = 5.0 Hz, 1H), 6.93-6.78 (m, 4H), 6.54-6.48 (m, 2H), 6.07-6.02 (m, 2H), 3.70 (s, 3H), 3.70 (s, 3H) ppm. **^{13}C-NMR (125 MHz, d_6-DMSO)**: δ = 159.5 (brd, *J* = 244.5 Hz), 138.2, 131.3, 131.1, 126.5, 124.3, 124.2, 123.2, 122.9, 122.4, 119.1, 119.1, 118.4, 115.7, 111.8, 111.7, 108.0, 106.8, 33.6, 33.6 ppm. **UV/Vis (Ethanol)**: λ_{max} = 391.0 nm.

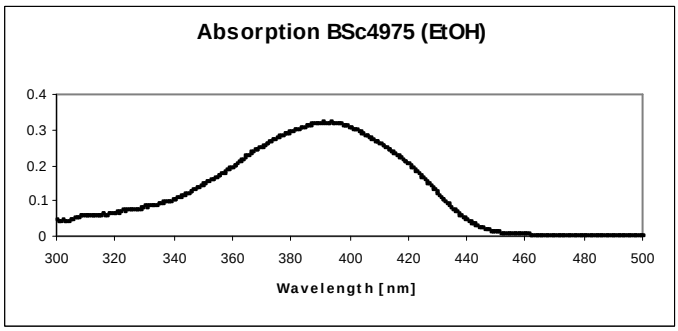

***In vitro* neuropathological staining of AD brain sections**: Tissues: hippocampus; Patient: male, 72 years old; CERAD Score: 3; NFTs-level: V.

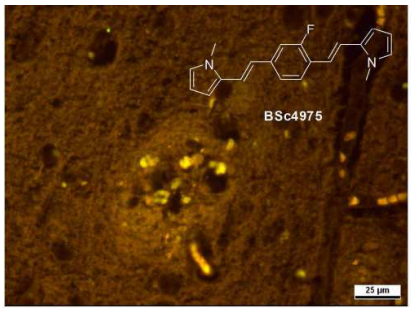

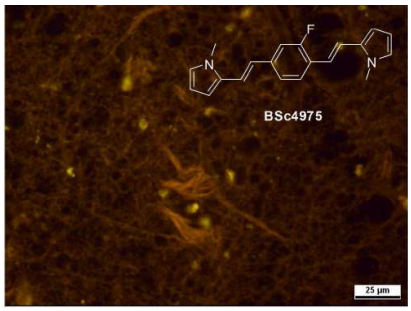

***In vitro* neuropathological staining of AD olfactory epithelium sections**: Tissues: olfactory epithelium; Patient: male, 78 years old; Braak: V, CERAD Score: 3.

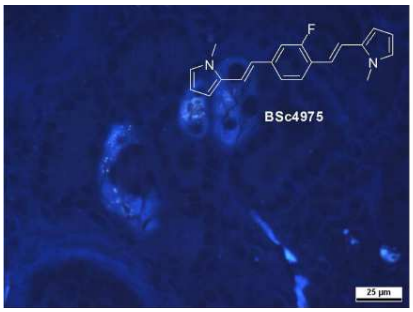

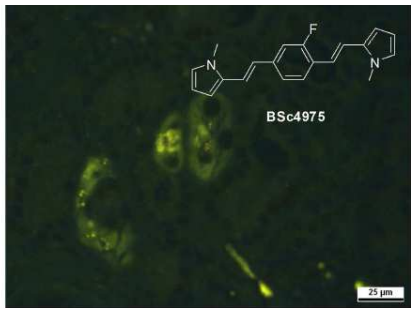

5,5'-(1*E*,1'*E*)-2,2'-(2-Fluoro-1,4-phenylene)bis(ethene-2,1-diyl)bis(*N*,*N*-dimethylthiophen-2-amine) (100c)

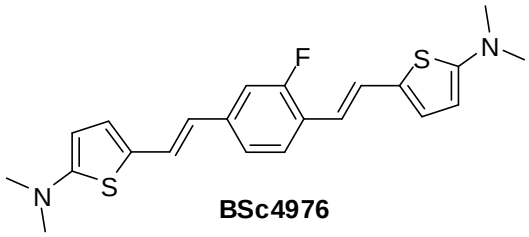

BSc4976

Yield: 39 %. **^{1}H-NMR (500 MHz, d_6-DMSO)**: δ = 7.55 (t, *J* = 8.0 Hz, 1H), 7.32-7.20 (m, 4H), 6.86 (dd, *J* = 10.5 Hz, *J* = 4.0 Hz, 2H), 6.42 (t, *J* = 16.0 Hz, 2H), 5.85-5.81 (m, 2H), 2.93 (s, 6H), 2.92 (s, 6H) ppm. **^{13}C-NMR (125 MHz, d_6-DMSO)**: δ = 158.6, 137.6, 129.3, 129.2, 126.3, 126.1, 123.9, 121.7, 119.9, 112.5, 111.5, 102.0, 41.9 ppm. **UV/Vis (Ethanol)**: λ_{max} = 409.5 nm.

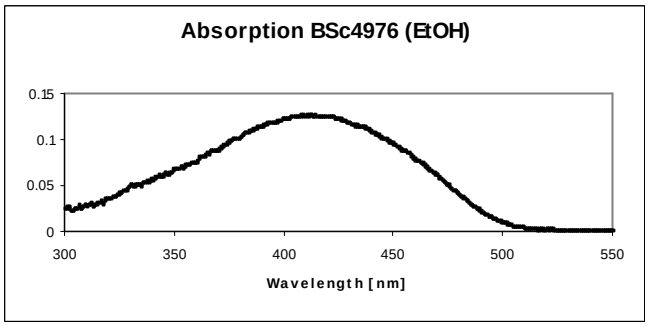

***In vitro* neuropathological staining of AD brain sections**: Tissues: hippocampus; Patient: male, 72 years old; CERAD Score: 3; NFTs-level: V.

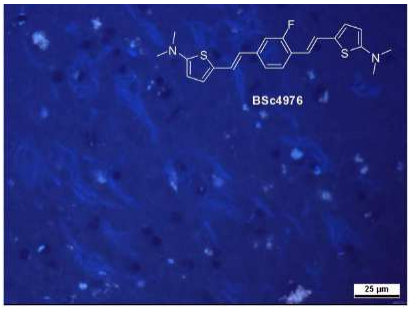

1,1'-(4,4'-(1*E*,1'*E*)-2,2'-(2-Fluoro-1,4-phenylene)bis(ethene-2,1-diyl)bis(4,1-phenylene))dipyrrolidine (100d)

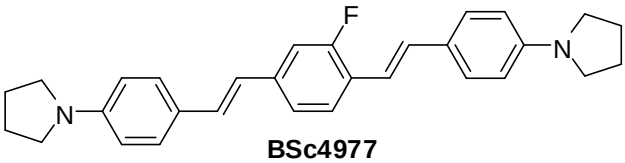

BSc4977

Yield: 62 %. **^{1}H-NMR (500 MHz, $CDCl_3$)**: δ = 7.53 (t, *J* = 8.0 Hz, 1H), 7.44 (dd, *J* = 14.5 Hz, *J* = 3.5 Hz, 4H), 7.23-7.00 (m, 5H), 6.89-6.60 (m, 5H), 3.38 (s, 8H), 2.07 (s, 8H) ppm. **UV/Vis (Ethanol)**: λ_{max} = 358.5 nm.

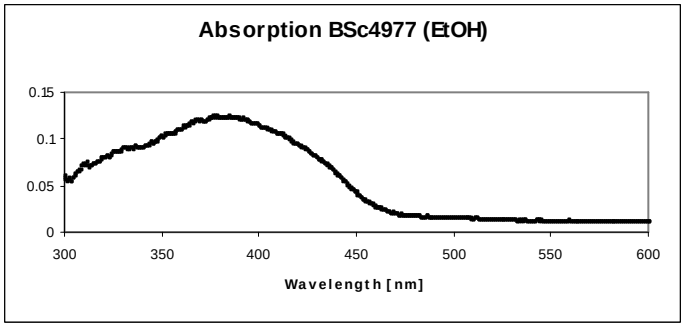

***In vitro* neuropathological staining of AD brain sections**: Tissues: hippocampus; Patient: male, 72 years old; CERAD Score: 3; NFTs-level: V.

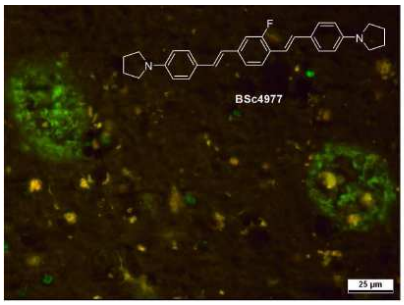

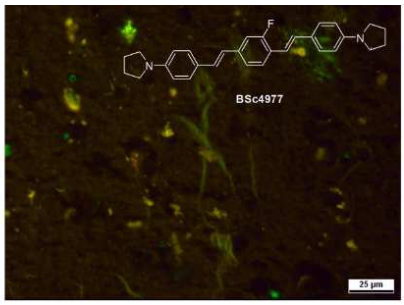

3,3'-(1*E*,1'*E*)-2,2'-(2-Fluoro-1,4-phenylene)bis(ethene-2,1-diyl)dipyridine (100e)

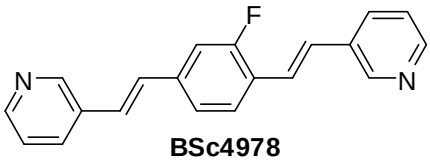

BSc4978

Yield: 66 %. **^{1}H-NMR (500 MHz, d_6-DMSO)**: δ = 8.81-8.76 (m, 2H), 8.50-8.45 (m, 2H), 8.07 (d, *J* = 8.0 Hz, 1H), 8.02 (d, *J* = 8.0 Hz, 1H), 7.80 (t, *J* = 8.0 Hz, 1H), 7.55-7.35 (m, 8H) ppm. **^{13}C-NMR (125 MHz, d_6-DMSO)**: δ = 160.0 (brd, *J* = 246.9 Hz), 148.7, 148.6, 148.4, 148.3, 138.5, 136.5, 132.7, 132.4, 132.3, 128.7, 127.8, 127.7, 127.6, 127.5, 126.6, 123.7, 123.1, 122.0, 113.4 (d, *J* = 22.6 Hz) ppm. **UV/Vis (Ethanol)**: λ_{max} = 349.5 nm.

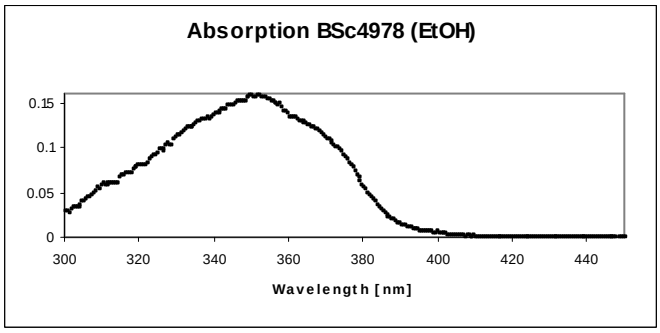

***In vitro* neuropathological staining of AD brain sections**: Tissues: hippocampus; Patient: male, 72 years old; CERAD Score: 3; NFTs-level: V.

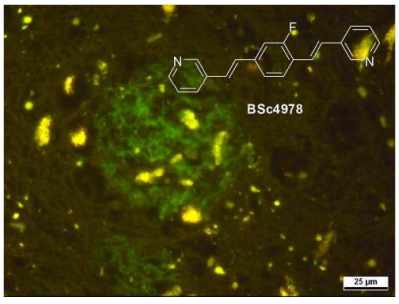

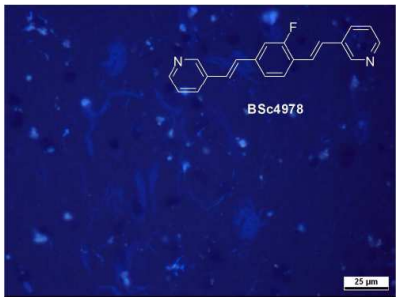

6.5.3.3. Synthesis of 1,2,4,5-tetrafluoro-3,6-bisstyrylbenzene derivatives

1,4-Bis(bromomethyl)-2,3,5,6-tetrafluorobenzene (102)

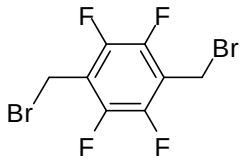

To a stirred solution of 2,3,5,6-tetrafluoro-*p*-xylene (1.78 g, 10.0 mmol, 1.0 eq) in $CHCl_3$ (30 mL) was added NBS (6.23 g, 35.0 mmol, 3.5 eq) and AIBN (0.23 g, 1.4 mmol, 0.14 eq) at room temperature. The reaction mixture was refluxed for 15 h. The cooled reaction mixture was then washed with H_2O and dried over $MgSO_4$. After filtration, the solvent was evaporated *in vacuo*, the residue was crystallized from cyclohexane to afford 2.37 g of target compound.

Yield: 71 %. **^{1}H-NMR (500 MHz, d_6-DMSO)**: δ = 4.73 (s, 4H) ppm. **^{13}C-NMR (125 MHz, d_6-DMSO)**: δ = 143.8 (brd, *J* = 249.3), 117.7, 17.7 ppm. **MS (EI, 70 eV)**: *m/z* = 336 $[M]^+$.

1,2,4,5-Tetrafluoro-3,6-bis(diethylphosphonylmethyl)benzene (103)

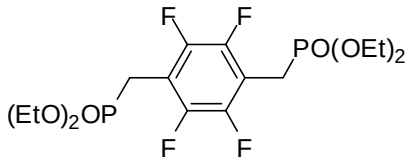

A mixture of triethyl phosphite (2.49 g, 15.0 mmol, 3 eq) and 1,4-bis(bromomethyl)-2,3,5,6-tetrafluorobenzene (1.68 g, 5.0 mmol, 1.0 eq) was heated to 160 °C for 6 h. The residue was crystallized from diethyl ether to afford the colorless solid, which was used in the next reaction without further purification.

^{1}H-NMR (500 MHz, d_6-DMSO): δ = 4.05-3.97 (m, 8H), 3.36 (d, *J* = 20 Hz, 4H), 1.18 (t, *J* = 7.0 Hz, 12H) ppm. **^{13}C-NMR (125 MHz, d_6-DMSO)**: δ = 144.2 (brd, *J* = 225.0 Hz), 110.8 (brs), 61.9 (t, *J* = 7.0 Hz), 20.9 (d, *J* = 138.9 Hz), 15.9 ppm. **MS (EI, 70 eV)**: *m/z* = 450 $[M]^+$.

General procedure for Wittig-Horner coupling

The *t*-BuOK (336 mg, 3.0 mmol, 3.0 eq) was added to a stirred solution of 1,2,4,5-tetrafluoro-3,6-bis(diethylphosphonylmethyl)benzene (450 mg, 1.0 mmol, 1.0 eq) in DMF (4 mL) at room temperature. The mixture was stirred for 5 min under argon. Then corresponding aldehyde

(2.0 mmol, 2.0 eq) was added to the mixture, which was further stirred at room temperature overnight. The reaction was then quenched with H_2O (15 mL), and the precipitates were filtered off, the residue was purified by column chromatography (SiO_2; dichloromethane: methanol = 10:1) to afford the corresponding compound in moderate yields (**Table 3.4**).

2,2'-(1*E*,1'*E*)-2,2'-(Perfluoro-1,4-phenylene)bis(ethene-2,1-diyl)bis(1-methyl-1*H*-pyrrole) (104a)

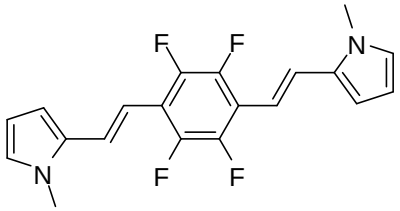

BSc4566

Yield: 69 %. **^{1}H-NMR (500 MHz, $CDCl_3$)**: δ = 7.36 (d, *J* = 16.5 Hz, 2H), 6.82 (d, *J* = 16.5 Hz, 2H), 6.70 (t, *J* = 2.0 Hz, 2H), 6.63 (dd, *J* = 4.0 Hz, *J* = 1.0 Hz, 2H), 6.20-6.18 (m, 2H), 3.70 (s, 6H) ppm. **^{13}C-NMR (125 MHz, $CDCl_3$)**: δ = 144.4 (brd, *J* = 238.6 Hz), 131.8, 124.9, 124.3, 114.6 (brs), 110.5, 109.0, 106.1, 34.0 ppm. **MS (EI)**: *m/z* = 360 $[M]^+$. **UV/Vis (Ethanol)**: λ_{max} = 406.5 nm.

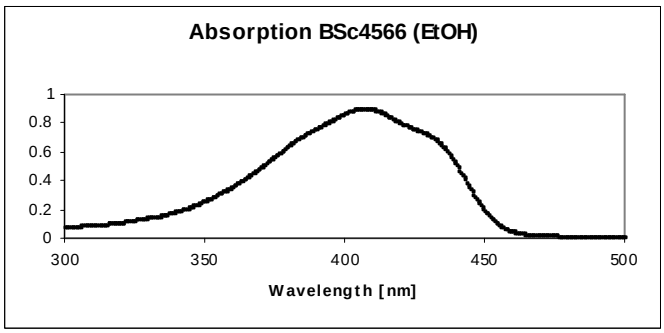

4,4'-(1*E*,1'*E*)-2,2'-(Perfluoro-1,4-phenylene)bis(ethene-2,1-diyl)bis(*N*,*N*-dimethylaniline) (104b)

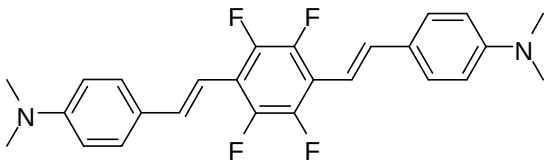

BSc4567

Yield: 65 %. **^{1}H-NMR (500 MHz, $CDCl_3$)**: δ = 7.47-7.39 (m, 6H), 6.88 (d, *J* = 16.5 Hz, 2H), 6.73 (d, *J* = 7.5 Hz, 4H), 3.02 (s, 12H) ppm. **UV/Vis (Ethanol)**: λ_{max} = 412.5 nm.

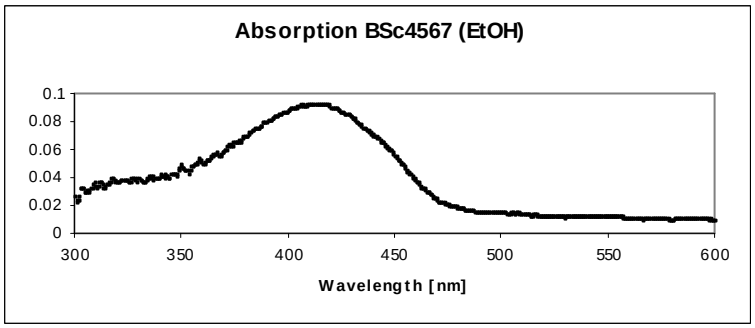

***In vitro* neuropathological staining of AD brain sections**: Tissues: hippocampus; Patient: male, 71 years old; CERAD Score: 3; NFTs-level: V.

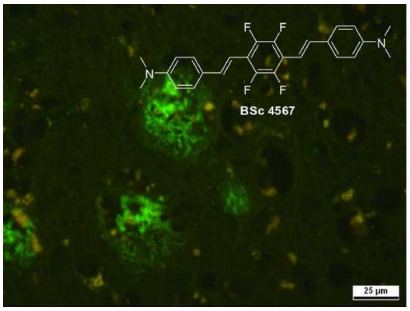

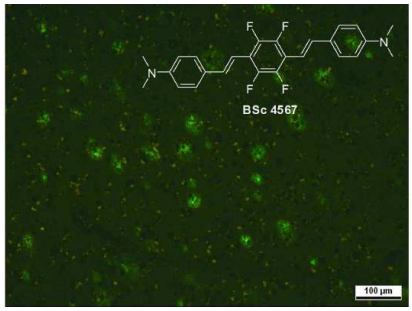

5,5'-(1*E*,1'*E*)-2,2'-(Perfluoro-1,4-phenylene)bis(ethene-2,1-diyl)di-2,2'-bithiophene (104c)

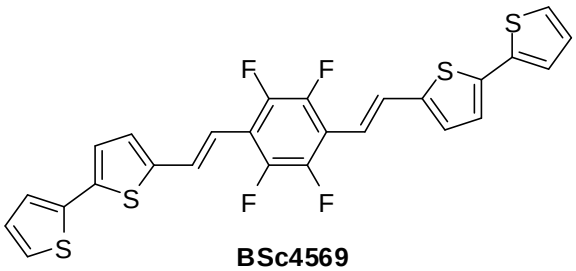

BSc4569

Yield: 66 %. **^{1}H-NMR (500 MHz, $CDCl_3$)**: δ = 7.56 (d, *J* = 16.5 Hz, 2H), 7.27-7.22 (m, 4H), 7.11 (d, *J* = 3.5 Hz, 2H), 7.07 (d, *J* = 3.5 Hz, 2H), 7.04 (dd, *J* = 5.0 Hz, *J* = 3.5 Hz, 2H), 6.85 (d, *J* = 16.5 Hz, 2H) ppm. **^{13}C-NMR (125 MHz, $CDCl_3$)**: δ = 141.2, 138.3, 137.1, 129.3, 128.0, 125.1, 124.3, 124.3, 124.2, 113.2 ppm. **UV/Vis (Ethanol)**: λ_{max} = 428.0 nm.

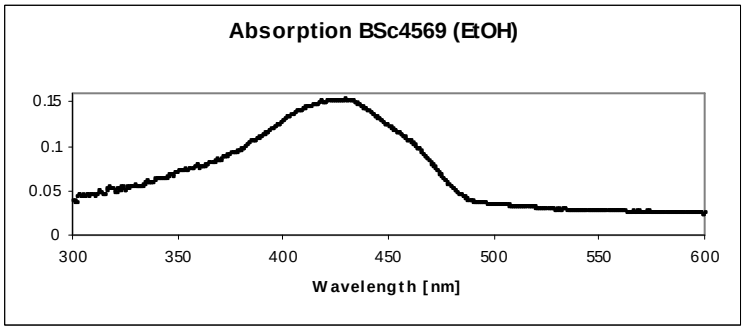

***In vitro* neuropathological staining of AD brain sections**: Tissues: hippocampus; Patient: male, 71 years old; CERAD Score: 3; NFTs-level: V.

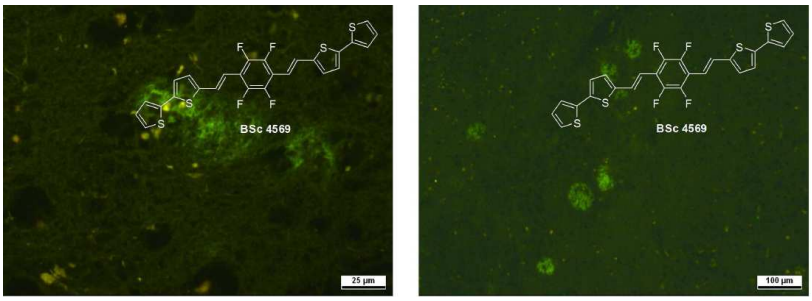

3,3'-(1*E*,1'*E*)-2,2'-(Perfluoro-1,4-phenylene)bis(ethene-2,1-diyl)dipyridine (104d)

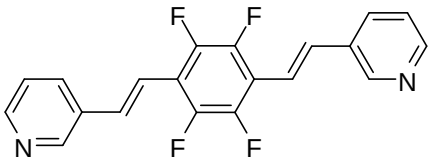

BSc4570

Yield: 62 %. **^{1}H-NMR (500 MHz, $CDCl_3$)**: δ = 8.76 (d, *J* = 2.0 Hz, 2H), 8.57 (dd, *J* = 4.5 Hz, *J* = 1.5 Hz, 2H), 7.90 (dt, *J* = 8.0 Hz, *J* = 2.0 Hz, 2H), 7.51 (d, *J* = 16.5 Hz, 2H), 7.34 (dd, *J* = 8.0 Hz, *J* = 4.5 Hz, 2H), 7.15 (d, *J* = 17.0 Hz, 2H) ppm. **^{13}C-NMR (125 MHz, $CDCl_3$)**: δ = 149.8, 149.0, 144.8(brd, *J* = 252.8 Hz), 133.6, 132.9, 132.4, 123.7, 116.0, 115.0 (brs) ppm. **UV/Vis (Ethanol)**: λ_{max} = 342.5 nm.

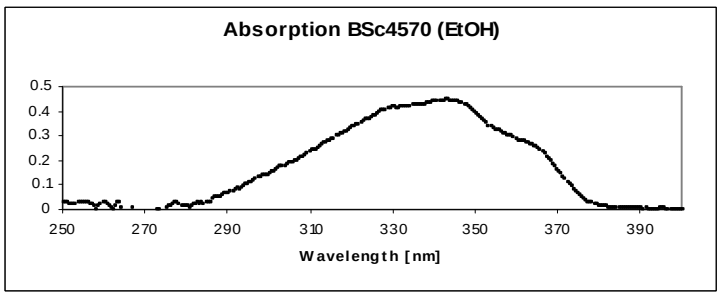

***In vitro* neuropathological staining of AD brain sections**: Tissues: hippocampus; Patient: male, 71 years old; CERAD Score: 3; NFTs-level: V.

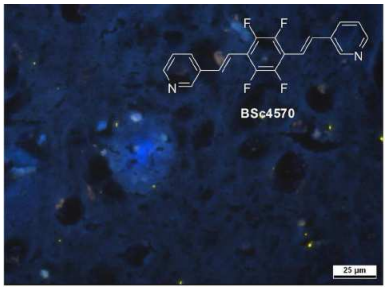

(4,4'-(1*E*,1'*E*)-2,2'-(Perfluoro-1,4-phenylene)bis(ethene-2,1-diyl)bis(4,1-phenylene))bis(methylsulfane) (104e)

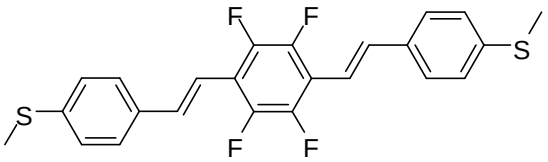

BSc4571

Yield: 59 %. **^{1}H-NMR (500 MHz, $CDCl_3$)**: δ = 7.50-7.43 (m, 6H), 7.26 (d, *J* = 7.5 Hz, 4H), 7.05 (d, *J* = 16.5 Hz, 2H), 2.52 (s, 6H) ppm. **UV/Vis (Ethanol)**: λ_{max} = 373.5 nm.

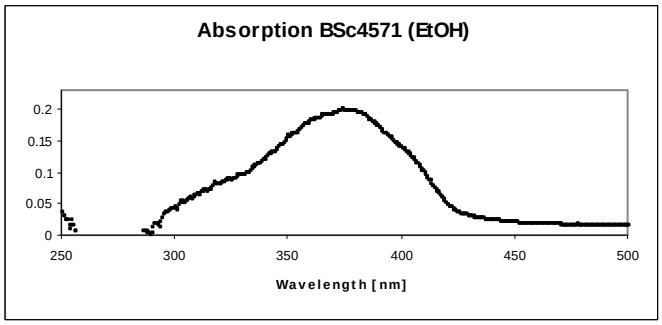

***In vitro* neuropathological staining of AD brain sections**: Tissues: hippocampus; Patient: male, 71 years old; CERAD Score: 3; NFTs-level: V.

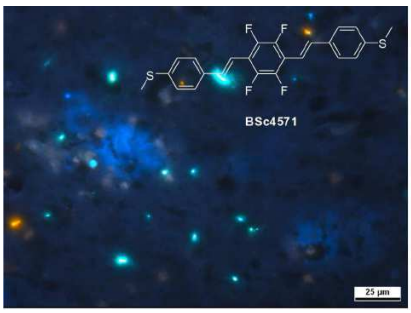

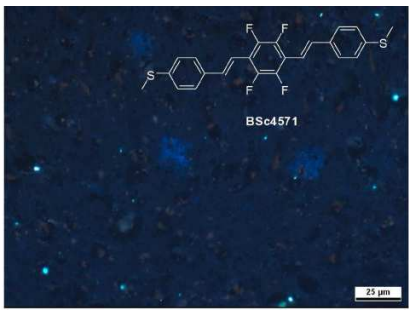

4,4'-(1*E*,1'*E*)-2,2'-(Perfluoro-1,4-phenylene)bis(ethene-2,1-diyl)dibenzonitrile (104f)

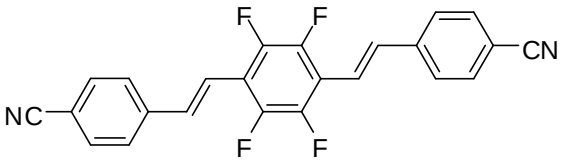

BSc4572

Yield: 53 %. **^{1}H-NMR (500 MHz, $CDCl_3$)**: δ = 7.69 (d, *J* = 8.0 Hz, 4H), 7.64 (d, *J* = 8.5 Hz, 4H), 7.53 (d, *J* = 17 Hz, 2H), 7.20 (d, *J* = 16.5 Hz, 2H) ppm. **UV/Vis (Ethanol)**: λ_{max} = 357.5 nm.

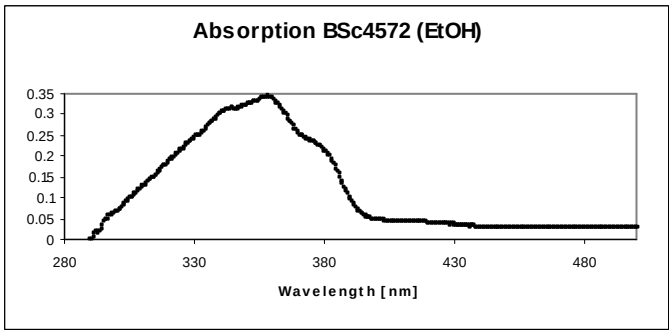

4,4'-(1*E*,1'*E*)-2,2'-(Perfluoro-1,4-phenylene)bis(ethene-2,1-diyl)bis(*N*,*N*-diethylaniline) (104g)

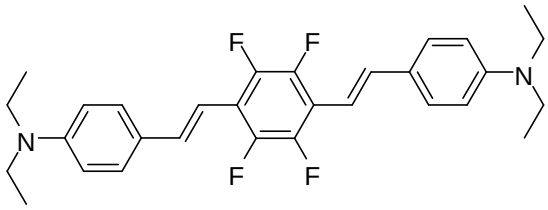

BSc4573

Yield: 59 %. **^{1}H-NMR (500 MHz, $CDCl_3$)**: δ = 7.44-7.38 (m, 6H), 6.85 (d, *J* = 16.5 Hz, 2H), 6.67 (d, *J* = 9.0 Hz, 4H), 3.43-3.37 (m, 8H), 1.20 (t, *J* = 7.0 Hz, 12H) ppm. **^{13}C-NMR (125 MHz, $CDCl_3$)**: δ = 148.1, 144.5 (brd, *J* = 243.8 Hz), 136.4, 128.4, 124.3, 114.6 (brs), 111.6, 109.0, 44.4, 12.6 ppm. **UV/Vis (Ethanol)**: λ_{max} = 422.0 nm.

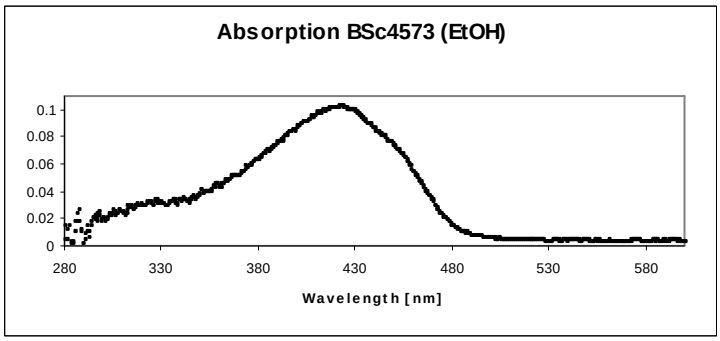

6.5.4. Synthesis of 1,4-bisstyryl-2-bromo-5-cyanobenzene derivatives

4-Bromo-2,5-dimethylbenzonitrile (105)

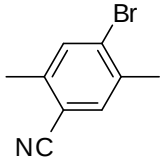

A mixture of 1,4-dibromo-2,5-dimethylbenzene (1.32 g, 5.0 mmol, 1.0 eq) and CuCN (0.448 g, 5.0 mmol, 1.0 eq) in DMF (10 mL) at 80 °C for 1 h. The reaction was then quenched with H_2O (15 mL) and extracted with EtOAc. The organic phase was dried over Na_2SO_4. After filtration, the solvent was evaporated *in vacuo*, the residue was purified by column chromatography (SiO_2; ethyl acetate: cyclohexane = 1:10) to afford 0.73 g of title compound.

Yield: 70 %. **^{1}H-NMR (500 MHz, $CDCl_3$)**: δ = 7.49 (s, 1H), 7.41 (s, 1H), 2.46 (s, 3H), 2.36 (s, 3H) ppm. **^{13}C-NMR (125 MHz, $CDCl_3$)**: δ = 140.5, 136.4, 134.0, 133.7, 130.0, 117.4, 111.7, 22.1, 19.6 ppm.

4-Bromo-2,5-bis(bromomethyl)benzonitrile (106)

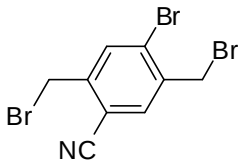

To a stirred solution of 4-bromo-2,5-dimethylbenzonitrile (2.10 g, 10.0 mmol, 1.0 eq) in $CHCl_3$ (30 mL) was added NBS (6.23 g, 35.0 mmol, 3.5 eq) and AIBN (0.23 g, 1.4 mmol, 0.14 eq) at room temperature. The reaction mixture was refluxed for 15 h. The cooled reaction mixture was then washed with H_2O and dried over $MgSO_4$. After filtration, the solvent was evaporated *in vacuo*, the residue was crystallized from cyclohexane to afford 2.89 g of target compound.

Yield: 79 %. **^{1}H-NMR (500 MHz, d_6-DMSO)**: δ = 8.20 (s, 1H), 8.12 (s, 1H), 4.77 (s, 2H), 4.73 (s, 2H) ppm. **^{13}C-NMR (125 MHz, d_6-DMSO)**: δ = 142.9, 138.8, 135.9, 135.1, 129.6, 115.8, 111.6, 32.2, 29.2 ppm. **MS (EI, 70 eV)**: *m/z* = 368 $[M]^+$.

Tetraethyl (2-bromo-5-cyano-1,4-phenylene)bis(methylene)diphosphonate (107)

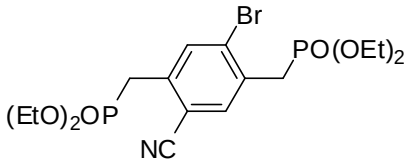

A mixture of triethyl phosphite (2.49 g, 15.0 mmol, 3.0 eq) and 4-bromo-2,5-bis(bromomethyl)benzonitrile (1.84 g, 5.0 mmol, 1.0 eq) was heated to 160 °C for 6 h. The residue was crystallized from cyclohexane to afford the colorless solid, which was used in the next reaction without further purification.

^{1}H-NMR (500 MHz, d_6-DMSO): δ = 7.81 (s, 1H), 7.80 (s, 1H), 4.03-3.95 (m, 8H), 3.46 (d, *J* = 6.0 Hz, 2H), 3.42 (d, *J* = 6.0 Hz, 2H), 1.20-1.15 (m, 12H) ppm.

General procedure for Wittig-Horner coupling

The *t*-BuOK (336 mg, 3 mmol, 3.0 eq) was added to a stirred solution of tetraethyl (2-bromo-5-cyano-1,4-phenylene)bis(methylene)diphosphonate (482 mg, 1 mmol, 1.0 eq) in DMF (4 mL) at room temperature. The mixture was stirred for 5 min under argon. Then corresponding aldehyde (2.0 mmol, 2.0 eq) was added to the mixture, which was further stirred at room temperature overnight. The reaction was then quenched with H_2O (15 mL), and the precipitates were filtered off, the residue was purified by column chromatography (SiO_2; dichloromethane: methanol = 10:1) to afford the corresponding compound in moderate yields (**Table 3.5**).

4-Bromo-2,5-bis(4-(diethylamino)styryl)benzonitrile (108a)

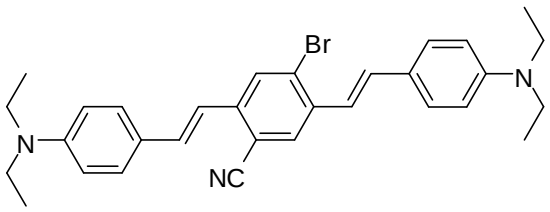

BSc4577

Yield: 77 %. **^{1}H-NMR (500 MHz, $CDCl_3$)**: δ = 7.94 (s, 1H), 7.83 (s, 1H), 7.44 (t, *J* = 9.0 Hz, 4H), 7.19-7.07 (m, 3H), 6.99 (d, *J* = 16.0 Hz, 1H), 6.67 (dd, *J* = 9.0 Hz, *J* = 3.5 Hz, 4H), 3.44-3.36 (m, 8H), 1.20 (td, *J* = 7.0 Hz, *J* = 1.5 Hz, 12H) ppm. **^{13}C-NMR (125 MHz, $CDCl_3$)**: δ = 148.3, 148.1, 139.9, 136.3, 133.6, 132.7, 129.7, 128.8, 128.7, 128.5, 123.8, 123.2, 120.0, 118.0, 117.2, 111.6, 111.5, 109.6, 44.4, 12.6 ppm. **MS (EI, 70 eV)**: *m/z* = 527 $[M]^+$. **UV/Vis (Ethanol)**: λ_{max} = 442.0 nm.

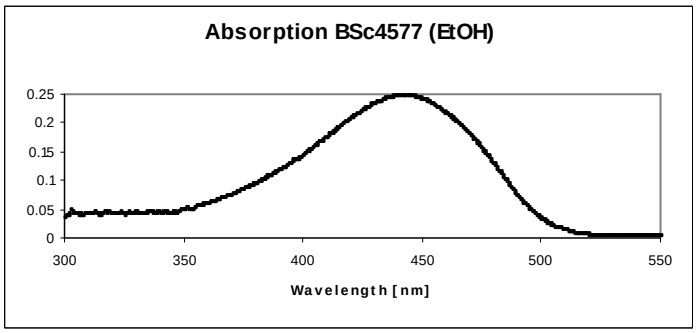

***In vitro* neuropathological staining of AD brain sections**: Tissues: hippocampus; Patient: male, 71 years old; CERAD Score: 3; NFTs-level: V.

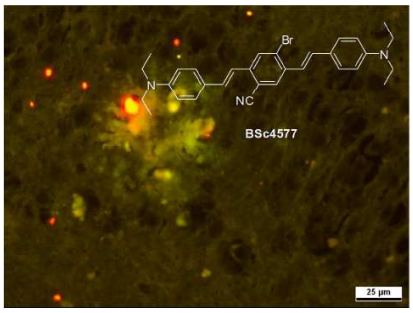

4-Bromo-2,5-bis((*E*)-2-(1-methyl-1*H*-pyrrol-2-yl)vinyl)benzonitrile (108b)

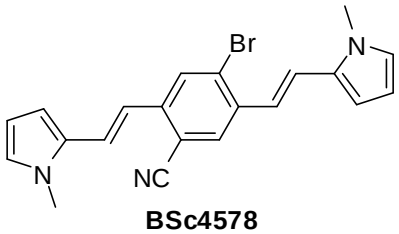

BSc4578

Yield: 73 %. **^{1}H-NMR (500 MHz, $CDCl_3$)**: δ = 7.87 (s, 1H), 7.80 (s, 1H), 7.19-6.91 (m, 4H), 6.74-6.68 (m, 2H), 6.65 (dd, *J* = 4.0 Hz, *J* = 1.0 Hz, 1H), 6.61 (dd, *J* = 4.0 Hz, *J* = 1.0 Hz, 1H), 6.22-6.17 (m, 2H), 3.76 (s, 3H), 3.75 (s, 3H) ppm. **MS (EI, 70 eV)**: *m/z* = 393 $[M+2]^+$. **UV/Vis (Ethanol)**: λ_{max} = 417.5 nm.

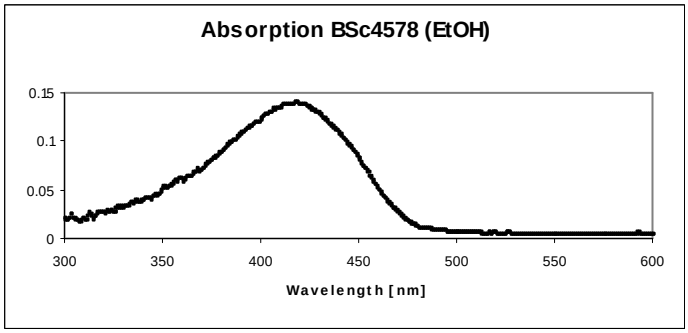

4-Bromo-2,5-bis((*E*)-2-(pyridin-3-yl)vinyl)benzonitrile (108c)

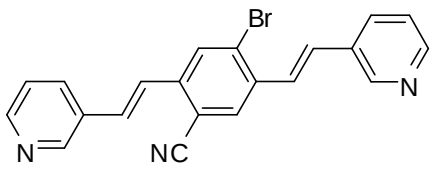

BSc4580

Yield: 82 %. **^{1}H-NMR (500 MHz, $CDCl_3$)**: δ = 7.78 (dd, *J* = 6.5 Hz, *J* = 2.0 Hz, 2H), 8.58 (td, *J* = 5.0 Hz, *J* = 1.0 Hz, 2H), 8.06 (s, 1H), 7.97-7.93 (m, 2H), 7.90 (dt, *J* = 8.0 Hz, *J* = 2.0 Hz, 1H), 7.49-7.39 (m, 2H), 7.38-7.33 (m, 2H), 7.28 (d, *J* = 16.0 Hz, 1H), 7.10 (d, *J* = 16.0 Hz, 1H) ppm. **^{13}C-NMR (125 MHz, $CDCl_3$)**: δ = 150.0, 149.7, 149.3, 148.9, 139.6, 136.8, 133.3, 133.1, 131.9, 131.5, 130.8 130.7, 130.2, 129.9, 129.2, 127.1, 124.5, 123.8, 123.7, 117.0, 111.0 ppm. **UV/Vis (Ethanol)**: λ_{max} = 341.5 nm.

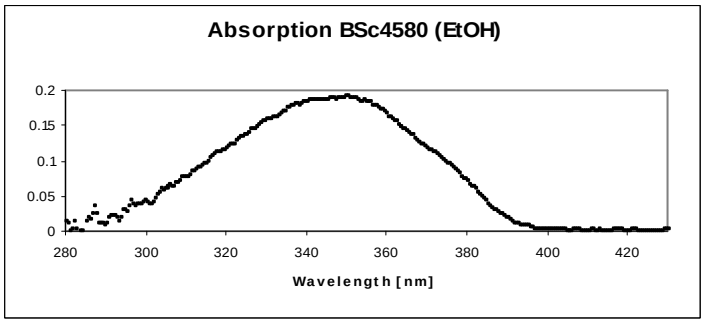

***In vitro* neuropathological staining of AD brain sections**: Tissues: hippocampus; Patient: male, 71 years old; CERAD Score: 3; NFTs-level: V.

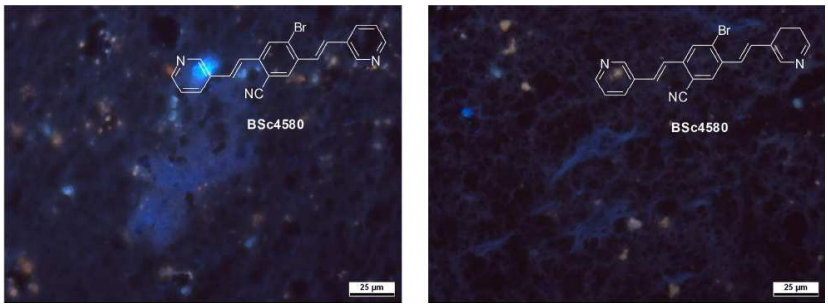

Dimethyl 5,5'-(1*E*,1'*E*)-2,2'-(2-bromo-5-cyano-1,4-phenylene)bis(ethene-2,1-diyl)bis (2-methoxybenzoate) (108d)

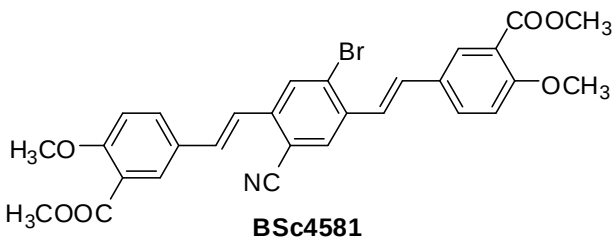

BSc4581

Yield: 66 %. **^{1}H-NMR (500 MHz, $CDCl_3$)**: δ = 8.01-7.96 (m, 3H), 7.87 (s, 1H), 7.71 (dd, *J* = 9.0 Hz, *J* = 2.5 Hz, 1H), 7.66 (dd, *J* = 9.0 Hz, *J* = 2.5 Hz, 1H), 7.27 (d, *J* = 16.5 Hz, 1H), 7.22 (s, 2H), 7.06-6.99 (m, 3H), 3.96-3.91 (m, 12H) ppm. **^{13}C-NMR (125 MHz, $CDCl_3$)**: δ = 166.3, 166.1, 159.7, 159.4, 139.7, 136.6, 132.7, 131.9, 131.8, 131.8, 130.9, 130.4, 130.4, 129.7,

128.9, 128.6, 128.2, 124.1, 121.4, 120.5, 120.5, 117.4, 112.5, 112.4, 110.4, 56.2, 52.2, 52.2 ppm. **UV/Vis (Ethanol)**: λ_{max} = 371.5 nm.

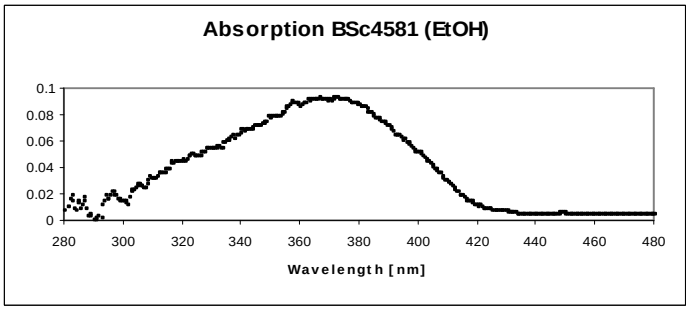

***In vitro* neuropathological staining of AD brain sections**: Tissues: hippocampus; Patient: male, 71 years old; CERAD Score: 3; NFTs-level: V.

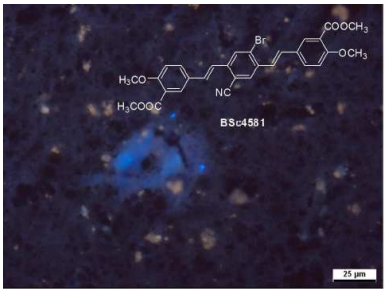

4-Bromo-2,5-bis(4-methoxystyryl)benzonitrile (108e)

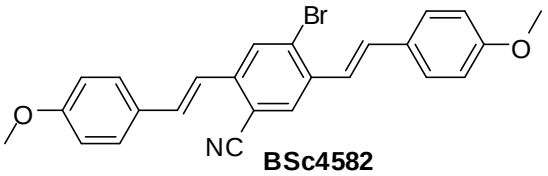

BSc4582

Yield: 69 %. **^{1}H-NMR (500 MHz, $CDCl_3$)**: δ = 7.98 (s, 1H), 7.87 (s, 1H), 7.54-7.49 (m, 4H), 7.24 (d, *J* = 16.5 Hz, 1H), 7.21 (s, 2H), 7.04 (d, *J* = 16.0 Hz, 1H), 6.95-6.91 (m, 4H), 3.85 (s, 3H), 3.85 (s, 3H) ppm. **^{13}C-NMR (125 MHz, $CDCl_3$)**: δ = 160.5, 160.2, 139.8, 136.6, 133.5, 132.6, 130.2, 129.4, 129.1, 128.8, 128.7, 128.4, 123.0, 120.3, 117.6, 114.4, 114.3, 110.3, 55.4 ppm. **UV/Vis (Ethanol)**: λ_{max} = 379.0 nm.

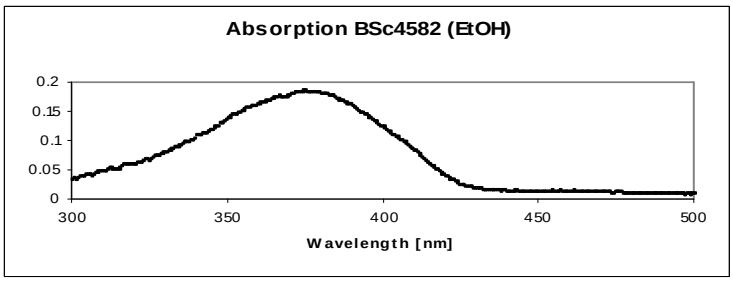

***In vitro* neuropathological staining of AD brain sections**: Tissues: hippocampus; Patient: male, 71 years old; CERAD Score: 3; NFTs-level: V.

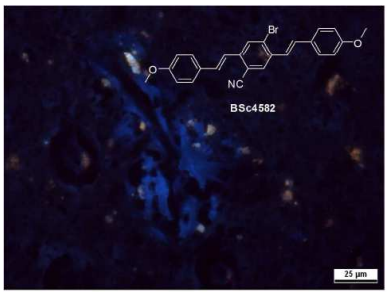

Dimethyl 5,5'-(1*E*,1'*E*)-2,2'-(2-bromo-5-cyano-1,4-phenylene)bis(ethene-2,1-diyl)bis (2-hydroxybenzoate) (108f)

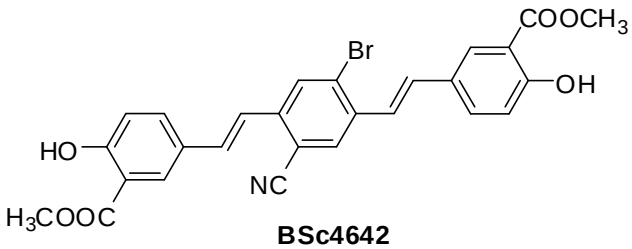

BSc4642

A 1.0 N solution of boron tribromide in dichloromethane (5.0 mL, 5.0 mmol, 5.0 eq) was added dropwise over 10 min to a stirred suspension of **108d** (561 mg, 1.0 mmol, 1.0 eq) in anhydrous dichloromethane (10 mL) at -20 °C. The reaction mixture was stirred for 12 h at room temperature. The reaction mixture was then quenched with 20 mL of water to afford **108f** as precipitates, which was filtered off and washed with water and ethyl acetate.

Yield: 97 %. **MS (EI, 70 eV)**: *m/z* = 535 $[M+2]^+$. **UV/Vis (Ethanol)**: λ_{max} = 372.5 nm.

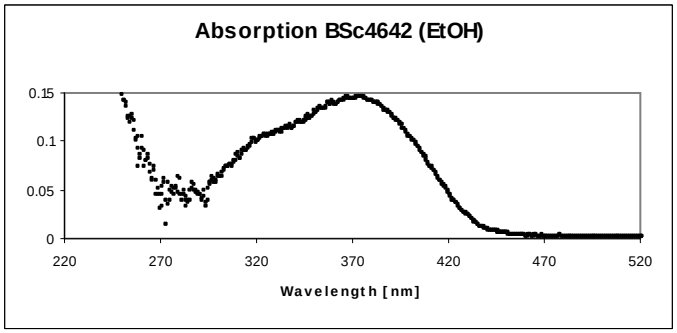

***In vitro* neuropathological staining of AD brain sections**: Tissues: hippocampus; Patient: male, 71 years old; CERAD Score: 3; NFTs-level: V.

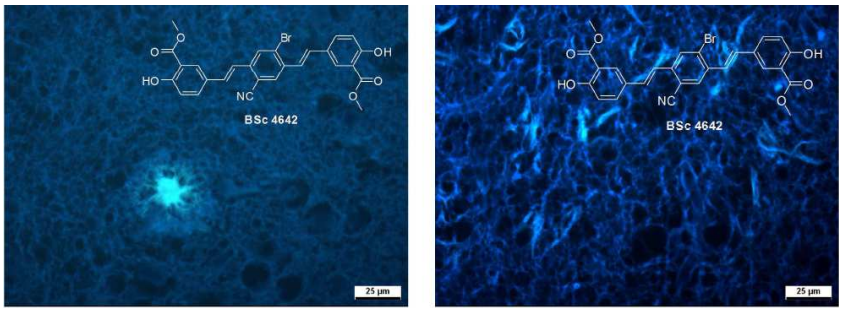

5,5'-(1*E*,1'*E*)-2,2'-(2-Bromo-5-cyano-1,4-phenylene)bis(ethene-2,1-diyl)bis(2-hydroxybenzoic acid) (108g)

To **108f** (106 mg, 0.2 mmol, 1.0 eq) was added 1.0 N NaOH (5.0 mL, 5.0 mmol, 25 eq), and the solution was stirred at 90 °C overnight. After cooling down to room temperature, the solution was quenched with 5 mL water and 1 mL 6.0 M HCl solution. Precipitates were filtered off and washed with water and ethyl acetate to afford **108g** without further purification.

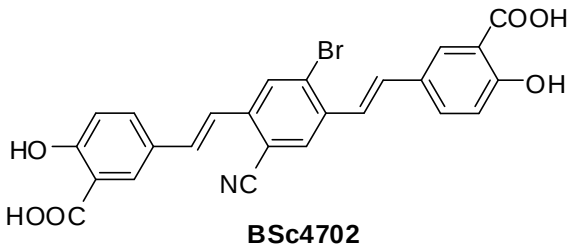

BSc4702

Yield: 84 %. **^{1}H-NMR (500 MHz, $CDCl_3$)**: δ = 8.31 (s, 2H), 8.04 (d, *J* = 2.0 Hz, 1H), 8.00 (d, *J* = 2.5 Hz, 1H), 7.86-7.80 (m, 2H), 7.66 (d, *J* = 16.0 Hz, 1H), 7.50 (d, *J* = 16.5 Hz, 1H), 7.20 (d, *J* = 16.0 Hz, 1H), 7.14 (d, *J* = 16.0 Hz, 1H), 7.06-7.00 (m, 2H) ppm. **UV/Vis (Ethanol)**: λ_{max} = 384.0 nm.

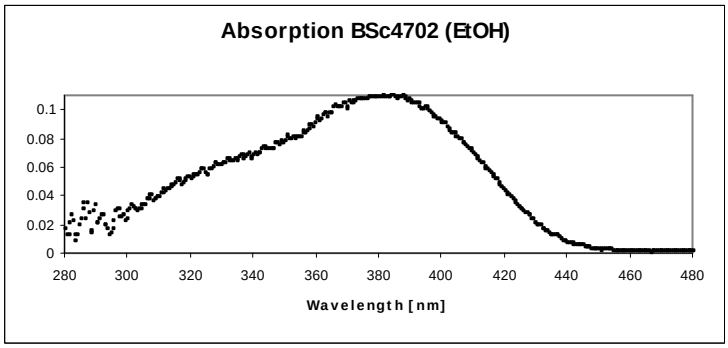

***In vitro* neuropathological staining of AD brain sections**: Tissues: hippocampus; Patient: male, 71 years old; CERAD Score: 3; NFTs-level: V.

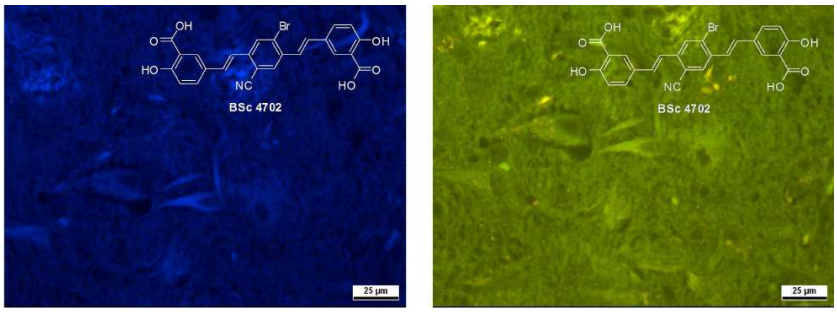

6.5.5. Synthesis of bis(arylvinyl)pyrimidine derivatives

6.5.5.1. Synthesis of aldehydes based on microwave irradiation

4-(Dimethylamino)-3-fluorobenzaldehyde (110)

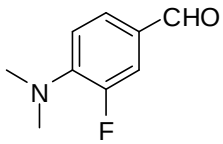

A mixture of 3,4-difluorobenzaldehyde (1.42 g, 10.0 mmol, 1.0 eq), 30 % dimethylamine solution (1.8 g, 12.0 mmol, 1.2 eq) and potassium carbonate (4.14 g, 30.0 mmol, 3.0 eq) in DMSO (5 mL) was stirred for 12 h at 60 °C under microwave irradiation. Reaction mixture was cooled down to room temperature, diluted with EtOAc (20 mL) and washed with water (2 x 10 mL). Organic layer was dried over Na_2SO_4. After filtration, the solvent was evaporated *in vacuo*, the residue was purified by column chromatography (SiO_2; ethyl acetate: cyclohexane = 1:1) to afford 1.47 g of title compound as yellow oil.

Yield: 88 %. **^{1}H-NMR (500 MHz, $CDCl_3$)**: δ = 9.74 (d, *J* = 2.0 Hz, 1H), 7.53-7.45 (m, 2H), 6.81 (t, *J* = 8.5 Hz, 1H), 3.04 (d, *J* = 2.0 Hz, 6H) ppm. **^{13}C-NMR (125 MHz, $CDCl_3$)**: δ = 189.5, 154.8 (d, *J* = 977.5 Hz), 145.2 (d, *J* = 32.0 Hz), 128.1, 127.7 (d, *J* = 23.5 Hz), 116.2 (d, *J* = 87.0 Hz), 115.9 (d, *J* = 16.5 Hz), 42.1 (d, *J* = 24.5 Hz) ppm.

4-(2-Hydroxyethylamino)benzaldehyde (113)

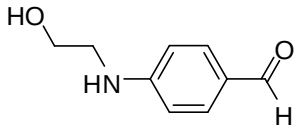

A mixture of 4-bromobenzaldehyde (1.01 g, 5.0 mmol, 1.0 eq), 2-aminoethanol (458 mg, 7.5 mmol, 1.5 eq), K_3PO_4 (2.12 g, 10.0 mmol, 2.0 eq), CuI (95 mg, 0.5 mmol, 0.1 eq), and proline (115 mg, 1.0 mmol, 0.2 eq) in 3 mL of DMSO was heated at 80 °C under microwave irradiation. Water was added to the reaction mixture. The mixture was then extracted with EtOAc twice. The combined organic layers were washed with brine, dried over Na_2SO_4. After filtration, the solvent was evaporated *in vacuo*. The residue was purified by column chromatography (SiO_2; ethyl acetate: cyclohexane = 1:1) to afford 0.84 g of title compound.

Yield: 93 %. **^{1}H-NMR (500 MHz, $CDCl_3$)**: δ = 9.62 (s, 1H), 7.62 (d, *J* = 9.0 Hz, 2H), 6.58 (t, *J* = 8.5 Hz, 2H), 5.03 (s, 1H), 3.84 (t, *J* = 5.0 Hz, 2H), 3.34 (t, *J* = 5.0 Hz, 2H), 3.05 (s, 1H) ppm. **^{13}C-NMR (125 MHz, $CDCl_3$)**: δ = 190.6, 153.6, 132.4, 126.1, 111.9, 60.7, 45.1 ppm

6.5.5.2. General procedures for synthesis of bis(arylvinyl)pyrimidine derivatives

A mixture of 4,6-dimethylpyrimidine (108 mg, 1.0 mmol, 1.0 eq), corresponding aldehyde (2 mmol, 2.0 eq), Aliquat 336 (60.6 mg, 0.15 mmol, 0.15 eq) and 5 N NaOH solution (5 mL) was stirred at 80 °C for 16 h. The reaction was then quenched with H_2O (10 mL). The precipitates were filtered off and washed with water, the residue was purified by column chromatography (SiO_2; ethyl acetate: cyclohexane = 1:2) to afford the corresponding compound in moderate yields (**Table 3.6**).

2,2'-(4,4'-(1*E*,1'*E*)-2,2'-(Pyrimidine-4,6-diyl)bis(ethene-2,1-diyl)bis(4,1-phenylene))bis(azanediyl)diethanol (115a)

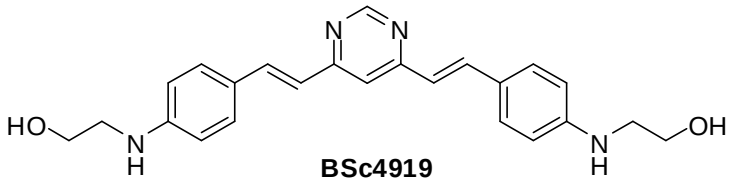

BSc4919

Yield: 82 %. **^{1}H-NMR (300 MHz, d_6-DMSO)**: δ = 8.85 (d, *J* = 0.9 Hz, 1H), 7.78 (d, *J* = 15.9 Hz, 2H), 7.49-7.41 (m, 5H), 6.88 (d, *J* = 15.9 Hz, 2H), 6.63 (d, *J* = 8.7 Hz, 4H), 6.15 (s, 2H), 4.70 (s, 2H), 3.57 (t, *J* = 6.0 Hz, 4H), 3.16 (t, *J* = 6.0 Hz, 4H) ppm. **^{13}C-NMR (75 MHz, d_6-DMSO)**: δ = 162.4, 157.6, 150.3, 137.2, 129.3, 122.8, 119.6, 114.5, 111.9, 59.4, 45.1 ppm. **UV/Vis (Ethanol)**: λ_{max} = 432.0 nm.

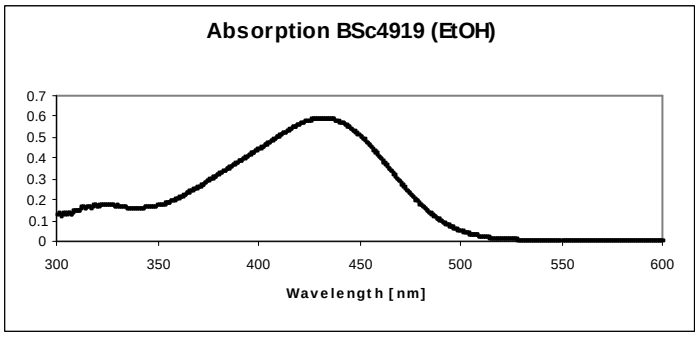

***In vitro* neuropathological staining of AD brain sections**: Tissues: hippocampus; Patient: male, 72 years old; CERAD Score: 3; NFTs-level: V.

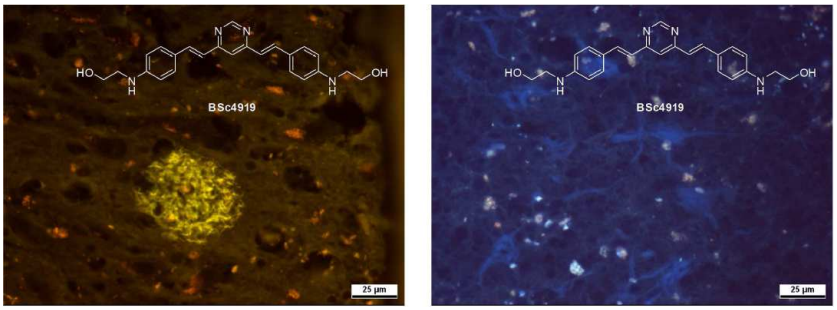

***In vitro* neuropathological staining of AD olfactory epithelium sections**: Tissues: olfactory epithelium; Patient: male, 78 years old; Braak: V, CERAD Score: 3.

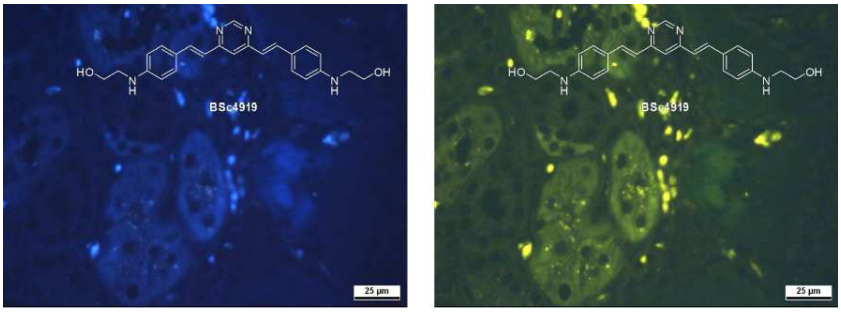

4,4'-(1*E*,1'*E*)-2,2'-(Pyrimidine-4,6-diyl)bis(ethene-2,1-diyl)bis(2-fluoro-*N*,*N*-dimethylaniline) (115b)

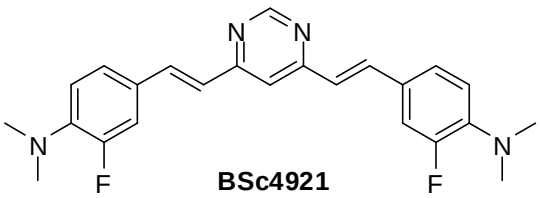

BSc4921

Yield: 77 %. **^{1}H-NMR (500 MHz, d_6-DMSO)**: δ = 8.97 (s, 1H), 7.82 (d, *J* = 16.0 Hz, 2H), 7.55-7.49 (m, 3H), 7.40 (dd, *J* = 8.5 Hz, *J* = 2.0 Hz, 2H), 7.12 (d, *J* = 16.0 Hz, 2H), 6.94 (t, *J* = 9.0

Hz, 2H) , 2.87 (s, 12H) ppm. **^{13}C-NMR (125 MHz, d_6-DMSO)**: δ = 162.2, 158.1, 153.4 (d, *J* = 933.0 Hz), 140.9 (d, *J* = 33.5 Hz), 135.2, 127.6 (d, *J* = 29.5 Hz), 124.9, 123.8, 117.6 (d, *J* = 14.0 Hz), 115.8, 114.4 (d, *J* = 36.5 Hz), 41.9 (d, *J* = 18.0 Hz) ppm. **UV/Vis (Ethanol)**: λ_{max} = 403.5 nm.

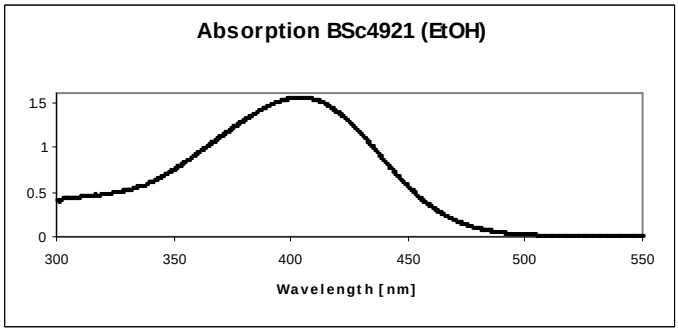

***In vitro* neuropathological staining of AD brain sections**: Tissues: hippocampus; Patient: male, 72 years old; CERAD Score: 3; NFTs-level: V.

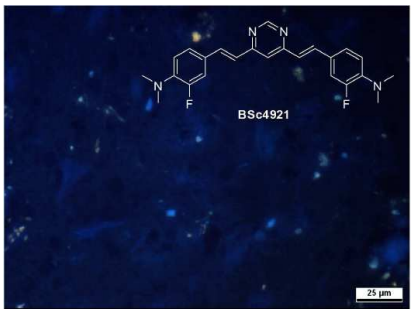

4,6-Bis((*E*)-2-(5-bromothiophen-2-yl)vinyl)pyrimidine (115c)

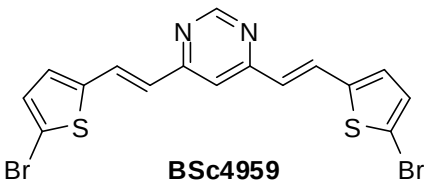

BSc4959

Yield: 62 %. **^{1}H-NMR (500 MHz, d_6-DMSO)**: δ = 9.00 (s, 1H), 8.01 (d, *J* = 16.0 Hz, 2H), 7.61 (s, 1H), 7.31 (d, *J* = 3.5 Hz, 2H), 7.27 (d, *J* = 4.0 Hz, 2H), 6.89 (d, *J* = 15.5 Hz, 2H) ppm. **^{13}C-NMR (125 MHz, d_6-DMSO)**: δ = 161.62, 158.2, 142.4, 131.7, 130.8, 128.6, 125.4, 116.4, 113.5 ppm.

5,5'-(1*E*,1'*E*)-2,2'-(Pyrimidine-4,6-diyl)bis(ethene-2,1-diyl)bis(*N*,*N*-dimethylthiophen-2-amine) (115d)

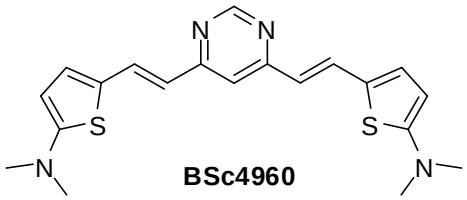

BSc4960

Yield: 96 %. **^{1}H-NMR (500 MHz, d_6-DMSO)**: δ = 8.75 (d, *J* = 1.0 Hz, 1H), 7.87 (d, *J* = 15.0 Hz, 2H), 7.24 (d, *J* = 1.0 Hz, 1H), 7.10 (d, *J* = 4.0 Hz, 2H), 6.30 (d, *J* = 15.0 Hz, 2H), 5.91 (d, *J* = 4.0 Hz, 2H) , 2.98 (s, 12H) ppm. **^{13}C-NMR (125 MHz, d_6-DMSO)**: δ = 161.9, 160.7, 133.3, 130.3, 124.2, 117.4, 114.0, 102.4, 41.8 ppm. **UV/Vis (Ethanol)**: λ_{max} = 490.0 nm.

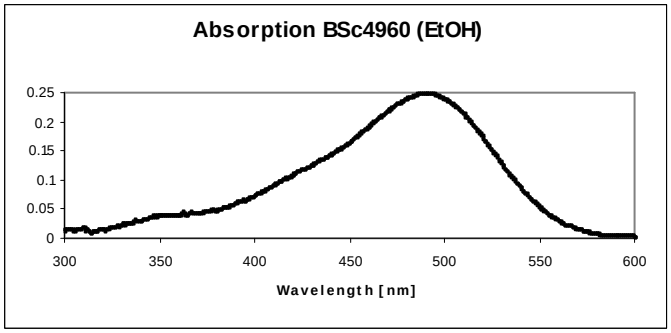

***In vitro* neuropathological staining of AD brain sections**: Tissues: hippocampus; Patient: male, 72 years old; CERAD Score: 3; NFTs-level: V.

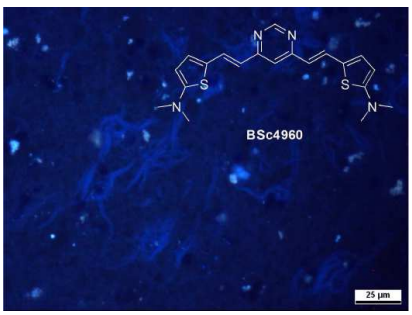

***In vitro* neuropathological staining of AD olfactory epithelium sections**: Tissues: olfactory epithelium; Patient: male, 78 years old; Braak: V, CERAD Score: 3.

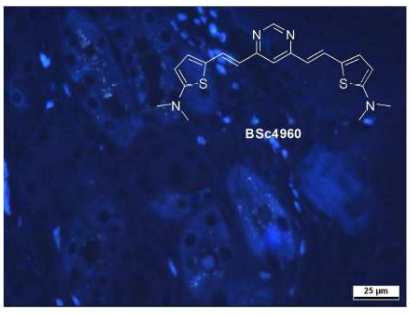

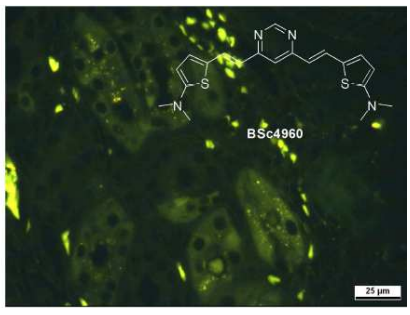

6.6. Synthesis of spiropyran derivatives

6.6.1. General procedures for synthesis of 5-substitute-2,3,3-trimethylindolenine

A mixture of substituted phenylhydrazine hydrochloride (10.0 mmol, 1.0 eq) and 3-methyl-2-butanone (1.03 g, 12.0 mmol, 1.2 eq) was dissolved in glacial acetic acid (20 mL) and then heated under reflux temperature for 12 h under argon. When it was cooled down to room temperature, the solvent was evaporated *in vacuo* and the residue was dissolved in dichloromethane (30 mL), washed with 10% aqueous Na_2CO_3 (2 × 30 mL), dried over Na_2SO_4. After filtration, the solvent was evaporated *in vacuo*. The crude product was purified by column chromatography (SiO_2; ethyl acetate: cyclohexane = 1:2) to afford the pure product as yellow liquid (yield: 73-88 %).

2,3,3-Trimethyl-3*H*-indole (118a)

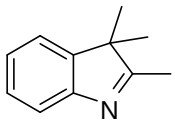

Yield: 81 %. **^{1}H-NMR (500 MHz, d_6-DMSO)**: δ = 7.42 (d, *J* = 7.5 Hz, 1H), 7.39 (d, *J* = 7.0 Hz, 1H), 7.26 (td, *J* = 7.5 Hz, *J* = 1.0 Hz, 1H), 7.16 (td, *J* = 7.5 Hz, *J* = 1.0 Hz, 1H), 2.19 (s, 3H), 1.22 (s, 6H) ppm. **^{13}C-NMR (125 MHz, d_6-DMSO)**: δ = 187.5, 153.5, 145.8, 127.2, 124.6, 121.4, 119.1, 53.0, 22.4, 14.9 ppm. **MS (EI, 70 eV)**: *m/z* = 159 $[M]^+$.

5-Fluoro-2,3,3-trimethyl-3*H*-indole (118b)

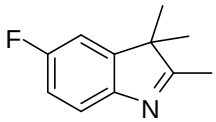

Yield: 73 %. **^{1}H-NMR (500 MHz, d_6-DMSO)**: δ = 7.49-7.44 (m, 1H), 7.01-6.95 (m, 2H), 2.28 (s, 3H), 1.30 (s, 6H) ppm. **^{13}C-NMR (125 MHz, d_6-DMSO)**: δ = 187.9 (d, *J* = 3.3 Hz), 161.3 (d, *J* = 242.4 Hz), 148.9, 147.4 (d, *J* = 8.4 Hz), 120.4 (d, *J* = 8.9 Hz), 114.2 (d, *J* = 22.3 Hz), 109.1 (d, *J* = 24.4 Hz), 54.2, 23.0, 15.3 ppm.

5-Bromo-2,3,3-trimethyl-3*H*-indole (118c)

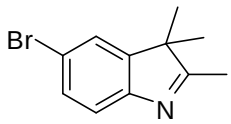

Yield: 86 %. **^{1}H-NMR (500 MHz, d_6-DMSO)**: δ = 7.66 (d, *J* = 2.0 Hz, 1H), 7.44 (dd, *J* = 8.5 Hz, *J* = 2.0 Hz, 1H), 7.36 (d, *J* = 8.5 Hz, 1H), 2.19 (s, 3H), 1.24 (s, 6H) ppm. **^{13}C-NMR (125 MHz, d_6-DMSO)**: δ = 188.6, 152.6, 148.4, 130.1, 124.9, 120.9, 117.7, 53.7, 22.1, 14.9 ppm.

5-Methoxy-2,3,3-trimethyl-3*H*-indole (118d)

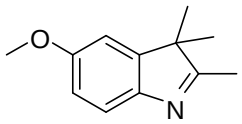

Yield: 88 %. **^{1}H-NMR (500 MHz, d_6-DMSO)**: δ = 7. 44 (d, *J* = 8.0 Hz, 1H), 6.85-6.80 (m, 2H), 3.82 (s, 3H), 2.26 (s, 3H), 1.29 (s, 6H) ppm. **^{13}C-NMR (125 MHz, d_6-DMSO)**: δ = 186.0, 158.0, 147.1, 120.0, 112.1, 108.2, 55.7, 53.7, 23.2, 15.2 ppm.

6.6.2. General procedures for synthesis of 1-alkyl/PEG-2,3,3-tetramethyl-3*H*-indolium

5-Substitute-1-alkyl -2,3,3-tetramethyl-3*H*-indolium

5-Substituted-2,3,3-trimethylindolenine (5 mmol, 1.0 eq) and methyl iodide (1.42 g, 10.0 mmol, 2.0 eq) were dissolved in anhydrous acetonitrile (15.0 mL). The reaction mixture was refluxed overnight. When it was cooled down to room temperature, the solvent was evaporated *in vacuo* and the residue was treated with ethyl acetate (30.0 mL). The final product was collected by filtration and washed with ethyl acetate. The colorless solid was used in the next reaction without further purification.

1,2,3,3-Tetramethyl-3*H*-indolium iodide (119a)

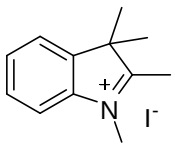

^{1}H-NMR (500 MHz, d_6-DMSO): δ = 7.93-7.89 (m, 1H), 7.84-7.81 (m, 1H), 7.65-7.59 (m, 2H), 3.97 (s, 3H), 2.77 (s, 3H), 1.53 (s, 6H) ppm. **^{13}C-NMR (125 MHz, d_6-DMSO)**: δ = 195.9,

142.0, 141.5, 129.2, 128.7, 123.1, 115.0, 53.8, 34.6, 21.6, 14.0 ppm. **MS (EI, 70 eV)**: *m/z* = 173 [*M*-H]$^+$. **mp**: 258–259 °C (MeCN).

5-Fluoro-1,2,3,3-tetramethyl-3*H*-indolium iodide (119c)

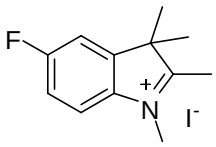

^{1}H-NMR (500 MHz, d_6-DMSO): δ = 7.96 (dd, *J* = 9.0 Hz, *J* = 4.5 Hz, 1H), 7.83 (dd, *J* = 8.0 Hz, *J* = 2.5 Hz, 1H), 7.50 (td, *J* = 9.0 Hz, *J* = 2.5 Hz, 1H), 3.96 (s, 3H), 2.75 (s, 3H), 1.54 (s, 6H) ppm. **^{13}C-NMR (125 MHz, d_6-DMSO)**: δ = 195.9, 162.5 (d, *J* = 245.4 Hz), 144.8 (d, *J* = 9.9Hz), 138.2, 116.9 (d, *J* = 9.6 Hz), 115.7 (d, *J* = 24.8 Hz), 111.2 (d, *J* = 25.9 Hz), 54.0, 34.8, 21.4, 14.1 ppm.

5-Bromo-1,2,3,3-tetramethyl-3*H*-indolium iodide (119d)

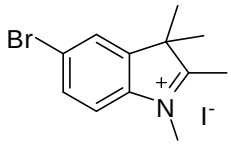

^{1}H-NMR (500 MHz, d_6-DMSO): δ = 8.16 (d, *J* = 1.5 Hz, 1H), 7.89-7.82 (m, 2H), 3.95 (s, 3H), 2.75 (s, 3H), 1.53 (s, 6H) ppm. **^{13}C-NMR (125 MHz, d_6-DMSO)**: δ = 196.4, 143.7, 141.3, 131.6, 126.6, 122.5, 117.0, 54.1, 34.8, 21.4, 14.1 ppm.

5-Methoxy-1,2,3,3-tetramethyl-3*H*-indolium iodide (119e)

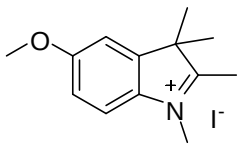

^{1}H-NMR (500 MHz, d_6-DMSO): δ = 7.80 (d, *J* = 9.0 Hz, 1H), 7.46 (d, *J* = 2.5 Hz, 1H), 7.14 (dd, *J* = 9.0 Hz, *J* = 2.5 Hz, 1H), 3.93 (s, 3H), 3.86 (s, 3H), 2.70 (s, 3H), 1.50 (s, 6H) ppm. **^{13}C-NMR (125 MHz, d_6-DMSO)**: δ = 193.1, 160.6, 143.6, 135.3, 116.0, 114.1, 109.2, 56.1, 53.7, 34.6, 21.8, 13.7 ppm.

1-Butyl-2,3,3-trimethyl-3*H*-indolium iodide (119b)

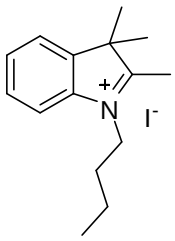

2,3,3-Trimethyl-3*H*-indole (318 mg, 2.0 mmol, 1.0 eq) and 1-iodobutane (552 mg, 3.0 mmol, 1.5 eq) were refluxed overnight in ethylmethylketone (10 mL). When it was cooled down to room temperature, the solvent was evaporated *in vacuo* and the residue was purified by column chromatography (SiO_2; dichloromethane: methanol = 20:1) to afford 502 mg of product as pale yellow solid.

Yield: 73 %. **^{1}H-NMR (500 MHz, d_6-DMSO)**: δ = 7.99-7.94 (m, 1H), 7.96-7.82 (m, 1H), 7.66-7.60 (m, 2H), 4.45 (t, *J* = 7.5 Hz, 2H), 2.84 (s, 3H), 1.86-1.77(m, 2H), 1.54 (s, 6H), 1.47-1.38 (m, 2H), 0.94 (t, *J* = 7.5 Hz, 3H) ppm. **^{13}C-NMR (125 MHz, d_6-DMSO)**: δ = 196.3, 141.8, 141.0, 129.3, 128.9, 123.4, 115.4, 54.1, 47.3, 29.2, 21.9, 19.2, 13.9, 13.5 ppm. **MS (EI, 70 eV)**: *m/z* = 215 $[M\text{-H}]^+$. **mp**: 135-136 °C.

1-(2-Methoxyethyl)-2,3,3-trimethyl-3*H*-indolium chloride (119g)

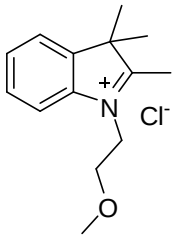

2-Methoxyethanol (0.76 g, 10.0 mmol, 1.0 eq) with THF (3 mL) was added dropwise to a solution of NaOH (0.52 g, 13.0 mmol, 1.3 eq) in 1.0 mL water at 0 °C. The solution of *p*-toluenesulfonyl chloride (2.1 g, 11.0 mmol, 1.1 eq) was then added to the mixture. After 12 hours of stirring at room temperature, the reaction was quenched by 2.5 mL water and extracted with dichloromethane (20 mL). The combined organic phases were washed successively with 2 N HCl (15 mL) and saturated NaCl solution (15 mL), dried over $MgSO_4$. After filtration, the solvent was evaporated *in vacuo*.

2,3,3-Trimethyl-indolenine (0.80 g, 5.0 mmol, 1.0 eq) and 2-methoxyethyl 4-methylbenzenesulfonate (2.3 g, 10.0 mmol, 2.0 eq) were dissolved in anhydrous acetonitrile (10.0 mL). The reaction mixture was refluxed for 4 days. The color of reaction mixture turned

to purple, and then it was cooled down to room temperature. The crude product was purified by column chromatography (SiO_2; dichloromethane: methanol: triethylamine= 10:1:0.1) to afford the purple liquid (yield: 23 %).

6.6.3. General procedures for synthesis of spiropyran derivatives

A mixture of corresponding substituted salicylaldehyde (1.1 mmol, 1.1 eq) and indolium derivatives (1.0 mmol, 1.0 eq) in EtOH (5 mL) was refluxed overnight. The solvent was evaporated *in vacuo* and the residue was purified by column chromatography (SiO_2; dichloromethane: methanol = 10:1) to furnish the corresponding compound in moderate yields (yield: 35-77 %).

***N*,*N*-Diethyl-1',3',3'-trimethylspiro[chromene-2,2'-indolin]-7-amine (120a)**

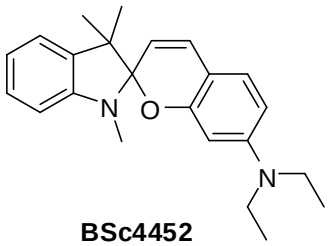

BSc4452

Yield: 77 %. **^{1}H-NMR (500 MHz, d_6-DMSO)**: δ = 7.11-7.04 (m, 2H), 6.90 (d, *J* = 8.5 Hz, 1H), 6.83 (d, *J* = 10.0 Hz, 1H), 6.74 (td, *J* = 7.5 Hz, *J* = 1.0 Hz, 1H), 6.53 (d, *J* = 7.5 Hz, 1H), 6.13 (dd, *J* = 8.5 Hz, *J* = 2.5 Hz, 1H), 5.88 (d, *J* = 2.5 Hz, 1H), 5.38 (d, *J* = 10.0 Hz, 1H), 3.27-3.20 (m, 4H), 2.65 (s, 3H), 1.21 (s, 3H), 1.06 (s, 3H), 1.01 (t, *J* = 7.0 Hz, 6H) ppm. **^{13}C-NMR (125 MHz, d_6-DMSO)**: δ = 155.5, 148.6, 148.0, 136.5, 129.15, 127.14, 127.2, 121.3, 118.5, 112.8, 107.0, 106.5, 104.0, 103.5, 96.3, 50.9, 43.5, 28.4, 25.7, 19.7, 12.4 ppm. **MS (EI, 70 eV)**: *m/z* = 348 $[M]^+$. **UV/Vis (Ethanol)**: λ_{max} = 549.0 nm.

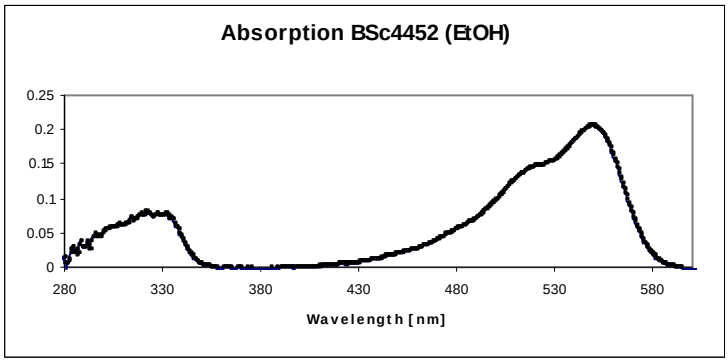

***In vitro* neuropathological staining of AD brain sections**: Tissues: hippocampus; Patient: male, 71 years old; CERAD Score: 3; NFTs-level: V.

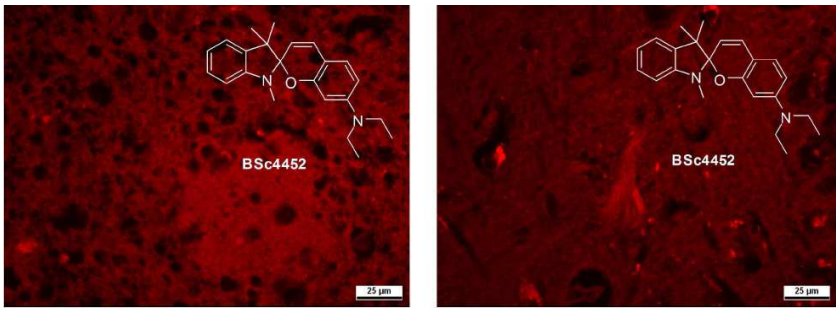

***In vitro* neuropathological staining of AD olfactory epithelium sections**: Tissues: olfactory epithelium; Patient: male, 78 years old; Braak: V, CERAD Score: 3.

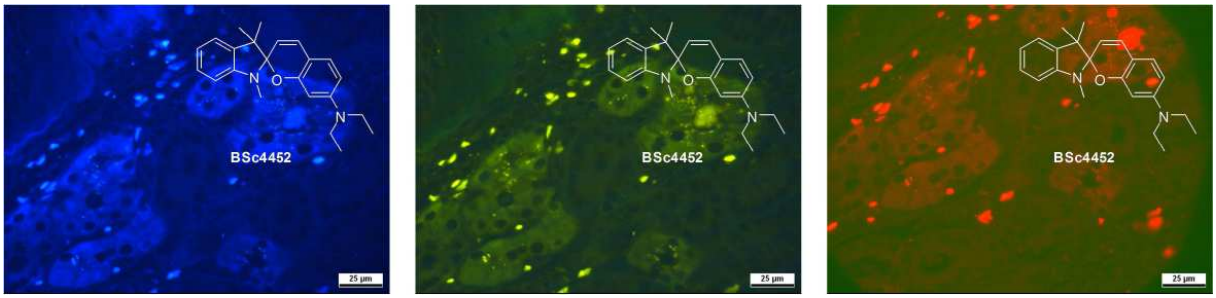

8-Methoxy-1',3',3'-trimethylspiro[chromene-2,2'-indoline] (120b)

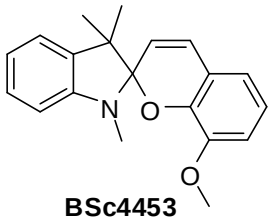

BSc4453

Yield: 46 %. **^{1}H-NMR (500 MHz, d_6-DMSO)**: δ = 7.10 (td, *J* = 8.0 Hz, *J* = 1.0 Hz, 1H), 7.07 (dd, *J* = 7.5 Hz, *J* = 1.0 Hz, 1H), 6.97 (d, *J* = 10.0 Hz, 1H), 6.84 (t, *J* = 5.0 Hz, 1H), 6.79-6.74 (m, 3H), 6.55 (d, *J* = 7.5 Hz, 1H), 5.74 (d, *J* = 10.5 Hz, 1H), 3.62 (s, 3H), 2.66 (s, 3H), 1.07-1.04 (s, 3H), 1.20 (s, 3H), 1.08 (s, 3H) ppm. **^{13}C-NMR (125 MHz, d_6-DMSO)**: δ = 147.7, 146.4, 142.8, 136.2, 129.1, 127.3, 121.4, 119.7, 119.5, 119.1, 118.9, 118.6, 113.1, 106.5, 103.6, 55.4, 51.3, 28.3, 25.7, 19.7 ppm. **MS (EI, 70 eV)**: *m/z* = 307 $[M]^+$. **UV/Vis (Ethanol)**: λ_{max} = 226.0 nm.

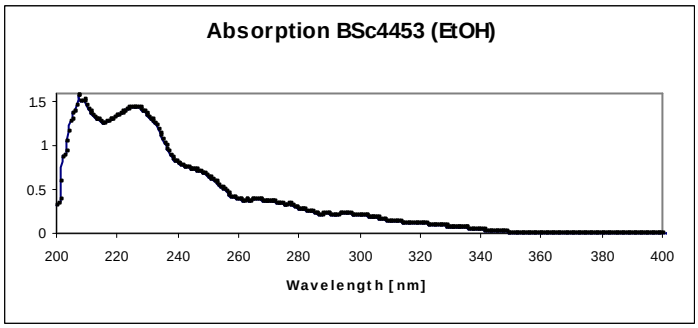

1',3',3'-Trimethylspiro[chromene-2,2'-indolin]-6-ol (120c)

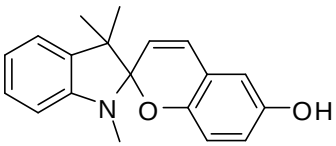

BSc4454

Yield: 45 %. **^{1}H-NMR (500 MHz, d_6-DMSO)**: δ = 8.88 (s, 1H), 7.11-7.04 (m, 2H), 6.91 (d, *J* = 10.0 Hz, 1H), 6.74 (td, *J* = 7.5 Hz, *J* = 1.0 Hz, 1H), 6.57 (d, *J* = 3.0 Hz, 1H), 6.54-6.48 (m, 3H), 5.72 (d, *J* = 10.0 Hz, 1H), 2.62 (s, 3H), 1.20 (s, 3H), 1.07 (s, 3H) ppm. **^{13}C-NMR (125 MHz, d_6-DMSO)**: δ = 150.5, 147.8, 146.6, 136.3, 129.3, 127.2, 121.3, 119.6, 118.8, 118.6, 116.1, 114.6, 112.7, 106.5, 103.0, 51.0, 28.5, 25.6, 19.9 ppm. **MS (EI, 70 eV)**: *m/z* = 293 $[M]^+$. **UV/Vis (Ethanol)**: λ_{max} = 231.5 nm.

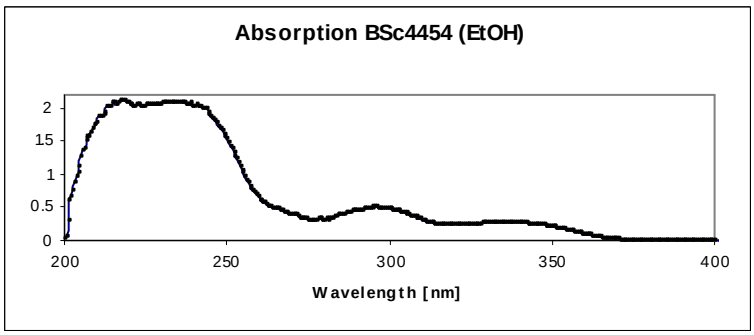

1',3',3'-Trimethyl-6-nitrospiro[chromene-2,2'-indoline] (120d)

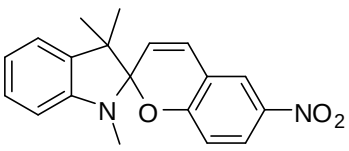

BSc4455

^{1}H-NMR (500 MHz, d_6-DMSO): δ = 8.20 (d, J = 3.0 Hz, 1H), 8.00 (dd, J = 9.0 Hz, J = 2.5 Hz, 1H), 7.20 (d, J = 10.5 Hz, 1H), 7.15-7.09 (m, 2H), 6.87 (d, J = 9.0 Hz, 1H), 6.80 (td, J = 7.5 Hz, J = 1.0 Hz, 1H), 6.60 (d, J = 7.5 Hz, 1H), 5.97 (d, J = 10.5 Hz, 1H), 2.66 (s, 3H), 1.20 (s, 3H), 1.10 (s, 3H) ppm. **^{13}C-NMR (125 MHz, d_6-DMSO)**: δ = 159.4, 147.4, 140.5, 135.9, 128.3, 127.7, 125.8, 122.8, 121.6, 121.5, 119.5, 118.9, 115.4, 107.0, 106.2, 51.9, 28.5, 25.7, 19.7 ppm. **MS (EI, 70 eV)**: *m/z* = 322 $[M]^+$.

***In vitro* neuropathological staining of AD brain sections**: Tissues: hippocampus; Patient: male, 71 years old; CERAD Score: 3; NFTs-level: V.

6-Fluoro-1',3',3'-trimethylspiro[chromene-2,2'-indoline] (120e)

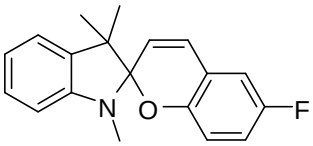

BSc4487

Yield: 47 %. **^{1}H-NMR (500 MHz, d_6-DMSO)**: δ = 7.14-7.03 (m, 3H), 7.00 (d, *J* = 10.0 Hz, 1H), 6.91 (td, *J* = 9.0 Hz, *J* = 3.0 Hz 1H), 6.77 (t, *J* = 7.5 Hz, 1H), 6.68 (dd, *J* = 9.0 Hz, *J* = 4.0 Hz, 1H), 6.55 (d, *J* = 7.5 Hz, 1H), 5.84 (d, *J* = 10.0 Hz, 1H), 2.64 (s, 3H), 1.21 (s, 3H), 1.08 (s, 3H) ppm. **^{13}C-NMR (125 MHz, d_6-DMSO)**: δ = 155.9 (d, *J* = 233.6 Hz), 150.0, 147.6, 136.1, 128.5, 127.3, 121.3, 120.7, 119.4 (d, *J* = 8.6 Hz), 118.9, 115.7 (d, *J* = 23.1 Hz), 115.3 (d, *J* = 8.0 Hz), 112.7 (d, *J* = 23.6 Hz), 106.7, 103.8, 51.3, 28.4, 25.5, 19.8 ppm. **MS (EI, 70 eV)**: *m/z* = 295 $[M]^+$. **UV/Vis (Ethanol)**: λ_{max} = 215.0 nm.

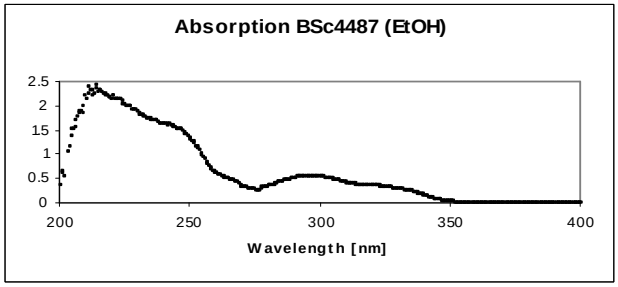

1',3',3'-Trimethylspiro[chromene-2,2'-indoline] (120f)

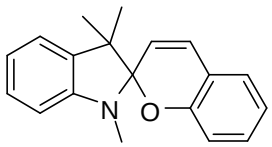

BSc4488

Yield: 53 %. **^{1}H-NMR (500 MHz, d_6-DMSO)**: δ = 7.16 (dd, *J* = 7.5 Hz, *J* = 1.5 Hz, 1H), 7.12-7.06 (m, 3H), 7.00 (d, *J* = 10.0 Hz, 1H), 6.82 (td, *J* = 7.5 Hz, *J* = 1.0 Hz, 1H), 6.76 (td, *J* = 7.5 Hz, *J* = 1.0 Hz, 1H), 6.65 (d, *J* = 8.5 Hz, 1H), 6.55 (d, *J* = 8.0 Hz, 1H), 5.74 (d, *J* = 10.5 Hz, 1H), 2.64 (s, 3H), 1.21 (s, 3H), 1.09 (s, 3H) ppm. **^{13}C-NMR (125 MHz, d_6-DMSO)**: δ = 153.9, 147.8, 136.2, 129.7, 129.2, 127.4, 126.8, 121.4, 120.1, 119.1, 118.8, 118.6, 114.2, 106.7, 103.8, 51.3, 28.5, 25.6, 19.8 ppm. **MS (EI, 70 eV)**: *m/z* = 277 $[M]^+$. **UV/Vis (Ethanol)**: λ_{max} = 217.5 nm.

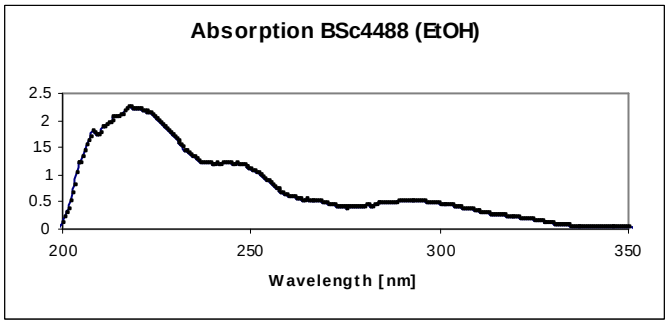

1',3',3',6-Tetramethylspiro[chromene-2,2'-indoline] (120g)

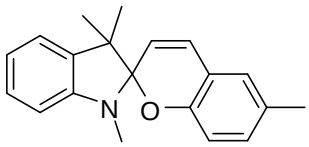

BSc4489

Yield: 64 %. **^{1}H-NMR (500 MHz, d_6-DMSO)**: δ = 7.11-7.04 (m, 2H), 6.97-6.92 (m, 3H), 6.88 (dd, *J* = 8.0 Hz, *J* = 2.0 Hz, 1H), 6.75 (td, *J* = 7.5 Hz, *J* = 1.0 Hz, 1H), 6.65-6.51 (m, 2H), 5.72 (d, *J* = 10.5 Hz, 1H), 2.62 (s, 3H), 2.18 (s, 3H), 1.19 (s, 3H), 1.07 (s, 3H) ppm. **^{13}C-NMR (125 MHz, d_6-DMSO)**: δ = 151.8, 147.9, 136.4, 130.2, 129.4, 128.8, 127.4, 127.2, 121.4, 119.3, 118.9, 118.4, 114.1, 106.7, 103.7, 51.3, 28.6, 25.7, 20.0, 19.9 ppm. **MS (EI, 70 eV)**: *m/z* = 291 $[M]^+$. **UV/Vis (Ethanol)**: λ_{max} = 208.0 nm.

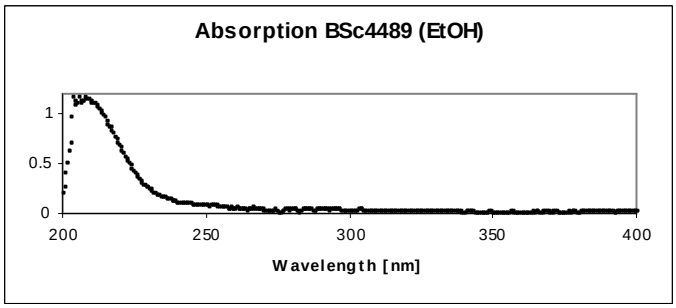

1'-Butyl-*N*,*N*-diethyl-3',3'-dimethylspiro[chromene-2,2'-indolin]-7-amine (120h)

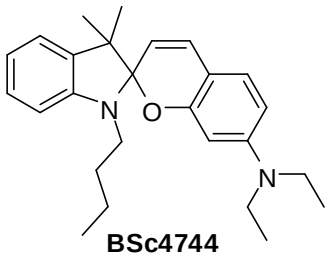

BSc4744

Yield: 61 %. **^{1}H-NMR (500 MHz, $CDCl_3$)**: δ = 7.17 (td, *J* = 7.5 Hz, *J* = 1.0 Hz, 1H), 7.09 (dd, *J* = 7.0 Hz, *J* = 1.0 Hz, 1H), 6.88 (d, *J* = 8.5 Hz, 1H), 6.82 (td, *J* = 7.5 Hz, *J* = 1.0 Hz, 1H), 6.74 (d, *J* = 10.0 Hz, 1H), 6.57 (d, *J* = 8.0 Hz, 1H), 6.16 (dd, *J* = 8.5 Hz, *J* = 2.5 Hz, 1H), 6.07 (d, *J* = 2.5 Hz, 1H), 5.41 (d, *J* = 10.5 Hz, 1H), 3.33-3.07 (m, 6H), 1.70-1.52 (m, 2H), 1.44-1.25 (m, 5H), 1.18 (s, 3H), 1.13 (t, *J* = 7.0 Hz, 6H), 0.93 (t, *J* = 7.0 Hz, 3H) ppm. **^{13}C-NMR (125 MHz, $CDCl_3$)**: δ = 156.0, 149.3, 148.1, 137.1, 129.1, 127.4, 121.6, 118.3, 114.1, 107.7, 106.2, 105.0, 103.4, 97.7, 51.7, 44.4, 43.6, 31.4, 26.2, 20.6, 20.1, 14.1, 12.7 ppm. **UV/Vis (Ethanol)**: λ_{max} = 550.0 nm.

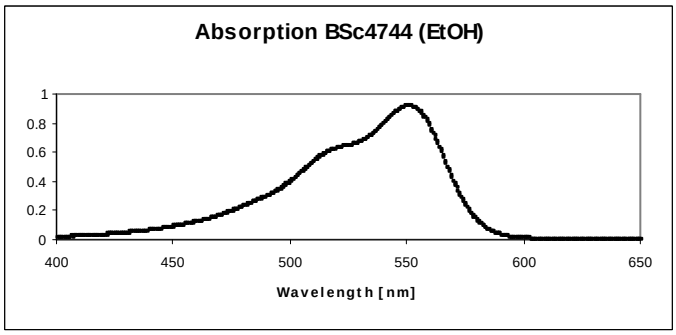

***In vitro* neuropathological staining of AD brain sections**: Tissues: hippocampus; Patient: male, 71 years old; CERAD Score: 3; NFTs-level: V.

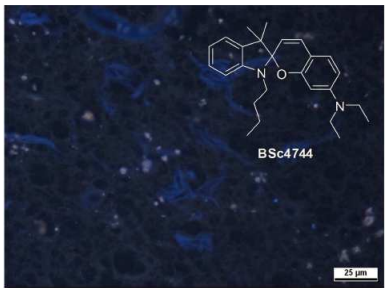

***In vitro* neuropathological staining of AD olfactory epithelium sections**: Tissues: olfactory epithelium; Patient: male, 78 years old; Braak: V, CERAD Score: 3.

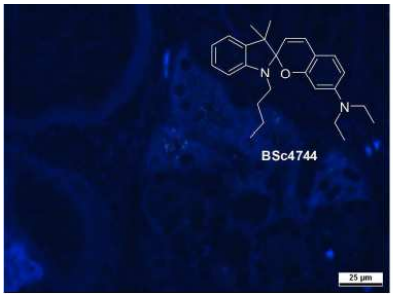

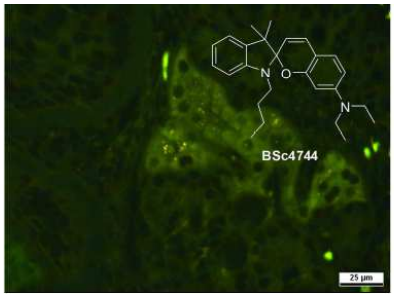

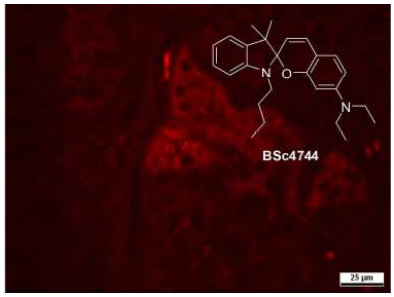

***N*,*N*-Diethyl-5'-fluoro-1',3',3'-trimethylspiro[chromene-2,2'-indolin]-7-amine (120i)**

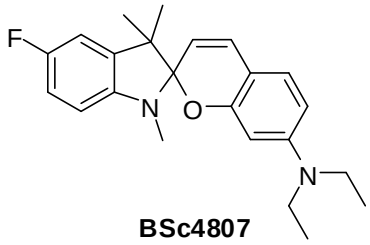

BSc4807

Yield: 41 %. **^{1}H-NMR (500 MHz, d_6-DMSO)**: δ = 6.96 (dd, *J* = 8.5 Hz, *J* = 2.5 Hz, 1H), 6.91-6.83 (m, 2H), 6.81 (d, *J* = 10.0 Hz, 1H), 6.47 (dd, *J* = 8.5 Hz, *J* = 4.0 Hz, 1H), 6.12 (dd, *J* = 8.5 Hz, *J* = 2.5 Hz, 1H), 5.88 (d, *J* = 2.5 Hz, 1H), 5.35 (d, *J* = 10.0 Hz, 1H), 3.25-3.17 (m, 4H), 2.62 (s, 3H), 1.21 (s, 3H), 1.07 (s, 3H), 1.00 (t, *J* = 7.0 Hz, 6H) ppm. **^{13}C-NMR (125 MHz, d_6-DMSO)**: δ = 156.5 (d, *J* = 231.6 Hz), 155.4, 148.9, 144.4, 138.7 (d, *J* = 7.4 Hz), 129.2, 127.5, 112.7, 112.5, 109.4 (d, *J* = 24.1 Hz), 106.9, 106.7 (d, *J* = 8.0 Hz), 104.3, 103.5, 96.3, 51.0, 43.5, 28.7, 25.3, 19.4, 12.3 ppm. **UV/Vis (Ethanol)**: λ_{max} = 549.0 nm.

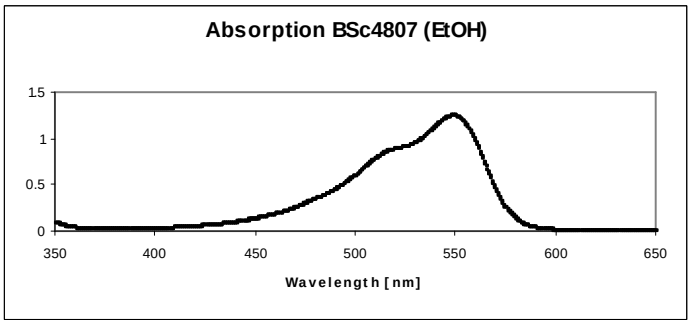

5'-Bromo-*N*,*N*-diethyl-1',3',3'-trimethylspiro[chromene-2,2'-indolin]-7-amine (120j)

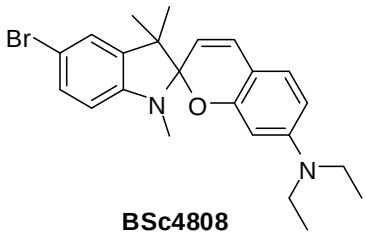

BSc4808

Yield: 53 %. **^{1}H-NMR (500 MHz, $CDCl_3$)**: δ = 7.25 (dd, *J* = 8.0 Hz, *J* = 2.0 Hz, 1H), 7.15 (d, *J* = 2.0 Hz, 1H), 6.87 (d, *J* = 8.5 Hz, 1H), 6.76 (d, *J* = 10.0 Hz, 1H), 6.39 (d, *J* = 8.5 Hz, 1H), 6.16 (dd, *J* = 8.5 Hz, *J* = 2.5 Hz, 1H), 6.05 (d, *J* = 2.5 Hz, 1H), 5.34 (d, *J* = 10.0 Hz, 1H), 3.31-3.25 (m, 4H), 2.72 (s, 3H), 1.30 (s, 3H), 1.15 (s, 3H), 1.12 (t, *J* = 7.0 Hz, 6H) ppm. **^{13}C-NMR (125 MHz, $CDCl_3$)**: δ = 155.8, 149.4, 147.6, 139.7, 130.1, 129.6, 127.5, 124.8, 112.7, 110.5, 108.1, 107.5, 104.5, 103.6, 97.3, 51.4, 44.3, 28.9, 25.8, 19.9, 12.7 ppm. **UV/Vis (Ethanol)**: λ_{max} = 554.0 nm.

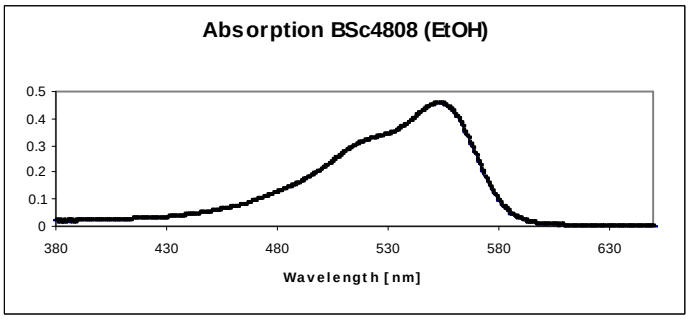

***In vitro* neuropathological staining of AD brain sections**: Tissues: hippocampus; Patient: male, 71 years old; CERAD Score: 3; NFTs-level: V.

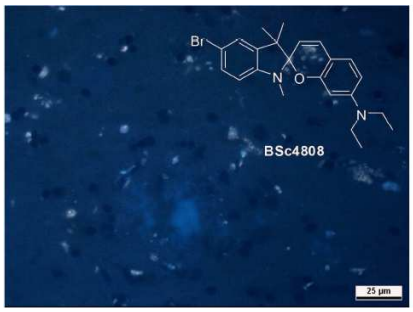

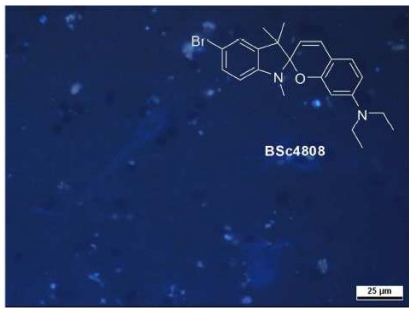

***N*,*N*-Diethyl-5'-methoxy-1',3',3'-trimethylspiro[chromene-2,2'-indolin]-7-amine (120k)**

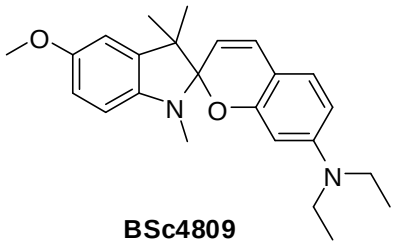

BSc4809

Yield: 55 %. **^{1}H-NMR (500 MHz, $CDCl_3$)**: δ = 6.86 (d, *J* = 8.5 Hz, 1H), 6.76-6.69 (m, 3H), 6.44 (d, *J* = 8.0 Hz, 1H), 6.15 (dd, *J* = 8.5 Hz, *J* = 2.5 Hz, 1H), 6.07 (d, *J* = 2.0 Hz, 1H), 5.32 (d, *J* = 10.0 Hz, 1H), 3.80 (s, 3H), 3.31-3.24 (m, 4H), 2.71 (s, 3H), 1.32 (s, 3H), 1.16 (s, 3H), 1.11 (t, *J* = 7.0 Hz, 6H) ppm. **^{13}C-NMR (125 MHz, $CDCl_3$)**: δ = 156.2, 153.6, 149.3, 142.9, 139.0, 129.2, 127.4, 113.5, 111.1, 109.7, 107.8, 106.8, 104.9, 103.5, 97.5, 55.9, 51.6, 44.3, 39.4, 25.9, 20.1, 12.7 ppm.

***In vitro* neuropathological staining of AD brain sections**: Tissues: hippocampus; Patient: male, 71 years old; CERAD Score: 3; NFTs-level: V.

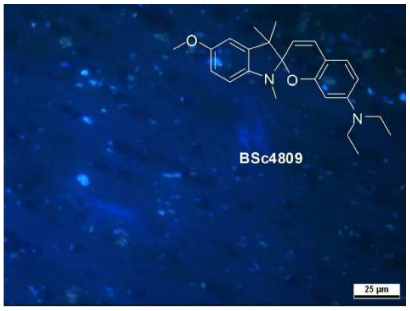

***N*,*N*-Diethyl-1'-(2-methoxyethyl)-3',3'-dimethylspiro[chromene-2,2'-indolin]-7-amine (120l)**

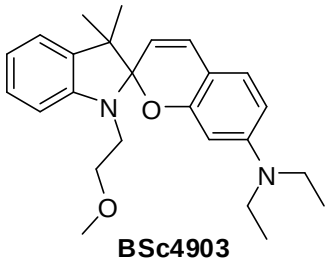

BSc4903

Yield: 35 %. **^{1}H-NMR (500 MHz, d_6-DMSO)**: δ = 7.09-7.03 (m, 2H), 6.89 (d, *J* = 8.5 Hz, 1H), 6.80 (d, *J* = 10.0 Hz, 1H), 6.72 (td, *J* = 7.5 Hz, *J* = 1.0 Hz, 1H), 6.57 (d, *J* = 7.5 Hz, 1H), 6.13 (dd, *J* = 8.5 Hz, *J* = 2.5 Hz, 1H), 5.87 (d, *J* = 2.0 Hz, 1H), 5.39 (d, *J* = 10.0 Hz, 1H), 3.51-3.13 (m, 11H), 1.21 (s, 3H), 1.04 (s, 3H), 1.01 (t, *J* = 7.0 Hz, 6H) ppm. **^{13}C-NMR (125 MHz, d_6-DMSO)**: δ = 155.2, 148.8, 147.2, 136.1, 129.0, 127.5, 127.1, 121.4, 118.2, 113.2, 106.8, 106.0, 104.2, 103.5, 96.5, 70.5, 58.1, 51.2, 43.5, 42.6, 25.9, 19.6, 12.4 ppm. **UV/Vis (Ethanol)**: λ_{max} = 551.0 nm.

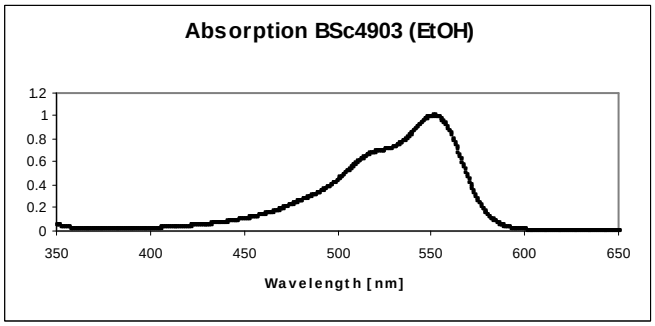

***In vitro* neuropathological staining of AD brain sections**: Tissues: hippocampus; Patient: male, 71 years old; CERAD Score: 3; NFTs-level: V.

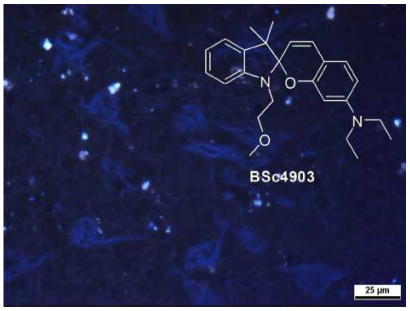

6.7. Synthesis of merocyanine derivatives

6.7.1. Synthesis of 3-ethyl-1,2,3-trimethyl-3*H*-indolium iodide

3-Ethyl-2,3-dimethyl-3*H*-indole (123)

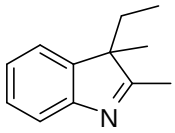

A mixture of phenylhydrazine hydrochloride (1.44 g, 10.0 mmol, 1.0 eq) and 3-methylpentan-2-one (1.2 g, 12.0 mmol, 1.2 eq) was dissolved in glacial acetic acid (20 mL) and then heated under reflux temperature for 12 h under argon. When it was cooled down to room temperature, the solvent was evaporated *in vacuo* and the residue was dissolved in dichloromethane (30 mL), washed with 10% aqueous Na_2CO_3 (2 × 30 mL), dried over Na_2SO_4. After filtration, the solvent was evaporated *in vacuo*. The crude product was purified by column chromatography (SiO_2; ethyl acetate: cyclohexane = 1:2) to afford 1.68 g of product as red liquid.

Yield: 96 %. **^{1}H-NMR (500 MHz, d_6-DMSO)**: δ = 7.54 (d, *J* = 7.5 Hz, 1H), 7.31 (td, *J* = 7.5 Hz, *J* = 2.5 Hz, 1H), 7.25-7.18 (m, 2H), 2.26 (s, 3H), 1.96-1.75 (m, 2H), 1.30 (s, 3H), 0.40 (t, *J* = 7.5 Hz, 3H) ppm. **^{13}C-NMR (125 MHz, d_6-DMSO)**: δ = 187.4, 153.9, 143.3, 127.6, 125.2, 121.6, 119.6, 58.4, 30.1, 22.3, 15.6, 8.5 ppm.

3-Ethyl-1,2,3-trimethyl-3*H*-indolium iodide (124)

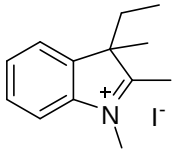

3-Ethyl-2,3-dimethyl-3*H*-indole (0.88 g, 5.0 mmol, 1.0 eq) and methyl iodide (1.42 g, 10.0 mmol, 2.0 eq) were dissolved in anhydrous acetonitrile (15.0 mL). The reaction mixture was refluxed overnight. When the reaction mixture was cooled down to room temperature, the solvent was evaporated *in vacuo* and the residue was treated with ethyl acetate (30.0 mL). The final product was collected by filtration and washed with ethyl acetate. The colorless solid was used in the next reaction without further purification.

^{1}H-NMR (500 MHz, d_6-DMSO): δ = 7.93-7.89 (m, 1H), 7.79-7.75 (m, 1H), 7.67-7.61 (m, 2H), 4.00 (s, 3H), 2.77 (s, 3H), 2.25-2.03 (m, 2H), 1.51 (s, 3H), 0.39 (t, *J* = 7.5 Hz, 3H) ppm. **^{13}C-**

NMR (125 MHz, d_6-DMSO): δ = 196.2, 142.8, 139.7, 129.5, 129.0, 123.6, 115.1, 58.9, 34.7, 29.7, 20.6, 14.0, 8.3 ppm.

6.7.2. Synthesis of 3-substitute-2-methylbenzo[*d*]oxazol-3-ium iodide

2,3-Dimethylbenzo[*d*]oxazol-3-ium iodide (127)

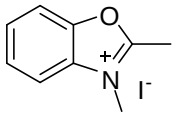

2-Methylbenzo[*d*]oxazole (0.67 g, 5.0 mmol, 1.0 eq) and methyl iodide (1.42 g, 10.0 mmol, 2.0 eq) were dissolved in anhydrous acetonitrile (15.0 mL). The reaction mixture was refluxed overnight. When the reaction mixture was cooled down to room temperature, the solvent was evaporated *in vacuo* and the residue was treated with ethyl acetate (30.0 mL). The final product was collected by filtration and washed with ethyl acetate. The colorless solid was used in the next reaction without further purification.

3-Butyl-2-methylbenzo[*d*]oxazol-3-ium iodide (130)

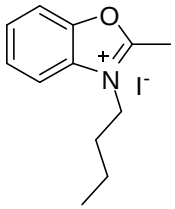

The mixture of 2-methylbenzo[*d*]oxazole (0.67 g, 5.0 mmol, 1.0 eq) and butyl iodide (1.84 g, 10.0 mmol, 2.0 eq) was stirred at 120 °C overnight. When the reaction mixture was cooled down to room temperature, the residue was treated with ethyl acetate (30.0 mL). The final product was collected by filtration and washed with ethyl acetate. The colorless solid was used in the next reaction without further purification.

6.7.3. Synthesis of merocyanine derivatives

A mixture of corresponding substituted aldehyde (1.1 mmol, 1.1 eq) and indolium derivatives (1.0 mmol, 1.0 eq) in EtOH (5 mL) was refluxed overnight. The solvent was evaporated *in vacuo* and the residue was purified by column chromatography (SiO_2; dichloromethane: methanol = 10:1) to furnish the corresponding compound with yields of 77-96 %.

(*E*)-1-Butyl-2-(4-(diethylamino)styryl)-3,3-dimethyl-3*H*-indolium iodide (121a)

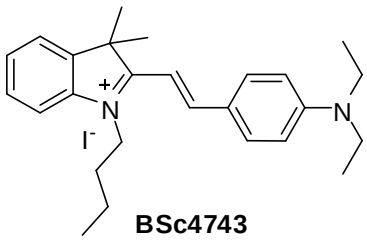

BSc4743

Yield: 96 %. **^{1}H-NMR (500 MHz, d_6-DMSO)**: δ = 8.32 (d, *J* = 16.5 Hz, 1H), 8.06 (d, *J* = 8.5 Hz, 2H), 7.77 (d, *J* = 7.5 Hz, 1H), 7.70 (d, *J* = 8.0 Hz, 1H), 7.54 (td, *J* = 7.5 Hz, *J* = 1.5 Hz, 1H), 7.46 (td, *J* = 7.5 Hz, *J* = 0.5 Hz, 1H), 7.21 (d, *J* = 16.0 Hz, 1H), 6.86 (d, *J* = 8.0 Hz, 2H), 4.50 (t, *J* = 7.5 Hz, 2H), 3.60-3.52 (m, 4H), 1.81-1.71 (m, 8H), 1.47-1.38 (m, 2H), 1.18 (t, *J* = 7.5 Hz, 6H), 0.93 (t, *J* = 7.5 Hz, 3H) ppm. **^{13}C-NMR (125 MHz, d_6-DMSO)**: δ = 179.0, 154.2, 152.6, 142.5, 141.0, 134.6 (brs), 128.7, 127.3, 122.7, 121.9, 113.4, 112.0, 104.0, 50.7, 44.7, 44.4, 29.8, 26.5, 19.2, 13.6, 12.5 ppm. **IR (KBr)**: $\tilde{\nu}$ = 3428, 2970, 1742, 1613, 1564, 1523, 1466, 1418, 1351, 1318, 1289, 1267, 1190, 1154, 1072, 838, 751, 715, 507 cm^{-1}. **MS (EI, 70 eV)**: *m/z* = 376 [*M*+H]$^{+}$. **Anal. calcd for $C_{26}H_{35}IN_2$**: C 62.15, H 7.02, N 5.58, found: C 62.28, H 7.00, N 5.66. **UV/Vis (Ethanol)**: λ_{max} = 558.0 nm.

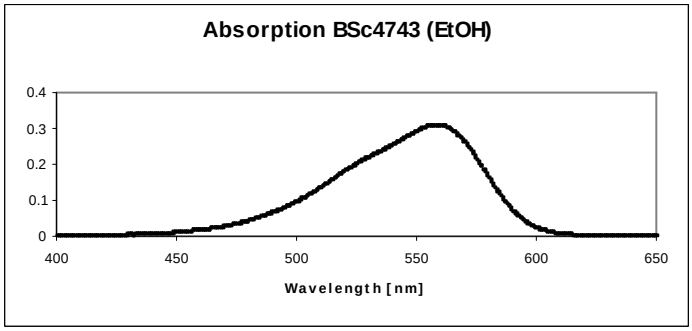

***In vitro* neuropathological staining of AD brain sections**: Tissues: hippocampus; Patient: male, 71 years old; CERAD Score: 3; NFTs-level: V.

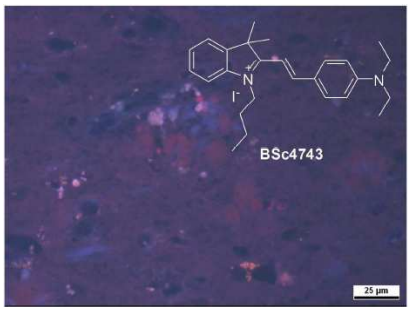

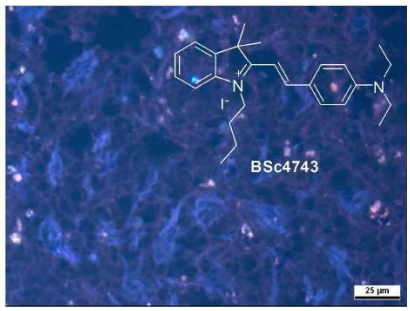

***In vitro* neuropathological staining of PD brain sections**: Tissues: midbrain; Patient: male, 76 years old.

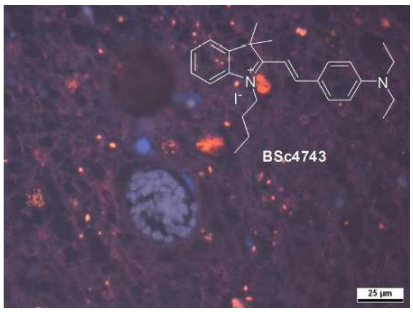

***In vitro* neuropathological staining of AD olfactory epithelium sections**: Tissues: olfactory epithelium; Patient: male, 78 years old; Braak: V, CERAD Score: 3.

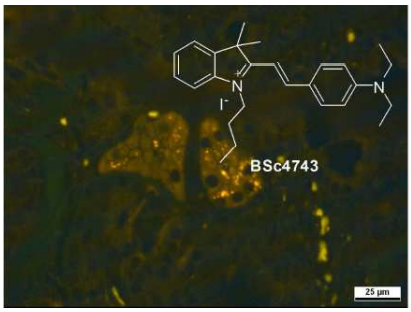

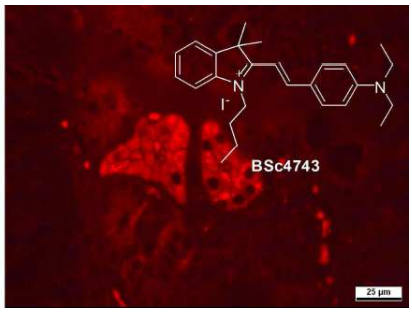

(*E*)-2-(4-(Dimethylamino)styryl)-1,3,3-trimethyl-3*H*-indolium iodide (121b)

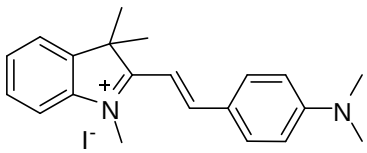

BSc4745

Yield: 93 %. **^{1}H-NMR (500 MHz, d_6-DMSO)**: δ = 8.30 (d, *J* = 16.5 Hz, 1H), 8.07 (d, *J* = 9.0 Hz, 2H), 7.77 (d, *J* = 7.5 Hz, 1H), 7.70 (d, *J* = 8.0 Hz, 1H), 7.55 (td, *J* = 7.5 Hz, *J* = 1.0 Hz, 1H), 7.48 (td, *J* = 7.5 Hz, *J* = 0.5 Hz, 1H), 7.25 (d, *J* = 16.5 Hz, 1H), 6.88 (d, *J* = 9.0 Hz, 2H), 3.96 (s, 3H), 3.16 (s, 6H), 1.75 (s, 6H). **^{13}C-NMR (125 MHz, d_6-DMSO)**: δ = 179.5, 154.3, 154.0, 142.4, 142.0, 133.8 (brs), 128.6, 127.4, 122.5, 122.2, 113.5, 112.1, 105.1, 50.8, 33.0, 26.1 ppm. **IR (KBr)**: $\tilde{\nu}$ = 3420, 2921, 1574, 1527, 1477, 1375, 1290, 1193, 1170, 1113, 832, 786, 728, 509 cm^{-1}. **MS (EI, 70 eV)**: *m/z* = 304 [*M*-H]$^{+}$. **Anal. calcd for $C_{21}H_{25}IN_2$**: C 58.34, H 5.83, N 6.48, found: C 58.59, H 5.82, N 6.41. **UV/Vis (Ethanol)**: λ_{max} = 547.5 nm.

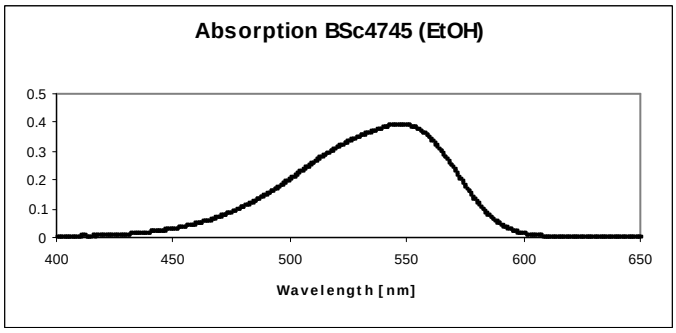

***In vitro* neuropathological staining of AD brain sections**: Tissues: hippocampus; Patient: male, 71 years old; CERAD Score: 3; NFTs-level: V.

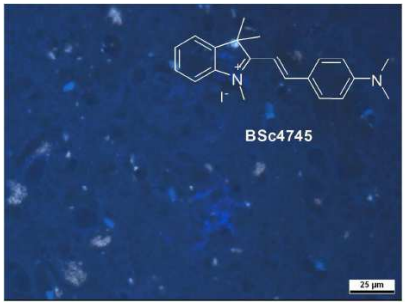

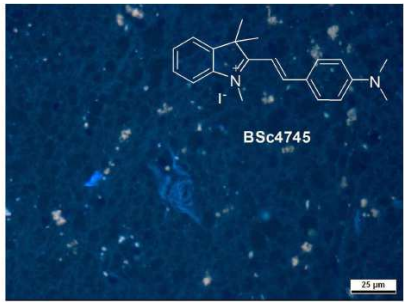

***In vitro* neuropathological staining of PD brain sections**: Tissues: midbrain; Patient: male, 76 years old.

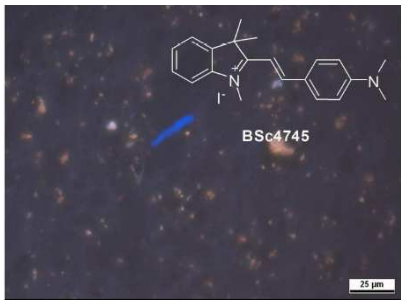

(*E*)-2-(4-Methoxystyryl)-1,3,3-trimethyl-3*H*-indolium iodide (121c)

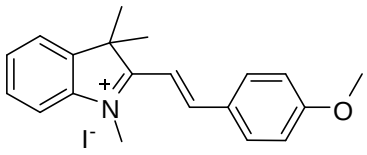

BSc4746

Yield: 77 %. **^{1}H-NMR (500 MHz, d_6-DMSO)**: δ = 8.40 (d, *J* = 16.0 Hz, 1H), 8.21 (d, *J* = 8.5 Hz, 2H), 7.87-7.83 (m, 2H), 7.64-7.57 (m, 2H), 7.54 (d, *J* = 16.0 Hz, 1H), 7.16 (d, *J* = 9.0 Hz, 2H), 4.11 (s, 3H), 3.90 (s, 3H), 1.78 (s, 6H) ppm. **^{13}C-NMR (125 MHz, d_6-DMSO)**: δ = 181.5,

163.7, 153.1, 143.2, 141.7, 133.0, 128.9, 128.8, 127.3, 122.7, 114.9, 114.7, 110.3, 55.8, 51.8, 34.1, 25.5 ppm. **IR (KBr)**: $\tilde{\nu}$ = 3435, 2927, 1585, 1564, 1526, 1478, 1298, 1271, 1256, 1171, 1126, 1035, 828, 761, 517 cm^{-1}. **MS (EI, 70 eV)**: *m/z* = 291 $[M\text{-H}]^+$. **Anal. calcd for $C_{20}H_{20}INO$**: C 57.29, H 5.29, N 3.34, found: C 57.01, H 5.24, N 3.25. **UV/Vis (Ethanol)**: λ_{max} = 426.0 nm.

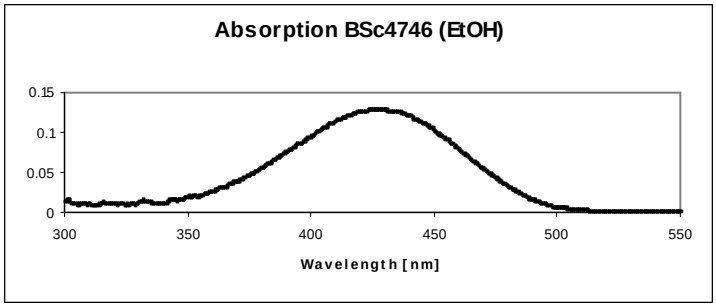

***In vitro* neuropathological staining of AD brain sections**: Tissues: hippocampus; Patient: male, 71 years old; CERAD Score: 3; NFTs-level: V.

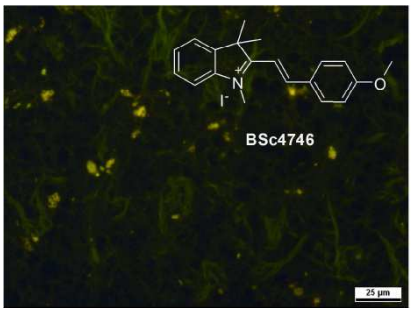

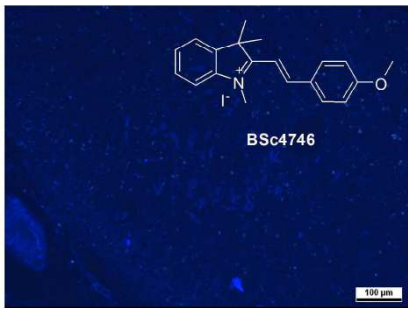

(*E*)-2-(4-(Diethylamino)styryl)-1,3,3-trimethyl-3*H*-indolium iodide (121d)

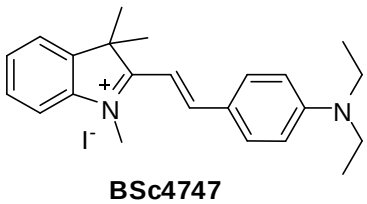

BSc4747

Yield: 92 %. **^{1}H-NMR (500 MHz, d_6-DMSO)**: δ = 8.26 (d, *J* = 15.5 Hz, 1H), 8.02 (d, *J* = 8.5 Hz, 2H), 7.74 (d, *J* = 7.5 Hz, 1H), 7.67 (d, *J* = 8.0 Hz, 1H), 7.53 (td, *J* = 7.5 Hz, *J* = 1.0 Hz, 1H), 7.46 (td, *J* = 7.5 Hz, *J* = 1.0 Hz, 1H), 7.19 (d, *J* = 15.5 Hz, 1H), 6.86 (d, *J* = 9.0 Hz, 2H), 3.93 (s, 3H), 3.57-3.51 (m, 4H), 1.73 (s, 6H), 1.17 (t, *J* = 7.0 Hz, 6H). **^{13}C-NMR (125 MHz, d_6-DMSO)**: δ = 179.4, 153.9, 152.6, 142.4, 142.1, 134.6 (brs), 128.7, 127.4, 122.6, 121.9, 113.4, 112.0, 104.6, 50.8, 44.5, 32.9, 26.3, 12.6 ppm. **IR (KBr)**: $\tilde{\nu}$ = 3420, 1924, 1574, 1526, 1479, 1404, 1353, 1270, 1191, 1112, 1073, 928, 783, 714, 506 cm^{-1}. **MS (EI, 70 eV)**: *m/z* = 334

[*M*+H]$^+$. **HRMS**: *m/z* [*M*]$^+$ calcd for $C_{23}H_{29}N_2$: 333.2331, found: 333.2336. **UV/Vis (Ethanol)**: λ_{max} = 548.0 nm.

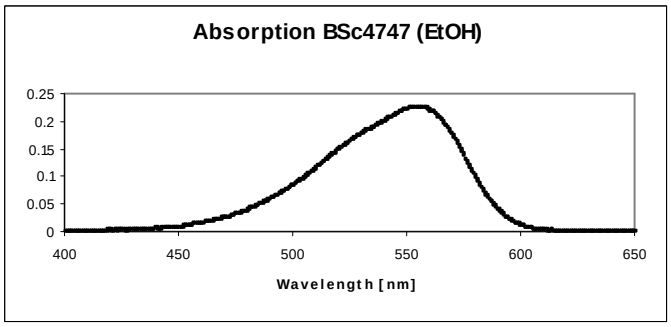

***In vitro* neuropathological staining of AD brain sections**: Tissues: hippocampus; Patient: male, 71 years old; CERAD Score: 3; NFTs-level: V.

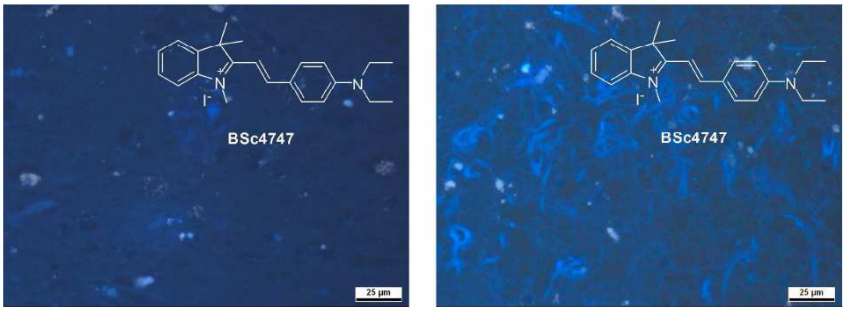

***In vitro* neuropathological staining of AD olfactory epithelium sections**: Tissues: olfactory epithelium; Patient: male, 78 years old; Braak: V, CERAD Score: 3.

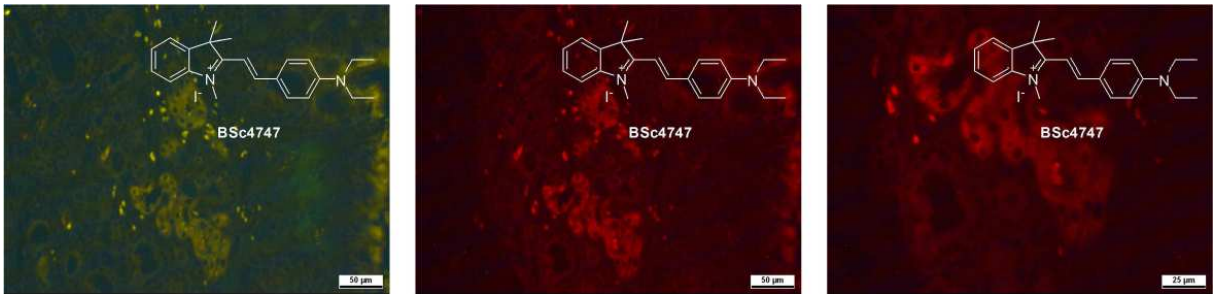

(*E*)-2-(4-Hydroxystyryl)-1,3,3-trimethyl-3*H*-indolium iodide (121e)

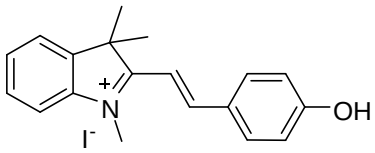

BSc4748

Yield: 83 %. **^{1}H-NMR (500 MHz, d_6-DMSO)**: δ = 8.33 (d, *J* = 16.0 Hz, 1H), 8.10 (d, *J* = 8.5 Hz, 2H), 7.81 (m, 2H), 7.60 (td, *J* = 7.5 Hz, *J* = 1.0 Hz, 1H), 7.55 (td, *J* = 7.5 Hz, *J* = 1.0 Hz, 1H), 7.41 (d, *J* = 16.5 Hz, 1H), 6.82 (d, *J* = 8.5 Hz, 2H), 4.06 (s, 3H), 1.76 (s, 6H) ppm. **^{13}C-NMR (125 MHz, d_6-DMSO)**: δ = 180.8, 164.1, 153.3, 142.9, 141.8, 133.6, 128.7, 128.4, 125.6, 122.6, 116.7, 114.3, 108.5, 51.5, 33.7, 25.6 ppm. **IR (KBr)**: $\tilde{\nu}$ = 3442, 3046, 1760, 1592, 1574, 1538, 1368, 1311, 1273, 1219, 1166, 1108, 940, 818, 766, 666, 483 cm^{-1}. **MS (EI, 70 eV)**: *m/z* = 277 [*M*-H]$^{+}$. **Anal. calcd for $C_{19}H_{20}INO$**: C 56.31, H 4.97, N 3.46, found: C 56.63, H 5.09, N 3.43. **UV/Vis (Ethanol)**: λ_{max} = 546.0 nm.

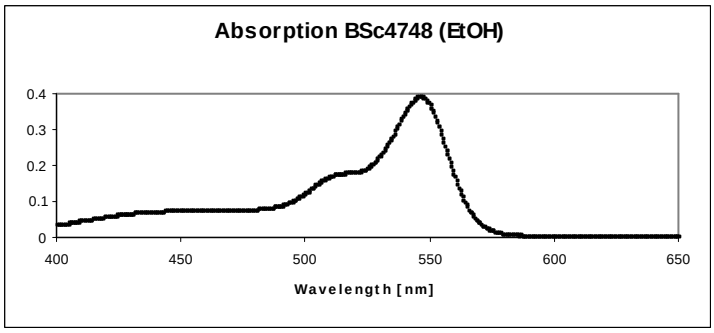

***In vitro* neuropathological staining of AD brain sections**: Tissues: hippocampus; Patient: male, 71 years old; CERAD Score: 3; NFTs-level: V.

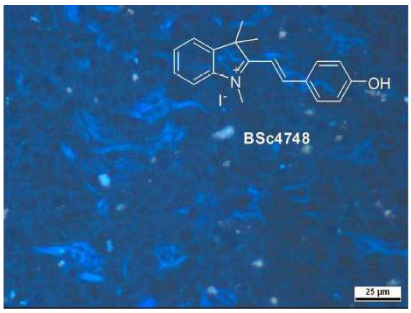

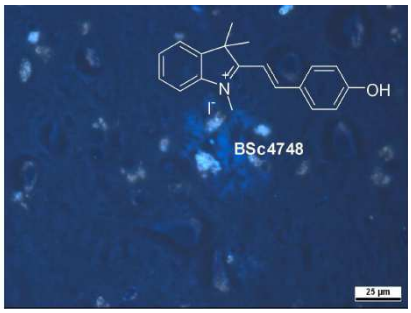

(*E*)-1,3,3-Trimethyl-2-(4-(4-methylpiperazin-1-yl)styryl)-3*H*-indolium iodide (121f)

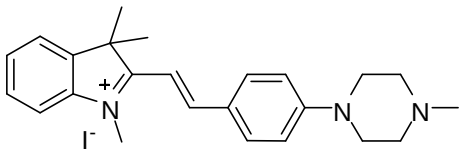

BSc4749

Yield: 91 %. **^{1}H-NMR (500 MHz, d_6-DMSO)**: δ = 8.30 (d, *J* = 16.0 Hz, 1H), 8.07 (d, *J* = 9.0 Hz, 2H), 7.79 (d, *J* = 7.5 Hz, 1H), 7.74 (d, *J* = 8.0 Hz, 1H), 7.56 (td, *J* = 7.5 Hz, *J* = 1.5 Hz, 1H), 7.51 (td, *J* = 7.5 Hz, *J* = 1.0 Hz, 1H), 7.32 (d, *J* = 16.0 Hz, 1H), 7.10 (d, *J* = 9.5 Hz, 2H), 4.00 (s, 3H), 3.53 (t, *J* = 5.0 Hz, 4H), 2.46 (t, *J* = 4.5 Hz, 4H), 2.25 (s, 3H), 1.75 (s, 6H) ppm.

^{13}C-NMR (125 MHz, d_6-DMSO): δ = 180.1, 154.2, 153.6, 142.7, 141.9, 133.7, 128.7, 127.8, 123.5, 122.6, 113.8, 113.5, 106.5, 54.1, 51.0, 46.0, 45.4, 33.3, 26.0 ppm. **IR (KBr)**: $\tilde{\nu}$ = 3434, 2919, 2802, 1568, 1520, 1479, 1439, 1375, 1291, 1242, 1190, 1172, 1114, 998, 918, 826, 786, 750, 640, 492 cm^{-1}. **MS (EI, 70 eV)**: *m/z* = 361.37 [*M*+H]$^+$. **HRMS**: *m/z* [*M*]$^+$ calcd for $C_{24}H_{30}N_3$: 360.2440, found: 360.2399. **UV/Vis (Ethanol)**: λ_{max} = 530.5 nm.

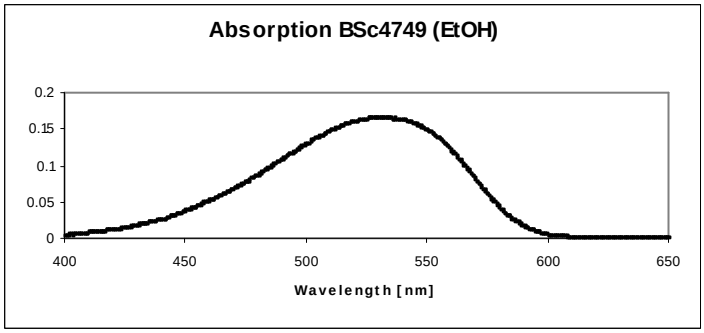

***In vitro* neuropathological staining of AD brain sections**: Tissues: hippocampus; Patient: male, 71 years old; CERAD Score: 3; NFTs-level: V.

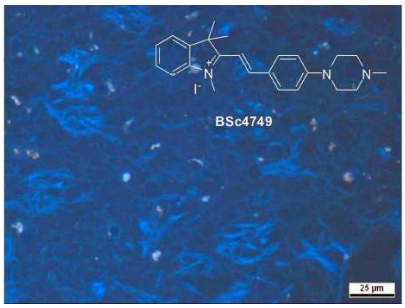

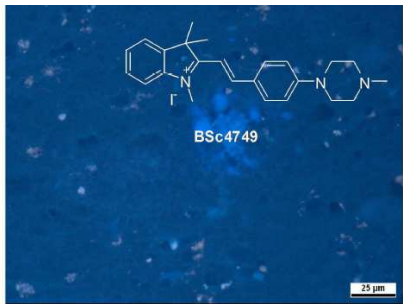

(*E*)-1,3,3-Trimethyl-2-(4-(pyrrolidin-1-yl)styryl)-3*H*-indolium iodide (121g)

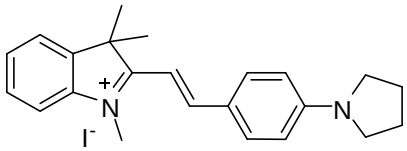

BSc4750

Yield: 96 %. **^{1}H-NMR (500 MHz, d_6-DMSO)**: δ = 8.30 (d, *J* = 15.5 Hz, 1H), 8.07 (d, *J* = 8.5 Hz, 2H), 7.76 (d, *J* = 7.5 Hz, 1H), 7.68 (d, *J* = 8.0 Hz, 1H), 7.54 (td, *J* = 7.5 Hz, *J* = 1.0 Hz, 1H), 7.46 (td, *J* = 7.5 Hz, *J* = 1.0 Hz, 1H), 7.22 (d, *J* = 15.5 Hz, 1H), 6.75 (d, *J* = 9.0 Hz, 2H), 3.95 (s, 3H), 3.48 (t, *J* = 7.5 Hz, 4H), 2.04-1.98 (m, 4H), 1.74 (s, 6H) ppm. **^{13}C-NMR (125 MHz, d_6-DMSO)**: δ = 179.1, 154.0, 151.9, 142.3, 142.0, 134.2 (brs), 128.5, 127.2, 122.5, 122.1, 113.3, 112.6, 104.5, 50.6, 47.8, 32.8, 26.2, 24.7 ppm. **IR (KBr)**: $\tilde{\nu}$ = 3429, 2925, 1614, 1576, 1529, 1477, 1396, 1293, 1188, 1114, 930, 817, 774, 706 cm^{-1}. **MS (EI, 70 eV)**: *m/z* =

332 $[M+H]^+$. **Anal. calcd for $C_{23}H_{27}IN_2$**: C 60.27, H 5.94, N 6.11, found: C 60.22, H 5.92, N 5.96. **UV/Vis (Ethanol)**: λ_{max} = 555.5 nm.

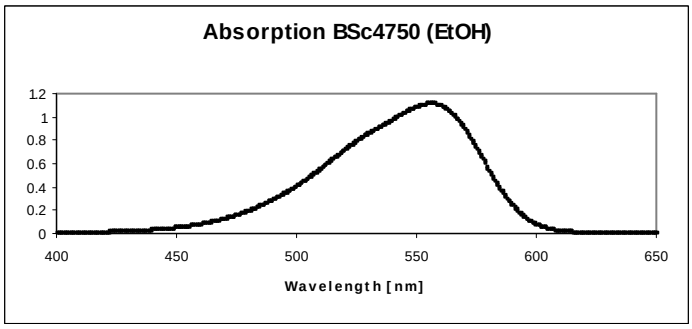

***In vitro* neuropathological staining of AD brain sections**: Tissues: hippocampus; Patient: male, 71 years old; CERAD Score: 3; NFTs-level: V.

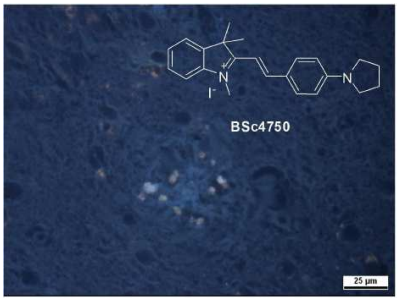

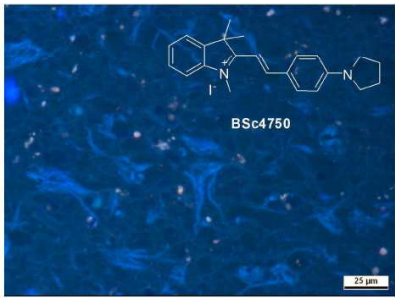

***In vitro* neuropathological staining of AD olfactory epithelium sections**: Tissues: olfactory epithelium; Patient: male, 78 years old; Braak: V, CERAD Score: 3.

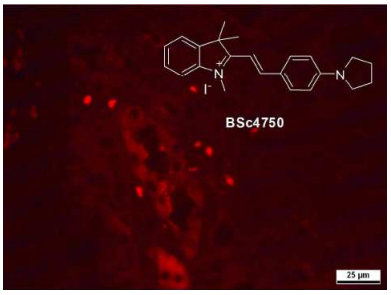

(*E*)-2-(2-(1*H*-Indol-5-yl)vinyl)-1,3,3-trimethyl-3*H*-indolium iodide (121h)

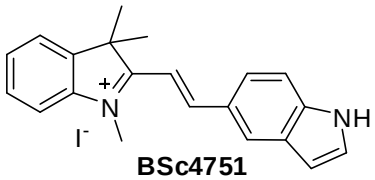

Yield: 87 %. **^{1}H-NMR (500 MHz, d_6-DMSO)**: δ = 11.67 (s, 1H), 8.56 (d, *J* = 16.5 Hz, 1H), 8.51 (s, 1H), 8.02 (dd, *J* = 8.5 Hz, *J* = 1.5 Hz, 1H), 7.86-7.81 (m, 2H), 7.64-7.55 (m, 4H),

7.52 (t, *J* = 8.0 Hz, 1H), 6.65-6.62 (m, 1H), 4.11 (s, 3H), 1.81 (s, 6H) ppm. **^{13}C-NMR (125 MHz, d_6-DMSO)**: δ = 181.2, 156.1, 143.0, 141.8, 139.07, 128.7, 1287.5, 128.1, 127.8, 126.5, 126.0, 123.0, 122.6, 114.4, 112.5, 109.1, 103.0, 51.6, 33.8, 25.6 ppm. **UV/Vis (Ethanol)**: λ_{max} = 457.5 nm.

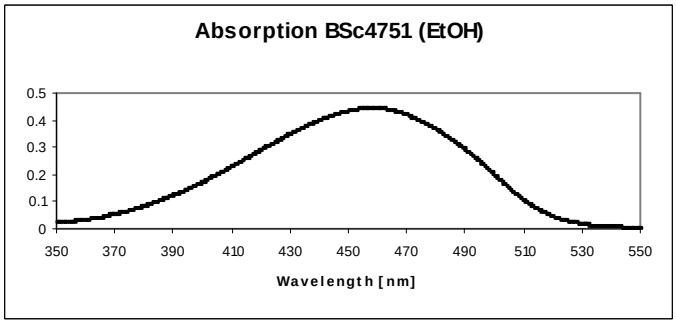

***In vitro* neuropathological staining of AD brain sections**: Tissues: hippocampus; Patient: male, 71 years old; CERAD Score: 3; NFTs-level: V.

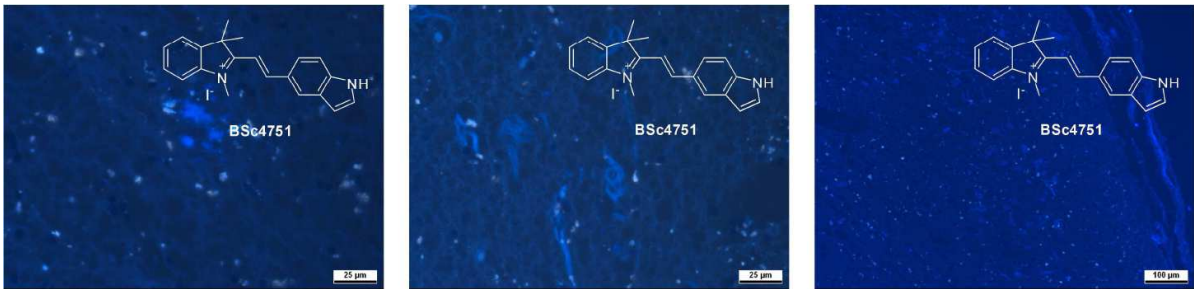

(*E*)-2-(4-(Diethylamino)styryl)-5-fluoro-1,3,3-trimethyl-3*H*-indolium iodide (121i)

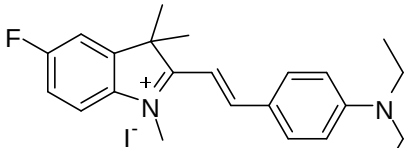

BSc4815

Yield: 81 %. **^{1}H-NMR (500 MHz, d_6-DMSO)**: δ = 8.27 (d, *J* = 15.5 Hz, 1H),8.04 (d, *J* = 8.5 Hz, 2H), 7.77 (dd, *J* = 8.5 Hz, *J* = 2.5 Hz, 1H), 7.71 (dd, *J* = 9.0 Hz, *J* = 4.5 Hz, 1H), 7.40 (td, *J* = 8.5 Hz, *J* = 2.5 Hz, 1H), 7.18 (d, *J* = 15.5 Hz, 1H), 6.87 (d, *J* = 9.5 Hz, 2H), 3.93 (s, 3H), 3.59-3.51 (m, 4H), 1.75 (s, 6H), 1.17 (t, *J* = 7.0 Hz, 6H) ppm. **^{13}C-NMR (125 MHz, d_6-DMSO)**: δ = 179.3, 161.4 (*J* = 243.1 Hz), 153.7, 152.4, 144.7 (*J* = 9.3 Hz), 138.3, 134.4 (brs), 121.8, 115.4 (*J* = 24.3 Hz), 114.8 (*J* = 9.1 Hz), 111.8, 110.6 (*J* = 13.3 Hz), 104.6, 50.9, 44.3, 33.1, 26.0, 12.4 ppm. **UV/Vis (Ethanol)**: λ_{max} = 554.0 nm.

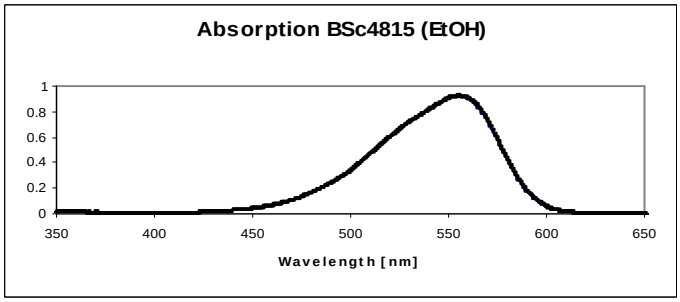

***In vitro* neuropathological staining of AD brain sections**: Tissues: hippocampus; Patient: male, 71 years old; CERAD Score: 3; NFTs-level: V.

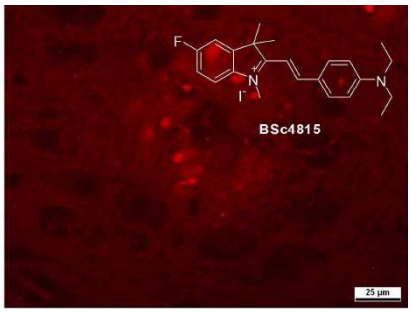

(*E*)-2-(4-(Diethylamino)styryl)-5-methoxy-1,3,3-trimethyl-3*H*-indolium iodide (121j)

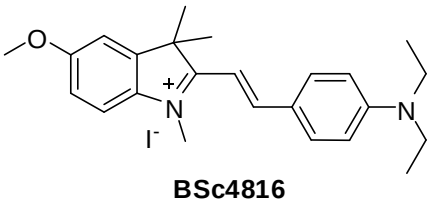

BSc4816

Yield: 89 %. **^{1}H-NMR (500 MHz, d_6-DMSO)**: δ = 8.20 (d, *J* = 16.0 Hz, 1H),8.00 (d, *J* = 9.0 Hz, 2H), 7.62 (d, *J* = 9.0 Hz, 1H), 7.43 (d, *J* = 2.0 Hz, 1H), 7.17 (d, *J* = 15.5 Hz, 1H), 7.09 (dd, *J* = 8.5 Hz, *J* = 2.5 Hz, 1H), 6.85 (d, *J* = 9.5 Hz, 2H), 3.94 (s, 3H), 3.86 (s, 3H), 3.56-3.49 (m, 4H), 1.74 (s, 6H), 1.17 (t, *J* = 7.0 Hz, 6H) ppm. **^{13}C-NMR (125 MHz, d_6-DMSO)**: δ = 177.9, 159.5, 152.1, 151.9, 144.4, 135.3, 133.7 (brs), 121.7, 114.4, 114.0, 111.6, 108.6, 104.9, 55.9, 50.8, 44.2, 33.0, 26.0, 12.4 ppm. **UV/Vis (Ethanol)**: λ_{max} = 553.0 nm.

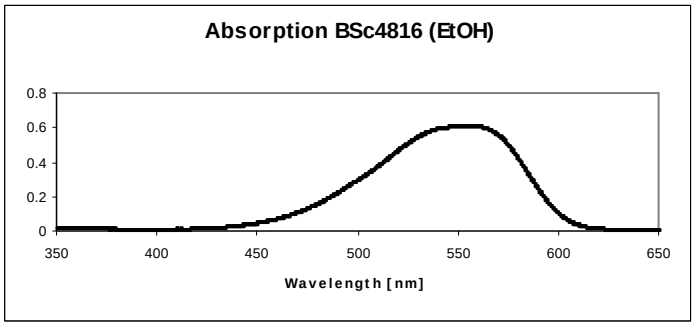

***In vitro* neuropathological staining of AD brain sections**: Tissues: hippocampus; Patient: male, 71 years old; CERAD Score: 3; NFTs-level: V.

***In vitro* neuropathological staining of PD brain sections**: Tissues: midbrain; Patient: male, 76 years old.

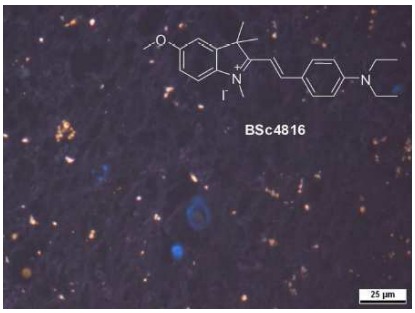

(*E*)-5-Bromo-2-(4-(diethylamino)styryl)-1,3,3-trimethyl-3*H*-indolium iodide (121k)

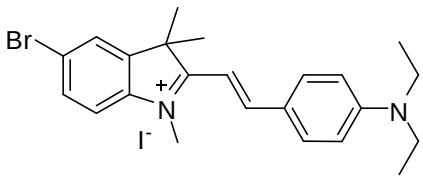

BSc4817

Yield: 92 %. **^{1}H-NMR (500 MHz, d_6-DMSO)**: δ = 8.30 (d, *J* = 15.5 Hz, 1H),8.10-8.02 (m, 3H), 7.73 (dd, *J* = 8.5 Hz, *J* = 1.5 Hz, 1H), 7.62 (d, *J* = 8.5 Hz, 1H), 7.17 (d, *J* = 15.5 Hz, 1H), 6.89 (d, *J* = 9.0 Hz, 2H), 3.91 (s, 3H), 3.60-3.53 (m, 4H), 1.75 (s, 6H), 1.18 (t, *J* = 7.0 Hz, 6H) ppm. **^{13}C-NMR (125 MHz, d_6-DMSO)**: δ = 178.9, 154.2, 152.7, 144.5, 141.4, 134.5 (brs), 131.3, 125.8, 122.0, 119.8, 115.0, 112.0, 104.2, 50.7, 44.4, 32.9, 26.0, 12.5 ppm. **UV/Vis (Ethanol)**: λ_{max} = 564.0 nm.

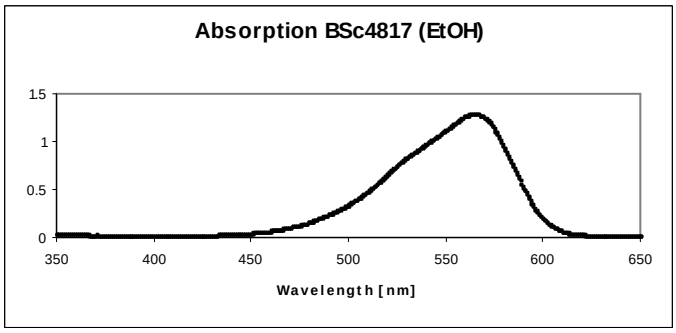

***In vitro* neuropathological staining of AD brain sections**: Tissues: hippocampus; Patient: male, 71 years old; CERAD Score: 3; NFTs-level: V.

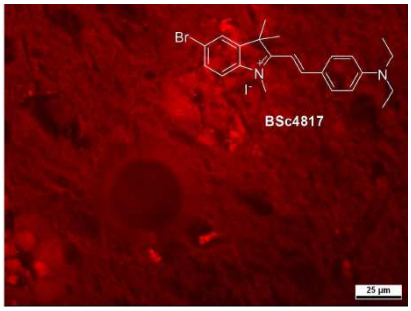

***In vitro* neuropathological staining of PD brain sections**: Tissues: midbrain; Patient: male, 76 years old.

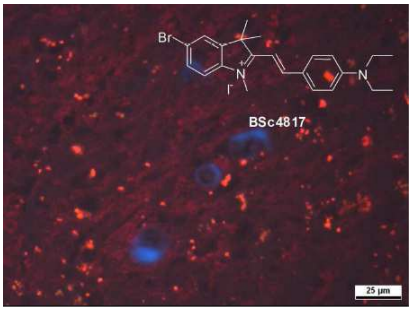

(*E*)-2-(4-(Diethylamino)styryl)-3-ethyl-1,3-dimethyl-3*H*-indolium iodide (123a)

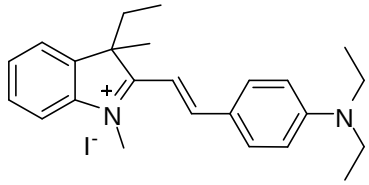

BSc4813

Yield: 93 %. **^{1}H-NMR (500 MHz, d_6-DMSO)**: δ = 8.26 (d, *J* = 15.5 Hz, 1H),8.03 (d, *J* = 8.5 Hz, 2H), 7.71-7.65 (m, 2H), 7.55 (td, *J* = 7.5 Hz, *J* = 1.0 Hz, 1H), 7.47 (td, *J* = 7.5 Hz, *J* = 1.0 Hz, 1H), 7.23 (d, *J* = 15.0 Hz, 1H), 6.86 (d, *J* = 9.0 Hz, 2H), 3.95 (s, 3H), 3.57-3.51 (m, 4H), 2.47-

2.25 (m, 2H), 1.73 (s, 3H), 1.17 (t, *J* = 7.0 Hz, 6H), 0.33 (t, *J* = 7.5 Hz, 3H) ppm. **^{13}C-NMR (125 MHz, *d*$_6$-DMSO)**: δ = 178.3, 153.4, 152.7, 142.9, 140.3, 134.7 (brs), 238.9, 127.45, 122.7, 121.9, 113.2, 112.1, 104.8, 55.9, 44.5, 33.6, 32.9, 25.8, 12.6, 8.5 ppm. **UV/Vis (Ethanol)**: λ_{max} = 556.5 nm.

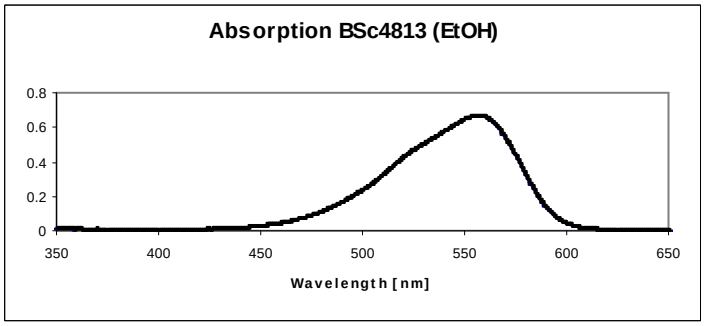

***In vitro* neuropathological staining of AD brain sections**: Tissues: hippocampus; Patient: male, 71 years old; CERAD Score: 3; NFTs-level: V.

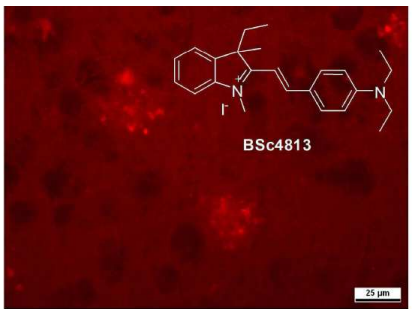

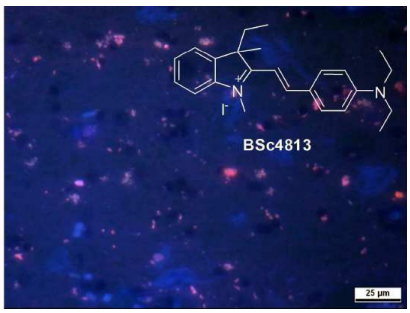

(*E*)-2-(4-(Dimethylamino)styryl)-3-ethyl-1,3-dimethyl-3*H*-indolium iodide (123b)

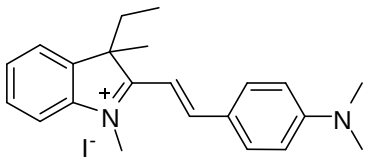

BSc4814

Yield: 90 %. **^{1}H-NMR (500 MHz, *d*$_6$-DMSO)**: δ = 8.31 (d, *J* = 16.0 Hz, 1H),8.07 (d, *J* = 8.5 Hz, 2H), 7.71 (t, *J* = 8.0 Hz, 2H), 7.56 (td, *J* = 7.5 Hz, *J* = 1.0 Hz, 1H), 7.49 (td, *J* = 7.5 Hz, *J* = 1.0 Hz, 1H), 7.29 (d, *J* = 15.5 Hz, 1H), 6.89 (d, *J* = 9.0 Hz, 2H), 4.00 (s, 3H), 3.17 (s, 6H), 2.46-2.28 (m, 2H), 1.74 (s, 3H), 0.34 (t, *J* = 7.5 Hz, 3H) ppm. **^{13}C-NMR (125 MHz, *d*$_6$-DMSO)**: δ = 178.5, 154.4, 153.5, 142.8, 140.3, 133.9 (brs), 128.7, 127.4, 122.6, 122.1, 113.3, 112.1, 105.2, 55.9, 33.4, 32.9, 25.6, 8.4 ppm. **UV/Vis (Ethanol)**: λ_{max} = 549.5 nm.

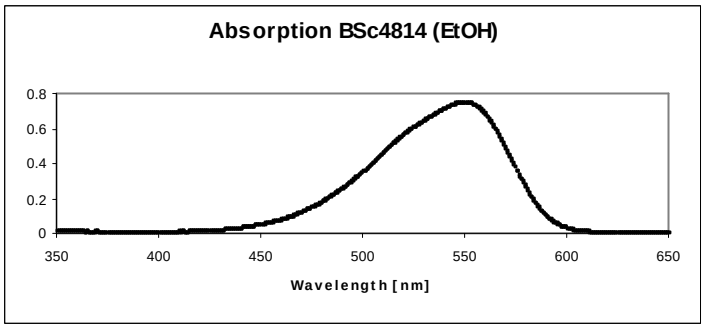

***In vitro* neuropathological staining of AD brain sections**: Tissues: hippocampus; Patient: male, 71 years old; CERAD Score: 3; NFTs-level: V.

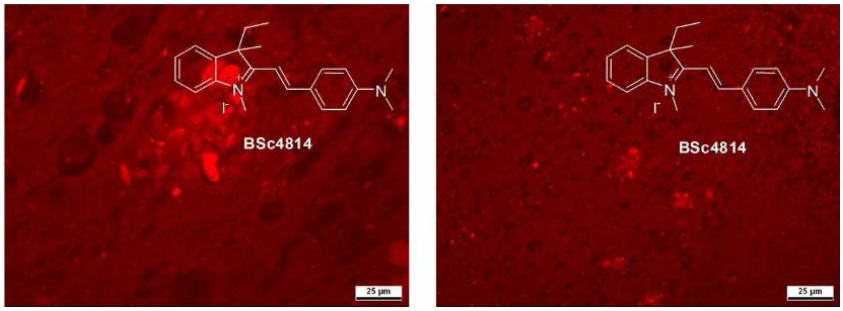

***In vitro* neuropathological staining of PD brain sections**: Tissues: midbrain; Patient: male, 76 years old.

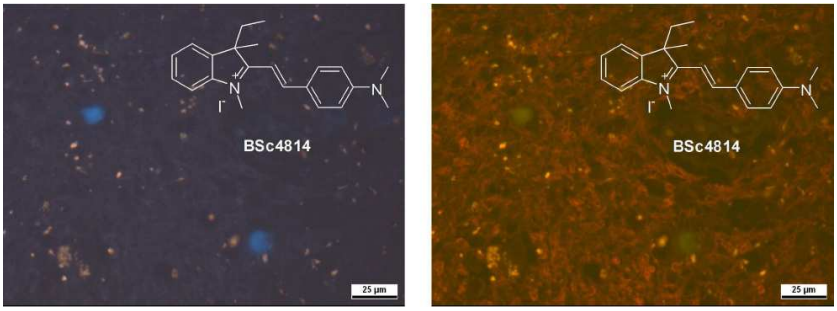

(*E*)-2-(2-(1*H*-Indol-5-yl)vinyl)-3-ethyl-1,3-dimethyl-3*H*-indolium iodide (123c)

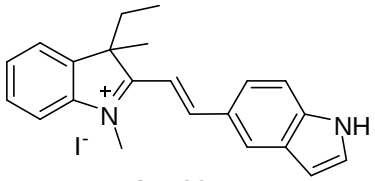

BSc4865

Yield: 80 %. **^{1}H-NMR (500 MHz, d_6-DMSO)**: δ = 11.68 (s, 1H), 8.57 (d, *J* = 16.0 Hz, 1H),8.51 (s, 1H), 8.02 (d, *J* = 9.0 Hz, 1H), 7.85 (d, *J* = 7.5 Hz, 1H), 7.81 (d, *J* = 7.5 Hz, 1H), 7.66-7.55 (m, 4H), 7.53 (t, *J* = 2.5 Hz, 1H), 6.64 (s, 1H), 4.15 (s, 3H), 3.58-2.37 (m, 2H), 1.81 (s, 3H),

0.37 (t, *J* = 7.0 Hz, 3H) ppm. **^{13}C-NMR (125 MHz, d_6-DMSO)**: δ = 180.56, 155.86, 142.56, 140.97, 139.17, 128.90, 128.59, 128.16, 127.87, 126.69, 125.97, 122.99, 122.79, 114.33, 112.51, 109.24, 103.07, 56.79, 33.81, 33.32, 25.07, 8.34 ppm. **UV/Vis (Ethanol)**: λ_{max} = 458.5 nm.

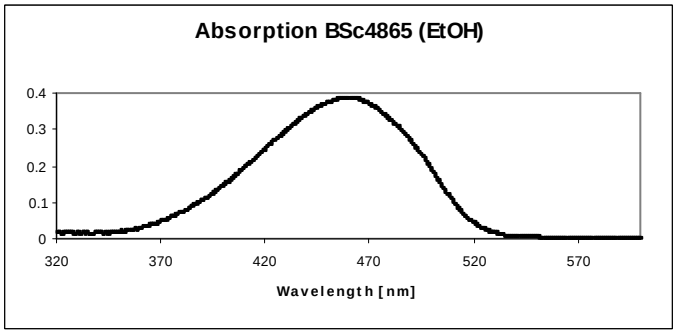

(E)-3-Ethyl-1,3-dimethyl-2-(4-(pyrrolidin-1-yl)styryl)-3*H*-indolium iodide (123d)

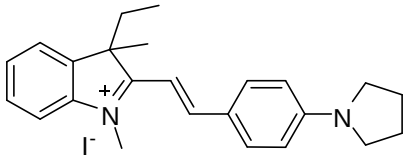

BSc4866

Yield: 94 %. **^{1}H-NMR (500 MHz, d_6-DMSO)**: δ = 8.29 (d, *J* = 15.5 Hz, 1H), 8.07 (d, *J* = 8.0 Hz, 2H), 7.74-7.67 (m, 2H), 7.56 (t, *J* = 7.5 Hz, 1H), 7.48 (t, *J* = 7.5 Hz, 1H), 7.26 (d, *J* = 15.5 Hz, 1H), 6.75 (d, *J* = 8.5 Hz, 2H), 3.97 (s, 3H), 3.49 (t, *J* = 6.0 Hz, 4H), 2.47-2.27 (m, 2H), 2.01 (t, *J* = 6.0 Hz, 4H), 1.74 (s, 3H), 0.35 (t, *J* = 7.5 Hz, 3H) ppm. **^{13}C-NMR (125 MHz, d_6-DMSO)**: δ = 178.1, 153.6, 152.0, 142.8, 140.2, 134.2, 128.7, 127.2, 122.6, 122.1, 113.1, 112.7, 104.7, 55.7, 47.8, 33.5, 32.8, 25.7, 24.7, 8.4 ppm. **UV/Vis (Ethanol)**: λ_{max} = 557.5 nm.

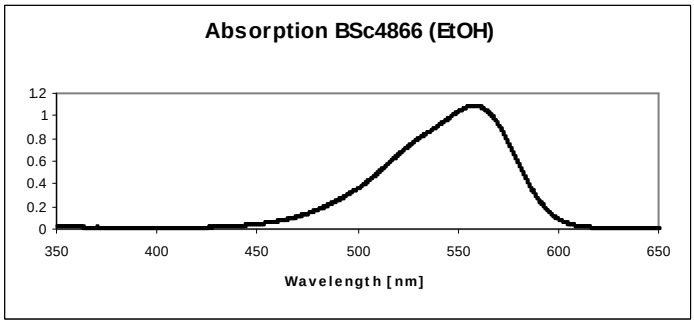

***In vitro* neuropathological staining of AD brain sections**: Tissues: hippocampus; Patient: male, 71 years old; CERAD Score: 3; NFTs-level: V.

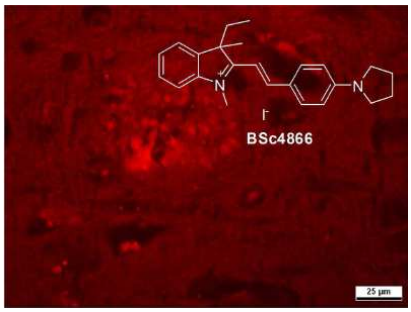

(*E*)-3-Methyl-2-(4-(pyrrolidin-1-yl)styryl)benzo[*d*]oxazol-3-ium iodide (129)

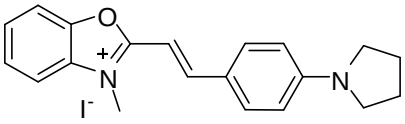

BSc4905

Yield: 79 %. **^{1}H-NMR (300 MHz, d_6-DMSO)**: δ = 8.22 (d, *J* = 15.9 Hz, 1H), 7.98-7.87 (m, 4H), 7.69-7.63 (m, 2H), 7.30 (d, *J* = 15.9 Hz, 1H), 6.72 (d, *J* = 9.0 Hz, 2H), 4.06 (s, 3H), 3.47-3.39 (m, 4H), 2.04-1.97 (m, 4H) ppm. **^{13}C-NMR (75 MHz, d_6-DMSO)**: δ = 163.0, 151.2, 151.1, 146.7, 133.2, 131.4, 127.4, 126.8, 120.7, 113.2, 112.3, 111.7, 95.6, 47.5, 31.5, 24.7 ppm. **UV/Vis (Ethanol)**: λ_{max} = 504.0 nm.

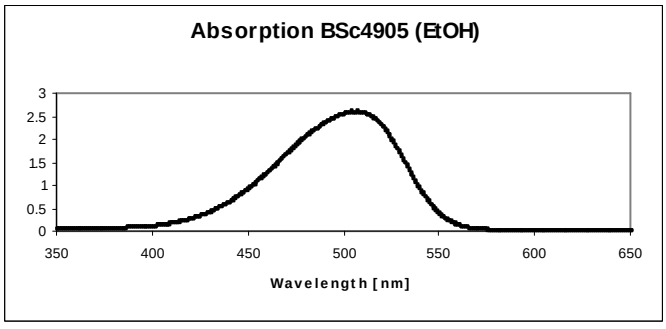

(*E*)-3-Butyl-2-(4-(pyrrolidin-1-yl)styryl)benzo[*d*]oxazol-3-ium iodide (131)

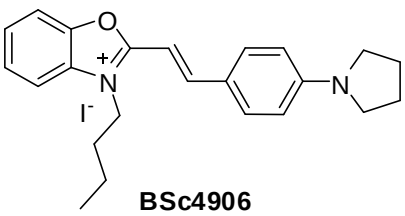

BSc4906

Yield: 83 %. **^{1}H-NMR (300 MHz, d_6-DMSO)**: δ = 8.24 (d, *J* = 15.0 Hz, 1H), 8.01-7.88 (m, 4H), 7.69-7.61 (m, 2H), 7.31 (d, *J* = 15.3 Hz, 1H), 6.71 (d, *J* = 8.7 Hz, 2H), 4.57 (t, *J* = 7.2 Hz, 2H), 3.47-3.40 (m, 4H), 2.04-1.97 (m, 4H), 1.91-1.78 (m, 2H), 1.53-1.38 (m, 2H), 0.94 (t, *J* = 7.2 Hz, 3H) ppm. **^{13}C-NMR (75 MHz, d_6-DMSO)**: δ = 162.7, 151.6, 151.3, 146.9, 133.3, 130.6, 127.4, 126.8, 120.7, 113.3, 112.3, 111.8, 95.3, 47.6, 44.7, 30.1, 24.7, 19.1, 13.5 ppm. **UV/Vis (Ethanol)**: λ_{max} = 509.0 nm.

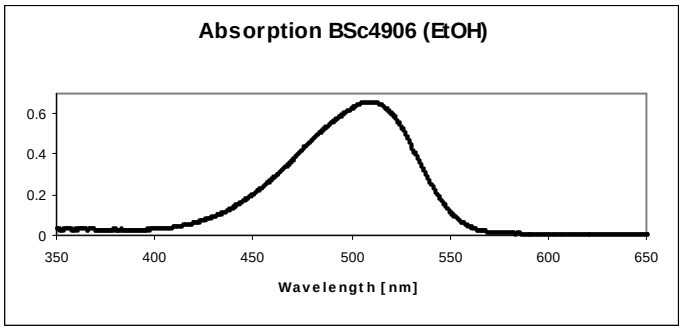

6.8. Synthesis of trimethine cyanine derivatives

6.8.1. Synthesis of 1-alkyl/PEG-2,3,3-tetramethyl-3*H*-indolium

1,2,3,3-Tetramethyl-5-nitro-3*H*-indolium iodide (134a)

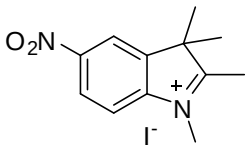

A mixture of (4-nitrophenyl)hydrazine hydrochloride (1.89 g, 10.0 mmol, 1.0 eq) and 3-methyl-2-butanone (1.03 g, 12.0 mmol, 1.2 eq) was dissolved in glacial acetic acid (20 mL) and then heated under reflux temperature for 12 h under argon. When the reaction mixture was cooled down to room temperature, the solvent was evaporated under reduced pressure and the residue was dissolved in dichloromethane (30 mL), washed with 10% aqueous Na_2CO_3 (2 × 30 mL), dried over Na_2SO_4. After filtration, the solvent was evaporated *in vacuo*. The crude product was purified by column chromatography (SiO_2; ethyl acetate: cyclohexane = 1:2) to afford the product as brown liquid.

2,3,3-Trimethyl-5-nitro-3*H*-indole (1.02 g, 5 mmol, 1.0 eq) and methyl iodide (1.42 g, 10.0 mmol, 2.0 eq) were dissolved in anhydrous acetonitrile (15.0 mL). The reaction mixture was refluxed overnight. When the reaction mixture was cooled down to room temperature, the solvent was evaporated *in vacuo* and the residue was treated with ethyl acetate (30.0 mL).

The final product was collected by filtration and washed with ethyl acetate. The colorless solid was used in the next reaction without further purification.

1-Decyl-2,3,3-trimethyl-3*H*-indolium bromide (134b)

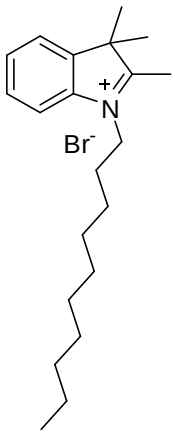

A solution of 2,3,3-trimethylindolenine (0.96 g, 6.0 mmol, 1.0 eq) and 1-bromodecane (4.2 g, 19 mmol, 3.1 eq) in 15 mL MeCN was heated under reflux temperature and argon overnight. When the reaction mixture was cooled down to room temperature, the solvent was evaporated under reduced pressure. The final product purified by column chromatography (SiO_2; dichloromethane: methanol = 10:1) to afford 1.12 g of 1-decyl-2,3,3-trimethyl-3*H*-indolium bromide as red waxy solid (yield: 49 %).

1-PEG-2,3,3-tetramethyl-3*H*-indolium (134c-e)

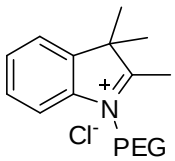

Polyethylene glycol (10.0 mmol, 1.0 eq) with THF (3 mL) was added dropwise to a solution of NaOH (0.52 g, 13.0 mmol, 1.3 eq) in 1.0 mL water in 0 °C. The solution of *p*-toluenesulfonyl chloride (2.1 g, 11.0 mmol, 1.1 eq) was then added to the mixture. After 12 hours of stirring at room temperature, the reaction was quenched with 2.5 mL water and extracted with dichloromethane (20 mL). The combined organic phases were washed successively with 2 N HCl (15 mL) and brine (15 mL), the organic phase was dried over $MgSO_4$ After filtration, the solvent was evaporated *in vacuo*.

2,3,3-Trimethyl-indolenine (5.0 mmol, 1.0 eq) and polyethylene glycol 4-methylbenzenesulfonate (10.0 mmol, 2.0 eq) were dissolved in anhydrous acetonitrile (10.0 mL). The reaction mixture was refluxed for 4 days. The color of the reaction mixture turned to purple, then it was cooled down to room temperature. The crude product was purified by column chromatography (SiO_2; dichloromethane: methanol = 10:1, 2 % triethylamine) to afford the purple liquid (Yield < 20 %).

6.8.2. Synthesis of 3-substitute-2-methylbenzo[*d*]thiazol-3-ium

2,3-Dimethylbenzo[*d*]thiazol-3-ium iodide (137a)

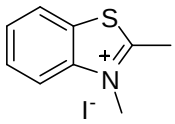

2-Methylbenzo[*d*]thiazole (0.75 g, 5.0 mmol, 1.0 eq) and methyl iodide (1.42 g, 10.0 mmol, 2.0 eq) were dissolved in anhydrous acetonitrile (15.0 mL). The reaction mixture was refluxed overnight. When the reaction mixture was cooled down to room temperature, the solvent was evaporated under reduced pressure and the residue was treated with ethyl acetate (30.0 mL). The final product was collected by filtration and washed with ethyl acetate. The colorless solid was used in the next reaction without further purification.

3-PEG-2-methylbenzo[*d*]thiazol-3-ium (137b-c)

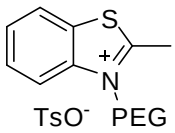

2-Methylbenzo[*d*]thiazole (5.0 mmol, 1.0 eq) and polyethylene glycol 4-methylbenzenesulfonate (10.0 mmol, 2.0 eq) were stirred at 130 °C for 2 days. The color of the reaction mixture turned to purple, then it was cooled to room temperature. The crude product was purified by column chromatography (SiO_2; dichloromethane: methanol = 10:1) to afford the waxy solid (Yield < 20 %).

6.8.3. General procedures for synthesis of trimethine cyanine

A solution of corresponding indolium / 3-substitute-2-methylbenzo[*d*]thiazol-3-ium / 3-substitute -2-methylbenzo[*d*]oxazol-3-ium (1.0 mmol, 1.0 eq) and triethyl orthoformate (296

mg, 2.0 mmol, 4.0 eq) in 1 mL of dry pyridine was refluxed for 16 h under argon. When the reaction mixture was cooled down to room temperature, the residue was purified by column chromatography (SiO_2; dichloromethane: methanol = 10:1) to afford the final product in moderate yields (yield: 29-83 %).

1,3,3-Trimethyl-2-((1*E*,3*E*)-3-(1,3,3-trimethylindolin-2-ylidene)prop-1-enyl)-3*H*-indolium iodide (135a)

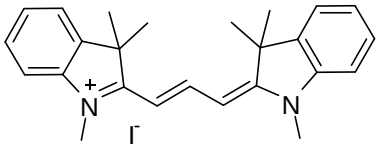

BSc4704

Yield: 83 %. **^{1}H-NMR (500 MHz, d_6-DMSO)**: δ = 8.34 (t, *J* = 13.5 Hz, 1H), 7.62 (d, *J* = 7.0 Hz, 2H), 7.46-7.42 (m, 4H), 7.32-7.27 (m, 2H), 6.44 (d, *J* = 13.5 Hz, 2H), 3.64 (s, 6H), 1.68 (s, 12H) ppm. **^{13}C-NMR (125 MHz, d_6-DMSO)**: δ = 174.4, 149.6, 142.7, 140.6, 128.7, 125.3, 122.5, 111.5, 102.7, 48.9, 31.4, 27.4 ppm. **UV/Vis (Ethanol)**: λ_{max} = 547.0 nm.

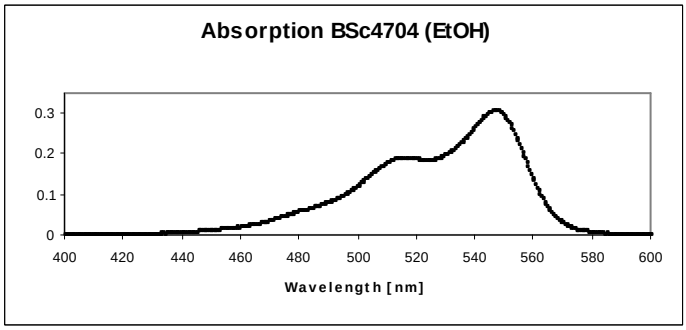

***In vitro* neuropathological staining of AD brain sections**: Tissues: hippocampus; Patient: male, 71 years old; CERAD Score: 3; NFTs-level: V.

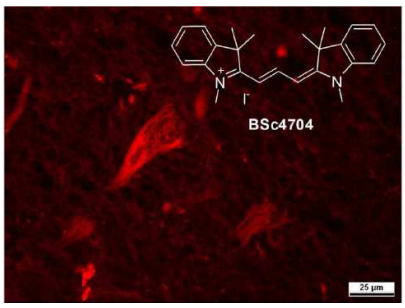

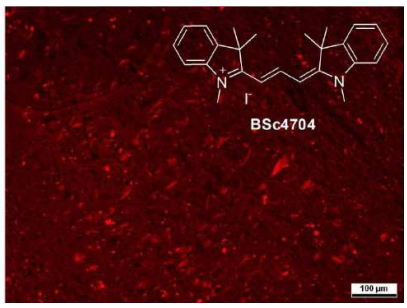

***In vitro* neuropathological staining of PD brain sections**: Tissues: midbrain; Patient: male, 76 years old.

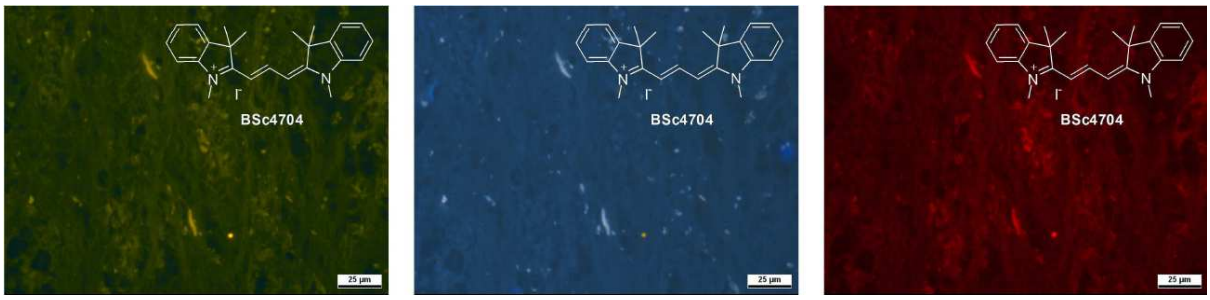

***In vitro* neuropathological staining of AD olfactory epithelium sections**: Tissues: olfactory epithelium; Patient: male, 78 years old; Braak: V, CERAD Score: 3.

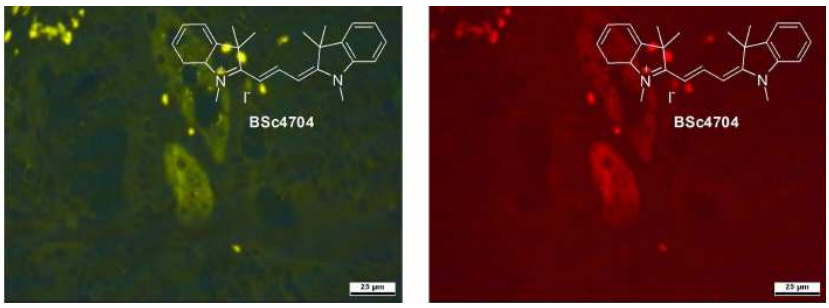

1,3,3-Trimethyl-5-nitro-2-((1*E*,3*E*)-3-(1,3,3-trimethyl-5-nitroindolin-2-ylidene)prop-1-enyl)-3*H*-indolium iodide (135b)

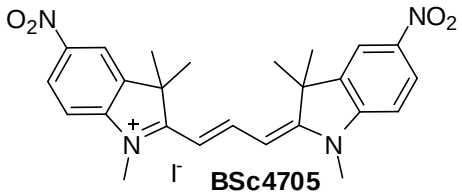

BSc4705

Yield: 53 %. **^{1}H-NMR (500 MHz, d_6-DMSO)**: δ = 8.60 (d, *J* = 2.5 Hz, 2H), 8.44 (t, *J* = 13.5 Hz, 1H), 8.38 (dd, *J* = 9.0 Hz, *J* = 2.5 Hz, 2H), 7.70 (d, *J* = 9.0 Hz, 2H), 6.74 (d, *J* = 13.5 Hz, 2H), 3.74 (s, 6H), 1.76 (s, 12H) ppm. **^{13}C-NMR (125 MHz, d_6-DMSO)**: δ = 178.5, 151.5, 147.8, 144.5, 141.9, 125.4, 118.2, 112.1, 105.7, 54.8, 49.0, 32.2, 26.8 ppm. **MS (EI, 70 eV)**: *m/z* = 446 $[M\text{-}1]^+$. **UV/Vis (Ethanol)**: λ_{max} = 567.0 nm.

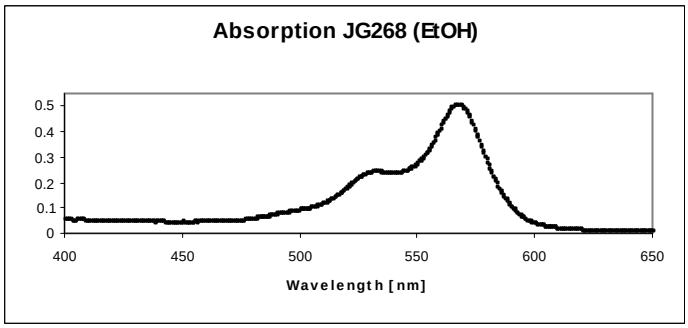

***In vitro* neuropathological staining of AD brain sections**: Tissues: hippocampus; Patient: male, 71 years old; CERAD Score: 3; NFTs-level: V.

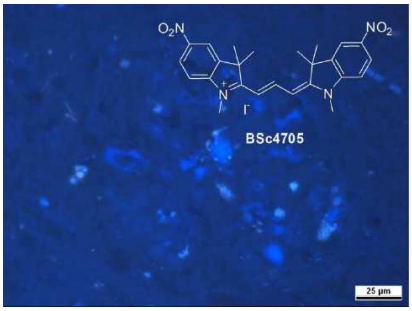

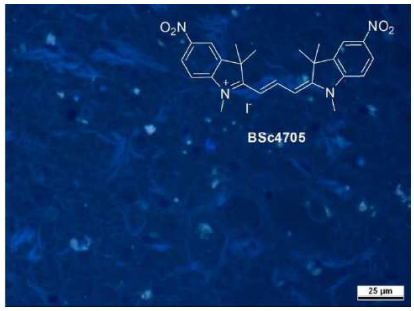

1-Decyl-2-((1*E*,3*E*)-3-(1-decyl-3,3-dimethylindolin-2-ylidene)prop-1-enyl)-3,3-dimethyl-3*H*-indolium bromide (135c)

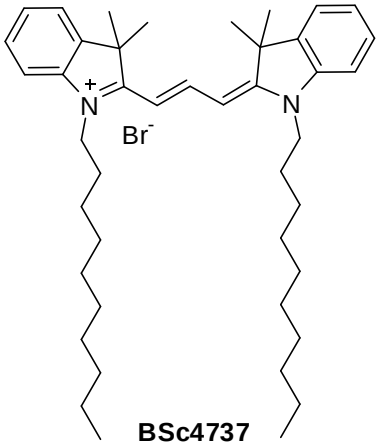

BSc4737

Yield: 68 %. **^{1}H-NMR (500 MHz, d_6-DMSO)**: δ = 8.35 (t, *J* = 13.5 Hz, 1H), 7.65 (d, *J* = 7.5 Hz, 2H), 7.47 (d, *J* = 7.5 Hz, 2H), 7.43 (td, *J* = 8.0 Hz, *J* = 1.0 Hz, 2H), 7.29 (td, *J* = 8.0 Hz, *J* = 1.0 Hz, 2H), 6.65 (d, *J* = 13.5 Hz, 2H), 4.15 (t, *J* = 7.5 Hz, 4H), 1.76-1.68 (m, 4H), 1.69 (s, 12H), 1.44-1.35 (m, 4H), 1.35-1.26 (m, 4H), 1.26-1.14 (m, 20H), 0.81 (t, *J* = 7.0 Hz, 6H) ppm. **^{13}C-NMR (125 MHz, d_6-DMSO)**: δ = 173.6, 149.7, 141.7, 140.5, 128.5, 125.1, 122.4, 111.5, 102.7, 48.7, 43.7, 31.1, 28.8, 28.7, 28.7, 28.5, 27.3, 26.9, 25.9, 21.9, 13.8 ppm. **UV/Vis (Ethanol)**: λ_{max} = 551.0 nm.

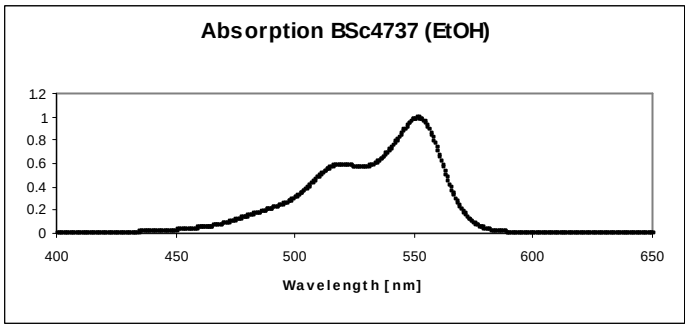

***In vitro* neuropathological staining of AD brain sections**: Tissues: hippocampus; Patient: male, 71 years old; CERAD Score: 3; NFTs-level: V.

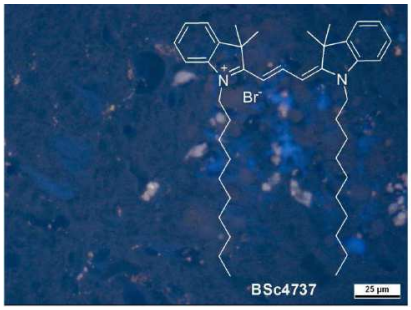

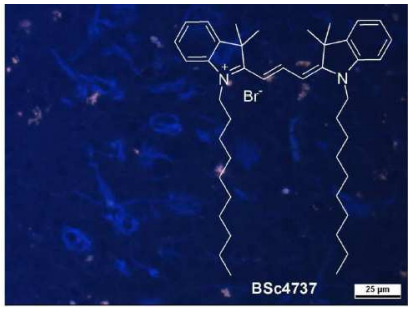

***In vitro* neuropathological staining of PD brain sections**: Tissues: midbrain; Patient: male, 76 years old.

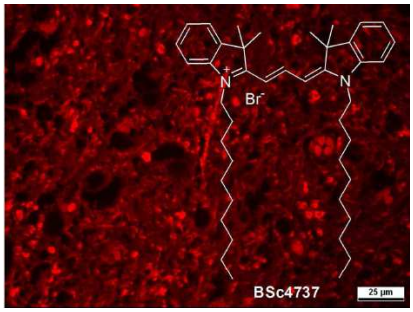

***In vitro* neuropathological staining of AD olfactory epithelium sections**: Tissues: olfactory epithelium; Patient: male, 78 years old; Braak: V, CERAD Score: 3.

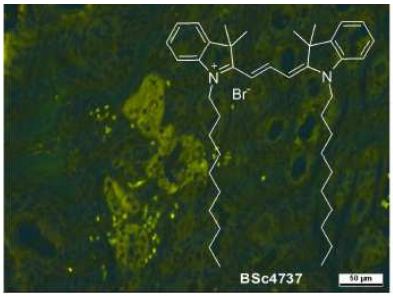

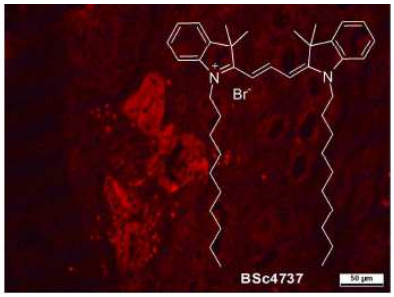

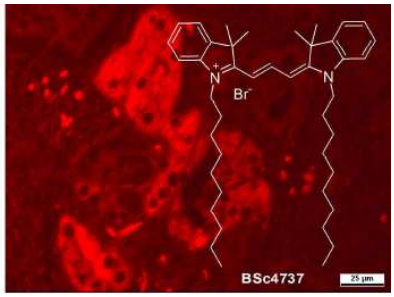

1-(2-(2-(2-Methoxyethoxy)ethoxy)ethyl)-2-((1*E*,3*E*)-3-(1-(2-(2-(2-methoxyethoxy)ethoxy)ethyl)-3,3-dimethylindolin-2-ylidene)prop-1-enyl)-3,3-dimethyl-3*H*-indolium chloride (135d)

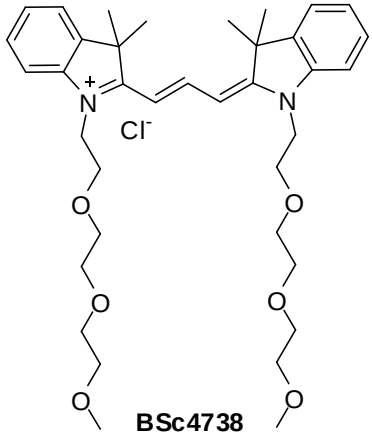

BSc4738

Yield: 38 %. **^{1}H-NMR (500 MHz, d_6-DMSO)**: δ = 8.38 (t, *J* = 13.0 Hz, 1H), 7.63 (d, *J* = 7.0 Hz, 2H), 7.46 (d, *J* = 8.0 Hz, 2H), 7.42 (td, *J* = 8.0 Hz, *J* = 1.0 Hz, 2H), 7.29 (td, *J* = 8.0 Hz, *J* = 1.0 Hz, 2H), 6.55 (d, *J* = 13.5 Hz, 2H), 4.34 (t, *J* = 5.0 Hz, 4H), 3.82 (t, *J* = 5.0 Hz, 4H), 3.55-3.50 (m, 4H), 3.44-3.40 (m, 4H), 3.39-3.36 (m, 4H), 3.31-3.27 (m, 4H), 3.16 (s, 6H), 1.70 (s, 12H) ppm. **^{13}C-NMR (125 MHz, d_6-DMSO)**: δ = 174.5, 149.7, 142.1, 140.3, 128.3, 125.0, 122.2, 111.9, 103.1, 71.1, 70.2, 69.7, 69.5, 67.1, 57.9, 48.8, 44.1, 27.4 ppm. **MS (EI)**: *m/z* = 622 $[M+1]^+$. **UV/Vis (Ethanol)**: λ_{max} = 551.5 nm.

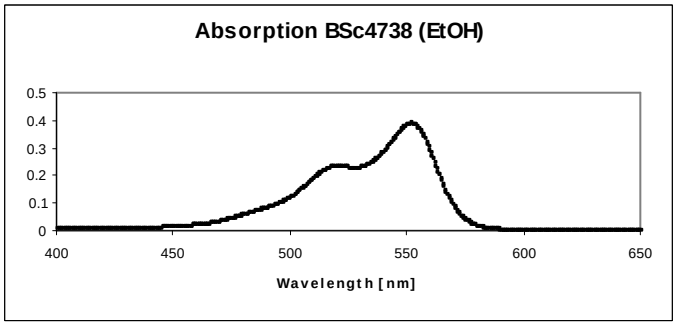

***In vitro* neuropathological staining of AD brain sections**: Tissues: hippocampus; Patient: male, 71 years old; CERAD Score: 3; NFTs-level: V.

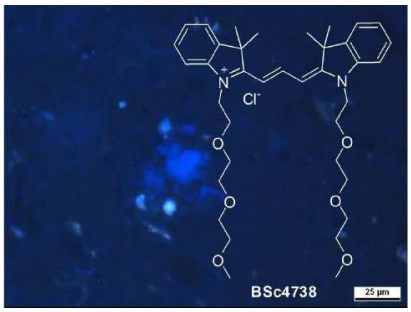

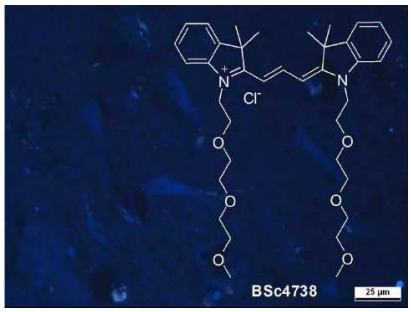

***In vitro* neuropathological staining of PD brain sections**: Tissues: midbrain; Patient: male, 76 years old.

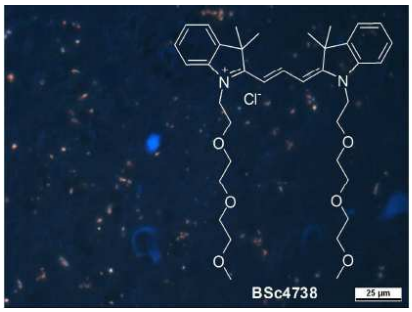

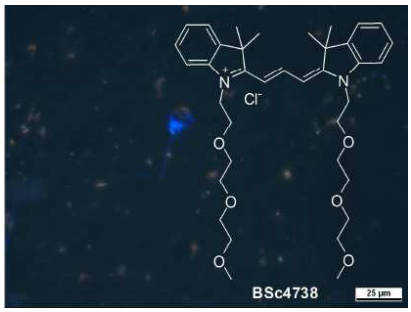

1-Butyl-2-((1*E*,3*E*)-3-(1-butyl-3,3-dimethylindolin-2-ylidene)prop-1-enyl)-3,3-dimethyl-3*H*-indolium iodide (135e)

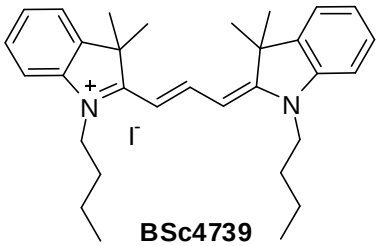

BSc4739

Yield: 61 %. **^{1}H-NMR (500 MHz, d_6-DMSO)**: δ = 8.36 (t, *J* = 13.5 Hz, 1H), 7.64 (d, *J* = 7.0 Hz, 2H), 7.49-7.41 (m, 4H), 7.30 (td, *J* = 7.5 Hz, *J* = 1.5 Hz, 2H), 6.58 (d, *J* = 13.5 Hz, 2H), 4.14 (t, *J* = 7.5 Hz, 4H), 1.77-1.71 (m, 4H), 1.70 (s, 12H), 1.48-1.40 (m, 4H), 0.94 (t, *J* = 7.5 Hz, 6H) ppm. **^{13}C-NMR (125 MHz, d_6-DMSO)**: δ = 173.7, 149.8, 141.8, 140.5, 128.5, 125.1, 122.4, 111.5, 102.5, 48.8, 43.6, 29.1, 17.4, 19.5, 13.7 ppm. **UV/Vis (Ethanol)**: λ_{max} = 550.5 nm.

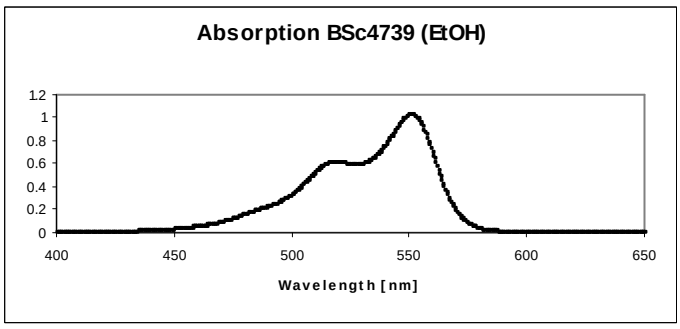

***In vitro* neuropathological staining of AD brain sections**: Tissues: hippocampus; Patient: male, 71 years old; CERAD Score: 3; NFTs-level: V.

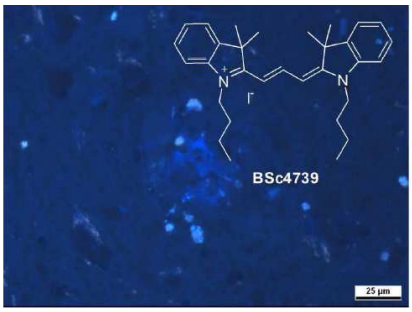

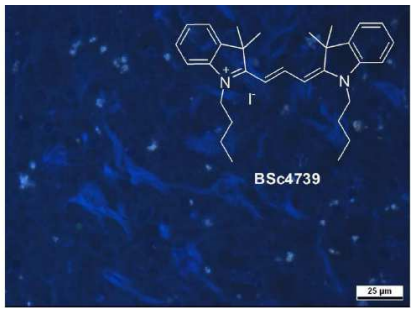

***In vitro* neuropathological staining of PD brain sections**: Tissues: midbrain; Patient: male, 76 years old.

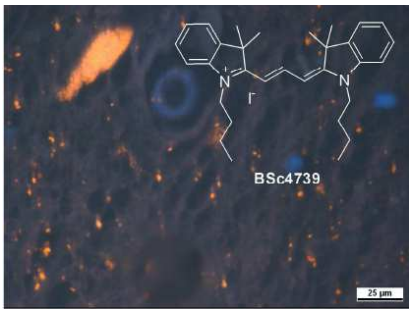

***In vitro* neuropathological staining of AD olfactory epithelium sections**: Tissues: olfactory epithelium; Patient: male, 78 years old; Braak: V, CERAD Score: 3.

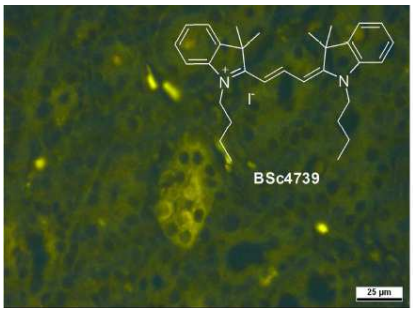

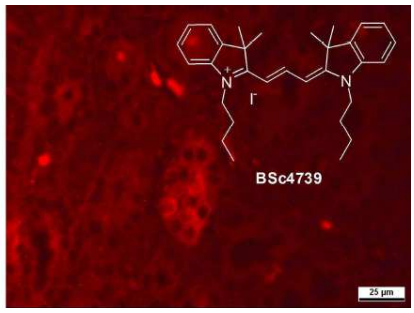

1-(2-Methoxyethyl)-2-((1*E*,3*E*)-3-(1-(2-methoxyethyl)-3,3-dimethylindolin-2-ylidene)prop-1-enyl)-3,3-dimethyl-3*H*-indolium chloride (135f)

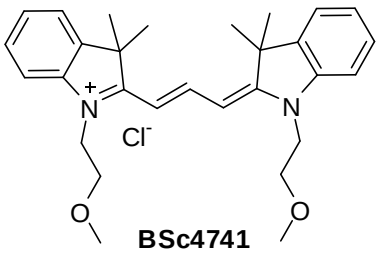

BSc4741

Yield: 29 %. **^{1}H-NMR (500 MHz, d_6-DMSO)**: δ = 8.39 (t, *J* = 13.0 Hz, 1H), 7.63 (d, *J* = 7.0 Hz, 2H), 7.48-7.40 (m, 4H), 7.29 (td, *J* = 8.0 Hz, *J* = 1.5 Hz, 2H), 6.53 (d, *J* = 13.5 Hz, 2H), 4.34 (t, *J* = 5.5 Hz, 4H), 3.26 (s, 6H), 1.70 (s, 12H) ppm. **^{13}C-NMR (125 MHz, d_6-DMSO)**: δ = 174.5, 149.9, 142.2, 140.3, 128.4, 125.0, 122.3, 111.8, 103.0, 68.8, 58.6, 48.8, 44.1, 27.4 ppm. **UV/Vis (Ethanol)**: λ_{max} = 550.0 nm.

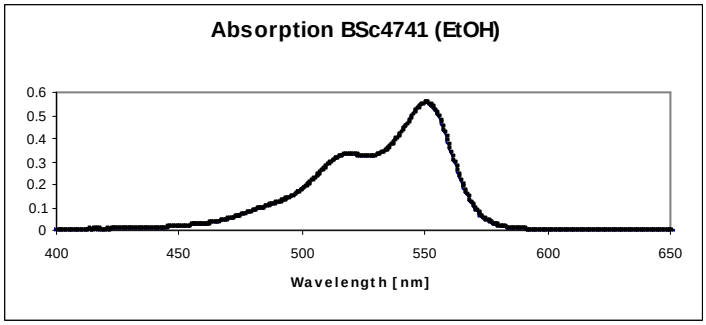

***In vitro* neuropathological staining of AD brain sections**: Tissues: hippocampus; Patient: male, 71 years old; CERAD Score: 3; NFTs-level: V.

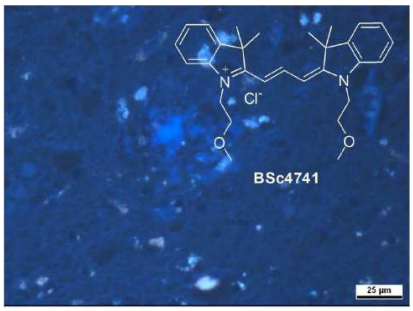

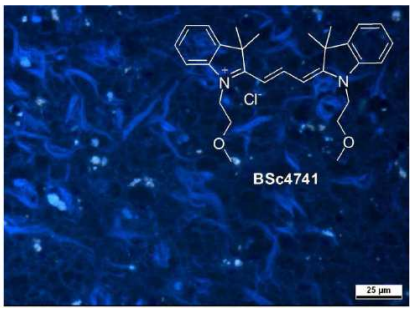

***In vitro* neuropathological staining of PD brain sections**: Tissues: midbrain; Patient: male, 76 years old.

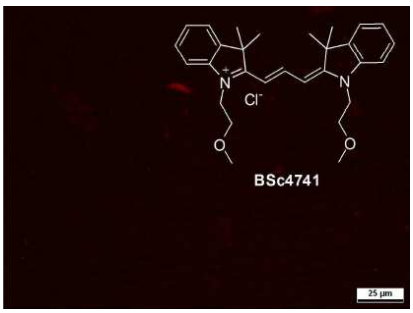

5-Bromo-2-((1*E*,3*E*)-3-(5-bromo-1,3,3-trimethylindolin-2-ylidene)prop-1-enyl)-1,3,3-trimethyl-3*H*-indolium iodide (135g)

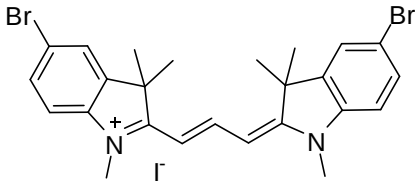

BSc4742

Yield: 58 %. **^{1}H-NMR (500 MHz, d_6-DMSO)**: δ = 8.30 (t, *J* = 13.5 Hz, 1H), 7.93 (d, *J* = 2.0 Hz, 2H), 7.64 (dd, *J* = 8.5 Hz, *J* = 2.0 Hz, 2H), 7.42 (d, *J* = 8.5 Hz, 2H), 6.45 (d, *J* = 13.5 Hz, 2H), 3.63 (s, 6H), 1.68 (s, 12H) ppm. **^{13}C-NMR (125 MHz, d_6-DMSO)**: δ = 174.1, 149.6, 142.7, 141.9, 131.2, 125.5, 117.4, 113.2, 103.1, 48.9, 31.5, 26.9, 26.2 ppm. **UV/Vis (Ethanol)**: λ_{max} = 556.0 nm.

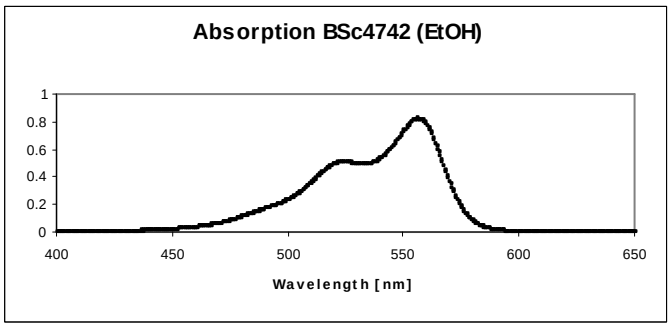

***In vitro* neuropathological staining of AD brain sections**: Tissues: hippocampus; Patient: male, 71 years old; CERAD Score: 3; NFTs-level: V.

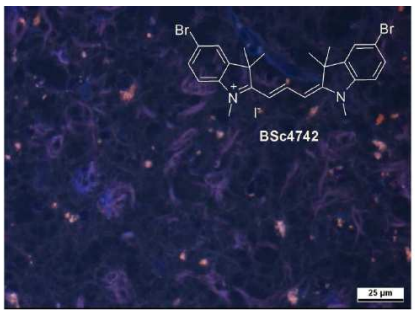

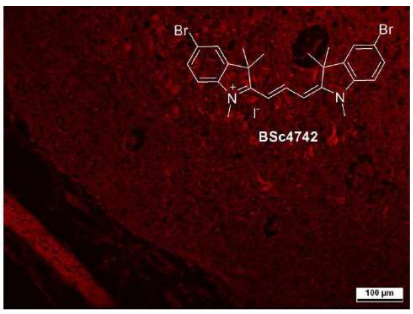

***In vitro* neuropathological staining of PD brain sections**: Tissues: midbrain; Patient: male, 76 years old.

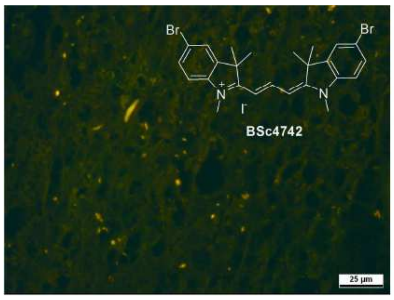

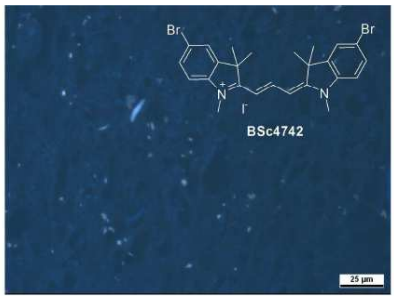

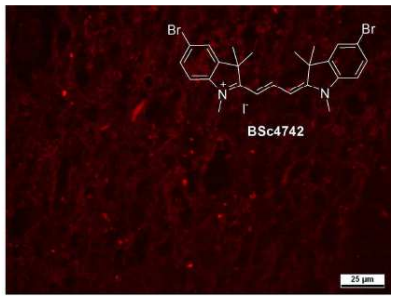

***In vitro* neuropathological staining of AD olfactory epithelium sections**: Tissues: olfactory epithelium; Patient: male, 78 years old; Braak: V, CERAD Score: 3.

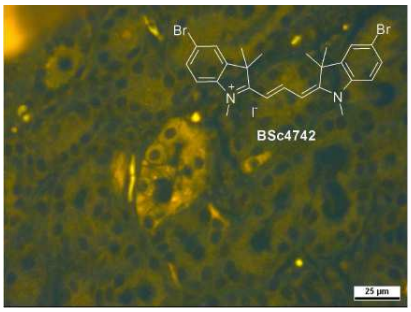

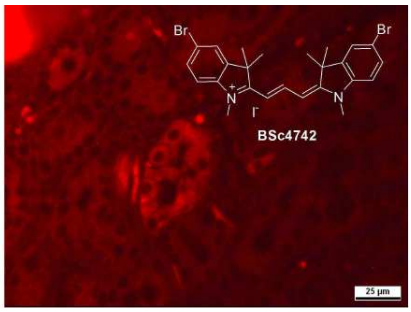

5-Fluoro-2-((1*E*,3*E*)-3-(5-fluoro-1,3,3-trimethylindolin-2-ylidene)prop-1-enyl)-1,3,3-trimethyl-3*H*-indolium iodide (135h)

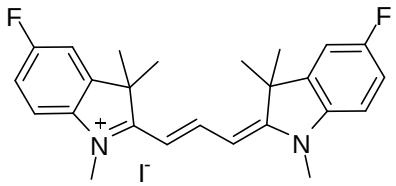

BSc4806

Yield: 43 %. **^{1}H-NMR (500 MHz, d_6-DMSO)**: δ = 8.28 (t, *J* = 13.5 Hz, 1H), 7.64 (dd, *J* = 8.0 Hz, *J* = 2.5 Hz, 2H), 7.48 (dd, *J* = 9.0 Hz, *J* = 4.0 Hz, 2H), 7.30 (td, *J* = 9.0 Hz, *J* = 2.5 Hz, 2H), 6.40 (d, *J* = 13.5 Hz, 2H), 3.63 (s, 6H), 1.69 (s, 12H) ppm. **^{13}C-NMR (125 MHz, d_6-DMSO)**: δ = 174.3, 160.2 (d, *J* = 240.4 Hz), 149.1, 142.5 (d, *J* = 8.6 Hz), 138.9, 115.0 (d, *J* = 24.3 Hz), 112.5 (d, *J* = 8.8 Hz), 110.5 (d, *J* = 25.5 Hz), 102.6, 49.0, 31.5, 27.0 ppm. **UV/Vis (Ethanol)**: λ_{max} = 547.0 nm.

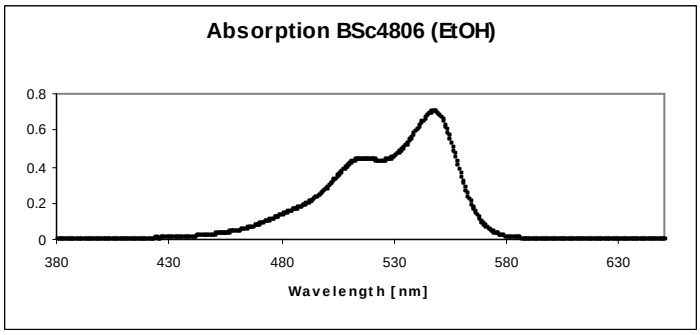

***In vitro* neuropathological staining of AD brain sections**: Tissues: hippocampus; Patient: male, 71 years old; CERAD Score: 3; NFTs-level: V.

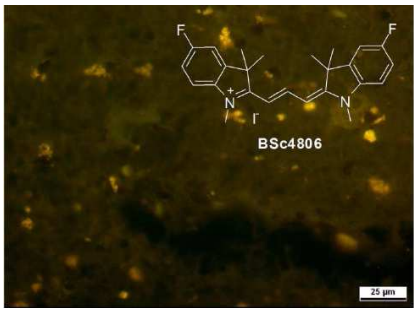

***In vitro* neuropathological staining of PD brain sections**: Tissues: midbrain; Patient: male, 76 years old.

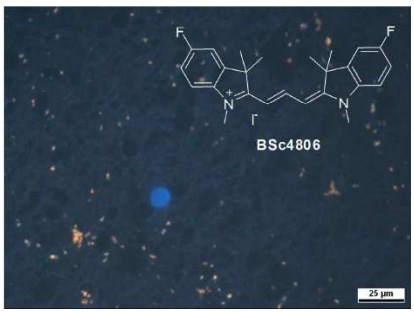

5-Methoxy-2-((1*E*,3*E*)-3-(5-methoxy-1,3,3-trimethylindolin-2-ylidene)prop-1-enyl)-1,3,3-trimethyl-3*H*-indolium iodide (135i)

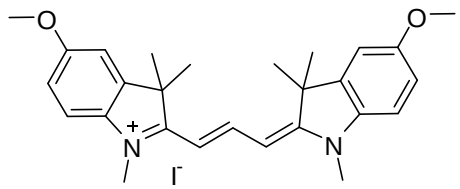

BSc4810

Yield: 51 %. **^{1}H-NMR (500 MHz, d_6-DMSO)**: δ = 8.23 (t, *J* = 13.5 Hz, 1H), 7.35 (d, *J* = 8.5 Hz, 2H), 7.29 (d, *J* = 2.5 Hz, 2H), 6.99 (dd, *J* = 8.5 Hz, *J* = 2.5 Hz, 2H), 6.32 (d, *J* = 13.5 Hz, 2H), 3.82 (s, 6H), 3.60 (s, 6H), 1.67 (s, 12H) ppm. **^{13}C-NMR (125 MHz, d_6-DMSO)**: δ = 172.9, 157.7, 147.6, 142.0, 136.1, 113.3, 111.9, 109.1, 101.8, 55.8, 48.8, 31.3, 27.2 ppm. **UV/Vis (Ethanol)**: λ_{max} = 574.0 nm.

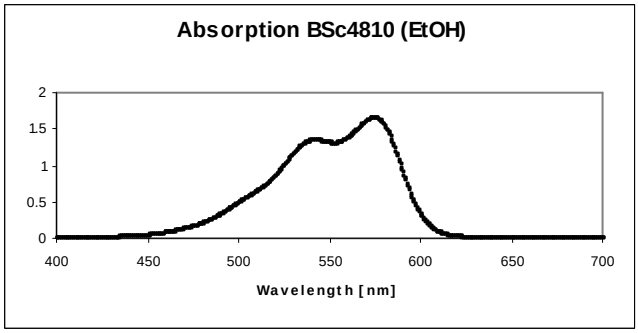

***In vitro* neuropathological staining of AD brain sections**: Tissues: hippocampus; Patient: male, 71 years old; CERAD Score: 3; NFTs-level: V.

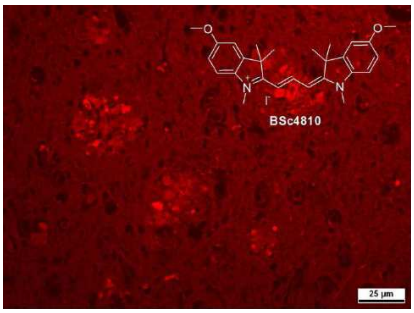

***In vitro* neuropathological staining of PD brain sections**: Tissues: midbrain; Patient: male, 76 years old.

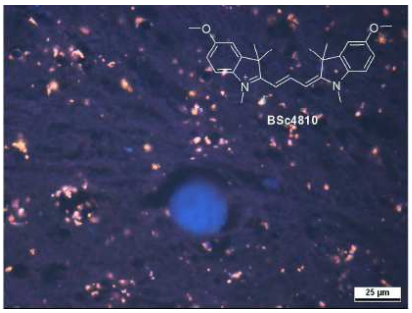

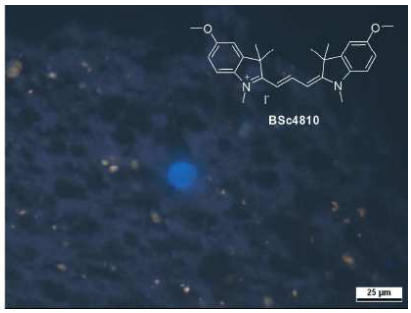

3-Ethyl-2-((1*E*,3*E*)-3-(3-ethyl-1,3-dimethylindolin-2-ylidene)prop-1-enyl)-1,3-dimethyl-3*H*-indolium iodide (135j)

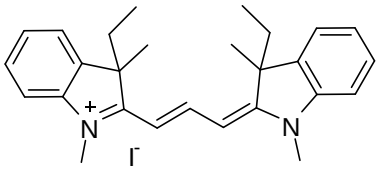

BSc4811

Yield: 67 %. **^{1}H-NMR (500 MHz, d_6-DMSO)**: δ = 8.29 (t, *J* = 13.5 Hz, 1H), 7.57 (d, *J* = 7.5 Hz, 2H), 7.48-7.42 (m, 4H), 7.33-7.28 (m, 2H), 6.48 (d, *J* = 13.5 Hz, 2H), 3.65 (s, 6H), 2.37-2.04 (m, 4H), 1.66 (s, 3H), 1.65 (s, 3H), 0.42-0.36 (m, 6H) ppm. **^{13}C-NMR (125 MHz, d_6-DMSO)**: δ = 172.9, 148.5, 143.5, 138.3, 128.7, 125.2, 122.4, 111.2, 103.0, 54.0, 34.1, 31.3, 26.9, 26.8, 8.6, 8.5 ppm. **UV/Vis (Ethanol)**: λ_{max} = 548.5 nm.

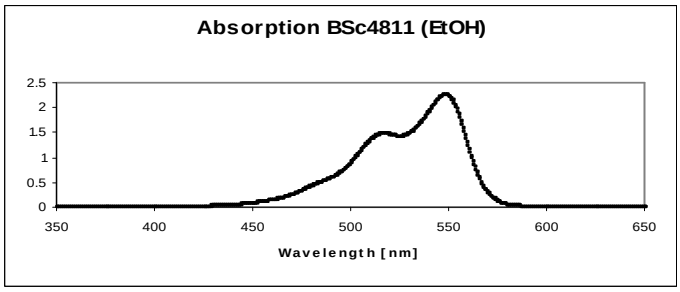

***In vitro* neuropathological staining of AD brain sections**: Tissues: hippocampus; Patient: male, 71 years old; CERAD Score: 3; NFTs-level: V.

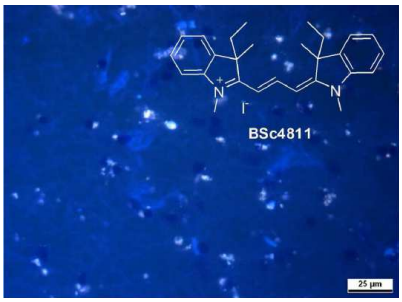

***In vitro* neuropathological staining of PD brain sections**: Tissues: midbrain; Patient: male, 76 years old.

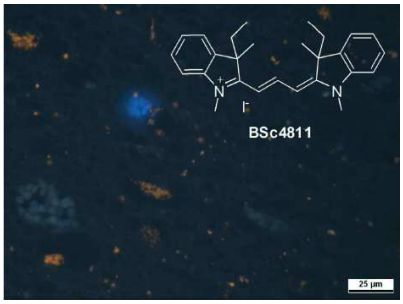

1-(2-(2-Methoxyethoxy)ethyl)-2-((1*E*,3*E*)-3-(1-(2-(2-methoxyethoxy)ethyl)-3,3-dimethylindolin-2-ylidene)prop-1-enyl)-3,3-dimethyl-3*H*-indolium 4-methylbenzene sulfonate (135k)

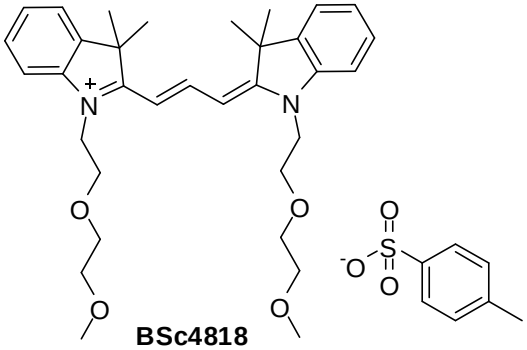

BSc4818

Yield: 34 %. **^{1}H-NMR (500 MHz, d_6-DMSO)**: δ = 8.38 (t, *J* = 13.5 Hz, 1H), 7.63 (d, *J* = 7.5 Hz, 2H), 7.51-7.39 (m, 6H), 7.29 (t, *J* = 7.5 Hz, 2H), 7.11 (d, *J* = 8.0 Hz, 2H), 6.54 (d, *J* = 13.0 Hz, 2H), 4.34 (t, *J* = 5.5 Hz, 4H), 3.81 (t, *J* = 5.5 Hz, 4H), 3.55-3.50 (m, 4H), 3.36-3.32 (m, 4H), 3.11 (s, 6H), 2.28 (s, 3H), 1.70 (s, 12H) ppm. **^{13}C-NMR (125 MHz, d_6-DMSO)**: δ = 174.5, 149.7, 145.7, 142.1, 140.3, 137.4, 128.3, 127.9, 125.4, 125.0, 122.2, 111.9, 103.1, 71.1, 70.0, 67.1, 58.0, 48.8, 44.1, 27.4, 20.7 ppm. **UV/Vis (Ethanol)**: λ_{max} = 550.5 nm.

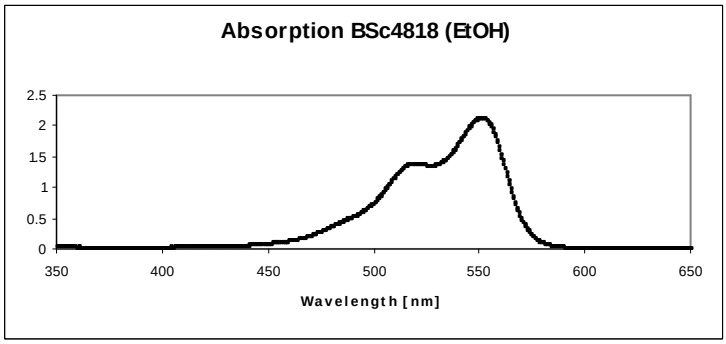

1-(3-Methoxypropyl)-2-((1*E*,3*E*)-3-(1-(3-methoxypropyl)-3,3-dimethylindolin-2-ylidene)prop-1-enyl)-3,3-dimethyl-3*H*-indolium chloride (135l)

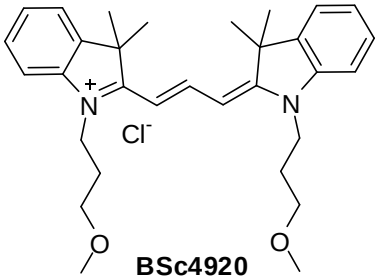

BSc4920

Yield: 35 %. **^{1}H-NMR (300 MHz, d_6-DMSO)**: δ = 8.38 (t, *J* = 13.5 Hz, 1H), 7.64 (d, *J* = 7.2 Hz, 2H), 7.50-7.40 (m, 4H), 7.35-7.24 (m, 2H), 6.48 (d, *J* = 13.5 Hz, 2H), 4.20 (t, *J* = 6.9 Hz, 4H), 3.39 (t, *J* = 5.7 Hz, 4H), 3.21 (s, 6H), 3.12-3.00 (m, 4H), 1.70 (s, 12H) ppm. **^{13}C-NMR (75 MHz, d_6-DMSO)**: δ = 174.0, 153.8, 149.7, 147.0, 141.5, 128.5, 125.1, 122.4, 111.3, 102.4, 68.5, 57.8, 48.9, 27.3, 26.9 ppm. **UV/Vis (Ethanol)**: λ_{max} = 550.0 nm.

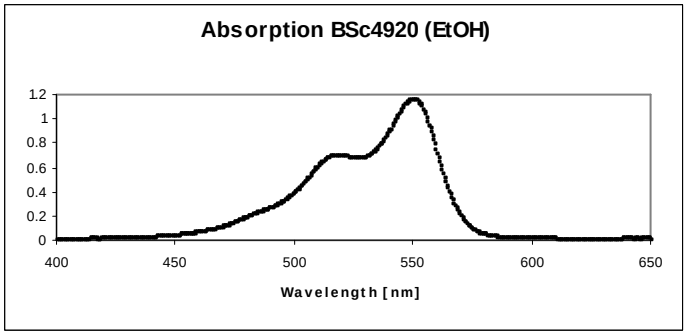

***In vitro* neuropathological staining of AD brain sections**: Tissues: hippocampus; Patient: male, 71 years old; CERAD Score: 3; NFTs-level: V.

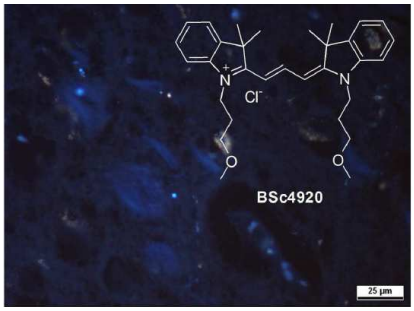

***In vitro* neuropathological staining of PD brain sections**: Tissues: midbrain; Patient: male, 76 years old.

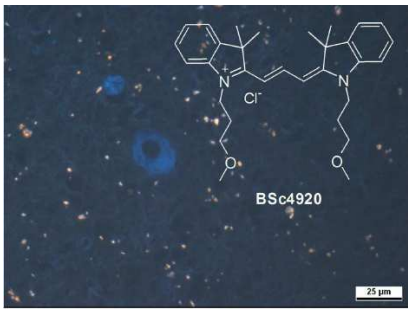

3-Methyl-2-((1*E*,3*E*)-3-(3-methylbenzo[*d*]thiazol-2(3*H*)-ylidene)prop-1-enyl)benzo[*d*]thiazol-3-ium iodide (138a)

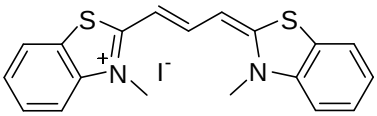

BSc4706

Yield: 72 %. **^{1}H-NMR (500 MHz, d_6-DMSO)**: δ = 7.96 (d, *J* = 8.0 Hz, 2H), 7.74-7.66 (m, 3H), 7.53 (t, *J* = 8.0 Hz, 2H), 7.37 (t, *J* = 8.0 Hz, 2H), 6.52 (d, *J* = 13.0 Hz, 2H), 3.80 (s, 6H) ppm. **^{13}C-NMR (125 MHz, d_6-DMSO)**: δ = 164.8, 145.9, 141.7, 127.9, 125.0, 124.71, 122.8, 113.4, 98.8, 33.4 ppm. **UV/Vis (Ethanol)**: λ_{max} = 558.0 nm.

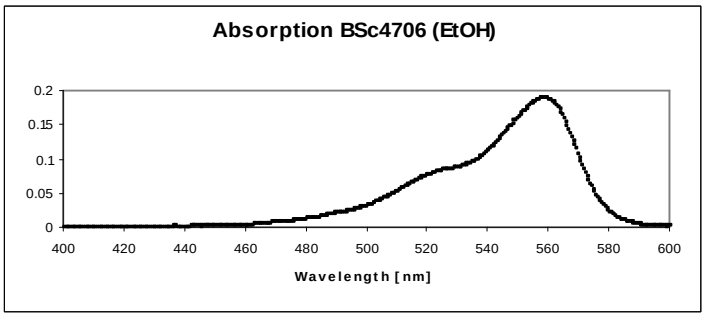

***In vitro* neuropathological staining of AD brain sections**: Tissues: hippocampus; Patient: male, 71 years old; CERAD Score: 3; NFTs-level: V.

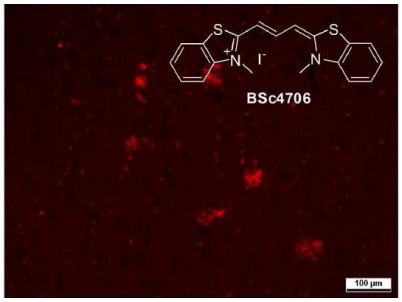

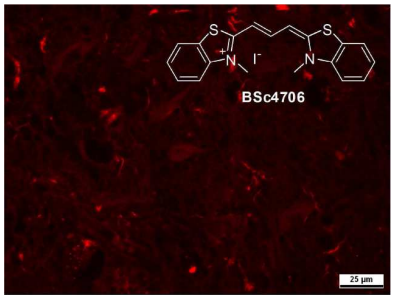

3-(2-Methoxyethyl)-2-((1*E*,3*E*)-3-(3-(2-methoxyethyl)benzo[*d*]thiazol-2(3*H*)-ylidene)prop-1-enyl)benzo[*d*]thiazol-3-ium 4-methylbenzenesulfonate (138b)

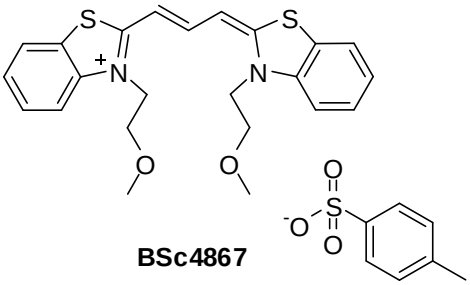

BSc4867

Yield: 37 %. **^{1}H-NMR (500 MHz, d_6-DMSO)**: δ = 7.85 (d, *J* = 8.0 Hz, 2H), 7.61 (t, *J* = 12.5 Hz, 1H), 7.53 (d, *J* = 8.0 Hz, 2H), 7.37 (d, *J* = 8.5 Hz, 2H), 7.32 (t, *J* = 7.5 Hz, 2H), 7.17 (t, *J* = 7.5 Hz, 2H), 7.15-7.08 (m, 4H), 4.48-4.40 (m, 4H), 3.83-3.76 (m, 4H), 3.20 (s, 6H), 2.30 (s, 3H) ppm. **^{13}C-NMR (125 MHz, d_6-DMSO)**: δ = 164.4, 146.9, 144.3, 142.2, 138.8, 128.4, 127.5, 126.0, 124.9, 124.7, 121.9, 113.8, 101.1, 70.2, 59.0, 47.4, 21.2 ppm. **UV/Vis (Ethanol)**: λ_{max} = 547.0 nm.

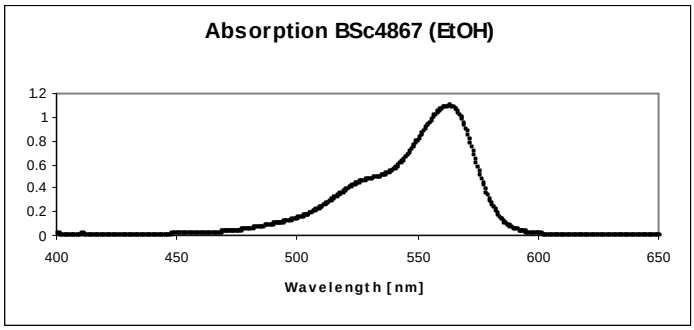

3-(2-(2-(2-Methoxyethoxy)ethoxy)ethyl)-2-((1*E*,3*E*)-3-(3-(2-(2-(2-methoxyethoxy)ethoxy) ethyl)benzo[*d*]thiazol-2(3*H*)-ylidene)prop-1-enyl)benzo[*d*]thiazol-3-ium 4-methyl benzenesulfonate (138c)

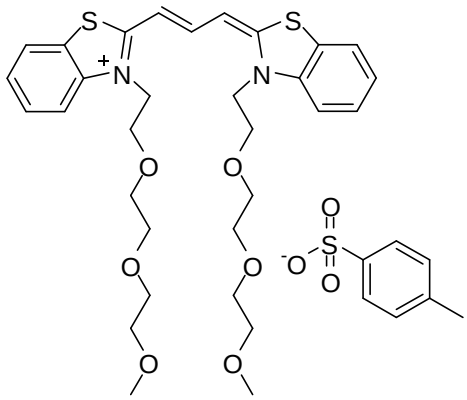

BSc4868

Yield: 34 %. **^{1}H-NMR (500 MHz, d_6-DMSO)**: δ = 7.82 (d, *J* = 8.0 Hz, 2H), 7.63 (t, *J* = 13.0 Hz, 1H), 7.54 (d, *J* = 8.0 Hz, 2H), 7.43 (d, *J* = 8.0 Hz, 2H), 7.32 (t, *J* = 7.5 Hz, 2H), 7.19 (t, *J* = 7.5 Hz, 2H), 7.16-7.09 (m, 4H), 4.50-4.40 (m, 4H), 3.90-3.85 (m, 4H), 3.52-3.34 (m, 16H), 3.28 (s, 6H), 2.29 (s, 3H) ppm. **^{13}C-NMR (125 MHz, d_6-DMSO)**: δ = 164.5, 147.0, 144.1, 142.3, 138.8, 128.4, 127.4, 126.0, 124.8, 124.7, 141.8, 114.1, 101.2, 71.7, 70.6, 70.2, 70.2, 68.6, 58.8, 47.4, 21.2 ppm. **UV/Vis (Ethanol)**: λ_{max} = 563.5 nm.

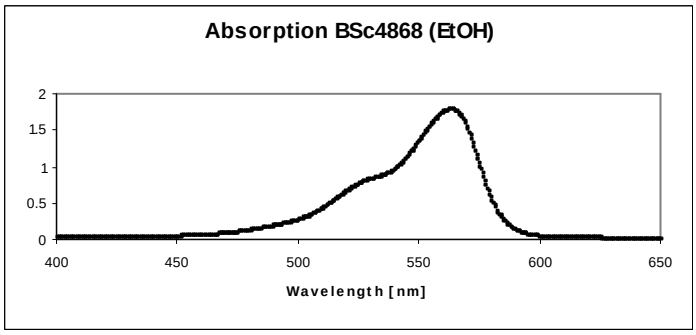

***In vitro* neuropathological staining of AD brain sections**: Tissues: hippocampus; Patient: male, 71 years old; CERAD Score: 3; NFTs-level: V.

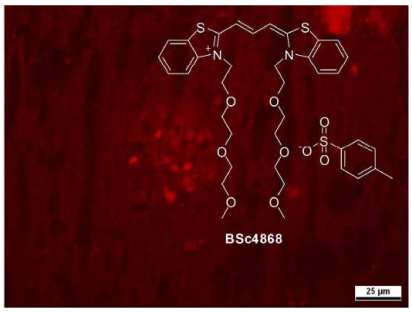

***In vitro* neuropathological staining of PD brain sections**: Tissues: midbrain; Patient: male, 76 years old.

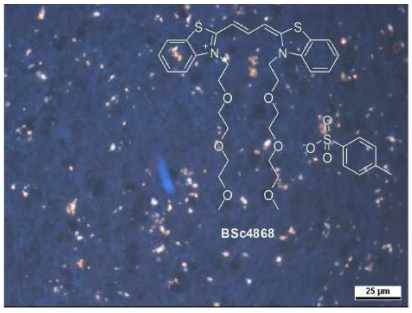

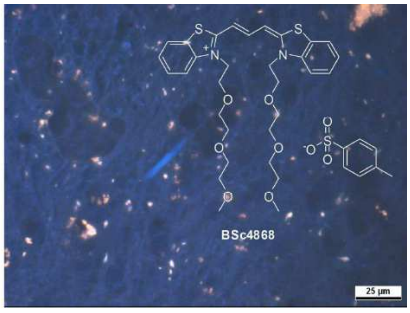

3-Methyl-2-((1*E*,3*E*)-3-(3-methylbenzo[*d*]oxazol-2(3*H*)-ylidene)prop-1-enyl)benzo[*d*]oxazol-3-ium iodide (138d)

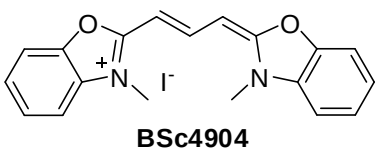

BSc4904

Yield: 70 %. **^{1}H-NMR (500 MHz, d_6-DMSO)**: δ = 8.28 (t, *J* = 13.5 Hz, 1H), 7.75 (d, *J* = 8.0 Hz, 2H), 7.70 (d, *J* = 7.5 Hz, 2H), 7.46 (td, *J* = 7.5 Hz, *J* = 1.0 Hz, 2H), 7.39 (td, *J* = 7.5 Hz, *J* = 1.0 Hz, 2H), 6.01 (d, *J* = 13.5 Hz, 2H), 3.73 (s, 6H) ppm. **^{13}C-NMR (125 MHz, d_6-DMSO)**: δ

= 162.0, 146.2, 145.7, 131.8, 125.7, 124.8, 111.1, 110.6, 84.8, 30.2 ppm. **UV/Vis (Ethanol)**: λ_{max} = 484.0 nm.

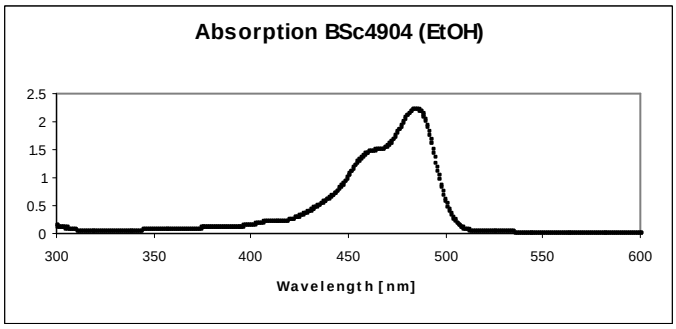

***In vitro* neuropathological staining of PD brain sections**: Tissues: midbrain; Patient: male, 76 years old.

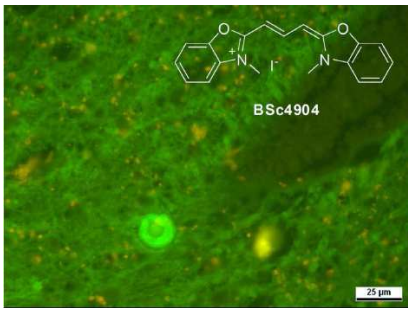

3-Butyl-2-((1*E*,3*E*)-3-(3-butylbenzo[*d*]oxazol-2(3*H*)-ylidene)prop-1-enyl)benzo[*d*]oxazol-3-ium iodide (138e)

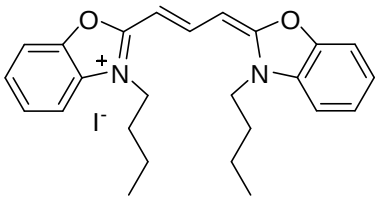

BSc4907

Yield: 68 %. **^{1}H-NMR (500 MHz, d_6-DMSO)**: δ = 8.32 (t, *J* = 13.5 Hz, 1H), 7.76 (d, *J* = 7.5 Hz, 2H), 7.70 (d, *J* = 7.5 Hz, 2H), 7.47 (td, *J* = 8.0 Hz, *J* = 1.0 Hz, 2H), 7.41 (td, *J* = 8.0 Hz, *J* = 1.0 Hz, 2H), 6.11 (d, *J* = 13.5 Hz, 2H), 4.21 (t, *J* = 7.5 Hz, 4H), 1.81-1.72 (m, 4H), 1.45-1.36 (m, 4H), 0.94 (t, *J* = 7.0 Hz, 6H) ppm. **^{13}C-NMR (125 MHz, d_6-DMSO)**: δ = 161.6, 146.3, 131.2, 125.8, 124.9, 111.3, 110.8, 85.0, 43.6, 29.4, 19.3, 13.5 ppm. **UV/Vis (Ethanol)**: λ_{max} = 486.5 nm.

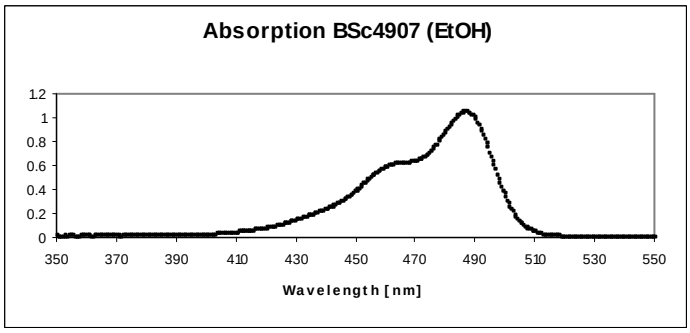

6.9. Synthesis of *N*-2-aryl-1,2,3-triazole derivatives

6.9.1. General procedures for azo coupling

To a mixture of 4-substituted-2-nitroanilinein (2.0 mmol, 1.0 eq), water (5 mL) and concentrated hydrochloric acid (HCl, 12 mol/L, 0.5 mL) at 0 ^{o}C, a solution of sodium nitrite (152 mg, 2.2 mmol, 1.1 eq) in water (5 mL) was added dropwise while the temperature was maintained below 5 ^{o}C. After stirring for 20 min, a solution of benzenediazonium chloride was prepared. Subsequently, the solution was added gradually to a mixture of aromatic compounds (2.2 mmol, 1.1 eq), sodium hydroxide (80 mg, 2 mmol, 1.0 eq), ethanol (5 mL) and water (20 mL) at 0-5 ^{o}C. After the addition of the above diazonium solution, the mixture was further stirred for 6 h until a lot of precipitates were produced. The reaction residue was extracted with EtOAc and washed with water. The crude product was purified by column chromatography (SiO_2; ethyl acetate: cyclohexane = 1:10) to furnish the corresponding compound.

(*E*)-4-((4-(Dimethylamino)phenyl)diazenyl)-3-nitrobenzonitrile (141a)

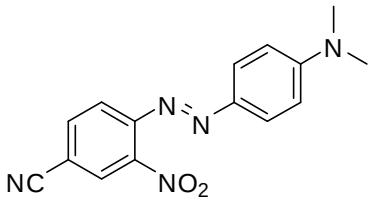

Yield: 21 %. **^{1}H-NMR (300 MHz, d_6-DMSO)**: δ = 8.60 (d, *J* = 1.8 Hz, 1H), 8.16 (dd, *J* = 8.4 Hz, *J* = 1.8 Hz, 1H), 7.85 (d, *J* = 8.4 Hz, 1H), 7.77 (d, *J* = 9.3 Hz, 2H), 6.88 (d, *J* = 9.3 Hz, 2H), 3.13 (s, 6H) ppm. **^{13}C-NMR (75 MHz, d_6-DMSO)**: δ = 154.3, 146.8, 146.5, 143.0, 136.6, 128.1, 126.7, 119.4, 117.2, 111.9, 110.6, 39.9 ppm.

(*E*)-*N*,*N*-Dimethyl-4-((2-nitrophenyl)diazenyl)aniline (141b)

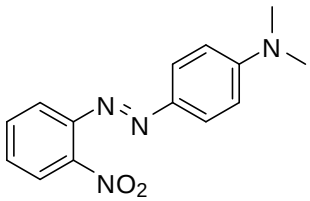

Yield: 32 %. **^{1}H-NMR (500 MHz, d_6-DMSO)**: δ = 7.98 (dd, *J* = 8.0 Hz, *J* = 1.0 Hz, 1H), 7.77-7.69 (m, 4H), 7.62-7.57 (m, 1H), 6.84 (d, *J* = 9.0 Hz, 2H), 3.08 (s, 6H) ppm. **^{13}C-NMR (125 MHz, d_6-DMSO)**: δ = 153.3, 146.8, 144.4, 142.5, 132.9, 129.3, 125.6, 123.6, 118.2, 111.5, 39.7 ppm.

(*E*)-*N*,*N*-Diethyl-4-((2-nitrophenyl)diazenyl)aniline (141c)

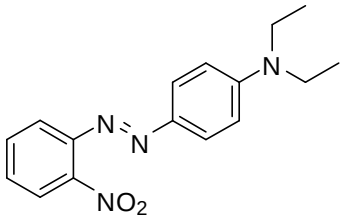

Yield: 28 %. **^{1}H-NMR (500 MHz, d_6-DMSO)**: δ = 7.96 (dd, *J* = 8.5 Hz, *J* = 1.0 Hz, 1H), 7.75-7.67 (m, 4H), 7.59-7.54 (m, 1H), 6.78 (d, *J* = 9.0 Hz, 2H), 3.47-3.37 (m, 4H), 1.12 (t, *J* = 7.0 Hz, 6H) ppm. **^{13}C-NMR (125 MHz, d_6-DMSO)**: δ = 151.0. 146.8. 144.5. 142.2. 132.8. 129.1. 126.0. 123.6. 118.2. 111.0. 44.1. 12.3 ppm.

(*E*)-*N*,*N*-Dimethyl-4-((4-methyl-2-nitrophenyl)diazenyl)aniline (141d)

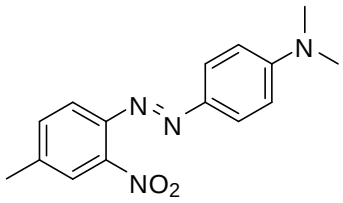

Yield: 41%. **^{1}H-NMR (500 MHz, d_6-DMSO)**: δ = 7.81 (d, *J* = 0.5 Hz, 1H), 7.72 (d, *J* = 9.5 Hz, 2H), 7.64 (d, *J* = 8.5 Hz, 1H), 7.58-7.54 (m, 1H), 6.84 (d, *J* = 9.0 Hz, 2H), 3.08 (s, 6H), 2.44 (s, 3H) ppm. **^{13}C-NMR (125 MHz, d_6-DMSO)**: δ = 153.1, 147.0, 142.5, 142.1, 140.1, 133.4, 125.3, 123.5, 117.8, 111.5, 39.7, 20.4 ppm.

(*E*)-*N*,*N*-Diethyl-4-((4-methyl-2-nitrophenyl)diazenyl)aniline (141e)

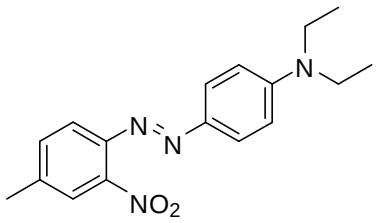

Yield: 34 %. **^{1}H-NMR (500 MHz, d_6-DMSO)**: δ = 7.78 (d, *J* = 1.0 Hz, 1H), 7.70 (d, *J* = 9.0 Hz, 2H), 7.62 (d, *J* = 8.5 Hz, 1H), 7.55-7.51 (m, 1H), 6.80 (d, *J* = 9.5 Hz, 2H), 3.49-3.42 (m, 4H), 3.42 (s, 3H), 1.14 (t, *J* = 7.5 Hz, 6H) ppm. **^{13}C-NMR (125 MHz, d_6-DMSO)**: δ = 150.8, 146.9, 142.2, 142.1, 139.8, 133.3, 125.7, 123.5, 117.8, 111.0, 44.1, 20.4, 12.3 ppm.

(*E*)-4-((4-Methoxy-2-nitrophenyl)diazenyl)-*N*,*N*-dimethylaniline (141f)

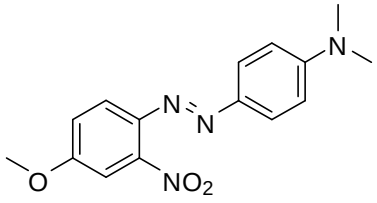

Yield: 31 %. **^{1}H-NMR (300 MHz, d_6-DMSO)**: δ = 7.75 (d, *J* = 9.0 Hz, 1H), 7.69 (d, *J* = 9.3, 2H), 7.57 (d, *J* = 2.7 Hz, 1H), 7.30 (dd, *J* = 9.0 Hz, *J* = 2.7 Hz, 1H), 6.83 (d, *J* = 9.3 Hz, 2H), 3.90 (s, 3H), 3.07 (s, 6H) ppm. **^{13}C-NMR (75 MHz, d_6-DMSO)**: δ = 159.8, 152.8, 148.6, 142.4, 137.5, 125.0, 119.0, 118.8, 111.5, 107.9, 56.3, 39.7 ppm.

(*E*)-*N*,*N*-Diethyl-4-((4-methoxy-2-nitrophenyl)diazenyl)aniline (141g)

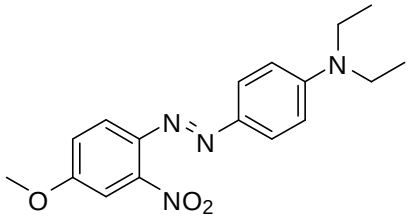

Yield: 37 %. **^{1}H-NMR (300 MHz, d_6-DMSO)**: δ = 7.74 (d, *J* = 9.0 Hz, 1H), 7.67 (d, *J* = 9.3, 2H), 7.56 (d, *J* = 2.7 Hz, 1H), 7.29 (dd, *J* = 9.0 Hz, *J* = 2.7 Hz, 1H), 6.80 (d, *J* = 9.3 Hz, 2H), 3.90 (s, 3H), 3.51-.341 (m, 4H), 1.15 (t, , *J* = 7.2 Hz, 6H) ppm. **^{13}C-NMR (75 MHz, d_6-DMSO)**: δ = 159.6, 150.5, 148.4, 142.0, 137.6, 125.4, 119.0, 118.8, 111.0, 107.8, 56.2, 44.0, 12.4 ppm.

6.9.2. General procedures for synthesis of *N*-2-aryl-1,2,3-triazole

2-Nitroazobenzene derivatives (1.0 mmol, 1.0 eq) and of sodium azide (325 mg, 5.0 mmol, 5.0 eq) were stirred for 2 days at 125° C in 2 mL DMSO. When the conversion had taken place, the mixture was cooled down and water was added to the mixture. The reaction residue was extracted with EtOAc and washed with water. The crude product was purified by column chromatography (SiO_2; ethyl acetate: cyclohexane = 1:10) to furnish the corresponding final compound in poor yields.

2-(4-(Dimethylamino)phenyl)-2*H*-benzo[*d*][1,2,3]triazole-5-carbonitrile (142a)

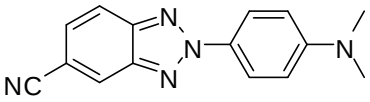

BSc 4954

Yield: 21 %. **^{1}H-NMR (500 MHz, $CDCl_3$)**: δ = 8.33 (m, 1H), 8.27 (d, *J* = 9.0 Hz, 2H), 8.00 (dd, *J* = 9.0 Hz, *J* = 1.0 Hz, 1H), 7.54 (dd, *J* = 8.0 Hz, *J* = 1.5 Hz, 1H), 6.99 (d, *J* = 9.0 Hz, 2H), 3.11 (s, 6H) ppm. **UV/Vis (Ethanol)**: λ_{max} = 390.5 nm.

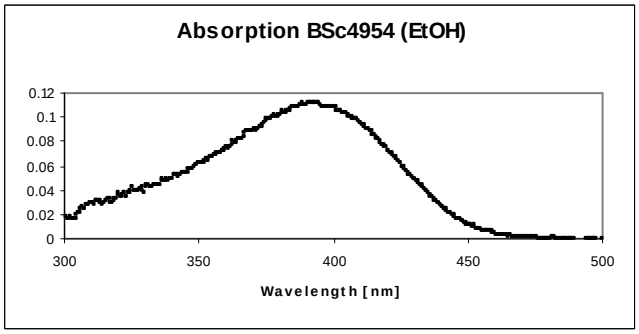

***In vitro* neuropathological staining of AD brain sections**: Tissues: hippocampus; Patient: male, 72 years old; CERAD Score: 3; NFTs-level: V.

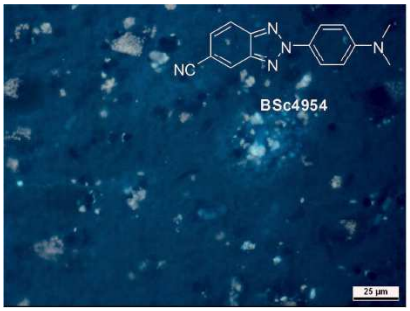

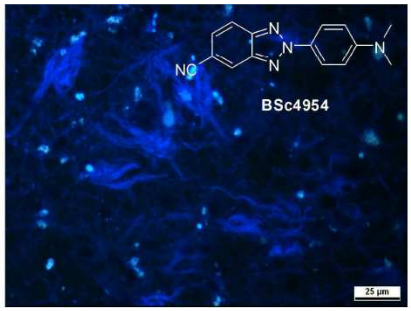

4-(2*H*-benzo[*d*][1,2,3]triazol-2-yl)-*N*,*N*-dimethylaniline (142b)

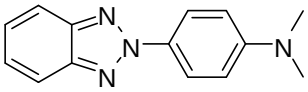

BSc 4955

Yield: 29 %. **^{1}H-NMR (500 MHz, d_6-DMSO)**: δ = 8.12 (d, *J* = 9.5 Hz, 2H), 7.97 (dd, *J* = 6.5 Hz, *J* = 3.0 Hz, 2H), 7.46 (dd, *J* = 6.5 Hz, *J* = 3.0 Hz, 2H), 6.90 (d, *J* = 9.5 Hz, 2H), 3.02 (s, 6H) ppm. **^{13}C-NMR (125 MHz, d_6-DMSO)**: δ = 150.7. 144.0. 129.0. 126.6. 121.1. 117.6. 112.0. 39.9 ppm. **UV/Vis (Ethanol)**: λ_{max} = 361.0 nm.

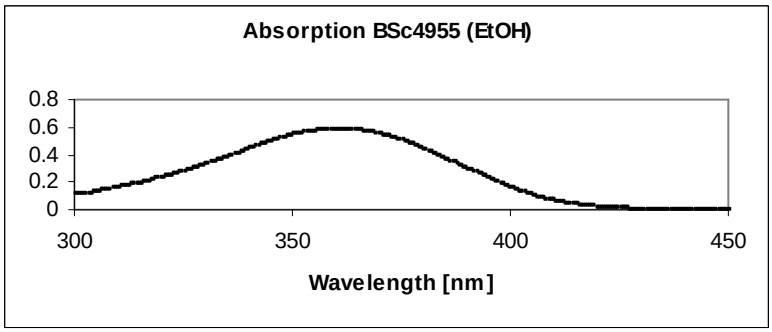

***In vitro* neuropathological staining of AD brain sections**: Tissues: hippocampus; Patient: male, 72 years old; CERAD Score: 3; NFTs-level: V.

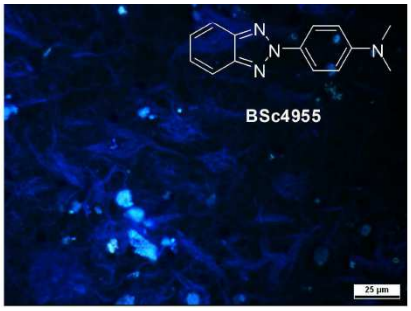

***In vitro* neuropathological staining of PD brain sections**: Tissues: midbrain; Patient: male, 76 years old.

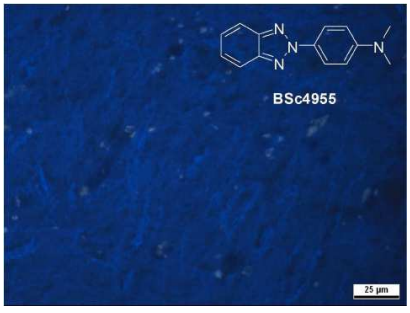

4-(2*H*-Benzo[*d*][1,2,3]triazol-2-yl)-*N*,*N*-diethylaniline (142c)

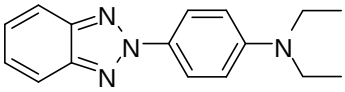

BSc 4956

Yield: 25 %. **^{1}H-NMR (500 MHz, d_6-DMSO)**: δ = 8.09 (d, *J* = 9.5 Hz, 2H), 7.96 (dd, *J* = 6.5 Hz, *J* = 3.0 Hz, 2H), 7.45 (dd, *J* = 6.5 Hz, *J* = 3.0 Hz, 2H), 6.84 (d, *J* = 9.5 Hz, 2H), 3.45-3.39 (m, 4H), 1.14 (t, *J* = 7.0 Hz, 6H) ppm. **^{13}C-NMR (125 MHz, d_6-DMSO)**: δ = 148.0, 143.9, 128.1, 126.5, 121.5, 117.5, 111.2, 43.8, 12.3 ppm. **UV/Vis (Ethanol)**: λ_{max} = 368.5 nm.

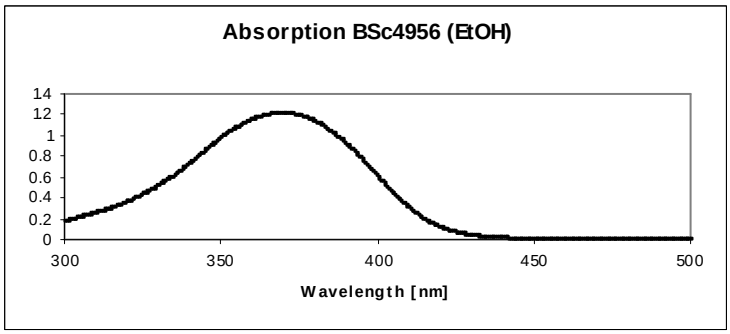

***In vitro* neuropathological staining of AD brain sections**: Tissues: hippocampus; Patient: male, 72 years old; CERAD Score: 3; NFTs-level: V.

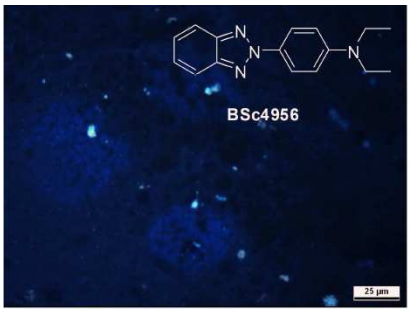

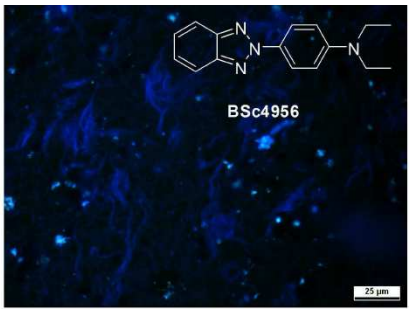

***In vitro* neuropathological staining of AD olfactory epithelium sections**: Tissues: olfactory epithelium; Patient: male, 78 years old; Braak: V, CERAD Score: 3.

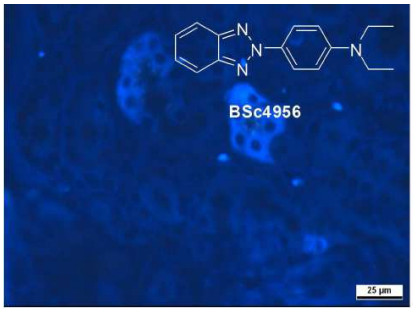

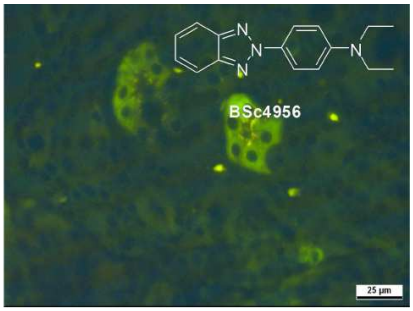

***N*,*N*-Dimethyl-4-(5-methyl-2*H*-benzo[*d*][1,2,3]triazol-2-yl)aniline (142d)**

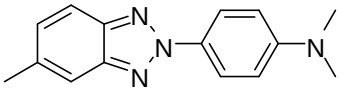

BSc 4957

Yield: 17 %. **^{1}H-NMR (500 MHz, d_6-DMSO)**: δ = 8.09 (d, *J* = 9.0 Hz, 2H), 7.85 (d, *J* = 8.5 Hz, 1H), 7.71 (d, *J* = 1.0 Hz, 1H), 7.29 (dd, *J* = 8.5 Hz, *J* = 1.5 Hz, 1H), 6.88 (d, *J* = 9.5 Hz, 2H), 3.00 (s, 6H), 2.45 (s, 3H) ppm. **^{13}C-NMR (125 MHz, d_6-DMSO)**: δ = 150.5, 144.5, 142.7, 136.3, 129.3, 129.1, 120.9, 117.1, 115.7, 112.0, 39.8, 21.5 ppm. **UV/Vis (Ethanol)**: λ_{max} = 359.5 nm.

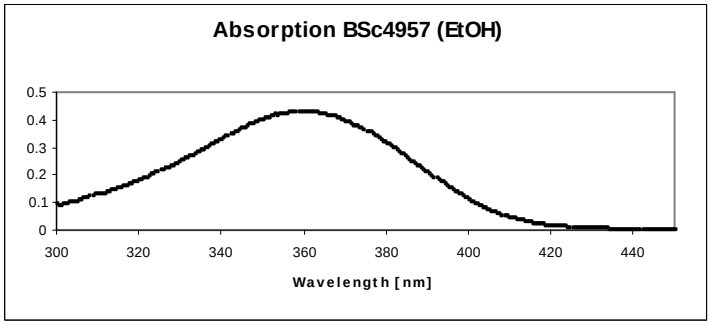

***In vitro* neuropathological staining of AD brain sections**: Tissues: hippocampus; Patient: male, 72 years old; CERAD Score: 3; NFTs-level: V.

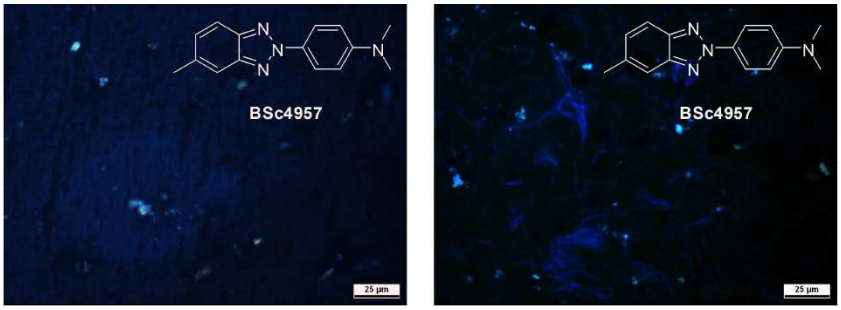

***N*,*N*-Diethyl-4-(5-methyl-2*H*-benzo[*d*][1,2,3]triazol-2-yl)aniline (142e)**

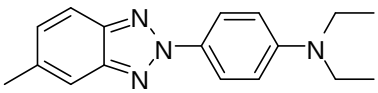

BSc 4958

Yield: 23 %. **^{1}H-NMR (500 MHz, d_6-DMSO)**: δ = 8.05 (d, *J* = 9.5 Hz, 2H), 7.84 (d, *J* = 8.5 Hz, 1H), 7.71-7.69 (m, 1H), 7.28 (dd, *J* = 8.5 Hz, *J* = 1.5 Hz, 1H), 6.82 (d, *J* = 9.0 Hz, 2H), 3.44-3.34 (m, 4H), 2.46 (s, 3H), 1.13 (t, *J* = 7.5 Hz, 6H) ppm. **^{13}C-NMR (125 MHz, d_6-DMSO)**: δ =

147.8, 144.4, 142.6, 136.2, 129.1, 128.2, 121.3, 117.0, 115.7, 111.2, 43.7, 21.5, 12.3 ppm. **UV/Vis (Ethanol)**: λ_{max} = 362.0 nm.

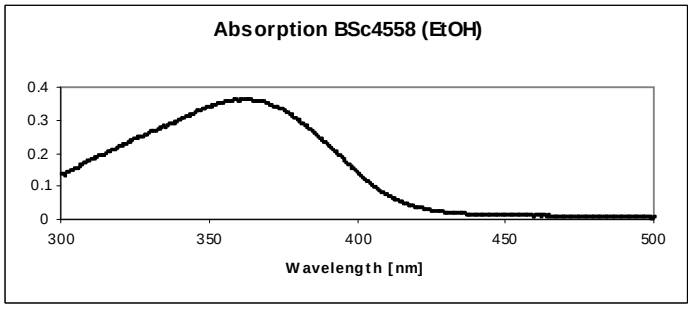

***In vitro* neuropathological staining of AD brain sections**: Tissues: hippocampus; Patient: male, 72 years old; CERAD Score: 3; NFTs-level: V.

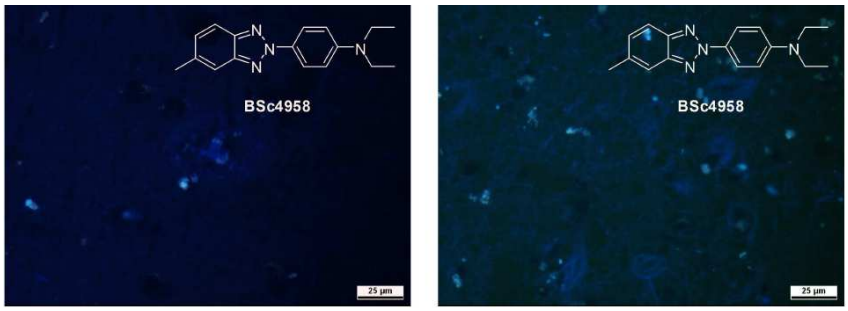

4-(5-Methoxy-2*H*-benzo[*d*][1,2,3]triazol-2-yl)-*N*,*N*-dimethylaniline (142f)

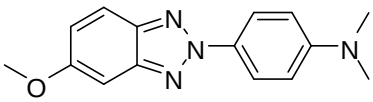

BSc5043

Yield: 14 %. **^{1}H-NMR (300 MHz, d_6-DMSO)**: δ = 8.05 (d, *J* = 9.3 Hz, 2H), 7.84 (dd, *J* = 9.3 Hz, *J* = 0.6 Hz, 1H), 7.29 (d, *J* = 2.1 Hz, 1H), 7.11 (dd, *J* = 9.3 Hz, *J* = 2.4 Hz, 1H), 6.89 (d, *J* = 9.3 Hz, 2H), 3.87 (s, 3H), 3.00 (s, 6H) ppm. **^{13}C-NMR (75 MHz, d_6-DMSO)**: δ = 158.4, 150.4, 145.0, 140.0, 129.2, 121.0, 120.7, 118.5, 112.1, 95.0, 55.5, 39.9 ppm. **UV/Vis (Ethanol)**: λ_{max} = 368.5 nm.

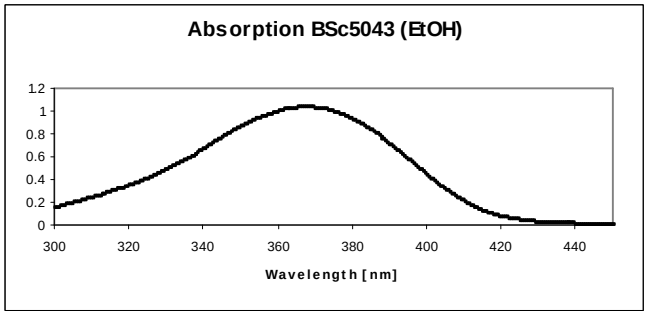

***N*,*N*-Diethyl-4-(5-methoxy-2*H*-benzo[*d*][1,2,3]triazol-2-yl)aniline (142g)**

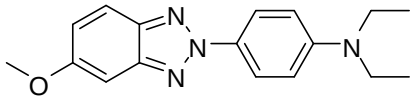

BSc5044

Yield: 17 %. **^{1}H-NMR (300 MHz, d_6-DMSO)**: δ = 8.01 (d, *J* = 9.3 Hz, 2H), 7.84 (d, *J* = 9.0 Hz, 1H), 7.28 (d, *J* = 2.7, 1H), 7.09 (dd, *J* = 9.3 Hz, *J* = 2.4 Hz, 1H), 6.81 (d, *J* = 9.3 Hz, 2H), 3.86 (s, 3H), 3.46-3.35 (m, 4H), 1.12 (t, *J* = 6.9 Hz, 6H) ppm. **^{13}C-NMR (75 MHz, d_6-DMSO)**: δ = 158.3, 147.6, 145.0, 140.0, 128.4, 121.0, 120.8, 118.4, 111.3, 95.0, 55.5, 43.8, 12.3 ppm.

6.10. *In vitro* neuropathological staining of brain sections

Four micrometers thick serial sections of paraffin-embedded brain sections or olfactory epithelium sections of AD patients were used in this study. The brain sections were deparaffinized and hydrated in distilled water. The tissue sections were treated with acid hemalum solution and wansed with running water. Then the sections immersed in 1 mM solution of the probe in DMSO for 10 minutes and then washed with methanol. The sections were differentiated in 1 % acetic acid for 20 min, afterwards washed with running water for 5 min. Finally, the sections were treated with Roti®-Mount FluorCare (from Sigma-Aldrich) and covered with a coverslip.

Table 6.1 Procedures for *in vitro* neuropathological staining of AD brain sections.

Steps	Procedures	Time	Notes
1	Acid Hemalum solution	10 min	Nuclear stain in histology
2	Washed with running water	5 min	
3	Stained the tissues	10 min	Keep in dark
4	Washed with methanol and/or DMSO		2-5 mL solvent
5	1 % acetic acid solution	20 min	Differentiate
6	Washed with running water	5 min	
7	Finalize		Treat with Roti®-Mount FluorCare protected with coverslip
8	Visualized by fluorescence microscopy	5 min	Detection by the DAPI- or FITC-filters

The sections were analyzed by fluorescence microscopy using a Axioskop microsocope with a HBO100 fluorescence illuminator (Carl Zeiss, Oberkochem, Germany) with the bandpass filter set 09 BP450-490, FT510, LP515, the filter set 02 G365, FT395, LP420 and the filter set 15 BP546, FT580, LP590 (all Carl Zeiss, Oberkochem, Germany).

6.11. *In vitro* binding affinity determined by *Thiazine Red R* displacement assay

Recombinant human microtubule associated tau protein purified from *E.coli* was aggregated at a concentration of 5 µM with arachidonic acid (100 µM) in 10 mM Tris, pH = 8, for 24 h at 37 °C. Synthetic $A\beta_{40}$ was aggregated at a concentration of 50 µM with arachidonic acid (100 µM) in 10 mM Tris, pH = 8, for three days at 37 °C, under shaking at 150 rpm. *Thiazine Red R* was added at the concentration corresponding to the K_d of the respective aggregated protein binding site to induce a fluorescent signal that could be inhibited by the addition of a displacer compound (K_d for aggregated tau = 18 nM, K_d for aggregated Aβ = 49 nM).

To determine the affinity of a displacer compound to the *Thiazine Red R* binding sites of the aggregated proteins, the compound was added at different concentrations to the assay ranging from 0.1 nM to 10000 nM. For the inhibition curve, the compound was measured together with the aggregated proteins and *Thiazine Red R*. The fluorescence of some dyes overlapped with the fluorescence of *Thiazine Red R* when measured at 595 nm. Therefore, compounds were also measured together with the aggregated proteins, but without *Thiazine Red R* (autofluorescence curve). Net-fluorescence was calculated by subtracting the fluorescence of the wells without *Thiazine Red R* from the fluorescence of wells containing *Thiazine Red R* (inhibition curve). As negative control *Thiazine Red R* and aggregated protein was used. As positive control, *Thiazine Red R*, reference compound with known activity and aggregated protein was used.

The assay was performed in Perkin Elmer OptiPlate 384, black, 45 mL assay volume. As assay buffer DPBS (no $CaCl_2$ no $MgCl_2$) (GIBCO N. 14020) was used. The tested compounds were diluted in DMSO and 2 µL of the solution was added to the assay (5% DMSO final). The assay was started by the addition of the aggregated protein (competitive condition). The plates were shortly shaken (1 min with Sterico variomag teleshake) and incubated at room temperature for 30 min. Measurements were performed with En: Vision (Perkin Elmer), at Excitation 531 nm / Emission 595 nm. Corresponding IC_{50} values (inhibitory concentration for 50% decrease) were calculated using the Levenburg Marquardt algorithm: y = A + ((B-A)/(1+((C/x)^D)))

Table 6.2 Descriptions of the equation.

Item	Description
A	The bottom plateau of the curve corresponds to the final minimum y value.
B	The top of the plateau of the curve corresponds to the final maximum y value.
C	The IC_{50} value represents the x value at which the half maximum y value is attained.
D	The slope factor. In this model a positive value is returned when y increases with increasing x and a negative value when y increases as x is decreasing.
x	Concentration of the tested compound (nM)
y	Net fluorescence in % of controls.

The obtained values are the average values of replicate experiments. The statistical presentation follows the guidelines laid out by G. Cumming.[234]

Determination of IC_{50} values for different compounds on aggregated proteins using the *Thiazine Red R* assay. Data represent average of technical replicates.

Table 6.3 IC_{50} values for different reference compounds.

Compounds	Aggr. tau - IC_{50} (nM)	Aggr. $A\beta_{40}$ - IC_{50} (nM)
Evans Blue	1.0	89
Congo Red	5.4	14
Hondson 1d[117]	8.8	13
BSB	18	78
MeXO4	246	140
Crystal Violet	1545	1280
FDDNP	1635	1467
IMPY	2707	5671
PIB	3255	5190
AZD2184	9802	>10000
FENE	>10000	>10000
BF-158	>10000	>10000

6.12. *In vivo* zebrafish embryo assay for cytotoxicity

The zebrafish were bred and maintained according to the methods described by Christiane Nuesslein-Volhard and Ralf Dahm.[157] In brief, the wild-type zebrafish were raised on 14-h light-10-h dark cycles at 26.0 ± 0.5°C. The embryos were obtained via natural mating and cultured in water. All experiments in this study were carried out according to the ethical and welfare principles in legislation on animal research in Germany. The embryos were collected and placed into 24-well plates, ten embryos per well. When the embryos were older than 6 hpf (> 50% epiboly) were treated with solutions containing 1, 5, 10 µM of the corresponding imaging probes in E2 solution. The phenotypes were examined using the Axio Scope. A1 microscope system from Carl Zeiss at 24 hpf and 72 hpf.

6.13. *In vitro* cell proliferation assay (HepG2)

Liver hepatocellular carcinoma cells HepG2 were maintained in DMEM/F12 1+1 supplemented with 10% fetal bovine serum. Cells were cultivated under sterile conditions in a humidified incubator (37 °C, 5 % CO_2, 95 % humidity) without antibiotics. Mycoplasma contamination could be excluded via routinely examinations (PCR). To determine the number of viable cells after probes incubation, the CellTiter 96®AQueous non-radioactive cell proliferation assay (Promega, Madison, USA) was used. The HepG2 cells were seeded in 96-well plates at a density of 12000 cells per cm^2. 24 hours later, the cells were incubated with 0.1 µM, 1 µM, 10 µM and 50 µM of potential compounds for 24 hours. Afterwards, cells were washed three times with PBS and CellTiter 96®AQueous non-radioactive cell proliferation assay reagent was added to the samples. The colorimetric assay is based on the reduction of a tetrazolium salt [3-(4,5-dimethylthiazol-2-yl)-5-(3-carboxymethoxyphenyl)-2-(4sulfophenyl)-2H-tetrazolium, inner salt (MTS) into a formazan product by intrinsic dehydrogenases of living cells. The amount of formazan product correlates directly to the number of metabolically active cells, and it was calculated after photometric analysis at λ=492 nm using a microplate reader (Tecan, Crailsheim, Germany). To quantify cell viability, absorbances of treated samples were normalized to untreated controls (percent of nontreated controls), which resulted in cell vitality. Thereby cell vitality values between 70 % and 120 % represent neither cytotoxic nor proliferative effects on HepG2 and loss of cell vitality over 30 % characterizes a substance as cytotoxic, according to the DIN ISO 10993-5:2009. Finally EC_{50} was calculated via the best-fitted trendline of cell vitality as a function of dye concentration. EC_{50} declares the dye concentration in which 50 % of the cells died after incubation with the probe.

References

(1) Citron, M. *Nat. Rev. Drug Discov.* **2010**, *9*, 387.
(2) Jakob-Roetne, R.; Jacobsen, H. *Angew. Chem. Int. Ed. Engl.* **2009**, *48*, 3030.
(3) Mucke, L. *Nature* **2009**, *461*, 895.
(4) Prince, M.; Bryce, R.; Ferri, C. *World Alzheimer Report 2011* **2011**.
(5) Wimo, A.; Prince, M. *World Alzheimer Report 2010* **2010**.
(6) Forsyth, E.; Ritzline, P. D. *Phys. Ther.* **1998**, *78*, 1325.
(7) Selkoe, D. J. *Physiol. Rev.* **2001**, *81*, 741.
(8) Ittner, L. M.; Gotz, J. *Nat. Rev. Neurosci.* **2011**, *12*, 67.
(9) Mandelkow, E. M.; Mandelkow, E. *Trends Cell Biol.* **1998**, *8*, 425.
(10) Brunden, K. R.; Trojanowski, J. Q.; Lee, V. M. *Nat. Rev. Drug Discov.* **2009**, *8*, 783.
(11) Gustaw-Rothenberg, K.; Lerner, A.; Bonda, D. J.; Lee, H. G.; Zhu, X.; Perry, G.; Smith, M. A. *Biomark. Med.* **2010**, *4*, 15.
(12) Seabrook, G. R.; Ray, W. J.; Shearman, M.; Hutton, M. *Mol. Interv.* **2007**, *7*, 261.
(13) Cotman, C. W.; Poon, W. W.; Rissman, R. A.; Blurton-Jones, M. *J. Neuropatho. Exp. Neurol.* **2005**, *64*, 104.
(14) Benilova, I.; Karran, E.; De Strooper, B. *Nat. Neurosci.* **2012**, *15*, 349.
(15) Nizzari, M.; Thellung, S.; Corsaro, A.; Villa, V.; Pagano, A.; Porcile, C.; Russo, C.; Florio, T. *J. Toxicol.* **2012**, *2012*, 187297.
(16) Zhang, H.; Ma, Q.; Zhang, Y. W.; Xu, H. *J. Neurochem.* **2012**, *120 Suppl 1*, 9.
(17) Chow, V. W.; Mattson, M. P.; Wong, P. C.; Gleichmann, M. *Neuromol. Med.* **2010**, *12*, 1.
(18) Bell, R. D.; Zlokovic, B. V. *Acta Neuropathol.* **2009**, *118*, 103.
(19) Hanger, D. P.; Anderton, B. H.; Noble, W. *Trends Mol. Med.* **2009**, *15*, 112.
(20) Borroni, B.; Colciaghi, F.; Pastorino, L.; Archetti, S.; Corsini, P.; Cattabeni, F.; Di Luca, M.; Padovani, A. *Eur. Neuropsychopharmacol.* **2002**, *12*, 195.
(21) Duyckaerts, C.; Delatour, B.; Potier, M. C. *Acta Neuropathol.* **2009**, *118*, 5.
(22) Höttecke, N.; Baumann, S.; Taghavi, A.; Braun, H. A.; Schmidt, B. *Front. Med. Chem.* **2009**, *4*, 730.
(23) Sambamurti, K.; Greig, N. H.; Utsuki, T.; Barnwell, E. L.; Sharma, E.; Mazell, C.; Bhat, N. R.; Kindy, M. S.; Lahiri, D. K.; Pappolla, M. A. *J. Neurochem.* **2011**, *117*, 359.
(24) Vassar, R. *Adv. Drug Deliv. Rev.* **2002**, *54*, 1589.
(25) Venugopal, C.; Demos, C. M.; Rao, K. S.; Pappolla, M. A.; Sambamurti, K. *CNS Neurol. Disord. Drug Targets* **2008**, *7*, 278.
(26) Ghosh, A. K.; Gemma, S.; Tang, J. *Neurotherapeutics* **2008**, *5*, 399.
(27) Cole, S. L.; Vassar, R. *Mol. Neurodegener.* **2007**, *2*, 22.
(28) Laird, F. M.; Cai, H.; Savonenko, A. V.; Farah, M. H.; He, K.; Melnikova, T.; Wen, H.; Chiang, H. C.; Xu, G.; Koliatsos, V. E.; Borchelt, D. R.; Price, D. L.; Lee, H. K.; Wong, P. C. *J. Neurosci.* **2005**, *25*, 11693.
(29) Pissarnitski, D. *Curr. Opin. Drug discov. Devel.* **2007**, *10*, 392.
(30) Van Broeck, B.; Van Broeckhoven, C.; Kumar-Singh, S. *Neurodegener. Dis.* **2007**, *4*, 349.
(31) Craig-Schapiro, R.; Fagan, A. M.; Holtzman, D. M. *Neurobiol. Dis.* **2009**, *35*, 128.
(32) Liu, F.; Zaidi, T.; Iqbal, K.; Grundke-Iqbal, I.; Merkle, R. K.; Gong, C. X. *FEBS Lett.* **2002**, *512*, 101.
(33) Medeiros, R.; Baglietto-Vargas, D.; LaFerla, F. M. *CNS Neurosci. Ther.* **2011**, *17*, 514.
(34) Binder, L. I.; Guillozet-Bongaarts, A. L.; Garcia-Sierra, F.; Berry, R. W. *Biochim. Biophys. Acta* **2005**, *1739*, 216.
(35) Meraz-Rios, M. A.; Lira-De Leon, K. I.; Campos-Pena, V.; De Anda-Hernandez, M. A.; Mena-Lopez, R. *J. Neurochem.* **2010**, *112*, 1353.
(36) Sergeant, N.; Delacourte, A.; Buee, L. *Biochim. Biophys. Acta* **2005**, *1739*, 179.

(37) Bulic, B.; Pickhardt, M.; Mandelkow, E. M.; Mandelkow, E. *Neuropharmacology* **2010**, *59*, 276.
(38) Jung, H. J.; Park, S. S.; Mok, J. O.; Lee, T. K.; Park, C. S.; Park, S. A. *Exp. Neurol.y* **2011**, *228*, 232.
(39) Mohorko, N.; Repovs, G.; Popovic, M.; Kovacs, G. G.; Bresjanac, M. *J. Neuropathol. Exp. Neurol.* **2010**, *69*, 405.
(40) McMillan, P.; Korvatska, E.; Poorkaj, P.; Evstafjeva, Z.; Robinson, L.; Greenup, L.; Leverenz, J.; Schellenberg, G. D.; D'Souza, I. *J. Comp. Neurol.* **2008**, *511*, 788.
(41) Denk, F.; Wade-Martins, R. *Neurobiol. Aging* **2009**, *30*, 1.
(42) LaFerla, F. M. *Biochem. Soc. Trans.* **2010**, *38*, 993.
(43) Yoshida, H.; Goedert, M. *J. Neurochem.* **2012**, *120*, 165.
(44) Iseki, E.; Yamamoto, R.; Murayama, N.; Minegishi, M.; Togo, T.; Katsuse, O.; Kosaka, K.; Akiyama, H.; Tsuchiya, K.; de Silva, R.; Andrew, L.; Arai, H. *Neurosci. Lett.* **2006**, *405*, 29.
(45) Shimazaki, M.; Nakano, H.; Kobayashi, K. *Psychogeriatrics* **2005**, *5*, 22.
(46) Arima, K.; Nakamura, M.; Sunohara, N.; Nishio, T.; Ogawa, M.; Hirai, S.; Kawai, M.; Ikeda, K. *Acta Neuropathol.* **1999**, *97*, 565.
(47) Shankar, S. K.; Yanagihara, R.; Garruto, R. M.; Grundke-Iqbal, I.; Kosik, K. S.; Gajdusek, D. C. *Ann. Neurol.* **1989**, *25*, 146.
(48) Uchihara, T.; Nakamura, A.; Yamazaki, M.; Mori, O. *Acta Neuropathol.* **2000**, *100*, 385.
(49) Bolander, A.; Kieser, D.; Voss, C.; Bauer, S.; Schon, C.; Burgold, S.; Bittner, T.; Holzer, J.; Heyny-von Haussen, R.; Mall, G.; Goetschy, V.; Czech, C.; Knust, H.; Berger, R.; Herms, J.; Hilger, I.; Schmidt, B. *J. Med. Chem.* **2012**, *55*, 9170.
(50) Klunk, W. E.; Bacskai, B. J.; Mathis, C. A.; Kajdasz, S. T.; McLellan, M. E.; Frosch, M. P.; Debnath, M. L.; Holt, D. P.; Wang, Y.; Hyman, B. T. *J. Neuropathol. Exp. Neurol.* **2002**, *61*, 797.
(51) Ghosh, A. K.; Brindisi, M.; Tang, J. *J. Nneurochem.* **2012**, *120 Suppl 1*, 71.
(52) Bjorklund, C.; Oscarson, S.; Benkestock, K.; Borkakoti, N.; Jansson, K.; Lindberg, J.; Vrang, L.; Hallberg, A.; Rosenquist, A.; Samuelsson, B. *J. Med. Chem.* **2010**, *53*, 1458.
(53) Park, S. Y. *Arch. Pharm. Res.* **2010**, *33*, 1589.
(54) Stachel, S. J.; Coburn, C. A.; Steele, T. G.; Jones, K. G.; Loutzenhiser, E. F.; Gregro, A. R.; Rajapakse, H. A.; Lai, M. T.; Crouthamel, M. C.; Xu, M.; Tugusheva, K.; Lineberger, J. E.; Pietrak, B. L.; Espeseth, A. S.; Shi, X. P.; Chen-Dodson, E.; Holloway, M. K.; Munshi, S.; Simon, A. J.; Kuo, L.; Vacca, J. P. *J. Med. Chem.* **2004**, *47*, 6447.
(55) Zhu, Y.; Xiao, K.; Ma, L.; Xiong, B.; Fu, Y.; Yu, H.; Wang, W.; Wang, X.; Hu, D.; Peng, H.; Li, J.; Gong, Q.; Chai, Q.; Tang, X.; Zhang, H.; Shen, J. *Bioorg. Med. Chem.* **2009**, *17*, 1600.
(56) Kukar, T. L.; Ladd, T. B.; Bann, M. A.; Fraering, P. C.; Narlawar, R.; Maharvi, G. M.; Healy, B.; Chapman, R.; Welzel, A. T.; Price, R. W.; Moore, B.; Rangachari, V.; Cusack, B.; Eriksen, J.; Jansen-West, K.; Verbeeck, C.; Yager, D.; Eckman, C.; Ye, W.; Sagi, S.; Cottrell, B. A.; Torpey, J.; Rosenberry, T. L.; Fauq, A.; Wolfe, M. S.; Schmidt, B.; Walsh, D. M.; Koo, E. H.; Golde, T. E. *Nature* **2008**, *453*, 925.
(57) Dovey, H. F.; John, V.; Anderson, J. P.; Chen, L. Z.; de Saint Andrieu, P.; Fang, L. Y.; Freedman, S. B.; Folmer, B.; Goldbach, E.; Holsztynska, E. J.; Hu, K. L.; Johnson-Wood, K. L.; Kennedy, S. L.; Kholodenko, D.; Knops, J. E.; Latimer, L. H.; Lee, M.; Liao, Z.; Lieberburg, I. M.; Motter, R. N.; Mutter, L. C.; Nietz, J.; Quinn, K. P.; Sacchi, K. L.; Seubert, P. A.; Shopp, G. M.; Thorsett, E. D.; Tung, J. S.; Wu, J.; Yang, S.; Yin, C. T.; Schenk, D. B.; May, P. C.; Altstiel, L. D.; Bender, M. H.; Boggs, L. N.; Britton, T. C.; Clemens, J. C.; Czilli, D. L.; Dieckman-McGinty, D. K.; Droste, J. J.; Fuson, K. S.; Gitter, B. D.; Hyslop, P. A.; Johnstone, E. M.; Li, W. Y.; Little, S. P.; Mabry, T. E.; Miller, F. D.; Audia, J. E. *J. Neurochem.* **2001**, *76*, 173.

(58) Siemers, E. R.; Quinn, J. F.; Kaye, J.; Farlow, M. R.; Porsteinsson, A.; Tariot, P.; Zoulnouni, P.; Galvin, J. E.; Holtzman, D. M.; Knopman, D. S.; Satterwhite, J.; Gonzales, C.; Dean, R. A.; May, P. C. *Neurology* **2006**, *66*, 602.
(59) Best, J. D.; Jay, M. T.; Otu, F.; Ma, J.; Nadin, A.; Ellis, S.; Lewis, H. D.; Pattison, C.; Reilly, M.; Harrison, T.; Shearman, M. S.; Williamson, T. L.; Atack, J. R. *J. Pharmacol. Exp. Ther.* **2005**, *313*, 902.
(60) Wolfe, M. S. *Neurotherapeutics* **2008**, *5*, 391.
(61) Imbimbo, B. P. *Drug Discov. Today* **2008**, *5*, 169.
(62) Wu, W. L.; Zhang, L. L. *Drug Dev. Res.* **2009**, *70*, 94.
(63) Panza, F.; Frisardi, V.; Imbimbo, B. P.; Capurso, C.; Logroscino, G.; Sancarlo, D.; Seripa, D.; Vendemiale, G.; Pilotto, A.; Solfrizzi, V. *CNS Neurosci. Ther.* **2010**, *16*, 272.
(64) Boutajangout, A.; Sigurdsson, E. M.; Krishnamurthy, P. K. *Curr. Alzheimer Res.* **2011**, *8*, 666.
(65) Hernandez, F.; Gomez de Barreda, E.; Fuster-Matanzo, A.; Lucas, J. J.; Avila, J. *Exp. Neurol.* **2010**, *223*, 322.
(66) Eldar-Finkelman, H. *Trends Mol. Med.* **2002**, *8*, 126.
(67) Takashima, A. *J. Pharmacol. Sci.* **2009**, *109*, 174.
(68) Kaidanovich-Beilin, O.; Lipina, T. V.; Takao, K.; van Eede, M.; Hattori, S.; Laliberte, C.; Khan, M.; Okamoto, K.; Chambers, J. W.; Fletcher, P. J.; MacAulay, K.; Doble, B. W.; Henkelman, M.; Miyakawa, T.; Roder, J.; Woodgett, J. R. *Mol. Brain* **2009**, *2*, 35.
(69) Phiel, C. J.; Wilson, C. A.; Lee, V. M.; Klein, P. S. *Nature* **2003**, *423*, 435.
(70) Monte, F. L.; Kramer, T.; Bolander, A.; Plotkin, B.; Eldar-Finkelman, H.; Fuertes, A.; Dominguez, J.; Schmidt, B. *Bioorg. Med. Chem. Lett.* **2011**, *21*, 5610.
(71) Kramer, T.; Schmidt, B.; Lo Monte, F. *Int. J. Alzheimers Dis.* **2012**, *2012*, 1.
(72) Noble, W.; Olm, V.; Takata, K.; Casey, E.; O, M.; Meyerson, J.; Gaynor, K.; LaFrancois, J.; Wang, L. L.; Kondo, T.; Davies, P.; Burns, M.; Nixon, V. R.; Dickson, D.; Matsuoka, Y.; Ahlijanian, M.; Lau, L. F.; Duff, K. *Neuron* **2003**, *38*, 555.
(73) Chirita, C.; Necula, M.; Kuret, J. *Biochemistry* **2004**, *43*, 2879.
(74) Honson, N. S.; Jensen, J. R.; Darby, M. V.; Kuret, J. *Biochem. Biophys. Res. Commun.* **2007**, *363*, 229.
(75) Schafer, K. N.; Murale, D. P.; Kim, K.; Cisek, K.; Kuret, J.; Churchill, D. G. *Bioorg. Med. Chem. Lett.* **2011**, *21*, 3273.
(76) Agdeppa, E. D.; Spilker, M. E. *AAPS J.* **2009**, *11*, 286.
(77) Willmann, J. K.; van Bruggen, N.; Dinkelborg, L. M.; Gambhir, S. S. *Nat. Rev. Drug Discov.* **2008**, *7*, 591.
(78) Massoud, T. F.; Gambhir, S. S. *Genes Dev.* **2003**, *17*, 545.
(79) Hampel, H.; Frank, R.; Broich, K.; Teipel, S. J.; Katz, R. G.; Hardy, J.; Herholz, K.; Bokde, A. L.; Jessen, F.; Hoessler, Y. C.; Sanhai, W. R.; Zetterberg, H.; Woodcock, J.; Blennow, K. *Nat. Rev. Drug Discov.* **2010**, *9*, 560.
(80) Cai, W.; Rao, J.; Gambhir, S. S.; Chen, X. *Mol. Cancer Ther.* **2006**, *5*, 2624.
(81) Cedazo-Minguez, A.; Winblad, B. *Exp. Gerontol.* **2010**, *45*, 5.
(82) Ametamey, S. M.; Honer, M.; Schubiger, P. A. *Chem. Rev.* **2008**, *108*, 1501.
(83) Jack, C. R., Jr.; Marjanska, M.; Wengenack, T. M.; Reyes, D. A.; Curran, G. L.; Lin, J.; Preboske, G. M.; Poduslo, J. F.; Garwood, M. *Neuroscientist.* **2007**, *13*, 38.
(84) Garcia-Alloza, M.; Bacskai, B. J. *Neuromol. Med.* **2004**, *6*, 65.
(85) Barrio, J. R.; Satyamurthy, N.; Huang, S.-C.; Petric, A.; Small, G. W.; Kepe, V. *Acc. Chem. Res.* **2008**, *42*, 842.
(86) Bacskai, B. J.; Klunk, W. E.; Mathis, C. A.; Hyman, B. T. *J. Cereb. Blood Fow. Metab.* **2002**, *22*, 1035.
(87) Zha, Z.; Choi, S. R.; Ploessl, K.; Lieberman, B. P.; Qu, W.; Hefti, F.; Mintun, M.; Skovronsky, D.; Kung, H. F. *J. Med. Chem.* **2011**, *54*, 8085.
(88) Cui, M.; Li, Z.; Tang, R.; Jia, H.; Liu, B. *Eur. J. Med. Chem.* **2011**, *46*, 2908.
(89) Lin, K. S.; Debnath, M. L.; Mathis, C. A.; Klunk, W. E. *Bioorg. Med. Chem. Lett.* **2009**, *19*, 2258.

(90) Cai, L.; Innis, R. B.; Pike, V. W. *Curr. Med. Chem.* **2007**, *14*, 19.
(91) Ryu, E. K.; Choe, Y. S.; Lee, K. H.; Choi, Y.; Kim, B. T. *J. Med. Chem.* **2006**, *49*, 6111.
(92) Cui, M.; Ono, M.; Kimura, H.; Liu, B.; Saji, H. *Bioorg. Med. Chem. Lett.* **2011**, *21*, 4193.
(93) Furumoto, S.; Okamura, N.; Iwata, R.; Yanai, K.; Arai, H.; Kudo, Y. *Curr. Top. Med. Chem.* **2007**, *7*, 1773.
(94) Vlassenko, A. G.; Benzinger, T. L.; Morris, J. C. *Biochim. Bophys. Acta* **2012**, *1822*, 370.
(95) Flaherty, D. P.; Walsh, S. M.; Kiyota, T.; Dong, Y.; Ikezu, T.; Vennerstrom, J. L. *J. Med. Chem.* **2007**, *50*, 4986.
(96) Nordberg, A. *Lancet Neurol.* **2004**, *3*, 519.
(97) Koivunen, J.; Verkkoniemi, A.; Aalto, S.; Paetau, A.; Ahonen, J. P.; Viitanen, M.; Nagren, K.; Rokka, J.; Haaparanta, M.; Kalimo, H.; Rinne, J. O. *Brain* **2008**, *131*, 1845.
(98) Klunk, W. E.; Engler, H.; Nordberg, A.; Wang, Y.; Blomqvist, G.; Holt, D. P.; Bergstrom, M.; Savitcheva, I.; Huang, G. F.; Estrada, S.; Ausen, B.; Debnath, M. L.; Barletta, J.; Price, J. C.; Sandell, J.; Lopresti, B. J.; Wall, A.; Koivisto, P.; Antoni, G.; Mathis, C. A.; Langstrom, B. *Ann. Neurol.* **2004**, *55*, 306.
(99) Mathis, C. A.; Wang, Y. M.; Holt, D. P.; Huang, G. F.; Debnath, M. L.; Klunk, W. E. *J. Med. Chem.* **2003**, *46*, 2740.
(100) Braskie, M. N.; Klunder, A. D.; Hayashi, K. M.; Protas, H.; Kepe, V.; Miller, K. J.; Huang, S. C.; Barrio, J. R.; Ercoli, L. M.; Siddarth, P.; Satyamurthy, N.; Liu, J.; Toga, A. W.; Bookheimer, S. Y.; Small, G. W.; Thompson, P. M. *Neurobiol. Aging* **2010**, *31*, 1669.
(101) Shoghi-Jadid, K.; Small, G. W.; Agdeppa, E. D.; Kepe, V.; Ercoli, L. M.; Siddarth, P.; Read, S.; Satyamurthy, N.; Petric, A.; Huang, S. C.; Barrio, J. R. *Am. J. Geriatr. Psychiatry* **2002**, *10*, 24.
(102) Verhoeff, N. P.; Wilson, A. A.; Takeshita, S.; Trop, L.; Hussey, D.; Singh, K.; Kung, H. F.; Kung, M. P.; Houle, S. *Am. J. Geriatr. Psychiatry* **2004**, *12*, 584.
(103) Kudo, Y.; Okamura, N.; Furumoto, S.; Tashiro, M.; Furukawa, K.; Maruyama, M.; Itoh, M.; Iwata, R.; Yanai, K.; Arai, H. *J. Nucl. Med.* **2007**, *48*, 553.
(104) Rowe, C. C.; Ackerman, U.; Browne, W.; Mulligan, R.; Pike, K. L.; O'Keefe, G.; Tochon-Danguy, H.; Chan, G.; Berlangieri, S. U.; Jones, G.; Dickinson-Rowe, K. L.; Kung, H. P.; Zhang, W.; Kung, M. P.; Skovronsky, D.; Dyrks, T.; Holl, G.; Krause, S.; Friebe, M.; Lehman, L.; Lindemann, S.; Dinkelborg, L. M.; Masters, C. L.; Villemagne, V. L. *Lancet Neurol.* **2008**, *7*, 129.
(105) Nordberg, A. *Neuropsychologia* **2008**, *46*, 1636.
(106) Newberg, A. B.; Wintering, N. A.; Plossl, K.; Hochold, J.; Stabin, M. G.; Watson, M.; Skovronsky, D.; Clark, C. M.; Kung, M. P.; Kung, H. F. *J. Nucl. Med.* **2006**, *47*, 748.
(107) Jensen, J. R.; Cisek, K.; Funk, K. E.; Naphade, S.; Schafer, K. N.; Kuret, *J. Alzheimer. Dis.* **2011**, *26 Suppl 3*, 147.
(108) Okamura, N.; Suemoto, T.; Furumoto, S.; Suzuki, M.; Shimadzu, H.; Akatsu, H.; Yamamoto, T.; Fujiwara, H.; Nemoto, M.; Maruyama, M.; Arai, H.; Yanai, K.; Sawada, T.; Kudo, Y. *J. Neurosci.* **2005**, *25*, 10857.
(109) Shin, J.; Lee, S. Y.; Kim, S. H.; Kim, Y. B.; Cho, S. J. *NeuroImage* **2008**, *43*, 236.
(110) Matsumura, K.; Ono, M.; Hayashi, S.; Kimura, H.; Okamoto, Y.; Ihara, M.; Takahashi, R.; Mori, H.; Saji, H. *MedChemComm* **2011**, *2*, 596.
(111) Matsumura, K.; Ono, M.; Kimura, H.; Ueda, M.; Nakamoto, Y.; Togashi, K.; Okamoto, Y.; Ihara, M.; Takahashi, R.; Saji, H. *ACS Med. Chem. Lett.* **2012**, *3*, 58.
(112) Ono, M.; Hayashi, S.; Matsumura, K.; Kimura, H.; Okamoto, Y.; Ihara, M.; Takahashi, R.; Mori, H.; Saji, H. *ACS Chem. Neurosci.* **2011**, *2*, 269.
(113) Fodero-Tavoletti, M. T.; Okamura, N.; Furumoto, S.; Mulligan, R. S.; Connor, A. R.; McLean, C. A.; Cao, D.; Rigopoulos, A.; Cartwright, G. A.; O'Keefe, G.; Gong, S.;

Adlard, P. A.; Barnham, K. J.; Rowe, C. C.; Masters, C. L.; Kudo, Y.; Cappai, R.; Yanai, K.; Villemagne, V. L. *Brain* **2011**, *134*, 1089.
(114) Volkova, K. D.; Kovalska, V. B.; Yu Losytskyy, M.; Veldhuis, G.; Segers-Nolten, G. M.; Tolmachev, O. I.; Subramaniam, V.; Yarmoluk, S. M. *J. Fuoresc.* **2010**, *20*, 1267.
(115) Chen, M.; Margittai, M.; Chen, J.; Langen, R. *J. Biol. Chem.* **2007**, *282*, 24970.
(116) Berriman, J.; Serpell, L. C.; Oberg, K. A.; Fink, A. L.; Goedert, M.; Crowther, R. A. *Proc. Natl. Acad. Sci. U. S. A.* **2003**, *100*, 9034.
(117) Honson, N. S.; Johnson, R. L.; Huang, W.; Inglese, J.; Austin, C. P.; Kuret, J. *Neurobiol. Dis.* **2007**, *28*, 251.
(118) Petkova, A. T.; Yau, W. M.; Tycko, R. *Biochemistry* **2006**, *45*, 498.
(119) Krebs, M. R.; Bromley, E. H.; Donald, A. M. *J. Struct. Biol.* **2005**, *149*, 30.
(120) Volkova, K. D.; Kovalska, V. B.; Balanda, A. O.; Losytskyy, M. Y.; Golub, A. G.; Vermeij, R. J.; Subramaniam, V.; Tolmachev, O. I.; Yarmoluk, S. M. *Bioorg. Med. Chem.* **2008**, *16*, 1452.
(121) Stsiapura, V. I.; Maskevich, A. A.; Kuzmitsky, V. A.; Turoverov, K. K.; Kuznetsova, I. M. *J. Phys. Chem.* **2007**, *111*, 4829.
(122) Clarke, C. E. *BMJ* **2007**, *335*, 441.
(123) Jankovic, J. *J. Neurol. Neurosurg. Psychiatry* **2008**, *79*, 368.
(124) Belin, A. C.; Westerlund, M. *FEBS J.* **2008**, *275*, 1377.
(125) Lees, A. J.; Hardy, J.; Revesz, T. *Lancet* **2009**, *373*, 2055.
(126) Dawson, T. M.; Dawson, V. L. *Science* **2003**, *302*, 819.
(127) Ross, O. A.; Farrer, M. J. *Biochem. Soc. Trans.* **2005**, *33*, 586.
(128) Henchcliffe, C.; Dodel, R.; Beal, M. F. *Prog. Neurobiol.* **2011**, *95*, 601.
(129) Davie, C. A. *Br. Med. Bull.* **2008**, *86*, 109.
(130) Berwick, D. C.; Harvey, K. *Trends Cell Biol.* **2011**, *21*, 257.
(131) Bisaglia, M.; Mammi, S.; Bubacco, L. *FASEB J.* **2009**, *23*, 329.
(132) Lamberto, G. R.; Torres-Monserrat, V.; Bertoncini, C. W.; Salvatella, X.; Zweckstetter, M.; Griesinger, C.; Fernandez, C. O. *J. Biol. Chem.* **2011**, *286*, 32036.
(133) Crews, L.; Tsigelny, I.; Hashimoto, M.; Masliah, E. *Neurotox. Res.* **2009**, *16*, 306.
(134) Cookson, M. R. *Annu. Rev. Biochem.* **2005**, *74*, 29.
(135) Fink, A. L. *Acc. Chem. Res.* **2006**, *39*, 628.
(136) Halliday, G. M.; Holton, J. L.; Revesz, T.; Dickson, D. W. *Acta Neuropathol.* **2011**, *122*, 187.
(137) Maries, E.; Dass, B.; Collier, T. J.; Kordower, J. H.; Steece-Collier, K. *Nat. Rev. Neurosci.* **2003**, *4*, 727.
(138) Vekrellis, K.; Xilouri, M.; Emmanouilidou, E.; Rideout, H. J.; Stefanis, L. *Lancet Neurol.* **2011**, *10*, 1015.
(139) Qin, Z.; Hu, D.; Han, S.; Hong, D. P.; Fink, A. L. *Biochemistry* **2007**, *46*, 13322.
(140) Necula, M.; Chirita, C. N.; Kuret, J. *J. Biol. Chem.* **2003**, *278*, 46674.
(141) Pavese, N.; Brooks, D. J. *Biochim. Biophys. Acta* **2009**, *1792*, 722.
(142) Tolosa, E.; Wenning, G.; Poewe, W. *Lancet Neurol.* **2006**, *5*, 75.
(143) Brooks, D. J. *J. Nucl. Med.* **2010**, *51*, 596.
(144) Schapira, A. H.; Bezard, E.; Brotchie, J.; Calon, F.; Collingridge, G. L.; Ferger, B.; Hengerer, B.; Hirsch, E.; Jenner, P.; Le Novere, N.; Obeso, J. A.; Schwarzschild, M. A.; Spampinato, U.; Davidai, G. *Nat. Rev. Drug Discov.* **2006**, *5*, 845.
(145) Brooks, D. J.; Pavese, N. *Prog. Neurobiol.* **2011**, *95*, 614.
(146) Brooks, D. J. *NeuroRx.* **2004**, *1*, 243.
(147) Chang, E.; Congdon, E. E.; Honson, N. S.; Duff, K. E.; Kuret, J. *J. Med. Chem.* **2009**, *52*, 3539.
(148) Chang, E.; Honson, N. S.; Bandyopadhyay, B.; Funk, K. E.; Jensen, J. R.; Kim, S.; Naphade, S.; Kuret, J. *Curr. Alzheimer Res.* **2009**, *6*, 409.
(149) Masuda, M.; Suzuki, N.; Taniguchi, S.; Oikawa, T.; Nonaka, T.; Iwatsubo, T.; Hisanaga, S.; Goedert, M.; Hasegawa, M. *Biochemistry* **2006**, *45*, 6085.
(150) Kramer, T.; Lo Monte, F.; Goring, S.; Okala Amombo, G. M.; Schmidt, B. *ACS Chem. Neurosci.* **2012**, *3*, 151.

(151) Peterson, R. T.; Nass, R.; Boyd, W. A.; Freedman, J. H.; Dong, K.; Narahashi, T. *Neurotoxicology* **2008**, *29*, 546.
(152) Lieschke, G. J.; Currie, P. D. *Nat. Rev. Genet.* **2007**, *8*, 353.
(153) Hill, A. J.; Teraoka, H.; Heideman, W.; Peterson, R. E. *Toxicol. Sci.* **2005**, *86*, 6.
(154) Zon, L. I.; Peterson, R. T. *Nat. Rev. Drug Discov.* **2005**, *4*, 35.
(155) Lawrence, C. *Aquaculture* **2007**, *269*, 1.
(156) McGrath, P. *Zebrafish: Methods for assessing drug safety and toxicity offers a practical guide for using zebrafish as a tool for toxicology studies* **2012**.
(157) Nuesslein-Volhard, C.; Dahm, R. *Zebrafish: A practical approach* **2002**.
(158) Lamason, R. L.; Mohideen, M. A.; Mest, J. R.; Wong, A. C.; Norton, H. L.; Aros, M. C.; Jurynec, M. J.; Mao, X.; Humphreville, V. R.; Humbert, J. E.; Sinha, S.; Moore, J. L.; Jagadeeswaran, P.; Zhao, W.; Ning, G.; Makalowska, I.; McKeigue, P. M.; O'Donnell, D.; Kittles, R.; Parra, E. J.; Mangini, N. J.; Grunwald, D. J.; Shriver, M. D.; Canfield, V. A.; Cheng, K. C. *Science* **2005**, *310*, 1782.
(159) Newman, M.; Verdile, G.; Martins, R. N.; Lardelli, M. *Biochim. Biophys. Acta* **2011**, *1812*, 346.
(160) Kimmel, C. B.; Ballard, W. W.; Kimmel, S. R.; Ullmann, B.; Schilling, T. F. *Dev. Dyn.* **1995**, *203*, 253.
(161) Atilla-Gokcumen, G. E.; Williams, D. S.; Bregman, H.; Pagano, N.; Meggers, E. *ChemBioChem* **2006**, *7*, 1443.
(162) Xi, Y.; Noble, S.; Ekker, M. *Curr. Neurol. Neurosci. Rep.* **2011**, *11*, 274.
(163) Rademakers, R.; Rovelet-Lecrux, A. *Trends Neurosci.* **2009**, *32*, 451.
(164) Mueller, T.; Vernier, P.; Wullimann, M. F. *Brain Res.* **2004**, *1011*, 156.
(165) Parng, C.; Ton, C.; Lin, Y. X.; Roy, N. M.; McGrath, P. *Neurotoxicol. Teratol.* **2006**, *28*, 509.
(166) Bai, Q.; Burton, E. A. *Biochim. Biophys. Acta* **2011**, *1812*, 353.
(167) Chen, M.; Martins, R. N.; Lardelli, M. *J. Alzheimer Dis.* **2009**, *18*, 305.
(168) Paquet, D.; Bhat, R.; Sydow, A.; Mandelkow, E. M.; Berg, S.; Hellberg, S.; Falting, J.; Distel, M.; Koster, R. W.; Schmid, B.; Haass, C. *J. Clin. Invest.* **2009**, *119*, 1382.
(169) Watanabe, K.; Nishimura, Y.; Oka, T.; Nomoto, T.; Kon, T.; Shintou, T.; Hirano, M.; Shimada, Y.; Umemoto, N.; Kuroyanagi, J.; Wang, Z.; Zhang, Z.; Nishimura, N.; Miyazaki, T.; Imamura, T.; Tanaka, T. *BMC Beurosci.* **2010**, *11*, 116.
(170) Ko, S. K.; Chen, X.; Yoon, J.; Shin, I. *Chem. Soc. Rev.* **2011**, *40*, 2120.
(171) McCollum, C. W.; Ducharme, N. A.; Bondesson, M.; Gustafsson, J. A. *Birth Defects Res. C. Embryo Today* **2011**, *93*, 67.
(172) Eimon, P. M.; Rubinstein, A. L. *Expert Opin. Drug Metab. Toxicol.* **2009**, *5*, 393.
(173) Rubinstein, A. L. *Expert Opin. Drug Metab. Toxicol.* **2006**, *2*, 231.
(174) Teraoka, H.; Dong, W.; Ogawa, S.; Tsukiyama, S.; Okuhara, Y.; Niiyama, M.; Ueno, N.; Peterson, R. E.; Hiraga, T. *Toxicol. Sci.* **2002**, *65*, 192.
(175) Serdons, K.; Terwinghe, C.; Vermaelen, P.; Van Laere, K.; Kung, H.; Mortelmans, L.; Bormans, G.; Verbruggen, A. *J. Med. Chem.* **2009**, *52*, 1428.
(176) Duan, X. H.; Liu, B. L. *Sci. China Ser. B. Chem.* **2008**, *51*, 801.
(177) Klunk, W. E.; Wang, Y.; Huang, G. F.; Debnath, M. L.; Holt, D. P.; Mathis, C. A. *Life Sci.* **2001**, *69*, 1471.
(178) Bolognesi, M. L.; Bartolini, M.; Tarozzi, A.; Morroni, F.; Lizzi, F.; Milelli, A.; Minarini, A.; Rosini, M.; Hrelia, P.; Andrisano, V.; Melchiorre, C. *Bioorg. Med. Chem. Lett.* **2011**, *21*, 2655.
(179) Mathis, C. A.; Bacskai, B. J.; Kajdasz, S. T.; McLellan, M. E.; Frosch, M. P.; Hyman, B. T.; Holt, D. P.; Wang, Y.; Huang, G. F.; Debnath, M. L.; Klunk, W. E. *Bioorg. Med. Chem. Lett.* **2002**, *12*, 295.
(180) Leuma Yona, R.; Mazeres, S.; Faller, P.; Gras, E. *ChemMedChem* **2008**, *3*, 63.
(181) Cashion, D. K.; Chen, G.; Kasi, D.; Kolb, H. C.; Liu, C.; Sinha, A.; Szardenings, A., Katrin; Wang, E.; Yu, C.; Zhang, W.; Gangadharmath, U., B. ; Walsh, J., C. *WO 2011119565* **2011**.
(182) Mohanakrishnan, A. K.; Srinivasan, P. C. *J. Org. Chem.* **1995**, *60*, 1939.

(183) Chen, X.; Yu, P.; Zhang, L.; Liu, B. *Bioorg. Med. Chem. Lett.* **2008**, *18*, 1442.
(184) Yamaguchi, Y.; Matsubara, Y.; Ochi, T.; Wakamiya, T.; Yoshida, Z. *J. Am. Chem. Soc.* **2008**, *130*, 13867.
(185) Kung, M. P.; Hou, C.; Zhuang, Z. P.; Cross, A. J.; Maier, D. L.; Kung, H. F. *Eur. J. Nucl. Med. Mol. Imaging* **2004**, *31*, 1136.
(186) Nagib, D. A.; MacMillan, D. W. *Nature* **2011**, *480*, 224.
(187) Mitronova, G. Y.; Belov, V. N.; Bossi, M. L.; Wurm, C. A.; Meyer, L.; Medda, R.; Moneron, G.; Bretschneider, S.; Eggeling, C.; Jakobs, S.; Hell, S. W. *Chem. Eur. J.* **2010**, *16*, 4477.
(188) Ban, H.; Gavrilyuk, J.; Barbas, C. F. *J. Am. Chem. Soc.* **2010**, *132*, 1523.
(189) Aginagalde, M.; Vara, Y.; Arrieta, A.; Zangi, R.; Cebolla, V. L.; Delgado-Camon, A.; Cossio, F. P. *J. Org. Chem.* **2010**, *75*, 2776.
(190) Real, M. D.; Sestelo, J. P.; Sarandeses, L. A. *Tetrahedron Lett.* **2002**, *43*, 9111.
(191) Criado, A.; Gomez-Escalonilla, M. J.; Fierro, J. L.; Urbina, A.; Pena, D.; Guitian, E.; Langa, F. *Chem. Commun.* **2010**, *46*, 7028.
(192) Plugge, M.; Alain-Rizzo, V.; Audebert, P.; Brouwer, A. M. *J. Photochem. Photobiol. A: Chem.* **2012**, *234*, 12.
(193) Gong, Y.-H.; Miomandre, F.; Méallet-Renault, R.; Badré, S.; Galmiche, L.; Tang, J.; Audebert, P.; Clavier, G. *Eur. J. Org. Chem.* **2009**, *2009*, 6121.
(194) Clavier, G.; Audebert, P. *Chem. Rev.* **2010**, *110*, 3299.
(195) Albota, M.; Beljonne, D.; Bredas, J. L.; Ehrlich, J. E.; Fu, J. Y.; Heikal, A. A.; Hess, S. E.; Kogej, T.; Levin, M. D.; Marder, S. R.; McCord-Maughon, D.; Perry, J. W.; Rockel, H.; Rumi, M.; Subramaniam, G.; Webb, W. W.; Wu, X. L.; Xu, C. *Science* **1998**, *281*, 1653.
(196) Strehmel, B.; Sarker, A. M.; Detert, H. *ChemPhysChem* **2003**, *4*, 249.
(197) Koronyo, Y.; Salumbides, B. C.; Black, K. L.; Koronyo-Hamaoui, M. *Neurodegener. Dis.* **2012**, *10*, 285.
(198) Koronyo-Hamaoui, M.; Koronyo, Y.; Ljubimov, A. V.; Miller, C. A.; Ko, M. K.; Black, K. L.; Schwartz, M.; Farkas, D. L. *NeuroImage* **2011**, *54 Suppl 1*, S204.
(199) Sato, K.; Higuchi, M.; Iwata, N.; Saido, T. C.; Sasamoto, K. *Eur. J. Med. Chem.* **2004**, *39*, 573.
(200) Flaherty, D. P.; Kiyota, T.; Dong, Y.; Ikezu, T.; Vennerstrom, J. L. *J. Med. Chem.* **2010**, *53*, 7992.
(201) Shin, K. J.; Roh, E. J.; Lee, Y. S. *US 20100190803* **2010**.
(202) Skovronsky, D. M.; Zhang, B.; Kung, M. P.; Kung, H. F.; Trojanowski, J. Q.; Lee, V. M. *Proc. Natl. Acad. Sci. U. S. A.* **2000**, *97*, 7609.
(203) Hefendehl, J. K.; Wegenast-Braun, B. M.; Liebig, C.; Eicke, D.; Milford, D.; Calhoun, M. E.; Kohsaka, S.; Eichner, M.; Jucker, M. *J. Neurosci.* **2011**, *31*, 624.
(204) Kieser, D. *Ph.D. Dissertation* **2011**, *Technische Universität Darmstadt*.
(205) Zhuang, Z. P.; Kung, M. P.; Hou, C.; Skovronsky, D. M.; Gur, T. L.; Plossl, K.; Trojanowski, J. Q.; Lee, V. M.; Kung, H. F. *J. Med. Chem.* **2001**, *44*, 1905.
(206) Jiang, H.; Liu, B.; Li, Y.; Wang, A.; Huang, H. *Org. Lett.* **2011**, *13*, 1028.
(207) Higuchi, M.; Iwata, N.; Matsuba, Y.; Sato, K.; Sasamoto, K.; Saido, T. C. *Nat. Neurosci.* **2005**, *8*, 527.
(208) Kim, H. M.; Yang, W. J.; Kim, C. H.; Park, W. H.; Jeon, S. J.; Cho, B. R. *Chem. Eur. J.* **2005**, *11*, 6386.
(209) Achelle, S.; Nouira, I.; Pfaffinger, B.; Ramondenc, Y.; Ple, N.; Rodriguez-Lopez, J. *J. Org. Chem.* **2009**, *74*, 3711.
(210) Li, Y.; Duan, Y.; Li, J.; Zheng, J.; Yu, H.; Yang, R. *Anal. Chem.* **2012**, *84*, 4732−4738.
(211) Keum, S.-R.; Ku, B.-S.; Lee, M.-H.; Chi, G.-Y.; Lim, S.-S. *Dyes Pigm.* **2009**, *80*, 26.
(212) Raymo, F. M.; Giordani, S. *J. Am. Chem. Soc.* **2001**, *123*, 4651.
(213) Volkova, K. D.; Kovalska, V. B.; Balanda, A. O.; Vermeij, R. J.; Subramaniam, V.; Slominskii, Y. L.; Yarmoluk, S. M. *Biochem. Biophys. Methods* **2007**, *70*, 727.

(214) Gu, J.; Anumala, U. R.; Lo Monte, F.; Kramer, T.; Heyny von Haussen, R.; Holzer, J.; Goetschy-Meyer, V.; Mall, G.; Hilger, I.; Czech, C.; Schmidt, B. *Bioorg. Med. Chem. Lett.* **2012**, *22*, 7667.
(215) Boto, R. E. F.; El-Shishtawy, R. M.; Santos, P. F.; Reis, L. V.; Almeida, P. *Dyes Pigm.* **2007**, *73*, 195.
(216) Sutharsan, J.; Dakanali, M.; Capule, C. C.; Haidekker, M. A.; Yang, J.; Theodorakis, E. A. *ChemMedChem* **2010**, *5*, 56.
(217) Zhang, W.; Arteaga, J.; Cashion, D. K.; Chen, G.; Gangadharmath, U.; Gomez, L. F.; Kasi, D.; Lam, C.; Liang, Q.; Liu, C.; Mocharla, V. P.; Mu, F.; Sinha, A.; Szardenings, A. K.; Wang, E.; Walsh, J. C.; Xia, C.; Yu, C.; Zhao, T.; Kolb, H. C. *J. Alzheimers. Dis.* **2012**, *31*, 601.
(218) Li, Q.; Lee, J. S.; Ha, C.; Park, C. B.; Yang, G.; Gan, W. B.; Chang, Y. T. *Angew. Chem. Int. Ed. Engl.* **2004**, *43*, 6331.
(219) Langhals, H.; Varja, A.; Laubichler, P.; Kernt, M.; Eibl, K.; Haritoglou, C. *J. Med. Chem.* **2011**, *54*, 3903.
(220) Karlsson, H. J.; Bergqvist, M. H.; Lincoln, P.; Westman, G. *Bioorg. Med. Chem.* **2004**, *12*, 2369.
(221) Yan, W.; Wang, Q.; Lin, Q.; Li, M.; Petersen, J. L.; Shi, X. *Chem. Eur. J.* **2011**, *17*, 5011.
(222) De Moor, O.; Dorgan, C. R.; Johnson, P. D.; Lambert, A. G.; Lecci, C.; Maillol, C.; Nugent, G.; Poignant, S. D.; Price, P. D.; Pye, R. J.; Storer, R.; Tinsley, J. M.; Vickers, R.; Well, R.; Wilkes, F. J.; Wilson, F. X.; Wren, S. P.; Wynne, G. M. *Bioorg. Med. Chem. Lett.* **2011**, *21*, 4828.
(223) Fischer, W.; Fritzsche, K.; Wolf, W.; Bore, L. *WO 2002024668A1* **2002**.
(224) Ying, W. *Future Neurol.* **2008**, *3*, 1.
(225) Illum, L. *Eur. J. Pharm. Sci.* **2000**, *11*, 1.
(226) Boländer, A. *Ph.D. Dissertation* **2012**, *Technischen Universität Darmstadt*.
(227) Arnold, S. E.; Lee, E. B.; Moberg, P. J.; Stutzbach, L.; Kazi, H.; Han, L. Y.; Lee, V. M.; Trojanowski, J. Q. *Ann. Neurol.* **2010**, *67*, 462.
(228) Fodero-Tavoletti, M. T.; Mulligan, R. S.; Okamura, N.; Furumoto, S.; Rowe, C. C.; Kudo, Y.; Masters, C. L.; Cappai, R.; Yanai, K.; Villemagne, V. L. *Eur. J. Pharmacol.* **2009**, *617*, 54.
(229) Volkova, K. D.; Kovalska, V. B.; Losytskyy, M. Y.; Fal, K. O.; Derevyanko, N. O.; Slominskii, Y. L.; Tolmachov, O. I.; Yarmoluk, S. M. *J. Fluoresc.* **2011**, *21*, 775.
(230) Volkova, K. D.; Kovalska, V. B.; Segers-Nolten, G. M.; Veldhuis, G.; Subramaniam, V.; Yarmoluk, S. M. *Biotech. Histochem.* **2009**, *84*, 55.
(231) Li, D.; Zhang, H.; Wang, C.; Huang, S.; Guo, J.; Wang, Y. *J. Mater. Chem.* **2012**, *22*, 4319.
(232) Santra, M.; Moon, H.; Park, M. H.; Lee, T. W.; Kim, Y. K.; Ahn, K. H. *Chem. Eur. J.* **2012**, *18*, 9886.
(233) Ono, M.; Watanabe, H.; Kimura, H.; Saji, H. *ACS Chem. Neurosci.* **2012**, *3*, 319.
(234) Cumming, G.; Fidler, F.; Vaux, D. L. *J. Cell Biol.* **2007**, *177*, 7.

Jiamin Gu
Kasinostraße 27
64293 Darmstadt

Darmstadt, 07.01.2013

Erklärung

Ich erkläre hiermit, dass ich meine Dissertation selbständig und nur mit den angegebenen Hilfsmitteln angefertigt habe.

Jiamin Gu

Jiamin Gu
Kasinostraße 27
64293 Darmstadt

Darmstadt, 07.01.2013

Erklärung

Ich erkläre hiermit, noch keinen Promotionsversuch unternommen zu haben.

Jiamin Gu

Curriculum Vitae

Personal Data

Name: Jiamin Gu

Date of Birth: 11 September 1983

Place of Birth: Suzhou, Jiangsu, China

Nationality: Chinese

Marital Status: Married

Education Background

1/2010 – present	Ph.D. thesis: ”Design, synthesis and evaluation of fluorescent probes for the diagnosis of Alzheimer's disease and Parkinson's disease.” Under the supervision of Prof. Dr. Boris Schmidt, Clemens-Schöpf Institute of Chemistry and Biochemistry, Technische Universität Darmstadt, Germany
9/2006 – 3/2009	Master of science Department. of Chemistry, Tongji University, China
9/2002 – 7/2006	Bachelor of Engineering College of Chemistry and Chemical engineering, Yangzhou University, China
9/1999 – 6/2002	Senior high school Suzhou No.3 High School, China
9/1996 – 6/1999	Junior high school Suzhou No.4 High School, China
9/1990 – 6/1996	Primary school Suzhou Taowu-Central Primary School, China

Work Experience

9/2009 – 12/2009	Suzhou Applica Technology Co.Ltd, China
3/2009 – 6/2009	WuXi AppTec Co.Ltd, China

Publications

See the list in the preamble of the thesis.